Year : 2012

INTEGRATED APPLICATION OF GEOCHEMICAL AND GEOPHYSICAL METHODS FOR HYDROGEOLOGICAL IMPACT ASSESSMENT FOR TUNNELING IN FRACTURED ROCK

MARZOCCHI Roberto

UNIL | Université de Lausanne
Faculté des géosciences
et de l'environnement
Institut de Minéralogie et de Géochimie
Centre d'Analyse Minérale

INTEGRATED APPLICATION OF GEOCHEMICAL AND GEOPHYSICAL METHODS FOR HYDROGEOLOGICAL IMPACT ASSESSMENT FOR TUNNELING IN FRACTURED ROCK

Thèse de doctorat

Présentée à la
Faculté des Géosciences et de l'Environnement de l'Université de Lausanne
par

Roberto MARZOCCHI
Diplômé en Ingénierie des eaux et du sol
de l'Université de Gênes (Italie)

Jury
Professeur Jean-Luc EPARD, Université de Lausanne, Président du jury
Professeur Hans-Rudolf PFEIFER, Université de Lausanne, Directeur de thèse
Docteur Sebastián PERA, Haute Ecole Spécialisée de la Suisse Italienne, expert
Professeur Klaus HOLLIGER, Université de Lausanne, expert
Professeur Torsten VENNEMANN, Université de Lausanne, expert
Docteur Laurent DECROUY, Université de Lausanne, expert

Lausanne, Février 2012

UNIL | Université de Lausanne
Faculté des géosciences
et de l'environnement
Institut de Minéralogie et de Géochimie
Centre d'Analyse Minérale

INTEGRATED APPLICATION OF GEOCHEMICAL AND GEOPHYSICAL METHODS FOR HYDROGEOLOGICAL IMPACT ASSESSMENT FOR TUNNELING IN FRACTURED ROCK

Thèse de doctorat

Présentée à la
Faculté des Géosciences et de l'Environnement de l'Université de Lausanne
par

Roberto MARZOCCHI
Diplômé en Ingénierie des eaux et du sol
de l'Université de Gênes (Italie)

Jury
Professeur Jean-Luc EPARD, Université de Lausanne, Président du jury
Professeur Hans-Rudolf PFEIFER, Université de Lausanne, Directeur de thèse
Docteur Sebastián PERA, Haute Ecole Spécialisée de la Suisse Italienne, expert
Professeur Klaus HOLLIGER, Université de Lausanne, expert
Professeur Torsten VENNEMANN, Université de Lausanne, expert
Docteur Laurent DECROUY, Université de Lausanne, expert

Lausanne, Février 2012

UNIL | Université de Lausanne
Faculté des géosciences et de l'environnement
bâtiment Amphipôle
CH-1015 Lausanne

IMPRIMATUR

Vu le rapport présenté par le jury d'examen, composé de

Président de la séance publique :	M. le Professeur Jean-Luc Epard
Président du colloque :	M. le Professeur Jean-Luc Epard
Directeur de thèse :	M. le Professeur Hans-Rudolf Pfeifer
Expert externe :	M. le Docteur Sébastián Pera
Expert interne :	M. le Professeur Klaus Holliger
Expert interne :	M. le Professeur Torsten Vennemann
Expert interne :	M. le Docteur Laurent Decrouy

Le Doyen de la Faculté des géosciences et de l'environnement autorise l'impression de la thèse de

Monsieur Roberto MARZOCCHI

Laurea specialistica : Ingegneria delle acque e della difesa del suolo

intitulée

INTEGRATED APPLICATION OF GEOCHEMICAL AND GEOPHYSICAL METHODS FOR HYDROGEOLOGICAL IMPACT ASSESSMENT FOR TUNNELING IN FRACTURED ROCK

Lausanne, le 17 février 2012

Pour le Doyen de la Faculté des géosciences et de l'environnement

Professeur Jean-Luc Epard, Vice-Doyen

Table of contents

List of figures

List of tables

Acknowledgments

I want to thank Prof. Hans-Rudolf Pfeifer for the help, support and encouragement he had given me during the last 3.5 years. In addition to scientific teaching, he had passed on me his enthusiasm and his passion for the scientific work.

Sincere thanks are due to Dr. Sebastian Pera co-tutor of my thesis for the support and encouragement. Although I was completely free and I could direct my research, he was able to give me good inputs and to lead my work during all the 3.5 years.

I am also thankful to all the members of the jury (Dr. Laurent Decrouy, Prof. Klaus Holliger and Prof. Torsten Venneman) for their feedbacks during the annual meetings organized to better define the PhD project.

It is also due a special remember of Prof. Gian Maria Zuppi, who initially conceived this project. He prematurely passed away on 12 May 2011. I had only a few of time to realize his competence, but during the first steps of my PhD, I have appreciated his simplicity and kindness.

I would also like to express my gratitude to Dr. Yama Tomonaga and Prof. Rolf Kipfer, of Swiss Federal Institute of Aquatic Science and Technology (EAWAG), for their fundamental scientific support concerning noble gas analysis. Their passion for the science was praiseworthy and their competences were precious to direct my efforts in the correct way.

I am also thankful to Morgane Tournier, Jean-Claude Lavanchy and Silwan Daouk for their precious supports during the geochemical analysis in Lausanne.

Special thanks are also due to Dr. Ludovic Baron, geophysical engineer at the geophysical institute of the Lausanne University (IG-UNIL), for the technical support and for the precious advices in interpreting geoelectrical results.

I am also thankful to AlpTransit Gotthard Ltd, Commissione Federale di Stima 13° Circondario and Federal Roads Office (FEDRO) for the agreements signed for tunnel access (Monte Ceneri base tunnel and San Fedele tunnel) and for the provided data. In particular, I would like to express my gratitude to the geologists that work with me during these years (Reto De Paoli, Pierre-François Erard, François Ghirlanda, Jean Frederic Kauffmann and Gianfranco Monti) for the helpfulness and interest demonstrated. Moreover, I am grateful to Geol. Jean Claude Bestenheider for the precious suggestions and information.

Finally, in Italian for my colleagues and friends…

Un ringraziamento speciale e davvero molto sentito lo devo a tutti i miei fantastici colleghi dell'Istituto Scienze della Terra. Cito solo i più giovani, sperando di non offendere nessuno, Mirko, Moreno, Claudio, Monia, Maurizio, Linda e Marie Louise. Mi hanno sempre incoraggiato e aiutato e con loro ho avuto il piacere di condividere piacevolissimi momenti al lavoro e non solo.

Doverosa menzione va ai compagni delle partite di calcetto del martedì, in particolare a Massimiliano, Marco e Alessio, per aver sopportato i miei piedi a banana.

Un ringraziamento speciale è destinato ai fantastici volontari del *Gruppolo d'Uva*: Paola, Michela, Roberta, Manju, Lorenzo, etc., per la gioia condivisa nel donare ritagli del proprio tempo e per i piacevoli momenti trascorsi assieme.

Giunto alla terza, spero ultima, tesi della mia vita, dedico per la prima volta un ringraziamento anche ai *genovesi*. Grazie di cuore alla mia strana famiglia, a chi c'è come a chi non c'è più, ai nonni Piera, Carlo, Alcide e Anna, alla mia prima maestra Elsa, nonché quinta nonna, ai miei genitori e infine, ma solo in quanto ultimi arrivati, ai miei fratellini Elena, Ennio, Pietro e Margherita, che in questi anni hanno molto apprezzato le vacanze in Svizzera.

Infine grazie a tutti i miei amici. Non volendo fare torto a nessuno cito solo chi in questi anni ha visitato la mia mansarda ticinese, nell'ordine Giovanni, Matteo, Vittorio, Francesca, Danilo, Anna e Victor.

Abstract

The interaction of tunneling with groundwater is a problem both from an environmental and an engineering point of view. In fact, tunnel drilling may cause a drawdown of piezometric levels and water inflows into tunnels that may cause problems during excavation of the tunnel. While the influence of tunneling on the regional groundwater systems may be adequately predicted in porous media using analytical solutions, such an approach is difficult to apply in fractured rocks. Numerical solutions are preferable and various conceptual approaches have been proposed to describe and model groundwater flow through fractured rock masses, ranging from equivalent continuum models to discrete fracture network simulation models. However, their application needs many preliminary investigations on the behavior of the groundwater system based on hydrochemical and structural data.

To study large scale flow systems in fractured rocks of mountainous terrains, a comprehensive study was conducted in southern Switzerland, using as case studies two infrastructures actually under construction: (i) the Monte Ceneri base railway tunnel (Ticino), and the (ii) San Fedele highway tunnel (Roveredo, Graubünden). The chosen approach in this study combines the temporal and spatial variation of geochemical and geophysical measurements. About 60 localities from both surface and underlying tunnels were temporarily and spatially monitored during more than one year. At first, the project was focused on the collection of hydrochemical and structural data. A number of springs, selected in the area surrounding the infrastructures, were monitored for discharge, electric conductivity, pH, and temperature. Water samples (springs, tunnel inflows and rains) were taken for isotopic analysis; in particular the stable isotope composition (δ^2H, $\delta^{18}O$ values) can reflect the origin of the water, because of spatial (recharge altitude, topography, etc.) and temporal (seasonal) effects on precipitation which in turn strongly influence the isotopic composition of groundwater. Tunnel inflows in the accessible parts of the tunnels were also sampled and, if possible, monitored with time. Noble-gas concentrations and their isotope ratios were used in selected locations to better understand the origin and the circulation of the groundwater. In addition, electrical resistivity and VLF-type electromagnetic surveys were performed to identify water bearing fractures and/or weathered areas that could be intersected at depth during tunnel construction.

The main goal of this work was to demonstrate that these hydrogeological data and geophysical methods, combined with structural and hydrogeological information, can be successfully used in order to develop hydrogeological conceptual models of the groundwater flow in regions to be exploited for tunnels. The main results of the project are: *(i)* to have successfully tested the application of electrical resistivity and VLF-electromagnetic surveys to asses water-bearing zones during tunnel drilling; *(ii)* to have verified the usefulness of noble gas, major ion and stable isotope compositions as proxies for the detection of faults and to understand the origin of the groundwater and its flow regimes (direct rain water infiltration or groundwater of long residence time); and *(iii)* to have convincingly tested the combined application of a geochemical and geophysical approach to assess and predict the vulnerability of springs to tunnel drilling.

Résumé

L'interférence entre eaux souterraines et des tunnels pose des problèmes environnementaux et de génie civile. En fait, la construction d'un tunnel peut faire abaisser le niveau des nappes piézométriques et faire infiltrer de l'eau dans le tunnel et ainsi créer des problème pendant l'excavation. Alors que l'influence de la construction d'un tunnel sur la circulation régionale de l'eau souterraine dans des milieux poreux peut être prédite relativement facilement par des solution analytiques de modèles, ceci devient difficile dans des milieux fissurés. Dans ce cas-là, des solutions numériques sont préférables et plusieurs approches conceptuelles ont été proposées pour décrire et modéliser la circulation d'eau souterraine à travers les roches fissurées, en allant de modèles d'équivalence continue à des modèles de simulation de réseaux de fissures discrètes. Par contre, leur application demande des investigations importantes concernant le comportement du système d'eau souterraine basées sur des données hydrochimiques et structurales.

Dans le but d'étudier des grands systèmes de circulation d'eau souterraine dans une région de montagnes, une étude complète a été fait en Suisse italienne, basée sur deux grandes infrastructures actuellement en construction: *(i)* Le tunnel ferroviaire de base du Monte Ceneri (Tessin) et *(ii)* le tunnel routière de San Fedele (Roveredo, Grisons). L'approche choisie dans cette étude est la combinaison de variations temporelles et spatiales des mesures géochimiques et géophysiques. Environs 60 localités situées à la surface ainsi que dans les tunnels soujacents ont été suiviès du point de vue temporel et spatial pendant plus de un an. Dans un premier temps le projet se focalisait sur la collecte de données hydrochimiques et structurales. Un certain nombre de sources, sélectionnées dans les environs des infrastructures étudiées ont été suivies pour le débit, la conductivité électrique, le pH et la température. De l'eau (sources, infiltration d'eau de tunnel et pluie) a été échantillonnés pour des analyses isotopiques; ce sont surtout les isotopes stables (δ^2H, δ^{18}O) qui peuvent indiquer l'origine d'une eaux, à cause de la dépendance d'effets spatiaux (altitude de recharge, topographie etc.) ainsi que temporels (saisonaux) sur les précipitations météoriques , qui de suite influencent ainsi la composition isotopique de l'eau souterraine. Les infiltrations d'eau dans les tunnels dans les parties accessibles ont également été échantillonnées et si possible suivies au cours du temps. La concentration de gaz nobles et leurs rapports isotopiques ont également été utilisées pour quelques localités pour mieux comprendre l'origine et la circulation de l'eau souterraine. En plus, des campagnes de mesures de la résistivité électrique et électromagnétique de type VLF ont été menées afin d'identifier des zone de fractures ou d'altération qui pourraient interférer avec les tunnels en profondeur pendant la construction.

Le but principal de cette étude était de démontrer que ces données hydrogéologiques et géophysiques peuvent être utilisées avec succès pour développer des modèles hydrogéologiques conceptionels de tunnels. Les résultats principaux de ce travail sont : i) d'avoir testé avec succès l'application de méthodes de la tomographie électrique et des campagnes de mesures électromagnétiques de type VLF afin de trouver des zones riches en eau pendant l'excavation d'un tunnel ; ii) d'avoir prouvé l'utilité des gaz nobles, des analyses ioniques et d'isotopes stables pour déterminer l'origine de l'eau infiltrée (de la pluie par le haut ou ascendant de l'eau remontant des profondeurs) et leur flux et pour déterminer la position de failles ; et iii) d'avoir testé d'une manière convainquant l'application combinée de méthodes géochimiques et géophysiques pour juger et prédire la vulnérabilité de sources lors de la construction de tunnels.

Riassunto

L'interazione dei tunnel con il circuito idrico sotterraneo costituisce un problema sia dal punto di vista ambientale che ingegneristico. Lo scavo di un tunnel può infatti causare abbassamenti dei livelli piezometrici, inoltre le venute d'acqua in galleria sono un notevole problema sia in fase costruttiva che di esercizio. Nel caso di acquiferi in materiale sciolto, l'influenza dello scavo di un tunnel sul circuito idrico sotterraneo, in genere, può essere adeguatamente predetta attraverso l'applicazione di soluzioni analitiche; al contrario un approccio di questo tipo appare inadeguato nel caso di scavo in roccia. Per gli ammassi rocciosi fratturati sono piuttosto preferibili soluzioni numeriche e, a tal proposito, sono stati proposti diversi approcci concettuali; nella fattispecie l'ammasso roccioso può essere modellato come un mezzo discreto o continuo equivalente. Tuttavia, una corretta applicazione di qualsiasi modello numerico richiede necessariamente indagini preliminari sul comportamento del sistema idrico sotterraneo basate su dati idrogeochimici e geologico strutturali.

Per approfondire il tema dell'idrogeologia in ammassi rocciosi fratturati tipici di ambienti montani, è stato condotto uno studio multidisciplinare nel sud della Svizzera sfruttando come casi studio due infrastrutture attualmente in costruzione: *(i)* il tunnel di base del Monte Ceneri (canton Ticino) e *(ii)* il tunnel autostradale di San Fedele (Roveredo, canton Grigioni). L'approccio di studio scelto ha cercato di integrare misure idrogeochimiche sulla qualità e quantità delle acque e indagini geofisiche. Nella fattispecie sono state campionate le acque in circa 60 punti spazialmente distribuiti sia in superficie che in sotterraneo; laddove possibile il monitoraggio si è temporalmente prolungato per più di un anno. In una prima fase, il progetto di ricerca si è concentrato sull'acquisizione dati. Diverse sorgenti, selezionate nelle aree di possibile influenza attorno alle infrastrutture esaminate, sono state monitorate per quel che concerne i parametri fisico-chimici: portata, conduttività elettrica, pH e temperatura. Campioni d'acqua sono stati prelevati mensilmente su sorgenti, venute d'acqua e precipitazioni, per analisi isotopiche; nella fattispecie, la composizione in isotopi stabili (δ^2H, $\delta^{18}O$) tende a riflettere l'origine delle acque, in quanto, variazioni sia spaziali (altitudine di ricarica, topografia, etc.) che temporali (variazioni stagionali) della composizione isotopica delle precipitazioni influenzano anche le acque sotterranee. Laddove possibile, sono state campionate le venute d'acqua in galleria sia puntualmente che al variare del tempo. Le concentrazioni dei gas nobili disciolti nell'acqua e i loro rapporti isotopici sono stati altresì utilizzati in alcuni casi specifici per meglio spiegare l'origine delle acque e le tipologie di circuiti idrici sotterranei. Inoltre, diverse indagini geofisiche di resistività elettrica ed elettromagnetiche a bassissima frequenza (VLF) sono state condotte al fine di individuare le acque sotterranee circolanti attraverso fratture dell'ammasso roccioso.

Principale obiettivo di questo lavoro è stato dimostrare come misure idrogeochimiche ed indagini geofisiche possano essere integrate allo scopo di sviluppare opportuni modelli idrogeologici concettuali utili per lo scavo di opere sotterranee. I principali risultati ottenuti al termine di questa ricerca sono stati: *(i)* aver testato con successo indagini geofisiche (ERT e VLF-EM) per l'individuazione di acque sotterranee circolanti attraverso fratture dell'ammasso roccioso e che possano essere causa di venute d'acqua in galleria durante lo scavo di tunnel; *(ii)* aver provato l'utilità di analisi su gas nobili, ioni maggiori e isotopi stabili per l'individuazione di faglie e per comprendere l'origine delle acque sotterranee (acque di recente infiltrazione o provenienti da circolazioni profonde); *(iii)* aver testato in maniera convincente l'integrazione delle indagini geofisiche e di misure geochimiche per la valutazione della vulnerabilità delle sorgenti durante lo scavo di nuovi tunnel.

Résumé grand public

"La NLFA (Nouvelle Ligne Ferroviaire à travers les Alpes) axe du Saint-Gothard est le plus important projet de construction de Suisse. En bâtissant la nouvelle ligne du Saint-Gothard, la Suisse réalise un des plus grands projets de protection de l'environnement d'Europe". Cette phrase, qu'on lit comme présentation du projet Alptransit est particulièrement éloquente pour expliquer l'utilité des nouvelles lignes ferroviaires transeuropéens pour le développement durable. Toutefois, comme toutes grandes infrastructures, la construction de nouveaux tunnels ont des impacts inévitables sur l'environnement. En particulier, le possible drainage des eaux souterraines réalisées par le tunnel peut provoquer un abaissement du niveau des nappes piézométriques. De plus, l'écoulement de l'eau à l'intérieur du tunnel, conduit souvent à des problèmes d'ingénierie. Par exemple, d'importantes infiltrations d'eau dans le tunnel peuvent compliquer les phases d'excavation, provoquant un retard dans l'avancement et dans le pire des cas, peuvent mettre en danger la sécurité des travailleurs. Enfin, l'infiltration d'eau peut être un gros problème pendant le fonctionnement du tunnel. Du point de vue de la science, avoir accès à des infrastructures souterraines représente une occasion unique d'obtenir des informations géologiques en profondeur et pour echantillonner des eaux autrement inaccessibles.

Dans ce travail, nous avons utilisé une approche pluridisciplinaire qui intègre des mesures d'étude hydrogéochimiques effectués sur les eaux de surface et des investigations géophysiques indirects, tels que la tomographie de résistivité électrique (TRE) et les mesures électromagnétiques de type VLF. L'étude complète a été fait en Suisse italienne, basée sur deux grandes infrastructures actuellement en construction, qui sont le tunnel ferroviaire de base du Monte Ceneri, une partie du susmentionné projet Alptransit, situé entièrement dans le canton Tessin, et le tunnel routière de San Fedele, situé a Roveredo dans le canton des Grisons. Le principal objectif était de montrer comment il était possible d'intégrer les deux approches, géophysiques et géochimiques, afin de répondre à la question de ce que pourraient être les effets possibles dû au drainage causés par les travaux souterrains. L'accès aux galeries ci-dessus a permis une validation adéquate des enquêtes menées confirmant, dans chaque cas, les hypothèses proposées.

À cette fin, nous avons fait environ 50 profils géophysiques (28 imageries électrique bidimensionnels et 23 électromagnétiques) dans les zones de possible influence par le tunnel, dans le but d'identifier les fractures et les discontinuités dans lesquelles l'eau souterraine peut circuler. De plus, des eaux ont été échantillonnés dans 60 localités situées la surface ainsi que dans les tunnels subjacents, le suivi mensuelle a duré plus d'un an.

Nous avons mesurés tous les principaux paramètres physiques et chimiques: débit, conductivité électrique, pH et température. De plus, des échantillons d'eaux ont été prélevés pour l'analyse mensuelle des isotopes stables de l'hydrogène et de l'oxygène (δ^2H, $\delta^{18}O$). Avec ces analyses, ainsi que par la mesure des concentrations des gaz rares dissous dans les eaux et de leurs rapports isotopiques que nous avons effectués dans certains cas spécifiques, il était possible d'expliquer l'origine des différents eaux souterraines, les divers modes de recharge des nappes souterraines, la présence de possible phénomènes de mélange et, en général, de mieux expliquer les circulations d'eaux dans le sous-sol.

Le travail, même en constituant qu'une réponse partielle à une question très complexe, a permis d'atteindre certains importants objectifs. D'abord, nous avons testé avec succès l'applicabilité des méthodes géophysiques indirectes (TRE et électromagnétiques de type VLF) pour prédire la présence d'eaux souterraines dans le sous-sol des massifs rocheux. De plus, nous avons démontré l'utilité de l'analyse des gaz rares, des isotopes stables et de l'analyses des ions majeurs pour la détection de failles et pour comprendre l'origine des eaux souterraines (eau de pluie par le haut ou eau remontant des profondeurs). En conclusion, avec cette recherche, on a montré que l'intégration des ces informations (géophysiques et géochimiques) permet le développement de modèles conceptuels appropriés, qui permettant d'expliquer comment l'eau souterraine circule. Ces modèles permettent de prévoir les infiltrations d'eau dans les tunnels et de prédire la vulnérabilité de sources et des autres ressources en eau lors de construction de tunnels.

Presentazione del lavoro

"L'asse NTFA (Nuova Trasversale Ferroviaria Alpina) del San Gottardo è il progetto edilizio più imponente della Svizzera. Con la costruzione della nuova ferrovia del San Gottardo la Svizzera realizza in Europa uno dei maggiori progetti per la tutela dell'ambiente." Questa frase che si legge come presentazione del progetto Alptransit è particolarmente eloquente allo scopo di spiegare l'utilità delle nuove linee ferroviarie trans-europee nell'ottica di uno sviluppo sostenibile. Tuttavia, come tutte le grandi infrastrutture, la costruzione di nuovi tunnel presenta alcuni inevitabili impatti sull'ambiente circostante. In particolare, il possibile drenaggio di acque sotterranee operato dal tunnel può causare un abbassamento del livello piezometrico. Inoltre il deflusso di acqua all'interno del tunnel comporta spesso problemi di tipo ingegneristico: consistenti infiltrazioni d'acqua in galleria possono infatti complicare le fasi di scavo, causando ritardo nell'avanzamento e, nei casi peggiori, ponendo a rischio la sicurezza dei lavoratori; infine eventuali infiltrazioni possono costituire un notevole problema anche nella fase di esercizio del tunnel stesso. Dal punto di vista prettamente scientifico, poter accedere a opere sotterranee rappresenta invece un'opportunità unica per ottenere informazioni geologiche in profondità e campionare acque altrimenti irraggiungibili.

Nel presente lavoro, si è scelto di utilizzare un approccio di studio multidisciplinare capace di integrare misure idrogeochimiche condotte sulle acque superficiali e indagini geofisiche indirette, quali la tomografia di resistività elettrica (ERT) e metodi elettromagnetici a bassissima frequenza (VLF-EM). Lo studio è stato condotto nel sud della Svizzera, utilizzando come casi di studio due infrastrutture in costruzione: il tunnel di base del Monte Ceneri, parte del già citato progetto Alptransit e situato interamente nel Canton Ticino e il tunnel autostradale di San Fedele, sito a Roveredo nel Canton Grigioni. Principale obiettivo è stato dimostrare come fosse possibile integrare i due approcci, geofisico e geochimico, allo scopo di rispondere alla domanda su quali possano essere gli eventuali effetti dovuti al drenaggio delle opere sotterranee. L'accesso alle gallerie di cui sopra ha permesso un'adeguata validazione delle indagini effettuate confermando, caso per caso, le ipotesi proposte.

A tale scopo si sono realizzati circa 50 profili geofisici (28 geoelettrici e 23 elettromagnetici) nelle zone di possibile influenza del tunnel con lo scopo di individuare fratture e discontinuità all'interno delle quali circolassero le acque sotterranee. Inoltre sono state campionate le acque in circa 60 punti spazialmente distribuiti sia in superficie che in sotterraneo con un monitoraggio su base mensile che, laddove possibile, è durato più di un anno. Sono stati misurati tutti i principali parametri chimico-fisici: portata, conduttività elettrica, pH, temperatura, e campioni d'acqua sono stati prelevati mensilmente per analisi sugli isotopi stabili di idrogeno e ossigeno (δ^2H, $\delta^{18}O$). Con queste analisi, come anche attraverso la misura delle concentrazioni dei gas nobili disciolti nell'acqua e dei loro rapporti isotopici condotte in alcuni specifici casi, è stato possibile spiegare l'origine delle diverse acque sotterranee, le modalità di ricarica, la presenza di eventuali fenomeni di mescolamento all'interno del sottosuolo e più in generale le tipologie di circuiti idrici sotterranei.

Il lavoro, pur inserendosi in un ambito molto complesso e costituendo solo una parziale risposta alla domanda iniziale, ha permesso il raggiungimento di alcuni importanti obiettivi. In primo luogo si è testata con successo l'applicabilità di indagini indirette di tipo geofisico (ERT e VLF-EM) per prevedere la presenza nel sottosuolo di acqua sotterranea all'interno degli ammassi rocciosi. Inoltre si è provata l'utilità di analisi su gas nobili, ioni maggiori e isotopi stabili per l'individuazione di faglie e per comprendere l'origine delle acque sotterranee (acque di recente infiltrazione o provenienti da circolazioni profonde). In conclusione, con questa ricerca si è dimostrato come l'integrazione delle suddette informazioni permetta di sviluppare opportuni modelli idrogeologici concettuali capaci di spiegare le modalità dei deflussi idrici sotterranei. Modelli, questi ultimi, che sono un indispensabile punto di partenza per una successiva applicazione di soluzioni numeriche o opportuni approcci stocastici (metodi parametrici) capaci di predire le eventuali venute d'acqua all'interno delle gallerie e la vulnerabilità di sorgenti e risorse idriche in genere.

1. General introduction

1.1 Significance of the study

"*Water is the driving force of all the nature*". This sentence was written in the XVI century by Leonardo da Vinci. Water in fact is the most distributed substance on the surface of our planet. In different amounts, it is present everywhere and plays an important role in the environment and human life (Table. 1.1). From total water resources, only 2.5% is constituted by fresh water, with the greater portion (68.7%) made up by permanent ice and snow cover in the Antarctic, Arctic, and mountainous regions. 30.1% is contained in the ground, while only about 0.3% of the total is concentrated in lakes, reservoirs, and rivers.

Table 1.1 - The distribution of water across the globe (Shiklomanov, 2000)

Location	**Volume [10^3 Km^3]**	**% of total hydrosphere**	**% of freshwater**	**Volume Recycled annually (km^3)**	**Renewal period years**
Ocean	1,338,000	96.5	–	505,000	2,500
Groundwater (gravity and capillary)	23,4001	1.7		16,700	1,400
Predominantly fresh groundwater	10,530	0.76	30.1		
Soil moisture	16.5	0.001	0.05	16,500	1
Glaciers and permanent snow cover:	24,064	1.74	68.7		
Antarctica	21,600	1.56	61.7		
Greenland	2,340	0.17	6.68	2,477	9,700
Arctic Islands	83.5	0.006	0.24		
Mountainous regions	40.6	0.003	0.12	25	1,600
Ground ice (permafrost)	300	0.022	0.86	30	10,000
Water in lakes:	176.4	0.013	–	10,376	17
Fresh	91.0	0.007	0.26		
Salt	85.4	0.006	–		
Marshes and swamps	11.5	0.0008	0.03	2,294	5
River water	2.12	0.0002	0.006	43,000	16 days
Biological water	1.12	0.0001	0.003		–
Water in the atmosphere	12.9	0.001	0.04	600,000	8 days
Total volume in the hydrosphere	1,386,000	100	–		
Total freshwater	35,029.2	2.53	100		

Table 1.1 shows in detail the different uses of groundwater constituting 98% of the liquid freshwater resources of the world. Since it is not easily renewable, its conservation and its stable availability for human uses in the next years (drinking water, industrial water, agricultural water, etc.) is a common concern (Figure 1.1).

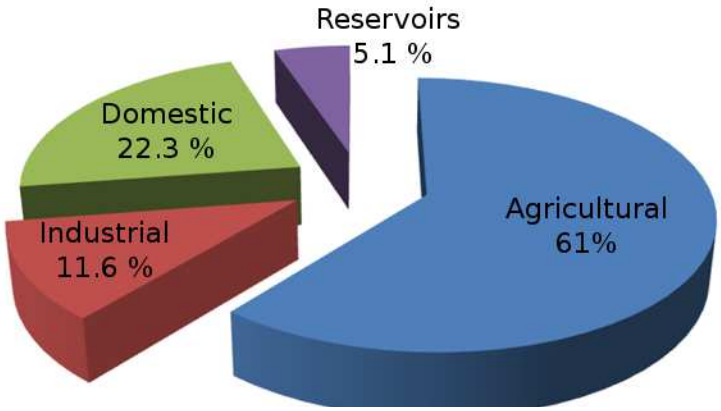

Figure 1.1- Predicted use of water in 2025 (Rosegrant et al., 2002)

Besides, for a sustainable economic development, in the European countries, there is an increasing need of new transport infrastructures such as the high capacity railways (EU commission, 2001). The construction of these railways, especially in mountainous regions (e.g. Alps, Apennines, Pyrenees, etc.), often implies excavation of tunnels. These underground infrastructures, in not properly planned, may have different impacts on the surrounding areas, of which one of the main ones is on the regional hydrogeological systems (Figure 1.2). In fact, water drainage through a tunnel is likely to cause a drawdown of the piezometric level, and hence a possible decrease of spring's discharge and well levels. Its impact can be in terms of both groundwater quantity and quality, and its effect can be manifested on the surface by alteration of the discharge of the hydrogeological basin, vegetation changes, subsidence phenomena (Zangler, 2008a; 2008b) and stability of slopes.

The study area is located in Ticino (Figure 1.3), southern Switzerland, is very interesting for both groundwater resources and construction of new tunnel infrastructures. In Ticino, in fact, groundwater is the most important source of drinking water (Pera et al., 2008). Moreover various tunnels were under construction while this study was undertaken (e.g. Monte Ceneri base tunnel, San Fedele tunnel, etc.), offering a unique opportunity to sample and study waters that otherwise are difficult to access (Figure 1.4).

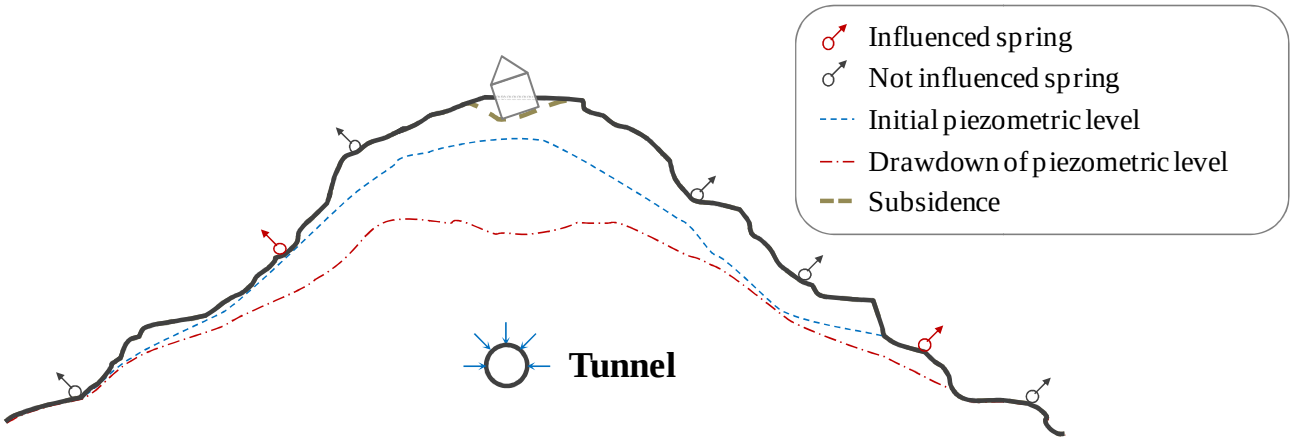

Figure 1.2 - Schematic view of the hydrogeological interferences of tunnel

Figure 1.3 - Position of the studied region, located in the southern Switzerland (CH), in the pre-alpine region (aerial photo from Google®)

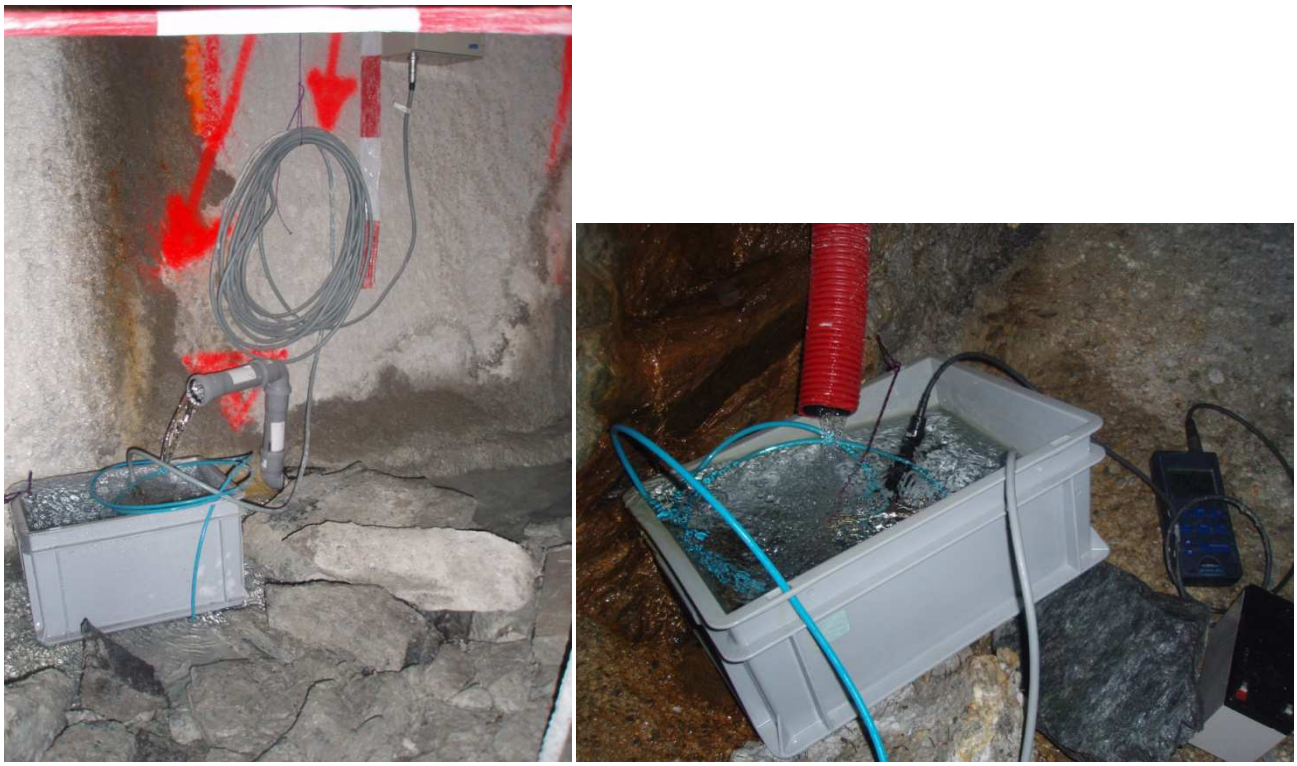

Figure 1.4 - Examples of sampling structures installed within the tunnel during the research project (Northern portal of the Monte Ceneri base tunnel)

1.2 Groundwater occurrence

Geological materials containing groundwater can be classified as aquicludes, aquitards and aquifers according to their increasing capacity to store and release water. On the basis od the origin of its porosity, three main types of aquifers can be distinguished (Fig. 1.5):

i. sediments with a homogeneous porous structure where water circulates within the voids among grains;
ii. fractured rocks with a inhomogeneous porosity derived from discontinuities within the rock

masses;

iii. karstified carbonate rocks and evaporites with large cavities and conduits originated by dissolution.

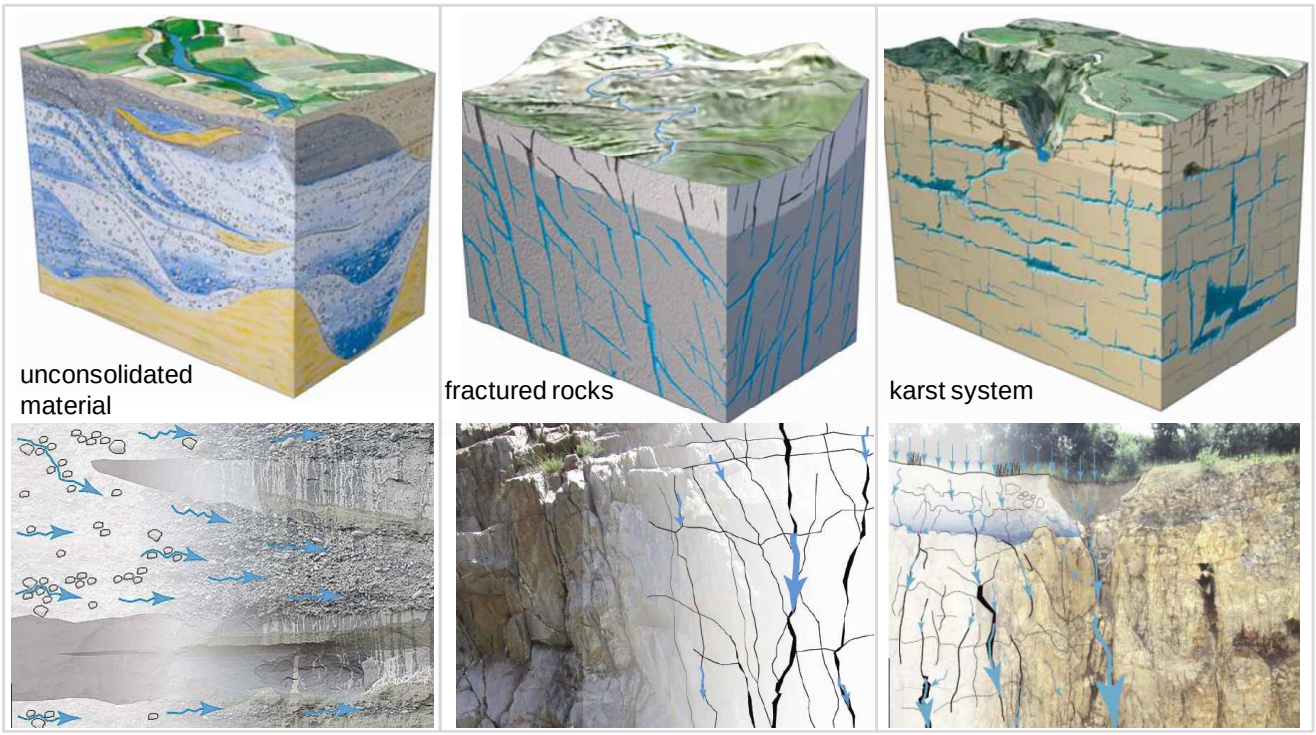

Figure1.5 - Typical patterns of groundwater systems (Brühlmann et al. 2004)

Concerning the presence of discontinuities in rock masses, they might be homogeneously distributed and developed, or have more developed fractures. According to different situations (Fig. 1.6) slightly and strongly heterogeneous fractured rock masses may be distinguished.

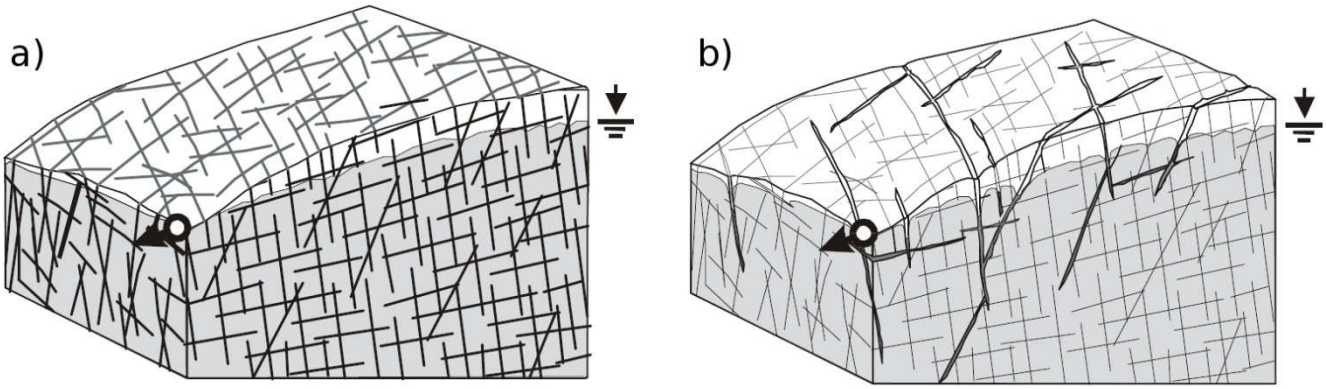

Figure 1.6 - Patterns for fractured rock masses according to Pochon and Zwahlen (2003). a) slightly and b) strongly heterogeneous fractured rock masses.

1.3 The scientific question

As previously described and shown in Figure 1.2, several geological and hydrogeological issues need to be addressed prior and during tunnel drilling in a complex geological context such as the Alpine region,. In particular:

i. impact of tunnel drilling on the local and regional groundwater system;
ii. possible water inflow into the tunnel that may occurs during its construction and that may be a problem during excavation or tunnel service.

1.4 State of the art: study approaches

Understanding the interaction between tunneling and groundwater, especially in fractured rock, is very complex, and currently the state of the art of the research in this field includes three possible approaches which can quantify tunnel drainage effects and related impacts:

i. analytical methods
ii. numerical methods
iii. parametric methods

The first method consists of the application of analytical equations to calculate the discharge of tunnel water inflows. Several equations are proposed in the literature to evaluate the discharge in steady or unsteady conditions (Muskat, 1937; Goodman et al., 1965; Lei, 1999; El Tani, 2003; Kolymbas and Wagner, 2007; Perrochet, 2005; etc.). They consider the presence of (i) a water table in initial conditions, (ii) some hydrogeological parameters of the underground (e.g. hydraulic conductivity, volumetric specific storage, etc.) and finally (iii) the tunnel radius. The tunnel is in practice considered as a drain excavated through homogeneous media. This approach is frequently used in engineering because it is the simplest way to quantify the expected discharge of the groundwater drained by the tunnel; although it may give good results in porous-media aquifer, this approach is probably inadequate to correctly predict the possible impact of tunneling in case of fractured rock masses or kartstic media, due to the high heterogeneity that may characterize these geological materials.

Alternative approaches that could be more suitable to fractured media are constituted by numerical or parametric models (Vincenzi et al, 2010). Numerical models can be used to estimate the potential tunnel inflows and the possible impact on the surrounding water resurgence points (springs, streams or wells). In fact, considering the correct boundary conditions and the hydrogeological parameters of the rock, these models allow the flow equations to be solved with numerical finite difference (e.g MODFLOW) or finite element (e.g. FEFLOW, Groundwater, etc.) methods. The correct estimation of hydrogeological parameters of medium and of boundary conditions is obviously fundamental in order to correctly describe the hydrogeological behaviour of rock masses.

The parametric methods consist of evaluating the potential hydrogeological impact of tunneling in terms of hazard. For instance, in recent years two possible applications have been proposed by Cesano (Cesano et al., 2000, Cesano 2001) and De Matteis (De Matteis et al. 2001, Torri et al., 2007; De Matteis 2008). The first is specifically suggested by the authors in order to obtain the tunnel inflow hazard distinguishing between major and minor inflows, while the second method evaluates the aquifer depletion hazard, caused by the new tunnel drilling and its impact on the surrounding water points (wells and springs). implementation of these methods can be facilitated using a Geographic Information System – GIS (Pancescu, 2006). Nevertheless, this approach requires a good knowledge of geological and hydrogeological parameters of the tunnel, rock masses, springs or wells, to formulate reliable hypothesis on the hydrogeological cycle.

In the following sections these three different approaches are presented in detail.

1.4.1 Analytical method

Some analytical formulas to calculate the water inflows into the tunnel are given. Due to their simplicity, in the engineering practice, they are often applied in tunnel design. The available equations in the literature can be grouped into:

i. steady state equations, where the discharge is calculated independently of the time, and dynamic equilibrium assumed;
ii. unsteady state equations (Figure 1.7) where the water level is evaluated at the different times after drilling.

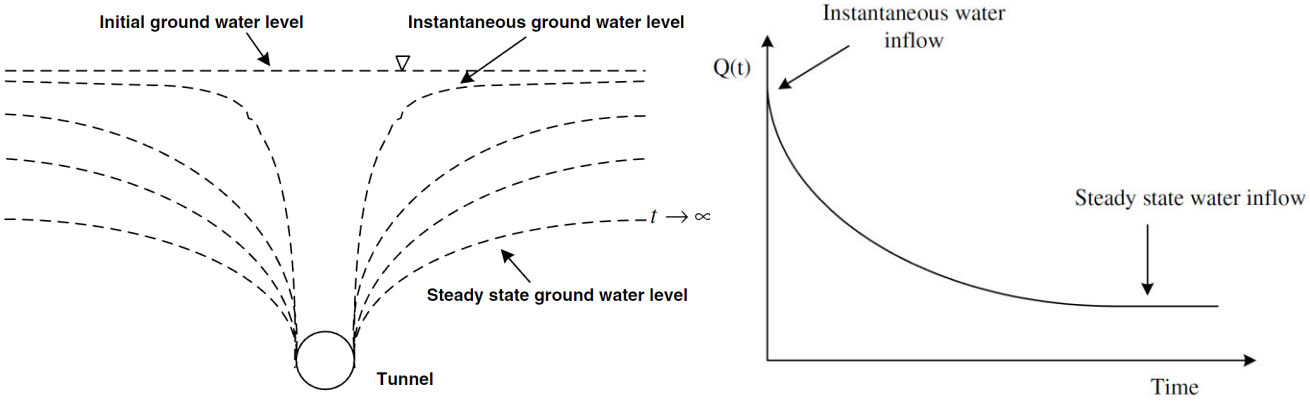

Water inflow and drawdown nearby a tunnel — Tunnel water inflow history

Figure 1.7 - Water inflows evaluation in unsteady condition, considering the position of the water table within the ground changing with time

- *Steady state equations*

A first equation has been proposed by Muskat (1937) and by Goodman et al. (1965):

$$Q = \frac{2\pi KL(H - h_t)}{\ln\left(\frac{2H - 2h_t}{r}\right)} \tag{1.1}$$

where Q represents the discharge drained by the tunnel [m^3/s], K is the permeability coefficient [m/s], L is the tunnel length [m], H is the water table elevation in initial conditions [m], h_t the elevation of the tunnel axis [m] and *r* is the tunnel radius [m].

Other similar steady state equations are also proposed by different authors:

a) Karlsud (2001):

$$Q = \frac{2\pi KL(H - h_t)}{\ln\left(2\frac{H - h_t}{r} - 1\right)} \tag{1.2}$$

b) Lombardi, 2002 (reported in El Tani, 2003):

$$Q = \frac{2\pi KL(H - h_t)}{\left[1 + 0.4\left(\frac{r}{H - h_t}\right)^2\right] ln\left(2\frac{H - h_t}{r}\right)} \tag{1.3}$$

c) El Tani (2003):

$$Q = \frac{2\pi KL(H - h_t)\left[1 - 3\left(\frac{r}{2(H - h_t)}\right)^2\right]}{\left[1 - \left(\frac{r}{2(H - h_t)}\right)^2\right] \ln\left(\frac{2(H - h_t)}{r}\right) - \left(\frac{r}{2(H - h_t)}\right)^2} \tag{1.4}$$

d) previously reported equations have been modified by Lei (1999), with the hypothesis of a water level above the terrain (subaqueous tunnels), with a constant hydraulic head above the tunnel.

$$Q = \frac{2\pi KL(H - h_t)}{\ln\left(\frac{H - D - h_t}{r} + \sqrt{\left(\frac{H - D - h_t}{r}\right)^2 - 1}\right)} \qquad (1.5)$$

In this case D is the water depth above the ground surface [m]. Terms of the various presented equations are shown in Figure 1.8.

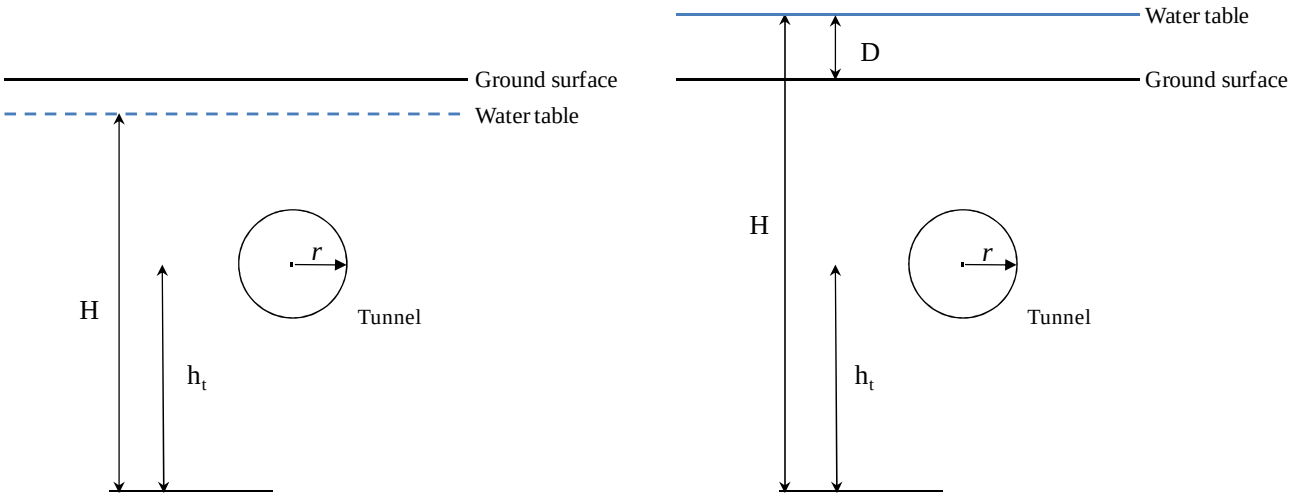

Figure 1.8 - Scheme of a generic tunnel with the notations commonly used in the analytical equations. At left generic case, at right a subaqueous tunnel.

e) Kolymbas and Wagner (2006) proposed another analytical formula valid for subaqueous tunnels.

$$Q = \frac{2\pi KL(D - h_a)}{\ln\left(\frac{h_1 + \sqrt{h_1^2 - r^2}}{r}\right)} \qquad (1.6)$$

Where h_1 is the ground surface elevation above the tunnel [m], h_a is the real head [m] evaluated above the tunnel as shown in Figure 1.9.

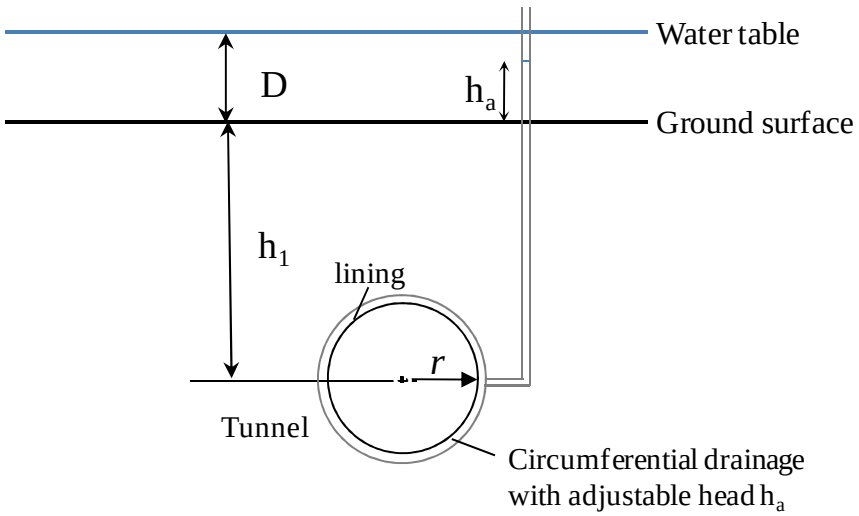

Figure 1.9 - Conceptual scheme used by Kolymbas and Wagner (2006).

- *Unsteady state equations*

a) The first equation to obtain the tunnel discharge as a function of the time was proposed by Jacob and Lohman (1952):

$$Q(t) = \frac{4\pi KL(H - h_t)}{\ln\left(\frac{2.25kLt}{Sr^2}\right)} \tag{1.7}$$

where *S* is the is the volumetric specific storage [1/m], and the other terms were already discussed and shown in Figure 1.8.

b) Finally we report the equations proposed by Perrochet (2005) considering instantaneous tunnel drilling:

$$Q(t) = \frac{2\pi KL(H - h_t)}{\ln\left(1 + \pi \frac{Kt}{Sr^2}\right)} \tag{1.8}$$

Perrochet (2005) has also proposed an approach to evaluate the tunnel inflows considering the velocity of drilling *v* using dimensionless parameters.

1.4.2 Numerical methods

Recently, various applications of numerical models have been carried out to investigate the impact of tunneling on groundwater (Zangler et al. 2008a; 2008b; Piccinini and Vincenzi, 2010; Vincenzi et al. 2010). Most groundwater numerical models in use are deterministic mathematical models that generally require the solution of partial differential equations for groundwater flow.

Existing methods to solve Flow Equations include: Finite Differences Methods (FDM) and Finite Element Methods (FEM) depending on the numerical regular or irregular grid used to solve the groundwater flow equation (Figure 1.10).

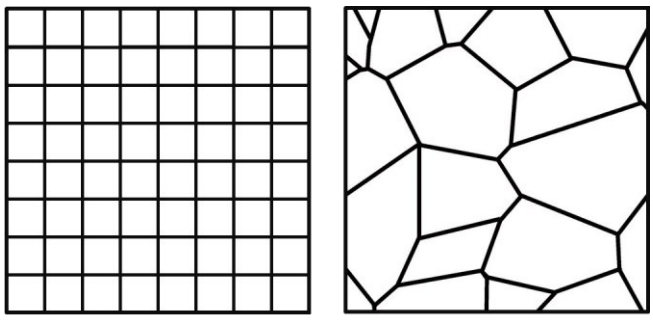

Figure 1.10 - Examples of grids used for numerical model (FDM and FEM methods)

Considering fractured rock masses we can summarize three possible approaches as a function of the conceptualization of the medium:

i. assuming the medium as an equivalent continuum with either single or double porosity based on prescribing effective hydraulic parameters: *Equivalent Porous Medium* (EPM) approach (McDonald and Harbugh, 1988);
ii. associating flow only to fractures needing to define the geometry of the fracture network: *discrete* approach (Therrien, 1992);
iii. combining approaches (i) and (ii) (*hybrid models*), that consists of treating minor fractures and the rock matrix as a continuum (~EPM) and explicitly modeling major fracture zones (Shapiro and Andersson 1983).

Each approach has advantages and disadvantages (easy or difficult geometry construction, higher or lower computational requirements, etc), nevertheless the main problem is constituted by the

correct definition of hydraulic parameters (essentially the hydraulic conductivity K) and of boundary conditions.

Parameters and boundary conditions are generally derived from a conceptual model. Moreover, parameters are changed also on the basis of (*i*) calibration processes, consisting of the comparison between simulated and measured data, and (*ii*) sensitivity analysis, consisting in varying each model parameter and understanding its influence on the model output.

1.4.3 Parametric methods

For fractured rock, the application of a numerical solution is often complex; moreover the water flow systems are not easy to interpret in a deterministic manner as it is possible using the analytical equations. Therefore, parametric approaches are often proposed in order to define, in probabilistic terms, the hazard of tunnel inflows and associated groundwater depletion. For instance, recently, two methods (Vincenzi et al., 2010) have been proposed and will be presented below:

i. the De Matteis method;
ii. the Cesano method.

- *De Matteis method*

This method (De Matteis et al. 2000) is a predictive probabilistic model to describe the drawdown hazard of water points (springs and eventually wells). In fact the output of this method is the *Drawdown Hazard Index* (DHI), which is an indicator of the groundwater depletion hazard due to the tunnel drilling.

It is based on a statistical general approach used also by Hudson (1992) to obtain one of the most common rock quality classification systems: the Rock Quality Designation (RQD) index. Some variables related to the geological environment of the tunnel and to the springs type, respectively, are considered and attended to obtain a value for the DHI.

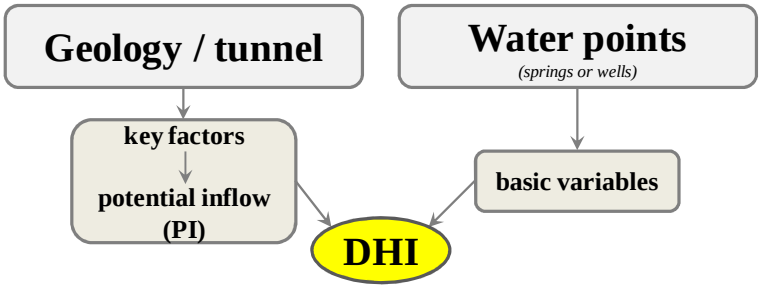

Figure 1.11 - Conceptual scheme of the DHI methods.

Key factors and potential inflow index

Summarizing, the following four parameters are named *key factors* (*kf*) and are related to the geological environment:

kf.1. the fracture frequency (FF) – it can be described by using one of the rock mass classification systems like the RQD or the Q index of Barton (2002) or the volumetric joint count (J_v) defined by Palmstrøm (1982) that is directly correlated with the fracture frequency as illustrated in Figure 1.12. Some simple theoretical correlation between RQD or Q and J_v are available in the literature (Hudson 1992; Barton, 2002). In Table 1.2 the numerical values assigned to the FF key factor are reported.

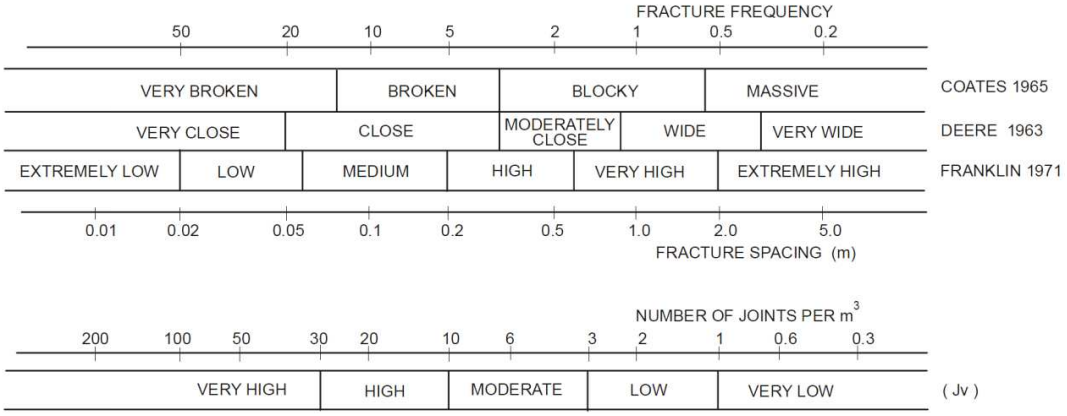

Figure 1.12 - Classification of joint spacing and J_v (from Palmstrøm 1982)

Table 1.2 - Numerical values of FF variable (modified from Torri et al 2007)

Frequency of fracturation	FF
High	1
Low	0.6
Absent	0.1

kf.2. the rock mass permeability (MK) - it is a parameter that describes the lithological units from a hydrogeological point of view, intending only the effective hydraulic conductivity of the rock mass, using for example the five classes (Table 1.3) of AFTES (2003) or a more detailed classification (Torri 2007) shown in Table 1.4.

Table 1.3 - Rock mass permeability classes using the A.F.T.E.S. classification (2003)

A.F.T.E.S. class	Rock mass permeability K_M (m/s)	Description
K1	$<10^{-8}$	Low permeability
K2	10^{-8} to 10^{-6}	Moderate permeability
K3	10^{-6} to 10^{-4}	High permeability
K4	$>10^{-4}$	Very high permeability
K5	Practically infinite	Karst conduits and caves

Table 1.4 - Numerical values of variable MK (from Torri et al 2007)

Degree of permeability	MK
Very high	0.9
High	0.8
From high to medium	0.7
Medium	0.5
From medium to low	0.4
Low	0.2
Very low	0.1

kf.3. the overburden (OV) – it is the thickness of the rock above the tunnel. An increase of this variable results in a decrease of the probability of water leakage into the tunnel. In Table 1.5 the numerical values assigned to the OV key factor are reported.

Table 1.5 - Numerical values of OV variable (from Torri et al 2007)

Tunnel depth	OV
< 50 m	0.9
50 to 100 m	0.5
100 to 500 m	0.2
> 500 m	0.1

kf.4. the amplitude of the plastic zone (PZ) – it describes the expected effect drilling on the surrounding rock masses and assumes values of 0 or 1 depending on the amplitude of this disturbed zone around the tunnel (Table 1.6).

Table 1.6 - Numerical values for the PZ variable (from Torri et al 2007)

Amplitude of the plastic zone	PZ
> tunnel diameter	1
< tunnel diameter	0

The four key factors are grouped as the potential inflow (PI) index that describes the probability of occurrence of water leakage into the tunnel independently of surrounding hydrogeological conditions. PI is evaluated with the following equation where each key factor is opportunely weighted:

$$PI = 0.41 \cdot FF + 0.22 \cdot MK + 0.17 \cdot OV + 0.20 \cdot PZ \qquad (1.9)$$

Basic variables

Other four parameters are called *basic variables* (*bv*) and are rather related to nearby water points (in particular springs) and to the possible impacts caused by tunnel drilling:

bv.1. distance from the tunnel (DT) –it is the planimetric distance of a water point from the tunnel that is inversely correlated with the potential depletion of water resources (Table 1.7).

Table 1.7 - Numerical values for the DT variable (from DeMatteis et al. 2001)

Distance from the tunnel	DT
< 100 m	1
100 to 200 m	0.8
200 to 400 m	0.6
400 to 600 m	0.4
600 to 800 m	0.2
> 800 m	0

bv.2. intersection with major faults (IF) - it is a variable which value is 1 in the case of permeability of the water point (spring or well) is related to structural elements such as a fault line, a karst conduit, etc.; 0 otherwise

bv.3. spring type (TS) –it is a variable for which the value depends of the hydrogeological flow path feeding the spring, defined for example, by a geochemical study. In Table 1.8 the numerical values assigned to the TS parameter by Torri et al. (2007) is reported.

Table 1.8 - Numerical values for the TS variable (from Torri et al 2007)

Spring type	TS
Deep fluid system	1
Intermediate fluid system	0.5
Shallow fluid system	0

bv.4. topographic effect (ET) – it is a parameter that depends on geomorphological features within nearby basins . ET values are reported in Table 1.9 derived from Torri et al. (2007) and obtained on the basis of the scheme shown in Figure 1.13. The slope effect take in account the position of the spring on the slope as compared to the tunnel, while the altitude effect takes in account the elevation of the spring compared to that of the tunnel.

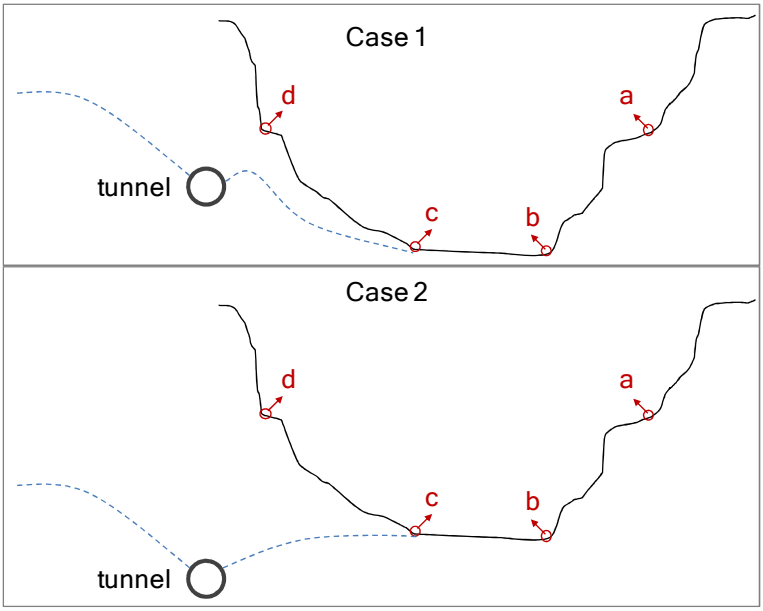

Figure 1.13 - Cases considered by Torri et al. (2007) to define the TS parameter following Table 1.9.

Table 1.9 - Numerical values of ET variable (from Torri et al 2007). See Figure 1.12.

Case & spring placement	Slope effect	Altitude effect	ET
1-a	0.2	1	1.2
1-b	0.2	0.2	0.4
1-c	1	0.2	1.2
1-d	1	1	2
2-a	0.2	1	1.2
2-b	0.2	1	1.2
2-c	1	1	2
2-d	1	1	2

Finally the DHI is evaluated with the following equation (that does not consider the topographic effect):

$$DHI = PI_m \cdot (DT + 1) \cdot (IF + 1) \cdot (TS + 1) \qquad (1.10)$$

Or with this equation proposed by Torri et al. (2007), considering also the ET parameter:

$$DHI = PI_m \cdot \frac{DT+1}{1.9} \cdot \frac{IF+1}{2} \cdot \frac{TS+1}{2} \cdot \frac{ET}{2} \qquad (1.11)$$

Using the first equation (1.10), the probabilistic results are shown in Table 1.10.

Table 1.10 - Different degree of probability associated with the DHI according to De Matteis et al 2001

DHI	Impact on springs flow rate
< 0.2	Not observed / Minimum drawdown
0.2 to 0.6	Partial drawdown
0.6 to 0.7	Partial / Complete drawdown
> 0.7	Complete drawdown

Using equation 11 (modified in Torri et al., 2007) the mean of the results is different and is expressed in Table. 1.11.

Table 1.11 - Different degree of probability associated with the DHI according to Torre et al 2007

DHI	Class	Probability of impact
< 0.1	1	Negligible
0.1 to 0.2	2	Low
0.2 to 0.3	3	Medium
> 0.3	3	High

The DHI method was applied in different cases (De Matteis et al., 2001; Torri et al. 2007; Perello et al., 2009; De Matteis et al., 2009, Vincenzi et al. 2010) to predict possible impact of underground infrastructures in a mountainous region (Torino-Lyon high velocity railway, Brenner base tunnel, Perthus tunnel, etc.) on nearby springs. The authors have also performed back analysis and sensitivity analysis, hence results appear realistic. Tested reliability of the model (equation 10) is about 100% in case of DHI<0.2 and DHI>0.7.(De Matteis et al. 2001): Obviously a correct application of this method depends on the collection of a large dataset and on their correct interpretation.

- *Cesano method*

This method (Cesano et al., 2000) was obtained with a systematic statistical analysis that has been carried out on a tunnel excavated in the hard rocks of southern Sweden. A number of topographical, hydrogeological (soil, rock and surface geophysics) and technical parameters (Figure 1.14) were taken into account and statistically analyzed in comparison with tunnel inflows, which distinguish between minor (diffuse dripping) and major localized inflows.

VARIABLE	DESCRIPTION
	TOPOGRAPHICAL PARAMETERS
OVERB	average thickness (m) of the soil layers above the hard rock terrain calculated for each 100-m section
TOPSTEEP	average steepness of the ground topography above each 100-m tunnel section
ROKSTEEP	average steepness of the bedrock basement topography above each 100-m tunnel section
TOPODISC	topographical high and low areas in the overburden above each 100-m section
ROCKDISC	topographical high and low areas in the rock basement above each 100-m section
TUNDEPTH	average depth (m) of the tunnel for each 100-m section of the tunnel
	SOIL PARAMETERS
TILL	Sq. km of till in the 500 m surrounding each 100-m tunnel section
PEAT	Sq. km of peat in the 500 m surrounding each 100-m tunnel section
GLACLAK	Sq. km of glacial lake sediments in the 500 m surrounding each 100-m tunnel section
GLAFLU	Sq. km of glacio-fluvial sediments in the 500 m surrounding each 100-m tunnel section
DISLAKE	distance (m) to surface water bodies from each 100-m tunnel section
	ROCK PARAMETERS
NO_FRACT	number of fractures for each 100-m tunnel section
DIP_0_45	number of fractures dipping < 45 for each 100-m tunnel section
DIP45_90	number of fractures dipping > 45 for each 100-m tunnel section
AMPHIB	number of amphibolite dikes for each 100-m tunnel section
GNEISS	number of fractures in gneiss for each 100-m section
CROSSZON	number of fracture zones in each 100-m tunnel section
MINERAL	number of fractures filled with minerals in each 100-m tunnel section
DISPLAST	distance (m) to measured structures of plastic deformation (e.g., foliation) from each 100-m tunnel section
DISRUPT	distance (m) to measured structures of ruptural deformations (e.g., major faults) for each 100-m tunnel section
	SURFACE GEOPHYSICAL PARAMETERS
MAG	average value of surface magnetic measurements along each 100-m tunnel section
SEIS	average value of surface seismic measurements along each 100-m tunnel section
ELECT	average value of surface electrical measurements along each 100-m tunnel section
	TECHNICAL PARAMETERS
WEEKS	number of weeks necessary to advance the tunnel face for each 100-m tunnel section
ROCKQUAL	rock quality in each 100-m tunnel section classified by the tunnel mapped into 3 classes
PREGROUT	number of pregrouted zones for each 100-m tunnel section

Figure 1.14 – Topographical, hydrogeological and technical parameters analyzed by Cesano et al. (2000).

The study of Cesano shows that many factors regulated the leakages. In particular the most important are the rock quality, the soil type, the number of fractures and the thickness of the overburden. Finally, also the pregrouting, even though it is not a natural parameter such as the previous, can influence the inflows. Using the data collected in the Bolmen tunnel (Sweden) during the last decade of the last century, Cesano suggest some linear correlation between the leakages and the different parameters.

This method has not been codified by the authors. Nevertheless Vincenzi et al. (2010) have reformulated it, proposing the following two equations to evaluate the Potential Inflows (PI), distinguishing between major and minor inflows:

- ✓ major inflows:

$$PI = 0.32 \cdot TSW + 0.29 \cdot BM + 0.28 \cdot T + 0.11 \cdot FF \qquad (1.12)$$

- ✓ minor inflows (diffuse dripping):

$$PI = 0.30 \cdot BM + 0.29 \cdot QC + 0.26 \cdot QA + 0.11 \cdot PV \qquad (1.13)$$

where:

- *TSW* is the Euclidean distance between the midpoint of each tunnel sector and the nearest main stream bed (or lake or reservoir) located above the tunnel;

- *BM* is the index considering the bedrock morphology underlying the Quaternary or morainic deposits;
- *T* is the topography index that can be evaluated like as the overburden parameter (*OV*) of the De Mattteis method (Table 1.5Table 1.5);
- *FF* is the fracture density (see the De Matteis method and Table 1.2);
- *QC* is the parameter considering the thickness and lithology of the Quaternary cover;
- *QA* is the parameter considering the percentage of area of Quaternary outcrops above the tunnel calculated on a buffer area around the tunnel of about 1000 m;
- *PV* is a parameter considering the presence of peaks and valleys. It is calculated from tunnel section subdivided for tunnel sector (e.g. 100 m). Value of 1 is assigned in presence of valley, 0 in presence of peaks above the considered tunnel sector. Otherwise intermediate values can be used.

The parametric methods are certainly a simplification of the problem; however they are suitable to estimate with appreciable certitude the possible impact of tunneling on the hydrogeological cycle, especially in complex environments.

1.5 Chosen research approach in this study

In the previous sections the state of the art of the available techniques to estimate the interaction of the tunnel with the hydrologic cycle are presented. Independently from the chosen approach the first problem is the formulation of a data supported Hydrogeological Conceptual Model (HCM), that is needed to define the parameters of the analytical formula, as well as parameters and boundary conditions of the numerical methods or finally to correctly estimate the potential inflows and hazard index of the parametric methods.

The main goal of this research has been the understanding of how hydrogeochemical data (groundwater monitoring, major ions, stable isotopes, noble gas groundwater analysis, etc.) and geophysical techniques (electrical resistivity tomography and very low frequency electromagnetic methods), combined with structural and hydrogeological information, can be integrated in order to develop hydrogeological conceptual models (Figure 1.15).

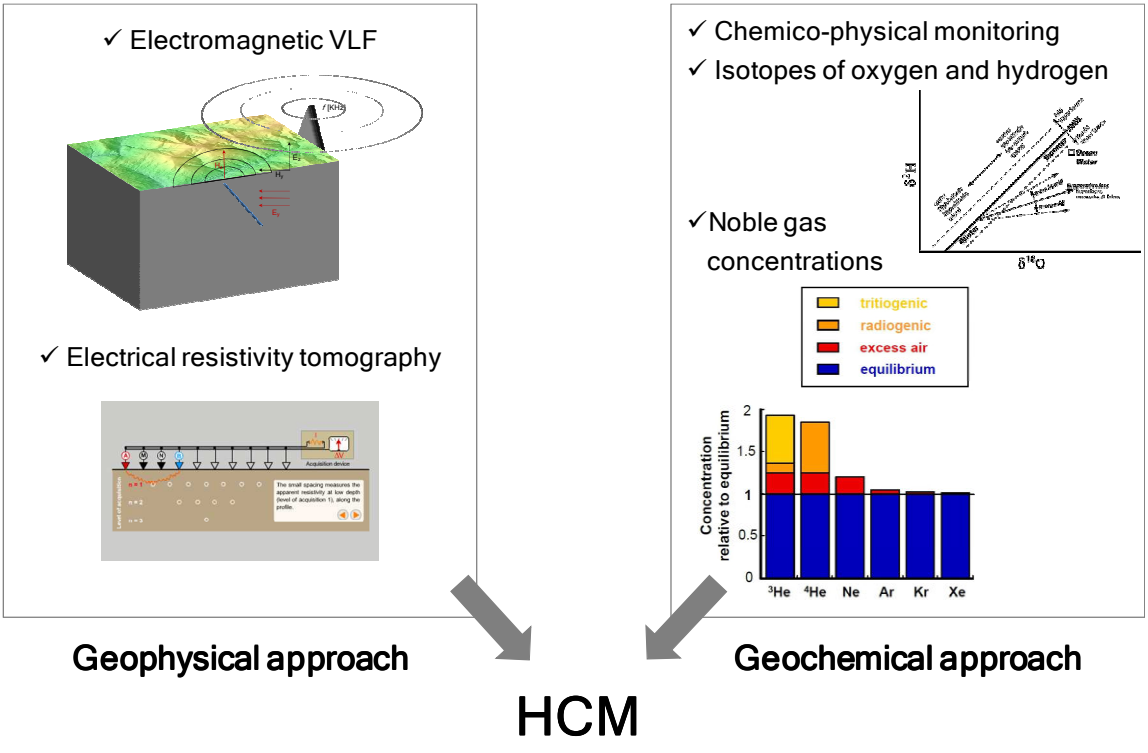

Figure 1.15 - Scheme of the chosen research approach.

Appendix A contains an already published paper that present more details about the chosen research approach. This publication is part of the proceedings of the session "Hydrogeological impacts of tunnels", GEOITALIA 2009, Rimini, September 2009 (session's conveners: Alessandro Gargini, Valentina Vincenzi, Michele Sapigni).

References

AFTES (2003). Caracterization of rock masses useful for the design and the construction of underground structures. Guidelines f Association Française des Tunnels et de l'Espace Souterrain (AFTES) 49 pp

Barton N. (2002). Some new Q-value correlations to assist in site characterisation and tunnel design. International Journal of Rock Mechanics & Mining Sciences 39:185–216

Brühlmann F., Conrad R. Haldimasnn P., Kempf T. (2004). Instructions pratiques pour la protection des eaux souterraines. Environnement pratique no. VU-2508-F. Federal office for the environment, Bern, 133p.

Cesano D. (2001). Water Leakage into underground construction in fractured rocks – Geological and Hydrogeological information as a basis for prediction. TRITA-AMI-PHD 1039 Licentiate thesis

Cesano D., Olofsson B., Bagtzoglou A.C. (2000). Parameters regulating groundwater inflows in hard rock tunnels – a statistical study of the Bolmen tunnel in Southern Sweden, Tunneling and Underground Space Technology 15(2):153-165

De Matteis A. (2008). Come prevenire e gestire venute d'acqua in galleria. Strade & Autostrade 1:66-70.

De Matteis A., Kalamaras G., Eusebio A., (2001). A System approach for evaluating springs drawdown due to tunneling, Proceedings of the AITES-ITA 2001 World Tunnel Congress, Milano

De Matteis A., Perello P., Delle Piane L., Torri R., Thiery M., Darmendrail X. Venturini G. (2005). Tunnels profonds et impact des acquifères: l'exemple du tunnel ferroviare Lyon-Turin, Proceedings of the 25th Géoline 2005, Lyon France

De Matteis A., Torri R., Looser M. (2007). Water Resources Management in Tunneling: insights in the decisionmaking process to improve tunnels environmental sustainability, Procedings of XXXV IAH Congress, Groundwater and Ecosystems, Lisbon 17-21 Sept. 2007, 8 pp.

El Tani M. (2003). Circular tunnel in a semi-infinite acquifer, Tunnelling and Underground Space Technology 18, 49-55

EU commission (2001). White Paper: European transport policy for 2010: time to decide, Technical document of the Commission of the European Communities

Goodman R.F., Moye D.G., Van Schaikwyk A., Javandel I. (1965). Ground water inflows during tunnel driving. Bulletin of the International Association of Engineering Geologists 2(1):39–56

Hoek E. (2007). Practical rock engineering – Notes available online (http://www.rocscience.com/hoek/PracticalRockEngineering.asp)

Hudson J.A. (1992). Rock Engineering Systems, theory and practice, Ellis Horwood, NY, 185 pp.

Pera S., Pozzoni M., Seno S. (2008). Stato della risorsa idrica nel Cantone Ticino - Rapporto relativo alla scheda Piano direttore sull'acqua (obiettivo 27). Istituto Scienze della Terra (SUPSI) pp. 83

Jacob C. E., Lohman S.W. (1952). Nonsteady flow to a well of constant drawdown in a extensive aquifer. Transaction of the American Geophysical Union 33(4):559-569

Karlsud K. (2001). Control of water leakage when tunneling under urban areas in the Oslo region. NFP Publication 12

Kolymbas D., Wagner P. (2006). Groundwater ingress to tunnels – The exact analytical solution, Tunneling and underground space technology 22:23-27

Lei S., (1999). An analytical solution for steady flow into a tunnel. Ground Water 37:23–26

McDonald M. G., Harbaugh A. W. (1988). A modular three dimensional finite difference groundwater flow model, U.S. Geological Survey Techniques of Water Resources Investigations, Book 6, Chapter A1, 586 pp.

Molinero J., Samper J., Juanes R. (2002). Numerical modeling of the transient hydrogeological response produced by tunnel construction in fractured bedrocks, Engineering geology 64:369-386

Muskat, M. (1937). The Flow of Homogeneous Fluid through Porous Media. Mc Graw Hill, pp. 175–181

Ohnishi Y, Ohtsu H., Takahashi K., Yasuda T., (2006). Research of Observational Method on the Groundwater in the Tunnel Excavation Using the SWING Method, Tunneling and underground space technology Tunnelling 21(3-4):p420

Palmstrøm A (1982). The volumetric joint count –a useful and simple measure of the degree of rock mass jointing, Proceedings of the IV congress international association of engineering geology , New Dehli, Volume 2:221-228

Palmstrøm A (2005). Measurements of and Correlations between Block Size and Rock Quality Designation (RQD), Tunnels and Underground Space Technology 20:362-377

Pancescu M. (2006). Phreatic aquifers vulnerability for Mostistea Plain using GIS technology, Proceedings International Conference Hydrology and Ecology: The Groundwater/Ecology Connection 11–14 September 2006, Karlovy Vary, Czech Republic, 267-272

Park K., Owatsiriwong A., Lee J. (2008). Analytical solution for steady-state groundwater inflow into a drained circular tunnel in a semi-infinite aquifer: A revisit, Tunneling and underground space technology 23:206-209

Pera S.,Pozzoni M., Seno S. (2008) Stato della risorsa idrica nel Cantone Ticino - Rapporto relativo alla scheda Piano direttore sull'acqua (obiettivo 27) Canobbio, settembre 2008

Perello P., Delle Piane L., Martinotti G., Spanò M., Gallará F. Fenelli A. (2001). Geological and hydrogeological investigation for the new Lyons railway, middle Susa Valley, Italian Western Alps, Proceedings of the AITES-ITA 2001 World Tunnel Congress, Milano

Perello P., Venturini G. Delle Piane L., De Matteis A. (2007). Groundwater inflows in Tunnels excavated in faulted rock mass. A case history from the Italian Western Alps, Felsbau 25(4):28-34

Perello P., Venturini G., De Matteis A., Bianchi, Giampino W., Delle Piane L., Damiano A. (2005). Determination of reliability in geological forecasting for linear underground structures: the method of R-index, Proceedings of the 25th Géoline 2005, Lyon France

Perrochet P. (2005). Confined flow into a tunnel during progressive drilling: An analytical solution. Ground Water 43(6):943–946

Perrochet P., De Matteis A. (2007). Modeling transient discharge into a Tunnel Drilled in a Heterogeneous formation, GROUND WATER, VOL. 45(6):786-790

Piccinini L., Vincenzi V. (2010). Impacts of a Railway Tunnel on the streams baseflow verified by Means of numerical modelling Aquamundi 1(2):123-134

Pochon, A., Zwahlen, F. (2003). Délimitation deszones de protection des eaux souterraines en milieu fissuré – Guide pratique. L'environnement pratique. Office fédéral de l'environnement, des forêts et du paysage, Office fédéral des eaux et de la géologie, Berne, 83 p.

Rosegrant M.W., Cai X., Cline S.A. (2002). Global water outlook to 2025 - Averting an Impending Crisis, Food policy report for the International Food Policy Research Institute (IFPRI), 28 pp

Shapiro A., Andersson J. (1983). Steady state fluid response in fractured rock: a boundary element solution for a coupled, discrete fracture continuum model. Water Resources Research 19(4):959-969

Song W., Hamm S., Cheoing J. (2006). Estimation of Groundwater Discharged into a Tunnel, Tunneling and underground space Tecnology 21, Proceedings of the ITA-AITES 2006 World Tunnel Congress and 32nd ITA General Assembly

Shiklomanov I.A. (2000). Appraisal and Assessment of World Water Resources. Water International, 25(1):11-32

Therrien R. (1992). Three dimensional analysis of variably –saturated flow and solute transport in discretely-fractured porous media, PhD. Thesis, University of Waterloo

Torri, R., De Matteis, A., Delle Piane, L. (2007). Drawdown hazard of springs and wells in tunneling: predictive model and Verification. Proc. XXXV IAH Congress, Groundwater and Ecosystems, Lisbon 17-21 Sept. 2007, 10 pp.

Vincenzi V., Piccinini L., Gargini A., Sapigni M. (2010). Parametric and numerical modelling tools to forecast hydrogeological impacts of a tunnel Aquamundi 1(2):135-153

Zangerl C., Evans K.F., Eberhardt E., Loew S. (2008a). Consolidation settlements above deep tunnels in fractured rock: part 1 – Investigation above the Gotthard highway tunnel, International journal of rock mechanics & mining sciences – 45:1195–1210

Zangerl C., Evans K.F., Eberhardt E., Loew S. (2008b). Consolidation settlements above deep tunnels in fractured rock: part 2 – Investigation above the Gotthard highway tunnel, International journal of rock mechanics & mining sciences 45:1211–1225

2. Stable isotopes of oxygen and hydrogen of rain and snow from the Ticino area. Groundwater recharge dynamics study through stable isotopic composition.

Abstract

The stable isotope composition of water is an important research tool in the field of hydrogeology, hydrology, climatology and paleoclimatology. In fact, isotopic fractionation occurs on water molecules during thermodynamic reactions such as the evaporation of surface water and the progressive raining out of water vapour air masses. Hence, the stable isotope composition of water can be useful to understand aquifer recharge, transit time of water in the rock as well as groundwater mixing.

Composite monthly samples of atmospheric precipitation were collected in six station of the canton Ticino (southern Switzerland) for one year (March 2010 – February 2011) and δ^2H and $\delta^{18}O$ values were monthly analyzed. From the collected data, a local meteoric water line for southern Switzerland, the so called "Ticino MWL", was obtained. The effect of the admixture of vapour from lakes is particularly visible and causes an increase of the deuterium excess during most of the months of the year. Several known parameters that influence the isotope composition of the rain were identified: (i) a high *amount* effect depending on the rain abundance, (ii) a *temperature* effect that both acts seasonally and also annually, and (iii) a pronounced *altitude* effect depending on the elevation. Different altitude gradients (H-δ^2H or H-$\delta^{18}O$) have been obtained on the basis of the collected rain data, and differences between the isotopic composition of meteoric water (rain and snow) and that of the groundwater was observed. On the basis of the stable isotope compositions, the aquifer recharge conditions are discussed.

2.1 Stable isotopes of hydrogen and oxygen: standards and measurements

2.1.1 Introduction

Each chemical element is defined by three numbers, that are:

i) the *Atomic Number* (*Z*) that is the number of protons contained in its nucleus;
ii) the *Number of Neutrons* (N);
iii) the *Atomic Weight* (A) that is given by the sum of number of protons and neutrons, considering that the weight of electrons is negligible.

As shown by Figure 2.1, using these numbers (N, Z, and A), it is possible distinguish isotopes, isotones and isobares. In particular an *isotope*(Z constant) is defined as a nuclide, which contains a different number of neutrons in its nucleus than some other nuclides of the same atomic species. Practically, it means that different isotopes of an element will have the same Z, but different N and thence A, since the mass of an element is given by both the number of protons and neutrons.

In the standard atomic table of the International Union of Pure and Applied Chemistry (*IUPAC*) the chemical elements are defined using the two following information:

i) the atomic number;
ii) the standard atomic weight.

The atomic number has been previously defined, while the standard atomic weights can be determined from the knowledge of the isotopic abundances and corresponding atomic masses of the nuclides of that element (*Wieser, 2006*).

The number of neutrons of various atoms can differ, but their ranges are limited by stability (it is practically difficult to have too many or too few neutrons in the nucleus). On the basis of stability, it is possible to distinguish between stable and unstable isotopes. The latter, called also radioactive nuclides, have a certain probability of decay; while the stable isotopes do not spontaneous disintegrate by any known mode of decay. Figure 2.1shows the stable and unstable isotopes and their trend varying the atomic number (Z). In particular for the light elements (Z up to 20) the greatest stability occurs with a N/Z ratio close to 1, whereas this ratio increases towards 1.5 for heavy elements.

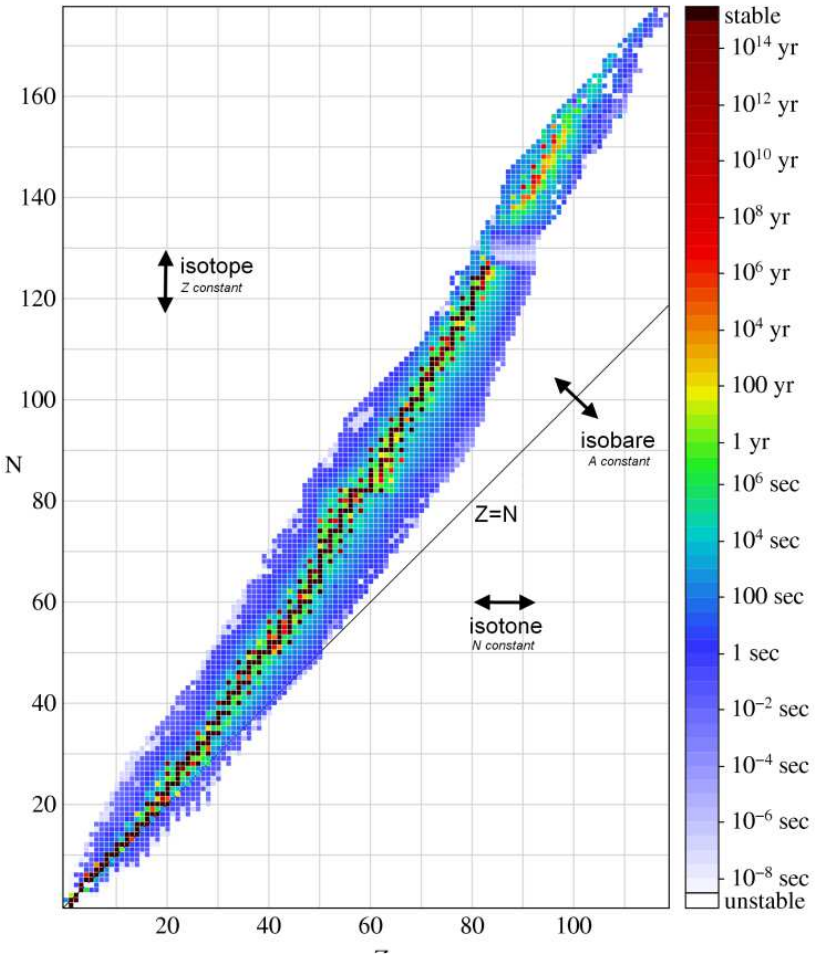

Figure 2.1 - Plot of Z vs. N for nuclides (data from the Nuclear Wallet Cards database version of 6/2/2009)

The two chemical elements of our interest are hydrogen and oxygen, which are the constituents of the water molecule. Hydrogen has one proton and oxygen has eight protons. The common hydrogen has one neutron and the common oxygen has eight neutrons too. The most abundant isotopes of these two elements are presented in Table 2.1.

Table 2.1 - Isotopic abundance of hydrogen and oxygen (from RosmanandTaylor 1998)

Element	Name	n° of neutrons	Atomic weight	Isotopic abundance	
^{1}H	*Hydrogen*	1	1.00782503	99.985	stable
^{2}H *(D)*	*Deuterium*	2	2.01410178	0.0115	stable
^{3}H *(T)*	*Tritium*	3	3.01604927	negligible	radioactive
^{16}O	*Oxygen*	16	15.9949146	99.757	stable
^{17}O	*Oxygen-17*	17	16.9991315	0.038	stable
^{18}O	*Oxygen-18*	18	17.9991604	0.205	stable

2.1.2 Stable hydrogen and oxygen isotopes in the water molecule

According with their isotopic composition, 18 different water molecules exist. However only light ($^{1}H_2{}^{16}O$) and heavy ($^{1}HD^{16}O$ and $^{1}H_2{}^{18}O$) are frequent; from Table 2.1 it is clear that the most common molecules are the light ones. Isotopic variations in natural systems are due to several processes occurring in the environment. During a chemical reaction, as an example, light molecules will, in general, react faster than the heavy ones, leading to a disproportionate accumulation of light isotopes with respect to heavy ones in one end of the reaction. The partitioning of isotopes between two substances with different isotopic ratios is called “isotope fractionation”. It may occur during chemical reactions and physical processes (i.e. state changes). In the next section, standards

definitions concerning stable isotopes of hydrogen and oxygen used in the following document are explained.

2.1.3Measuring isotope fractionation

Stable environmental isotopes are measured using the isotope abundance ratio *R* that is defined by the following expression:

$$R = \frac{\text{abundance of rare isotope}}{\text{abundance of most common isotope}} \qquad (2.1)$$

For instance, considering the oxygen, the ratio ($R={}^{18}O / {}^{16}O$) is about 0.00204, assuming that ^{18}O has a terrestrial abundance of 0.204%, while ^{16}O represents 99.796% of terrestrial oxygen. Fractionation processes will modify this ratio slightly for any given compound containing oxygen, but these variations are seen only at the fifth or sixth decimal. Measuring an absolute isotope ratio or abundance is not easily done and requires some rather sophisticated mass spectrometric equipment. Moreover, measuring this ratio on a routine basis would lead to tremendous problems in comparing data sets from different laboratories (Clark and Fritz, 1997).

To eliminate possible confusion in reporting isotopic abundances on non-corresponding scales, in 1961, Craig suggested that isotopic composition of water, determined by mass spectrometry, is expressed in per mil (‰) deviation from the *Standard Mean Ocean Water* (SMOW). Nowadays, the *Vienna Standard Mean Ocean Water* (VSMOW), managed by the *International Atomic Energy Agency* (IAEA), has replaced the SMOW.

These deviations, called delta values, are written as follows for deuterium and 18 oxygen:

$$\delta^{2}H = \frac{m\left({}^{2}H/{}_{1}H\right)_{sample} - m\left({}^{2}H/{}_{1}H\right)_{reference}}{m\left({}^{2}H/{}_{1}H\right)_{reference}} \times 1000 \qquad (2.2)$$

and

$$\delta^{18}O = \frac{m\left({}^{18}O/{}_{16}O\right)_{sample} - m\left({}^{18}O/{}_{16}O\right)_{reference}}{m\left({}^{18}O/{}_{16}O\right)_{reference}} \times 1000 \qquad (2.3)$$

Mathematically, the analytical error *m* between the apparent and the true ratios is cancelled. δ-values can be positive or negative numbers. Negative numbers show impoverishment in heavy isotope, while positive ones indicate enrichment in the sample respect to the standard(Gat et al, 2001).

Isotope fractionation occurs during any thermodynamic reaction due to differences in reaction rates of different molecular species. Two different types of fractionation are distinguishable:

i) equilibrium fractionation: is a reversible process that occurs during the chemical reactions at equilibrium;
ii) kinetic fractionation: is an irreversible process that occurs in kinetic (time dependant) reactions.

The kinetic effects are usually stronger than the equilibrium ones; however the mathematical description of the two fractionations type is similar. The result is an unequal concentration of one isotope over the other on one side of the reaction. It is expressed by the fractionation factor, α, which is the ratio of the isotope abundance ratios for the reactants and products:

$$\alpha = \frac{R_{reac}}{R_{prod}} \qquad (2.4)$$

e.g. for the oxygen in the water-vapour reaction:

$$\alpha_{W-V}{}^{18}O = \frac{\left({}^{18}O/{}^{16}O\right)_{water}}{\left({}^{18}O/{}^{16}O\right)_{vapour}} \qquad (2.5)$$

αvalues maybe obtained fromδvalues as follows:

$$\alpha_{W-V}{}^{18}O = \frac{\delta^{18}O_{water} + 1000}{\delta^{18}O_{vapour} + 1000} \qquad (2.6)$$

As isotope fractionation effects are small ($\alpha \approx 1$) deviation of $\alpha$from 1 is used. This quantity, named enrichment factor, is defined byεas follows:

$$\varepsilon_{A-B} = (\alpha_{A-B} - 1) \times 1000 = \left(\frac{R_A}{R_B} - 1\right) \times 1000 \qquad (2.7)$$

whereεrepresents the enrichment ($\varepsilon > 0$) or the depletion ($\varepsilon < 0$) of the rare isotope with respect to the most abundant one. It is important to point out that since ε is an approximation of the fractionation factor α, it may lead to significant errors, especially for hydrogen isotopes for which fractionations are large compared to other elements such as oxygen.

2.2 Stable isotopes in the hydrological cycle

2.2.1 The meteoric water line

Harmon Craig, in 1961, published the first δ^2H‰ -δ^{18}O correlation diagram, based on about 400 water samples of rivers, lakes and meteoric precipitations from various countries,obtaining the following best fit line:

$$\delta^2 H = 8\ \delta^{18}O + 10 \qquad (2.8)$$

Delta values in equation (2.8) are not expressed against VSMOW, since it was not introduced until over a decade later, as well as the monitoring of stable isotope composition of precipitation worldwide (IAEA Global Network for Isotopes in Precipitation – GNIP; Clark and Fritz, 1997).

Later Rozanski et al. (1993) performed statistical analysis of GNIP data (period 1960-1987). Long-term means weighted by the amount of precipitation were calculated considering only the years for which more than 70% of precipitation samples were analyzed and at least one year of observation was available. The resulting correlation is expressed by the following equation and shown in Figure 2.2:

$$\delta^2 H = 8.13\ \delta^{18}O + 10.8 \qquad (2.9)$$

The flux of moisture from the oceans and its return via rainout and runoff is close to a dynamic equilibrium, at least on an annual basis and global scale. Only major climatic shifts will seriously change the storage of fresh water in glacial, groundwater and surface water reservoirs. Within the existing cycle, however, significant variability does exist in stable isotope composition of the different reservoirs. Evaporation from the oceans, rainout, re-evaporation, snow and ice accumulation and melting, and runoff vary under different climatic regimes. Hence, it is possible to individually differentiate MWL for the various regions.

The slope of the MWL depends on the fractionation equilibrium. In particular the slope of about 8 is due to the equilibrium condition during condensation of the precipitation that occurs in clouds. Evaporation generally shifts isotopic compositions along a line with slope lower than 8 (Figure 2.2). Nevertheless the kinetic effects are more important and determine changes in the MWL intercept with the δ^2H –axis, which is called *deuterium excess* (Figure 2.2). It is mainly dependent on the mean relative humidity of the air above the evaporation source. For instance a deuterium excess of about 10‰ is correlated to the mean relative humidity of 85% during the evaporation from the ocean. The deuterium excess is generally in inverse proportion to the relative

humidity (Merlivat and Jouzel, 1979). Therefore, a decrease of relative humidity causes an increase of the deuterium excess; nevertheless increased deuterium excess in precipitation can also be interpreted as due to a significant addition of re-evaporated moisture from continental basins to the water vapour travelling inland (Macharavan and Krishnamurthy, 1995). Examples of deuterium enriched precipitation derived in this way are known from the Region of Great Lakes (USA-Canada, Machavaran and Krishnamurthy, 1995) and from the Amazon basin (Salati et al., 1979).

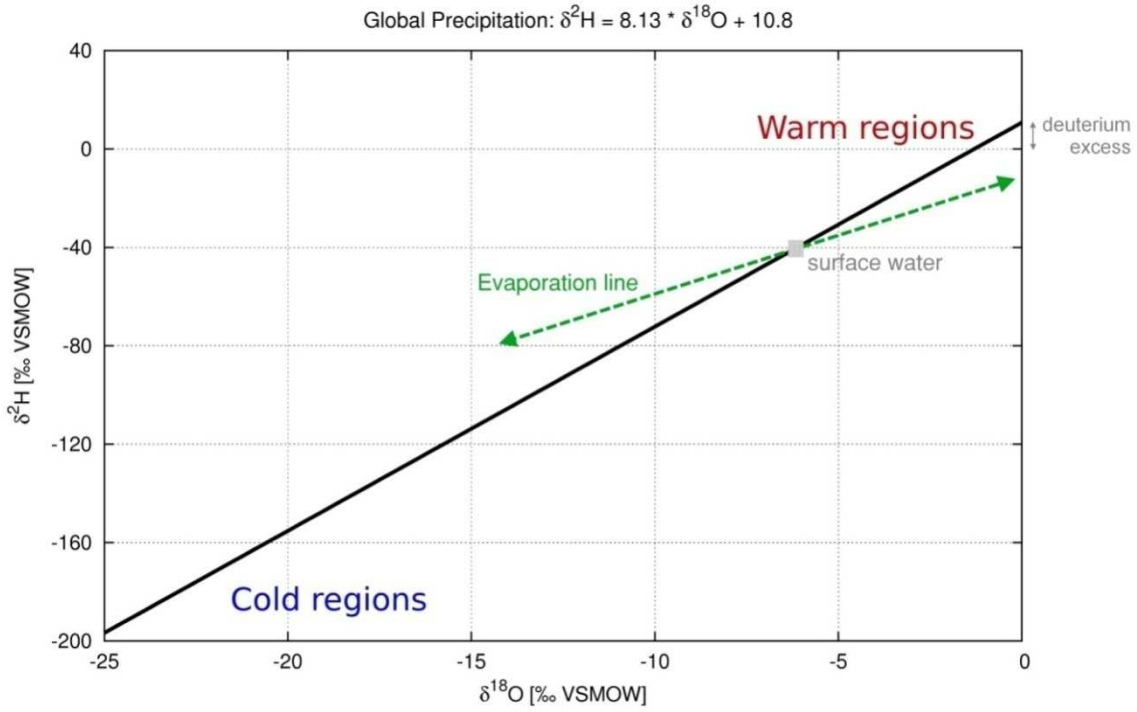

Figure 2.2 - The meteoric relationship for ^{18}O and ^{2}H in precipitation. MWL was obtained by Rozanski et al. (1993), while comments were elaborated based on Gat et al. (2001).

2.2.2 δ²H - δ¹⁸O in precipitation

As precipitation is conventionally considered the main input of surface and ground water in the hydrological cycle, a starting point for comparing water isotopic composition from any sample is constituted by the meteoric water line (MWL). Variations in $\delta^{2}H$ and $\delta^{18}O$ of meteoric water are controlled by two main processes of the global water cycle:

i) the evaporation of surface water characterized by the isotopic fractionation effect between various water vapor molecules;
ii) the progressive raining out of the vapour masses as they move towards continental regions.

In particular, stable isotope composition is controlled by a series of temperature-based mechanisms that drive this rainout processes (Dansgaard ,1964; Vogel et al., 1975; Yurtsever and Gat 1981; Dray et al., 1997; Gonfiantini et al. 2001; Marechal and Etcheverry, 2003) and are here summarized.

- *Seasonal effects*

Seasonal variations in temperature lead to variations in isotope composition of precipitations as schematically shown in Figure 2.3 for the Locarno Monti meteorological station (Ticino).

Generally the temperature effect is more evident, but frequently an influence of the amount of precipitation on the T-$\delta^{18}O$ (or $\delta^{2}H$) relationship is also observable (Clark and Fritz, 1997). A less pronounced anticorrelation between the monthly amount of precipitation and the proportion of heavier isotopes in the water is registered and it is called *amount effect* (Dansgaard, 1964). These variations are an important tool to study groundwater dynamics, watershed response to precipitation, and the recharge (Gat et al., 2001, Maloszeski et al., 2002).

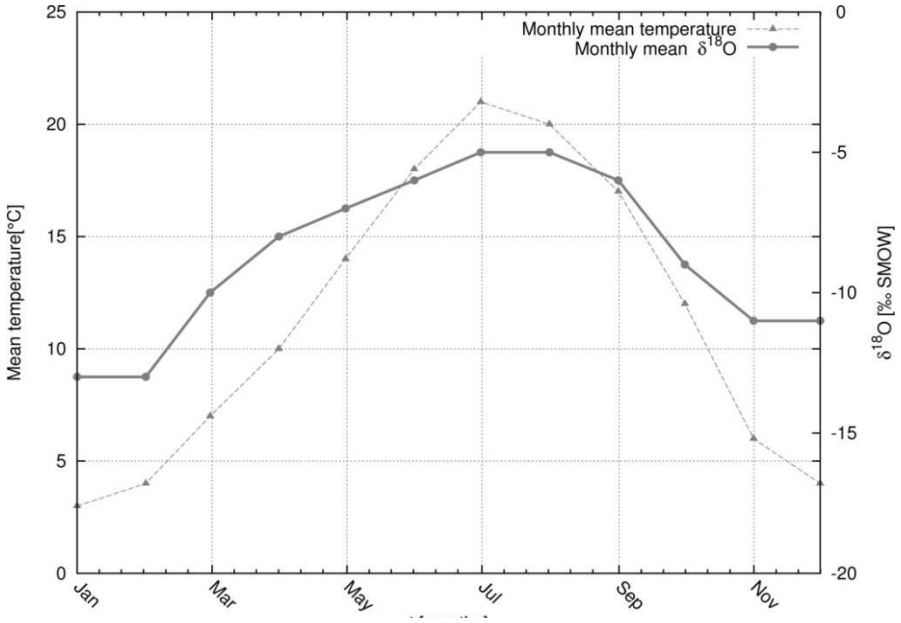

Figure 2.3 - Temperature effect on the $\delta^{18}O$ for the Locarno Monti (Ticino) meteorological station.

- *Continental effects*

As a vapour mass moves from its source region across the continent, as a rule, its isotopic composition evolves becoming more and more depleted in heavier isotopes (^{2}H and ^{18}O), this is the so called *continental effect*.

- *Screen effects*

Orographic barriers influence composition and distribution of nearby precipitation. Often, on the windward side of a mountain, precipitations occur due to the rising air motion of a large-scale flow of moist air across the mountain ridge, resulting in adiabatic cooling and finally in condensation; while, on the leeward side of the same mountain, precipitations can be absent or they may be due to water sources of different origin. This effect acts on spatial distribution and abundance of precipitation, having consistent outcomes also on their stable isotope composition.

- *Altitude effects*

As a rule, precipitation changes with altitude becoming more and more depleted in ^{18}O and ^{2}H at higher elevations. For example, the observed effect on $\delta^{18}O$ generally varies between –0.1‰ and -0.6‰ per 100 m of altitude (Figure 2.24). Values in this range have also been reported for other mountainous regions in northern and southern Switzerland by Pearson et al. (1991). Altitude gradient isotope composition may be used for the identification of the elevation at which groundwater recharge takes place (Blavoux and Letolle, 1995; Pastorelli et al., 1999; Ofterdinger, 2001).

- *Admixture of secondary moisture*

Another effect recognized in rain is the addition of secondary moisture (Machavaram and Krishnamurthy, 1995). It is normally due to the presence of a main reservoir of water close to the region where precipitations occur. These reservoirs can be constituted by enclosed seas (e.g the Mediterranean Sea) or by lakes (e.g. region of great lakes in the US). The effect is normally an increase of the deuterium excess.

2.3 Context of the study

δ^2H and$\delta^{18}O$ are often used in groundwater studies as natural tracers (Blavoux and Letolle, 1995; Ofterdinger, 2001; Hildebrand et al., 2005; Paternoster, 2008) due to their ability in distinguishing different types of waters. In this chapter, the main effects controlling the isotopic signature of rain are identified and discussed, with particular attention to recharge process.

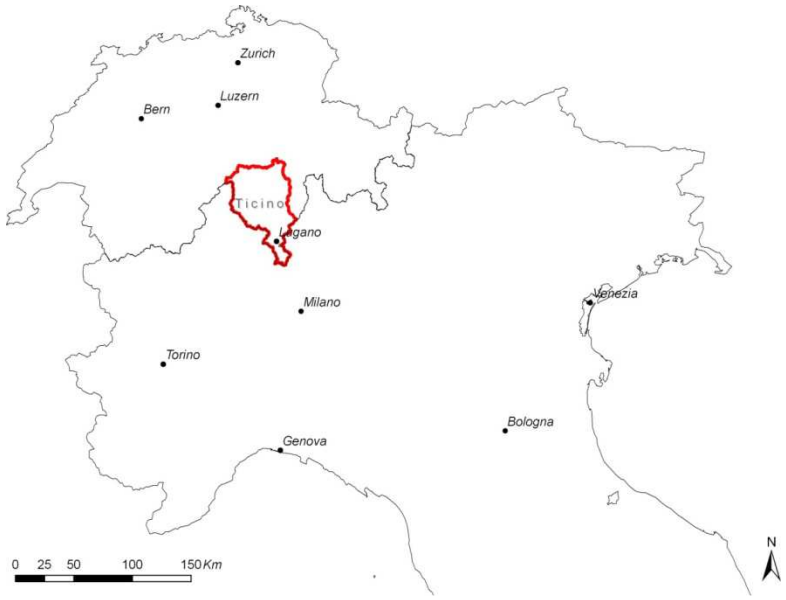

Figure 2.4 - Location of the studied region, in the southern part of the Swiss Alps.

Stable isotope composition of precipitation can be strongly influenced by the topography (*screen effect),* air mass origin and by the so-called climatic controls (rain or snowfall) in southern Italian and Swiss alps (Moser et al., 1972; Novel et al., 1999; Aouad-Rizk et al., 2005). Moreover, the presence of large lakes (Maggiore, Como and Ceresio), located between the Po Valley and the chain of the Alps in the *prealpine* region, can also appreciably influence the stable isotope composition of meteoric water (Machavaram and Krishnamurthy, 1995; Salati et al., 1979). Figure 2.5 illustrates more in detail the expected screen effect in the studied region, the orography of the studied region and the presence of lakes.

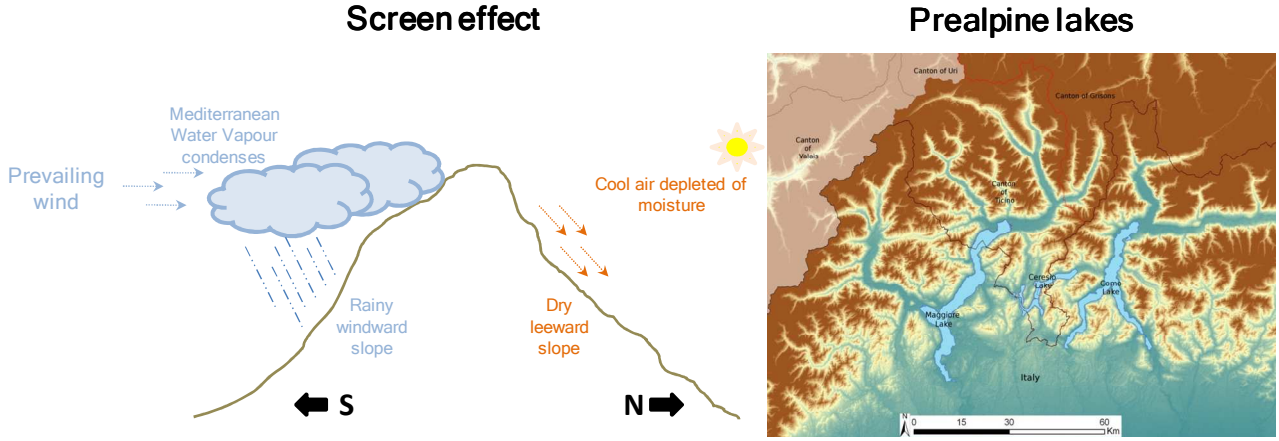

Figure 2.5 - Schematic view of the screen effect and map of the studied region. The southern side of the Alps (Swiss cantons of Ticino and Grisons and Northern Italy) and the prealpine lake system are evidenced.

Since 1961, the δ^2H *(‰VSMOW)* and the $\delta^{18}O$ *(‰VSMOW)* values of the meteoric waters have been collected by the International Atomic Energy Agency (IAEA) Water Resources Program and by the World Meteorological Organization (WMO), that created the Global Network of Isotopes in Precipitation (GNIP). Moreover in Switzerland, since 1993, the Network for the Observation of Isotopes in the Water Cycle (*NISOT*) of the national groundwater observation

program NAQUA is commissioned to survey the content of hydrogen and oxygen isotopes in precipitation (Schürch et al, 2003). It is managed by the Federal Office for the Environment (FOEN) in conjunction with the Climate and Environmental Physics group at the University of Bern. Available data for Switzerland, in particular values collected in the Locarno Monti meteorological station since 1983, allow for an estimation of the local Meteorological Water Line (MWL) referred as *Locarno MWL* (Marzocchi et al., 2010, appendix A).

Although Locarno station data are enough in order to obtain a reliable meteoric water line, they are not able to fully explain isotopic variations in rain due to the local and seasonal effects, and obviously it is not possible to define an altitude gradient based on a single station. On the other hand, the relationships proposed by Pearson et al. (1991) are difficult to apply to southern Switzerland, since there is a considerable difference in altitude gradients due to screen effects (Marechal and Etcheverry, 2003). Three altitude gradients elevation-$\delta^{18}O$ are reported in literature (Pastorelli et al., 2001; Ofterdinger et al. 2001, Bestenheider, 2006) for areas close to the Ticino canton (Figure 2.6) (see appendix A), but all these relationships are obtained with a small datasets, and, not exactly for the region of study (Monte Ceneri region). Therefore, in order to estimate it in the Monte Ceneri region, stations at different elevation were established for precipitation sampling.

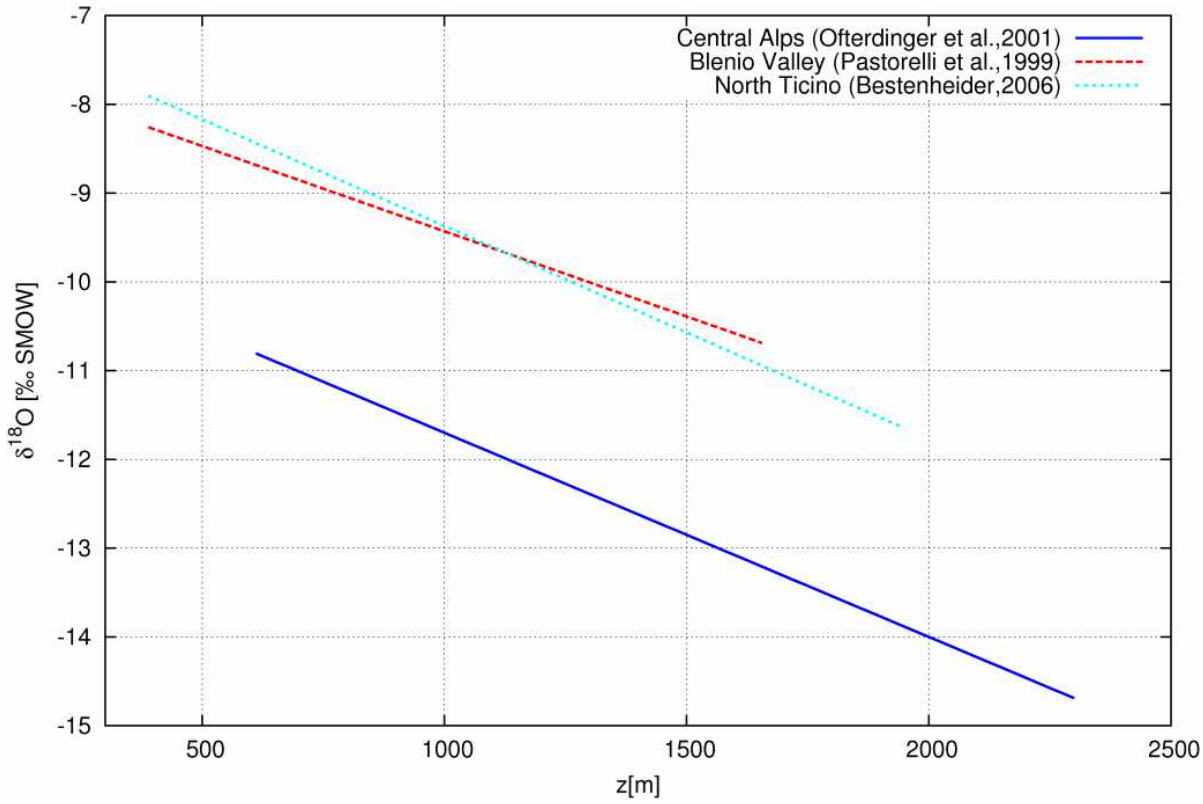

Figure 2.6 - Stable isotope-recharge altitude relationships obtained with data of area close to the Canton Ticino, from different authors.

2.4 Methods

Seasonal variations in isotopic composition of precipitation due to the amount of rain and the temperature may be used as a tool to understand groundwater recharge and flow dynamics. Thence these effects will be analyzed in detail in the further sections.

2.4.1 Monitoring network and stable isotope measurements

A monitoring network for rain isotopic data in Canton Ticino was established since March 2010; it is constituted by six stations placed at different latitude and altitude based on six rain gauges of the hydrological network operated by Institute of Earth Science, part of the University of

Applied Science of the southern Switzerland (IST-SUPSI).In Figure 2.7the rain gauges locations are shown, while in Table 2.2 geographical coordinates and altitudes are reported.

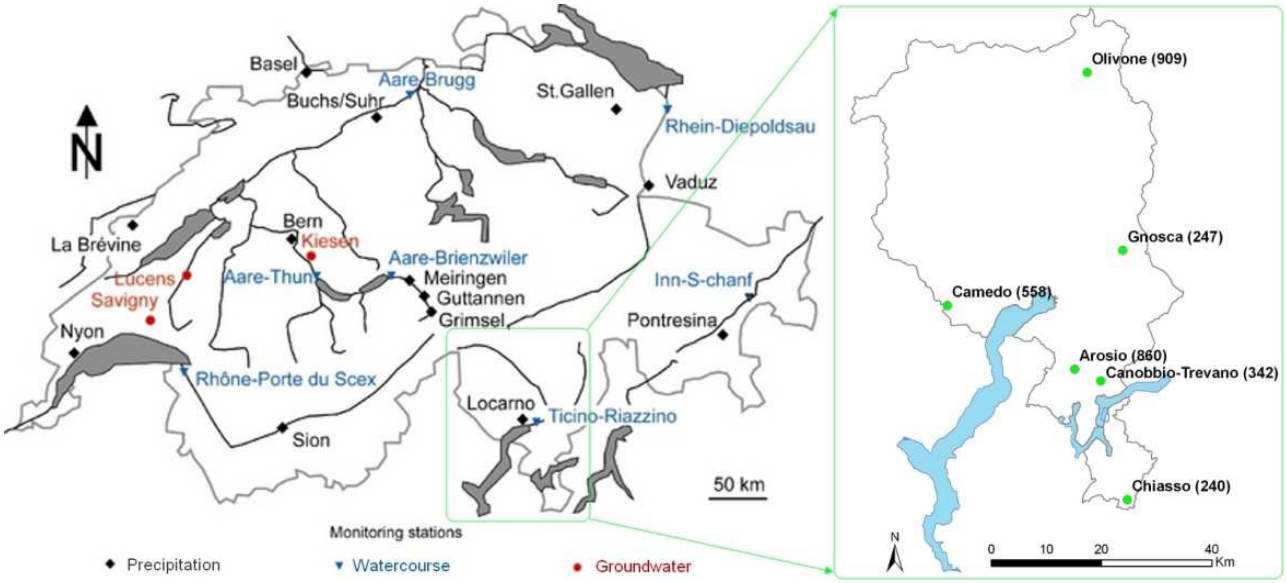

Figure 2.7 - Location of the stations used for the measurementof stable isotopes of meteoric precipitationsof the Swiss Network for Isotope measurements (ISOT module, http://www.bafu.admin.ch), left, and of rain gauges used for this research project, right.

Table 2.2- Swiss coordinates /CH1903 / LV03) of the rain gauges used for the stable isotope relative abundance's analysis

Name	East	North	altitude [m a.s.l.]
Arosio	713130	100610	860
Camedo	690050	112110	558
Chiasso	722690	77090	240
Gnosca	721880	122072	247
Olivone	715410	54120	909
Canobbio-Trevano	717900	98520	342

Precipitation samples were collected in 10 l high density polyethylene (HDPE) container (Figure 2.8), taking care to avoid evaporation effects using paraffin oil according to the technical procedure for precipitation sampling for isotopic analyses published by the IAEA-WMO (appendix B6).

Each container represents the integrated precipitation in the selected station for a one-month period. From each container, at the end of every month, a 30 ml quote was taken in airtight brown glass bottles. Glass instead of plastic was used to avoid isotopic exchange which may happen in the plastic bottles (Spangenberg and Vennemann, 2008). Oxygen and hydrogen stable-isotope composition of water was determined at the Stable Isotopes Laboratory of the University of Lausanne using a Wavelength-Scanned Cavity Ring Down Spectroscopy (WS-CRDS) based analyzer (Picarro L1102-*i* Isotopic Water Liquid Analyzer). Because memory effects are known to affect the analytical measurements, eight injections per sample were made of which only the last four were used for data reduction and normalization. For calibration, internal laboratory standards calibrated to VSMOW were inserted repeatedly within each analytical sequence (about each 11 samples), as well as at the beginning and at the end of the sequence. For the set of standards measured at the beginning and at the end of the sequence, 12 injections were made of which only the last five injections were used for calculations. Typical reproducibility for this method is approximately ±0.08 ‰ and ± 0.8 ‰ for $\delta^{18}O$ and $\delta^{2}H$, respectively.

The results obtained for the first year (March 2010 – February 2011) are reported as δ values relative to the Vienna Standard Mean Ocean Water, as defined in the previous sections. Appendix B contains all the data measured in rain and groundwater.

Figure 2.8 - Example of a rain gauge used for the monitoring (Arosio), with the 10 l HDPE containers used to collect water. The full container is replaced every month by a new one with the paraffin oil.

2.4.2 Numerical model to evaluate groundwater recharge

Groundwater recharge was mathematically calculate by using two different models:

- *The SOCONT model*

The first approach consists of the application of the SOCONT model(Berod, 1994; Consuegra and Vez 1996, Schaefli et al., 2005) and successfully applied in some mountain basins of Ticino canton (Pozzoni and Salvadè, 2008). It is a conceptual parametric model that simulates the discharge (Q_{total}) from a hydrological basin, as the sum of the runoff (Q_{quick}) derived from net rainfall and the base-flow (Q_{base}) derived from infiltrated rainfall infiltrated in the underground (Figure 2.9).

The model was applied to a section of Vedeggio river basin upstream of the village of Isone (Figure 2.10)that is representative of the region where the Monte Ceneri base tunnel is placed. Hydrological data was available from IST network (IST, 2010) which has monitored rain and discharge data since 1981 in Isone (Figure 2.10). Other necessary climatic data (temperature, sun radiance, relative humidity), were instead obtained from Lugano meteorological station (MeteoSwiss), and temperature is obviously corrected considering the altitude gradient. The evapotranspiration is simulated using a short term formula over 10 days (Turc, 1961).

Two steps are distinguished. First, parameters values to be used in the model (A, β and k) are obtained through a calibration procedure performed on different hydrological years, using discharge observed in the Vedeggio stream basin outlet.

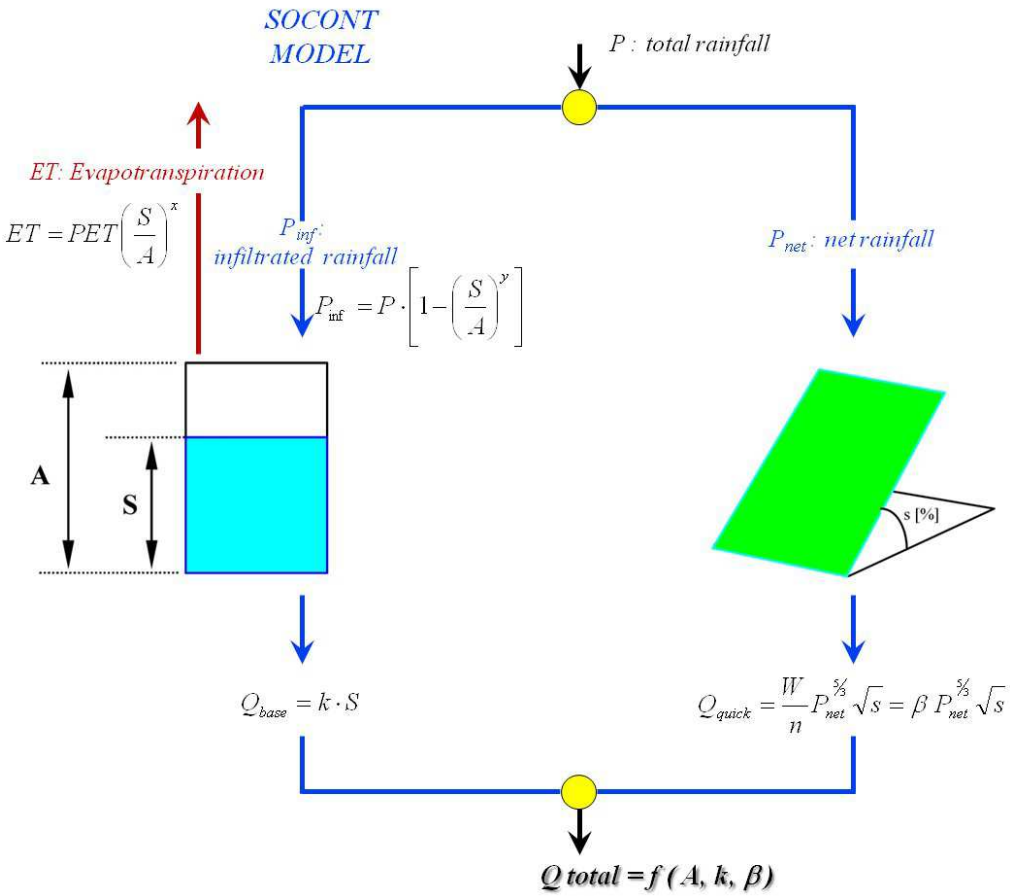

Figure 2.9 - Conceptual scheme of the adopted parametric hydrologic model. A (mm) is the maximum storage capacity of the reservoir; *S* (mm) is the actual storage; *PET* is the potential evapotranspiration evaluated with the Turc (1961) formulation, *s* id the slope of the catchment. According to previous studies (Consuegra and Vez, 1996), the exponent *x* and *y*can be set to 0.5 and 2, respectively. The parameters A, k and β are calibrated by the model.

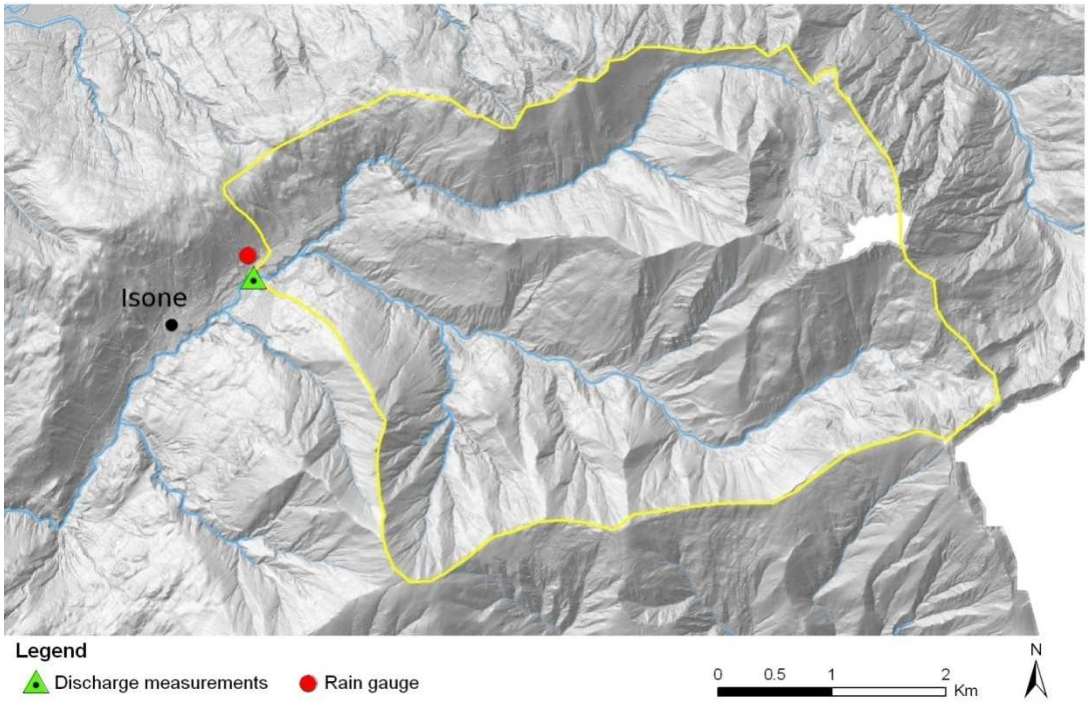

Figure 2.10 - Vedeggio basin upstream of the village of Isone. The exact location of the discharge measurement station and the rain gauge are shown by a green triangle and a red circle respectively.

Then, the parameters obtained from the calibration process are applied on the other years to reproduce the steam runoff (validation). The calibration and validation quality is evaluated on the basis of two factors:

i) the so called NS coefficient (Nash and Suttcliffe, 1970),
ii) a bias estimator, so called PBIAS,

which are expressed by the following equation 2.10:

$$NS = 1 - \frac{\sum_{i=1}^{n}\left(Q_i^{sim} - Q_i^{obs}\right)^2}{\sum_{i=1}^{n}\left(Q_i^{obs} - Q_{mean}\right)^2} \qquad PBIAS = \frac{\sum_{i=1}^{n}\left(Q_i^{sim} - Q_i^{obs}\right)}{\sum_{i=1}^{n} Q_i^{obs}} \qquad (2.10)$$

where Q_i^{sim} is the runoff simulated by the model on the daily time-step, Q_i^{obs} is the real runoff measured in the stream and Q_{mean} is the average discharge measured. NS of 1 corresponds to a perfect match of modeled discharge to the observed data, while PBIAS of 0 corresponds to a perfect correspondence of volumes.

- *The Soil Water Balance (SWB) code*

A second approach to simulate the groundwater recharge is constituted by the application of the Soil Water Balance code developed by US Geological Survey for the estimation of groundwater recharge (Westenbroek et al., 2010),.

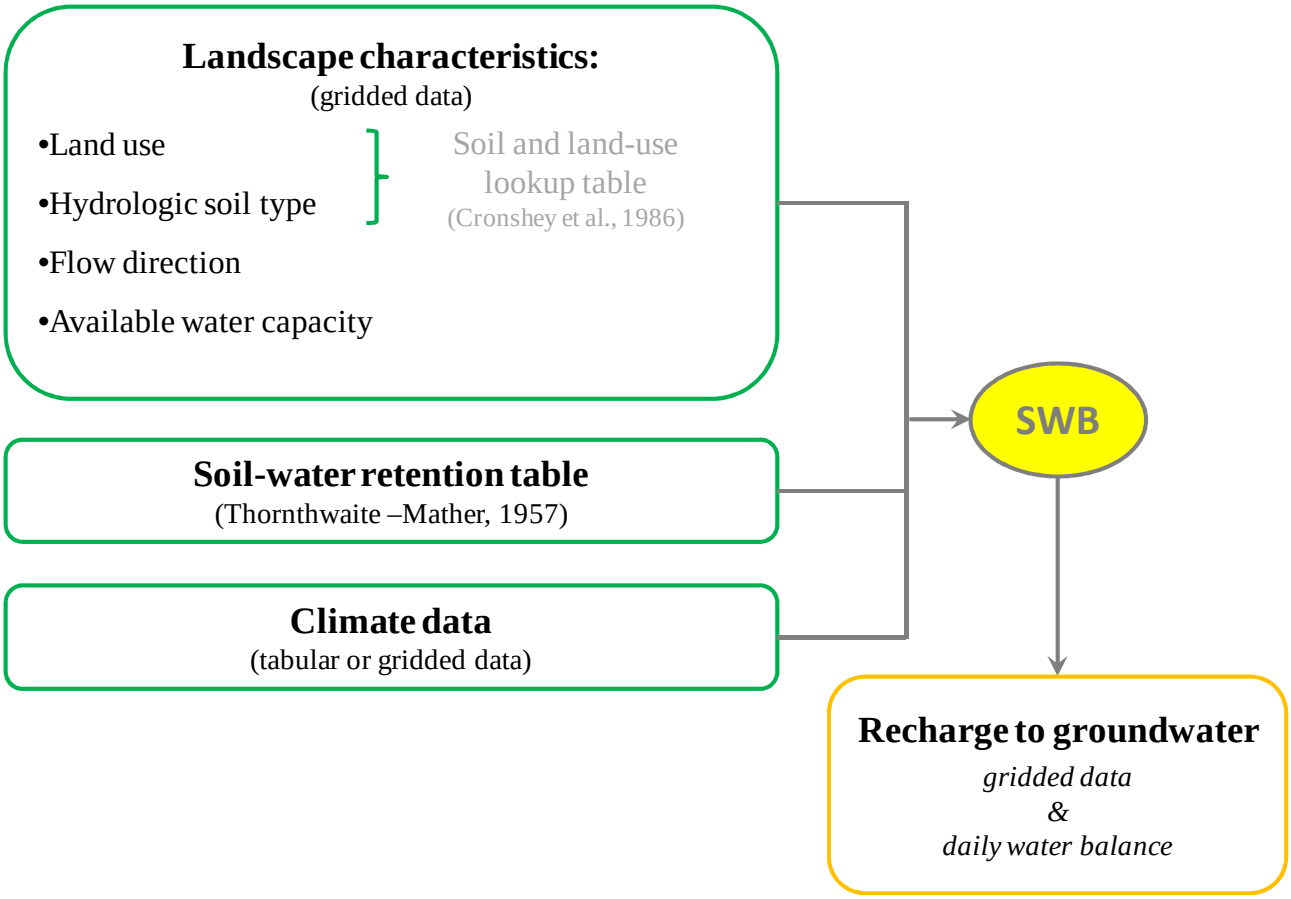

Figure 2.11 - Schematic representation of the input and output data of the SWB code. Soil and land-use lookup table are defined according to Cronshey et al. (1986).

In this case, groundwater recharge (R) is obtained by mass balance using equation (2.11) on each cell of a grid raster map of terrain:

$$R = \left(P + SM + inflow\right) - \left(Int + runoff + ET\right) - \Delta Soil\ \ Moisture \qquad (2.11)$$

where *P* is the precipitation as rain, *SM* is the snowmelt, *inflow* is the water coming from the outflow of adjacent cells calculated by use of a flow-direction grid derived from a digital elevation model, *Int* is the interception due to the vegetation, *runoff* is calculated by the application of the Natural Resources Conservation Service (NRCS) curve number (CN) method (Cronshey et al., 1986), *ET* is the evapotranspiration calculated on a daily basis using the temperature minimum, maximum and mean values and the Thornthwaite-Mather formulation (1957) and finally the *soil-moisture* term represent the amount of water held in soil storage for a given grid cell, and its variation Δ are tabulated by means of the soil-water-balance methods published also in Thornthwaite and Mather (1957). A schematic flowchart of the SWB code is shown in the following Figure 2.11.

Although this method, seems more suitable for a hydrogeological purpose; nevertheless it has some limitations. A main limit is given by the adoption of the NRCS-CN method to estimate run-off; in fact, this approach has been developed to evaluate floods and not designed to simulate daily flows of ordinary magnitude. Moreover this second approach does not allow a simple calibration based on the observed discharge such as the SOCONT model, but its results are only obtained on the basis of a reclassification of the land–cover map (Chow et al. 1988).This method is applied in the same area in order to compare the results obtained from both.

2.5 Results and discussion

2.5.1 Meteorological regime

As consequence of regional characteristics, precipitation rates and temperature are strongly variable within the area. Figure 2.12 and Figure 2.13 show the trends of the two parameters interpolated on the basis of the available data[1] for year 2010. Concerning seasonal distribution of precipitation autumn and winter (from October to March), are slightly dryer respect to spring-summer (from April to October), as also evidenced by mean values elaborated from MeteoSwiss for the 1961-1990 period for the meteorological stations southern Switzerland [Begert et al., 2005].

Figure 2.13 shows temperature seasonal variability in the 2010. July was the hottest month and December was particularly cold and characterized by snow precipitations almost in all the Ticino canton, also at lower depth.

[1]The used data were rain and temperature data of (i) IST rain gauges [IST, 2010], (ii) MeteoSwiss pluviometric and meteorological stations and for the contiguous Italian territory from the (iii) Agenzia Regionale per la Protezione dell'Ambiente della Lombardia (ARPAL) and (iii) Agenzia Regionale per la Protezione dell'Ambiente del Piemonte (ARPAP) pluviometric /meteorological stations respectively of the Lombardia and Piemonte regions. For the temperature interpolation, specific altitude gradients are evaluated for every month.

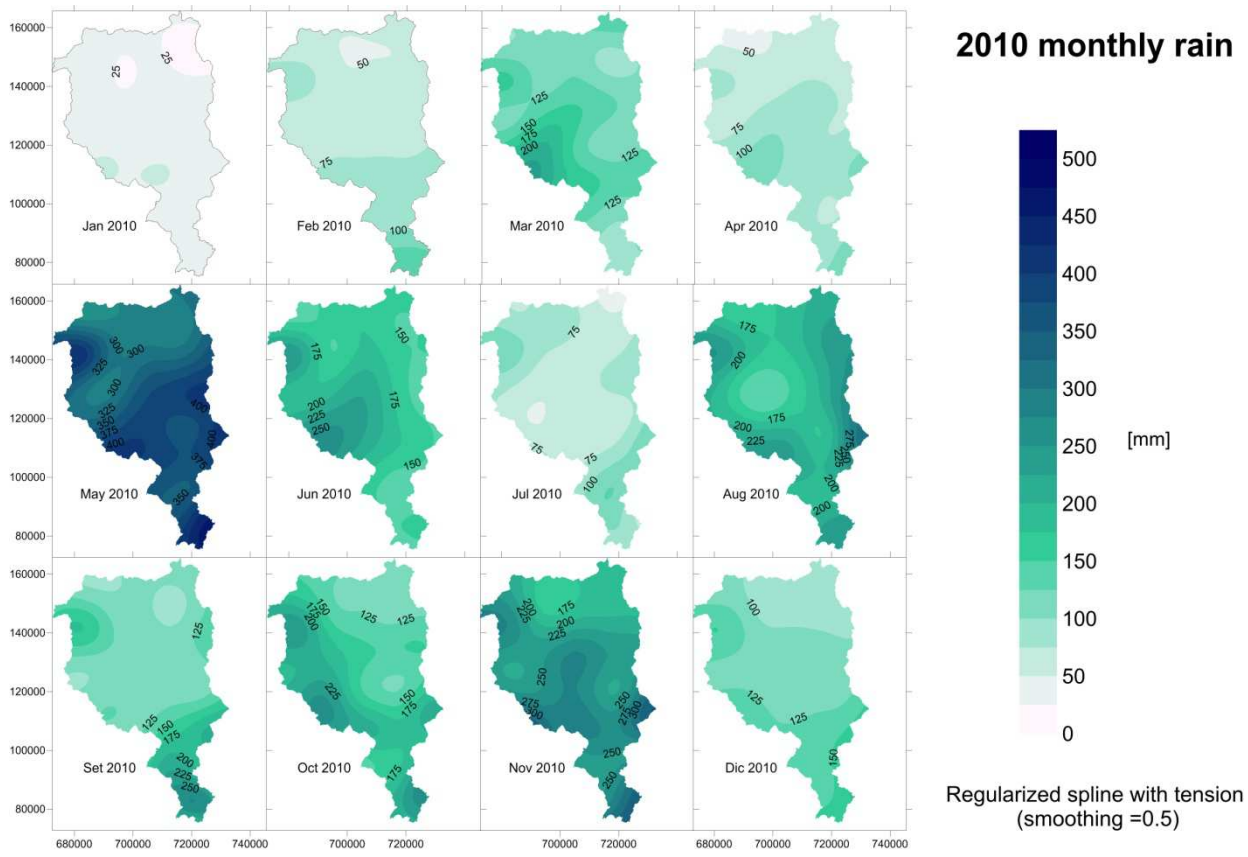

Figure 2.12 - Monthly interpolated rain.

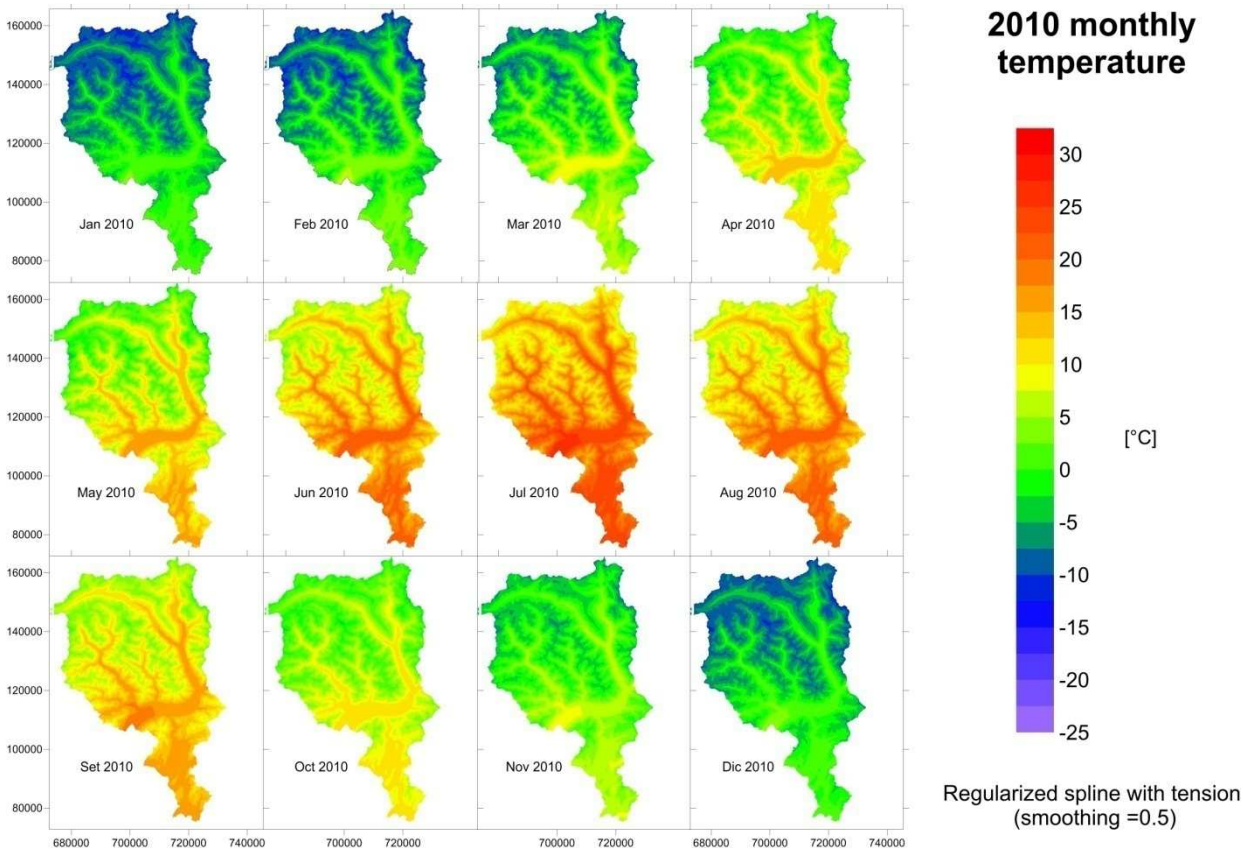

Figure 2.13 - Monthly interpolated temperature.

2.5.2The $\delta^{18}O$ - δD relationship

The data collected from March 2010 to February 2011 are presented in the appendix B and graphically represented in Figure 2.14, on the $\delta^{18}O$ - $\delta^{2}H$ graph, comparing them with the following meteoric water lines (MWL):

- ✓ the Global MWL (Rozanski et al., 1993);
- ✓ the Mediterranean MWL (Gat and Carmi, 1970);
- ✓ the Locarno MWL (Marzocchi et al., 2010, see appendix A).

Precipitation values, plot between Locarno and Mediterranean MWL, are not represented by none of them. For each of the analyzed6 rain gauges a linear best fit line has been calculated and the corresponding equations are reported in Table 2.3.

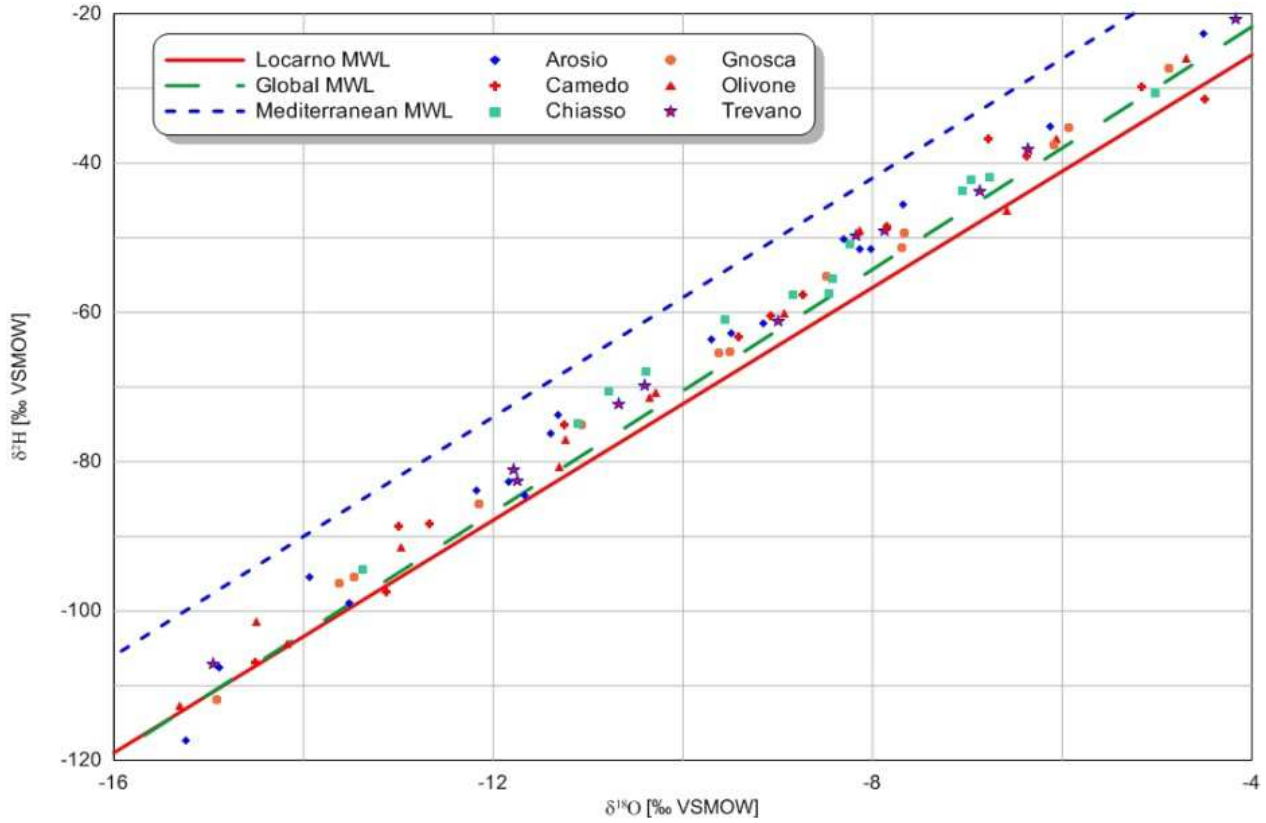

Figure 2.14 - Rain data of the six rain gauges from March 2010 to February 2011 compared to different MWLs.

Obtained lines are similar for all stations. Intercepts of the MWL with the $\delta^{2}H$ axis at $\delta^{18}O=0$, so-called deuterium excesses (~12‰), are close to that of the Global MWL (10‰), or slightly higher, probably due to Mediterranean influences (Sappa and Vitale, 2007):

$$\delta^{2}H = (8.03 \pm 0.09)\delta^{18}O + (12.65 \pm 0.92) \qquad (2.12)$$

It can be considered as the meteoric water line characteristic of the studied region, and is therefore called “Ticino MWL”.

If the annual mean weighted averages in the selected rain gauges (see equation 2.16) are considered, then the following correlation is obtained:

$$\delta^{2}H = (9.17 \pm 0.36)\delta^{18}O + (24.33 \pm 3.58) \qquad (2.13)$$

It is not representative of the real long term rain isotopic composition because rely on an insufficient data set.

Table 2.3 - Meteoric Water Lines for each rain gauge (March 2010 and February 2011).

Station	MWL	R^2	Number of samples
Arosio	$\delta^2H = (8.29\pm0.20)\cdot\delta^{18}O+(15.93\pm1.94)$	0.98	12
Camedo	$\delta^2H = (7.91\pm0.33)\cdot\delta^{18}O+(11.19\pm3.27)$	0.98	12
Chiasso	$\delta^2H = (7.57\pm0.24)\cdot\delta^{18}O+(9.33\pm2.19)$	0.99	12
Gnosca	$\delta^2H = (8.10\pm0.15)\cdot\delta^{18}O+(12.49\pm1.48)$	0.99	12
Olivone	$\delta^2H = (7.98\pm0.22)\cdot\delta^{18}O+(11.10\pm2.42)$	0.97	12
Trevano	$\delta^2H = (8.03\pm0.15)\cdot\delta^{18}O+(13.04\pm0.15)$	0.99	11

2.5.3 Seasonal effects

Concerning seasonal effects δ^2H and $\delta^{18}O$ correlations were obtained for all the rain gauges and shown in Figure 2.15 and Table 2.4.

Table 2.4 - Seasonal meteoric water lines obtained combining the data collected in the 6 rain gauges.

Period	Months	MWL	R^2	Number of samples
Winter	1–3	$\delta^2H = (8.08\pm0.16)\cdot\delta^{18}O+(11.03\pm1.77)$	0.99	20
Spring	4–6	$\delta^2H = (8.33\pm0.27)\cdot\delta^{18}O+(15.23\pm2.21)$	0.98	17
Summer	7–9	$\delta^2H = (7.75\pm0.17)\cdot\delta^{18}O+(11.55\pm1.43)$	0.99	18
Fall	10–12	$\delta^2H = (8.61\pm0.38)\cdot\delta^{18}O+(20.45\pm4.73)$	0.96	21

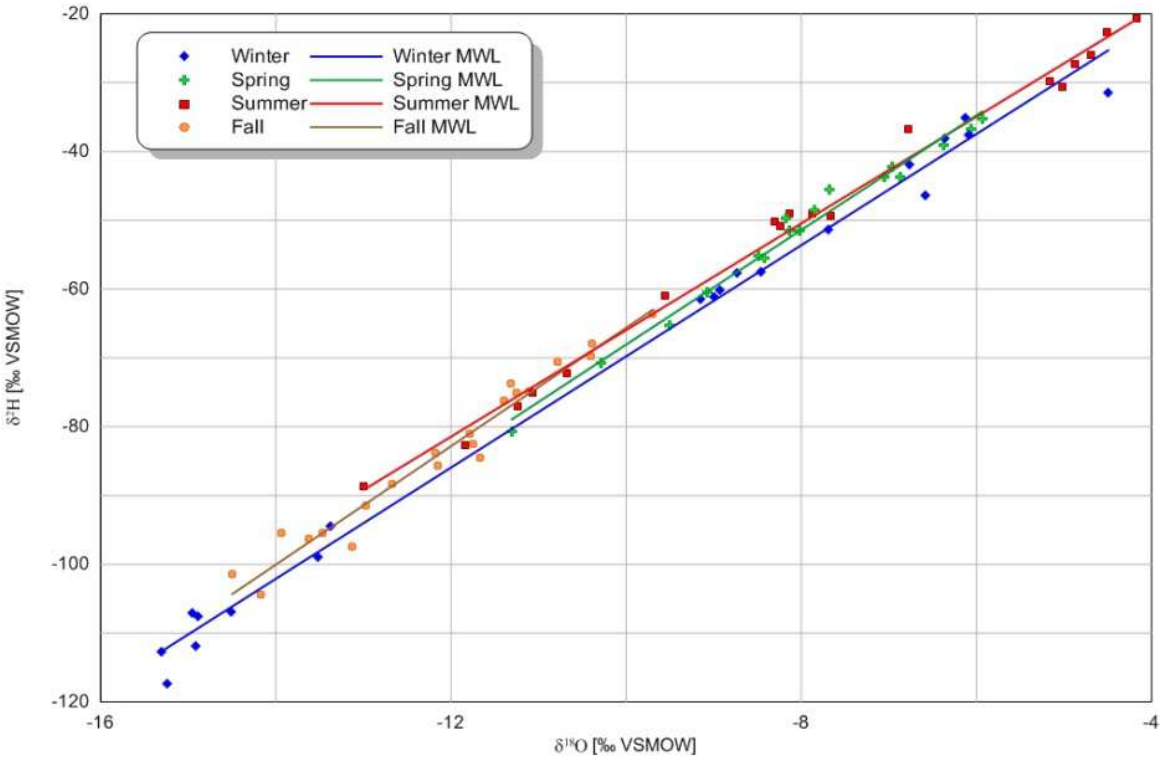

Figure 2.15 - Relative abundance of ^2H and ^{18}O in the six rain gauges subdivided for different seasons and seasonal meteoric water line reported in Table 2.4.

The MWL obtained from winter and summer rain data plot close to the global MWL, while differences are visible in MWL from fall and spring precipitation. The fall MWL has a slightly higher slope, and a higher deuterium excess. It is probably due to the Mediterranean origin of the water vapour, but also to "interpolation effects", due to the presence of too few data. As shown in Figure 2.16, indeed, no one of the fall rain has a so high deuterium excess such as expressed by fall MWL; also spring samples form a seasonal MWL that seem characterized by a little higher deuterium excess.

The deuterium excess is always higher than 10, a value of global MWL that is normally used as reference (Craig 1961). It is particularly high in spring and fall and this can be a typical effect

caused by an admixture of a secondary moisture due to the presence of the Maggiore, Como and Ceresio lakes in the studied region (Machavaram and Krishnamurthy, 1995; Coulomb et al., 2008), or to moisture fluxes coming from the Mediterranean Sea (Sappa and Vitale, 2007). Winter precipitation is instead characterized by generally lower deuterium excess. In fact, in the studied area, during winter, evaporation from lakes decreases because of lower temperatures (Figure 2.17) as well as the Mediterranean moisture fluxes are less frequent.

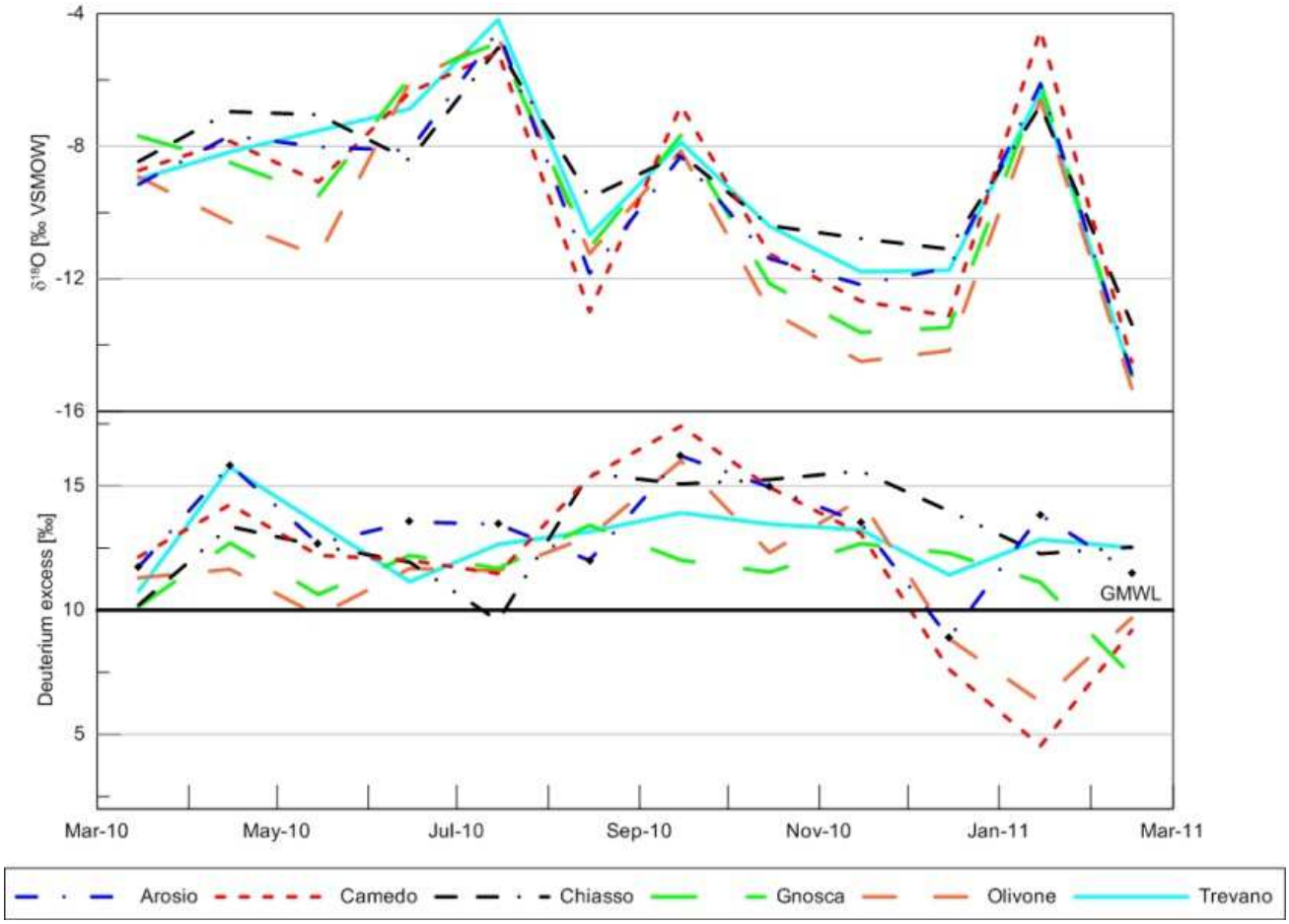

Figure 2.16 - Above, annual (March 2010- February 2011) trend of relative abundance of ^{18}O; below, the annual trend of deuterium-excess.

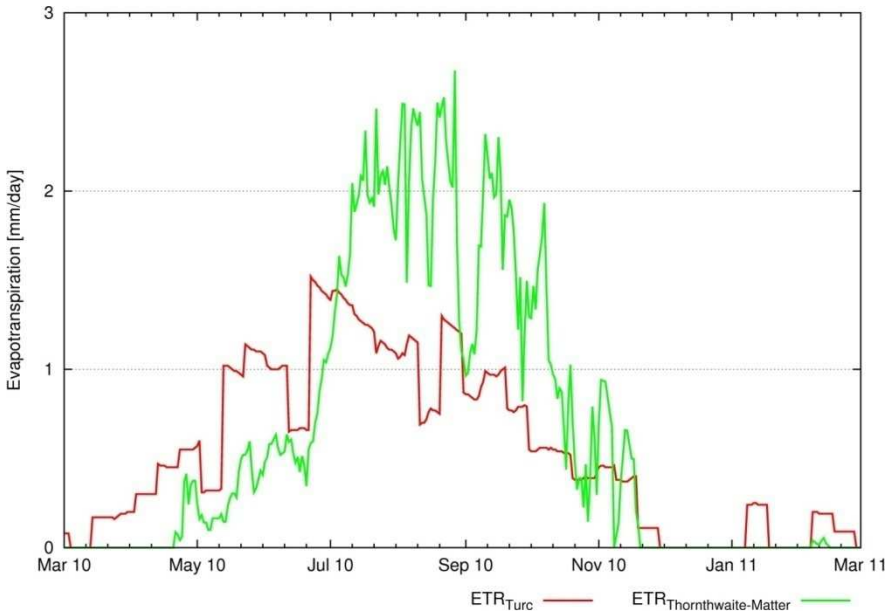

Figure 2.17 - Daily evapotranspiration evaluated for the Vedeggio basin using the Turc (1961) and Thornwaite-Mather formulas.

To analyze the seasonal temperature and amount effects, $\delta^{18}O$ data, and average monthly temperature in the Arosio rain gauge can be used. In fact, as shown by the data reported in Appendix B.1, the behaviors in all the station is similar.

Observing the $\delta^{18}O$ trend, a combined effect of temperature and amount of precipitations is visible. Two exceptions are constituted by the lower $\delta^{18}O$ measured in August 2010 and the unexpected high $\delta^{18}O$ measured in January 2011 registered in all the rain gauges. While the values of August can be explained with the amount effect typical of abundant precipitation registered in this month, the values of January are difficulty explained observing the daily temperature and the amount of precipitation for January and February 2011 (Figure 2.19). The February rain has been more abundant and more depleted in stable isotopes($\delta^{18}O \approx -14‰$; $\delta^{2}H \approx -110‰$), while in January an unexpected high isotope content was measured($\delta^{18}O \approx -6‰$; $\delta^{2}H \approx -35‰$). Excluding an error of measurement, unlikely in 6 stations at the same time, it is possible conclude that $\delta^{2}H$ and $\delta^{18}O$ values measured in January 2011 are probably the effect of a singular meteorological event, probably of southern origin, that is not very representative of the typical winter rain.

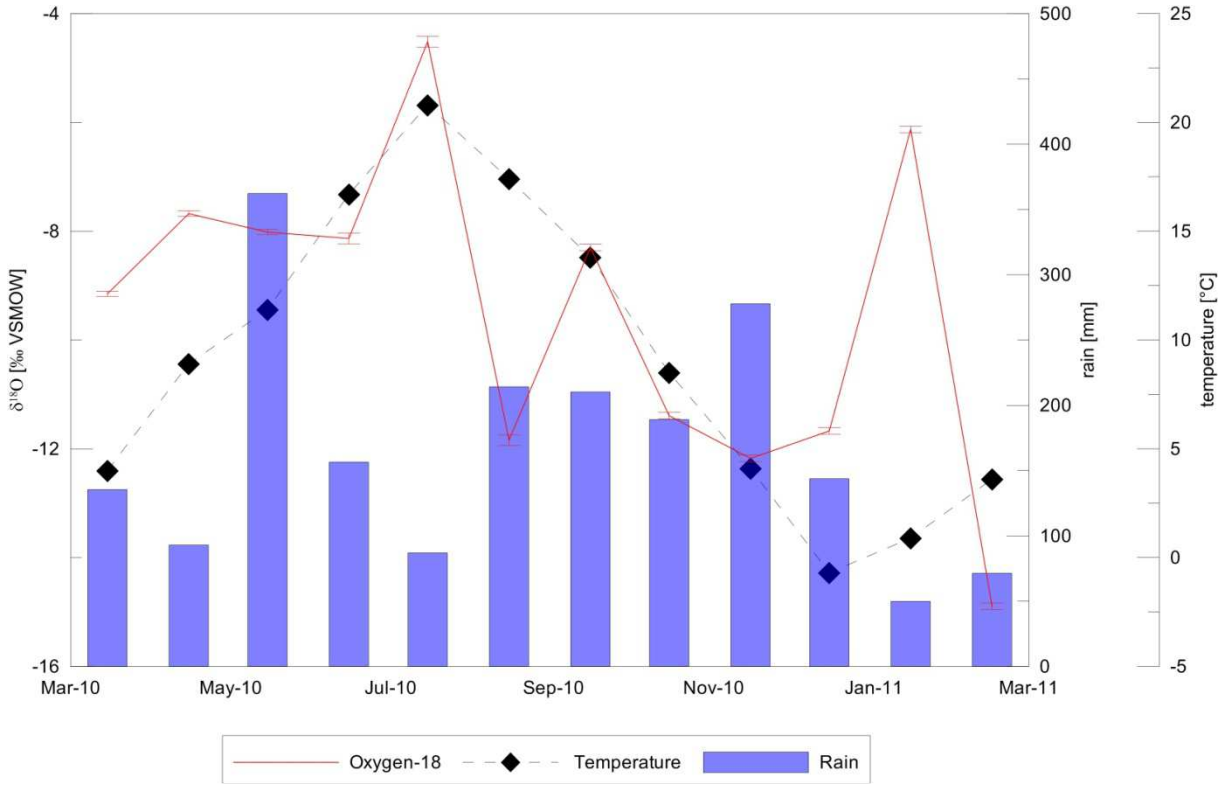

Figure 2.18 - Annual trend (March 2010- February 2011) of the relative abundance of ^{18}O in the Arosio rain gauge, compared with registered monthly precipitation and temperature.

The seasonal variations of stable isotope values in precipitation were also analyzed with the statistical software R [*R Development Core Team*, 2011]. For each station, the linear correlations between *(i)* mean monthly stable isotope composition ($\delta^{2}H$ or $\delta^{18}O$), *(ii)* mean monthly temperature and *(iii)* rain amount were examined. Results are summarized in Figure 2.20, where *p* is the monthly rain amount expressed in mm, and *T* the monthly mean temperature expressed in °C.

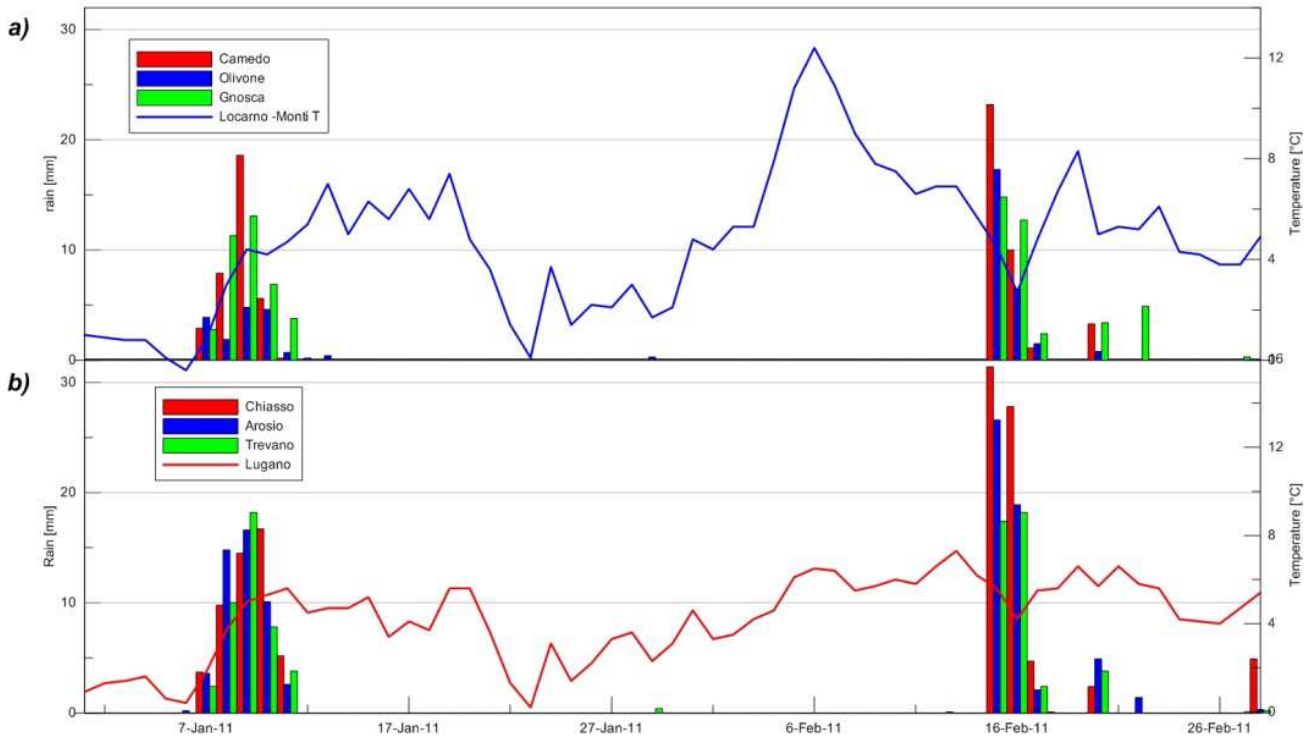

Figure 2.19 - Detailed analysis of the precipitations registered in January and February 2011 respectively for the Northern (*a*) and Southern (*b*) rain gauges compared with the temperature registered in Locarno Monti and Lugano [MeteoSwiss].

For each station the correlation with the mean monthly temperature and the rain amount is low. This fact is due to the reciprocal influence of temperature and rain abundance and to the restricted dataset. Moreover, with this approach, other effects that could influence the δ-values, such as the differences in the water vapour source regions, cannot be considered. In fact, there are not indexes to consider the so-called continentality (distance from the sea or the point of origin of the evaporated water). As most rain in the studied area comes from Mediterranean region, and unfortunately in Northern Italy data were only sporadically collected between 2002 and 2004 (Longinelli and Selmo,2003; Longinelli et al., 2006); therefore continentality effects are difficult to evaluate.

A multiple regression, considering the rain amount and the temperature as independent variables and the relative isotope abundances ($\delta^{18}O$ or $\delta^{2}H$) as dependent variable was also tried. Resulting correlations are shown in Table 2.5. Correlation coefficients(R^2) are generally higher with respect to the single correlations of Figure 2.30, even though they remain low (0.23÷0.52).

Finally, a triple regression among the rain amount, temperature and rain gauges elevation (m a.s.l) as independent variables and the $\delta^{2}H$ or $\delta^{18}O$ values as dependent variable was on all 71 samples analyzed. The resulting regression lines are reported in the following equations:

$$\delta^{2}H = -0.068 \cdot p[mm] + 1.685 \cdot T[°C] + \left(1.27 \times 10^{-4}\right) \cdot H[ma.s.l.] - 66.882 \qquad R^2 = 0.31 \qquad (2.14)$$

$$\delta^{18}O = -0.008 \cdot p[mm] + 0.197 \cdot T[°C] + \left(1.2 \times 10^{-5}\right) \cdot H[ma.s.l.] - 9.9 \qquad R^2 = 0.30 \qquad (2.15)$$

where H is the elevation of the monitoring rain gauge expressed in meters above sea level.

No significant increase of the correlation coefficient (R^2) has been registered with respect to the double correlation.

In Figure 2.21 the correlation between $\delta^{18}O$ and temperature is given for the Locarno Monti station with the data collected since 1972 to 2010. The more extended dataset give a more reliable correlation. Simply analyzing monthly data is clear the combined effect also of amount resulting in a correlation coefficient lower (R^2 = 0.583), while considering average data, obviously the amount

effect is mediate resulting in a higher correlation coefficient (R^2 = 0.959). Nevertheless, the correlation equations do not differ sensibly.

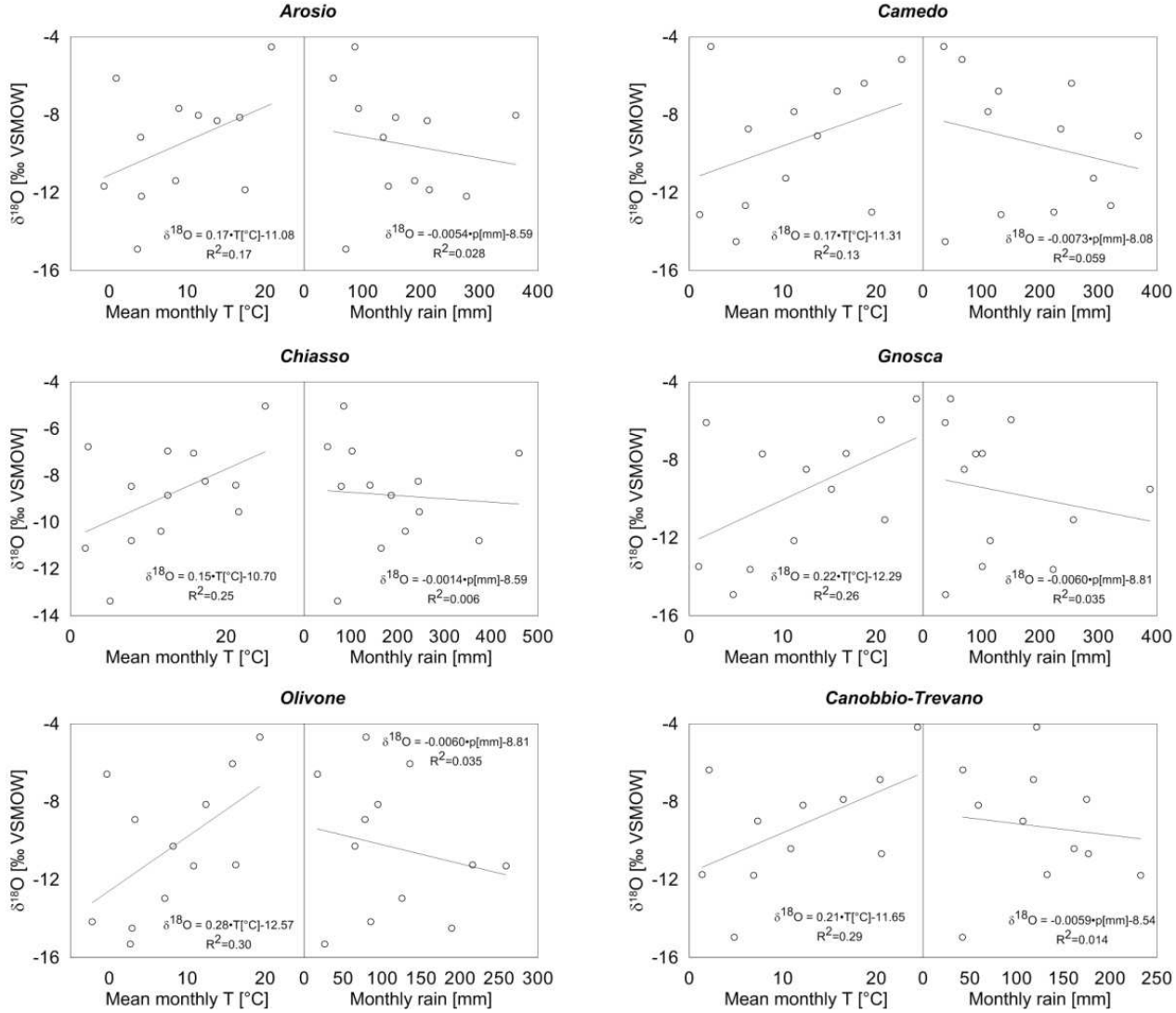

Figure 2.20 - Monthly correlation of $\delta^{18}O$ with temperature and rain amount in the six measuring stations.

Table 2.5 - Multiple correlations obtained in each rain gauge and relative coefficient of determination

Rain gauge	Regression lines	R^2	Sample
Arosio	$\delta^2H = (-0.068)\cdot p\ [mm] + (1.685)\cdot T\ [°C] + (-66.882)$	0.247	12
	$\delta^{18}O = (-0.008)\cdot p\ [mm] + (0.197)\cdot T\ [°C] + (-9.9)$	0.238	
Camedo	$\delta^2H = (-0.062)\cdot p\ [mm] + (1.829)\cdot T\ [°C] + (-72.076)$	0.257	12
	$\delta^{18}O = (-0.009)\cdot p\ [mm] + (0.195)\cdot T\ [°C] + (-9.878)$	0.220	
Chiasso	$\delta^2H = (-0.017)\cdot p\ [mm] + (1.212)\cdot T\ [°C] + (-69.582)$	0.277	12
	$\delta^{18}O = (-0.003)\cdot p\ [mm] + (0.159)\cdot T\ [°C] + (-10.23)$	0.282	
Gnosca	$\delta^2H = (-0.090)\cdot p\ [mm] + (2.206)\cdot T\ [°C] + (-79.679)$	0.390	12
	$\delta^{18}O = (-0.012)\cdot p\ [mm] + (0.267)\cdot T\ [°C] + (-11.251)$	0.385	
Olivone	$\delta^2H = (-0.183)\cdot p\ [mm] + (3.174)\cdot T\ [°C] + (-75.951)$	0.546	12
	$\delta^{18}O = (-0.024)\cdot p\ [mm] + (0.379)\cdot T\ [°C] + (-10.662)$	0.514	
Trevano	$\delta^2H = (-0.119)\cdot p\ [mm] + (1.933)\cdot T\ [°C] + (-68.885)$	0.377	11
	$\delta^{18}O = (-0.015)\cdot p\ [mm] + (0.238)\cdot T\ [°C] + (-10.182)$	0.370	

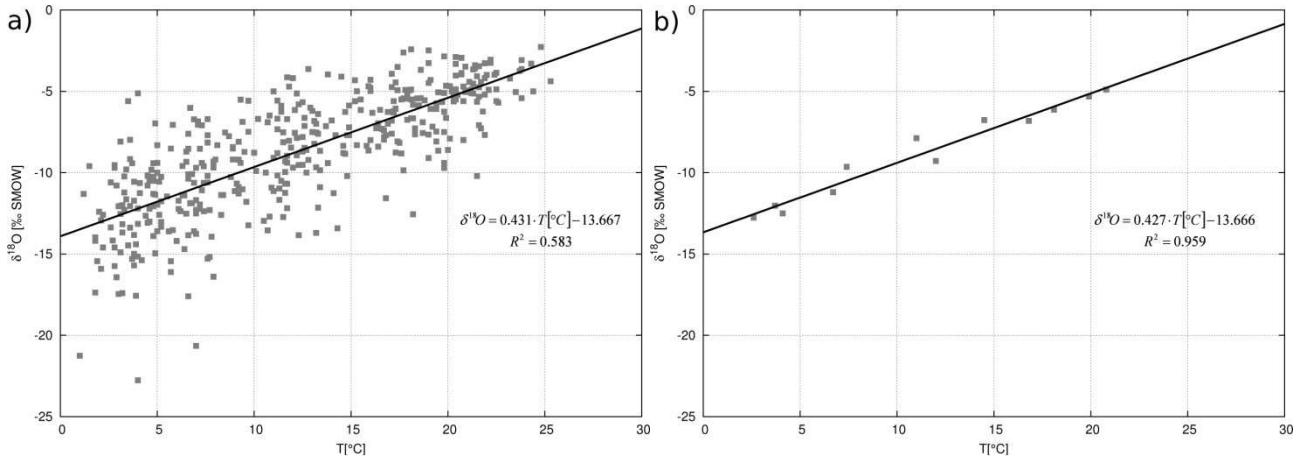

Figure 2.21 - Correlations between monthly temperature and $\delta^{18}O$ for Locarno Monti. a) monthly data collected since 1972 to 2010, b) long term average of monthly data.

2.5.4 Precipitation altitude gradients

Given the $\delta^{18}O$ and $\delta^{2}H$ mean monthly composition of rainfall for each rain gauges, the mean weighted $\delta^{18}O$ and $\delta^{2}H$ annual composition were obtained using the following equation:

$$\delta X_{mwa} = \frac{\sum_{i=1}^{12} P_i \delta X_i}{\sum_{i=1}^{12} P_i} \qquad (2.16)$$

where P_i is the precipitation registered during the i-th month, and δX is respectively $\delta^{2}H$ and $\delta^{18}O$.

Using the mean weighted isotopic composition, a linear regression between the altitudes at which rain has been collected and $\delta^{18}O$ or $\delta^{2}H$ values was obtained. Annual data collected in the Canobbio-Trevano rain gauge were not considered, because of the missing of data in last May, due to the blocking of the rain gauge.

In the previous section the screen effect caused by orographic barriers has been already discussed, from a theoretical point of view. In the studied region, it is particularly significant considering the Alps barrier that divides the southern from the central and northern Switzerland. Nevertheless, on the basis of rain amount and distribution (Figure 2.12) and stable isotope composition (Figure 2.23 and Figure 2.25), two different subregions can be also identified in canton Ticino (southern Switzerland): "*Sotto-Ceneri*" and "*Sopra-Ceneri*". In particular, the "*Sotto-Ceneri*" rain gauges are placed at the South (Chiasso and Arosio) with respect to the Monte Ceneri ridge (Figure 2.22) and the "*Sopra–Ceneri*" rain gauges are placed at North (Camedo, Gnosca, Olivone). Three different altitude-isotope relationships (one general, one for the "*Sotto-Ceneri*", one for the "*Sopra-Ceneri*") were obtained considering respectively the deuterium and the oxygen-18 and are reported in Figure 2.23.

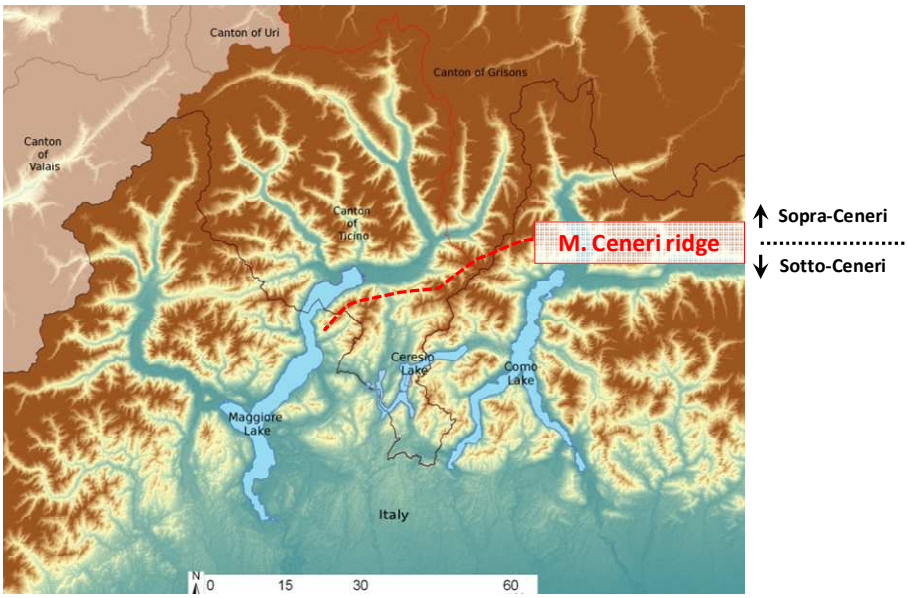

Figure 2.22 - The studied region and evidenced the Monte Ceneri orographic barrier, with the sketching subdivision in "*Sopra-Ceneri*" / "*Sotto-Ceneri*" regions.

The obtained general relationship (Figure 2.24) shows differences with respect to previously reported ones for northern and central Switzerland (Pearson et al., 1991) and those for the Blenio Valley and for the Gotthard region (Pastorelli et al., 2001; Ofterdinger et al. 2001, Bestenheider, 2006).

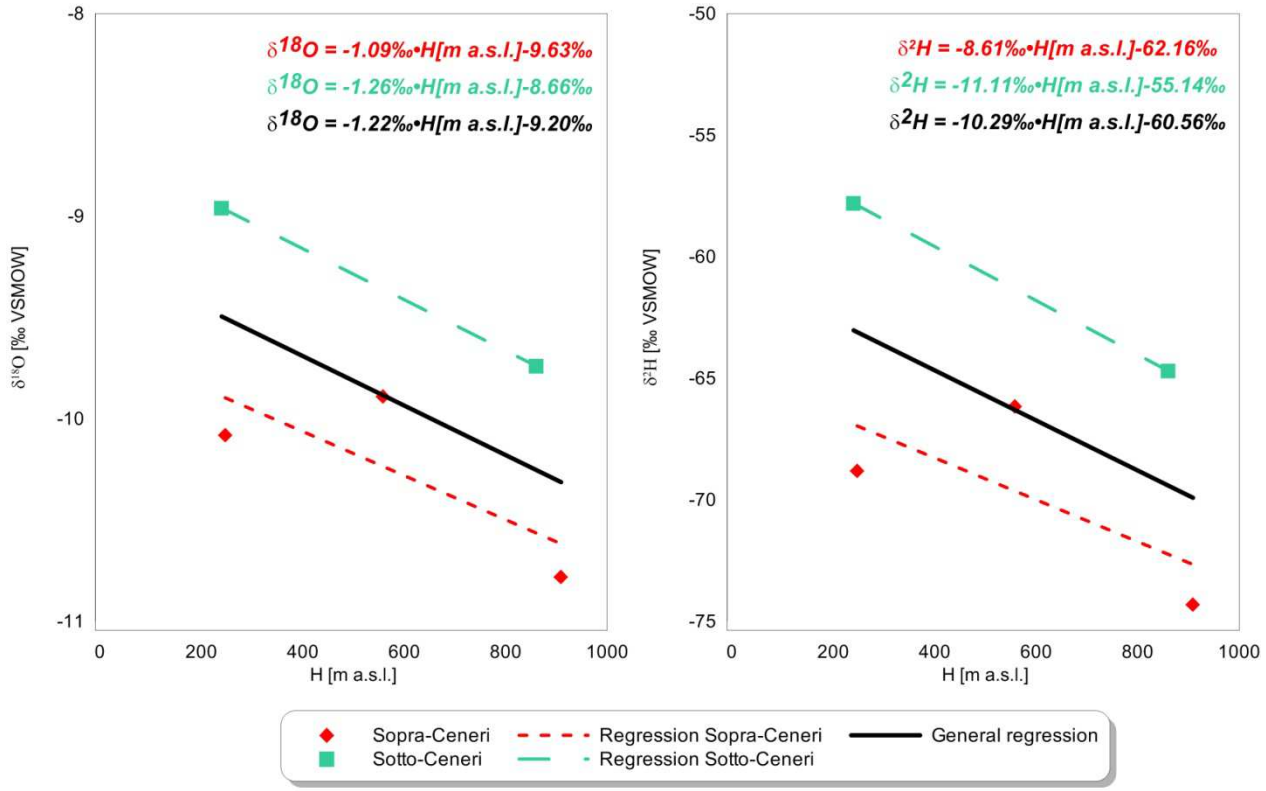

Figure 2.23 - Isotopic altitude gradient obtained with the collected data. On the left H-$\delta^{18}O$, on the right H-$\delta^{2}H$ (left: $\delta^{18}O$, right: $\delta^{2}H$)

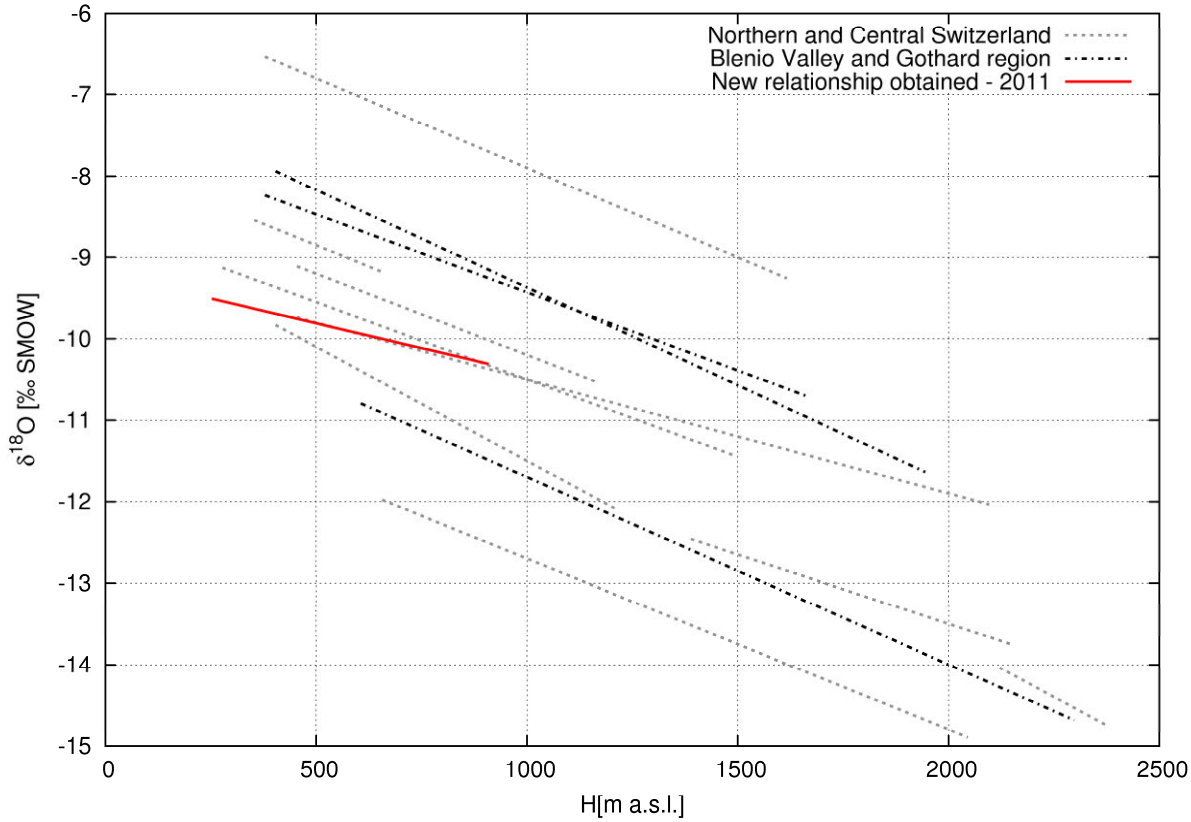

Figure 2.24 - New obtained altitude-isotope gradient, compared with other available relationships for the northern and central Switzerland (Pearson et al., 1991), Blenio valley and Gotthard region (Pastorelli et al. 1999; Oftendinger et al. 2004; Bestenheider, 2006).

2.6 Groundwater recharge

In previous sections, δ^2H and $\delta^{18}O$ values from rain data were discussed; nevertheless, in order to apply hydrological observations (rain) to the hydrogeological cycle (groundwater) some remarks need to be made.

As shown by Figure 2.25, groundwater (springs and tunnel inflows) samples are aligned close to the Ticino MWL, on a line expressed by the equation:

$$\delta^2H = (7.78 \pm 0.32)\delta^{18}O + (13 \pm 2.93) \qquad R^2 = 0.95 \qquad (2.15)$$

Nevertheless, as a preliminary observation, comparing isotopic composition of groundwater samples and that measured in the monthly rain samples, a few differences are observable.(Figure 2.25). These differences are also visible comparing the altitude gradient in precipitation with the mean yearly relative isotope abundance in springs and tunnel inflows Practically, altitude gradient obtained from precipitation data do not fit with groundwater data (springs and tunnel inflows), and often the altitude of infiltration estimated using the stable isotope composition is lower than the elevation of springs (Figure 2.26).

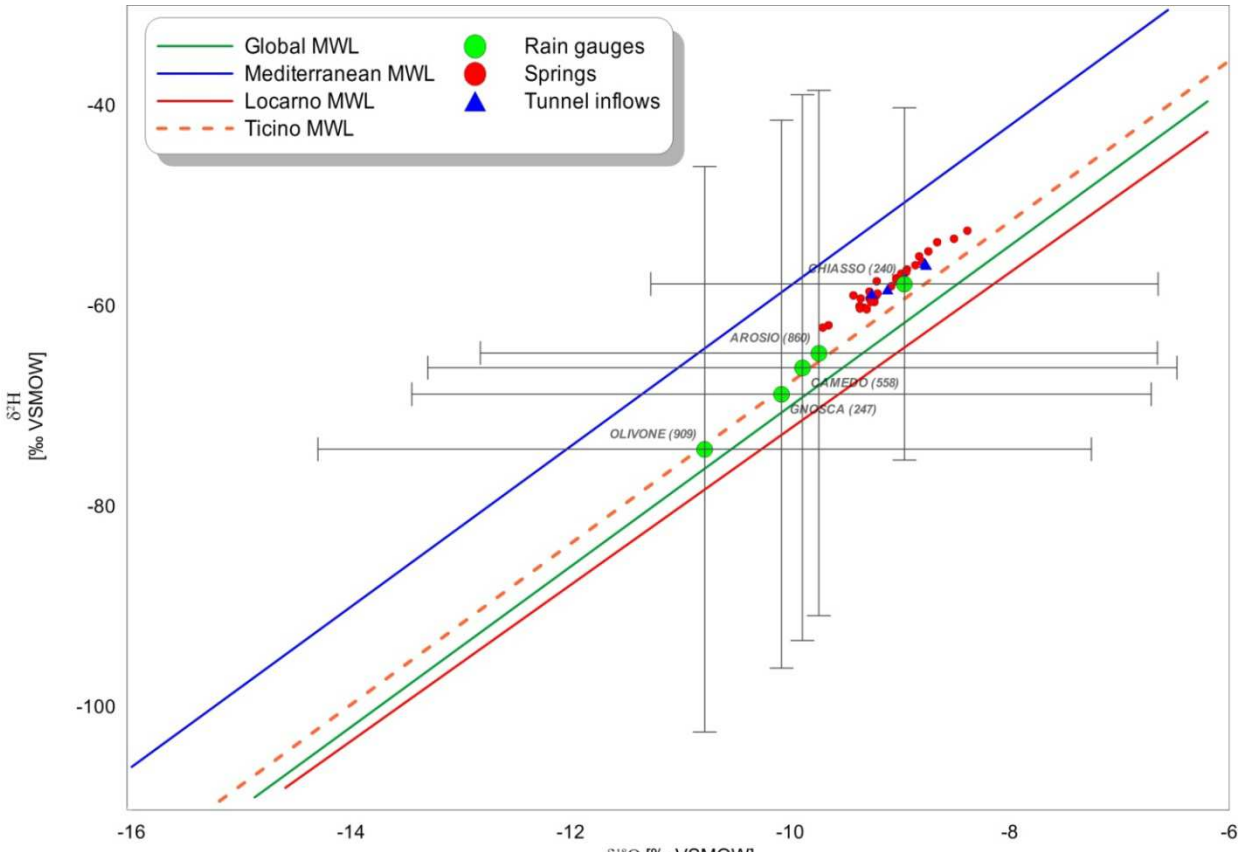

Figure 2.25 - Mean annual isotope abundance of groundwater and yearly weighted average of collected rain. The standard deviation given by the average of mean monthly stable isotope data is also shown. All data are compared with various meteoric water lines: Ticino (here obtained), Locarno (Marzocchi et al., 2010), global (Rozanski et al., 1993) and Mediterranean (Gat and Carmi, 1970).

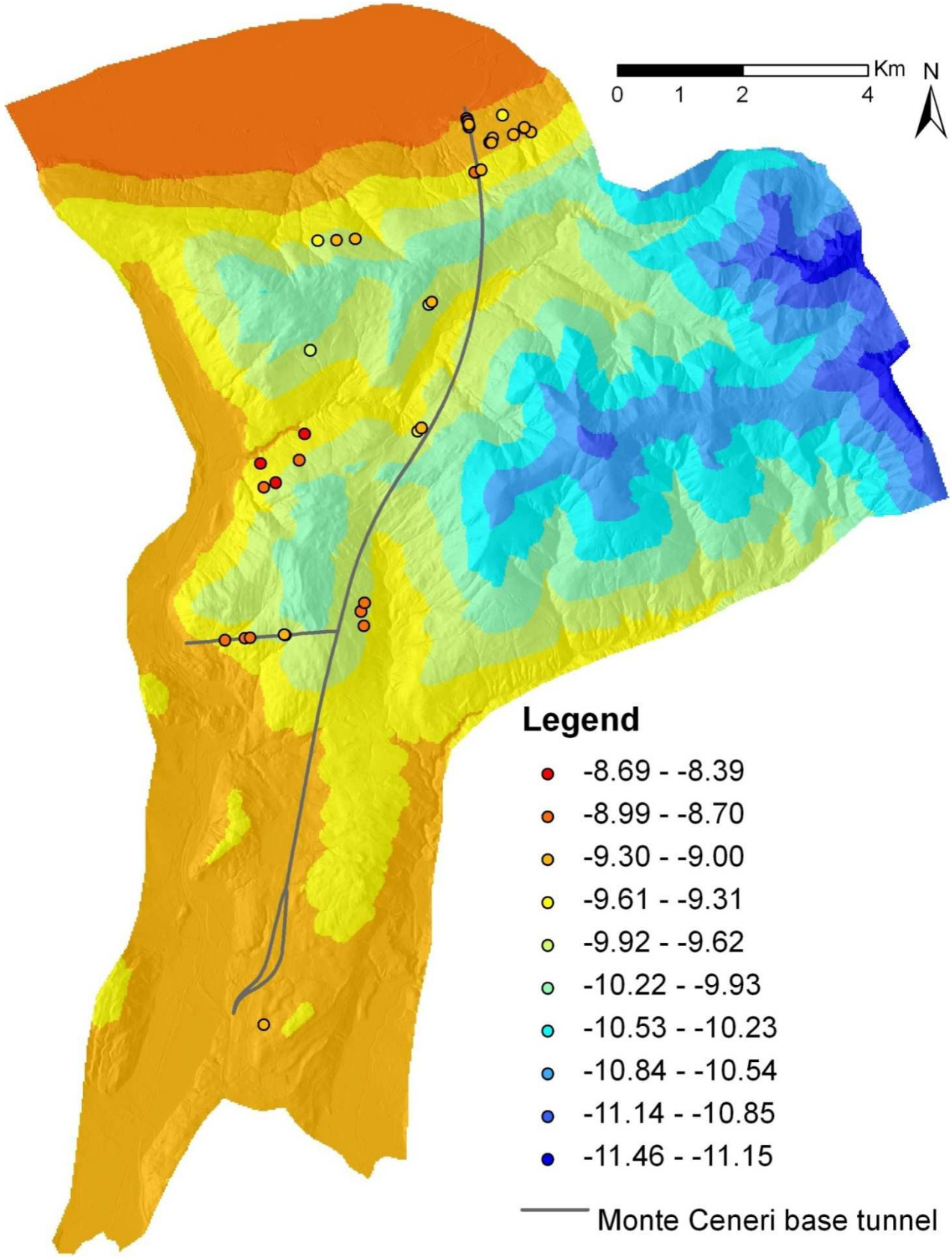

Figure 2.26 - Mean annual $\delta^{18}O$ in precipitations (altitude gradient with colors varying from low altitudes shown in red to higher ones shown in blue) and groundwater (yearly average in springs and water inflows) for the Monte Ceneri region (Magadino plain in the north, Lugano in the south).

2.6.1 Recharge estimation by numerical models

As discussed in previous sections isotopic composition of meteoric water varies throughout the year. Since recharge may vary spatially and temporally due to geological or climatic conditions. Two hydrological models SOCONT and SWB, were applied for a calculation of meteoric water effectively infiltrating.

Concerning the SOCONT model, the calibration was made comparing the simulated and observed discharges during the years 1981-2000 in the Vedeggio stream. Results are reported in Table 2.6.Using obtained coefficients (A, k and β) ; the model was validated on the years 2000-2011 obtaining a NS of 0.730 and a PBIAS of 0.079. These values are typical of a model that appreciably simulates the stream runoff as it is also shown in Figure 2.27 for the stable isotope monitoring period (March 2010-Februar 2011).On the basis of the obtained results, the monthly recharge in the Vedeggio basin was estimated as the increase of the underground storage capacity S (Figure 2.9).

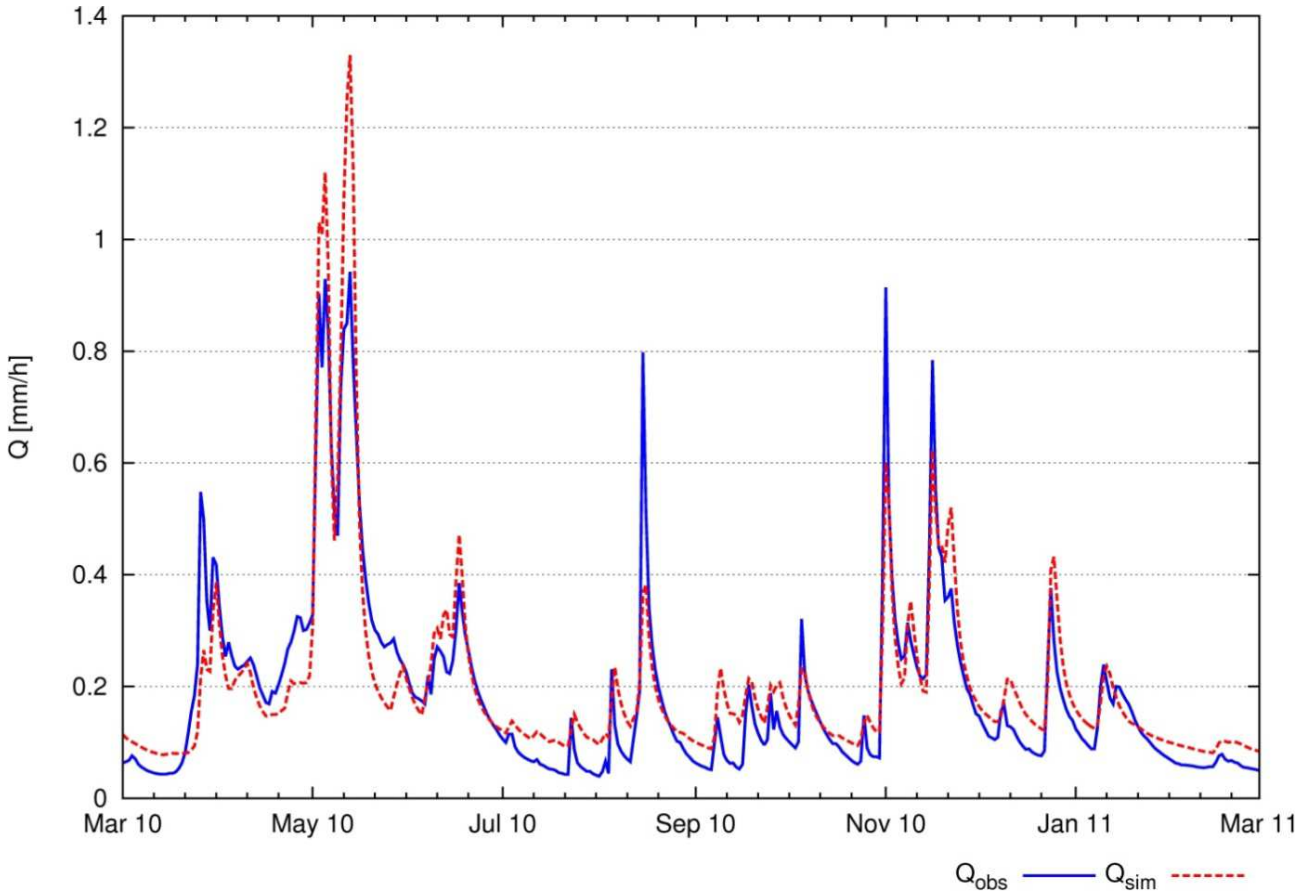

Figure 2.27 - Observed and simulated discharge in the Vedeggio river (Isone) during the year of observation. As shown also by NS and PBIAS the agreement of the model with observed data is good.

Table 2.6 - Results of the calibration process: *(i)* model coefficients (A, k and β) and *(ii)* calibration parameters (NS and PBIAS).

A	350 mm
k	-7.54 h^{-1}
β	330
NS	0.627
PBIAS	0.117

The SWB model was applied after having conveniently (Cronshey et al., 1986) reclassified the land-use map obtaining all the needed inputs (Figure 2.11), and monthly results are shown in Figure 2.28.

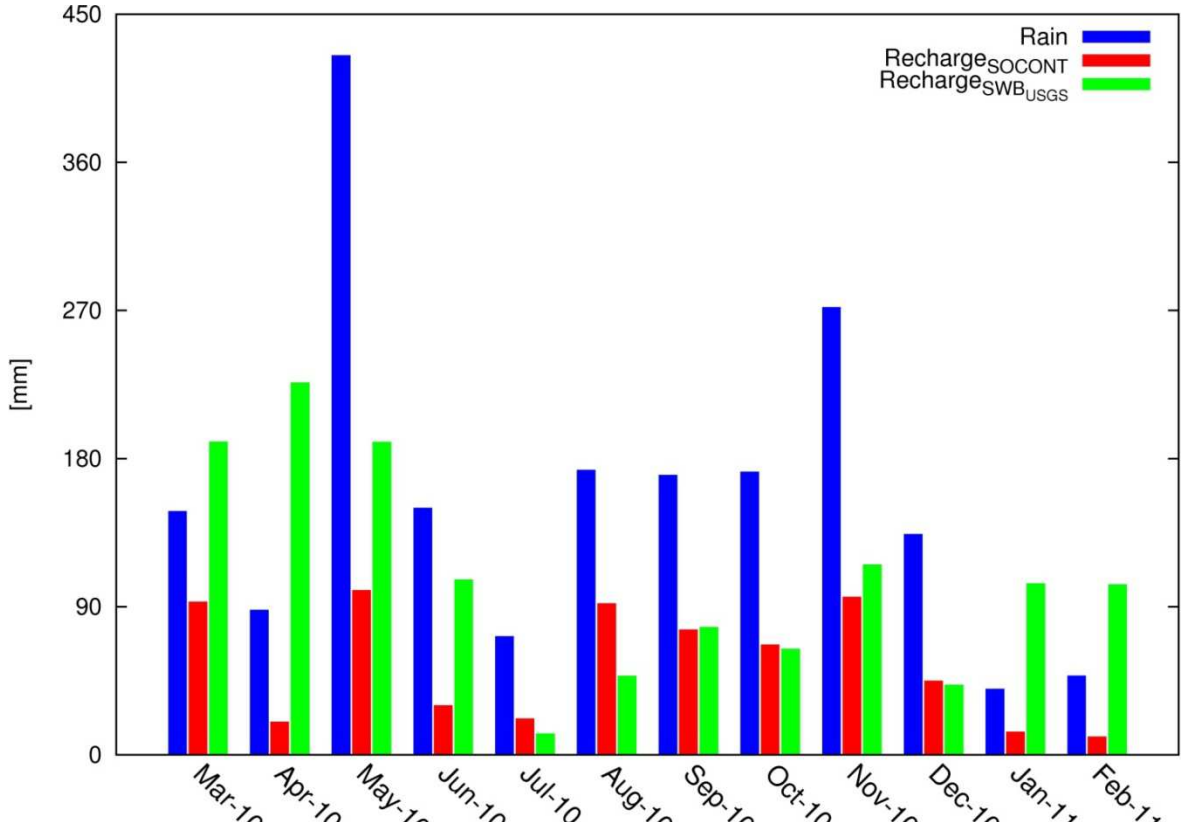

Figure 2.28 - Monthly hydrologic balance for the period of observation using the two different approaches previously described.

From the application of both hydrological models a daily and consequently monthly water balance was estimated. In Figure 2.28 the monthly rain and simulated recharge from both models for the period of observation (March 2010 - February 2011) are reported. Although similar results for recharge are obtained since May to December due to rain contributions; consistent differences instead occur during winter and spring (March and April of 2010; January and February 2011). In this period the two models do not agree in estimating recharge due to the snowmelt. In particular, is opinion of the authors that the SWB code overestimate snowmelt recharge, probably because it neglect the sublimation effects due to the dry winds and it do not consider that the layer of soil through which infiltration occurs, during these months, is frozen. On the contrary, the SOCONT model underestimates this contribution as well observable by the higher simulated base-flow respect of the observed ones, in January and February 2011 (Figure 2.27), because it underestimates the soil retention effect.

2.6.2 Stable isotope evidences on groundwater recharge

Groundwater recharge estimation using numerical model was demonstrated to be difficult, nevertheless useful indication concerning groundwater recharge can be obtained comparing collected rain and groundwater data. Although groundwater from springs and inflows have their origin in meteoric recharge, differences in isotopic composition may be noted. Seasonal effects, evaporation during runoff, mixing during infiltration modify isotopic composition of groundwater.

To understand the differences between precipitation and groundwater stable isotope composition, the last eleven years of data (2000-2010) for Locarno station were analyzed.

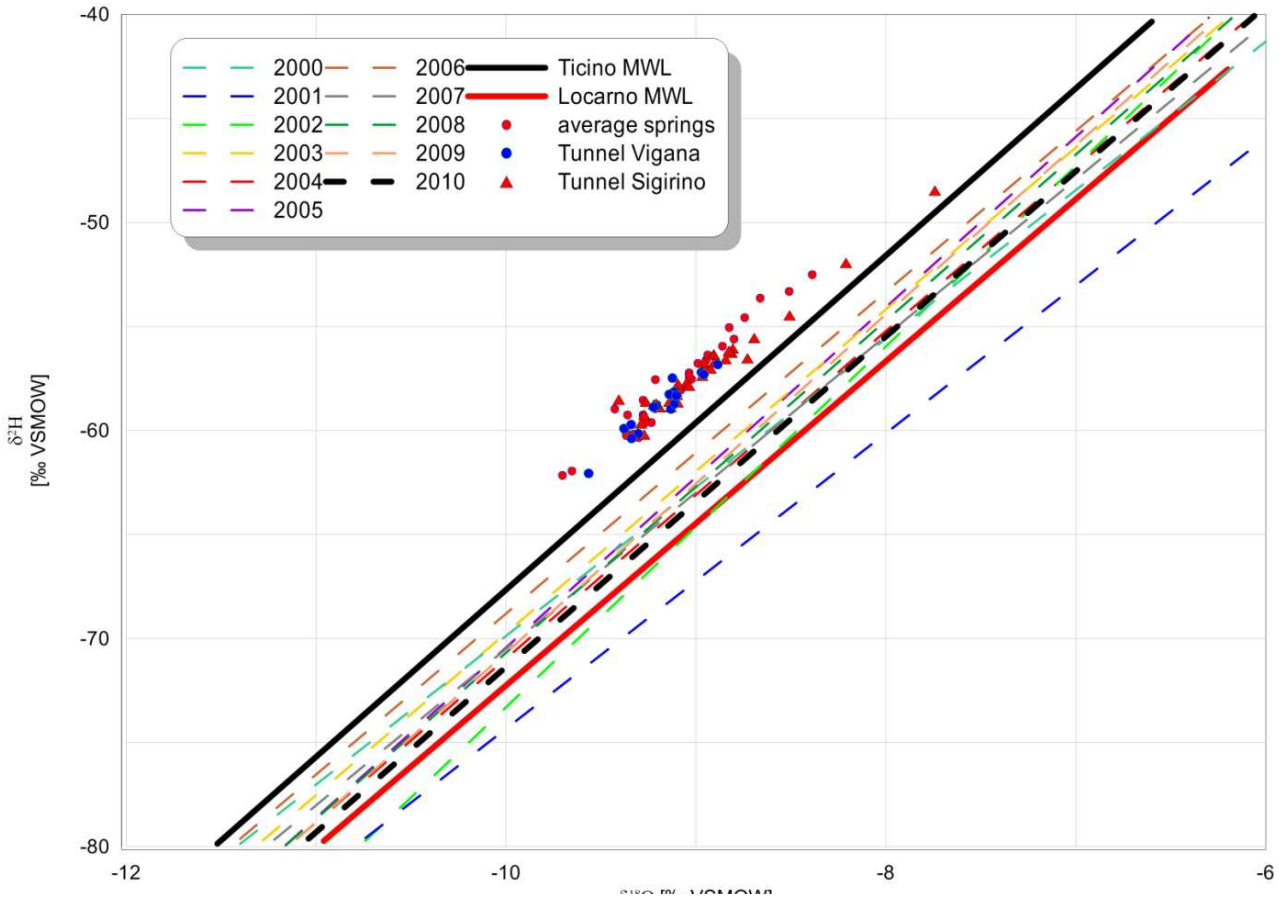

Figure 2.29 - Individual Locarno annual lines, since 2000 to2010, compared with the Locarno MWL and the Ticino MWL obtained using the selected rain gauges since March 2010 to February 2011. The 2010 Locarno MWL is evidenced using an higher width in order to compare it with the Ticino MWL obtained in the same time interval. Large differences are however visible.

Obtained MWLs for each year are shown in Figure 2.29. Two observations can be made on the basis of analyzed data. First, most of the Locarno annual MWLs, except that of the 2001 year, are characterized by an higher deuterium-excess with respect to the general Locarno MWL (Marzocchi et al., 2010 and Appendix A). Second, differences between the Locarno MWL and the Ticino MWL are also observed. Such differences cannot be justified only by the small dataset for Ticino MWL. In fact, a comparison of the 2010 Locarno annual MWL with the Ticino MWL (March 2010-Februar 2011) confirms however the difference in terms of deuterium excess.

Table 2.7 - Available data from GNIP Locarno station. Not all the data are available; in a few months; even if rain amount is not null, any stable isotope data are available.

Year	Available monthly observations	Rainy months (>5mm/month)
2000	10/12	11/12
2001	9/12	11/12
2002	12/12	12/12
2003	10/12	10/12
2004	11/12	12/12
2005	10/12	10/12
2006	10/12	12/12
2007	11/12	12/12
2008	12/12	12/12
2009	11/12	12/12
2010	10/12	12/12

Locarno data seem not to be representative of precipitation responsible of recharge in the Monte Ceneri base tunnel area, nor that of the Roveredo region that were the areas studied in this thesis.

Excluding the effect only of the restricted dataset, it is important to note that rain amount and temperature have an effect also on the groundwater recharge. In fact, only a part of the precipitation effectively feeds the aquifer, while a considerable amount of rain feeds directly the surface waters as runoff and a part of it evaporates because of the evapotranspiration effect. The latter has considerable importance in the studied region, which is covered by woods up to 49% (Mossi, 2005).

Considering seasonal MWLs (Figure 2.30, Table 2.4) and the monthly δ^2H and $\delta^{18}O$ collected in the Arosio rain gauge (Figure 2.31) and comparing them with δ^2H and $\delta^{18}O$ of groundwater (springs and tunnel inflows), we see that recharge generally occurs during summer and spring,. In fact, there is a high correspondence between stable isotope composition of groundwater and precipitation of May (~20% of the annual rain) and fall (from October to December). On the contrary, winter precipitation contributes poorly to groundwater recharge because soil frost and snow cover often inhibits infiltration (Bayard, 2003) and only a part of snowfall effectively infiltrates. In fact, a consistent fraction of the snowpack sublimate during the warmer and windy days and most of the snowmelt directly produce run-off.

Considering also that δ^2H and $\delta^{18}O$ values of snowfall (Figure 2.31), measured in rain gauges, are different from that of snowmelt due to sublimation (Taylor et al, 2001; Lee et al. 2010), it is reasonable to conclude that winter precipitation do not influence sensibly stable isotope composition of groundwater.

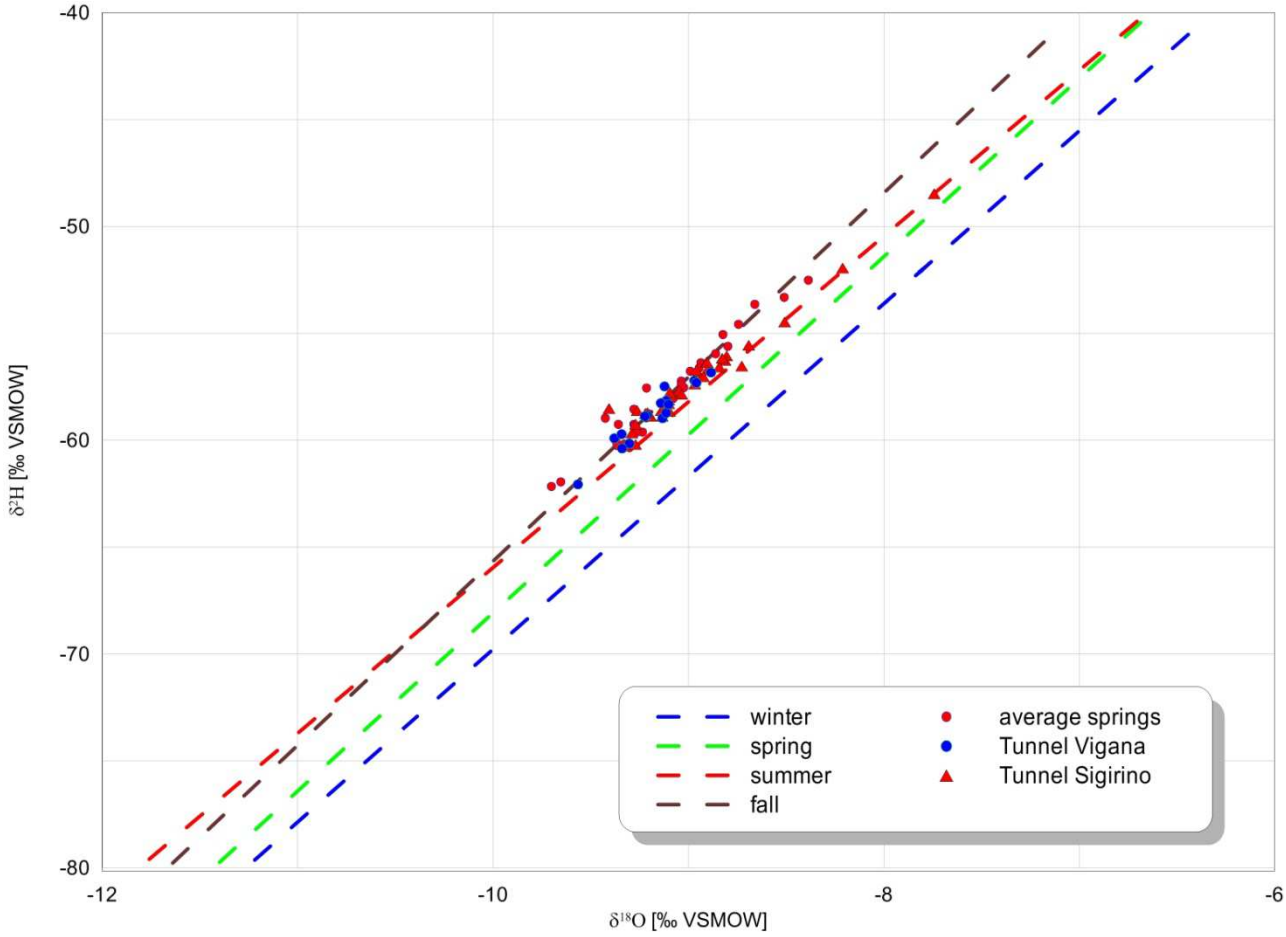

Figure 2.30 - Seasonal local meteoric water lines compared to relative isotope abundance in groundwater samples.

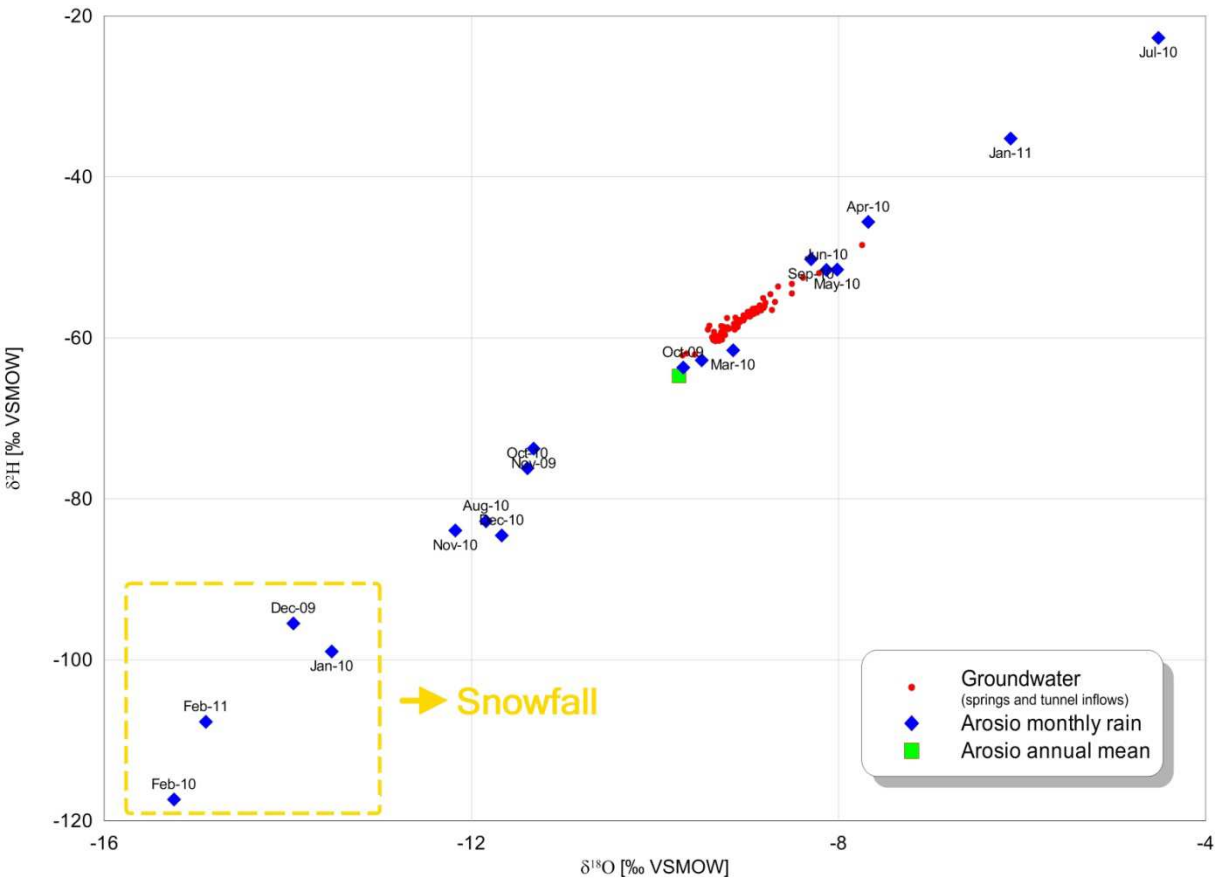

Figure 2.31 - Monthly rain in the Arosio rain gauges. The months of snowfall are evidenced with the yellow shaped rectangle.

2.6.3 Suggested altitude gradients for groundwater

Yearly weighted average δ^2H and $\delta^{18}O$ (Figure 2.25) in rains are used in order to estimate the altitude gradient for precipitation. In the light of the considerations done in the previous sections, the obtained δX-altitude relationships, even if adequate for precipitation, cannot instead be applied to groundwater. Although the line slope (^{18}O altitude gradient of about -0.12‰/100 m and a ^{2}H gradient of -1.03‰/100 m) is effectively representative of the altitude effect also of groundwater, intercepts with the y-axis of the equations (Figure 2.23) are instead only valid for rain. Because of the seasonal effects on groundwater recharge, to use these equation to estimate altitude of infiltration of groundwater causes an underestimation of altitudes, as well shown by Figure 2.26.

According to paragraph 2.6.2, not all the months equally contribute to recharge. In particular, from a comparison of monthly collected stable isotope composition of groundwater and rain (Figure 2.31), it is possible to identify which months have a higher contribution to recharge. Generally, winter does not seem to contribute sensibly. During these months in fact, the first soil layer is frozen, precipitation are mainly snowfall remaining as a snowpack, which melting, occurring in spring, mainly contribute to run-off (Figure 2.27) and not to infiltration.

On the basis of this observation, new altitude-stable isotope relationships have been proposed, considering δ^2H or $\delta^{18}O$ weighted average from March to November 2010.

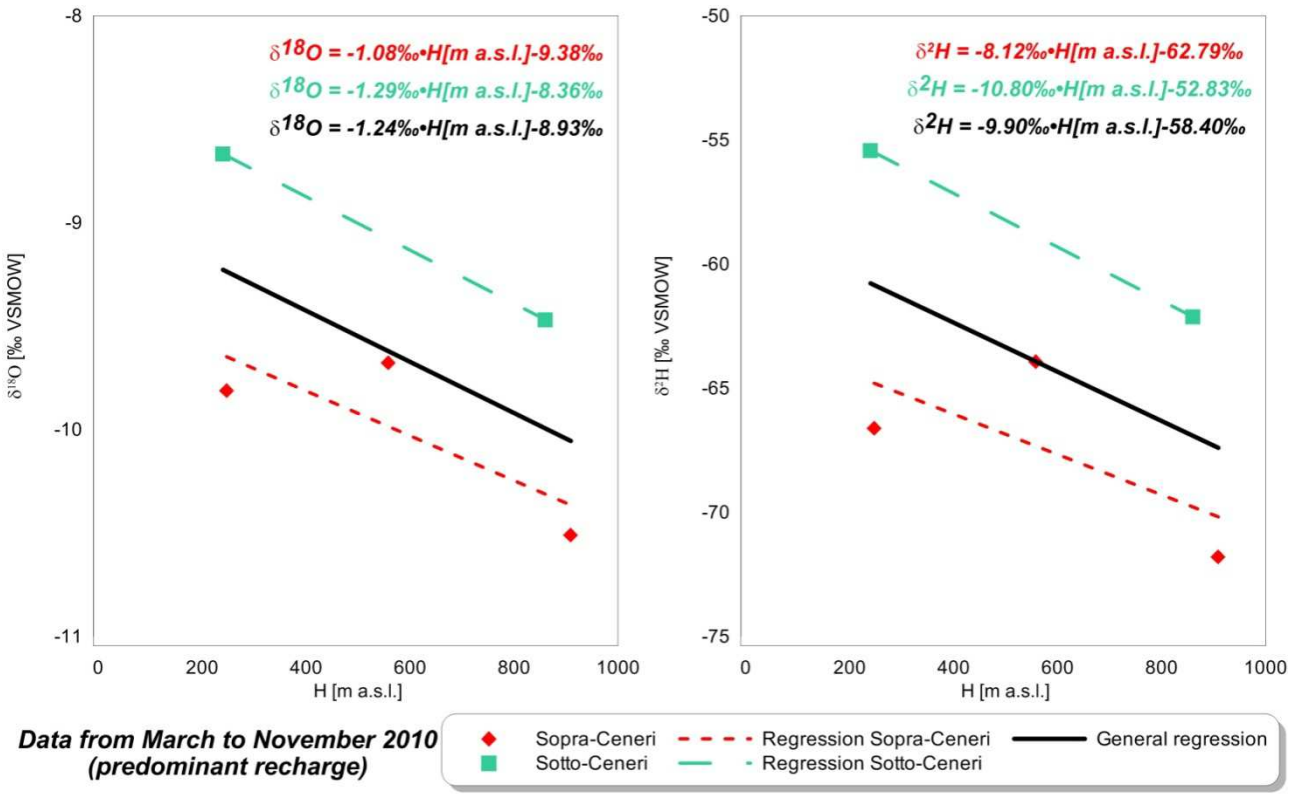

Figure 2.32 - Isotopic altitude gradient obtained with only the collected data that seem contribute to groundwater recharge (rain collected from March to November 2010). On the left H-$\delta^{18}O$, on the right H-$\delta^{2}H$.

Results are reported in Figure 2.32. As can be seen from the reported equations, the slopes do not differ sensibly (only in the second decimal of the per-mil) from those reported in Figure 2.23, obtained on all the months. On the contrary, the intercept with the $\delta^{18}O$ (or $\delta^{2}H$) sensibly decrease and seem to better represent isotopic composition of monitored groundwater (springs and tunnel inflows). The obtained equations will be thence used in the next chapters with the aim of estimate the mean altitude of infiltration for a few selected springs (see chapter 6).

2.7 Conclusions

As rain is conventionally considered the starting point of the hydrological cycle, the first step of this study was to establish a monitoring network for $\delta^{2}H$ and $\delta^{18}O$ in precipitation, in 6 stations of the Southern part of the Swiss Alps (Figure 2.7) from March 2010 to February 2011. It is important to note that this data-set (only 12 months) is statistically restricted. Nevertheless combining the collected $\delta^{2}H$ and $\delta^{18}O$ data with that coming from the NISOT network (Locarno Monti station) collected since 1983, it has been possible to acquire useful information concerning the stable isotope composition of potential groundwater. Main conclusions and remarks obtained from this analysis are summarized as follows.

i) A local meteoric water line, so named "*Ticino MWL*" (eq.2.12), has been obtained as a starting point to compare with groundwater samples from the studied region.
ii) A higher deuterium excess respect to Global MWL has been observed, as the result of mixture of vapour probably originating from the local lakes and the Mediterranean Sea. The effect has been noted during almost all year with the exception of winter months (Figure 2.16).
iii) An amount and a temperature effect have been observed on precipitations (Figure 2.18). Single and multiple correlations have been considered (Figure 2.20 and Table 2.5), even if the restricted dataset has not been able to completely describe these combined effects. In fact, it is important to note that during the 12 months of observations two exceptional

months (August 2010 and January 2011) have been registered. Even though they should be not representative of the general pattern, these anomalous events have nevertheless a considerable influence on the statistical correlations. Moreover, not always the two effects (temperature and amount) act at the same time; defining which effects are predominant for the different months would be possible only with a observation period of more than one year that would allow to extract sub-datasets of months not influenced by the other effect or to calculate different averages of the data. Therefore, analyzing the more complete dataset of Locarno Monti (NISOT network), the temperature effect has been more reliably described. The increase of T causes a proportional increasing of δ^2H and $\delta^{18}O$ in rain as expressed by the equation reported in Figure 2.21.

iv) Differences between the stable isotope signature of precipitation (rain and snow) and the effective groundwater recharge have been observed. In fact, only a fraction of precipitation effectively infiltrates and reaches the groundwater. Precipitation data have been compared with recently infiltrated groundwater, where effects of water-rock interaction can be considered insignificant, and three main reasons have been identified to describe differences in stable isotope composition of rain and groundwater:
    a. evaporation effects;
    b. seasonal effects on recharge (higher during humid season, practically zero during winter, etc.);
    c. different δ^2H and $\delta^{18}O$ of the snowfall (measured in rain gauges) and snowmelt that infiltrates (groundwater recharge).

   The application of two different numerical models has been tested in order to estimate from a quantitative point of view recharge to groundwater. Although similar results for recharge are obtained since May to December; consistent differences instead occur during winter and spring. In this period the two models do not agree in estimating recharge due to the snowmelt. Nevertheless, individuating the most reliable model on the basis of hydrological data only, has been almost impossible. In practice the application of these numerical models has one more time evidenced the high complexity of infiltration/run-off phenomena at the basin scale, without giving more realistic information concerning infiltration.

v) A ^{18}O altitude gradient of about -0.12‰/100 m and a ^{2}H gradient of -0.99‰/100 m have been determined based on the stable isotope composition of precipitation. A screen effect due to the presence of the Monte Ceneri ridge has been observed, and two different correlations between stable isotope composition and altitude can be obtained at north and at south of the Monte Ceneri ridge (Figure 2.23). Although obtained relationships are able to well describe the altitude effect on isotope composition of rain of the southern part of the Swiss Alps, these equations have been demonstrated not to be adapted to describe the groundwater infiltration phenomena. Using these equations, it is practically impossible to estimate the correct altitude of infiltration of groundwater (Blavoux and Letolle, 1995). For this reason after the analysis of groundwater recharge, other relationships have been proposed. These equations even though obtained on a restricted dataset, hence improvable, have been demonstrated to be more adapted to describe the altitude of recently infiltrated groundwater of the studied area and therefore has been applied in the next chapters of this thesis to estimate mean altitude of infiltration of recently infiltrated groundwater (see chapter 6).

References

Aouad-Rizk A., Job J.L., Nakjem W., Travi Y., Blavoux B., Gourcy L. (2005). Oxygen-18 and deuterium contents over Mount Lebanon related to air mass trajectories and local parameters, in IAEA-TECDOC-1453:75-82

Bayard D. (2003).The effect of seasonal soil frost on the alpine groundwater recharge including climate change aspects, PhD thesis EPFL n. 2709, Lausanne 235 pp.

Begert M., Schlegel T., Kirchhofer W. (2005). Homogeneous Temperature and Precipitation Series of Switzerland from 1864 to 2000.International Journal of Climatology 25:65-80.

Bérod D., (1994). Contribution à l'estimation des crues à l'aide de méthodes déterministes, PhD Thesis EPFL N°1319, Lausanne, 165 pp.

Bestenheider J.C. (2006).Captazioni nella Galleria OFIBLE, a 300 m e a 1210 m dal portale della finestra di Torre, Technical Hydrogeological study for the Torre (TI) town

Blavoux B., Letolle R. (1995) Apport des techniques isotopiques à la connaissance des eaux souterraines, Géochroniques 54, 12-15

Chow V. T, Maidment D. R., Mays L. W (1988).Applied Hydrology. McGraw-Hill, Inc. 570 pp

Clark I., Fritz P. (1997). Environmental isotopes in Hydrogeology, CRC Press LLC, Lewis Publishers

Consuegra D., Vez E., (1996). AMIE: Analyse et Modélisation Intégrées du cheminement des Eaux en zones habitées, modélisation hydrologique, Application au bassin versant de la Haute Broye, HYDRAM, EPFL, Lausanne

Coulomb C.V., Gasse F., Sonzogni C. (2008). Seasonal evolution of the isotopic composition of atmospheric water vapour above a tropical lake: deuterium excess and implication for water recycling Geochimica et Cosmochimica Acta 72:4661-4674

Craig, H. (1961). Isotopic variation in meteoric waters. Science 133:1702–1703.

Cronshey R.G., McCuen R.H. (1986). Urban Hydrology for Small Catchments. Technical Release 55. USDA, Natural Resources Conservation Service

Dansgaard W. (1964). Stable isotopes in precipitation, Tellus 16:436-469

Epstein S., Sharp R., Gow A.J., (1965). Six year record of oxygen and hydrogen isotope variations in South Pole, Journal of Geophysical Research 70:1809-1814

Gat J.R., Carmi H. (1970).Evolution of the isotopic composition of atmospheric waters in the Mediterranean Sea area. Journal of Geophysical Research 75:3039–3040.

Gat J.R., Mook W.G., Meijer H.A.J. (2001).Atmospheric water – Environmental isotopes in the hydrological cycle. Principle and applications. IHP-V, Technical document N. 39, UNESCO, Paris, 113pp

IST (2010). Annuario idrologico del Canton Ticino 2009. Institute of Earth Science (SUPSI)

Lee J., Feng X., Faiia A.M., Posmentier E.S., Kirchner J. W., Osterhuber R., Taylor S., (2010). Isotopic evolution of a seasonal snow cover and ist melt by isotopic exchange between liquid water and ice, Chemical Geology 270:126-134

Longinelli A., Selmo E. (2003). Isotopic composition of precipitation in Italy: a first overall map, Journal of Hydrology 270:75-88

Longinelli A., AnglesioE., Flora O., Iacumin P., Selmo E. (2006). Isotopic composition of precipitation in Northern Italy: reverse effect of anomalous climatic events. Journal of Hydrology 329:471-476

Machavaram M.V., Krishnamurthy R.V. (1995). Earth surface evaporative process: a case study from the great lakes in region of the United States based on deuterium excess in precipitation. Geochimica et Cosmochimica Acta 59(20):4279-4283

Maloszeski P., Stichler W., Zuber A., Rank D. (2002).Identifying the flow systems in a karstic-fissured-porous aquifer, the Schneealpe, Austria, by modelling of environmental 18O and 3H isotopes Journal of Hydrology 256:48-59

Maréchal J.C., Etcheverry D. (2003). The use of 3H and 18O tracers to characterize water inflows in Alpine tunnels, Applied Geochemistry 18:339-351

Marzocchi R., Pera S., Pfeifer H.R. (2010). Hydrogeological interferences in tunneling - A comprehensive study, Aquamundi 1(3):1-14

Merlivat L., Jouzel J. (1979). Global climatic interpretation of the deuterium - oxygen-18 relationship for precipitation. Journal of geophysical research 84(8):5029-5033

MeteoSwiss, IDAWEB data service – Free available data for research project

Moser H., Silva, C., Stichler, W., Stowhas, L.(1972). Measuring the isotopic content in precipitation in the Andes, in The Role of Snow and Ice in Hydrology, Proceedings of the Banff Symposium, Unesco-WMO-IAHS, 1:15–23

Mossi R. (2005) L'evoluzione del paesaggio ticinese: un'analisi quantitativa. Dati, statistiche e società. 2:92-97

Nash J.E., Sutcliffe J.V. (1970). River flow forecasting through conceptual models. Part I, a discussion of principles. Journal of Hydrology, 10 :282-290

Novel J.P., Dray M., Ferhi A., Jusserand C., Nicoud G., Olive P., Puig J.M., Zuppi G.M. (1999). Homogénéisation des signaux isotopiques, ^{18}O et ^{3}H, dans un système hydrologique de haute montagne: la Vallée d'Aoste (Italie), Revue des sciences de l'eau 12(1):3-21

Ofterdinger U.S., Balderer W., Loew S., Renard P. (2004). Environmental isotopes as indicator for ground water recharge to fractured granite, Ground Water 42(6):868-879

Pastorelli S., Marini L., Hunziker J.C. (1999). Water chemistry and isotope composition of the Acquarossa thermal system Ticino Switzerland, Geothermics 28:75-93

Paternoster M., Liotta M., Favara R., (2008). Stable isotope ratios in meteoric recharge and groundwater at Mt. Vulture volcano, southern Italy, Journal of Hydrology 348:87– 97

Pearson F.J., Balderer W., Loosli H.H., Lehmann B.E., Matter A., Peters T., Schmassmann H., Gautschi A. (1991). Applied Isotope Hydrogeology – A case study in Northern Switzerland. Elsevier Science Publishers, 439 pp.

Pozzoni M., Salvadé G. (2008). An Hydrological Model to Optimize Hydropower Production. Proceedings of the European Geoscience Meeting. Vienna. 13-18 april 2008

RosmanK. J. R., TaylorP. D. P. (1998). Isotopic compositions of the elements 1997 (Technical Report) Pure and Applied Chemistry.70(1):217-235

RozanskiK., Araguas L., Gonfiantini R. (1993).Isotopic patterns in modern global precipitation. In: Climate change in continental isotopic record (SwartP.K., Lohman K.L., McKenzie J.A., Savin S.). Geophysical Monograph series 78:1-37

R Development Core Team (2011). R: A Language and Environment for Statistical Computing, R Foundation for Statistical Computing - Vienna, Austria (http://www.R-project.org)

Salati E., Olio A. D., Matsui E., Gat J.R., (1979). Recycling of water in the Amazon Basin : An isotopic study, Water Resources Research., 15(5):1250-1258

Sappa G., Vitale S. (2007). Approccio multisistema alla individuazione delle aree di ricarica di un acquifero, Ingegneria e Geologia degli acquiferi, 22:79-92

Schaefli B., Hingray B.,Niggli M., Musy A. (2005).A conceptual glacio-hydrological model for high mountainous catchments. Hydrology and Earth System Sciences, 9:95–109

Schurch M., Kozel R., Schotterer U., Tripet JP, (2003). Observation of isotopes in the water cycle: the Swiss National Network (NISOT), Environmental geology 45(1):1-11

Sheppard S.M.F. (1986).Characterization and isotopic variations in natural waters. In: J.W. Valley, H.P. Taylor, Jr. and J.R. O'Neil, Editors, Stable Isotopes in High Temperature Geological Processes Reviews in Mineralogy**16:**165–183

Spangenberg J.E., Vennemann T.W. (2008). The stable hydrogen and oxygen isotope variation of water stored in polyethylene terephthalate (PET) bottles, Rapid Commun. Mass Spectrom. 22: 672–676

Taylor S., Feng X., Kirchner J.W., Osterhuber R., Klaue B., Renshaw C. E. (2001). Isotopic evolution of a seasonal snowpack and its melt. Water resources research 37(3):759-769

Thornthwaite C.W., Mather J.R., (1957). Instructions and tables for computing potential evapotranspiration and the water balance. Publication in Climatology 10(3):185-311

Turc L. (1961).Estimation of irrigation water requirements, potential evapotranspiration: a simple climatic formula evolved up to date. Annales Agronomiques, 12:13-49.

Yurtsever Y. (1975). Worldwide survey of isotopes in precipitation. IAEA report, Vienna

Westenbroek S.M., Kelson V.A., Dripps W. R., Hunt R.J., Bradbury K.R. (2010). SWB – A modified Thornthwaite-Mather Soil-Water Balance code for estimating groundwater recharge. USGS Techniques and Methods 6-A31, 60 pp

Wieser M. E. (2006). Atomic Weight of the elements 2005 (IUPAC technical report report), Pureand Applied Chemistry, 78(11):2051–2066

3. Electrical resistivity tomography and VLF electromagnetic surveys: methodology and initial applications in southern Switzerland

Abstract

Geophysical techniques are often used in geological and hydrogeological investigations in order to obtain information of the subsurface in a non-invasive manner. In particular, due to the high resistivity contrast between most rocks and groundwater, geoelectrical and electromagnetic techniques can be used to detect groundwater in fractured rock masses. During a comprehensive study in southern Switzerland to understand the impacts on the hydrogeological cycle due to the drilling of new tunnels, geoelectrical (ERT) and electromagnetic (VLF-EM) surveys were made to assess water-bearing zones in fractured rock masses. Concerning the geoelectrical surveys, different electrical arrangements were assessed including different arrays (dipole-dipole and Wenner-Schlumberger) and different length of surveys (230 or 470 m). In this chapter, the two methodologies are presented in detail, focusing on the interpretation of the measurements. Moreover, the first applications of both methods are presented and compared and respective advantages and disadvantages are discussed.

3.1 Introduction

As outlined in the first chapter, a comprehensive study was conducted in southern Switzerland, a mountainous region where several new tunnels are being drilled, in order to understand the impact of the construction of underground infrastructures on the hydrological cycle. In this chapter, the geophysical techniques applied in our research are presented; they are:

- ✓ the Electrical Resistivity Tomography (ERT);
- ✓ the Very Low Frequency Electromagnetic method (VLF-EM).

Moreover, the results of the first campaign that was conducted crossing the main probable tectonic discontinuities localized in the Monte Ceneri base tunnel region (Southern Switzerland) that were inferred based on the available geological information (Reinhard, 1962; Bächlin, 1974) as well as morphological observations are presented.

3.2 Geophysical surveys: methodologies and equipments

3.2.1 Generalities

The ability to reliably predict the hydraulic properties of the subsurface is one of the most important and challenging goals in geophysics (Kirsch, 2006). Geophysical methods are used to obtain more accurate information about subsurface conditions, such as the type and depth of materials (Francese et al., 2009), to detect fractured zones and groundwater (Pagano, 1996; Macedo and Lima 2004; Fazzito et al., 2009; Bersan et al. 2010), to determine the depth to bedrock (Di Maio et al., 2007; Piegari et al. 2009), to detect saline intrusions of water (Kruse et al., 1998), etc.

The considered electrical and electromagnetic geophysical prospecting techniques are based on the direct or indirect injections of electric current in the soil and the measurement of the conductivity response of the underground. These measurements provide indirect information concerning the geology of the studied zone, due to the different electrical properties of soil and rocks.

There is a large variety of techniques available measuring:

- ✓ the electrical resistivity,
- ✓ the electrical potential;
- ✓ the electromagnetic field.

In the case study considered here, the ERT method has been chosen since it is able to give an image of the subsurface structure on the basis of the high electrical resistivity contrast between the intact and fractured, water-logged crystalline rock masses at our site. Moreover, a VLF-EM instrument was also used, which is able to detect steeply dipping high conductivity bodies in a resistive medium.

3.2.2 The ERT method

- *Resistivity technique*

DC resistivity methods (e.g., Bhattacharya and Patra, 1968; Kirsch, 2006; Chapellier et al., 2010) are all the techniques of survey that investigate the underground using an electric current. In practice, they consist of introducing an electric current in the terrain with two or more electrodes, so-called "*current electrode*" (A, B), and then measuring of the potential difference created by the current flow, using two different electrodes, so-called "*potential electrodes*" (M, N). By changing the distances between the electrodes (A, B, M, N) it is possible to investigate the terrain at different depths.

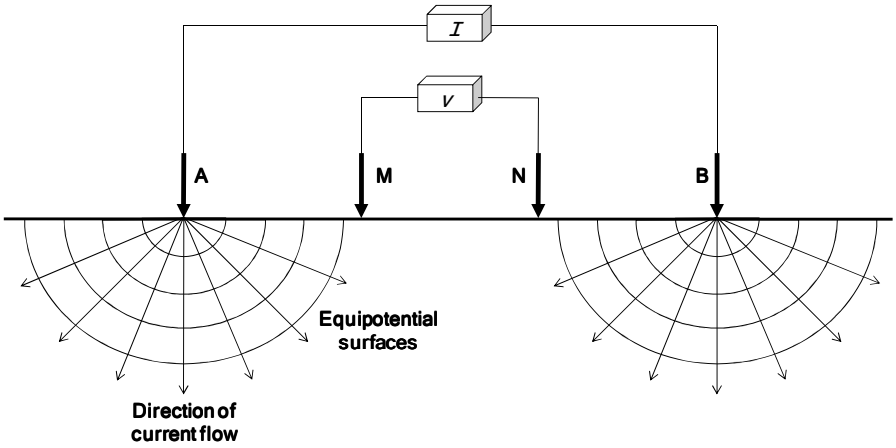

Figure 3.1 - Physical principle of the geoelectrical prospecting.

The measured parameter is the resistivity of the terrain. In particular the resistivity ρ is the physical property which determines the capacity of this material to be opposed to the flow of the electrical current. The resistivity ρ is the ohmic resistance of a cylinder of unit section and length. Therefore, the resistance R, measured in Ohm (Ω), is expressed by the following equation know as Ohm's law:

$$R = \rho \frac{L}{s} \tag{3.1}$$

where L is the length and s the cross-sectional area of a "cylinder" expressed in m, and ρ is the resistivity of the material expressed in Ohm·m (Ω·m).

Measuring the voltage difference between the potential electrodes, M and N (ΔV_{MN}), and knowing the current intensity introduced in the terrain through the current electrodes A and B, (I_{AB}) it is possible obtain the terrain resistivity using the following relationship:

$$\rho = K \frac{\Delta V_{MN}}{I_{AB}} \tag{3.2}$$

where K is the geometric factor, defined as follows:

$$K = 2\pi \left(\frac{1}{AM} - \frac{1}{BM} - \frac{1}{AN} + \frac{1}{BN} \right)^{-1} \tag{3.3}$$

For a given geological situation, the resistivity depends obviously by the material, but also by the porosity, by the permeability and, above all, by the ionic charge of the interstitial fluid and material.

The simplest application of DC resistivity surveys is the vertical electrical sounding. In this case the four electrodes above mentioned (A,B,M,N) are used in succession with an increasing electrode separation. Obviously the center of the configuration and its orientation remain fixed, and correspond to the point where the vertical sounding is obtained. Different quadripole configurations (Dipole-Dipole, Wenner, Schlumberger, Pole-Pole, etc.) are possible, depending on the mutual position of the current and potential electrodes (Kirsch, 2006).

ERT is the natural evolution of vertical electrical soundings. The physical principle is the same; the only difference is that through an automatic acquisition method it is possible to vary at each time the center of the quadripole, using a multicore cable with an high number of connected electrodes (16,24,32,48, etc.). In this way, it is possible to obtain not only a vertical sounding under the center of the quadripole, but also a 2D profile along the section where the multi-core cable is spread out.

The problem of ERT is a more complex interpretation of the obtained data. In fact in the field one obtains values of *apparent resistivity*, that is, the resistivity that an equivalent homogeneous underground that would give the same resistance value for the same electrode arrangement. After an inversion process (Figure 3.2), the result is a modeled 2D section of terrain resistivity.

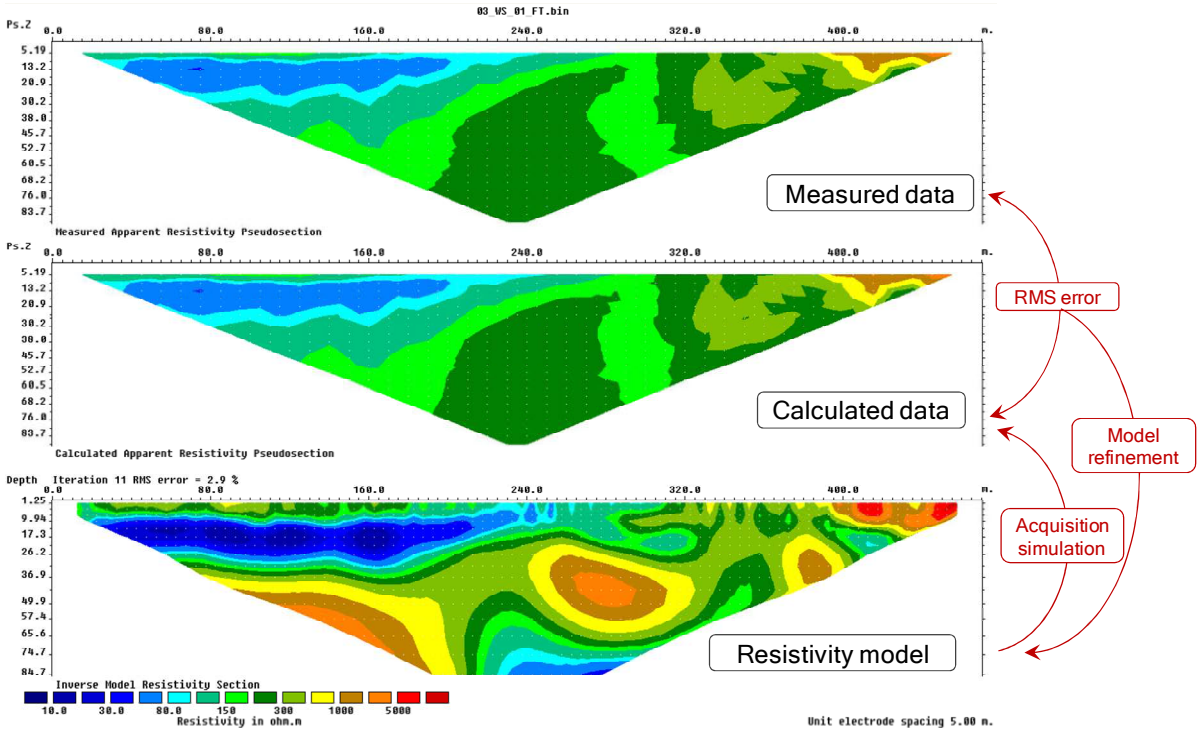

Figure 3.2 - Principle of the inversion of the measured apparent resistivity data.

The purpose of the inversion is, in this case, to find a 2D resistivity model of the underground that gives a response that is similar to the measured apparent resistivity values.

In particular the inversion procedure is based on the: (i) model parameters and on (ii) the model response. In the case, the model parameters are the resistivity values of the model cells that give the interpolated 2D resistivity section. The model responses are the calculated apparent resistivity data; they are obtained simulating an acquisition of the data with the same electrode configuration used in the field.

The model response is compared to the measured data and the initial model is modified such that the sum of the square error E is minimized, according to the smoothness constrained least-squares method. The scheme of the optimization procedure is summarized by the following Figure

3.3 and substantially governed by the Gauss-Newton equation that in his default formulation (deGroot-Hedlin and Constable 1990, Sasaki 1992) is given by the following equation:

$$\left(\mathbf{J}^{\mathrm{T}}\mathbf{J} + u\mathbf{F}\right)\Delta\mathbf{q} = \mathbf{J}^{\mathrm{T}}\mathbf{g} \qquad (3.4)$$

where **q**, **J**, **g** are expressed in Figure 3.3, *u* is called damping factor and **F** is the matrix for the smoothed constrained method (Ellis and Oldenburg, 1994) also vectors. Other possible options are to include the smoothness constrain directly on the model resistivity values, called "include smoothing of model resistivity" or the so called "robust inversion" where the equation 3.4 is modified so that resistivity of cell blocks (**q** vector) and errors (**g** vector) have the same magnitude (Loke, 2004).

The procedure is stopped when the sum of the squared errors does not change significantly. At the end of the iterative procedure a numerical estimation of the final differences between the measured and the calculated apparent resistivity data, so-called Root Mean Square (RMS) statistical error, is given to the user and is a good indication of the consistence of the model as well explained in the following sections.

Various implementation of the least–square procedure as well as various options for model construction are available in the RES2DINV software (Locke, 2004).

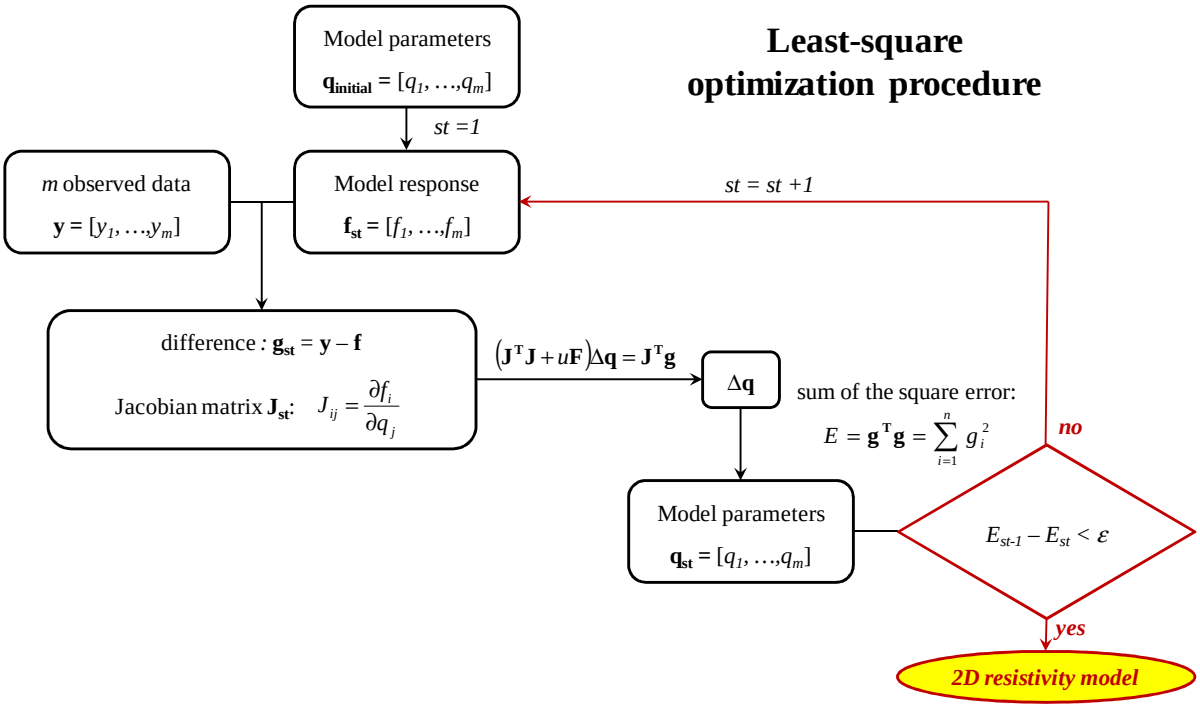

Figure 3.3 - Conceptual scheme of the least-square optimization procedure upon Loke (2004). The iterative procedure is summarized for different subsequent steps.

Finally, in the RES2DINV software three algorithm have been implemented for the least-square optimization procedure: (i) a quasi-Newton optimization technique (Loke and Baker, 1996), the conventional Gauss Newton method and (iii) a compromise between these two methods (Loke and Dahlin, 2002) using the conventional method for the first 2 or 3 iterations (*st*) and the quasi-Newton method for the last steps.

- *Interpretation of geophysical results*

The resistivity of subsurface materials substantially depends on *(i)* the water content and the resistivity of the water, which in turn depends on its salinity, *(ii)* the clay content, and the *(iii)* the ore content. Resistivity is a widely varying parameter which changes not only with the lithology but also within a given formation depending on its geological history (Stummer, 2003). For example, the resistivity values of the metamorphic crystalline rocks of the studied area (gneiss, paragneiss,

orthogneiss, amphibolites, etc) are very high, generally between 1000 and 20'000 Ω·m. The presence of water in micro-fractures of the rock matrix reduces the resistivity. The presence of water near disturbed zones, such as big fractures or faults filled by permeable materials, can therefore be easily detected by a resistivity profile. The evaluation of resistivity values in unconsolidated materials, such as moraine type glacial deposits, is more complex and again strongly dependent on the presence or absence of water In fact the resistivity of a moraine deposit under dry condition is often high and comparable with that of the surrounding crystalline rocks from which the glacial sediments have been derived, while the conductivity increases in presence of water in the unconsolidated material.

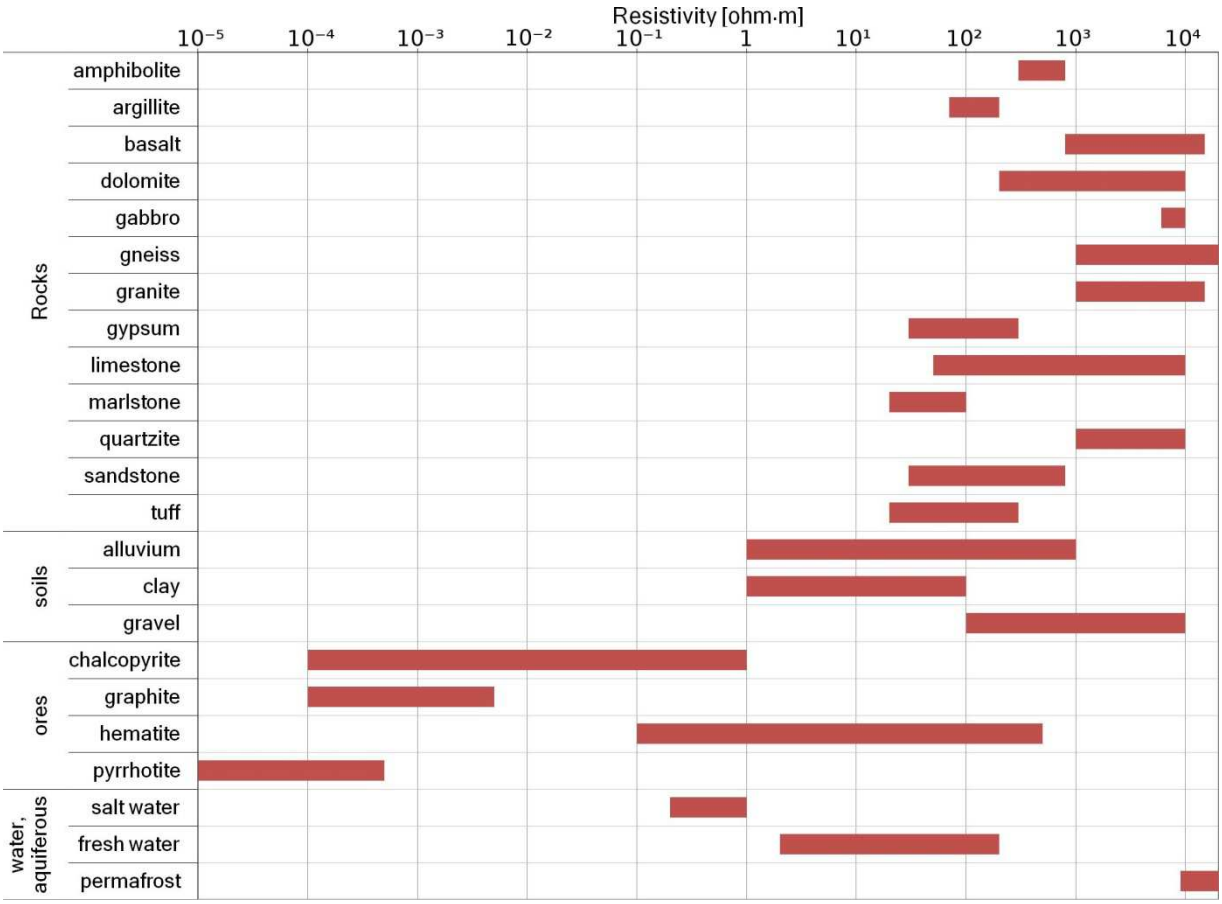

Figure 3.4 - Typical ranges of electrical resistivity of various earth materials (adopted from Stummer, 2003; Chapellier et al., 2010).

Figure 3.4 shows the ranges of resistivity values found for the most common rocks, soils, minerals, and aquifers (Stummer, 2003; *online course of geophysics* by Chapellier et al. provided by the University of Lausanne and by the Institute Français du Pétrol).

Depending on the purpose of the electrical tomography it is very important to adapt the color scale to represent the resistivity model in order to conveniently detect the geological and hydrogeological interesting informations. For example, for the study purpose, which is the groundwater detection, a scale that uses 14 electrical resistivity intervals from 10 to 10'000 Ω·m (Figure 3.2) has been chosen. It enables to distinguish intact dry rock, more humid rocks, and disturbed zones that can be considered as preferable groundwater pathways, as well as the presence of aquifers in the unconsolidated material encountered in our investigations.

- *Carrying out of the survey*

The resistivity measurements were performed using an IRIS-SYSCAL PRO System (Figure 3.5) with a multi-electrode cable consisting of 48 electrodes spaced at 10-m intervals and total length of 470 m.

Figure 3.5 - IRIS SYSCAL PRO used for the geophysical surveys. The big picture shows the equipment with the spread-out multicore cable, while the small insert picture shows in more detail the used instrument.

Two different configurations (Wenner-Schlumberger and Dipole-Dipole) were tested. Using the PROSYS software, the apparent resistivity data were filtered, removing the acquisition errors and the rough surface topography was incorporated into the model. The RES2DINV software (Loke, 2004) was used for the inversion of the field data in order to obtain a 2D resistivity model corresponding to the apparent resistivity data collected in field. Moreover, using the RES2DINV a further editing of field data is possible by removing for the different levels of acquisition the data points that have clearly erroneous resistivity values.

After a number of tests, a finite difference method was selected for the inversion. The elements of the Jacobian matrix have been calculated using the Gauss-Newton equation including smoothing of model resistivity. The optimization method follows a Gauss-Newton approach in its conventional form; the initial damping factor is equal to 0.3 and the minimum damping factor is set to 0.03.

In order to assess the accuracy of the obtained 2D models, an estimation of their consistency is needed; without that the interpretation of the resulting resistivity model is difficult, non-representative and dangerous (Marescot et al. 2003). The resulting resistivity section in fact is not unique and it is essential to carefully consider the reliability of the obtained model. In the literature different approaches are proposed to treat this problem and to give the user quantitative indices of the reliability. An example is the calculation of the Depth Of Investigation (DOI) index carrying out two inversions using different resistivity values for the starting reference model (Oldenburg and Li, 1999; Marescot et al. 2003). However, this approach is not widely implemented in the RES2DINV software. For this reason, instead to consider two parameters that are normally available from the commercial version of the software (Figure 3.6) have been used:

i) the Root Mean Square (RMS) error;
ii) the smoothed sensitivity of blocks.

The first parameter has previously been described and denotes the difference, in statistical terms, between the apparent resistivity measured in field and that calculated apparent resistivity

simulating the same acquisition scheme on the 2D resistivity model. It is a good parameter for assessing the consistency of the entire model (Tassone et al., 2010). For instance, considering the conducted surveys, RMS errors lower than 10% can be considered as being representative of a reliable model of terrain resistivity, RMS values between 10 and 20% are representative of an acceptable resistivity model that needs some extra attention, and RMS statistical errors higher than 20% are typical of a bad resistivity models due to high noise levels or other problems.

The smoothed sensitivity, also called subsurface sensitivity, depends on the measured data set and it is a surface normalized measure of amount of information about the resistivity of a model block cell, in which the underground is discretized for the numerical iterations needed to obtain the resistivity model (Loke, 2004). High smoothed sensitivity values depend only on the amount of available apparent resistivity data for unit of area and therefore are able to identify the doubtful part of the models. Hence, it can be useful to represent a transparent filter superimposed to the 2D resistivity model in case of low smoothed sensitivities. After a number of tests, a threshold value of 0.2 was chosen. It allows individuating the most probable erroneous interpolation of the inverted data and the low reliable part of the 2D resistivity sections. In practice, by using this transparent filter, the areas of the 2D resistivity section having low smoothed sensitivities can be identified, allowing a critical and accurate interpretation of the results coming from the inversion of field apparent resistivity data.

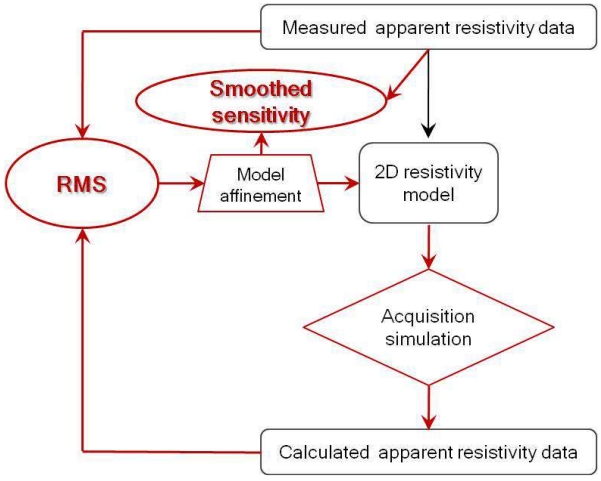

Figure 3.6 - Conceptual scheme of the inversion of resistivity data and significance of the indexes used in this work to check the consistency of the model.

3.2.3 The VLF-EM method

The VLF-EM method is useful for the detection of elongated, steeply dipping low-resistivity bodies. The principle of the VLF-EM is to use the electromagnetic field at very low frequencies (15-30 kHz) generated by radio transmitters to reveal conductive bodies located in the underground. These VLF transmitters are operating in a number of countries for long-distance military communications (Figure 3.7).

The electromagnetic field emitted from these antennas consists of a primary horizontal magnetic field component H_y, that at large distance from the transmitter source can be regarded as a plane wave and a vertical electric field E_z, perpendicular to the propagation direction. The conductivity variations whose strike is relatively parallel to the propagation direction of the EM waves, for example a conductive fracture in the underground perpendicular to the profile direction generates a horizontal electric field component E_y in the propagation direction and consequently a vertical magnetic field H_z (Figure 3.8).

Station identification				
Station	**Location**	**Country**	**Coordinates**	
3SA	Changde	China	29N04	111E43
3SB	Datong	China	39N56	113E15
DHO	Burlage	Germany	53N05	007E37
EWB	Odessa	Ukraine	46N29	030E44
FTA	Assise	France	48N32	002E34
FUO	Croix	France	44N45	000W48
GBR	Rugby	UK	52N22	001W11
GBZ	Rugby	UK	52N22	001W11
GQD	Rugby	UK	52N22	001W11
HWU	Le Blanc	France	46N37	001E05
ICV	Tavolara	Italy	40N55	009E45
JAP	Yosami	Japan	34N58	137E01
JJH	Kure	Japan	34N14	132E34
JJI	Ebino	Japan	32N05	131E51
JXN	Helgeland	Norway	66N25	013E01
JXZ	Helgeland	Norway	66N25	013E01
NAA	Cutler ME	USA	44N39	067W17
NAK	Annapolis	USA	38N59	076W28
NAU	Aguada	Puerto Rico	18N23	67W11
NBA	Balboa	Panama	09N04	079W39
NDT	Yokosukaichi	Japan	34N58	137E01
NEJ	Seattle	USA	47N41	122W15
NHB	Kodiak	Alaska	57N45	152W30
NLK	Oso Wash	USA	48N12	121W00
NPC	Seattle	USA	47N35	122W32
NPG	S Francisco	USA	38N06	122W16
NPL	S Diego	USA	32N44	117W05
NPM	Pearl Harbor	Hawai	21N25	158W09
NPN	Guam	Guatamala	13N34	144E50
NSS	Washington	USA	38N59	076W27
NWC	North West Cape	Australia	21S47	114E09
RAM	Moscow	Russia	55N49	037E18
RCV	Rostov	Russia	47N18	039E48
TBA	Antalya	Turkey	36N53	030E43
UBE	Petrolovsk	Russia	52N59	158E39
UGK	Kaliningrad	Russia	54N42	020E30
UMB	Rostov	Russia	57N14	039E48
UMS	Moscow	Russia	55N49	037E18
UNW	Kaliningrad	Russia	54N45	020E30
UPD	Murmansk	Russia	68N58	033E05
VTI	Bombay	India	19N00	073E00
VTX	Vijayanarayanam	India	08N26	077E44

Figure 3.7 - VLF transmitters operating in the world (from the WADI ABEM® user manual).

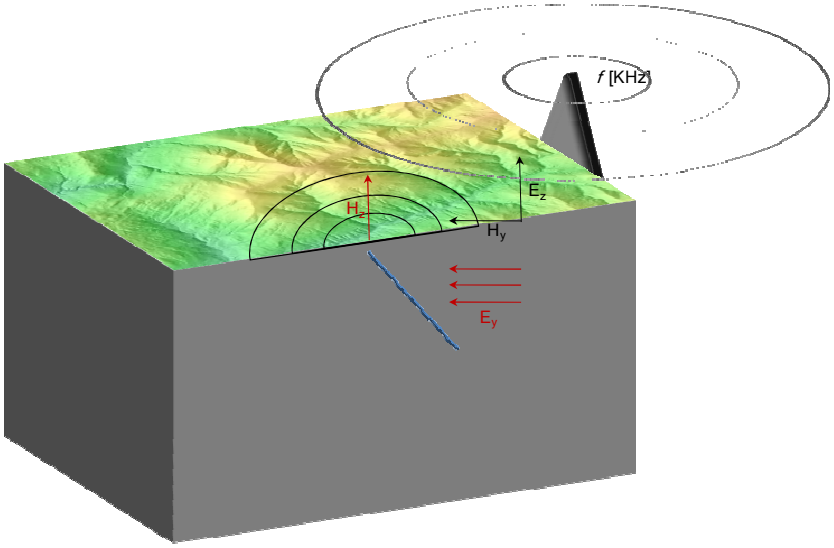

Figure 3.8 - Physical principle of the VLF-EM method. The ellipsoid represents the plane wave resulting of the electromagnetic field emitted from a generic VLF source transmitter.

The instrument measures the real (*in-phase*) and the imaginary (*quadrature*) components of the ratio between the vertical inducted magnetic component field (H_z) and the primary one (H_y). These components are defined as *tilt angle* α and *ellipticity e*, respectively, as shown in Figure 3.9; finally the ratio between the inducted and the primary magnetic field is frequently also called *tipper* (ABEM, 1993).

$$\mathrm{Re}\left(\frac{H_z}{H_y}\right) = \tan(\alpha)\cdot 100\ \%$$

$$\mathrm{Im}\left(\frac{H_z}{H_y}\right) = e\cdot 100\ \%$$

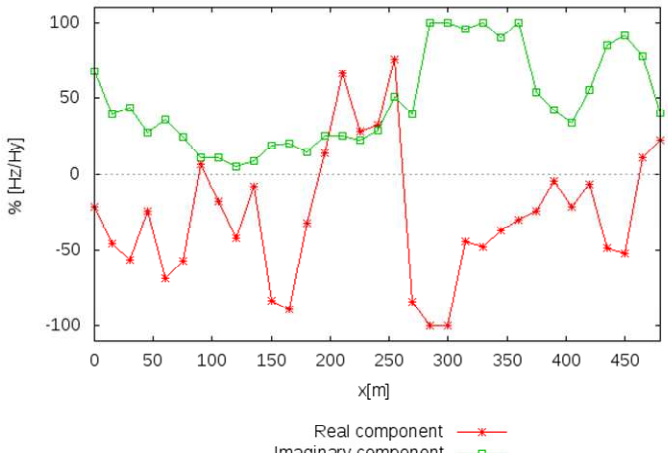

Figure 3.9 - Raw data obtained with the VLF-EM instrument and main EM quantity definitions.

Different filters exist in order to obtain an interpretation of the raw data. The first, in order of time, and simplest filter was proposed by Fraser (1969). It consists in the first derivative of the raw data. From the *n* stations measured in the field it is possible to apply this filter on *n-3* interpolated points using the following formulation:

$$fr_{i\cdot\Delta x+\Delta x/2} = \left(H_{(i+2)\cdot\Delta x} + H_{(i+1)\cdot\Delta x}\right) - \left(H_{(i-1)\cdot\Delta x} + H_{i\Delta x}\right) \qquad (3.5)$$

where H a synthetic notation for the real ratio between the vertical and the horizontal magnetic component field (H_z/H_y) measured in field.

The effect of the Fraser filter is, first of all, the noise reduction. Moreover, it allows for obtaining more simple graphs with peaks in correspondence of the conductive zones as shown by the following Figure 3.10.

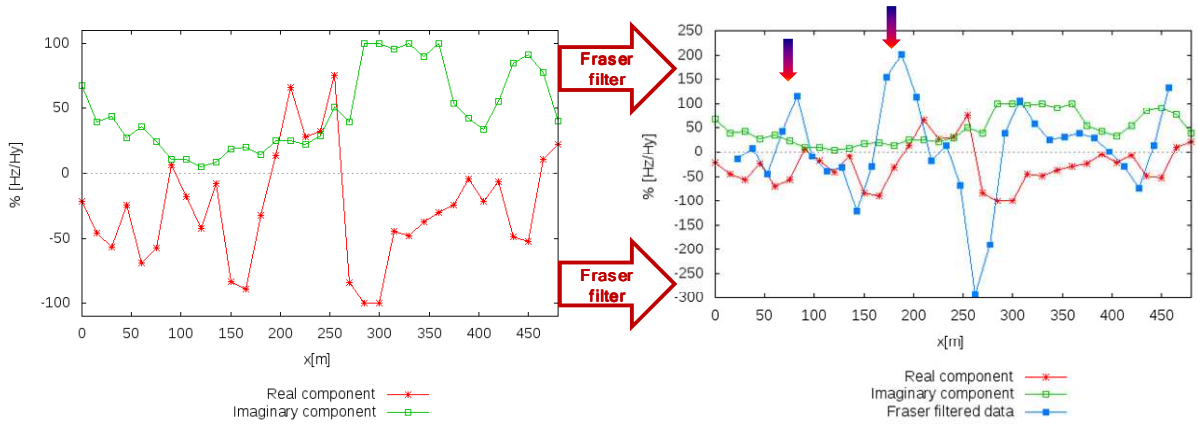

Figure 3.10 - Illustration of the effect of the Fraser filter. The higher conductive zone are represented with peaks in the Fraser filtered data.

A second filter, which is based on the Fraser, was proposed in 1977 by Karous and Hjelt (1977). It is a consequence of the Biot-Savart law.

$$\vec{\mathbf{B}} = \frac{\mu_0}{4\pi}\frac{\vec{\mathbf{I}}}{d} \qquad (3.6)$$

where **B** is the net magnetic field, μ_0 is the magnetic constant, **I** is the current density, d is the length of considered electric wire.

By filtering the in-phase data, it is possible to obtain an apparent current density pseudo-section that is more attractive and allows a qualitative interpretation of the underground resistivity variations. In particular, as shown by Karous and Hjelt (1977), it is possible to define the apparent current density **I** that flows in the underground because of the VLF-EM field:

$$I_0 = \frac{4\pi}{\mu_0}\sum_{i=-n}^{n+1} K_{i0}^{-1}\,\mathrm{Re}\left(\frac{H_z}{H_y}\right) \tag{3.7}$$

where K represents specific coefficients introduced by the authors. From a computational point of view the current intensity is defined as following:

$$\begin{aligned} I[i\cdot\Delta x,\, j\cdot\Delta x] = {} & -0.102\,H_{i\cdot\Delta x-3\,j\cdot\Delta x} + 0.059\,H_{i\cdot\Delta x-2\,j\cdot\Delta x} - 0.561\,H_{i\cdot\Delta x-j\cdot\Delta x} \\ & + 0.561\,H_{i\cdot\Delta x+j\cdot\Delta x} - 0.059\,H_{i\cdot\Delta x+2\,j\cdot\Delta x} + 0.102\,H_{i\cdot\Delta x+3\,j\cdot\Delta x} \end{aligned} \tag{3.8}$$

where H is the measured real tipper and I is the calculated apparent current density in the underground. Therefore, from the data measured at the surface it is possible obtain information about current intensity as shown in Figure 3.11.

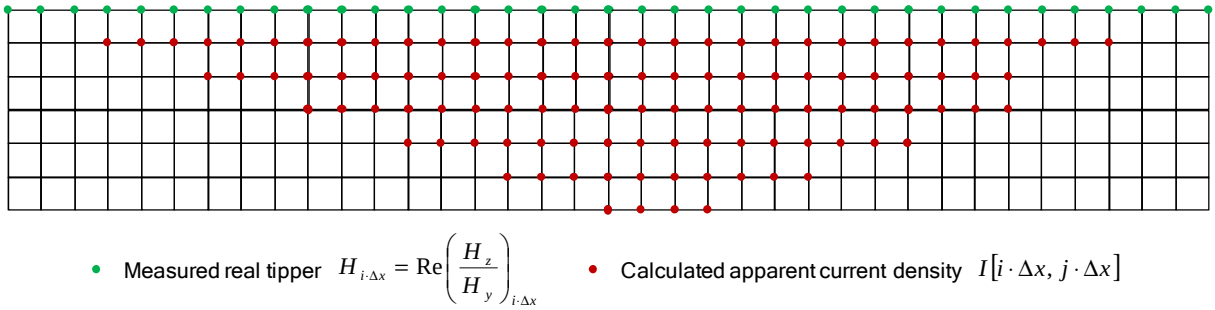

Figure 3.11 - Schematic representation of the Karous and Hjelt filter and of its application on the measured data (green points) to obtain the underground apparent current density information (red points).

Finally, by interpolating the gridded intensity data it is possible to obtain a pseudo-section (Figure 3.12).

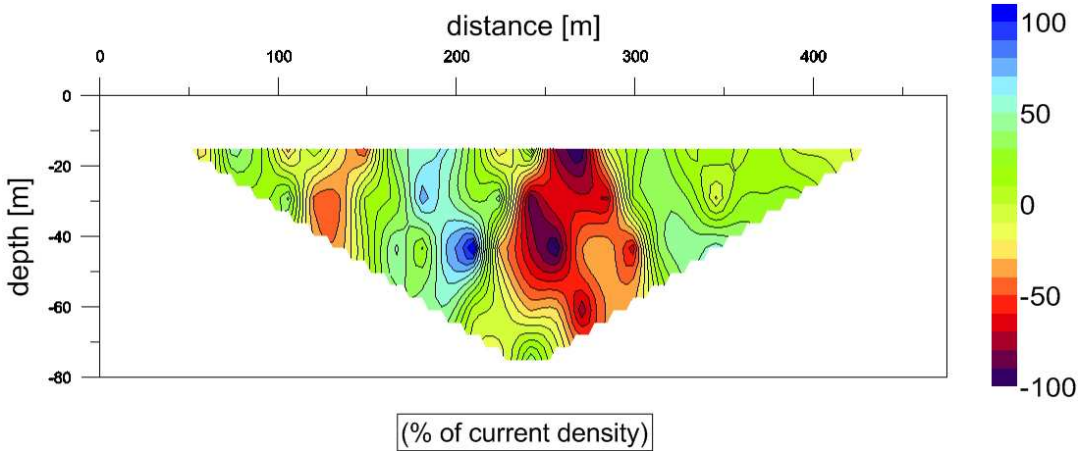

Figure 3.12 - Apparent current pseudo-sections using the previous raw data (Figure 3.9).

High current densities are typical of conductive zones, while low current densities are typical of the more resistive ones, even if there is no direct numerical relationship between the values of the current density of a pseudo-sections and the resistivity of the underground.

Finally, Chouteau et al. (1996) have introduced a filter that allows for transforming the in-phase data in apparent resistivity knowing the first apparent resistivity value. The filter is expressed by the following equation:

$$\sqrt{\rho_{j+1/2}} = -\sqrt{\omega\mu}\cdot\Delta x\cdot\mathrm{Re}\left(\frac{H_z}{H_y}\right) + \sqrt{\rho_{j-1/2}} \tag{3.9}$$

where ω is the angular frequency and μ is the magnetic permeability equal to μ_0.

The main advantage of the VLF-EM method is that this instrument may be carried by a single operator because of its weigh is only about 5 kg. Moreover, magnetic field measurements do not require ground contact and can be made in about a minute at each station. Station spacing may vary from 5 to 20 meters depending on the geologic objective, obviously the interspacing between measurement stations (Δx), also determine the resolution of the underground information as shown in the explanation of the Karous and Hjelt filter (Figure 3.11).

Nevertheless, VLF-EM method has some disadvantages:

- ✓ It does not allow for a quantitative interpretation of the underground resistivity such as the ERT. Some efforts has been made in order to obtain an inversion of the data (SasaKi, 1989; Becken andPedersen, 2003; Monteiro Santos et al., 2006), but nowadays these are not yet well developed techniques;
- ✓ The depth of the surveys (d) is in inverse proportion to the conductivity of the media and defined from the following relationship (Table 3.1):

$$d = 503.292\sqrt{\frac{\rho}{f}} \qquad (3.10)$$

For the fractured rocks which are analyzed here and which are characterized by high current resistivity, this method can be give good results, but it is probably not well adapted for all the subsurface materials and becomes unreliable for unconsolidated material in presence of a conductive water table.

Table 3.1 - Depth of surveys with a frequency of EM of 22.5 kHz for different resistivity values.

Resistivity[ohm·m]	d[m]
10	11
100	34
1000	106
2000	150
3000	184
4000	212
5000	237

- ✓ VLF measurements are sensitive to interferences from pipelines, utilities, fences, and other linear elements. Also topographic effects and unfavorable ionosphere conditions can bias the data. Moreover no methods for removing bad data exist.
- ✓ a quantitative indicator of the quality of the data is not available.

Considering all this, the VLF-EM method can be used primarily as a reconnaissance tool to identify anomalous areas for further investigation with other geophysical methods or drilling. Nevertheless a comparison with the ERT technique, also performed during this project, is useful for a better understanding of the advantages and limitations of this simple EM technique.

To treat the VLF-EM data various software packages exist. The first one, called RAMAG, has been developed by the ABEM® company and allows to download the data from the instrument. It allows also to treat the data with the Karous-Hjelt filter. Nevertheless the RAMAG software, in our opinion, is not flexible, since it does not give any numerical output to the user and it has some restrictive options for the generation of graphical output. For these reasons, this package is used only to download the raw data.

Another software for the treatment of the data is the numerical code KHFFILT, which has been developed by Pirttijärvi (2004) and is open source. It allows to apply the Fraser and the Karous-Hjelt filters and to obtain numerical and graphical representations of the filtered data. Finally, specific numerical codes have been implemented to perform the filters in order to have more specific options to treat and represent the data. In particular, the interpolation of the gridded data obtained from the Karous-Hjelt filter is a sensitive question. Using the numerical results of the implemented numerical codes, and an interpolation software, such as Surfer®, it is possible exclude

from the graphical output the insignificant data, that are the data out of the numerical grid represented in Figure 3.11.

Figure 3.13 - The ABEM® WADI VLF-EM instrument used in this research project.

The VLF-EM surveys were carried out using a VLF WADI ABEM instrument (Figure 3.13), using spacings between measurements points varying from 5 to 20 m. The length of the profiles was always the same as that of the resistivity profiles, while the maximum depth of investigation depends on this length as on its being inversely proportionally to the conductivity of the media (Table 3.1).

3.3 Surveys

3.3.1 Introduction

In this project, two campaigns of measurements were undertaken. In a first step, the methods discussed above have been applied to the assessment of water-bearing zones during tunnel drilling. In a second step, the potential of the geoelectrical techniques, integrated with hydrogeochemical data, have been tested to assess the groundwater circulation and the vulnerability of springs located above the drilled tunnels.

The key results of these two campaigns are presented in the chapters 4 and 6, while the remainder of this chapter presents the results of a preliminary measurement campaign in October 2009 conducted in the Monte Ceneri base tunnel region (Figure 3.14) in areas where geomorphological evidences allow to identify possible fracture zones. The detailed position of all these geophysical surveys is shown in Figure 3.16.

3.3.2 Geology and geomorphology settings

As shown in Figure 3.16, the south-alpine basement is separated from the Penninic nappes of the Central Alps by the Insubric Line, also known also as *Periadriatic Line*, which is one of the main tectonic features of the Alpine chain (Schmid et al. 1989, Schmid, 1993). The Ceneri base tunnel (Figure 3.14) is entirely located within the crystalline basement of the southern Alps from the Vigana north portal in the Magadino alluvial plain, to the Vezia south portal in the Vedeggio alluvial plain and it crosses two distinct tectonic zones: (i) the Strona-Ceneri zone (amphibolites, Ceneri orthogneiss and paragneiss, Giumello gneiss) in the North and (ii) the Val Colla zone (S. Bernardo orthogneisses, Stabiello paragneisses, schists and phylonites) in the South. These two zones are separated by the Val Colla Line, also known also as Caslano-Taverne-Gazzirola Line, a geologic fault that according to the classification of Buergi et al. (1999) is mainly composed of mylonites, of the Paleozoic era, with a thickness of 600 m (Pini and Rossi, 2010).

The thickness of the rocks above the tunnel ranges from about ten meters near the north portal to 850 m in the Ceneri zone and to 250 m in the Val Colla zone. All expected lithologies of the tunnel are shown in Figure 3.15. Cleavages run through the entire rock mass, even if, as shown by

several literature studies (Ofterdinger, 2001; Maréchal and Etcheverry, 2003, Masset and Loew, 2010), in crystalline rocks such as gneisses, a higher fracture density with open discontinuities is registered in the uppermost layers (100-200 m depth), while increase in stress leads to decreases fracturation in direct proportion to the depth of the rock cover (Marzocchi et al, 2010). Moreover, the rock masses of the region are generally covered by alluvial, detrital, fluvial, and/or glacial sediments; yet, the tunnel excavation will encounter unconsolidated materials only in two small areas around the north and south entry portals.

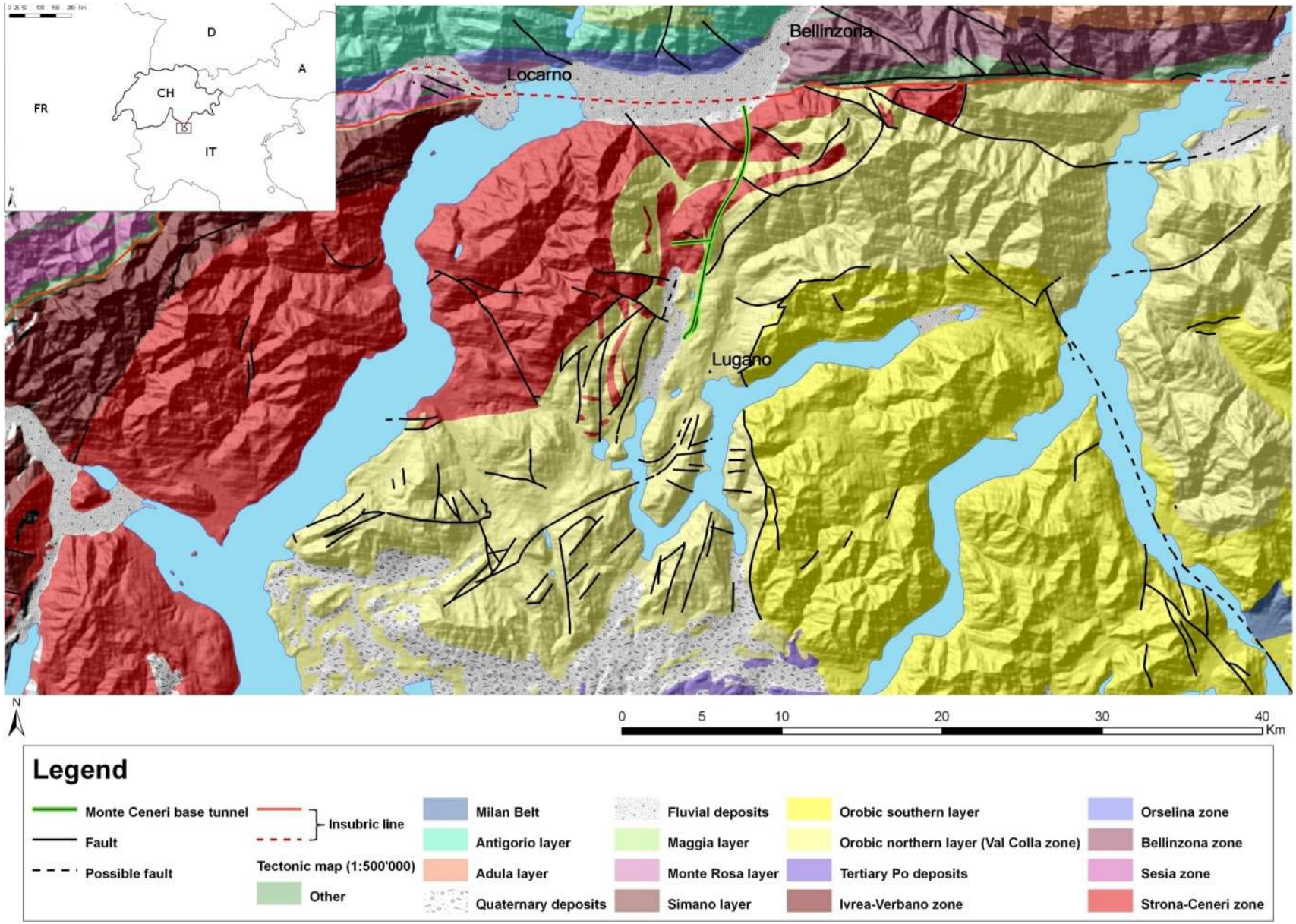

Figure 3.14 - Tectonic sketch map of the studied area (Sources of the data: *Swiss Federal Office of Topography, CGIAR-CSI, Alptransit Inc.*)

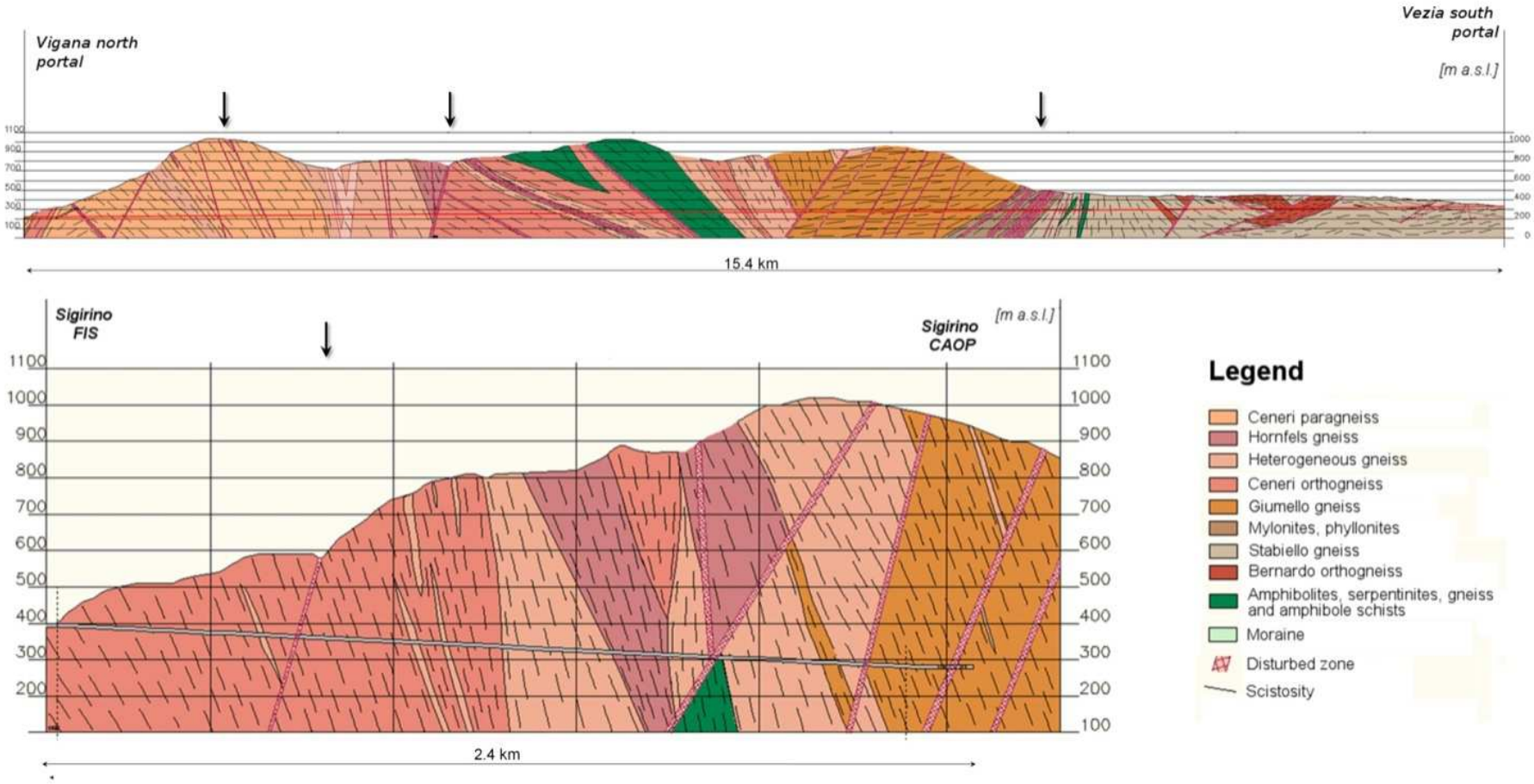

Figure 3.15 - Expected geological profile of the Ceneri base tunnel (upper side) and Sigirino exploration tunnel (below). [*data* kindly offered byAlptransit Inc.]. The investigated areas are shown by the black arrows. Now only the Sigirino exploration tunnel has been entirely excavated

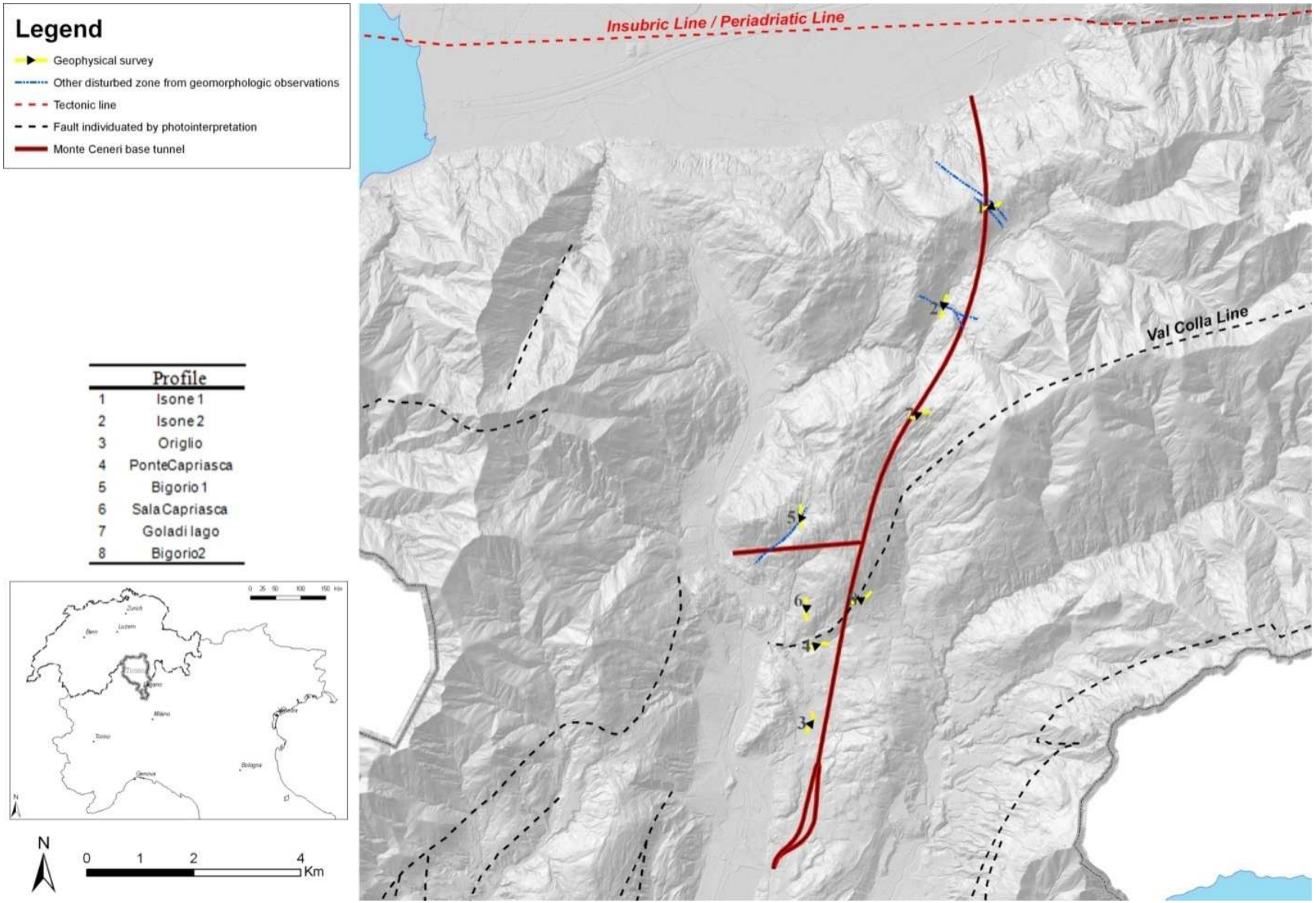

Figure 3.16 - High resolution shaded relief map of the studied area. Superimposed the main faults are shown, identified by photo-interpretation, the main tectonic line and other disturbed zones were identified by geomorphologic observations.

The main rock schistosity is nearly parallel to the slope in the northern part, with planar sub-vertical structures, while in the southern part it is south or south/east dipping with planar structures that follow sub-horizontal trends (Pini et al., 2007; Rossi et al. 2009). The deformations associated with the alpine orogenesis are of brittle nature with several kataclastic structures, such as fault zones and fractures, which, in the overlying landscape, morphologically correspond to incisions in the slope.

The geological maps (Reinhard, 1962; Bächlin, 1974) only indicate a few fractures in the Isone region and in the Monte Ceneri base tunnel area. Nevertheless, simply showing the high resolution shaded relief map and comparing it with geological map two additional tectonic disturbed zones have been identified and hence investigated with geophysical surveys. In Figure 3.16 the potential disturbed zone and the detailed location of the geophysical surveys carried out in the first phase (October 2009) are shown, superimposed to the shaded relief map obtained from a high resolution (2 m x 2 m) digital terrain model.

3.4 Results and interpretation

3.4.1 Introduction

In this section the results of three interesting surveys and other observations coming from additional geophysical investigations are discussed. Two of the surveys have been carried out above the Val Colla line; one of them close to the Sigirino access tunnel, and for this reason it will be discussed in the next chapter 5.

For each survey are shown:

1) the 2D resistivity section derived from ERT with the above explained transparent filter superimposed on the areas where smoothed sensitivity is lower than 0.2;
2) the VLF-EM results in terms of
    a. two lines representing the scattered surface raw data (real and imaginary components);
    b. a line representing the Fraser filtered data;
    c. a pseudo-section of the underground which represent the percentage of current density that flows in the subsurface, obtained applying the Karous-Hjelt filter.
3) a geological interpretation of the geophysical results, reporting also morphological and hydrogeological logs.

Details of the interpretation are presented with emphasis on the usefulness of the geophysical results as well as on the problems related to their application.

3.4.2 Val Colla line

As mentioned in the previous front matter geological section, a main tectonic line that will intersect the Monte Ceneri Base tunnel axis is the Val Colla Line. Therefore two different profiles located in the Ponte Capriasca and Bigorio towns were carried out with the idea to cross this main tectonic line in the few accessible zones where it is possible (Figure 3.17).

The first survey at Ponte Capriasca was carried out in a direction perpendicular to the fault zone in the first (~0-120 m) and last (~370-470 m) part, while in the middle part (120-370 m) the survey direction is about parallel to the expected fault zone (Figure 3.17).

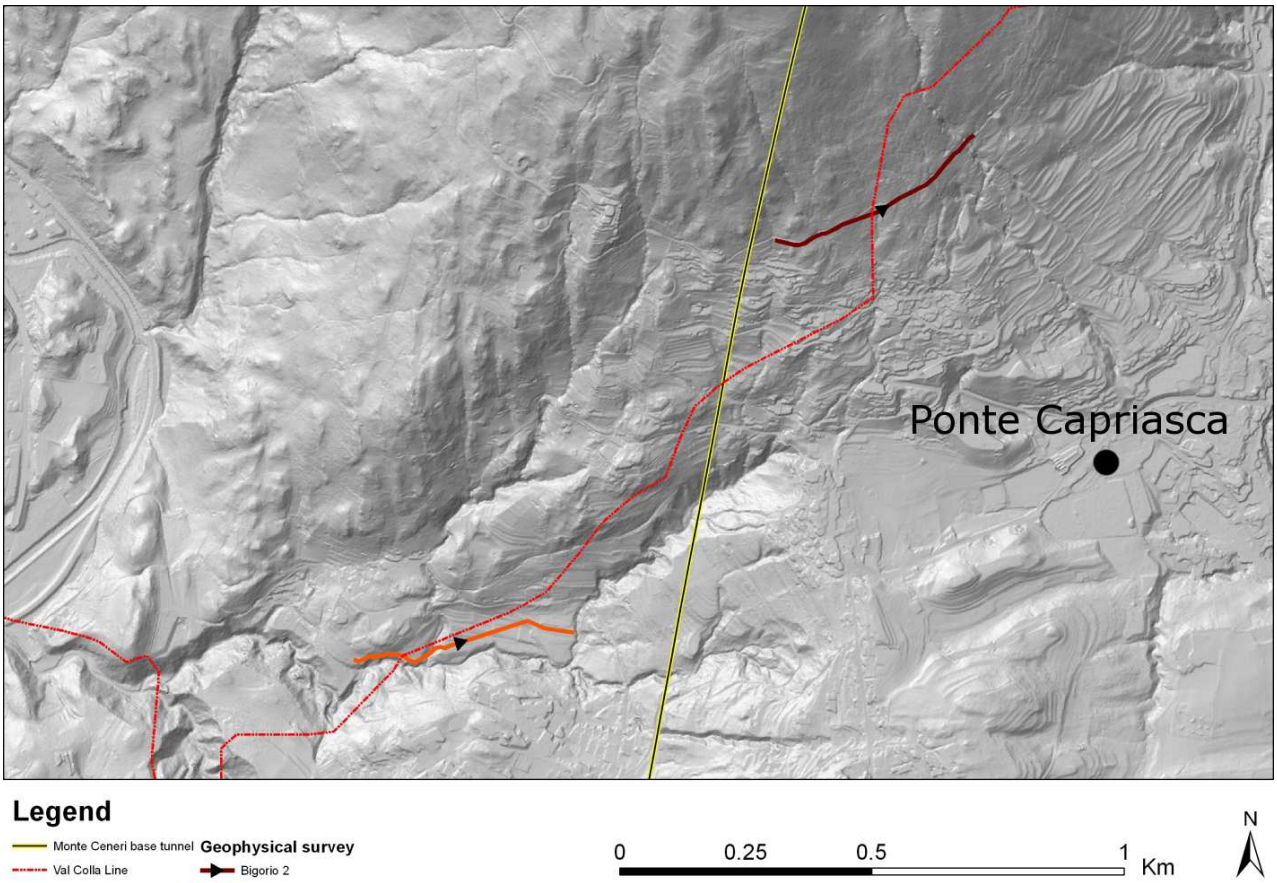

Figure 3.17 - Detailed position of the surveys carried out crossing the Val Colla line.

From a geomorphological point of view, the first part of the profile (0-150 m) was carried out parallel to a deeply incised creek, in a steep area characterized by outcropping rock that is highly fractured; after crossing the stream (~160 m) the survey was realized on a moraine deposit. On the basis of the geological map (Reinhard et al., 1962), mylonites (Buergi et al. 1999) forming the Val Colla line are expected under this moraine deposit. Parallel to the profile, about 50 m to the south, there is another deeply incised creek.

The 2D resistivity section (Figure 3.18) shows two different conductive zones: the first (120-150 m) is also visible on the VLF-EM pseudo-section could correspond to the expected disturbed zone (the Val Colla line), while the second one (~360 m later distance on the profile) is present about in the middle of the moraine deposit and it is perhaps related to the change in the profile direction that in the last part is again perpendicular to the expected fault zone. In the middle of the ERT profile, there is an anomalous area, characterized by higher conductivities that can be related to the presence of the expected fault zone under the moraine deposit with the same direction of the survey. These observations emphasize the problems related to the 3D geometry of the conductive subsurface bodies, which not always may be well shown by a 2D profile. The suggested procedure is to do a survey crossing orthogonally the investigated structure, however, from a logistical point of view, this is often difficult. Therefore, the interpretation of results is more complex and doubtful, even though possible.

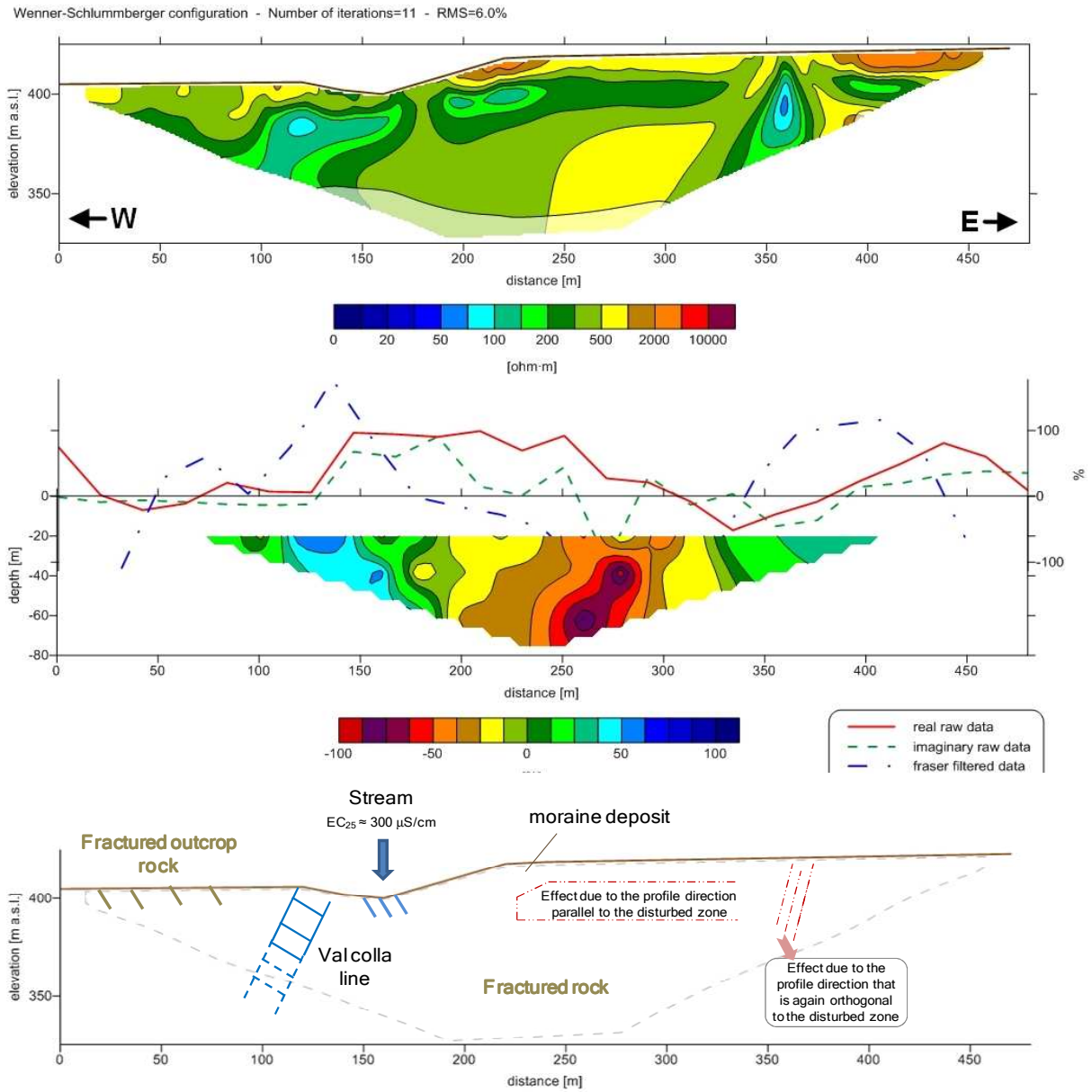

Figure 3.18 - Ponte Capriasca survey: resistivity model of the underground derived from ERT (above), VLF-EM results (middle), and geological interpretation of the profile (below).

In this case VLF-EM data appear reasonable and there is a detectable correspondence with electrical resistivity results. The expected crossing of the conductive zone (probably related to the Val Colla line) is in fact clearly visible also in the VLF-EM current density pseudo-section.

The second survey (Bigorio 2) was carried out crossing the expected fault zone, called Val Colla line, in this case, orthogonally (Figure 3.17).

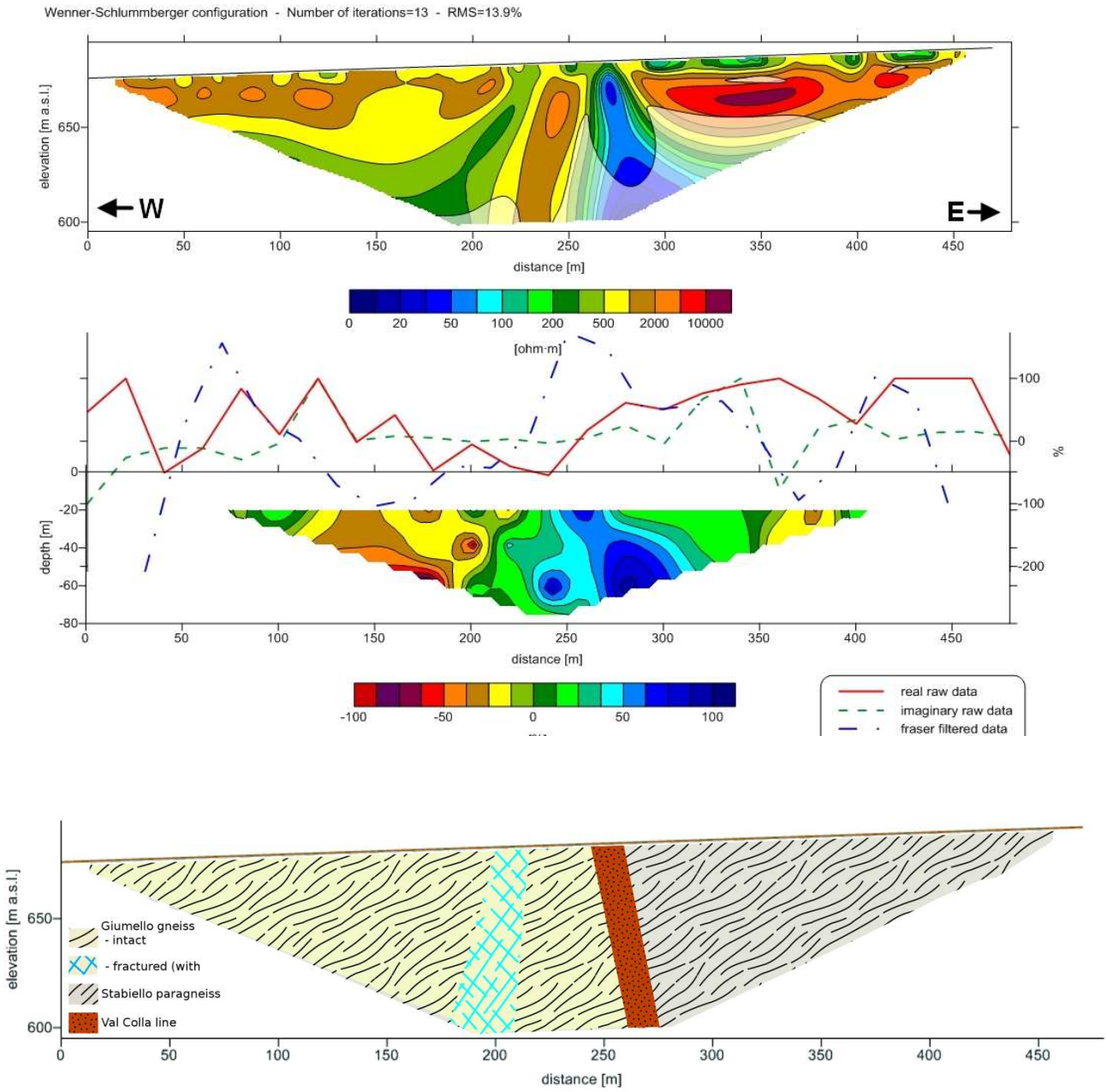

Figure 3.19 - Bigorio2 survey: resistivity model of the underground derived from ERT (above), VLF-EM results (middle), and geological interpretation of the profile (below).

From the geological map (Reinhard et al., 1962), it is possible to note that the first part (~0-200 m lateral distance) of the profile was realized on the Giumello gneisses (Strona-Ceneri zone), while the second part (~ 200-480 m distance), after the crossing of the possible disturbed zone, was carried out over the Stabiello, so called Ceneri paragneisses (Val Colla zone).

Two more conductive zones are observable (Figure 3.19) in correspondence of the Val Colla line crossing. The first one is characterized by lower resistivity values (100-300 ohm·m) and by an immersion on the west; while the second one is characterized by higher conductivity values (10-100 ohm·m), that probably denote a higher water presence, and by an immersion on the east. The data near the boundary of the 2D resistivity section seem to be influenced by interpolation errors, as shown by low smoothed sensitivity values in few areas of the section.

In this case, also the differences between the two types of crystalline rock masses seem visible in the 2D resistivity section. In particular the Stabiello paragneiss has higher resistivity values with respect to the Giumello gneisses. These differences can be related to difference in the mineral components (e.g., the Giumello gneiss is characterized by the presence of aluminosilicate minerals), or to different levels fracturing and water content. VLF-EM data appear adequate, even if a

probable noise effect has been registered at least in the first 100 m of the profile due to the presence of few houses and electrical cables. A correspondence with the ERT resistivity values is, however, discernable, at least in the middle of the profile. Here, the presence of a conductive zone, perhaps in correspondence of the Val Colla fault, seems to be confirmed by VLF-EM results that identify a sizeable area with high current density values about in the same position of the ERT results.

3.4.3 Sigirino tunnel mylonites

More interesting results are those obtained from the survey conducted at Bigorio (Bigorio 1 survey), crossing a creek that flows deeply incised in the rock. Downstream the Sigirino access tunnel has already been excavated below the same creek (Figure 3.20 and Figure 3.15). Nevertheless, the planimetric distance between the profile and the tunnel axis is about 800 m (Figure 3.20), and also the depth of investigation (~100 m in the middle of the profile) it is not sufficient to reach the tunnel that was drilled more than 200 m below the surface (Figure 3.15).

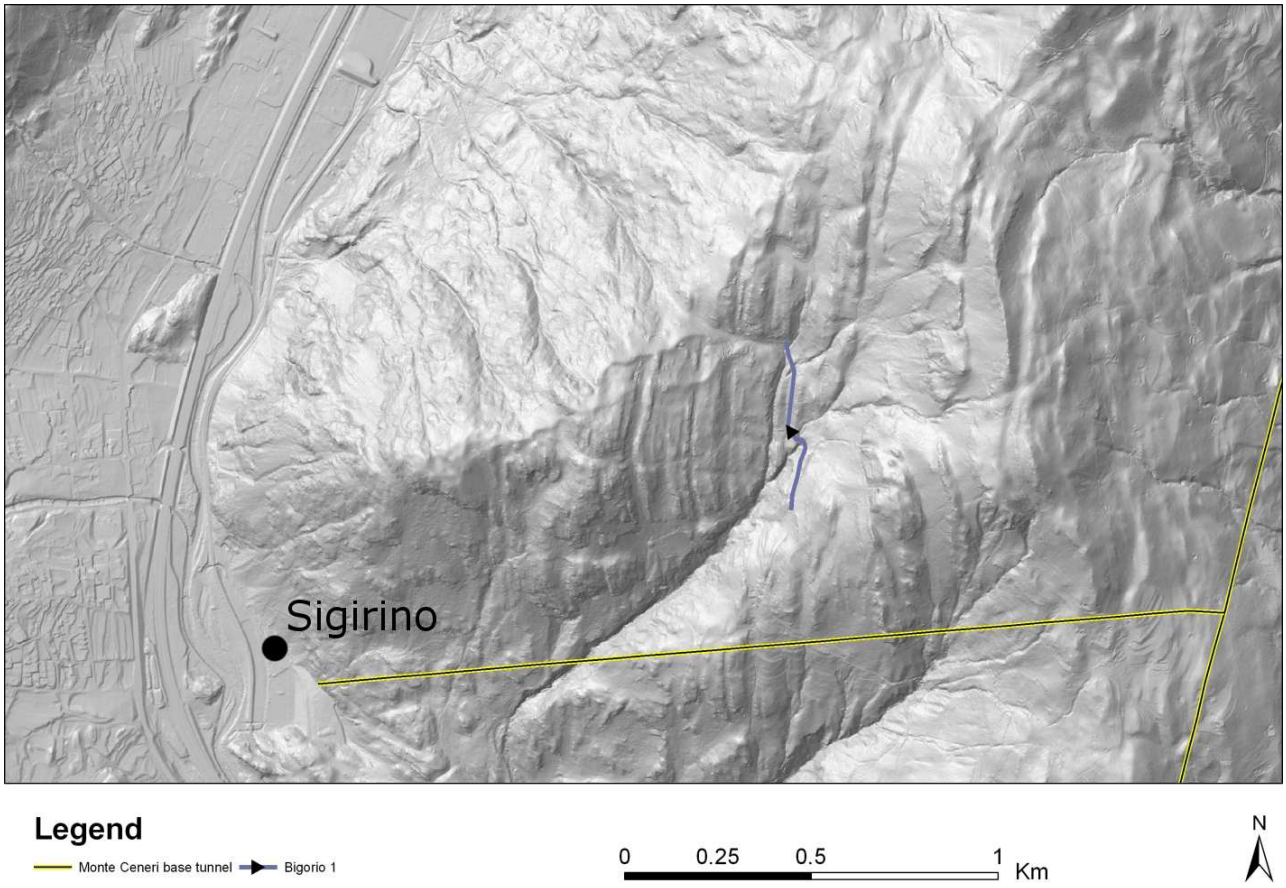

Figure 3.20 - Detailed position of the surveys carried out crossing the Sigirino access tunnel mylonites. Planimetric view and geological expect section with evidenced the disturbed zone.

The whole survey was carried out on the outcropping rock. In fact, the resistivity model of the underground, at least in the shallow layers, is characterized by very high resistivity values (3000-10’000 ohm·m) typical of the intact crystalline rock masses. This occurrence could be the clue to explain problems in electric current transit at depth. The low smoothed sensitivity values shown in few parts of the 2D section conceivably support this hypothesis. Nevertheless, the high resistivity at the surface can be also related to the dry conditions typical of the outcropping rocks present on the site (precipitation water quickly infiltrates, hence rocks, at the time of survey, were practically dry). In this case the resistivity model may be considered reliable and three deeper conductive zones have been observed (Figure 3.21). They are probably related to the presence of water. The first and the third high conductivity areas are individuated exactly below two little creeks crossed by the profile, and visible by morphological field observations (Figure 3.20). The zone in the middle of the profile,

instead, does not have a morphological evidence at the surface, but seems to be also related to the presence of groundwater bearing fractures.

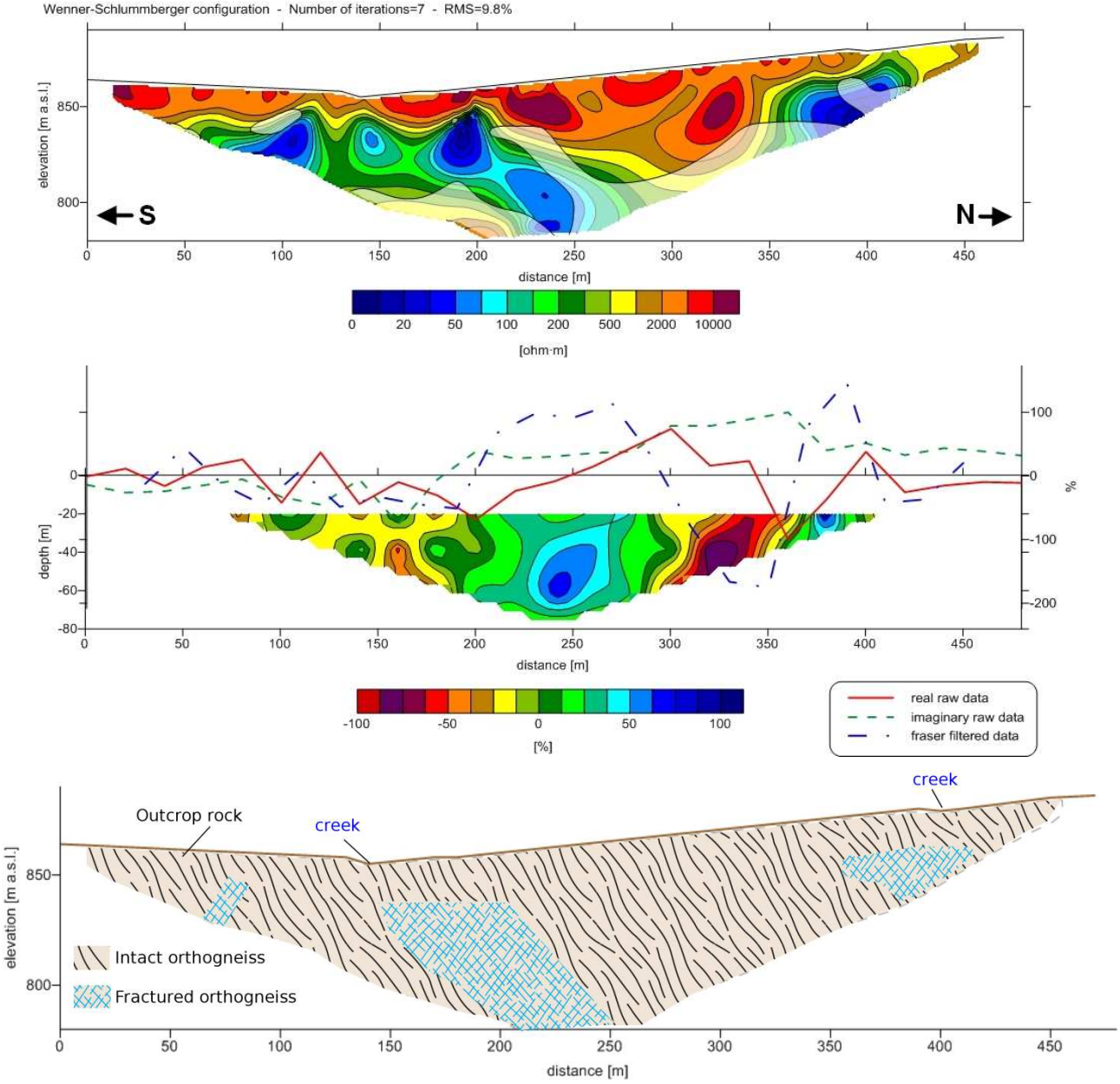

Figure 3.21 - Bigorio1 survey: resistivity model of the underground derived from ERT (above), VLF-EM results (middle), and geological interpretation of the profile (below).

Concerning VLF-EM data, in field, the element of noise are not distinguished from results, in fact the raw data appear reasonable. Moreover, the results are in agreement with the 2D resistivity section. In fact also in the current density pseudo-section at least two zones characterized by high current densities can be observed about in the same position of that individuated in the resistivity model. The direction of the individuated possible fault zone and also the immersion at north is correctly shown by the mylonites detected digging the Sigirino access tunnel (Figure 3.15).

Finally, it is important to note that these results are in agreement also with the hydrogeological model available from geochemical data that will be presented in the following chapter 6.

3.4.4 Other surveys

The surveys carried out in Origlio, Sala Capriasca and Gola di Lago (Figure 3.16) show good results from a geophysical point of view. RMS values are generally low and smoothed sensitivity

values are high. Nevertheless, interesting hydrogeological structures related to the tunnel construction were not identified; hence these data are not presented in this section.

Conversely, the two surveys carried out in Isone (Figure 3.16) have revealed a few problems related to the application of geophysical methods. The survey called Isone 1 was in fact carried out close to an aerial for radio transmission. Even though it is dismissed, its earth electrical connections have caused high electrical noises. Therefore, after a consistent filtering process of bad data, the obtained results are reliable, but only to ~30 m depth.

Figure 3.22 - Aerial for radio transmission present close to the survey line called Isone 1.

Finally, the survey called Isone 2 is characterized by unclear results due to the survey direction that is not perpendicular to the geological structures to investigate. As the Ponte Capriasca survey, the geological interpretation of the surveys is possible, but complex and doubtful.

3.5 Remarks

The geophysical results obtained from the ERT and VLF-EM techniques have demonstrated that these methods can be useful for the detection of fractures and disturbed zones that are normally the preferential hydraulic pathways in the rock masses. Hence they can be applied for the hydrogeological problems related to tunneling.

Few problems concerning (i) electrical noise and (ii) survey's location are evidenced and hence they have been taken in account for the other geophysical campaigns that will be presented in chapter 4 and 6. Concerning ERT surveys, two different configurations, the Wenner-Schlumberger (WS) and the Dipole-Dipole (DD), have been tested. Always better results have been obtained with the WS configuration. Therefore this latter configuration is chosen for the other campaigns.

Concerning the VLF-EM method different spaces have been tested for data acquisition, observing the best results with a distance between acquisition points of about 15 m. The VLF-EM instrument is effectively able to detect and map electrical conductive zones and it works quite well, at least over the crystalline rocks, which are high resistivity bodies. Nevertheless a few problems have been encountered in areas characterized by the presence of electrical structures, both in the subsoil or aerial; those generally cause a high noise. On the contrary, the ERT method can be also affected by electrical noise, but it is only due to the presence metallic objects in contact with the surface (e.g. a wire netting) or in the underground (e.g. a earth electrical connection), but often it is possible to conveniently filter the data and thence obtain a quite reliable resistivity model of the underground, at least of the first layers.

A further advantage of the use of ERT technique with respect to the VLF-EM method is the presence of few indexes of the reliability of the results; for instance the RMS statistical error and

the smoothed sensitivity that has been applied in our work. These indicators are in fact very useful, especially for the non expert user, allowing a correct interpretation of the results.

On the contrary VLF-EM noise effects are only visible from a qualitative point of view; Walen (2003) suggest that data which have a saw-tooth appearance can be considered suspicious, nevertheless does not exists any numerical index to quantify this effect.

Finally it is important to note that geoelectrical surveys are more expensive than VLF-EM profiles. In fact, the ERT method requires at least three or preferably four people for the displacement of instrument and electrical cables, while a VLF-EM exploration could be carried out by a single operator that employ less time. Nevertheless the 2D resistivity profiles obtained with the ERT technique are more reliable and more interpretable.

References

Bächlin R., Bianconi F., Codoni A., Dal Vesco E., Knoblauch P., Kündig E., Reinhard M., Spaenhauer F., Spicher A., Trommsdorff V., Wenk E. (1974). Atlante geologico della Svizzera 1:25'000 – Foglio 1313 Bellinzona

Bhattacharya P.K., Patra H. P. (1968). Direct current geoelectric sounding: Principles and interpretation, Elsevier Pub. Co., 139 pp

Beken M., Pedersen L.B. (2003). Transformation of VLF anomaly maps into apparent resistivity and phase, Geophysics 68(2),497-505

Bersan M., Pilla G., Dolza G., Torrese P., Ciancetti G. (2010). The uprising of deep saline waters into the oltrepò pavese (northern italy) aquifer: early results. Italian Journal of Engineering Geology and Environment 1:7-22

Buergi C., Parriaux A., Franciosi G., Rey J.Ph. (1999). Cataclastic rocks in underground structures – terminology and impact on the feasibility of projects (initial results), Engineering geology 51:225-235

Chapellier D., Tacchini G., Baron L., Onnet R., Marescot L, Mari JL., Perret F., Rochat S. Furrer J. (2010). Online course of geophysics – Available online http://www-ig.unil.ch/cours/

deGroot-Hedlin C., Constable S. (1990). Occam's inversion to generate smooth, two-dimensional models for magnotelluric data. Geophysics, 55:1613-1624

Di Maio R., Piegari E., Scotellaro C., Soldovieri M.G. (2007). Resisitivity tomographies to define thickness and water contento of pyroclastic covers at Mt. di Vezzi (Ischia island, Italy). Italian Journal of Engineering Geology and Environment, 2:65-72

Ellis R.G., Oldenburg D.W. (1994). Applied geophysical inversion. Geophysical journal international, 116:5-11

Fazzito S.Y., Rapalini A.E., Cortés J.M., Terrizzano C.M. (2009). Characterization of Quaternary faults by electric resistivity tomography in the Andean Precordillera of Western Argentina. Journal of South American Earth Sciences, 28:217-228

Francese R., Mazzarini F., Bistacchi A., Morelli G., Pasquarè G., Praticelli N., Robain H., Wardell N., Zaja A. (2009). A Structural and Geophysical Approach to the Study of Fractured Aquifer in the Scansano-Magliano in Toscana Ridge, Southern Tuscany, Italy. Hydrogeology journal, 17(5): 1233-1246

Franz L., Romer R.L. (2007). Caledonian high pressure metamorphism in the Strona-Ceneri Zone (southern Alps of southern Switzerland and northern Italy), Swiss Journal of Geosciences, 100(3):457-467

Fraser D.C. (1969). Contouring of VLF-EM data. Geophysics, 34:958-967

Karous M., Hjelt S.E. (1977). Determination of apparent current density from VLF measurements. Department of geophysics, University of Oulu, Contribution No. 89, 19 pp

Kirsch R. (2006). Groundwater Geophysics - A Tool for Hydrogeology, Springer-Verlag Berlin Heidelberg, 548 pp.

Kruse S.E., Brudzinski M.R., Geib T.L.(1998). Use of electrical and electromagnetic techniques to map seawater intrusion near the Cross-Florida Barge Canal, Environmental and Engineering Geosc. 4:331- 340.

Loke M.H. (2004). Tutorial:2-D and 3-D electrical imaging surveys. Copyright (1966-2004) M.H.Loke, 136pp.

Loke M.H., BarkerR.D. (1996). Rapid least-squares inversion o apparent resistivity pseudosections using a quasi-Newton method. Geophysical prospecting 44:131-152

Loke M.H., Dahlin T. (2002). A comparison of the Gauss-Newton and quasi-Newton methods in resistivity imaging inversion. Journal of Applied Geophysics, 49:149-162.

Macedo L., Lima A.S., (2004). Groundwater exploration by VLF techniques: a case study in granitic terrains of Northwestern Portugal. In: Proceedings of the "2004 Fractured Rock Conference", National Ground Water Association, USA

Maréchal J.C. , Etcheverry D. (2003). The use of ^{3}H and ^{18}O tracers to characterize water inflows in Alpine tunnels, Applied Geochemistry 18:339-351

Marescot L., Loke M.H., Chapellier D., Delaloye R., Lambiel C., Reynard E. (2003). Assessing reliability of 2D resistivity imaging in mountain permafrost studies using the depth of investigation index method, Near surface Geophysics, 1:57-67

Masset O., Loew S. (2010). Hydraulic conductivity distribution in crystalline rocks, derived from inflows to tunnels and galleries in the Central Alps, Switzerland. Hydrogeology Journal 18: 863–891

Marzocchi R., Pera S., Pfeifer H.R. (2010). Hydrogeological interferences in tunneling - A comprehensive study, Aquamundi1(3):1-14

Monteiro Santos F.A., Mateus A., Figueiras J., Gonçalves M.A. (2006). Mapping groundwater conrtamination around a landfill facility using the VLF-EM method – A case study, Applied Geophysics 60:115-125

Ofterdinger U.S. (2001). Ground water flow systems in the Rotondo Granite, Central Alps (Switzerland), Phd thesis of Natural Science, Swiss federal institute of technology (ETH) – Zurich 177 pp.

Oldemburg D.W., Li Y. (1999). Estimating depth of investigation in dc resistivity and IP surveys. Geophysics 64:403-416

Pagano A. (1996). Indagine geofisica VLF (Very Low Frequncy) preliminare allo scavo della galleria per Mergoscia, Cantone Ticino. Tecnical reports of IST

Piegari E., Cataudella V., Di maio R.,Milano L., Nicodemi M., Soldovieri M.G. (2009). Electrical resisitivity tomography and statistical analysis in landslide modeling: a conceptual approach. Journal of Applied Geophysics, 68:151-158

Pini O., Erard P.F., Del Col A. (2007). Percer la base du Ceneri. Traces 22:16-22

Pini O., Rossi D. (2009). The ceneri railway base tunnel (15.4 km) in the southern swiss alps (gotthard alptransit), Proceedings of the ITA–AITES world tunnel congress

Pirttijärvi M. (2004). Karous-Hjelt and Fraser filtering of VLF measurements. manual of the KHFFILT program - Available online in the webpage of "free geophysical software by Markku Pirttijärvi" (http://cc.oulu.fi/~mpi/Softat/)

Reinhard M., Bächlin R., Graeter P., Lehner P., Spicher A. (1962). Atlante geologico della Svizzera 1:25'000 – Foglio 1333 Foglio Tesserete

Rossi D., Bühler T., Drack E. (2009).Ceneri base tunnel, Tunnel 4:49-63

Sasaki Y. (1989). Two dimensional joint inversion of magnotelluric and dipole-dipole resistivity data Geophysics 54(2):254-262

Sasaki Y. (1992) Resolution of resistivity tomography inferred from numerical simulation. Geophysical Prospecting, 40:453-464.

Schmid S.M. (1993). Ivrea zone and adjacent southern Alpine basement, In:Von Raumer J.F. & Neubauer F. (Eds.): Pre-mesozoic geology in the alp, Springer, Heidelberg 567-583

Schmid S. M., Aebli H. R., Heller F., Zingg A. (1989). The role of the Periadriatic Line in the tectonic evolution of the Alps. Geological Society, London, Special Publications, 45:153-171

Schumacher M.E. (1996). Geological interpretation of the seismic profiles through the a Southern Alps. In: O.A. Pfiffner, P. Lehner, P. Heitzmann, St. Mueller and A. Steck, Editors, Deep Structure of the Swiss Alps — Results from the National Research Program 20 (NRP 20), Birkhäuser, Basel

Stummer P. (2003). New developments in electrical resistivity imaging – PhD dissertation of Swiss Federal Institute of Technology Zurich No. 15034 199pp.

Tassone A., Santomauro M., Menichetti M. Cerredo M.E., Remesal M.B., Lippai H., Lodolo E., Vilas J.F., (2010). Imaging subsurface lithological and structural features by resistivity tomography: North Beagle Channel (Tierra del Fuego, Argentina). Revista Mexicana de Ciencias Geológicas 27(3):562-572

Walen P. A. (2003). VLF Survey planning and interpretation software – For the Abem Wadi and other instruments that record VLF dip angle measurements – RAMAG Instruction manual, Copyright P.A. Walen

4. Integration of electrical tomography, VLF-EM surveys, and tracer tests, to asses water-bearing zones during tunnel drilling

Roberto Marzocchi[1,2], Sebastian Pera[1], Hans-Rudolf Pfeifer[2], and Klaus Holliger [3]

[1]IST, Institute of Earth Science, University of Applied Sciences and Arts of Southern Switzerland (SUPSI), Campus Trevano, CH-6952 Canobbio, Switzerland
[2]IMG, Centre of Mineral Analysis, Faculty of Geosciences and Environment, University of Lausanne (UNIL), Anthropole, CH-1015 Lausanne, Switzerland
[3]IG., Institute of Geophysics, Faculty of Geosciences and Environment, University of Lausanne (UNIL), Amphipole, CH-1015 Lausanne, Switzerland

Abstract

Tunnel drilling may result in hydrogeological interferences that cause both environmental and engineering problems. Geophysical methods, especially in fractured rock masses, are useful proxies to detect groundwater bearing fractures. In this chapter, are presented the results of a study carried out in a mountainous region of the southern Switzerland (Ticino and Grison), applying the Electrical Resistivity Tomography (ERT) and the Very Low Frequency Electromagnetic (VLF-EM) techniques. With this study the usefulness of the 2D ERT to detect water bearing fracture zones was demonstrated; in the light of the obtained results, hydrogeological conceptual models of the region, where the north portal of the Ceneri (Alptransit project) and the San Fedele (A13 Swiss Highway) tunnels have been drilled, were formulated. The correctness of the conceptual models was demonstrated on the basis of tunnel geological logs and also of a tracers test realized in one case study. Geological and hydrogeological settings of the two selected case studies, geophysical results, and a detailed discussion on the hydrogeological conceptual model formulated and on tunnel geological logs used as its validation are presented in this chapter.

4.1 Introduction

In fractured rock masses, the interaction of tunneling with groundwater is a very complex problem, both from an environmental as well as from an engineering point of view (Marechal, 1998; Gargini et al. 2008; Scesi and Gattinoni, 2009; Masset and Loew, 2010). In fact, tunnel drilling may cause a drawdown of groundwater levels and/or affect the discharge rates of springs. Moreover, inflows in tunnels may be a problem during excavation or tunnel service. While the influence of tunneling on the regional groundwater systems may be adequately predicted in porous media by using analytical solutions (Goodman et al., 1965; Lei, 1999; El Tani, 2003; Kolymbas and Wagner, 2007; Perrochet and DeMatteis, 2007), this approach is difficult to apply in the case of fractured rocks.

In this work, the possible application of different geophysical techniques to detect water bearing fractures and thus forecast water inflows in the tunnels excavating through fractured rock masses was investigated. Geophysics, in particular electrical and electromagnetic techniques, have been widely used in groundwater investigations, because of the correlation of electrical properties with geologic formations in general and their water content in particular (Flathe, 1955, 1970; McNeill, 1990; Kirsch, 2006). During this study, the application of 2D Electrical Resistivity Tomography (ERT), which can provide information concerning the groundwater presence in fractured rock masses (Di Maio et al., 2007; Piegari et al. 2009; Fazzito et al., 2009) was tested in detail. Moreover the Very Low Frequency Electromagnetic (VLF-EM) method, which is able to detect elongated, steeply dipping and high-conductivity bodies in the underground and therefore frequently used in hydrogeological studies (Pagano, 1996; Macedo and Lima 2004, Bersan et al. 2010), was also tried. Moreover tracer tests, which are a common tool to evaluate groundwater flow and transport processes, recharge and mixing processes, or sources of contamination (Käss 1998)

were also applied. They are frequently used in hydrogeology (Maloszewski et al., 1999; Schudel et al, 2002) and their applicability to tunneling has been confirmed by a recent work (Vincenzi et al., 2009). In the course of this study, a number of geophysical surveys (Marzocchi et al., 2010) were carried out in areas surrounding two tunnels in the southern part of the Switzerland while they were being drilled: the Monte Ceneri (Ticino) and the San Fedele tunnel (Grison). The objective was to understand whether the integration of these methods may be useful to obtain a hydrogeological model of the area where tunnels were excavated. The availability of geological logs collected during tunnel drilling, as well as the tracer test conducted in one case study, allowed to verify the interpretations or eventually to individuate critical situations.

4.2 Geological and hydrogeological setting

Currently, there are various important tunnel projects in southern Switzerland which constitute a unique opportunity to perform research in the field of tunneling and underground structures. The attention here is focused on the Monte Ceneri base tunnel (Ticino) and on the San Fedele tunnel (Roveredo, Grisons), which are shown in Figure 4.1. On the tectonic map of this figure, an important element is the Insubric line, also known also as Periadriatic Lineament, which is one of the main tectonic features of the Alpine chain and, in the study zone, marks a first-order tectonic boundary between the south-alpine basement and the main body of the Alps (Schmid et al. 1989). The Monte Ceneri base tunnel, in this case its north portal, is located within the crystalline south alpine basement; while the Roveredo tunnel, also called San Fedele tunnel, lies within the Alpine basement, and in particular the lower Penninic nappes of the Central Alps (Schmidt et al., 2004).

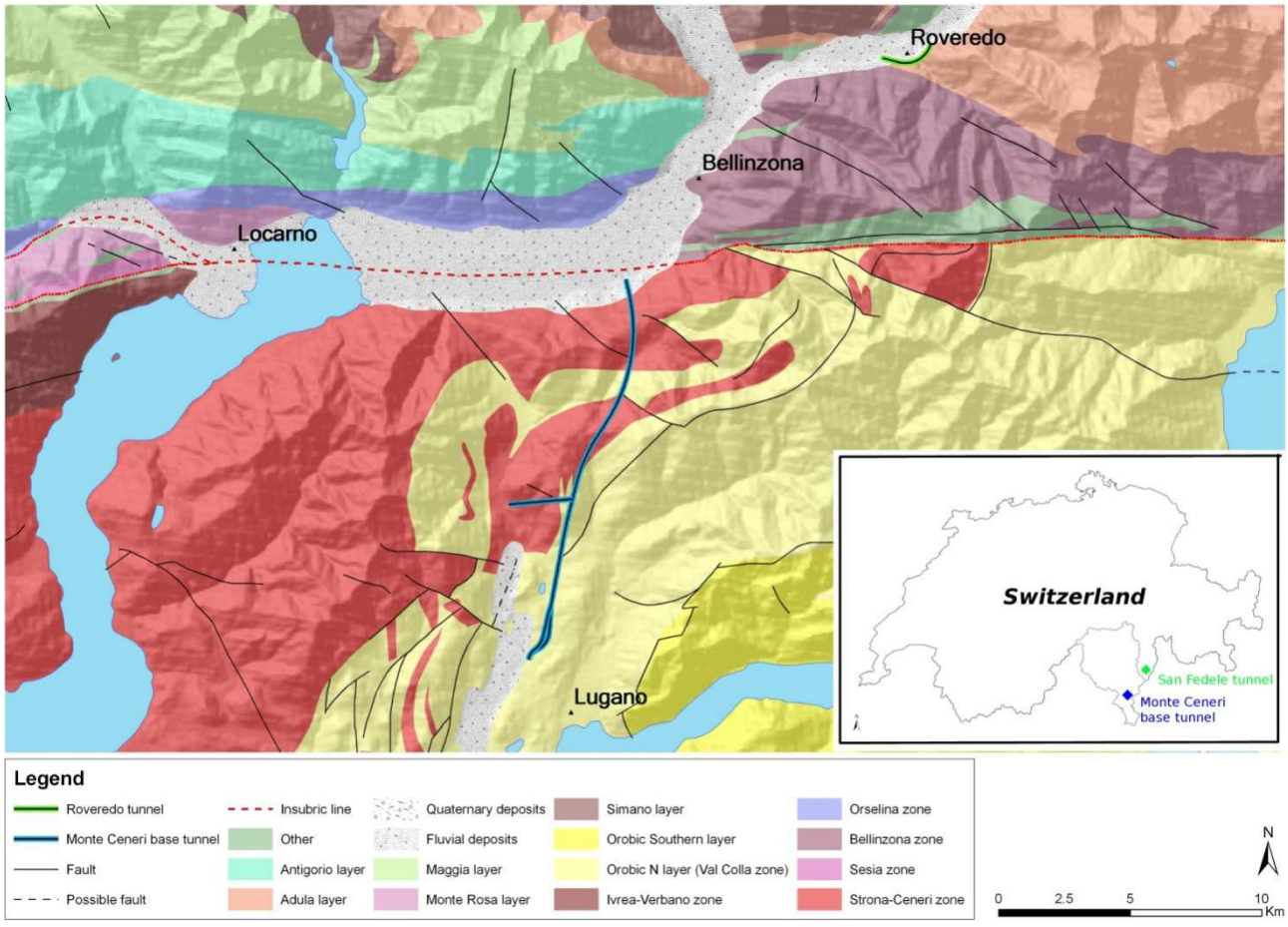

Figure 4.1 - Tectonic map (original scale 1:500'000) of the studied area (Sources of the data: Swiss Federal Office of Topography, CGIAR-CSI, Alptransit Inc.)

4.2.1 Monte Ceneri tunnel north portal

The Ceneri base tunnel, which is entirely located within the metamorphic south-alpine rocks, crosses two different tectonic zones: (i) the Strona-Ceneri zone (amphibolites, Ceneri orthogneiss and paragneiss, Giumello paragneiss) in the north and (ii) the Val Colla zone (S. Bernardo orthogneisses, Stabiello paragneisses, schists and phylonites) in the south. These two zones are separated by Val Colla Line, also known as Caslano-Taverne-Gazzirola Line, a fault that, according to the Buergi et al. (1999) classification, is mainly composed of mylonites of the Paleozoic era with a thickness of about 600 m (Pini and Rossi, 2009).

The northern portal is located near Vigana. The first part was excavated in unconsolidated material. After about 20 m the drilling was conducted in fractured rock, in particular through the Ceneri orthogneiss (100-150 m), followed by the Ceneri paragneiss that widely outcrops in this region. The thickness of overburden above the tunnel increases from about 10 m near the north portal to about 200 m at the progressive distance from the portal of about 600 meters. A sketch of a geological profile along the tunnel is presented in Figure 4.2 (profile and plan views):

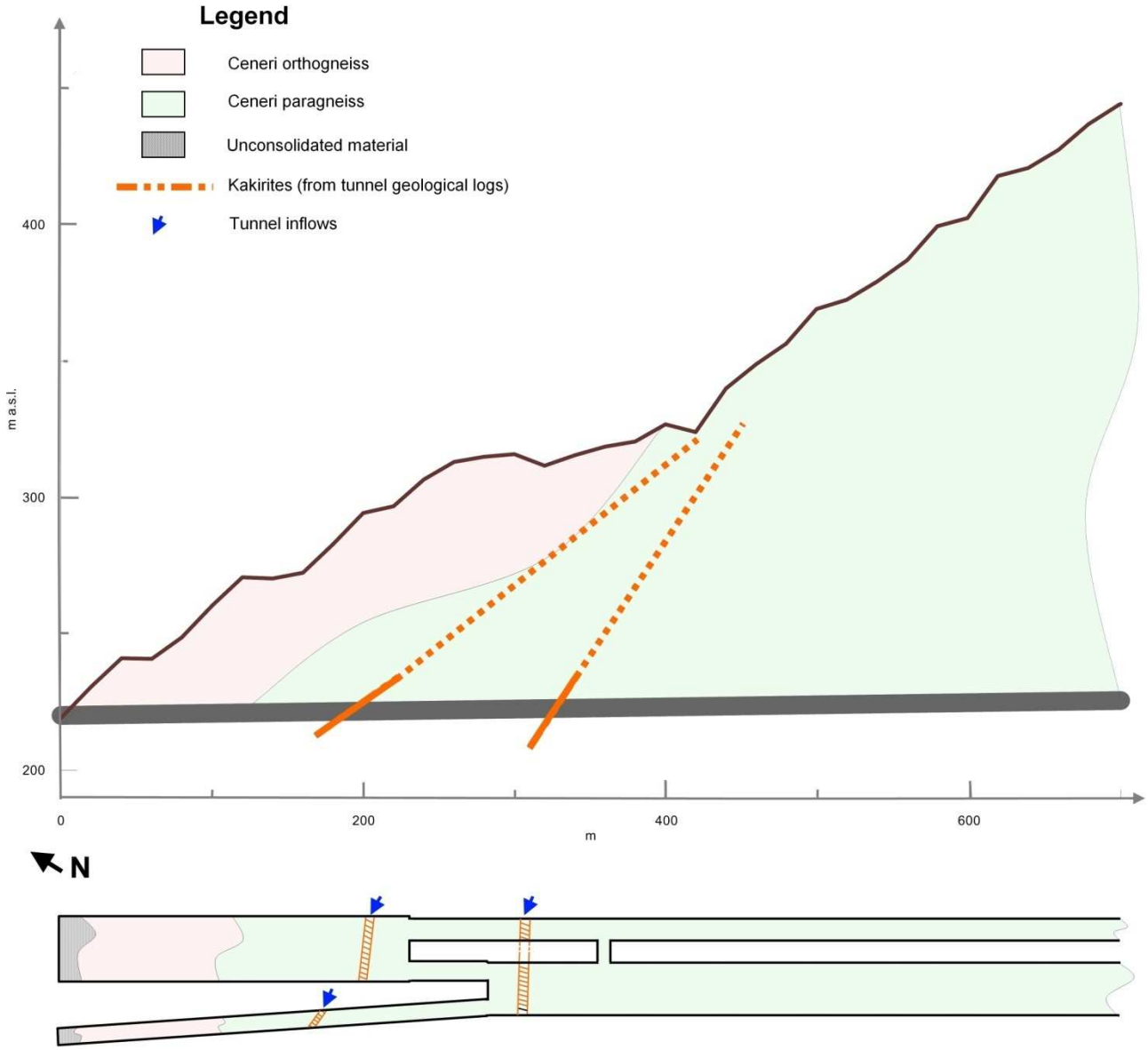

Figure 4.2 - Geological sketch section of the Monte Ceneri north portal, drawn based on geological logs obtained during tunnel drilling and kindly provided by Alptransit Inc. Above: cross section, below plan. For the classification of cataclastic structures the reader can refer to Buergi et al. (1999).

From a hydrogeological point of view, the orthogneisses and paragneisses show generally low hydraulic conductivity k [$L \cdot T^{-1}$]. The values of k at the tunnel depth, estimated on the basis of

geological knowledge, drilling, Lugeon tests, pumping tests, and variable head tests performed by tunnel designer, are in fact in the range of 10^{-7}-10^{-10} m/s. Nevertheless, the presence of two main cataclastic zones (kakirites) is associated with consistent water inflows according to Buergi et al., (1999). Moreover there is a marked change in rock schistosity that was registered upstream from the second encountered cataclastic structure shown in Figure 4.2. Downstream, rock planes have steep inclinations, generally dipping more than 60-70 degrees, while, just upstream in the kakirites the schistosity is about horizontal.

The total discharge drained by the northern portal of the tunnel is continuously registered (every half hour) since June 2010 at the tunnel exit. Moreover, weekly specific discharges of local inflows are also manually measured by Alptransit Inc. geologists allowing a complete understanding of the inflow and discharge trends. The automatically registered data of total discharge were filtered to remove statistical outliers that are probably due to external water contributions or to measuring errors. Hence, the daily average tunnel discharge shown in Figure 4.3 was obtained. In particular, from these data, two main features of the hydrogeological conditions within the tunnel can be identified:

i) the gneissic crystalline rock masses are characterized by an high permeability anisotropy. In fact, at least three distinct discharge peaks are observable. Two discharge's peaks were observed during summer 2010, when the western tube (see plan in Figure 4.2) had crossed the second cataclastic zone, and a last peak has been observed during January 2011 when the eastern tube had crossed the same cataclastic zone;

ii) the trend of total tunnel discharge is compared with the monthly precipitations collected in the Giubiasco rain gauge, belonging to the cantonal hydrologic network. The influence of rain on aquifer recharge is clearly evidenced (Figure 4.7). In fact, a low and constant increase of the drained tunnel discharge between October and December 2010 in correspondence with a humid period was observed; and similarly a constant decrease of the drained groundwater rate between January and June 2011 was measured as consequence of the tunnel drainage effects and a long-lasting drier period.

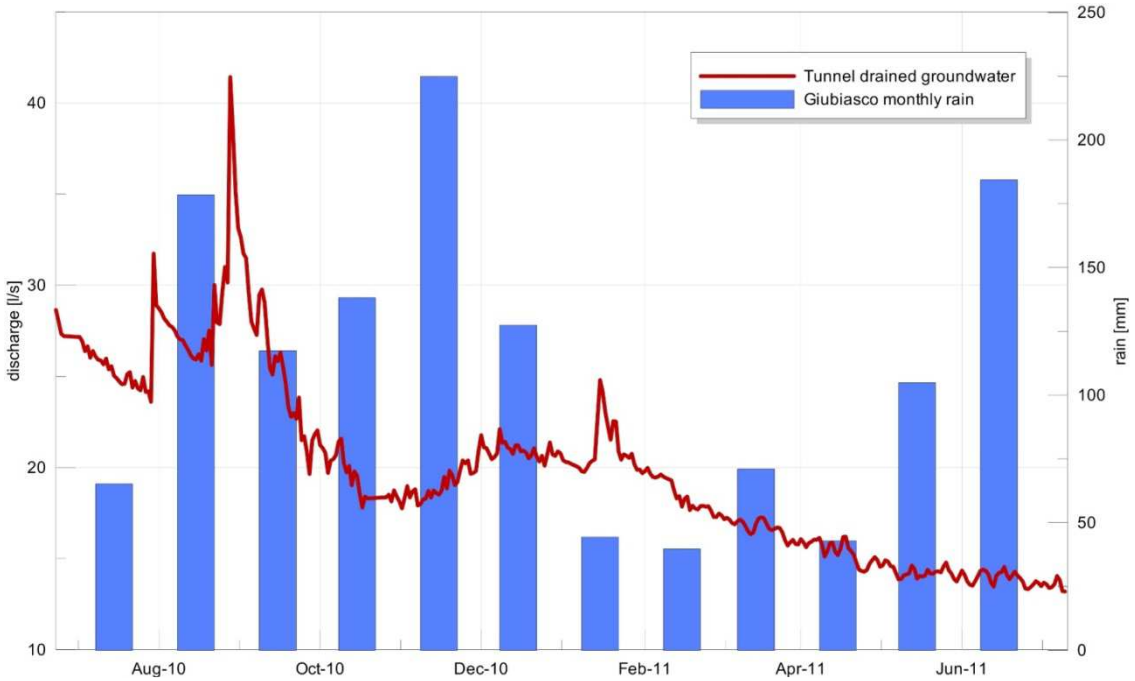

Figure 4.3 - One year trend of drained water [l/s] measured at the northern entrance of the Ceneri tunnel and corresponding monthly rain collected in the Giubiasco rain gauge.

4.2.2 San Fedele Tunnel

The Roveredo (Grisons) site, where the San Fedele tunnel has been excavated, is located at north of the Insubric Line in the lower Penninic nappes of the main alpine basement (Schmid et al, 2004) and crosses two major tectonic zones: (i) the Bellinzona zone in the west of the Traversagna

valley and (ii) the Adula zone in the east of the Traversagna valley. Both of these zones are mainly characterized by the presence of gneiss with layers of schists, amphibolites, and hornblende-gneiss. The initial parts of the tunnel are drilled through unconsolidated materials. In particular, the western portal is drilled through the alluvial materials of the Moesa valley (Valasc zone). More details about the schistosity are shown in Figure 4.4 in which the expected geological profile is reported.

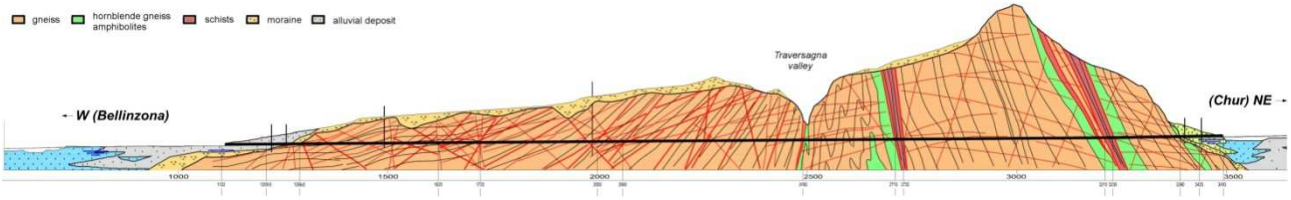

Figure 4.4 - Expected geological profile of the San Fedele tunnel (from Federal Roads Office).

The Traversagna valley represents a discontinuity between the two tectonic zones. A critical question was the presence of the Traversagna stream about 45 m above the tunnel crossing. In fact, a hydrogeological connection between the stream and the tunnel could not been excluded, even though the outcroping rocks exhibit a high resistance to the glacial and fluvial erosion, as demonstrated by the almost vertical faces formed along the river axis. Another critical zone, from a hydrogeological point of view, was the western portal that is partially (~50 m) excavated in unconsolidated material.

4.3 Geophysical surveys: equipment and methodology

The ERT method was chosen since it is able to give an image of the subsurface on the basis of the high electrical resistivity contrasts between intact, dry crystalline rock masses (1000-10’000 ohm·m) and the hydraulically active zones (10-1’000 ohm·m) as evidenced by several studies (Di Maio et al., 2007; Piegari et al. 2009; Fazzito et al., 2009).

Previous applications in the same region (Marzocchi et al., 2010) have confirmed the capabilities of this method to detect water-bearing fractures. During the first surveys, two different configurations (Wenner-Schlumberger and Dipole-Dipole) were tested showing consistently better results with the Wenner-Schlumberger configuration, which was therefore chosen for the geoelectrical campaign described in this chapter.

The resistivity measurements were performed using an IRIS-SYSCAL PRO System with a multi-electrode cable with outlet spacing of 10 m. 48 or 24 electrodes were used, obtaining total lengths of respectively 470 or 230 m. The depth of investigation, using a Wenner-Schlumberger configuration is about 1/5 of the total length at the center of the 2D profile (Kirsch, 2009). Using the PROSYS software, the apparent resistivity data were filtered to remove the acquisition errors and the rough surface topography was incorporated into the model. Finally, the RES2DINV software (Loke, 2004) was used for the inversion of the data in order to obtain a 2D resistivity profile of the probed subsurface region.

After a number of tests, a finite difference method was selected for the forward modeling part of the inversion procedure and the elements of the Jacobian matrix were calculated using the Gauss-Newton algorithm including smoothing of model resistivity (Table 4.1).

Table 4.1 - Main parameters used in the inversion process

Initial damping factor:	0.3000
Minimum damping factor:	0.0300
Robust data and model constrain:	no
Type of mesh:	finest
Model refinement:	half-width cells
Type of optimization method:	Gauss-Newton
Factor to increase model depth range:	1.0000

The result of the ERT method application is a 2D electrical resistivity section of the underground. In order to assess the accuracy of the obtained models, their consistency has to be estimated (Marescot et al. 2003). The resulting resistivity section is in fact not unique and it is fundamental to carefully consider the reliability of the obtained model. Various approaches have been proposed to treat this problem and give to the user quantitative indexes of the reliability of the model. An example is the calculation of Depth Of Investigation (DOI) index, carrying out two inversions, using different resistivity values for the starting reference model (Oldemburg and Li, 1999; Marescot et al. 2003). However, this approach is not widely implemented in the RES2DINV software. For this reason, two parameters that are normally available from the commercial version of the software (Figure 4.5) are used:

i) the Root Mean Square (RMS) statistical error;
ii) the smoothed sensitivity of blocks.

The first parameter indicates the cumulative difference, in statistical terms, between the apparent resistivity measured in field and that calculated simulating the same acquisition scheme on the 2D resistivity model and it is a good parameter of the consistency of the entire model (Tassone et al., 2010).

The smoothed sensitivity, also referred to as subsurface sensitivity, depends on the measured data set. It is a normalized measure of amount of information about the resistivity of a model block cell in which the underground is discretized for the numerical iterations needed to obtain the resistivity model (Loke, 2004). High smoothed sensitivity values depend only on the amount of available apparent resistivity data per unit area and therefore are able to identify doubtful part of the models. Hence, a transparent template over the 2D resistivity model is superimposed wherever the smoothed sensitivities are low. After a number of tests a threshold value of 0.2 has been chosen. This value allows us to identify the most probable erroneous interpolations of the inverted data and generally less reliable parts of the model. By using this approach, an area of the 2D resistivity section having low smoothed sensitivities can be identified allowing for a critical and accurate interpretation of the results coming from the inversion of field apparent resistivity data.

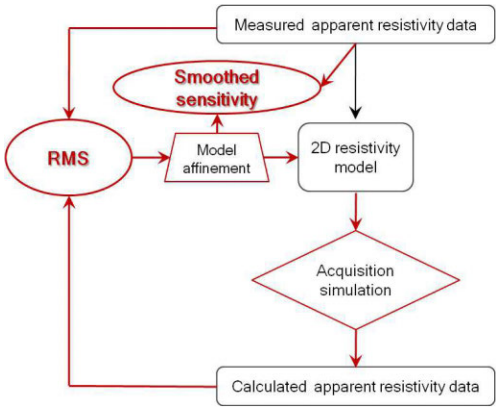

Figure 4.5 - Conceptual scheme of the inversion of resistivity data and significance of the indexes used in this work to quantify the consistency of the model.

In addition to this, the VLF-EM technique was also used. This method is able to detect steeply dipping high conductivity bodies in a resistive medium, as demonstrated by the surveys conducted in mountainous regions in the first step of the research project (Marzocchi et al., 2010).

The VLF-EM surveys were carried out using a VLF WADI ABEM instrument. After a number of tests, a spacing of 15 m between measurement points was chosen. The length of the profiles was always the same at that of the resistivity profiles; the maximum depth of investigation depends not only by this length, but it is also in inverse proportion to the conductivity of the geological media; for instance is high in presence of crystalline rock, while for more conductive media it appreciably decreases (Al-Oufi et al., 2008).

Different filter techniques are available in the literature (Fraser, 1969; Karous and Hjelt, 1977) and allow to conveniently analyse VLF-EM field data for obtaining qualitative information of the

underground. The Fraser filter has two effects: (i) to reduce the noise level and (ii) to give to the user a more understandable scattered data graph with peaks in correspondence of the underground conductive structures. The Karous-Hjelt filter allows us to obtain a 2D pseudo-section contouring the data of percent of current density that can flow in the underground; high current densities are typical of conductive zones, while low are typical of the more resistive ones. This pseudo-section allows for a qualitative interpretation of the subsoil and, in this work, has been compared with the resistivity 2D model. The WADI® module was used to download the data from the instrument to the computer, while specifically developed numerical codes was used to filter the raw VLF-EM data and obtain pseudo-sections and curves that may be qualitatively compared with the results of the ERT measurement.

4.4 Results and interpretations

4.4.1 Monte Ceneri tunnel north portal

Above the northern portal of the Ceneri base tunnel 5 surveys were made. Three of them were conducted in March 2010 during the first phases of tunnel excavation, which, from a hydrogeological point of view, is likely to correspond to mildly disturbed conditions. Conversely, the last two profiles have been acquired in October 2010 in completely disturbed conditions, as clearly evidenced by the tunnel water discharge graph (Figure 4.3). The locations of the surveys are shown in Figure 4.6. In Figure 4.7 the resistivity sections and the filtered VLF-EM data of the initially carried out surveys (Vigana1, Vigana2 and Vigana3) are shown. On the Vigana1 resistivity section the presence of a local perched aquifer corresponding to a glacial moraine can be observed in the middle of the resistivity section. Most likely, it is the origin of groundwater arriving in the tunnel. The first part of the survey (0-200 m) has been conducted on the outcrop rock as evidenced by the higher electrical resistivity values.

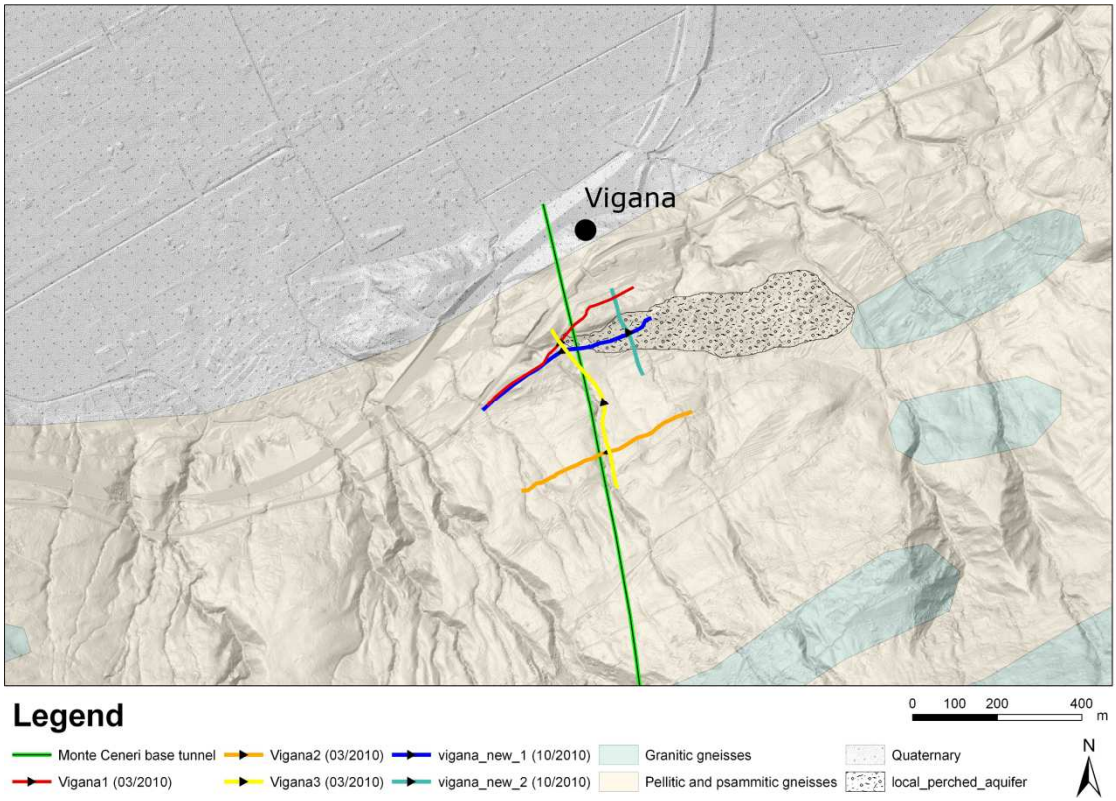

Figure 4.6 - Location of the five geophysical surveys conducted above the north portal of the Ceneri base tunnel (green line). An arrow individuates, for each profile, the survey sense.

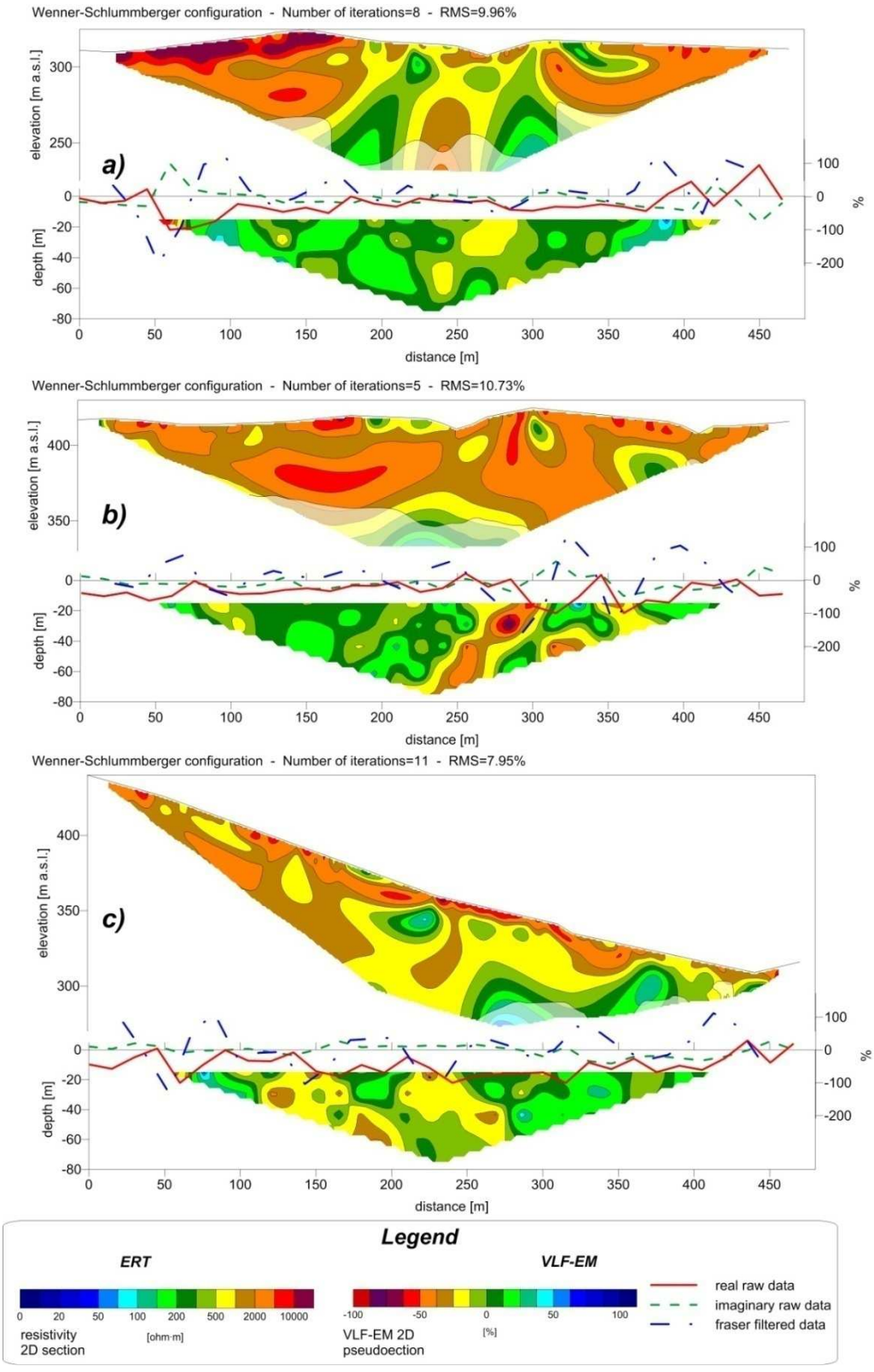

Figure 4.7 - Results of geophysical surveys conducted above the north portal: a) Vigana1; b) Vigana2; c) Vigana3. For each survey, above the 2D electrical resistivity section result of the geoelectrical survey, and below a pseudo current density cross-section result of the VLF-EM survey are reported. Superimposed to the VLF-EM pseudosection is also reported the raw data (real and imaginary component) and those filtered with the Fraser (1969) algorithm (only real component). In both the cases a similar color scale has been used: in blue are represented the more conductive zones, while in red the most resistive ones.

The Vigana2 resistivity section is generally characterized by higher electrical resistivity values. An increasing of conductivity, even though with a high level of uncertainty evidenced by the low smoothed sensitivity values, seems to be present at greater depth. The Vigana3 resistivity section,

resulting from a survey conducted along the slope direction is the most interesting. In fact, it seems able to identify the more humid zones that correspond effectively to the segment of tunnel where consistent water inflows have been registered during tunnel excavation.

A qualitative interpretation of the data coming from the above described surveys (Vigana1, Vigana2 and Vigana3) is shown in Figure 4.8 reconstructing the expected hydrogeological situation along the Vigana3 profile. The integration of the Vigana2 and Vigana3 are characterized by higher electrical conductivities at depth. This can be due to limited electric current flow through the weakly conductive fractured rock masses present at the surface. However, considering the generally acceptable smoothed sensitivity of geoelectrical data and the usually low RMS errors, the most probable hypothesis is given by a general increase of the water content in fractured rock masses with depth shown in Figure 4.8. This evidence corresponds to the data coming from piezometric head measurements conducted in the available geological inspection boreholes.

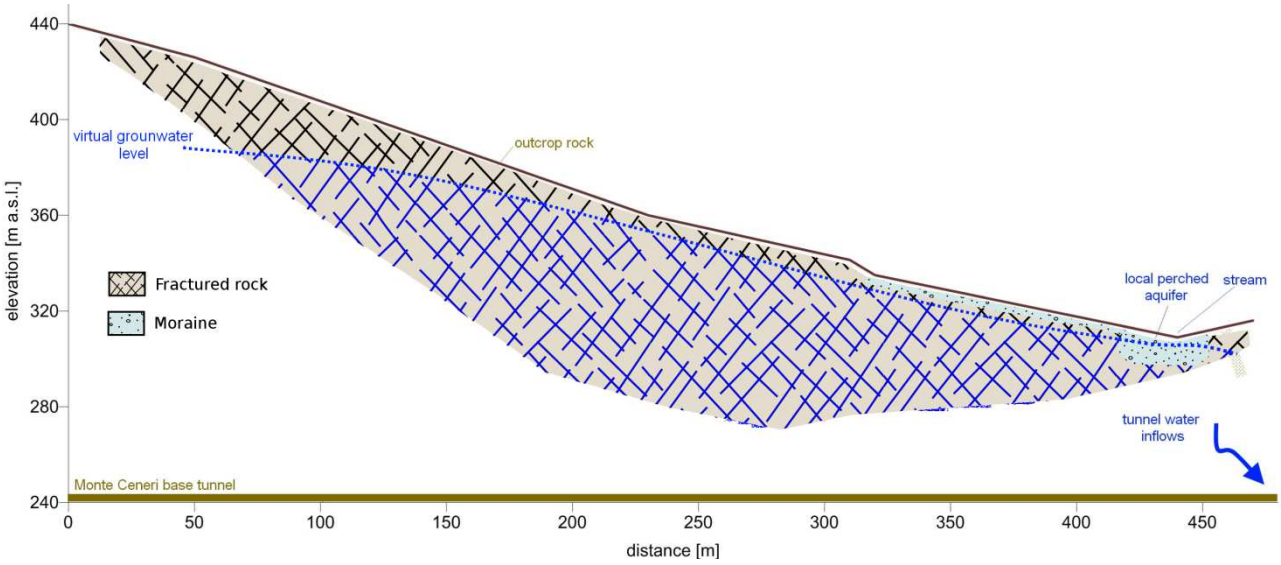

Figure 4.8 - Hydrogeological interpretation of the ERT results represented along the Vigana3 survey

The results of the first campaign (Figure 4.7) indicate that the VLF –EM method, in this zone, is not particularly suitable to the definition of hydrogeological conditions. This is probably due to the presence of infrastructures in the underground and also aerial, which cause a high level of ambient noise. Conversely, more detailed information concerning the presence of water bearing fracture zones are available from the ERT profiles, which are able to clearly identify the electrical conductive zones where groundwater is most likely present. For this reason, not any VLF-EM surveys were made in the second phase of the work and instead the efforts were concentrated on the electrical resistivity investigations.

The local perched aquifer identified by the three resistivity sections is placed just behind an antislope, where a stream flows. With the objective to better understand the mechanism of interferences between tunnel and the individuated local perched aquifer, two additional geoelectrical surveys were carried out above the local aquifer (Figure 4.6) and results are shown in Figure 4.9.

A first survey, named Vigana_new_1, has been conducted parallel to the slope. The second half of this survey was conducted practically on the same location of the Vigana1, while the first half, instead of above the outcrop rock, was carried out remaining above the local aquifer, visible in the middle of the Vigana1 and at the end of the Vigana3 resistivity sections.

A second survey has been conducted on the slope direction intersecting the stream and the corresponding humid zone. Unfortunately, due to logistic problems, the length of this last profile is only 230 m. The results of these two geoelectrical surveys add useful information in order to better define the geological model. In particular from the Vigana_new_1 resistivity section, the local perched aquifer is clearly visible in the first half of the section, as well as in the middle of the resistivity section. Comparing the results with which of the survey conducted few months before

(Vigana1), the tunnel drainage effect seem visible by a decreasing, even though low, of the electrical conductivity in the middle of the profile. Moreover, from the Vigana_new_2 resistivity section, groundwater bearing fracture zones seem clearly visible as an electrical conductive zone located below the outcrop rock, starting from the local aquifer. A possible hydrogeological interpretation of the Vigana_new_2 resistivity section is shown in Figure 4.10. The represented fracture zone can be linked to that observed within the tunnel at depth, which explains the constant and consistent groundwater inflows registered in the tunnel (Figure 4.3). The local perched aquifer is in fact wide and a constant recharge is probably furnished by the stream that flows on the slope (Figure 4.18).

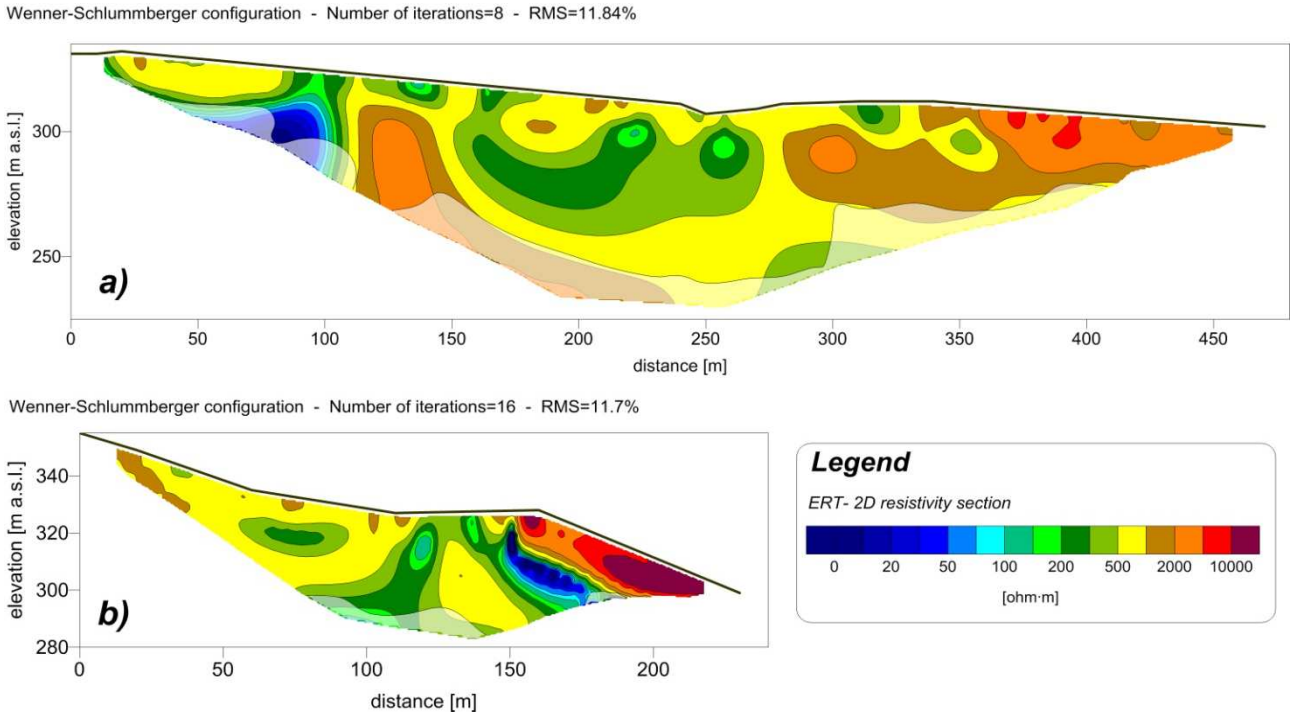

Figure 4.9 - 2D electrical resistivity sections of the two last carried out surveys. a) Vigana_new_1, b) Vigana2_new_2

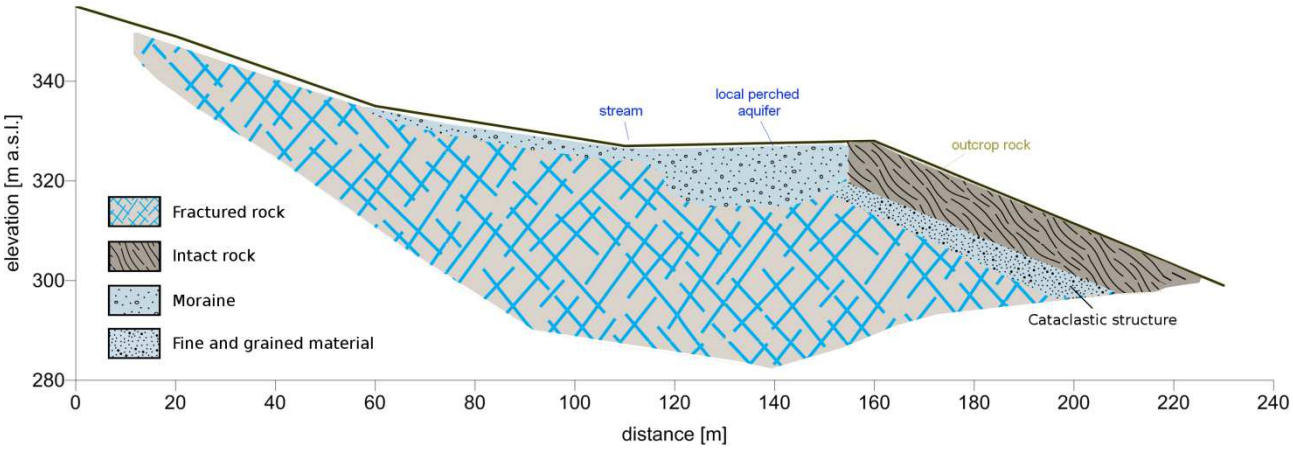

Figure 4.10 - Hydrogeological interpretation of the ERT results represented along the Vigana_new_2 survey.

4.4.2 San Fedele Tunnel

Parallel to the San Fedele Tunnel six geoelectrical surveys were acquired. The morphology of the area surrounding the tunnel is characterized by several escarpments and an in general near-vertical slope. Especially at the NE side of the tunnel, where it crosses the Traversagna valley, it is practically impossible to carry out surveys exactly above the tunnel axis. Therefore an image of the underground environment exactly where the tunnel pass through has not been possible. The location of geophysical survey lines and tunnel axis is shown in Figure 4.11

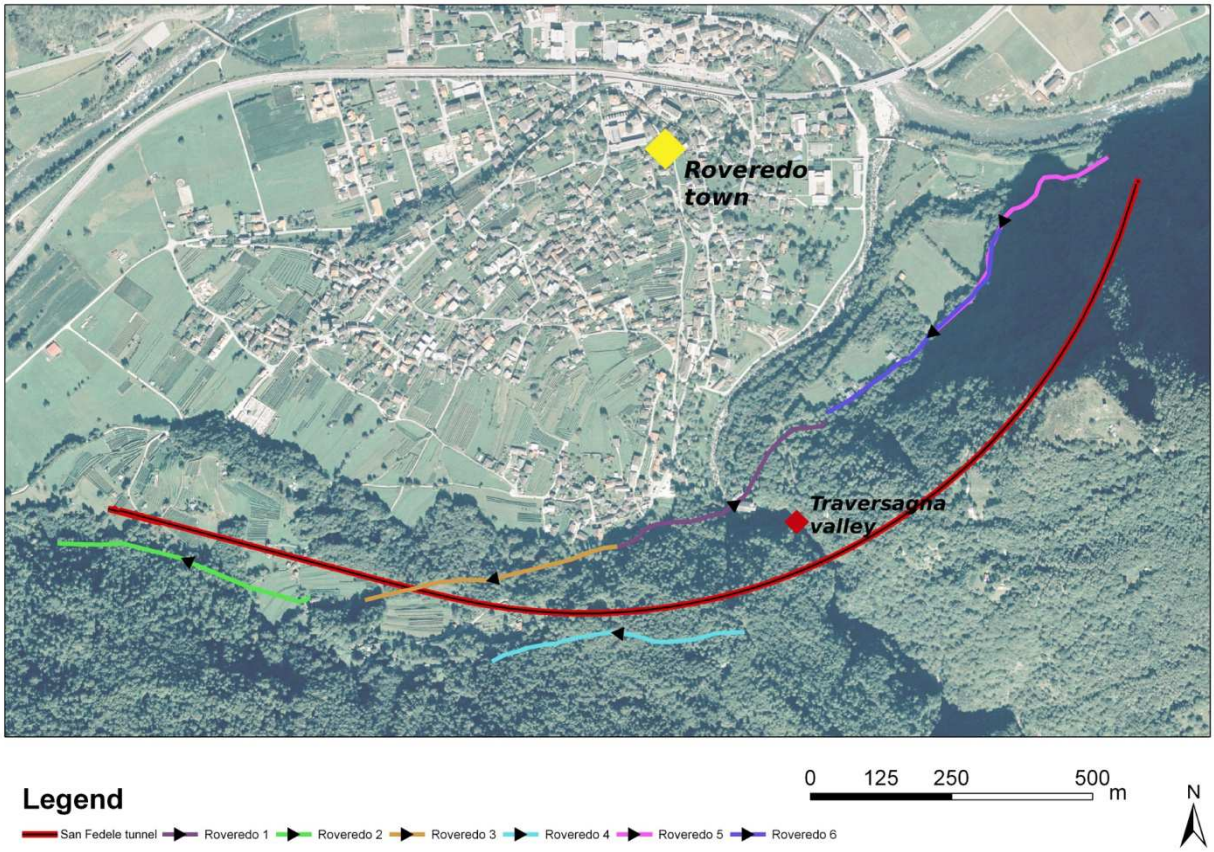

Figure 4.11 - Geoelectrical surveys and tunnel locations

All the surveys are 470 m long. Most of the geoelectrical resistivity sections (Roveredo3, Roveredo4, Roveredo5 & Roveredo6) show high electrical resistivity values typical of the low permeable rock masses. A few easily recognizable noise effects are found in the last two profiles (Roveredo5 & Roveredo6), because of the presence of a metallic pipe in the underground. The VLF-EM data do not show any anomaly, with a flat signal and showing quasi uniform pseudo-current density cross-sections. Obviously, ERT results are clearer and give more detailed informations about the rock permeability. For instance, in almost all of the 2D resistivity sections, a general decrease of the resistivity with depth was observed. Considering the generally acceptable smoothed sensitivity of geoelectrical data and the usually low RMS errors, the most probable hypothesis is given by a general increase of the water content in fractured rock masses with the depth. For a generally dry period, such as the 2010 winter (IST, 2011), this seems to be a realistic assumption.

At the time of writing, the geological inspection tunnel (small diameter of 4.5 m) had been completely excavated and geological logs collected during tunnel drilling are available. Geophysical results are in good agreement with the hydrogeological conditions found in the tunnel. Effectively, the tunnel drilling has been conducted in almost dry conditions. No consistent water inflows were measured crossing the fractured rock masses neither in the Bellinzona nor in the Adula zones. Only occasional lateral drippings were encountered, but obviously their detection has been practically impossible with the resolution of the resistivity measurements.

In Figure 4.12 the most interesting results of the conducted geophysical surveys (the Roveredo1 and Roveredo2 profiles) are shown. The Roveredo1 survey was used to investigate the hydrogeological conditions corresponding to the Traversagna valley crossing; while the Roveredo2 survey was used, in the region of the south-west portal, to investigate the position of the interface between unconsolidated material and fractured rock masses in place.

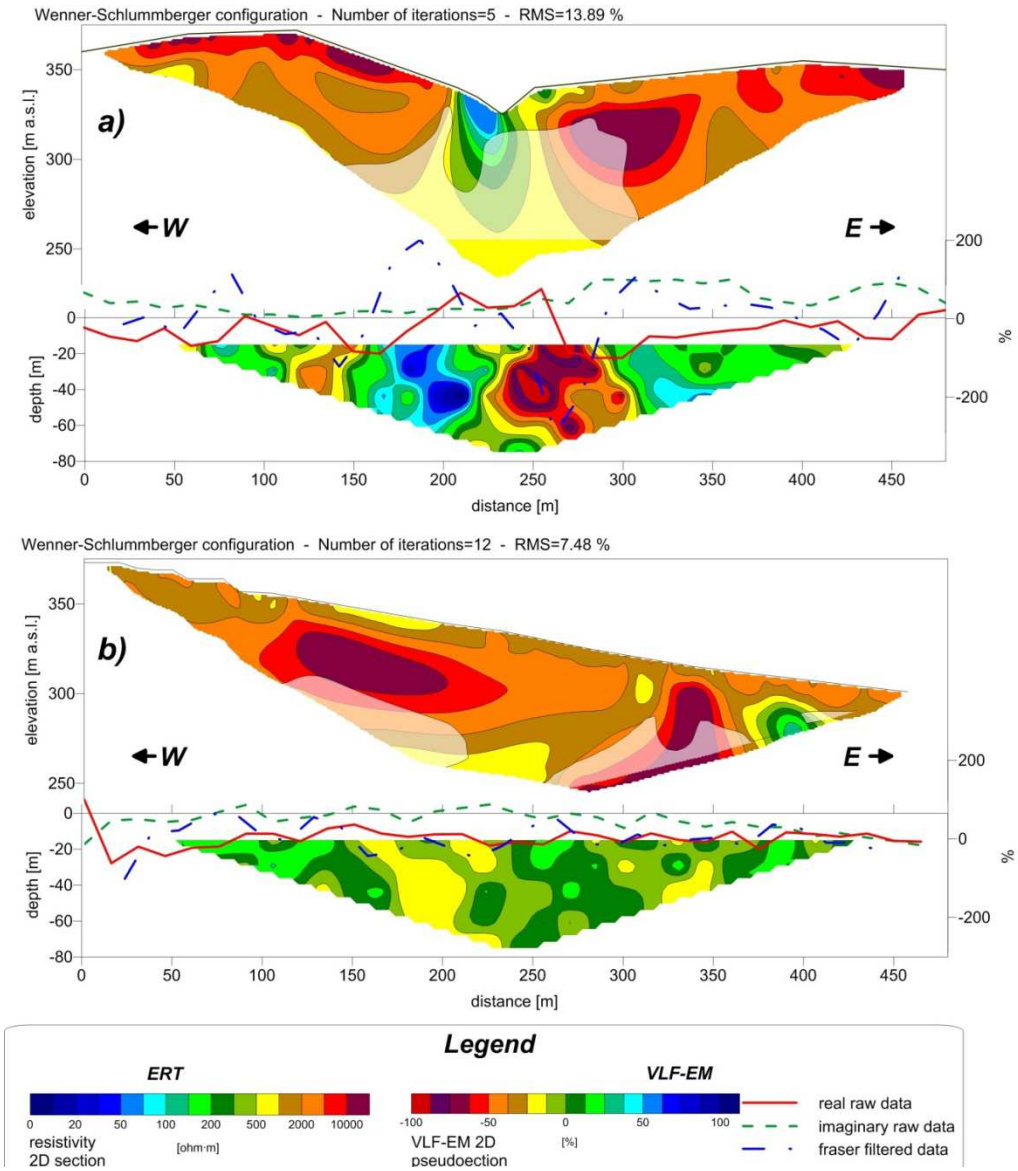

Figure 4.12 - Results of two geophysical surveys conducted close to the San Fedele tunnel: (a) the Roveredo1 profiles, conducted crossing the Traversagna valley, (b) the Roveredo2 profiles carried out close to the South-West portal. Details concerning the graphical representation are already described in Figure 4.7.

Concerning the Roveredo1 survey, the tunnel crosses the Traversagna valley at a depth of about 45 m under the river channel. Where the tunnel passes through, the valley is practically inaccessible, and hence the geophysical exploration has been carried out at south respect of the tunnel axis (Figure 4.11). Moreover, because of the terrain morphology, also in the selected location, a number of electrodes, in particular the three in correspondence of the river crossing, are not used. For this reason, the smoothed sensitivity in the middle of the profile is lower than the threshold value of 0.2. Nevertheless, the error between obtained and calculated apparent resistivity data is relatively low (RMS=6%), denoting a good agreement of obtained resistivity model with field apparent resistivity collected data. The 2D resistivity section (Figure 4.12) seems confirm the presence of a disturbed zone at the left side of the valley, characterized by lower resistivity values (100-500 ohm·m). This conductive zone is confined to the uppermost part of the underground, while at depth the electrical resistivity increases, probably in response to the decreasing water content in the fractured rock masses. In this case, there is a partial correspondence with VLF-EM data. In fact, the possible disturbed zone identified at the left side of the stream is also noticeable from the VLF apparent current density pseudo-section as well as from peak of Fraser filtered data (Figure 4.12). Obviously, the geometry of the conductive zone is not well defined as showing the 2D resistivity section and it is impossible observe the conductivity increasing with the depth.

A hydrogeological interpretation of the Roveredo1 survey is shown in the following Figure 4.13.

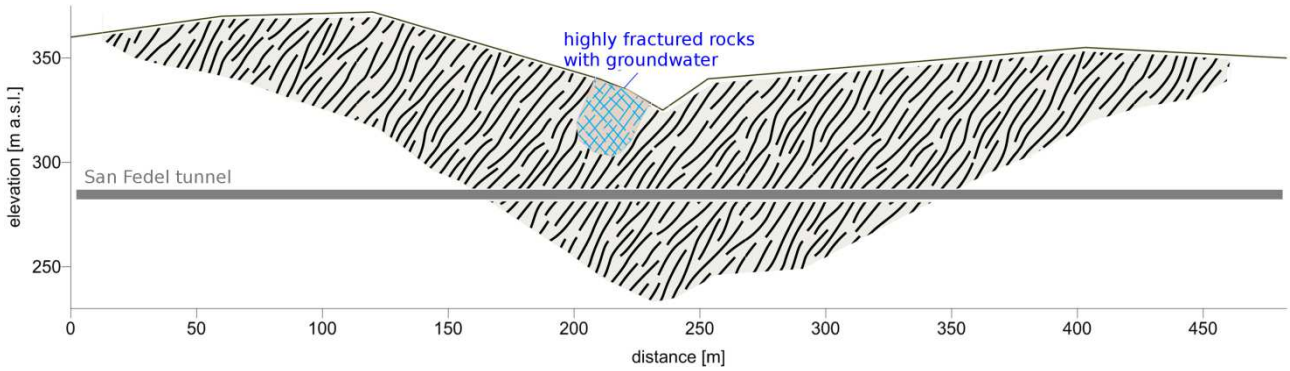

Figure 4.13 - Qualitative interpretation of results of Roveredo1 geophysical surveys.

This interpretation is in agreement with the geological logs collected during the drilling of the tunnel. The discontinuity between the two tectonic zones has, however, been confirmed by a change of the rock schistosity, but water inflows are not been encountered.

For the Roveredo 2 survey the interpretation is shown in Figure 4.14. The expected position of the fractured rock in place and of the unconsolidated soil that is placed above it, have been represented. A conductive zone in the unconsolidated material is visible; hence it can be interpreted as the presence of groundwater within the unconsolidated alluvial materials of the Moesa valley, outlining a supposed position of the water table shown in Figure 4.14

VLF-EM data are not able to identify the position of the interface between unconsolidated materials and fractured rock masses. In fact, it is important to point out that for the purpose of identifying the different layers of soil and the near horizontal interfaces only the ERT is an adapt method, while VLF-EM is only able to identify steeply dipping high conductive bodies in the underground.

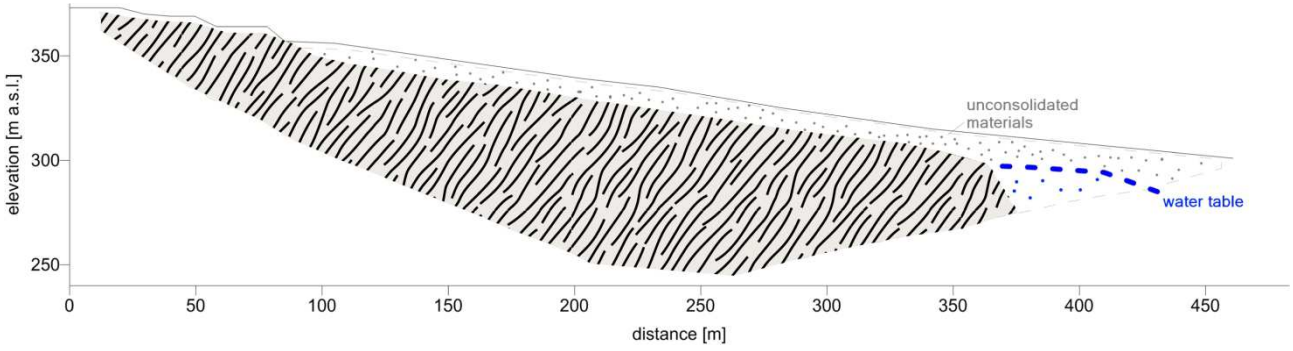

Figure 4.14 - Qualitative interpretation of results of the Roveredo 2 geoelectrical survey.

Also in this case, the tunnel geological logs are in good agreement with interpretations derived from the geoelectrical results. In particular, the interface between bedrock and unconsolidated material has been correctly imaged. The drilling of the western portal has been conducted below the piezometric level. Nevertheless, few water inflows are encountered at the interface between the alluvial material and the crystalline rocks, which, close to the surface, are generally more fractured and characterized by a higher permeability. This consideration is in agreement with the interpretations of the resistivity sections. It is important to point out that the position of the water table within the unconsolidated material, represented in Figure 4.14 seems slightly overestimate the real position of the water table. In fact, at the time of construction, it is lightly lower (~ 20 m below the terrain compared to the ~15 m that were interpreted from the resistivity 2D section). However, the survey line positions (Figure 4.11) are not exactly above the tunnel axis, and this fact is the probable reason of the slight difference between the interpreted and the real water table position.

4.5 Conceptual model of the water circulations and tracer test

When excavating the north portal of the Monte Ceneri base tunnel, consistent water inflows were observed (Figure 4.3). Integrating the results of geophysical surveys, a conceptual model of groundwater circulations was obtained and is shown in Figure 4.15.

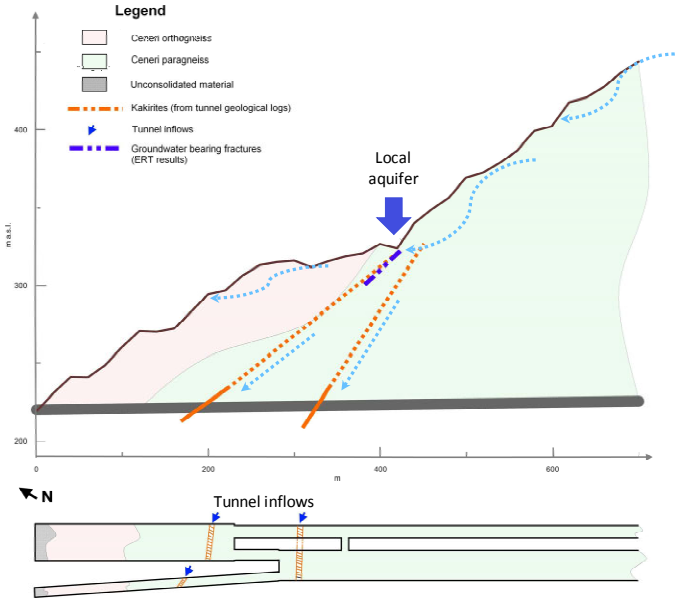

Figure 4.15 - Qualitative interpretation of groundwater circulations in the area where the northern portal of the Ceneri base tunnel is excavated (above: cross section, below: plan). The model is obtained from results of the geophysical surveys as well as of artificial tracer test and is in good agreement with tunnel geological logs.

The water of creeks and groundwater circulating in the highly fractured gneisses of the uppermost part of rock have a recharge effect on a perched local aquifer localized above the tunnel axis. Hence groundwater present in this local aquifer reach the tunnel through fractures present upstream of the cataclastic structures (kakirites) crossed by the tunnel, causing the consistent water inflows registered during tunnel drilling.

This model is in accordance with the tunnel geological logs collected during tunnel drilling in correspondence of the cataclastic structures, as well as with surface geomorphological observations.

In particular, Figure 4.16 shows the position of the first fault. The geometry of the structure (strike and dip) is in agreement with the direction of the conductive zone identified by the Vigana_new_2 resistivity section (Figure 4.9 and Figure 4.10). Moreover, there are two further hydrogeological observations that are also in agreement with the previous formulated conceptual model:

i) the western tube was excavated in the first months of 2010, while the eastern tube has been drilled only after more than one year; the initial water level in this second tube at the time of drilling has been obviously lower than in the first excavated tunnel, nevertheless inflows are permanently observed in correspondence of the fault zone until concluding the tunnel excavation;

ii) at the time of writing , the two tubes are completely excavated. A perceptible increasing of the water level about in correspondence of the fault zone is however clearly visible, even though the drawdown of the water table reach about the bottom of the tunnel.

Figure 4.17 shows the position of the second main cataclastic zone. The fault (75 degree of dip) is roughly perpendicular to the tunnel axis; just upstream these kakirites, the most consistent water inflows are registered drilling the tunnel tubes and also after the excavation of both the tunnel tubes (the eastern and western ones). An unambiguous observation, in agreement with the proposed model, is that groundwaters infiltrates from the eastern wall of the tunnel. In fact groundwater inflows were intercepted since summer 2010 in the western tube, while drilling the eastern tube, these waters have completely intercepted within this second excavated tube.

Also in this case, it is clear that the water inflows are due to groundwater bearing fractures. In fact, even though the drawdown of the water table is generally arrived as far as the bottom of the tunnel, water inflows upstream this kakirite zone are still consistent and about constant.

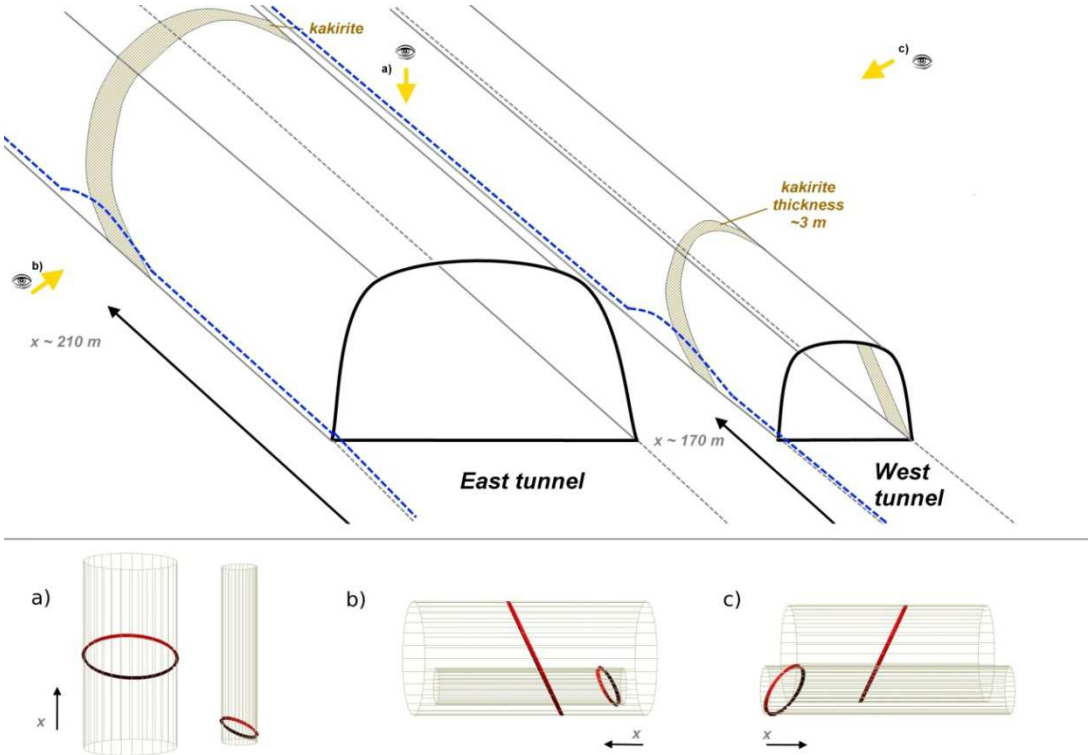

Figure 4.16 - The first cataclastic zone (kakirites) encountered at the progressive distance of about 170 m from the tunnel portal in the western tunnel tube, and of about 210 m in the eastern tube. Above, a 3D schematic view of the fault is shown, emphasizing the hydrogeological logs completely excavated the two tubes. Below, various geometrical views of the fault respect of the tunnel axis are represented. The structure geometry differs in the two tubes.

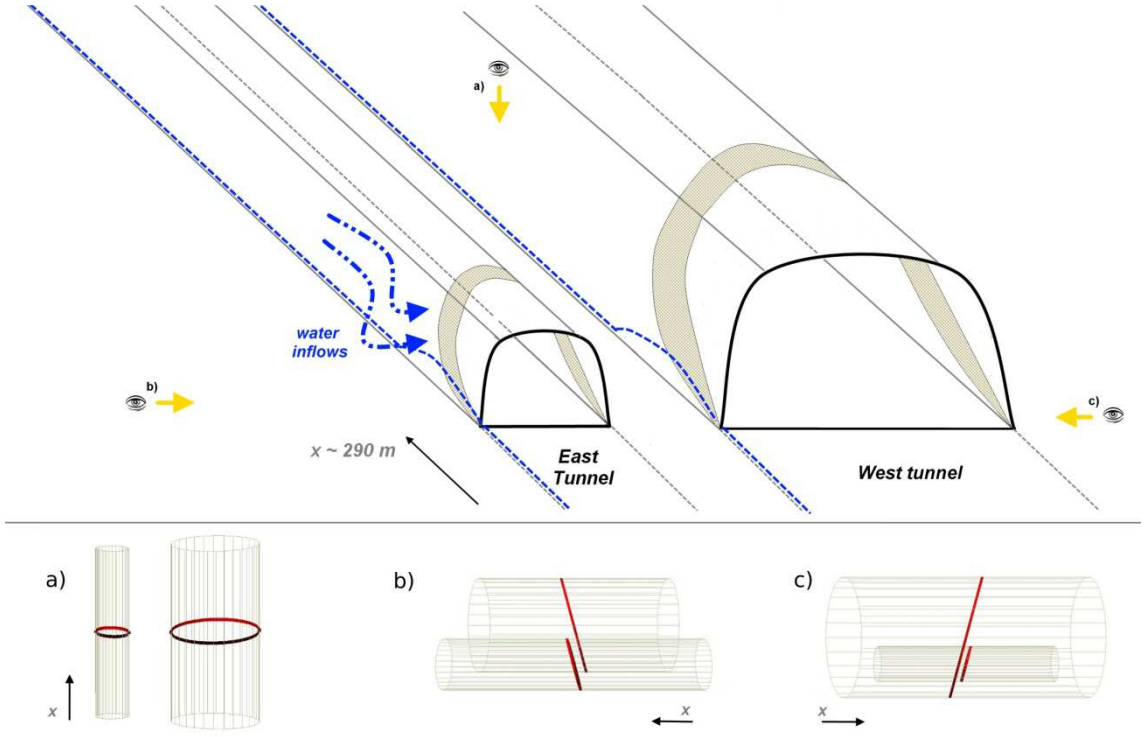

Figure 4.17 - The second cataclastic zone (kakirites) encountered at the progressive distance of about 290 m from the tunnel portal. Above, a 3D schematic view of the fault is shown, emphasizing the position of the consistent water inflows registered just upstream the cataclastic structure, also at the end of the tunnel drilling. Below, various geometrical views of the fault respect of the tunnel axis are represented.

However, an artificial tracer test was performed in order to have a further check of the hydrogeological model verifying the supposed interconnection between the local perched aquifer at the surface and the tunnel. Practically two different tracers were injected at two different times on the same point (Figure 4.18 and Figure 4.19), at the northern limit of the perched local aquifer, close to the outcrop rocks that form the above mentioned antislope. In particular 200 g of fluorescent dyes uranine (CAS 518-47-8) was injected on 16 February 2011 and a 1 Kg of sulforhodamine G (CAS 5873-16-5) on 6 April 2011. The two tracers were chosen because of their favorable physical properties and proven safety for humans and nature (Käss,1998; Behrens et al., 2002).

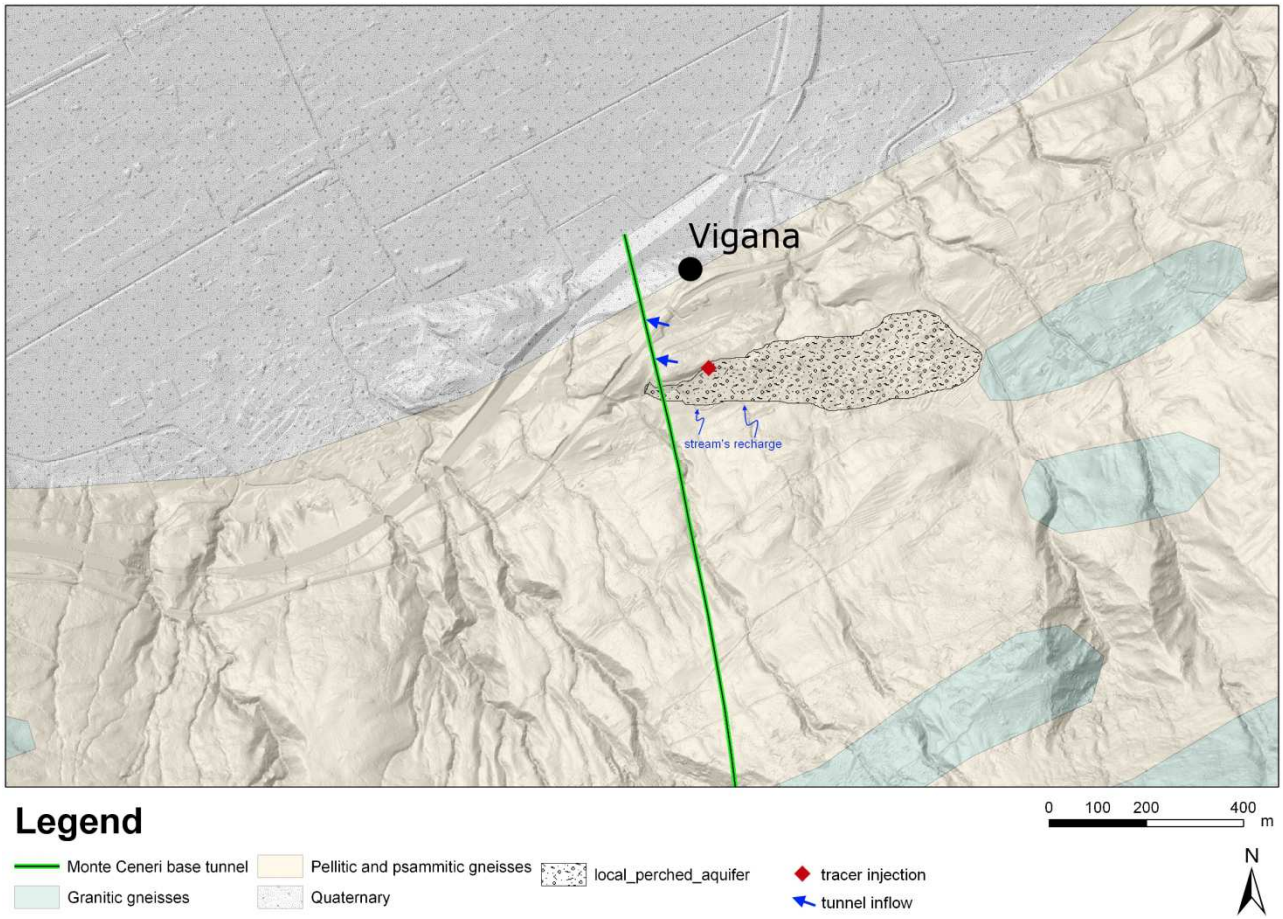

Figure 4.18 - Resulting hydrogeological model superimposed on the geological map (1:250,000). The perched local aquifer is probably recharged by stream evidenced by blue arrows. The location of the tunnel inflows (Figure 4.16and Figure 4.17) and tracer injection point are also represented.

As shown in detail by Figure 4.19, monitoring inside the tunnel has included:

i) two fluorometers (Schnegg and Flynn, 2002) for a continuous measurement of the tracer concentrations. They were placed in order to get an optimal result at the exit of two geological inspection boreholes where the two main inflows have been drained;
ii) eight charcoal bags placed at almost all of the main different water inflows;
iii) finally, due to few problems of ferrous hydroxide ($Fe(OH)_2$) within the optical tube of a fluorometer also a manual sampling of water inflows was performed since April 2011 in correspondence of the two fluorometers.

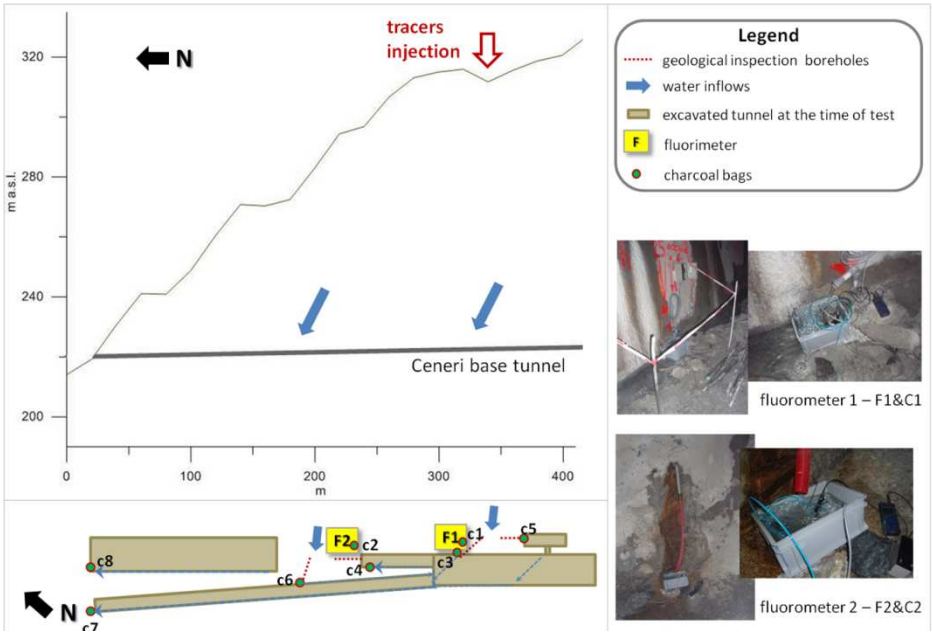

Figure 4.19 - Scheme of the tracer test. The point where tracer are injected and measurement sites are evidenced respectively in the cross section and in the plan.

Charcoal bags and manual samples were analyzed at the Hydrogeologic Center (CHYN) of the University of Neuchatel (Switzerland) with a specific spectrofluorometer. In particular, the charcoal bags were dried, dipped in an eluent for 12-14 h (10 g KOH per 100 ml of 96% ethanol) and then analyzed with the spectrofluorometer, while 40 ml of water for each collected manual samples are directly analyzed with the spectrofluorometer.

Figure 4.20 shows the signal registered in the fluorometers and in the manual samples; while Figure 4.21shows measured concentrations in the charcoal bags.

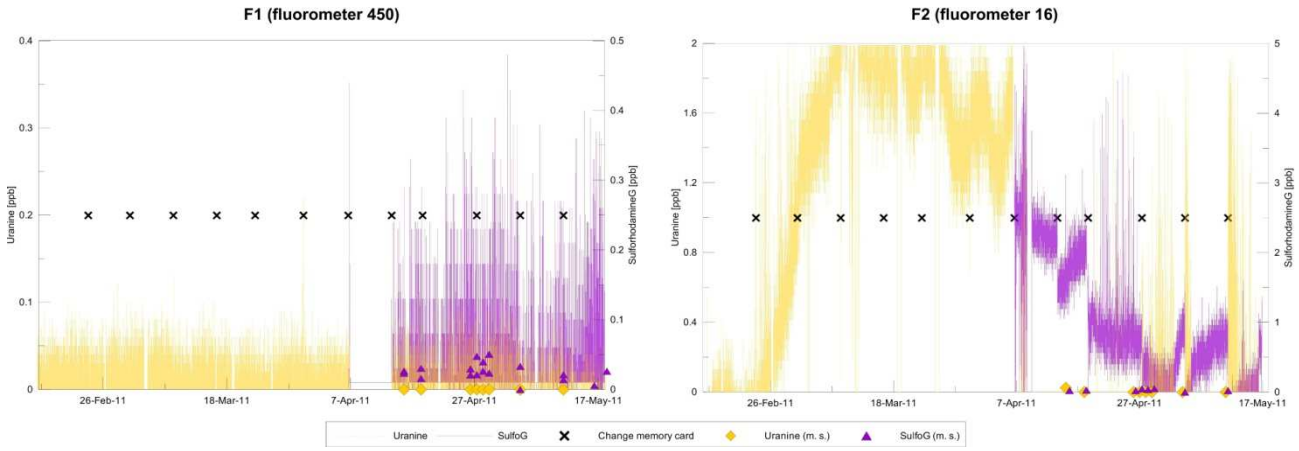

Figure 4.20 - The results of the two fluorometers used for the tracer test and of analysis on the manual samples. The detection limit is 0.01 ppb for the uranine, while 0.05 for the sulforhodamine G. The high signal of tracers registered in the F2 fluorometer are mainly due to the formation of a ferrous hydroxide layer of the optical tube. Since April, every week, when the memory card was changed (black crosses superimposed on the graphs) the optical tube was partially cleaned with a brush, causing instant decreasing of the read values, clearly visible on the right graph. The manual samples analysis, reported on the same graph and on Table 4.2 confirm the anomalous signal registered by fluorometers.

From the data registered in the first fluorometer (F1) any signal of neither uranine nor sulforhodamine G have been detected. Also in the manual samples collected after the second tracer injection (Table 4.2), the uranine is not yet detectable and the sulforhodamine G is below the detection limit (0.05 ppb). Nevertheless the uranine concentrations in the fluocaptors (Figure 4.21) placed in correspondence of the first fluorometer (C1) and close to this (C3) seem to demonstrate that the uranine, even though in low concentrations, is arrived at the sampling points, placed

upstream the second cataclastic zone (Figure 4.17). Conversely, no sulforhodamine G has been detected in charcoal bags.

Concerning the second fluorometer (F2), the signal is highly disturbed due to a Fe-dioxide layering of its optical tube. This layer causes an increasing of the turbidity in the water and consequently anomalous signals. From manual samples (Table 4.2) the sulforhodamine G seem arrived only in very low concentrations at the end of April (about one month since the tracer injection). Finally, in the charcoal bags (C2) the Uranine was detected since the first week after tracer injection, with a "peak" one month after, as shown in Figure 4.21. On the contrary, no sulforhodamine G has been detected in the C2 charcoal bag.

Table 4.2 - Manual sample analysis

Location	Date	Uranine (ppb) Detection limit = 0.01 ppb	Sulfo G (ppb) Detection limit = 0.05 ppb
F1	15/4/2011	n.d.	0.026
F1	18/4/2011	n.d.	0.016
F1	26/4/2011	n.d.	0.029
F1	27/4/2011	n.d.	0.021
F1	28/4/2011	n.d.	0.026
F1	29/4/2011	n.d.	0.024
F1	4/5/2011	n.d.	0.033
F1	11/5/2011	n.d.	0.014
F1	16/5/2011	n.d.	0.006
F1	18/5/2011	n.d.	0.026
F1	26/5/2011	n.d.	0.025
F1	30/5/2011	n.d.	0.015
F1	7/6/2011	n.d.	0.031
F1	14/6/2011	n.d.	0.022
F1	21/6/2011	n.d.	0.023
F1	30/6/2011	n.d.	0.014
F2	15/4/2011	0.024	0.0231
F2	18/4/2011	n.d.	0.0300
F2	26/4/2011	n.d.	0.0206
F2	27/4/2011	n.d.	0.0475
F2	28/4/2011	n.d.	0.0393
F2	29/4/2011	n.d.	0.0503
F2	4/5/2011	n.d.	n.d.
F2	11/5/2011	n.d.	0.0211
F2	23/5/2011	n.d.	0.0281

The first injected tracer (uranine), even though in low concentrations, has effectively arrived in correspondence to the two inflows, confirming the proposed hydrogeological model. On the contrary, the second injection with sulforhodamine G failed. This can be due to a dry period after the tracer injection and to the fact that tunnel drainage effects, by the time of test, were more pronounced. Finally as demonstrated by previous literature works (Schudel et al., 2002; Vincenzi et al., 2009), the sulforhodamine G exhibits often higher adsorption effects compared to uranine.

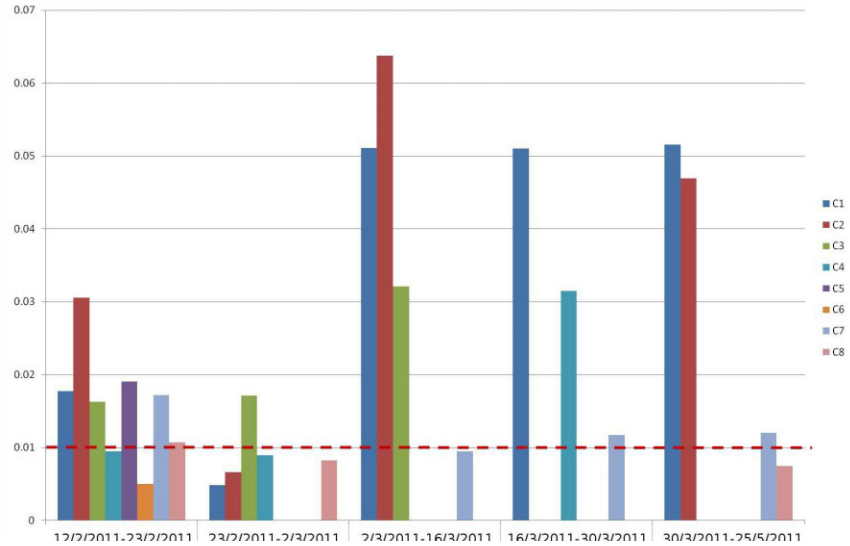

Figure 4.21 - Uranine concentrations in charcoal bags (the detection limit is 0.01 ppb). Sulforhodamine G has been analyzed only after the injection, thus in the last period (30/3-2011 – 25/5/2011), and no tracer has been detected.

4.6 Conclusions

The application of 2D ERT and VLF-EM techniques was tested for identifying water-bearing zones in two case studies in the Southern Switzerland: the north portal of the Monte Ceneri base tunnel (Ticino) and the San Fedele tunnel (Grison). In both cases, geological logs collected during tunnel drilling allow to check whether hydrogeological interpretations are in agreement with field data. A tracer test has also been conducted on the north portal of the Monte Ceneri base tunnel to verify a hydrogeological connection between a local perched aquifer and the tunnel.

At the north portal of the Ceneri base tunnel, conductive zones in the 2D resistivity sections were identified. They can be related to the presence of water upstream of the cataclastic structures identified by geological logs during the tunnel excavation. From geoelectrical surveys water-bearing fractures were identified. They act as preferential pathways for groundwater flows, especially in the upper zone of the gneiss masses where the north portal has been excavated. A hydrogeological connection between a local perched aquifer consisting of moraine deposit and the deeper tunnel is observed. Thence, the conducted tracer test has confirmed the assumption obtained in the light of resulting 2D resistivity sections. The used tracer, even though in very low concentrations, arrived from the local aquifer to the tunnel, since the first week after tracer injection, with a concentration peak one month after.

For the San Fedele tunnel, geological logs collected during tunnel drilling have generally confirmed the hydrogeological interpretation available from geophysical results. Most of the 2D resistivity sections denote high electrical resistivity typical of the fractured gneiss rock with low water content. Indeed, the tunnel crossed almost dry fractured rock masses. The Roveredo1 ERT profile successfully predicted that, at the designed depth, the crossing of the Traversagna valley would be on dry conditions, even though both the ERT and VLF-EM surveys detected a more conductive zone on the left (W) side of the Traversagna valley, probably caused by the tectonic discontinuity placed in the valley and effectively shown from geological tunnel logs.

In agreement with the finding for Roveredo2 geoelectrical survey, the expected water inflows are located at the rock/unconsolidated material interface, which is also in agreement with tunnel hydrogeological logs. Certainly the occasional lateral dripping associated with the presence of local discontinuities, are too small to be detected with available methods; nevertheless their influence on excavation phases and environment are not of considerable importance.

The geophysical results obtained from the ERT and VLF-EM techniques have demonstrated that these methods are useful for the detection of fracture zones that are normally the preferential

hydraulic pathways through the rock masses. Therefore they can be applied for the hydrogeological problems related to tunnelling.

Apart from these main conclusions, the carried out geophysical investigations also revealed other findings of general relevance concerning the two applied method. For the ERT surveys, the Wenner-Schlumberger (WS) and the Dipole-Dipole (DD) were tested, with consistently better results for the Wenner-Schlumberger configuration. The presence of indexes of the reliability of the results, notably the RMS statistical error and the smoothed sensitivity, is very useful, especially for the non-expert user, allowing a more accurate interpretation of the 2D resistivity model, taking in account possible critical situations.

For VLF-EM method different distances between stations where the data are acquired were tested, observing the best results with distances of 10/15 m. The VLF-EM instrument is effectively able to detect and map electrical conductive vertical structures and it works quite well, at least over the crystalline rocks that are resistivity bodies, while it has a few problems in the areas characterized by the presence of electrical structures, both in the subsoil or aerial, those generally cause a high electromagnetic noise. The ERT method gives in general more quantitative and exact results, but also the VLF-EM technique, that is absolutely not expensive, could be applied with appreciably results, at least for preliminary investigations, preferably combining them with a ERT surveys if a conductive zone has been indentified, or if other specific purposes (e.g. water table detection, or low permeable bedrock detection) are required.

Acknowledgments

The authors would like to thank AlpTransit Gotthard Ltd and the Federal Roads Office (FEDRO) for the agreements signed for access to data and utilization of study cases. In particular, special thanks are due to all the geologists (R. De Paoli, P. F. Erard and F. Ghirlanda, J.F. Kauffmann, G. Monti) for the helpfulness demonstrated giving us the tunnel geological logs, and mainly for the demonstrated interest. A mention is also due for all the colleagues of Institute of Earth Science (M. Baruffini, S. Beatrizzotti, M. Pozzoni, L. Soma, A. Spataro, M.L. Vogt) that assist us carrying out the field work and to Dr. Eng. Ludovic Baron of Institute of Geophysics (Unil) for the technical support.

References

Al Oufi A., Mustafa H.A., Al-Tarazi E., Abu Rajab J. (2008). Exploration of the extension of two lava tubes, faults and dikes using very low frequency-electromagnetic technique in NE Jordan, Acta Geophysica 56(2):466-484

Behrens H., Beims U., Dieter H., Dietze G., Eikmann T., Grummt T., Hanisch H., Henseling H., Käss W., Kerndorff H., Leibundgut C., Müller-Wegener U., Ronnefahrt I., Scharenberg B., Schleyer R., Schloz W., Tilkes F. (2001). Toxicological and ecotoxicological assessment of water tracers. Hydrogeology Journal 9(3):321–325

Bersan M., Pilla G., Dolza G., Torrese P., Ciancetti G. (2010). The uprising of deep saline waters into the oltrepò pavese (northern italy) aquifer: early results. Italian Journal of Engineering Geology and Environment 1:7-22

Buergi C., Parriaux A., Franciosi G., Rey J.Ph. (1999). Cataclastic rocks in underground structures – terminology and impact on the feasibility of projects (initial results), Engineering geology 51:225-235

Di Maio R., Piegari E., Scotellaro C., Soldovieri M.G. (2007). Resisitivity tomographies to define thickness and water contento of pyroclastic covers at Mt. di Vezzi (Ischia island, Italy). Italian Journal of Engineering Geology and Environment, 2:65-72

El Tani M. (2003). Circular tunnel in a semi-infinite aquifer. Tunnelling and Underground Space Technology 18, no. 1:49–55

Fazzito S.Y., Rapalini A,E., Cortés J,M., Terrizzano C,M. (2009). Characterization of Quaternary faults by electric resistivity tomography in the Andean Precordillera of Western Argentina. Journal of South American Earth Sciences, 28:217-228

Flathe H. (1955). Possibilities and Limitations in Applying Geoelectrical Methods to Hydrogeological Problems in the Coastal Areas of North-West Germany. Geophysical Prospecting, 3:95-110

Flathe H. (1970). Interpretation of Geoelectrical Resistivity Measurements for Solving Hydrogeological Problems. In Morely, E. W. (ed.), Mining and Groundwater Geophysics: Geological Survey of Canada Economic Geologica Report, 26:580-597

Fraser D.C. (1969). Contouring of VLF-EM data. Geophysics, 34:958-967

Gargini A., Vincenzi V., Piccinini L., Zuppi G.M., Canuti P. (2008). Groundwater flow systems in turbidites of the Northern Appennines (Italy): natural discharge and high speed railway tunnel drainage, Hydrogeology Journal 16:1577-1599

Goodman R.F., Moye D.G., Van Schaikwyk A.,Javandel I. (1965). Ground water inflows during tunnel driving. Bulletin of the International Association of Engineering Geologists, 2(1): 39–56

IST (2011). Annuario idrologico del Canton Ticino 2010, Istituto scienze della terra, SUPSI

Karous M., Hjelt S.E. (1977). Determination of apparent current density from VLF measurements. Department of geophysics, University of Oulu, Contribution No. 89, 19 pp

Käss W. (1998) Tracing technique in geohydrology Balkem, Rotterdam, 600 pp.

Kolymbas D., Wagner P. (2007). Groundwater ingress to tunnels – The exact analytical solution Tunnelling and Underground Space Technology 22:23–27

Kirsch R. (2006). Groundwater Geophysics - A Tool for Hydrogeology, Springer-Verlag Berlin Heidelberg, 548 pp.

Lei S. (1999) An analytical solution for steady flow into a tunnel. Ground Water 37:23–26

Loke M.H. (2004). Tutorial:2-D and 3-D electrical imaging surveys. Copyright (1966-2004) M.H.Loke, 136pp.

Macedo L, Lima A.S. (2004). Groundwater exploration by VLF techniques: a case study in granitic terrains of Northwestern Portugal. In: Proceedings of the "2004 Fractured Rock Conference", National Ground Water Association, USA

Maloszewski P, Herrmann A, Zuber A (1999) Interpretation of tracer tests performed in fractured rock of the Lange Bramke basin, Germany. Hydrogeology Journal 7(2):209–218

Maréchal J.C. (1998). Les circulations d'eau dans les massifs cristallins alpins et leurs relations avec les ouvrages souterrains [Groundwater flow in Alpine crystalline massifs and its relations to underground constructions]. PhD Thesis EPFL no. 1769, Lausanne, Switzerland, 296 pp

Marescot L., Loke M.H., Chapellier D., Delaloye R., Lambiel C., Reynard E. (2003). Assessing reliability of 2D resistivity imaging in mountain permafrost studies using the depth of investigation index method, Near surface Geophysics, 1:57-67

Marzocchi R., Pera S., Pfeifer H.R. (2010). Prospezioni geoelettriche e elettromagnetiche VLF per la detenzione di fratture in ammassi rocciosi. Applicazione allo studio dell'impatto idrogeologico delle opere in sotterraneo, Proceedings of the 29° Convegno Nazionale GNGTS, Prato 26 - 28 october 2010, 432-435

Masset O., Loew S.(2010). Hydraulic conductivity distribution in crystalline rocks, derived from inflows to tunnels and galleries in the Central Alps, Switzerland. Hydrogeology Journal 18: 863–891.

McNeill J. D. (1990). Use of Electromagnetic Methods for Groundwater Studies. In: Ward, S. H. (Ed.). Geotechnical and Environmental Geophysics, vol 1: Review and Tutorial, Society Of Exploration Geophysicists Investigations 5:107-112

Pagano A. (1996). Indagine geofisica VLF (Very Low Frequncy) preliminare allo scavo della galleria per Mergoscia, Cantone Ticino. Technical report of Institute of Earth Science (SUPSI)

Perrochet P., Dematteis A. (2007). Modeling transient discharge into a tunnel drilled in a heterogeneous formation. Ground Water, 45(6):786-790

Piegari E., Cataudella V., Di Maio R., Milano L., Nicodemi M., Soldovieri M.G. (2009). Electrical resistivity tomography and statistical analysis in landslide modeling: a conceptual approach. Journal of Applied Geophysics, 68, 151-158

Pini O., Rossi D. (2009). The Ceneri railway base tunnel (15.4 km) in the southern Swiss alps (Gotthard Alptransit). Proceedings of the ITA–AITES World Tunnel Congress (WCG`09). Budapest, Hungary 23-28 May 2009

Scesi L., Gattinoni P. (2009). Water circulations in Rocks, Springer Dordrecht HeidelbergLondon New York, 165 pp. ISBN 978-90-481-2416-9

Schmid S. M., Aebli H. R., Heller F., Zingg A. (1989). The role of the Periadriatic Line in the tectonic evolution of the Alps. Geological Society, London, Special Publications, 45:153-171

Schmid S.M., Fügenschuh B., Kissling E., Schuster R. (2004) Tectonic map and overall architecture of the Alpine orogen. Eclogae Geologicae Helvetiae, 97:93–117

Schnegg P.A., Flynn R. (2002). Online field fluorometers for hydrogeological tracer tests. In: Isotope und Tracer in der Wasserforschung, Technische Universität Bergakademie Freiberg, Germany, 19:29–36

Shudel B., Biaggi D., Dervey T., Kozel R., Müller I., Ross J.H., Shindler U. (2002). Utilisation des treceurs artificiels en hydrogéologie – Guide pratique, Rapport de l'OFEG, Série Géologie, 3, 77 pp

Tassone A., Santomauro M., Menichetti M. Cerredo M.E., Remesal M.B., Lippai H., Lodolo E., Vilas J.F., (2010). Imaging subsurface lithological and structural features by resistivity tomography: North Beagle Channel (Tierra del Fuego, Argentina). Revista Mexicana de Ciencias Geológicas 27(3):562-572

Vincenzi V., Gargini A., Goldscheider N. (2009). Using tracer tests and hydrological observations to evaluate effetc of tunnel drainage on groundwater and surface waters in the northern Apennines (Italy), Hydrogeology Journal 17:135-150

5. Noble-gas and stable-isotope data to determine origin and groundwater flow regimes: application to a tunnel in the southern Swiss Alps

Roberto Marzocchi[1,2], Yama Tomonaga[3], Sebastian Pera[1], Hans-Rudolf Pfeifer[2], Rolf Kipfer[3,4], Laurent Decrouy[5] and Torsten Vennemann[5]

[1]IST, Institute of Earth Science, University of Applied Sciences and Arts of Southern Switzerland (SUPSI), Campus Trevano, CH-6952 Canobbio, Switzerland

[2]IMG-Centre d'Analyse Minérale, Faculty of Geosciences and Environment, University of Lausanne (UNIL), Anthropole, CH-1015 Lausanne, Switzerland

[3]Eawag, Swiss Federal Institute of Aquatic Science and Technology, CH-8600 Duebendorf, Switzerland

[4]Institute of Geochemistry and Petrology, Swiss Federal Institute of Technology (ETH), CH-8092 Zurich, Switzerland

[5] IMG, Laboratoire des Isotopes Stables, Faculty of Geosciences and Environment, University of Lausanne (UNIL), Anthropole, CH-1015 Lausanne, Switzerland

Abstract

Tunnel drilling offers a unique opportunity to sample and study deep waters that otherwise are difficult to access. Understanding of the deep groundwater flow is of primary importance to assess possible negative impacts of tunneling on hydrogeological systems. During this study, water was sampled for noble-gas analysis from tunnel inflows in the Monte Ceneri base tunnel (Canton Ticino, southern Switzerland), which passes through an area mainly characterized by metamorphic rocks (gneiss). Furthermore, water was sampled from springs located in the same geological environment.

Noble gas concentrations and isotope ratios, as well as stable isotope composition of hydrogen and oxygen (δ^2H and $\delta^{18}O$) and major ions measured in the water allow a hydrogeological conceptual model to be established for the case study, identifying the most probable origin of groundwater sampled at different locations. ^3He, ^4He, and ^{20}Ne concentrations and the isotope compositions of terrigenic helium for the studied region, allow to distinguish old groundwater strongly enriched in helium of crustal origin or mixing with surface water that circulates preferably through cataclastic structures. Noble gas concentrations and isotope ratios are useful proxies for the characterization of faults that may be critical for tunnel drilling due to their active hydrogeological role and to their influence on the mechanics of the rocks.

5.1 Introduction

Tunnel drilling is a technological and environmental issue that needs to be addressed to avoid a negative impact on water resources; at the same time it offers a unique opportunity to sample waters that are otherwise difficult to access and hence unknown. In order to assess the hydrogeology of construction sites, the groundwater chemistry is often used to investigate residence time, origin, and flow pattern of groundwater in fractured rock (Cook et al., 2003; Teed et al., 2005; Demlie et al, 2008). Nevertheless, due to the complexity of water–rock interaction, straightforward data interpretation and comprehensive understanding of the underground water circulation is not always possible. Noble gases (He, Ne, Ar, Kr, and Xe) are chemically inert and are, therefore, ideal proxies to study physical processes and flow dynamics in aquifers (e.g., Beyerle, 1999; Morikawa, 2004; Klump et al. 2006; Althaus et al., 2009). Atmospheric noble gases enter surface waters by gas exchange at the air/water interface, and their concentrations are often found at their solubility equilibrium with the atmosphere. The amount of gas transferred from the atmosphere to the water depends mainly on the temperature and salinity conditions of the exchanging water body as described by Henry's Law (Ozima and Podosek, 1983; Kipfer et al., 2002). Therefore, deviations from the expected equilibrium concentrations (e.g., due to the accumulation of radiogenic and terrigenic noble-gas species) can be used to understand the transport dynamics within aquatic systems. Groundwaters are known to accumulate non-atmospheric noble gases, in particular He, that may be found in excess with respect to the expected equilibrium concentrations. Non-atmospheric He in aquifers can be tritiogenic ^3He, produced by the decay of tritium (^3H), or

terrigenic ^{4}He and ^{3}He emanating from solid earth. An additional source of noble-gas excess with respect to the expected equilibrium concentrations is the so called "excess air", which is essentially due to the partial dissolution of entrapped air bubbles within the quasi-saturated zone (Heaton and Vogel, 1981; Holocher et al., 2002, 2003, Klump et al, 2007).

For instance, noble-gas concentrations and their isotope ratios have been used in lakes and groundwaters to determine residence times, mixing processes, and the origin of water and geogenic fluids (Tolstikhin et al., 1996; Mahara and Igarashi, 2003; Althaus et al., 2009; Holzner et al., 2009, Tomonaga et al. 2011). Experimental evidence indicates that crustal emission of He into the atmosphere is focused on particular geological structures such as faults (Oxburgh and O'Nions 1987, O'Nions and Oxburgh 1988; Kennedy et al., 1997; Mahara and Igarashi, 2002; Kulongoski et al., 2003; Kennedy and Van Soest, 2007; Pik and Marty, 2009).

Enrichment in tritiogenic ^{3}He can be useful to date groundwater that was recharged during the last 50 years. In fact tritium has been released in large amounts during the nuclear bomb tests in the mid-sixties. Hence, groundwaters infiltrated during this time were highly enriched in ^{3}H that is actually decayed forming ^{3}He. On the other hand, terrigenic ^{4}He and ^{3}He can be useful to understand the origin of deep groundwater and can be indicative of the presence of geological structures fostering migration of fluids from the lithosphere. Furthermore, the $^{3}He/^{4}He$ ratios allow for identification of the source of terrigenic He (from mantle and crust) and hence of deep water flow systems (Kipfer et al. 1994; Tomonaga et al., 2011).

The stable-isotope composition of water is another important research tool in the field of hydrogeology, as well as of hydrology, climatology and paleoclimatology (Maloszeski et al., 2002; Maréchal and Etcheverry, 2003; Oftendinger et al., 2004; Paternoster et al., 2008). In fact, differences in isotope composition of water molecules are related to isotope fractionation (Sheppard, 1986) during any physico-chemical reaction. The stable-isotope composition of water can, therefore, be used to trace the hydrological cycle.

The isotope fractionation occurs during *(i)* the evaporation of surface water, and *(ii)* the progressive raining out of the vapour masses (as a rule, the isotopic composition of precipitations becomes more depleted in ^{2}H and ^{18}O and at higher elevations and after successive rains; Gat et al. 2001). Rain has a specific isotope composition that depends on the origin of the vapour, the amount of precipitation, the temperature of condensation and the altitude effects. Measurements of stable-isotope composition of water can therefore be useful to understand aquifer recharge, transit time of water in the rock as well as groundwater mixing (Eichinger et al., 1984; Maloszewski et al., 1990; Blavoux and Letolle, 1995).

In this study, major-ion composition, noble-gas concentrations, oxygen and hydrogen isotope compositions were measured in samples collected from the inflows of the Ceneri railway base tunnel and from springs located in the same geological environment in order to develop a hydrogeological conceptual model (HCM) for the investigated area located in Canton Ticino (southern Switzerland).

5.2 Geological settings of the sampling site

The studied Ceneri railway base tunnel is entirely located within the south-alpine crystalline basement (Figure 5.1). The tunnel project crosses two different tectonic zones: *(i)* the Strona-Ceneri zone (amphibolites, Ceneri orthogneiss, Giumello paragneiss) in the North and *(ii)* the Val Colla zone (S. Bernardo orthogneisses, Stabiello paragneisses, schists and phylonites) in the South. These two zones are separated by the Val Colla Line (known also as Caslano – Taverne – Gazzirola Line) which has a thickness of approximately 600 m (Pini and Rossi, 2009). According to the classification by Buergi et al. (1999), this geological structure is mainly composed of mylonites of the Paleozoic era.

Until now, the tunnel has been drilled from different access points and in different directions. The main construction site is the Sigirino access tunnel, from which the base tunnel is excavated both in the south and north directions. At the two ends of the tunnel (i.e., the Vigana portal in the

north and the Vezia portal in the south) two more construction sites are planned. The north portal of the base tunnel (Figure 5.2) is located near the village of Vigana. The first part is excavated in unconsolidated material. After about 20 meters, the tunnel traverses fractured rocks, in particular the Ceneri orthogneiss (100 to 150 m) followed by the Ceneri paragneiss, which widely outcrops in this region. The thickness of the rock above the tunnel increases from about 10 m (near the north portal) to about 100 m at a distance from the portal of about 400 meters. From the hydrogeological point of view, orthogneiss or paragneiss generally show low hydraulic conductivity; values between 10^{-7} and 10^{-10} m/s were in fact measured from prospective boreholes. The main water inflows are linked with two main cataclastic zones that cross the tunnel at 170 m and 300 m, respectively (Figure 5.3). These zones, according to Buergi et al. (1999), are classified as kakirites.

The Sigirino access tunnel was entirely excavated in fractured rocks. In particular it passes through Ceneri orthogneisses and gneisses, hornfels, amphibolites and also Giumello paragneisses (Figure 5.3). The permeability of these rocks is generally low and the tunnel was mainly excavated under dry conditions. Only occasional lateral drippings were observed in the first 100 m of rocks (with high discharge related to precipitations), as well as downstream or upstream to the main cataclastic structures (mylonites and kakirites) being crossed by the tunnel. Position and dip of these structures are represented in Figure 5.3.

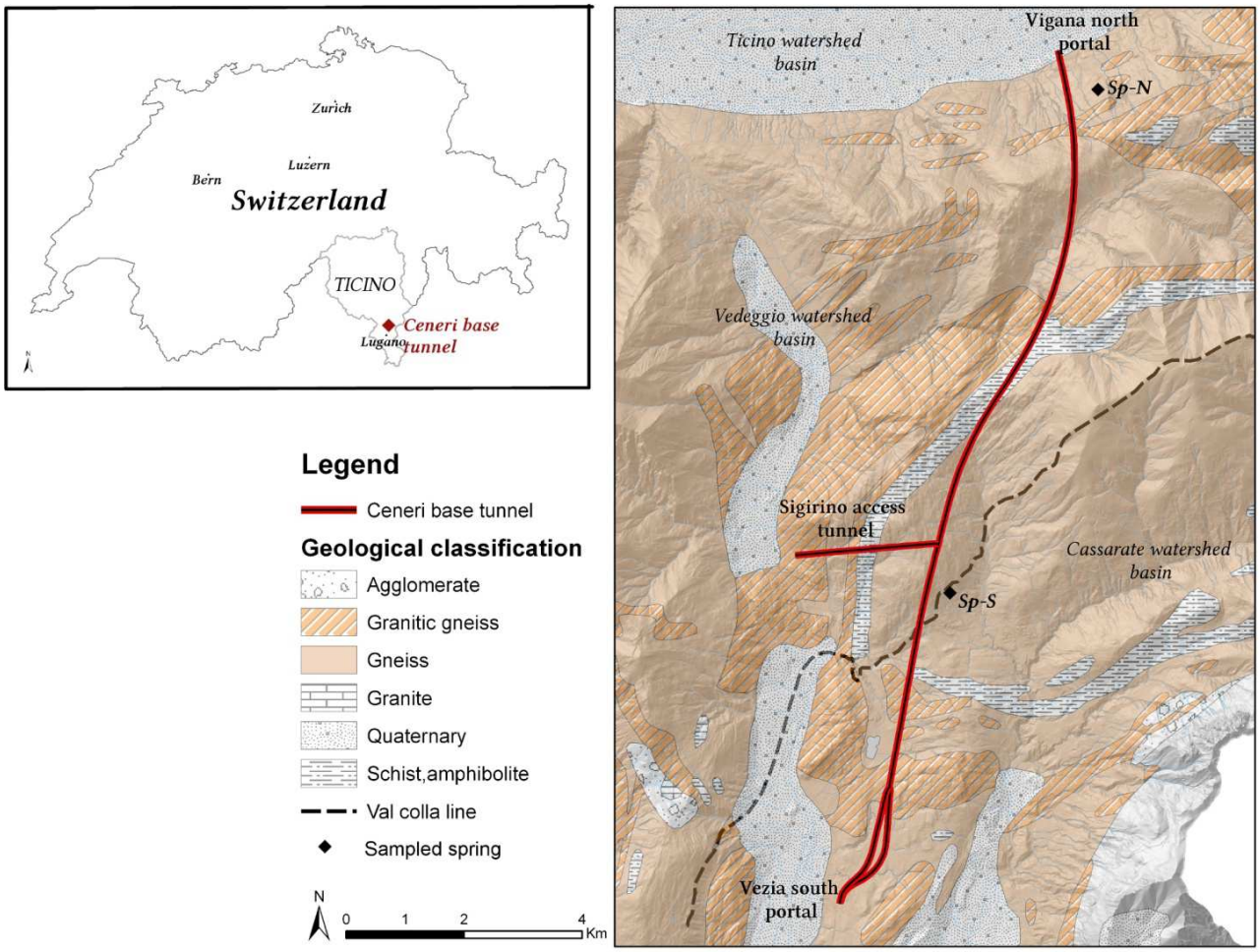

Figure 5.1 - Geological map (based on the 1:200'000 geological map of the Switzerland) of the region surrounding the Monte Ceneri base tunnel. The tunnel axis and the construction sites are shown in red. The locations of the two sampled springs (Sp-N and Sp-S), located up on the surface of the Ticino and Cassarate watershed, are represented by black squares.

5.3 Methods

Eight water inflows were sampled for noble-gas and geochemical analysis at the Vigana and Sigirino sites (Figure 5.2 and Figure 5.3). Samples from two springs located in the same geological environment (fractured gneiss) were also collected. The two springs are situated at the surface in two different hydrological basins and have been identified in previous studies as susceptible to be affected by drilling operations (Colombi and Baumer, 1995).

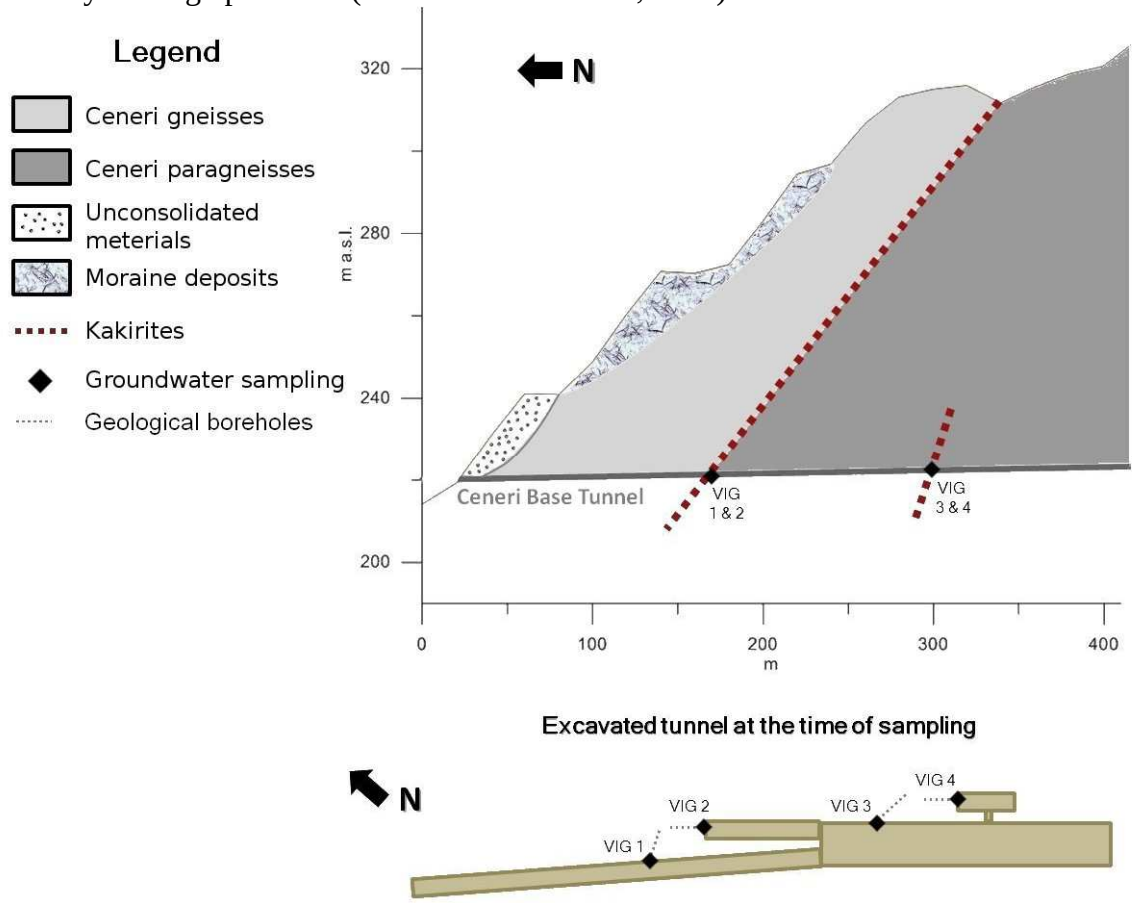

Figure 5.2 - Schematic view of the Vigana north portal (January 2011) and sampled tunnel inflows location. The sampled waters are likely to originate from two main water inflows, as confirmed by the measured noble-gas concentrations. Therefore in this figure they are grouped as “VIG 1&2” and “VIG 3&4”. Above a geological cross section is reconstructed from tunnel geological information kindly provided by Alptransit Inc. (http://www.alptransit.ch), from the Geological Atlas 1:25’000 of Switzerland (Bächlin et al., 1974), and from geophysical surveys carried out (see chapter 4).Below a plan of the excavated part of the tunnel at the time of sampling with exacted location of the sampled waters.

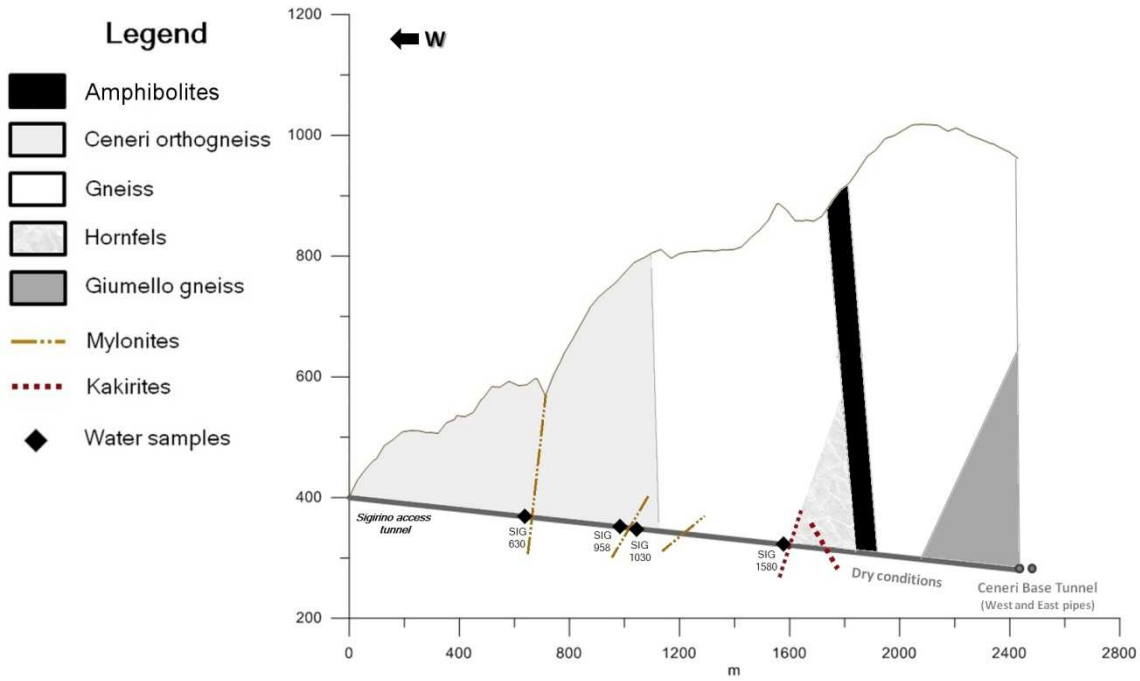

Figure 5.3 - Schematic view of the Sigirino access tunnel. The sampled water inflows are named on the basis of the progressive distance from the portal. The geological profile is reconstructed from tunnel geological information kindly provided by Alptransit Inc., and from the Geological Atlas 1: 25'000 of Switzerland (Reinhard et al. 1962) and geophysical surveys carried out (see chapter 4).

Sampling sites for noble-gas analysis are listed with the respective physico-chemical parameters and discharge rates in Table 5.1.

Major ions (F-, Cl-, NO_2^-, NO_3^-, SO_4^-, Li^+, Na^+, NH_4^+, K^+, Mg^{2+}, and Ca^{2+}) have been determined by ion chromatography on a dual Dionex ICS-2100-1100 system of Centre d'Analyse Minérale of University of Lausanne. Organic (TOC) and inorganic carbon (TIC) were measured by a C-analyzer (LiquiTOC Elementar Inc.), and HCO_3^- has been calculated from TIC. The detection limit for all the ions is 0.01 mg/L and 0.02 mg/L for organic and inorganic carbon; while the uncertainties of measurement is about 15% for both the ions and the carbon analyses, resulting in not good ionic balance (Table 5.2).

Oxygen and hydrogen stable-isotope compositions of water were measured at the Stable Isotopes Laboratory of the University of Lausanne using a Wavelength-Scanned Cavity Ring Down Spectroscopy (WS-CRDS) based analyzer (Picarro L1102-*i* Isotopic Water Liquid Analyzer). Because memory effect is known to affect the analytical measurements, eight injections per sample were effectuated of which only the last four were used for data reduction and normalization. For calibration, internal laboratory standards calibrated to VSMOW were inserted repeatedly within each analytical sequence (each 12-13 samples) as well as at the beginning and at the end of the sequence. For the set of standards measured at the beginning and at the end of the sequence, 12 injections were made of which the last five injections were used for normalization. Results are expressed using the δ-values with respect to the Vienna Standard Mean Ocean Water (VSMOW) (i.e., δ^2H and $\delta^{18}O$) as follows:

$$\delta = \frac{R_{sample} - R_{VSMOW}}{R_{VSMOW}} \times 1000 \qquad (5.1)$$

where R_{sample} is the stable-isotope ratio ($^2H/^1H$ or $^{18}O/^{16}O$) of the sample and R_{VSMOW} is the ratio of VSMOW. Typical reproducibility for this method is approximately ±0.08 ‰ and ± 0.8 ‰ for $\delta^{18}O$ and δD, respectively.

An extensive description of the methods applied for sampling and analysis of dissolved noble gases and tritium in water are given in Beyerle et al. (2000). The water (~25 g) is collected in small copper tubes that are closed by two special metal clamps in order to avoid degassing and contamination of the sample. The noble-gas analyses were carried out at the Noble Gas Laboratory

of the Swiss Federal Institute of Science and Technology in Zurich (ETHZ). Noble gases are extracted from the sample under ultrahigh vacuum (UHV) conditions. After purification noble-gas concentrations and isotope ratios are determined in two static mass spectrometers according to the experimental protocols presented in Beyerle et al. (2000). Typical analytical uncertainties of the measurements of He, Ne, Ar, Kr, and Xe concentrations are ±0.3%, ±0.9%, ±0.3%, ±0.8%, and ±1.0%, respectively. For the isotope ratios $^{3}He/^{4}He$, $^{20}Ne/^{22}Ne$, and $^{40}Ar/^{36}Ar$ the typical precisions are ±0.7%, ±0.3%, and ±0.2% (Beyerle et al., 2000).

5.4 Results

5.4.1 Major ions

Ionic composition of major element measured in water samples are presented in Table 5.2 and Figure 5.4 and Figure 5.5.

The variation of the different hydrochemical parameters are best illustrated using a Piper diagram (Piper, 1953) such as the one shown in Figure 5.4. In this diagram, four main hydrogeochemical facies (Back, 1966) can be recognized: (*i*) Ca^{2+}-HCO_3^-, (*ii*) Ca^{2+}-SO_4^{2-} , (*iii*) Na^{+}-HCO_3^- and (*iv*) Na^{+}-SO_4^{2-}. These facies can also be described using the Schmassmann classification (Table 5.2). This method allows a more detailed distinction between various samples, especially the ones from Sigirino tunnel.

Table 5.1 - Locations (site, distance from the tunnel portal for tunnel inflows, elevation) of the sampled waters (SIG and VIG: tunnel inflows, SP-N, Sp-S: spring at the surface). For each sampling site, discharge (Q), water temperature (T), pH, electrical conductivity normalized for the temperature of 25°C (EC_{25}), and stable isotope composition (δ^2H and $\delta^{18}O$) are given.

Sample	Site	Distance from the tunnel portal [m]	Elevation [m a.s.l.]	Q [L/m]	T [°C]	pH	EC_{25} [µS/cm]	$\delta^{18}O$ (‰VSMOW)	δ^2H (‰VSMOW)
SIG 630	Sigirino	630	370	<0.1	n.a.	8.50	190	-9.22±0.06	-58.79±0.5
SIG 958	Sigirino	958	360	0.1÷0.2	n.a.	8.55	189	-9.32±0.06	-59.78±0.5
SIG 1030	Sigirino	1030	360	0.1÷0.2	n.a.	9.35	290	-9.36±0.06	-60.97±0.5
SIG 1580	Sigirino	1580	350	0.1÷0.2	n.a.	9.25	550	-9.02±0.06	-56.50±0.5
VIG 1	Vigana	170	240	1	12.5	8.20	262	-9.11±0.06	-58.71±0.5
VIG 2	Vigana	200	240	18	12.3	8.55	248	-8.89±0.06	-56.82±0.5
VIG 3	Vigana	280	240	30	12.7	8.95	230	-9.12±0.06	-57.48±0.5
VIG 4	Vigana	320	240	300÷360	13.0	7.70	172	-9.10±0.06	-58.31±0.5
Sp - N	Spring (North)	-	570	80	9.6	6.30	76	-8.96±0.06	-59.02±0.5
Sp - S	Spring (South)	-	800	191	8.4	6.65	84	-9.27±0.06	-59.01±0.5

Table 5.2 - Major ion composition of the collected samples.

Sample	Li^+ [mg/L]	Na^+ [mg/L]	NH_4^+ [mg/L]	K^+ [mg/L]	Mg^+ [mg/L]	Ca^+ [mg/L]	HCO_3^- [mg/L]	$CO3^{2-}$ [mg/L]	F- [mg/L]	Cl^- [mg/L]	NO_3^- [mg/L]	SO_4^- [mg/L]	Ionic balance [%]	TDI [mg/L]	Hydrochemical facies (Back, 1966)	Schmassmann classification
SIG 630	0.02	30.51	0.92	1.20	0.66	12.98	53.56	1.20	3.18	0.99	0.87	16.16	18	122	$Na\text{-}HCO_3$	$Na\text{-}Ca\text{-}HCO_3\text{-}SO_4$
SIG 958	0.02	33.70	0.58	0.60	0.23	9.44	38.61	0.83	3.54	1.89	2.91	26.92	14	119	$Na\text{-}HCO_3$	$Na\text{-}Ca\text{-}HCO_3\text{-}SO_4$
SIG 1030	0.02	51.61	0.10	0.81	0.28	15.24	16.89	1.29	5.74	8.18	0.40	93.67	4	195	$Na\text{-}SO_4$	$Na\text{-}Ca\text{-}SO_4$
SIG 1580	0.05	105.02	0.06	1.09	0.25	2.24	132.51	6.61	14.63	2.16	0.39	26.14	11	291	$Na\text{-}HCO_3$	$Na\text{-}HCO_3\text{-}F$
VIG 1	<0.01	4.60	1.00	3.80	3.60	29.00	30.10	0.15	0.50	9.60	0.50	36.00	15	118	$Ca\text{-}SO_4$	$Ca\text{-}SO_4\text{-}HCO_3$
VIG 3	<0.01	6.70	0.17	7.00	3.31	22.54	30.18	0.62	0.30	5.71	0.10	35.68	13	112	$Ca\text{-}SO_4$	$Ca\text{-}SO_4\text{-}HCO_3\text{-}SO_4$
Sp-N	<0.01	3.82	n.a.	0.92	2.00	7.11	31.51	<0.01	0.10	2.34	5.63	13.47	-15	72	$Ca\text{-}HCO_3$	$Ca\text{-}Na\text{-}Mg\text{--}HCO_3\text{-}SO_4$
Sp-S	<0.01	3.02	n.a.	1.58	2.18	20.80	44.59	<0.01	0.07	0.85	2.83	20.26	6	93	$Ca\text{-}HCO_3$	$Ca\text{-}HCO_3\text{-}SO_4$

The two analyzed springs (Sp-N, Sp-S) are low mineralized and characterized by Ca^{2+}-HCO_3^- hydrochemical facies, which are typical from water circulating within fractured gneiss (Dubois, 1993; Derron, 1999), even though some Ca^{2+}-HCO_3^--SO_4^{2-} waters were recognized in other springs located near the northern end of the tunnel (Marzocchi et al., 2010). This is typical of metasediments and paragneiss containing intercalations of gypsum or other minerals that release sulfates in groundwater, such as pyrite (Dematteis, 1995). Sulfates are also present in samples collected at the Vigana site (VIG1,VIG 3) where the tunnel is located in the first section of bed rock, characterized by higher fracturing (Ofterdinger, 2001; Maréchal and Etcheverry, 2003; Masset and Low, 2010).

However, most of the samples collected in the Sigirino tunnel are Na^+-HCO_3^--SO_4^{2-} waters. From the diagram with the halite dissolution line (Figure 5.5) it is clear that all the samples collected in the Sigirino site are characterized by a high content of sodium not correlated with the chloride, which is a typical index of the ion exchange between water and surrounding rocks, hence of very slow groundwater circulations (Calmbach et al. 1994, Zuppi et al., 2004). As shown by the diagram with calcium-carbonate dissolution line (Figure 5.5), the SIG 1580 inflow, exhibits high bicarbonate concentrations not directly correlated to calcium ones. The fluoride ion is also significantly present in this sample (Table 5.2).The Sigirino inflow collected at a distance of 1030 m from the entrance (SIG 1030) is instead a Na-Ca-SO_4 groundwater clearly different from the other waters, as well evidenced by Figure 5.4.

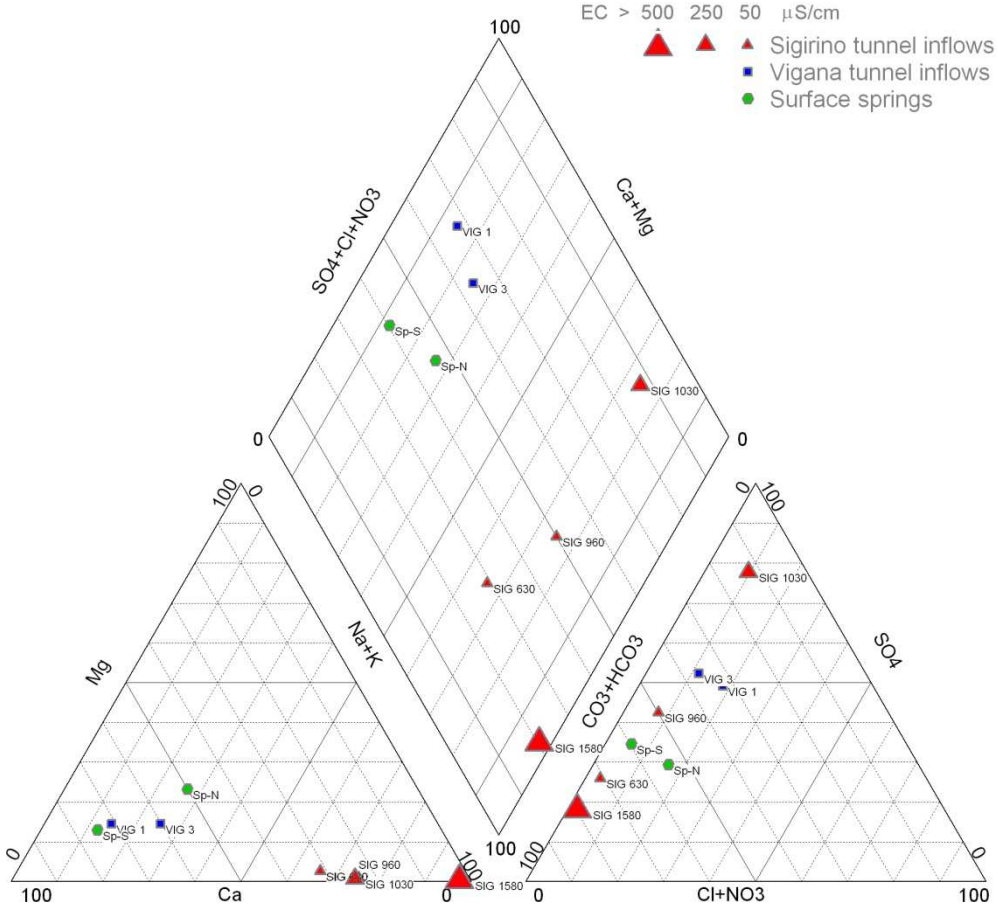

Figure 5.4 - Piper diagram of the concentrations of the major cations and anions measured the collected water samples.

Generalizing the results of major ions analysis the following observations can be made. First of all, the spring waters generally exhibit low total dissolved solids and are undersaturated to all conceivable minerals, as it is typical of water with a little contact and/or short transit time within the rock. Inflows collected within the north portal, even though more mineralized (higher EC_{25} with respect to Vigana) have a hydrogeological facies (Ca^{2+}-HCO_3^--SO_4^{2-}) similar to that of the surface springs in the surrounding area and are typical recently recharged groundwaters in paragneiss or metasediments. The hydrogeological facies of the groundwater collected in the Sigirino site (Na^+-

Ca^{2+}-HCO_3^- and Na^+-SO_4^{2-}) are rather typical of deep and old groundwater circulations with a high content in sodium, an indicator of a prolonged contact of the water with the surrounding rock matrix, resulting in chemical exchanges.

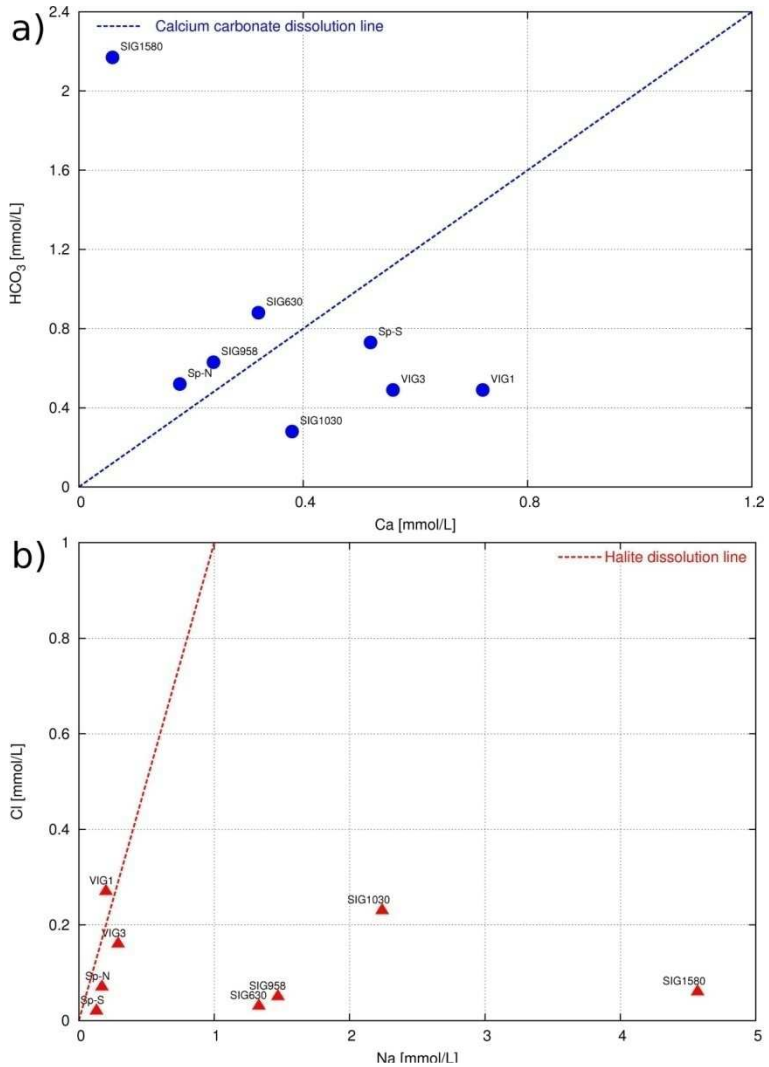

Figure 5.5 - Calcium versus bicarbonate (a) and sodium versus chloride (b) plots. In the first diagram a high content of bicarbonate ion in the SIG 1580 sample is shown, while in the other diagram all the samples collected within the Sigirino access tunnel are characterized by a higher content of sodium typically due to water-rock interaction (ion exchange).

5.4.2 δ^2H *and* δ^{18}O *data*

The relative abundances of oxygen and hydrogen stable isotopes in the tunnel inflows (Vigana and Sigirino, respectively) and surface spring waters were measured. The data are already presented in Table 5.1 and shown in Figure 5.5.

Looking at the relative abundances of stable isotopes of oxygen and hydrogen and comparing them with the local and global meteoric water lines (Gat and Carmi, 1970; Rozanski et al., 1993;) it is clear that all the samples are placed close to the Ticino MWL (Figure 5.6) defined in chapter 2. The latter is characterized by an increased value of deuterium excess, probably due to the seasonal effect on groundwater recharge (see chapter 2). All the samples are derived from meteoric infiltration, even if, considering only these data, hypothesis on age of water and different circulations are not possible.

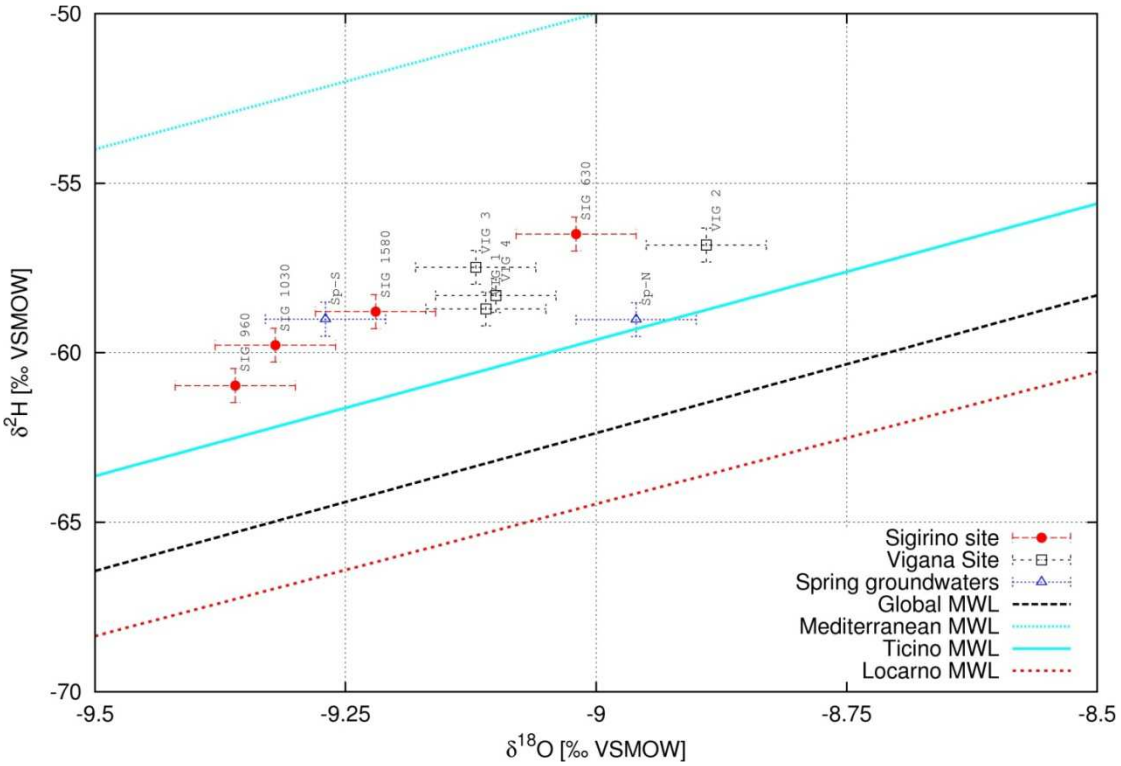

Figure 5.6 - $\delta^{18}O$ vs. $\delta^{2}H$ in the collected water samples.

A year of monitoring (summer 2009-summer 2010) of $\delta^{2}H$ and $\delta^{18}O$ in the Sigirino inflows and springs was also done. The seasonal trends are shown in Figure 5.7.

The $\delta^{18}O$ in the samples collected within the Sigirino access tunnel shows low variations over the year. In particular, the SIG 630, except one value, is the most stable. SIG 958 continuously decreases throughout the year of observation, but the variations are very small. Generally the standard deviations of $\delta^{18}O$ in the samples collected in the Sigirino access tunnel vary between 0.10 and 0.30‰.

On the contrary, trends of the stable isotope data of springs show higher variability (standard deviation of $\delta^{18}O$ between 0.24 and 0.50 ‰).

In particular observing $\delta^{18}O$ behaviour in the spring placed in the Ticino watershed (Sp-N) two high peaks in September 2009 and June 2010 was noted. These peaks seem to denote a mixing with enriched rain due to local infiltration; however any seasonal trend seems visible. Concerning the spring of the Cassarate watershed (Sp-S), seasonal trends can be observed, with lower values in spring and higher values during fall. Comparing the seasonal trends in springs with rain data collected in Locarno (Schürch et al, 2003), shown in Figure 5.7*b*, a mean residence time of about 2-3 months, or eventually 14-15 months, can be hypothesized. In fact the higher $\delta^{18}O$ in springs was measured in September 2009 and corresponds to rain of the previous summer, while the lowest $\delta^{18}O$ values were registered in May 2010 and correspond to the previous winter. Considering also the discharge variability (see chapter 6 and appendix B), highly correlated with precipitations, and the very low mineralization of these waters, the first hypothesis (~ 2-3 months of residence time) is the most probable.

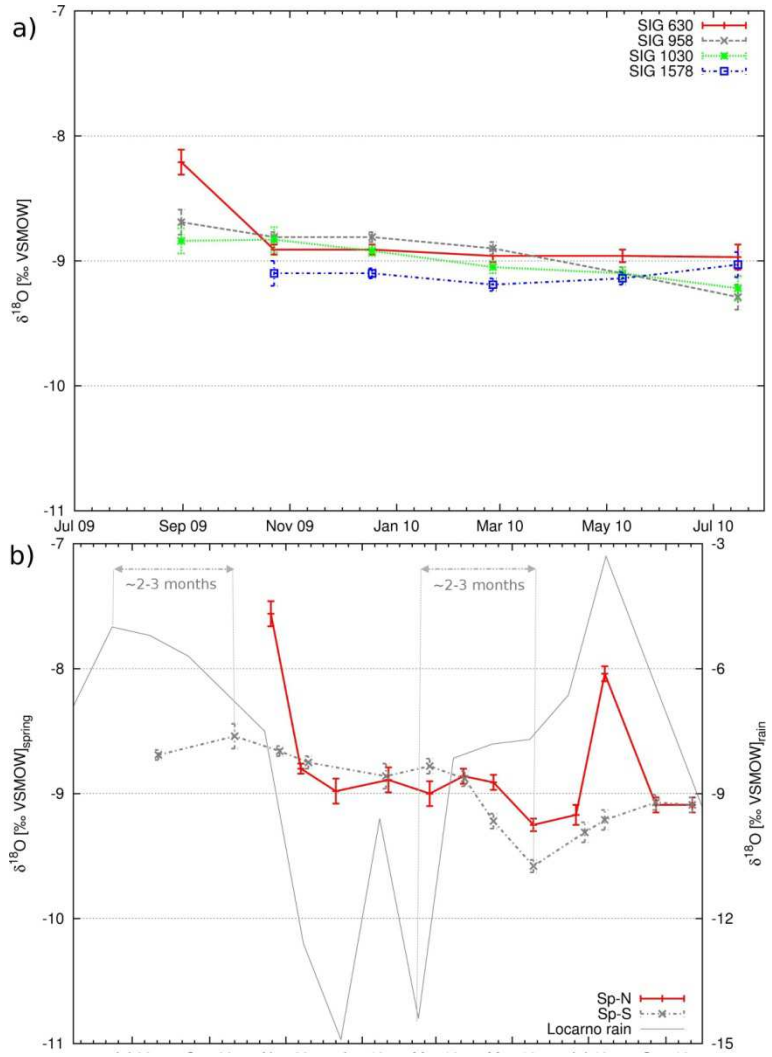

Figure 5.7 - $\delta^{18}O$ seasonal trends in the collected water samples: a) Sigirino access tunnel samples; b) groundwaters of springs.

Concerning the Vigana tunnel, groundwater inflows were only sampled sporadically during excavation phases and the available results cannot show any clear seasonal trends. Seasonal variations seem however visible from samples collected in different months.

5.4.3 Noble-gas concentrations and isotope ratios

Supposing an average temperature of infiltration of ~ 9°C and an average elevation of ~ 790 m a.s.l. (mean altitude of the region above the Monte Ceneri base tunnel), the He concentration expected for air saturated water (ASW) is about $4.34 \cdot 10^{8} cm^{3}STP/g$. All samples acquired for noble-gas analysis are hence characterized by He supersaturations with respect to the atmospheric equilibrium concentration (Table 5.3). Such a He excess is common in groundwaters and can be explained by the presence of excess air or the accumulation of tritiogenic or terrigenic He (Kipfer et al., 2002). The highest He concentration is found in sample SIG 1030.

Table 5.3 - Noble-gas concentrations and isotope ratios measured in water samples.

Sample	He (10^{-8} cm^3_{STP}/g)	$^3He/^4He$ (10^{-6})	$^{20}Ne/^4He$ (-)	Ar ($10^{-4} cm^3_{STP}/g$)	Kr (10^{-8} cm^3_{STP}/g)	Kr (10^{-8} cm^3_{STP}/g)
SIG 630	16.32±0.09	1.43±0.01	2.82±0.01	4.90±0.04	9.15±0.08	1.17±0.02
SIG 958	5.45±0.03	1.18±0.01	3.01±0.01	3.17±0.02	7.15±0.06	1.02±0.01
SIG 1030	664.72±3.78	0.03±0.00	0.03±0.01	3.24±0.02	6.51±0.05	0.86±0.01
SIG 1580	7.40±0.04	0.72±0.01	1.98±0.01	n.a.	n.a	n.a
VIG 1	6.30±0.03	1.37±0.02	3.71±0.01	4.00±0.02	8.99±0.03	1.29±0.04
VIG 2	6.09±0.03	1.37±0.02	3.71±0.01	3.93±0.02	8.61±0.03	1.23±0.04

VIG 3	6.76±0.04	1.82±0.02	3.66±0.01	4.19±0.02	9.12±0.03	1.30±0.04
VIG 4	5.94±0.01	1.73±0.01	3.59±0.002	4.23±0.01	9.45±0.05	1.34±0.01
Sp - N	5.65±0.03	1.36±0.01	3.77±0.01	3.96±0.02	8.69±0.04	1.26±0.04
Sp - S	6.40±0.03	1.39±0.05	3.65±0.01	3.99±0.02	8.93±0.03	1.29±0.04

Almost all the samples taken at the Sigirino site have $^{3}He/^{4}He$ ratios lower than the ASW $^{3}He/^{4}He$ ratio of $1.38 \cdot 10^{-6}$. The observed low $^{3}He/^{4}He$ ratios are indicative for the accumulation of terrigenic He of crustal origin ($^{3}He/^{4}He \sim 10^{-8}$). The measured $^{20}Ne/^{4}He$ ratios are plotted against the $^{3}He/^{4}He$ ratios in Figure. 5.8. The isotope composition of the SIG 1030 sample is characterized by a very low $^{20}Ne/^{4}He$ ratio, close to 0, which suggests the prevalence of He emanating from the (deep) lithosphere (Kipfer et al., 2002). Therefore, the corresponding $^{3}He/^{4}He$ isotope ratio of $\sim 3 \cdot 10^{-8}$ can be considered as the isotope signature of terrigenic He for the studied region.

Hence, that all the points of Figure 5.8, lying between the ASW and the SIG 1030 points, can be considered as a mixing of recently recharged groundwater, at atmospheric equilibrium, and very old groundwater coming from deeper circulations. All the remaining samples (SIG 1580, SIG 958 and SIG 630) from the Sigirino site lie near this mixing line. However, sample SIG 630 is affected by a slight deviation from this mixing line, whereby the $^{3}He/^{4}He$ ratio seems to be higher as expected. The measured $^{3}He/^{4}He$ ratio is even higher than ASW. In the light of the determined $^{3}He/^{4}He$ ratio of terrigenic He it is reasonable to relate the higher $^{3}He/^{4}He$ ratio of sample SIG 630 to the presence of tritiogenic ^{3}He produced by the decay of ^{3}H in groundwaters that recharged during the last 50 years.

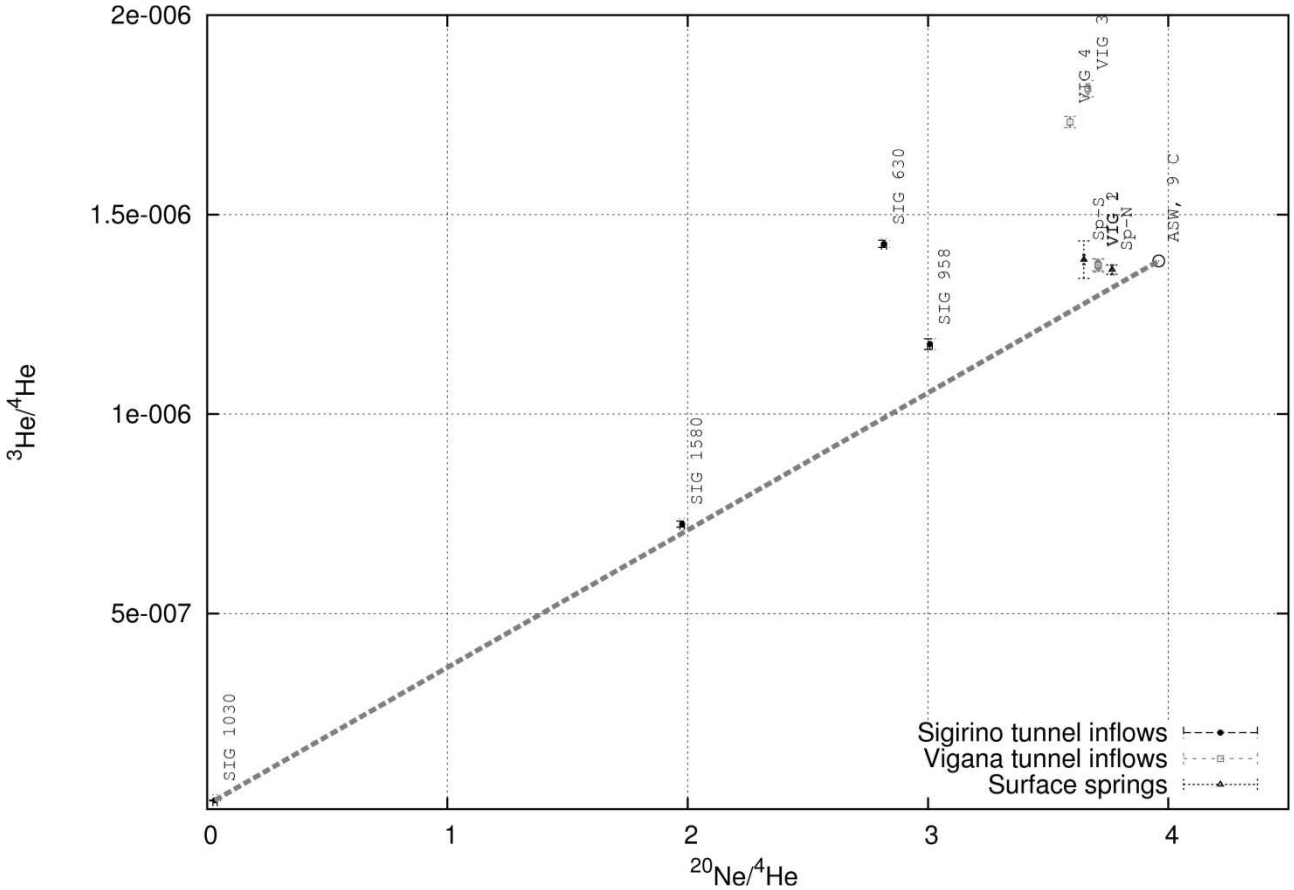

Figure 5.8 - Plot of the $^{20}Ne/^{4}He$ ratios against the $^{3}He/^{4}He$ ratios. Different symbols are used to distinguish the sampling locations (Sigirino site, black dots; Vigana site, empty squares; Springs, black triangles). The values for air saturated water (ASW) are calculated for a temperature of 9°C and 0 g/kg salinity. The waters superimposed on the dashed line represent a mixing of recently recharged groundwater, at atmospheric equilibrium, and very old groundwater coming from deeper circulations (SIG 1030).

On the contrary, the absence of significant amounts of tritiogenic ^{3}He (or any excess ^{3}He) in samples SIG 1030, SIG 958, and SIG 1580, and the He isotope signature becoming more crustal

with increasing distance from the Sigirino portal, suggest that these groundwaters are strongly or completely separated from the modern hydrological regime.

At the Vigana site (north portal) geological logs within the tunnel suggest that the groundwaters originate from two different inflows (Figure 5.2). The results of noble-gas analysis confirm this hypothesis. In fact, VIG 1 and VIG 2 are close to ASW, while VIG 3 and VIG 4 are characterized by higher $^{3}He/^{4}He$ ratios indicative for a contribution of tritiogenic ^{3}He (Figure 5.9). Such, a different He isotope signature of samples VIG 3 and VIG 4 is probably linked to longer and slower flows through the fractured rock masses.

The two water samples acquired from surface springs (Sp-N and Sp-S) are isotopically close to ASW (Figure 5.9) and can be considered as "young" groundwaters recently recharged by a rapid flow in the subsoil. No tritiogenic ^{3}He is present, similarly to the first tunnel inflow collected within the Vigana North portal (VIG 1 and VIG 2). Therefore, samples VIG 1 and VIG 2 are likely to be related to a fast flow regime which transports water in a relatively short time span from near-surface regions into the tunnel.

5.4.4 Noble-gas temperatures

Noble-gas equilibrium concentrations in water mainly depend on temperature and salinity of the water, and on the ambient atmospheric pressure that is normally related to the altitude of infiltration (Stute et al., 1992, 1995; Aeschbach-Hertig et al., 1999, 2000). Hence, for a given set of salinity and atmospheric pressure, from the noble-gas concentrations measured in the collected groundwater samples, it is possible to reconstruct the so called "noble-gas temperature" (NGT) in a straightforward manner. The NGT reflects the temperature of the considered water mass at the time when the last gas exchange with the atmosphere occurred (i.e., for groundwaters: the temperature of recharge).

Table 5.4 - Noble-gas temperatures calculated from noble-gas concentrations measured in the collected groundwater samples.

Sample	T [°C]
SIG 630	17.3 ± 1.1
SIG 958	16.9 ± 0.6
SIG 1030	24.6 ± 1.0
SIG 1580	n.a.
VIG 1	11.1 ± 0.2
VIG 2	13.2 ± 0.4
VIG 3	11.8 ± 0.3
VIG 4	9.9 ± 0.2
Sp-N	11.7 ± 0.4
Sp-S	9.4 ± 0.2

In the course of this study, the numerical code NOBLE90 implemented in MATLAB (Aeschbach-Hertig et al., 1999, 2000; Peeters et al., 2003) was adopted. It also corrects the measured noble-gas concentration for excess air formation (Heaton and Vogel, 1981; Klump, 2007; Klump et al., 2007, 2008; for a review see Kipfer et al., 2002). NGTs are calculated considering the closed system equilibration model (Aeschbach-Hertig et al., 2000), using the concentrations of Ar, Kr and Xe, which are the most temperature sensitive noble gases, and taking into account excess air; results are reported in Table 5.4.

The samples, collected in the Sigirino tunnel, are characterized by higher noble-gas temperatures. The highest NGT was calculated for the SIG 1030 inflow: about 25°C (i.e., almost 10°C higher than the NGTs of SIG 630 and SIG 958). Such a high NGT strongly suggests that the sampled groundwater has been exposed to a geothermal gradient (frequently encountered in deep circulation systems). Combined with a long residence time within the aquifer, this exposition fostered a secondary gas exchange. Therefore, the calculated NGT for sample SIG 1030 relates more to the host rock temperature and less to the original infiltration temperature. This is in

agreement with the observed strong accumulation of terrigenic He: the water inflows sampled in the deep part of the Sigirino tunnel are old groundwaters that are almost completely separated from the modern hydrological cycle.

Samples SIG 630 and SIG 958 show NGTs of about 17°C. These temperatures are higher than the NGT determined for the nearby spring Sp-S of about 9°C and suggest a mixing of old and recently infiltrated water. Again, this is in agreement with the He isotope data indicating the presence of tritiogenic ^{3}He from the decay of ^{3}H. On the contrary, NGTs of the inflows collected the Vigana tunnel site, are similar to the average annual values at the earth surface, indicating the prevalence of recently recharged groundwaters.

5.5 Discussion

On the basis of noble-gas concentrations and isotope ratios, and hydrogeochemical data, and considering also geological information, a hydrogeological conceptual model (HCM) can be elaborated, distinguishing two main different flow systems present in the Monte Ceneri base tunnel area. Surface springs (Sp-N and Sp-S samples) represent waters from shallow flow systems, generally originated from infiltration within the first layer of rock, characterized by intense fracturation and higher hydraulic conductivity (Ofterdinger, 2001; Maréchal and Etcheverry, 2003; Masset and Loew, 2010). In fact, the noble-gas analyses show concentrations substantially at atmospheric equilibrium and close to the expected ASW values. This is in agreement with the low value of total dissolved solids and the observed seasonal variations, even if attenuated, of δ^2H and δ^{18}O. The same geochemical characteristics are found in VIG1 and VIG2 samples that are located at about 180 m from the tunnel portal. As observed by geological logs and geophysical surveys (see chapter 4), these inflows are located upstream of a cataclastic fault zone filled by fine-grained material, which forms a natural barrier for the present groundwater. These inflows also represent water from a shallow flow system.

In contrast, in some faults filled by low hydraulic conductivity material and, above all, not directly connected to the surface, in particular in the SIG 1030 sample, groundwater with terrigenic He was sampled. It is rather characteristic of deeper and very “old” groundwaters. Their hydrogeochemical characteristics are quite different from the other groundwaters sampled in the same geological environment, at the surface (spring waters) and at depth (other tunnel inflows). Even though the amount of these groundwaters, in the studied case is low, it is not possible to exclude that the groundwater flows could be higher, especially related to the transition zones, frequently encountered upstream and downstream of cataclastic structures, such as mylonites, cataclasites and kakirites (Buergi et al., 1999).

Considering these two waters as the regional extremes (recently infiltrated and very old groundwaters), other flow systems resulting from mixing or enrichment in ^{3}He due to radioactive decay of tritium were identified. For instance, a second flow system was found at the north portal of the tunnel (Vigana site) and is represented by samples VIG3 and VIG4. Chemical data of these samples do not denote large differences respect of the other samples collected in the Vigana north portal. These inflows are in fact always linked to recently recharged water; nevertheless, in this case, water circulations through fractures are longer, hence slower, giving the tritium the time to decay, forming the measured enrichment in ^{3}He.

Concerning the Sigirino access tunnel, the other sampled waters (SIG 958 and SIG 1580) as well evidenced by noble gas isotope ratios (Figure 5.8) are the result of mixing between different ratios of *(i)* the above mentioned deep waters that flow close to faults, not directly connected with the surface and *(ii)* newly recharged waters coming from a slow infiltration from the surface into the low permeable deeper fractured rock masses.

Finally the SIG 630 sample shows the presence of ^{3}He of tritiogenic origin and hence can be considered as the result of a mixing between deep waters and those infiltrating and circulating through the fractures present upstream of a cataclastic zone at about 600 m from the tunnel entrance (see chapter 3).

5.6 Conclusions

Noble gases, δ^2H and $\delta^{18}O$, and major-ion concentrations were used to understand, even though on a local scale, the groundwater flow dynamics in fractured rocks and to determine residence times, mixing processes, and the origin of water otherwise unknown. Different flow systems were distinguished and the hydrogeological role of cataclastic structures was clearly evidenced.

Groundwater circulation through faults that are generally filled by fine-grained and low permeable material (SIG 1030) was characterized. This flow system is separated from the surface and carries groundwater with a strong terrigenic He signature of crustal origin ($^3He/^4He \sim 3.22 \cdot 10^{-8}$). Other tunnel inflows (SIG 958 and SIG 1568) are the results of a mixing between older and more recently recharged groundwater. In fact the noble gas isotope composition of these waters is placed on a "mixing line" between the isotope composition characterizing terrigenic He (SIG 1030) and the isotope composition of air saturated water (ASW).

The He isotope composition of crustal origin typical for the studied region, as well as the obtained mixing line, are also of considerable importance in order to distinguish water from springs (Sp-N and Sp-S) or tunnel inflows (VIG1 and VIG2) that rapidly recharge through more permeable fault systems. Faults are critical zones for tunnelling, due to their active hydrogeological role (Masset and Low, 2010) and to their influence on the rock's mechanic (Schubert et al., 2006) having negative effects on the excavation stability. Noble-gas analysis, especially in the light of the terrigenic helium isotope composition individuated with the present study, allows for straightforward identification and characterization of fault systems and their hydrological regime present in the underground.

Stable isotopes, in particular their seasonal variations compared to the stable-isotope composition of precipitation, are useful to obtain information about the groundwater residence time. Especially in case of recently recharged groundwaters, quantitative information is directly available, as demonstrated by results of δ^2H and $\delta^{18}O$ monitoring of springs; while in presence of older groundwater the seasonal variations of δ^2H and $\delta^{18}O$ have been much more attenuated.

The differences between the various aquifers can be assessed by using the traditional hydrogeochemical data, even though a clear and unambiguous interpretation of groundwater origin and flow regimes, using only these data, is not possible. In contrast, the use of noble-gas concentrations and isotope ratios combined with the observations coming from a monitoring of δ^2H and $\delta^{18}O$ allow for a better understanding of the underground flow system in the fractured rock masses of the investigated region supporting the formulation of well-supported HCM.

Acknowledgements

The authors would like to thank AlpTransit Gotthard Ltd for the agreements signed for access to data and utilization of case study. In particular, a special thanks is due to all the geologists (R. De Paoli, P. F. Erard) for the helpfulness demonstrated. The stable isotope and noble gas analyses have been partially financed by the Herbette Foundation (University of Lausanne).

References

Aeschbach-Hertig W., Schlosser P., Stute M., Simpson H.J., Ludin A., Clark J.F. (1998). A 3H/3He Study of Ground Water Flow in a Fractured Bedrock Aquifer, Groundwater 36:671-670.

Aeschbach-Hertig W., Peeters F., Beyerle U., Kipfer R. (1999). Interpretation of dissolved atmospheric noble gases in natural waters. Water Resource Research 35:2779-2792.

Aeschbach-Hertig W., Peeters F., Beyerle U., Kipfer R. (2000). Paleotemperature reconstruction from noble gases in ground water taking into account equilibration with entrapped air. Nature 405:1040-1044.

Althaus R., Klump S., Onnis A., Kipfer R., Purtschert R., Stauffer F., Kinzelbach W. (2009). Noble gas tracers fort the characterization of flow dynamics and origin og groundwater. A case study in Switzerland. Journal of Hydrology 370:64-72.

Bächlin R., Bianconi F., Codoni A., Dal Vesco E., Knoblauch P., Kündig E., Reinhard M., Spaenhauer F., Spicher A., Trommsdorff V., Wenk E. (1974). Geological Atlas of Switzerland. Map 66 Bellinzona (LK 1313).

Bayer R., Schlosser P., Bönisch G., Rupp H., Zaucker F., Zimmek G. (1989). Performance and blank components of a mass spectrometric system for routine measurement of helium isotopes and tritium by the 3He ingrowth method. Sitzungsberichte der Heidelberger Akademie der Wissenschaften Mathemathischnaturwissenschaftliche Klasse 5. Springer-Verlag.

Beyerle U. (1999). Groundwater Dynamics, Paleoclimate and Noble Gases. Ph.D. thesis No. 13078, Swiss Federal Institute of Technology (ETHZ).

Beyerle U., Aeschbach-Hertig W., Hofer M., Imboden D. M., Baur H. and Kipfer R. (1999). Infiltration of river water to a shallow aquifer investigated with 3H/3He, noble gases and CFCs. Journal of Hydrology. 220(3–4):169–185.

Beyerle U., Aeschbach-Hertig W., Imboden D.M., Baur H., Graf T., Kipfer R. (2000): A mass spectrometric system for the analysis of noble gases and tritium from water samples. Environmental Science & Technology, 34:2042–2050.

Blavoux B., Letolle R., (1995). Apport des rechniques isotopiques à la connaissance des eaux souterraines, Géochroniques 54 :12-15.

Buergi C., Parriaux A., Franciosi G. Rey J.Ph. (1999). Cataclastic rocks in underground structures – terminology and impact on the feasibility of projects (initial results), Engineering geology 51:225-235.

Calmbach, L., Krull, L., Pfeifer, H.-R. (1995). Etude des sources bicarbonatées sodiques dans la galérie d'amenée d'eau de Jaman (Préalpes Vaudoises). Bulletin d'hydrogéologie 13:33- 51.

Colombi A., Baumer A. (1995). Galleria di base del Monte Ceneri, Situazione idrogeologica, Rapporto idrogeologico. Alptransit tecnhnical report of the "Studio di geologia Dr. A. Baumer".

Cook P.G., Solomon D.K.(1997). Recent advances in dating young groundwater: chlorofluorocarbons, 3H/3He and 85Kr. Journal of Hydrology 191:245-265.

Cook P.G., Favreau G., Dighton J.C., Tickell S. (2003). Determining natural groundwater influx to a tropical river using radon, chlorofluorocarbons and ionic environmental tracers. Journal of Hydrology, 277(1-2):74-88.

Dematteis A. (1995). Typologie géochimique des eaux des aquifères carbonatés des chaînes alpines d'Europe centrale et méridionale. Ph.D. thesis No.1419, Ecole Polytechnique Fédérale Lausanne, 226 pp.

Demlie M., Wohnlich S., Ayenew T. (2008). Major ion hydrochemistry and environmental isotope signatures as a tool in assessing groundwater occurrence and its dynamics in a fractured volcanic aquifer system located within a heavily urbanized catchment, central Ethiopia. Journal of Hydrology 353:175–188.

Derron, M.-H. (1999). L'interaction eau-roche-sol à basse température dans les Alpes. Ph.D.thesis, University of Lausanne, 209 pp.

Dubois J.D. (1993). Typologie des aquifers du Cristallin: Exemple des massif des Aguilles Rouges et du Mont Blanc (France, Italie et Suisse). Ph.D. thesis No.950, Ecole Polytechnique Fédérale Lausanne,324 pp.

Eichinger L, Merkel B, Nemeth G, Salvamoser J, Stichler W (1984). Seepage Velocity Determinations in Unsaturated Quarternary Gravel. Recent investigations in the Zone of Aeration, Vol.1. TU München, 303-313.

Gat JR, Mook WG, Meijer HAJ (2001). Atmospheric water – Environmental isotopes in the hydrological cycle. principle and applications. IHP-V, Technical document N. 39, UNESCO, Paris, 113pp.

Heaton T.H.E., Vogel J.C. (1981). "Excess air" in groundwater. Journal of Hydrology 50:201-216.

Holocher J., Peeters F., Aeschbach-Hertig W., Hofer M., Brennwald M., Kinzelbach W., Kipfer R. (2002). Experimental investigations on the formation of excess air in quasi-saturated porous media. Geochimica et Cosmochimica Acta 66(23):4103–4117.

Holocher J., Peeters F., Aeschbach-Hertig W., Kinzelbach W., Kipfer R. (2003). Kinetic model of gas bubble dissolution in groundwater and its implications for the dissolved gas composition. Environmental Science & Technology . 37(7):1337–1343.

Holzner C.P., Aeschbach-Hertig W., Simona M., Veronesi M., Imboden D.M., Kipfer R. (2009). Exceptional mixing events in meromictic Lake Lugano (Switzerland/Italy), studied using environmental tracers. Limnology and Oceanography, 54(4):1113–1124.

Kennedy B.M., Kharaka Y.K., Evans W.C., Ellwood A., DePaolo D.J., Thordsen J., Ambats G., Mariner R.H.(1997). Mantle fluids in the San Andreas fault system, California. Science 278:1278–1281.

Kennedy B.M., Van Soest M.C. (2007). Flow of mantle fluids through the ductile lower crust: Helium isotopes trends. Science 318:1433–1436.

Kipfer R., Aeschbach-Hertig W., Peeters F., Stute M. (2002). Noble gases in lakes and ground waters. In Porcelli D., Ballentine C. and Wieler, R., editors, Noble Gases in Geochemistry and Cosmochemistry. Reviews in Mineralogy and Geochemistry, 47:615–700.

Klump S., Kipfer R., Cirpka O. A., Harvey C. F., Brennwald M. S., Ashfaque K. N., Badruzzaman A. B. M., Hug S. J., Imboden D. M. (2006). Groundwater Dynamics and Arsenic Mobilization in Bangladesh Assessed Using Noble Gases and Tritium, Environmental Science & Technology 40(1):243–250.

Klump S. (2007). The formation of excess air in groundwater studied using noble gases as conservative tracers in laboratory and field experiments. Ph.D. thesis No. 17168, Swiss Federal Insitute of Technology (ETHZ), doi:10.3929/ethz-a-005415312.

Klump S., Tomonaga Y., Kienzler P., Kinzelbach W., Baumann T., Imboden D.M., Kipfer R. (2007). Field experiments yield new insights into gas exchange and excess air formation in natural porous media. Geochimica et Cosmochimica Acta, 71:1385–1397.

Klump S., Cirpka O., Surbeck H., Kipfer, R. (2008). Experimental and numerical studies on excess-air formation in quasi-saturated porous media. Water Resource Research, 44:W05402.

Kulongoski J.T., Hilton D.R., Izbicki J.A. (2003). Helium isotope studies in the Mojave Desert, California: implications for groundwater chronology and regional seismicity. Chemical Geology 202:95-113.

Leybourne M.I., Clark I.D., Goodfellow W. D. (2006). Stable isotope geochemistry of ground and surface waters associated with undisturbed massive sulfide deposits; constraints on origin of waters and water-rock reactions. Chemical Geology 231:300-325.

Mahara Y., Igarashi T. (2003). Changes in isotope ratio and content of dissolved helium through groundwater evolution. Applied Geochemistry 18:719–738.

Maloszewski P, Moser H, Stichler W, Bertleff B, Hedin K, (1990). Modelling of groundwater pollution by river bank filtration using oxygen-18 data Groundwater monitoring and management IAHS Publ. No. 173:153-161.

Maloszeski P., Stichler W., Zuber A. and Rank D. (2002). Identifying the flow systems in a karstic-fissured-porous aquifer, the Schneealpe, Austria, by modelling of environmental 18O and 3H isotopes Journal of hydrology 256:48-59.

Mamyrin B.A. and Tolstikhin I.N. (1984). Helium Isotopes in Nature, volume 3 of Developments in Geochemistry, 1st ed. Elsevier, Amsterdam, New York, Tokyo.

Maréchal J.C., Etcheverry D. (2003). The use of 3H and 18O tracers to characterize water inflows in Alpine tunnels. Applied Geochemistry 18:339-351.

Marzocchi R., Pera S., Pfeifer H.R. (2010). Hydrogeological interferences in tunneling - A comprehensive study, Aquamundi 1(3):1-14.

Masset O., Loew S.(2010). Hydraulic conductivity distribution in crystalline rocks, derived from inflows to tunnels and galleries in the Central Alps, Switzerland. Hydrogeology Journal 18: 863–891.

Massmann G., Sültenfuß J., Dünnbier U., Knappe A., Taute T., Pekdeger A. (2008). Investigation of groundwater residence times during bank filtration in Berlin: a multi-tracer approach. Hydrological processes 22:788-801.

Morikawa, N. (2004). Dissolved helium distribution in deep groundwaters from the Tono area, central Japan: a tool for tracing groundwater flow in fractured granite. Limnology 5:61–69.

Ofterdinger U.S., (2001). Ground water flow systems in the Rotondo Granite, Central Alps (Switzerland). Ph.D. thesis No. 14108, Swiss Federal Institute of Technology (ETHZ).

Ofterdinger U.S., Balderer W., Loew S., Renard P., (2004). Environmental isotopes as indicator for grond water recharge to fractured granite, Ground Water 42/6:868-879.

O'Nions,R.K.,Oxburgh,E.R.,(1988), Helium,volatile fluxes and the development of continental crust. Earth and Planetary Science Letters 90:331–347.

Oxburgh, R., O'Nions, R.K. (1987). Helium loss, tectonics, and terrestrial heat budget, Science, 237:1583-1588.

Ozima, M., Podosek, F.A. (1983). Noble gas geochemistry. Cambridge, London, New York: Cambridge Univ. Press.

Paternoster M., Liotta M., Favara R., (2008). Stable isotope ratios in meteoric recharge and groundwater at Mt. Vulture volcano, southern Italy, Journal of Hydrology 348, 87– 97.

Peeters F., Beyerle U., Aeschbach-Hertig W., Holocher J., Brennwald M.S., Kipfer R.(2003). Improving noble gas based paleoclimate reconstruction and groundwater dating using 20Ne/22Ne ratios. Geochimica et Cosmochimica Acta, 67(4):587-600.

Pik R., Marty B. (2009). Helium isotopic signature of modern and fossil fluids associated with the Corinth rift fault zone (Greece): Implication for fault connectivity in the lower crust. Chemical Geology 266:67-75.

Pini O., Rossi D.(2009). The Ceneri railway base tunnel (15.4 km) in the southern Swiss alps (Gotthard Alptransit). Proceedings of the ITA–AITES World Tunnel Congress (WCG`09). Budapest, Hungary 23-28 May

Piper, A.M. (1953). A Graphic Procedure in the Geochemical Interpretation of Water Analysis. Washington D.C.: United States Geological Survey. ISBN ASIN: B0007HRZ36.

Reinhard M., Bächlin R., Graeter P., Lehner P., Spicher A. (1962). Geological Atlas of Switzerland. Map 39 Tesserete (LK 1333).

Rossi D., Bühler T., Drack E. (2009).Ceneri base tunnel. Tunnel 4:49-63.

Schurch M., Kozel R.; Schotterer U., Tripet J.P. (2003). Observation of isotopes in the water cycle: the Swiss National Network (NISOT), Environmental geology 45(1):1-11.

Schubert W., Fasching A., Goricki A. (2006). Tunnelling in Fault Zones – State of the Art. In Lee, In-Mo, Yoo, Chungsik & You, KwangHo (eds.), Safety in Underground Space; Proceedings of the ITA-AITES 2006 World Tunnel Congress and 32nd ITA General Assembly, 22-27 April, Seoul, Korea, Elsevier.

Sheppard S.M.F (1986). Characterization and isotopic variations in natural waters. In: J.W. Valley, H.P. Taylor, Jr. and J.R. O'Neil, Editors, Stable Isotopes in High Temperature Geological Processes. Reviews in Mineralogy, 16:165–183.

Solomon D.K., Poreda R.J., Schiff S.L., Cherry J.A. (1992). Tritium and helium-3 as Groundwater Age Tracers in the Borden Aquifer. Water Resources Research 28(3):741-755.

Stute M., Schlosser P., Clark J.F., Broecker W.S. (1992). Paleotemperatures in the Southwestern United States derived from noble gases in ground water. Science 256:1000–1003.

Stute M., Forster M., Frischkorn H., Serejo A., Clark J.F., Schlosser P., Broecker W.S., Bonani G.(1995). Cooling of tropical Brazil (5°C) during the last glacial maximum. Science, 269:379-383.

Teed S.O., Weaver T.R., Cartwright I. (2005). Distinguishing groundwater flow paths in different fractured-rock aquifers using groundwater chemistry: Dandenong Ranges, southeast Australia. Hydrogeology Journal 13:771786.

Tolstikhin I.N., Kamenskiy I.L. (1969). Determination of ground-water ages by the T-3He method. Geochemistry International, 6:810–811.

Tolstikhin I.N., Lehmann B.E., Loosli H.H., Gautschi A. (1996). Helium and argon isotopes in rocks, minerals, and related groundwaters: a case study in northern Switzerland. Geochimica et Cosmochimica Acta 60(9):1497–1514.

Tomonaga Y., Brennwald M. S., Kipfer R. (2011). Spatial distribution and flux of terrigenic He dissolved in the sediment pore water of Lake Van (Turkey). Geochimica et Cosmochimica Acta, 75(10):2848–2864.

Zuppi G.M., Novel J.P., Bray M., Darmendrail X., Fudral S., Jusserand C., Nicoud G. (2004). Eaux fortement minéralisées et circulations profondes dans le socle. Exemple des Alpes franco-italiennes. C.R. Geoscience 336:1371-1378.

6. Geochemical and geophysical approach to assess vulnerability of springs to tunnel drilling

Roberto Marzocchi[1,2], Sebastian Pera[1], Hans-Rudolf Pfeifer[2], Torsten Vennemann[3], Laurent Decrouy[3] and Klaus Holliger[4]

[1] IST, Institute of Earth Science, University of Applied Sciences and Arts of Southern Switzerland (SUPSI), Campus Trevano, CH-6952 Canobbio, Switzerland

[2] IMG, Centre of Mineral Analysis, Faculty of Geosciences and Environment, University of Lausanne (UNIL), Anthropole, CH-1015 Lausanne, Switzerland

[3] IMG, Laboratoire des Isotopes Stables, Faculty of Geosciences and Environment, University of Lausanne (UNIL), Anthropole, CH-1015 Lausanne, Switzerland

[4] IG, Institute of Geophysics, Faculty of Geosciences and Environment, University of Lausanne (UNIL), Amphipole CH-1015 Lausanne, Switzerland

Abstract

The construction of new underground infrastructures is a permanent issue in mountainous regions and may cause environmental impacts on the surrounding regions. Understanding on the interferences of tunnelling on the hydrogeological resources, such as wells, streams and springs, is an important and largely open question and addressing it requires a number of indirect investigations on the hydrogeological environment, such as hydro-geochemical analysis and geophysical surveys. In this chapter, are presented the results of studies on seven springs in Sant'Antonino, in the region surrounding the north portal of the Monte Ceneri base tunnel. On these springs, the physico-chemical parameters are monitored and other geochemistry data are analyzed in detail. Moreover Electrical Resistivity Tomography (ERT) was applied in order to identify preferential pathways for groundwater circulation, its links with springs' localization and recharge area. At the end, using the data coming from this combined approach, for these springs was formulated a hydrogeological conceptual model, which has been used such as test to assess the springs' vulnerability to tunnel drilling using a parametric method.

6.1 Introduction

The construction of new tunnels in mountainous regions is nowadays a constant requirement, contributing frequently to the sustainable development, for instance by increasing the rail freight capacity. Nevertheless, it may also have environmental impacts, among which negative ones on the hydrogeological cycle. Understanding the interaction between tunneling and groundwater, especially in fractured rock masses, is a very complex matter. Nowadays, the state of the art of the research in this field includes substantially three possible approaches: (*i*) analytic (e.g. Goodman et al., 1965; Lei, 1999; El Tani, 2003; Kolymbas & Wagner, 2007; Perrochet & DeMatteis, 2007), (*ii*) numerical (e.g. Vincenzi et al., 2010), and (*iii*) parametric methods.

This latter approach consists in evaluating the potential impact of tunneling in terms of hazard. In recent years two possible applications have been proposed: to obtain the tunnel inflow hazard distinguishing between major and minor inflows (Cesano et al., 2000) and to evaluate the aquifer depletion hazard caused by the new tunnel drilling and its impact on the surrounding surface springs (De Matteis et al. 2001, Torri et al., 2007; De Matteis 2008). Parametric methods can be easily implemented using a Geographic Information System – GIS (Pancescu, 2006), facilitating the assessment of springs and wells vulnerability to the tunnel construction. This approach does, however, require good knowledge of geology and groundwater flow system in order to formulate reliable hypothesis on the hydrogeological cycle that may be considered as a basic *Hydrogeological Conceptual Model* (HCM). Having a well-founded HCM, a parametric method, even though it is clearly an oversimplification of the problem, is particularly suitable for estimating the possible impact of tunneling.

In this work, a combined approach was used to obtain a data-supported groundwater circulation model in fractured rock by integrating hydrogeochemical and geophysical data necessary to evaluate springs' vulnerability to tunnel drilling according with De Matteis et al. (2001) method.

6.2 Geological and hydrogeological settings

The Ceneri base tunnel, which is entirely located within the crystalline south-alpine basement, crosses two different tectonic zones: (i) the Strona-Ceneri zone (amphibolites, Ceneri orthogneiss and paragneiss, Giumello paragneiss) in the north and (ii) the Val Colla zone (S. Bernardo orthogneisses, Stabiello paragneisses, schists and phylonites) in the south. These two zones are separated by Val Colla Line, also known as Caslano-Taverne-Gazzirola Line, a fault that according to the Buergi et al. (1999) classification is mainly composed of mylonites of the Paleozoic era, with a thickness of about 600 m (Pini and Rossi, 2009).

The northern portal is located near Vigana (Figure 6.1). The first part was excavated in the unconsolidated material and after about 20 meters of drilling it reached fractured crystalline rocks, in particular the Ceneri orthogneiss (100-150 m) and subsequently the Ceneri paragneiss which widely outcrops in this region. The thickness of the rock above the tunnel increases from about 10 m, near the northern portal, to 800 m at a distance from the portal of about 2 kilometers. A geological sketch map of the tunnel is represented in Figure 6.2. It is important to note also that this segment of tunnel is excavated below a creek flowing northward.

As shown by several studies (Ofterdinger, 2001; Maréchal and Etcheverry, 2003, Masset and Loew, 2010), in crystalline rocks, such as gneisses, a higher fracturation with open discontinuities is registered in the uppermost part (100-200 m depth), due to stress release. For this reason, water circulation in the upper part is favored since fracturation increases the hydraulic conductivity. In fact, from exploration boreholes carried out in the uppermost 100 m, the rock is often highly fractured and groundwater was frequently encountered. The groundwater level was identified about 10-20 m below the surface. Consistent water inflows (from 10 to 20 l/s every 100 m of tunnel) were registered in the first kilometer of tunnel.

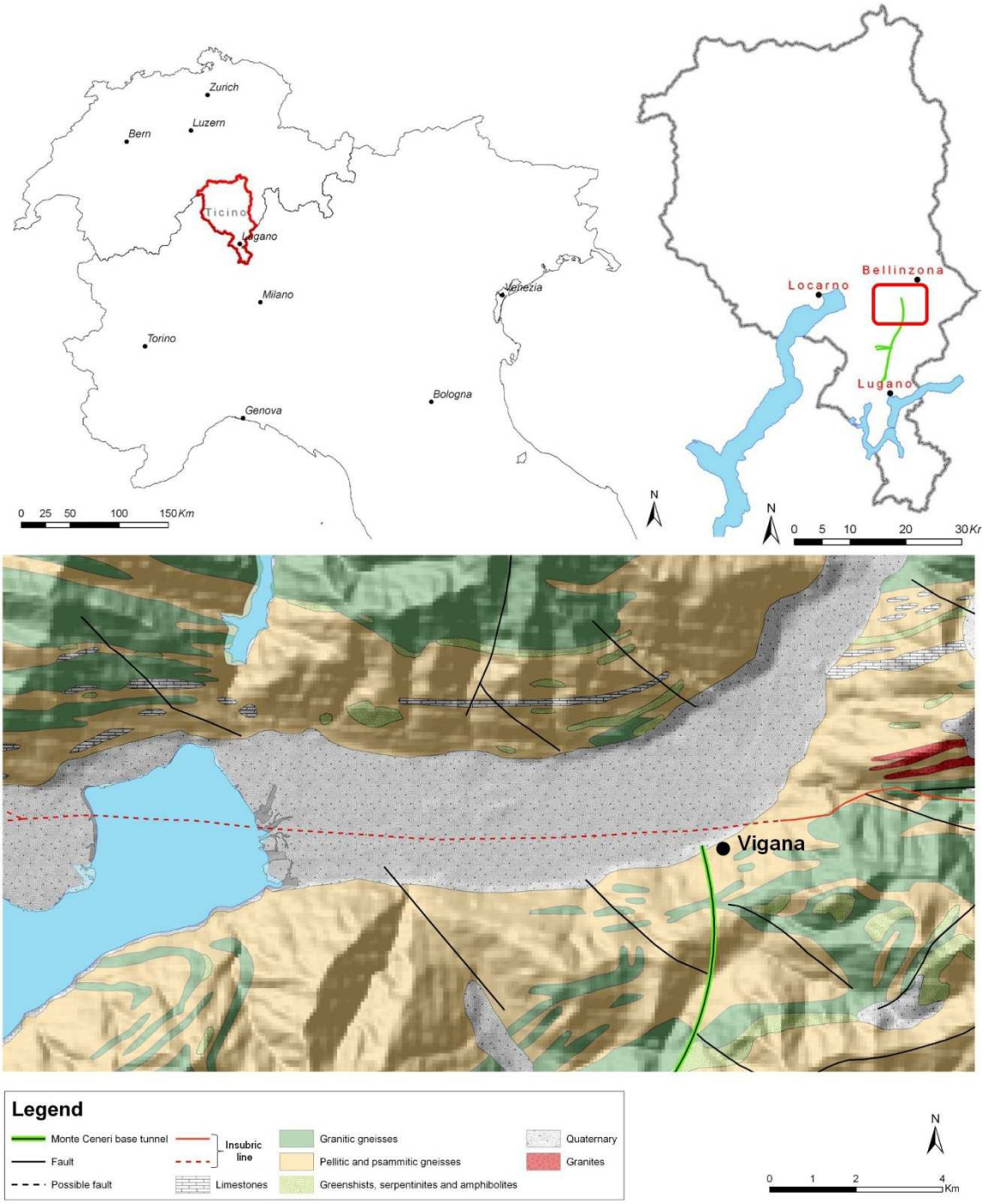

Figure 6.1 - Monte Ceneri base tunnel location and geological map of the considered region (based on the 1:200'000 geological map of the Switzerland) with superimposed the position of the Insubric Line individuated in Swiss tectonic map (1:500'000). Part of the tunnel axis is also shown[Sources of the data: Swiss Federal Office of Topography, CGIAR-CSI, Alptransit Inc.].

A series of cataclastic structures, which can be defined as *kakirites* and *cataclasites* using the classification proposed by Buergi et al. (1999), have been recognized in the tunnel geological logs. Their presence is associated to the Insubric Line, also called Periadriatic lineament, which marks a first-order tectonic boundary between the south-alpine basement and the main body of the Alps (Schmid et al. 1989; Schmid et al, 2004), in correspondence of the Ticino alluvial plain, as shown in Figure 6.1.

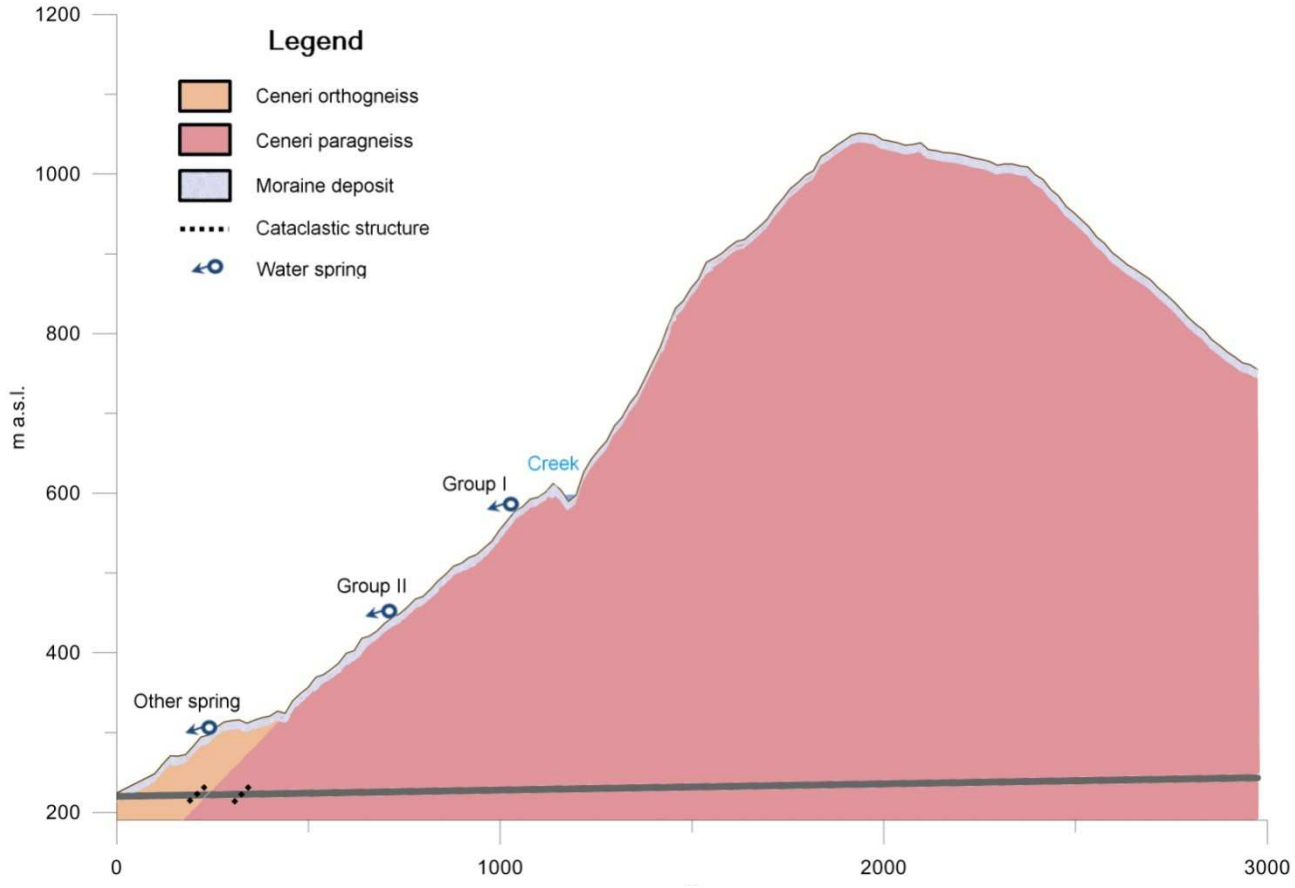

Figure 6.2 - Geological sketch profile of the north portal of the Monte Ceneri base tunnel, reconstructed by tunnel geological logs. The monitored springs (Marzocchi et al., 2010) are placed on three different levels. In this paper, only two groups of them are selected, because they are closer to the tunnel axis and thence higher influences can be expected. A creek flowing on the slope direction is placed above the tunnel axis for the first hundreds of meters and cross the tunnel axis at a progressive distance of 1 Km as evidenced by the profile.

6.3 Climate

The climatic regime of the studied area is typical of the southern Alpine region. The precipitation rate in Ticino is higher compared to that of the northern Switzerland and the Mediterranean area (Begert et al, 2005). Rainfall peaks are normally present in spring and autumn, and also the summer is normally not a dry season; only during the winter season the precipitations are normally lower and snowy, nevertheless it is difficult identify annual drought continuing seasons that could be defined as recession periods for the spring's discharge (Figure 6.4).

Mean yearly precipitations in the closest rain gauges of cantonal hydrologic network, Isone and Giubiasco, are 1498 and 1810 mm/year respectively (data are collected since 1979 in the Isone and since 1988 in the Giubiasco rain gauge).

In our region, the recent years are quite humid, as well shown by the comparison of the precipitations in the previous cited rain gauges during the last ten years that in Figure 6.3 are compared with the mean yearly values. For example annual precipitations in 2009 are about 106% of the long-term means, and in 2010 about 109%. Other details about the annual data and the meteorological trends are reported on the annual hydrologic report for the Ticino canton (IST, 2010) that is yearly published by the Institute of Earth Science (SUPSI).

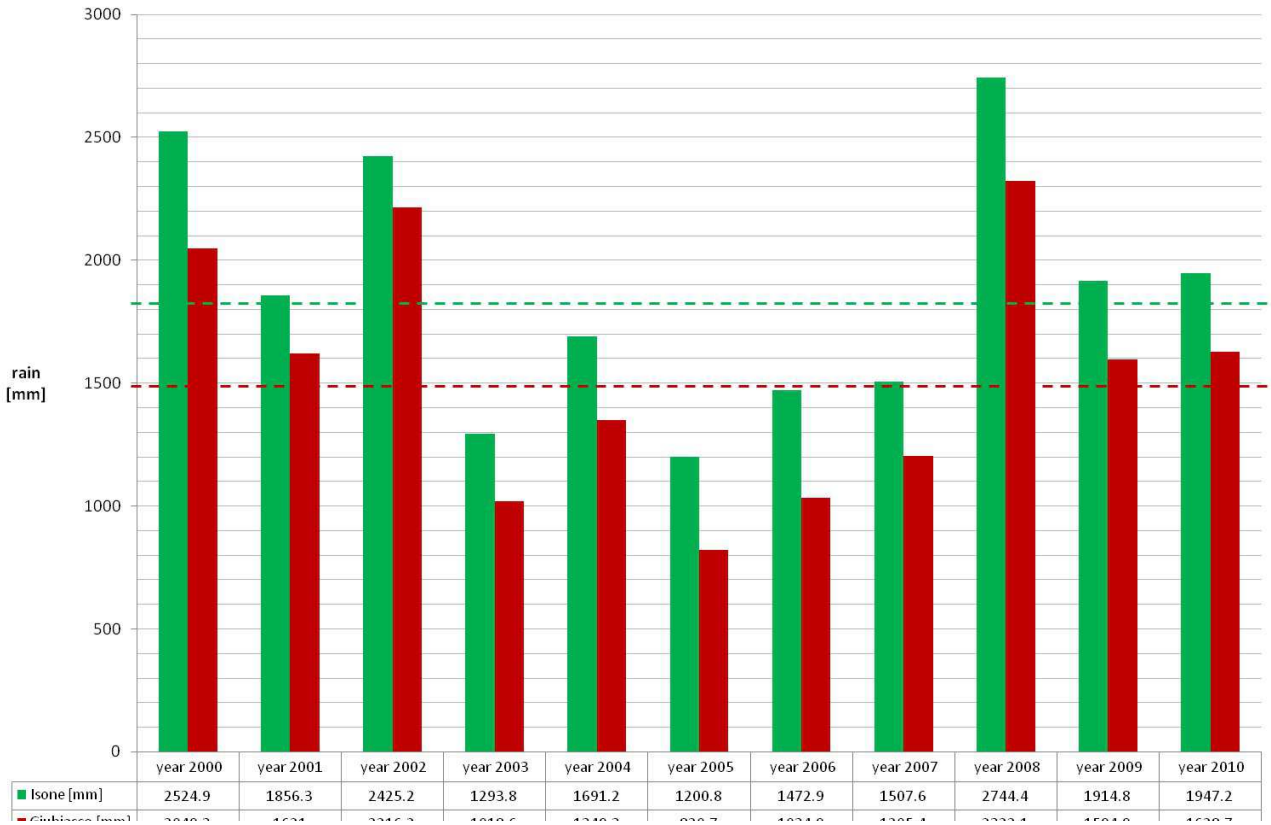

Figure 6.3 - Annual rain measured in the closest rain gauges (Isone and Giubiasco) since 2000.

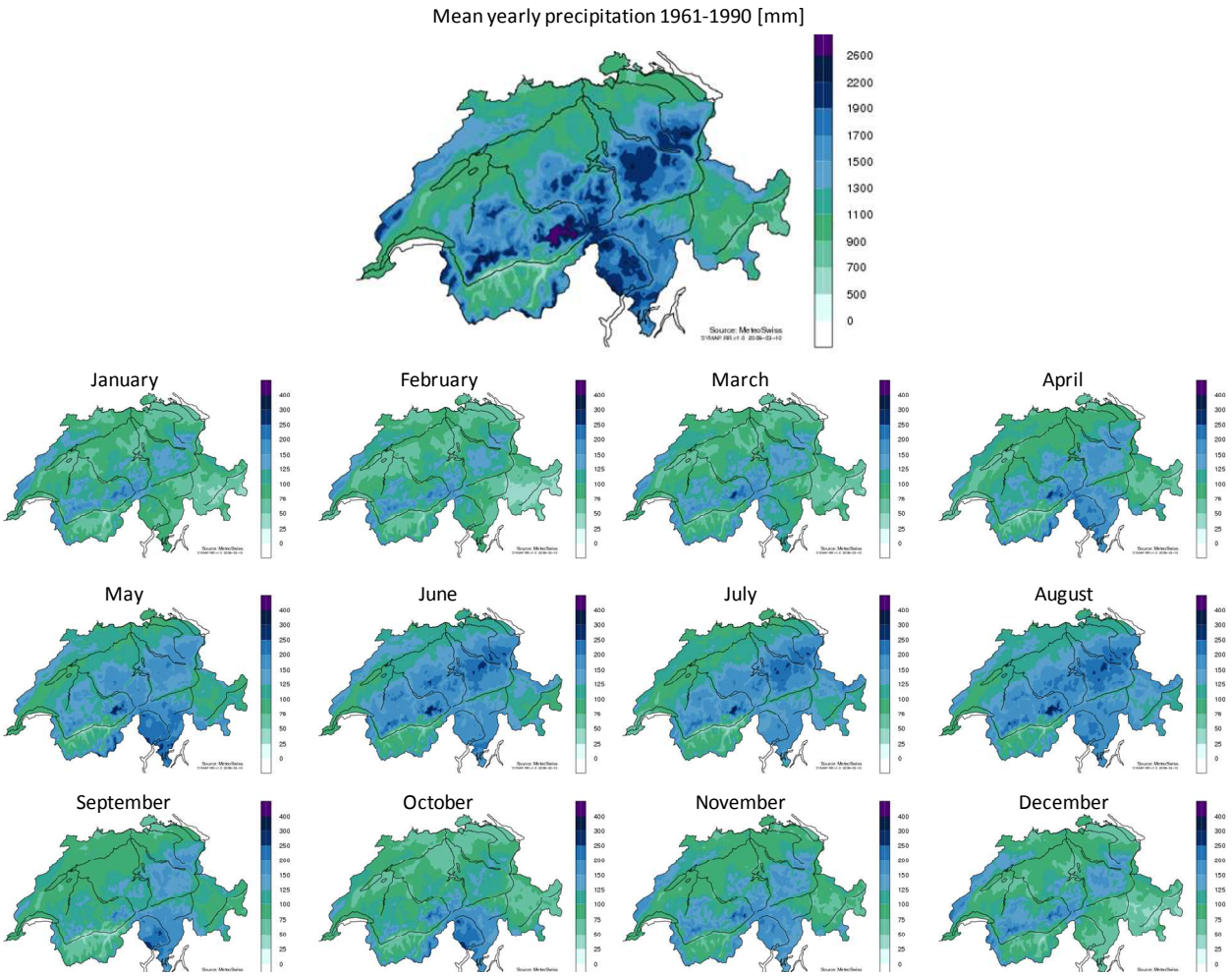

Figure 6.4 - Long-term (1961-1990) statistics on precipitation elaborated by MeteoSwiss. Mean yearly and monthly values 1961-1990 [mm]. Observing the mean monthly values is clear that is difficult find a specific drought season during the year, and thence a spring recession period [Sources of the data: MeteoSwiss].

6.4 Methods

From the about 750 springs present in the Monte Ceneri region, 30 were selected by Colombi and Baumer (1995) to be monthly monitored during drilling operations on the basis of criteria of *(i)* relevance (use and discharge) and *(ii)* distance from the tunnel. On these springs, a monitoring network (Marzocchi and Pera, 2009, Marzocchi et al., 2010) of physico–chemical parameters (discharge, electrical conductivity, temperature and pH) and geochemical data (major ions and stable isotopes of oxygen and hydrogen) was established.

The region surrounding the northern portal is particularly interesting from the hydrogeological point of view as previous shown in chapters 4 and 5. Hence, in this region, 7 springs are chosen, among the monitored ones, on the basis of their accessibility for the geoelectrical surveys. In this work, the possible integration of geochemical and geophysical approaches in order to formulate a HCM for the selected springs and assess their vulnerability to tunnel drilling is presented.

From a morphological point of view (Figure 6.2 and Figure 6.5) the 7 considered springs can be divided in two different groups:

- ✓ the first is composed by the SAN4, SAN5 and SAN6 springs. They are placed at a higher elevation above sea level and exactly above the tunnel axis.
- ✓ the second group is composed by SAN7, SAN8, SAN9 and SAN1 springs. They are placed at lower elevations and to the east of the tunnel axis.

From a geological point of view, they are localized close to fractured outcrops.

Discharge (Q), electrical conductivity (EC), temperature (T) and pH were measured on a monthly basis during a year and samples for stable isotope measurements were taken. Moreover, two geochemical analyses of major ions in a dry and a wet season were made.

Discharges have been measured with volumetric methods (keeping the time employed in order to fill a known volume tank), while EC, pH and temperature have been taken using a pH/conductivity meter, EC is normalized at the standard temperature of 25°C. Definition of mean annual discharge values, but also of temperature, EC and pH, is not always a simple process in presence of irregular and/or low frequency of measurements. Seasonal average can be an approach that takes in account eventual temporal irregularity in data collecting (Gargini et al. 2008). In this work, the chosen approach was to perform an average on the time domain of the collected data using the following equation:

$$p_m = \frac{\int_{t_0}^{t_1} p\,dt}{\Delta t} \qquad (6.1)$$

where the physical parameter p is integrated on the time domain (from t_0 to t_1) and divided by the time interval Δt (= $t_0 - t_1$). The calculations were done using the R statistical software (R Development Core Team, 2011) and in particular the zoo package (Zeileis and Grothendieck, 2005), specifically implemented to manage irregular time series and compute statistical parameters.

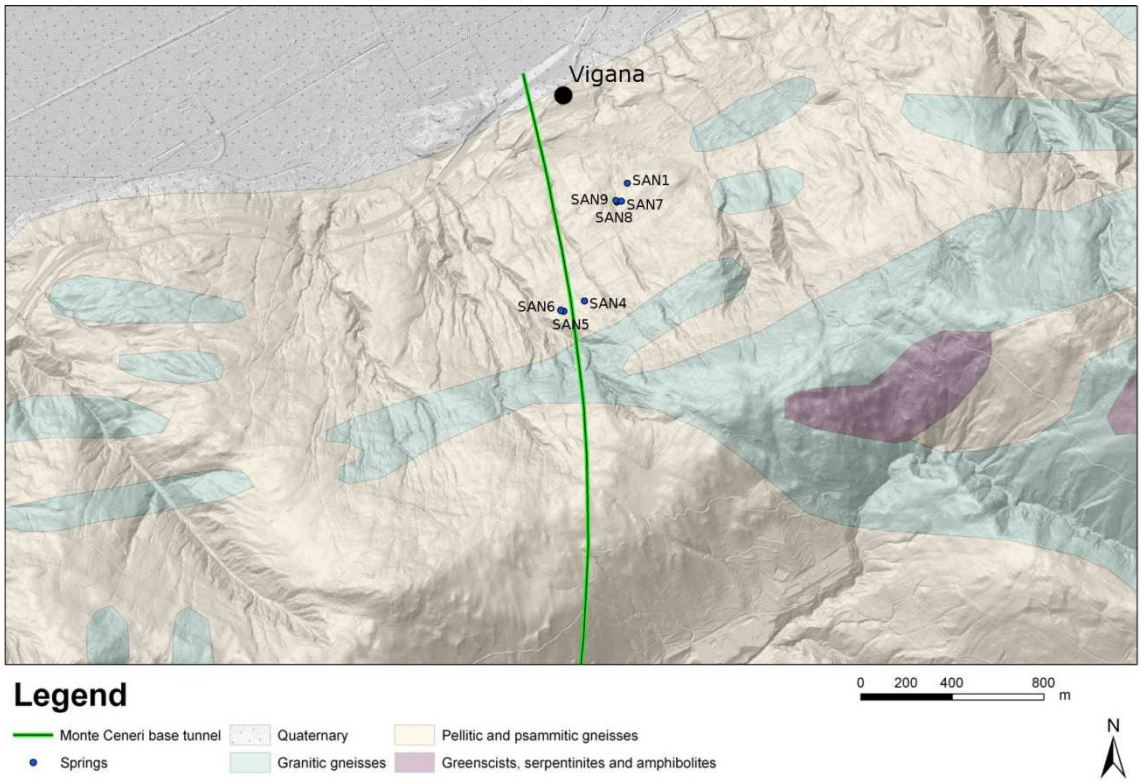

Figure 6.5 - Location of the seven selected springs in the region surrounding the north portal of the Monte Ceneri base tunnel [Source of the data: Swisstopo, Cantonal database and Alptransit Inc.].

Major ions (F^-, Cl^-, NO_2^-, NO_3^-, SO_4^-, Li^+, Na^+, NH_4^+, K^+, Mg^{2+}, and Ca^{2+}) have been determined by ion chromatography on a dual Dionex ICS-2100-1100 system of IMG-Centre d'Analyse Minérale of University of Lausanne. Organic (TOC) and inorganic carbon (TIC) were measured by a C-analyzer (LiquiTOC Elementar Inc.), and HCO_3^- has been calculated from TIC. The detection limit for all the ions is 0.01 mg/L and 0.02 for organic and inorganic carbon; while the uncertainty of the measurement is 15% for both the ions and the carbon analyses, resulting in not good ionic balance as shown in Table 6.2.

Oxygen and hydrogen stable-isotope composition measurements of water were carried out at the Stable Isotopes Laboratory of the University of Lausanne using a Wavelength-Scanned Cavity

Ring Down Spectroscopy (WS-CRDS) based analyzer (Picarro isotopic H2O L1102-i). Because memory effect is known to affect the analytical measurements, 8 injections per samples were effectuated of which only the last four were used for data reduction and normalization. For calibration, internal laboratory standards calibrated to VSMOW were inserted repeatedly within each analytical sequence (each 12-13 samples) as well as at the beginning and at the end of the sequence. For the set of standards measured at the beginning and at the end of the sequence, 12 injections were effectuated of which the last five injections were used for calculations. Results are expressed using the δ-values with respect to the Vienna Standard Mean Ocean Water (VSMOW) (i.e., δD and $\delta^{18}O$) as follows:

$$\delta = \frac{R_{sample} - R_{VSMOW}}{R_{VSMOW}} \times 1000 \qquad (6.2)$$

where R_{sample} is the stable-isotope ratio ($^2H/^1H$ or $^{18}O/^{16}O$) of the sample and R_{VSMOW} is the ratio of VSMOW. Typical reproducibility for this method is approximately ±0.08 ‰ and ± 0.8 ‰ for $\delta^{18}O$ and δD, respectively.

Physico-chemical parameter monitoring as well as geological and geomorphological observations are useful tools to investigate the springs' characteristics; however, they give poor information about the geometry of the flow system and the possible existence of preferential flow paths within their watershed. Therefore, 2D Electrical Resistivity Tomography (ERT) was applied, since it is able to give an image of the subsoil on the basis of the electrical resistivity contrast between the unweathered crystalline rock (1'000-10'000 ohm·m) and the weathered zones eventually bearing groundwater (10-1'000 ohm·m), as evidenced by several literature studies (Di Maio et al., 2007; Piegari et al. 2009; Fazzito et al., 2009, chapter 4).

The resistivity measurements were performed using an IRIS-SYSCAL PRO System with a multi-electrode cable with outlet spacing of 10 m. 48 or 24 electrodes were used resulting total profile lengths of 470 or 230 m, respectively. With previous investigations conducted in the same region, two different configurations (Wenner-Schlumberger and Dipole-Dipole) were tested obtaining always better results, in terms of consistency of the resistivity model, with the Wenner-Schlumberger configuration, which hence has been applied. The investigated depth, using a Wenner-Schlumberger configuration is about 1/5 of the total length at the center of the 2D profile (Kirsch, 2006).

Using the PROSYS software, the apparent resistivity data were filtered, to remove the acquisition errors and the rough surface topography was incorporated into the model. Finally, the RES2DINV software (Loke, 2004) was used for the inversion of the data in order to obtain a 2D resistivity profile of the probed subsurface region.

Concerning the inversion method, after a number of tests, a finite difference algorithm was chosen; the elements of the Jacobian matrix are thence calculated using the Gauss-Newton algorithm including smoothing of model resistivity.

In order to assess the accuracy of the 2D obtained resistivity sections, two parameters, which are available from the inversion software, have been considered:

i) the Root Mean Square (RMS) statistical error;
ii) the smoothed sensitivity of blocks.

The first parameter indicates the cumulative difference, in statistical terms, between the apparent resistivity measured in field and that calculated simulating the same acquisition scheme on the 2D resistivity section, and it is a good parameter of the consistency of the entire model (Tassone et al., 2010).

The smoothed sensitivity, also referred to as subsurface sensitivity, depends on the measured data set. It is a normalized measure of amount of information about the resistivity of a model block cell in which the underground is discretized for the numerical iterations needed to obtain the resistivity model (Loke, 2004). After a number of tests the chosen approach has been to represent a transparent template over the 2D resistivity model wherever the smoothed sensitivities are lower than a threshold value of 0.2. More detail about the adopted inversion algorithm and the parameters used to assess the reliability of the 2D model are reported in chapters 3 and 4.

Finally, in this chapter the De Matteis method (De Matteis et al. 2001, Torri et al., 2007; De Matteis 2008) was chosen between the various parametric method (chapter 1). Using this approach, for each spring, a numerical index of the probability of occurrence, or better hazard of drawdown, that is called Drawdown Hazard Index (DHI) has been calculated. In particular, as expressed by following equation (6.3) DHI is given by the product of:

i) the probability of potential inflow (PI)
ii) other parameters related to the spring hydrogeological characteristics.

In particular, PI is related to the tunnel geological conditions, as expressed by the following equation:

$$PI = 0.41 \cdot FF + 0.22 \cdot MK + 0.17 \cdot OV + 0.20 \cdot PZ \qquad (6.3)$$

where FF is the factor considering the expected fracture frequency at the tunnel depth , MK the rock permeability, OV the overburden, PZ the plastic zone radius.

Therefore the PI is correlated with the other parameters related to springs in order to obtain the DHI:

$$DHI = PI \cdot (IF + 1) \cdot (ST + 1) \cdot (DT + 1) \qquad (6.4)$$

where IF is the intersection of main faults, ST the spring type and DT the distance from the tunnel.

6.5 Results

6.5.1 Geochemistry

The data of physico-chemical and stable isotope monitoring are graphically represented in the Figure 6.6.

- *Discharge*

The discharge regime of the analyzed springs is mainly influenced by the direct recharge regime and in particular by the hydrologic and more generally climatic conditions of the studied site that are previously analyzed in detail. This is a consequence of the predominantly shallow nature of the groundwater circulating through fractured crystalline rocks of the site (Colombi and Baumer, 1995). Concerning springs discharges, the mean values for the year 2010 (Table 6.1) were evaluated using equation (*6.1*). It is important to note that, as previously demonstrated, from the hydrological point of view, 2010 is a humid year. Discharges of the analyzed springs are generally low, according to the Meinzer (1923) classification; in fact these springs belong to VI and VII classes. It is typical of the fractured gneiss; indeed in this type of rocks there is a high density of springs, but with low or very low discharges. Obviously this fact is correlated with small drainage areas, and in particular smaller for the first group of springs (~ 40'000 m^3/year of discharge) and slightly higher for the second group (~ 160'000 m^3/year of discharge). The Discharge Variability Index (Meinzer, 1923; Gargini et al, 2008) is generally very high as well shown also by Figure 6.6. The only exception is constituted by the SAN6 spring that, in accordance to the Meinzer variability classification could be considered as a quasi *constant spring*. Nevertheless, despite the springs' discharges of springs are very variable and not so high, it is important to point out that they all have reservoirs big enough to maintain discharges, even though low, during drought periods like in the 2003 summer (Bestenheider, 2005).

- *Electrical conductivity (EC), pH and temperature*

The electrical conductivities (EC_{25}) of the spring waters are generally low (Table 6.1), which is typical of shallow aquifers in fractured crystalline gneiss rocks. Moreover, variations in discharge are often accompanied by changes in spring water conductivity. Observing the EC_{25} behavior in correspondence of the discharge peak occurred during May 2010 as a result of intense rain events it is possible to note two different behaviors: in Group I (SAN4, SAN5, SAN6 springs), increasing the discharge, a decrease, even though less pronounced, of electrical conductivity has been registered. It denotes a possible "*dilution effect*" due to the aquifer recharge as consequence of rain contributions.

On the contrary, in group II (SAN7, SAN8, SAN9, SAN1), an increase in EC_{25}, even if low, was registered. This kind of behavior can be named "*piston effect*", assuming that water that falls on a slope is transmitted downstream with a pressure wave and causes a sudden exfiltration on the drainage area. Practically, infiltrating water to the aquifer act as a piston on residential groundwater in the fracture system (Kies et al. 2005); it is a common effect, especially in conduit systems (karst systems and crystalline fractured rocks), and it is typically characterized by an increase in conductivity corresponding to the increase in discharge.

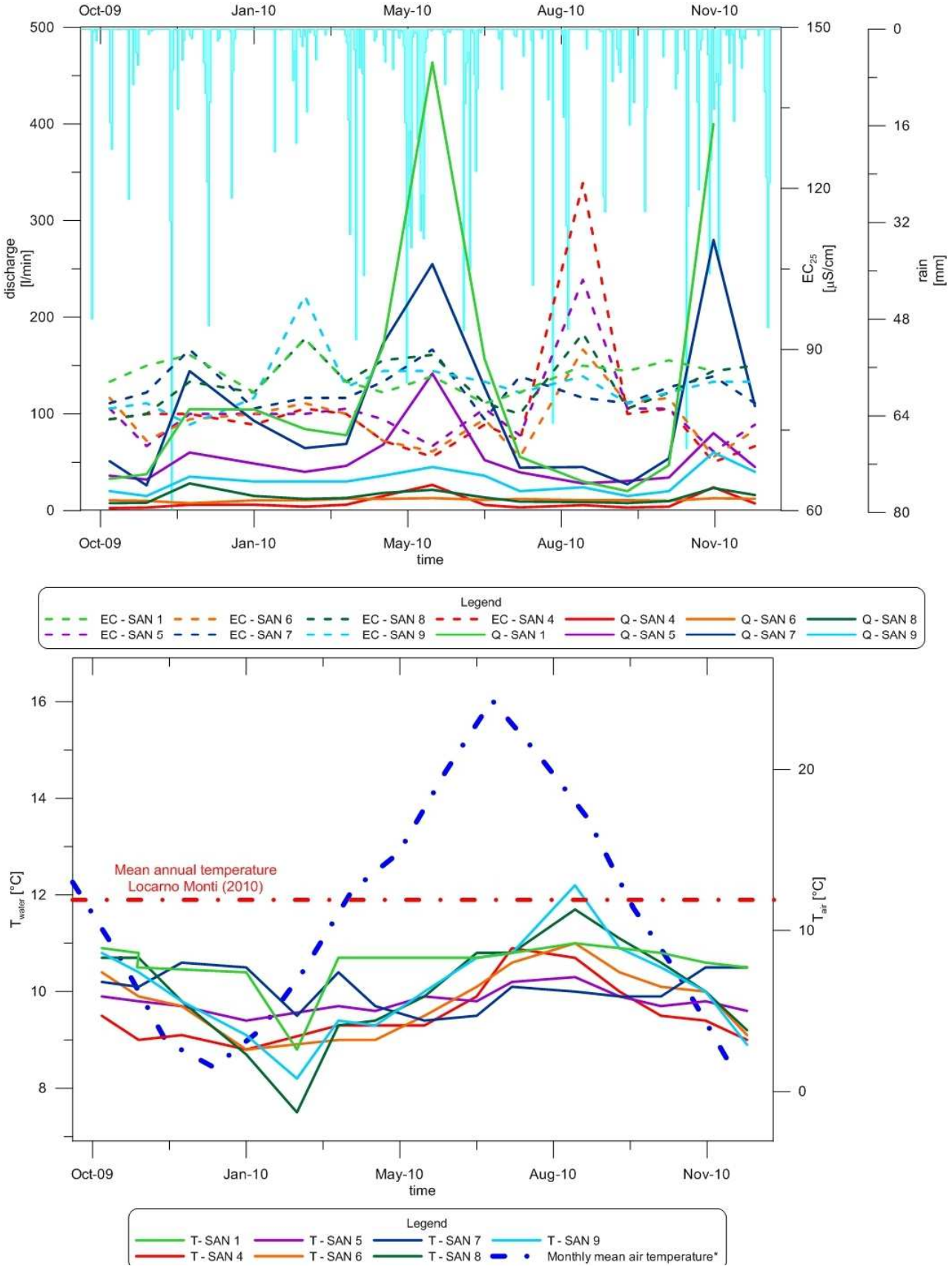

Figure 6.6 – Discharge (Q), electrical conductivity (EC) and temperature (T) on the selected springs correlated with the precipitations collected in the Giubiasco rain gauges (IST-SUPSI) and the temperature in Locarno Monti meteorological station (Meteoswiss).

pH remains constant throughout the year in both groups with values ranging between 6.2 and 7.2, which are typical values of slightly acid or neutral waters. Concerning temperature (Table 6.1

and Figure 6.6) the springs of first group (SAN4, SAN5, SAN6 springs) are more constant ranging from 8.8 to 11°C ; while in group II seasonal temperature variability is observed ranging from 7.5 to 12.2°C.

The mean air temperature available from the Locarno meteorological station (366 m a.s.l) is 11.5°C (MeteoSwiss), while in 2010 year the mean temperature has been 11.9 °C. It is important to note that there are few differences between the locations of the temperature monitoring point and that of water springs. In fact the Locarno Monti meteorological station is placed on a southern slope of a mountain and closest to the Maggiore Lake, while the analyzed springs are in a northern slope of the mountain with a lower solar radiance, at higher elevations and further away from the lake.

To take in account these differences that unavoidably change the mean yearly temperature of the spring site, (Figure 6.6) is needed in order to compare the temperature of spring with the mean monthly and yearly air temperature in Locarno Monti (MeteoSwiss).

In Table 6.1 a statistical summary of the collected data is reported, while raw data of physico-chemical monitoring are presented in appendix B.

Table 6.1 – Mean values and variability resulting from monitoring conducted on the selected water springs. The statistical computation on discharge, temperature, pH and EC are obtained on the 2010 year in order to compare them with the precipitation collected in the same monitoring time, while the stable isotope are monitored for an hydrologic season (from October 2009 to September 2010).

Spring	Elevation (m a.s.l.)	Q_{Max} (l/m)	Q_{min} (l/m)	Q_m (l/m)	Meinzer Class	DVI (%)	T_m (°C)	pH	EC_{25} (µS/cm)	δ18O (‰ VSMOW)	δD (‰ VSMOW)
SAN 4	582	27.5	3	9.2	VII	256%	9.6	6.50	79	-9.00	-57.40
SAN 5	568	142	28	55	VII	207%	9.8	6.50	79	-8.80	-55.54
SAN 6	560	12.8	9	11.3	VII	33%	9.7	6.50	77	-8.97	-56.64
SAN 7	448	280	27	112	VI	226%	10	6.25	82	-9.25	-59.48
SAN 8	438	23	7.7	14	VII	110%	9.9	6.50	85	-9.36	-59.90
SAN 9	435	60	15	32	VI	140%	10	6.40	85	-9.36	-60.12
SAN 1	420	464	20	145	VI	306%	10.5	6.55	85	-9.24	-59.07

- *Major ion analysis*

Results of analysis of major ions on collected samples are reported in Table 6.2; while in Figure 6.7 the major cations and anions are represented in % respect of the total according to the Schmassmann classification. This classification is frequently used by hydrogeologists (Högl,1980, Dubois, 1992; Hesske, 1995): the major ions concentrations are elaborated in meq/l and hence expressed as percentage of the total cations and anions respectively. Finally, the waters are classified only on the basis of the cations and the anions more abundant than 20% by descending sorting.

Table 6.2 - Chemical analysis of major ions of the selected springs in a dry (November 2009) and an humid (May 2010) season. As evidenced by charge balance the analysis of the SAN7 spring carried out in November 2009 are probably not representative.

Spring	**Date**	**pH**	**T (°C)**	**EC_{25} (µS/cm)**	**Q (l/min)**	**Na (mg/l)**	**K (mg/l)**	**Mg (mg/l)**	**Ca (mg/l)**	**F (mg/l)**	**Cl (mg/l)**	**NO3 (mg/l)**	**SO4 (mg/l)**	**HCO3 (mg/l)**	**TDI (mg/l)**	**Charge balance**	**Schmassmann classification**
SAN4	13/11/09	6.65	9.0	70	3	3.45	0.77	2.11	15.52	0.10	2.81	5.18	12.39	49.32	91.64	-5%	$Ca\text{-}HCO_3$
SAN 5	13/11/09	6.60	9.8	72	32	3.82	0.92	2.00	7.11	0.10	2.34	5.63	13.47	31.51	66.94	-15%	$Ca\text{- }Na\text{-}Mg\text{-}HCO_3$
SAN 6	13/11/09	6.60	9.9	73	10	3.87	0.93	2.11	15.97	0.12	2.34	5.20	13.72	62.29	106.59	-11%	$Ca\text{-}HCO_3$
SAN 7	13/11/09	6.45	10.1	82	26	4.28	0.95	1.87	6.79	0.11	4.9	3.75	16.06	73.21	111.94	-42%	$Ca\text{- }Na\text{-}Mg\text{-}HCO_3$-
SAN 8	13/11/09	6.80	10.7	78	8	4.07	0.81	1.82	11.16	0.11	4.25	3.56	16.08	11.49	53.39	+12%	$Ca\text{-}HCO_3\text{-}SO_4\text{-}Cl$
SAN 9	13/11/09	6.40	10.4	80	15	4.08	0.91	1.91	16.28	0.11	4.13	3.71	15.90	30.87	77.93	+7%	$Ca\text{-}HCO_3$
SAN 1	13/11/09	6.50	11.6	87	118	3.53	1.60	2.38	13.28	0.12	1.98	5.53	20.02	15.27	63.74	+3%	$Ca\text{-}HCO_3\text{-}SO_4$
SAN 4	18/5/10	6.71	9.3	70	26.5	3.90	0.72	1.92	6.50	0.04	1.40	4.29	11.89	16.42	30.66	+3%	$Ca\text{- }Na\text{-}Mg\text{-}HCO_3\text{-}SO_4$
SAN 5	18/5/10	6.43	9.9	72	141.7	4.17	0.98	1.95	6.78	0.06	1.30	4.16	11.29	21.48	30.69	+1%	$Ca\text{- }Na\text{-}Mg\text{-}HCO_3\text{-}SO_4$
SAN 6	18/5/10	6.30	9.5	71	12.8	4.07	0.82	1.92	6.68	0.06	1.24	4.25	11.51	13.57	30.54	+10%	$Ca\text{- }Na\text{-}Mg\text{-}HCO_3\text{-}SO_4$
SAN 7	18/5/10	6.26	9.4	90	255	6.43	1.29	2.03	7.21	0.06	8.25	3.61	13.17	9.94	42.04	+7%	$Ca\text{- }Na\text{-}Cl\text{-}HCO_3\text{-}SO_4$
SAN 8	18/5/10	6.5	9.9	89	21.4	5.89	0.91	1.99	7.63	0.06	8.66	3.46	12.10	8.19	40.70	+9%	$Ca\text{- }Na\text{-}Mg\text{-}Cl\text{-}HCO_3\text{-}SO_4$
SAN 9	18/5/10	6.49	10	86	45	5.41	0.98	2.03	7.63	0.06	7.03	3.08	12.47	8.07	38.68	+11%	$Ca\text{- }Na\text{-}Mg\text{-}HCO_3\text{-}SO_4$
SAN 1	18/5/10	6.29	10.7	85	464	3.92	1.71	2.57	7.71	0.06	1.59	10.71	15.36	5.75	43.63	+12%	$Na\text{-}Mg\text{-}Ca\text{-}NO_3$

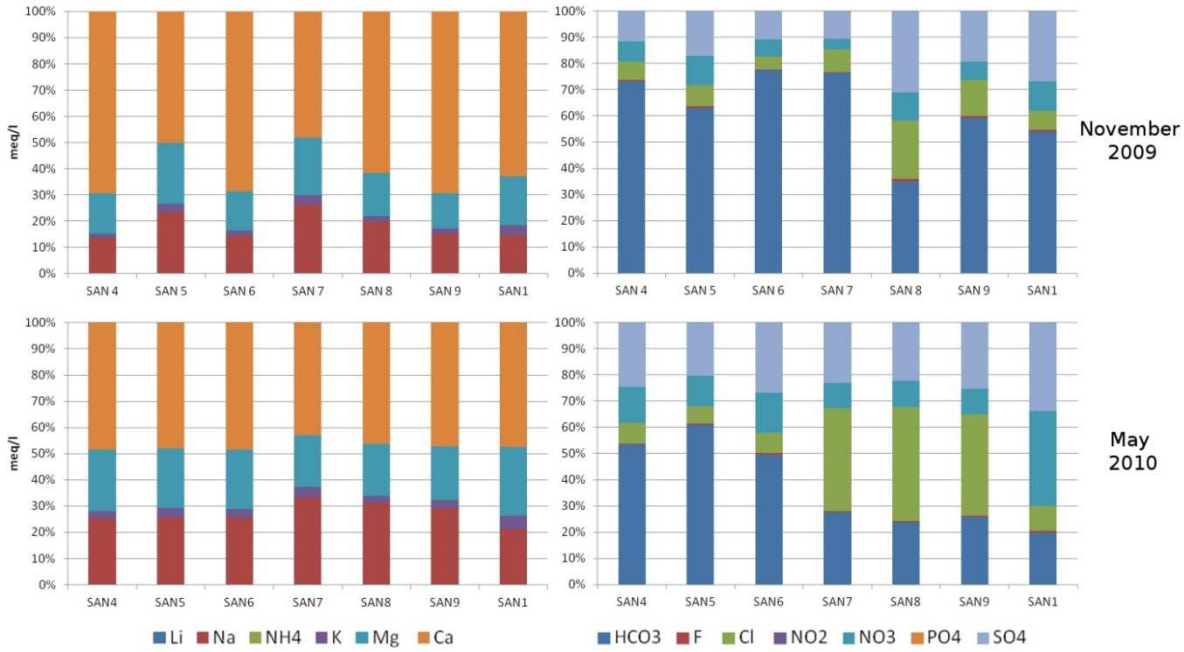

Figure 6.7 - Percent of the major ions in meq/l according to the Schmasmann geochemical classification.

Observing the major ions in the 7 considered springs, the two groups of springs can be distinguished and a few observations can be made. Almost all springs are characterized by a high content of sodium, magnesium and calcium cations. Concerning anions, in the first group a high predominance of bicarbonate ion (HCO_3^-) has been observed, while in the second group there is a sensibly higher content in sulfates (SO_4^{2-}), and especially in May a higher content of chloride ion (Cl^-).

Both the groups are typical of water circulating within fractured gneiss (Dubois, 1993; Derron, 1999); in the second group the presence of sulfates (SO_4^{2-}) is distinctive also of other springs close to the northern portal of the tunnel and of water samples collected from tunnel inflows (see chapter 5) and is perhaps due to the presence of gypsum bands or other minerals that release sulfates in groundwater (De Matteis, 1995). The increment of Cl^- content in may, as preliminary hypothesis, can be related to the dilution of salt normally used for winter road maintenance (NaCl or $CaCl_2$).

On the basis of major ions analyzed, also saturation indexes (SI) were calculated using PHREQC-2 software (Parkhurst and Appelo, 1999) for all conceivable mineral species (Table 6.3). All the springs are under-saturated respect of about all analyzed species, confirming that the springs are the rising up of shallow groundwater aquifers.

Table 6.3 - Saturation indexes (SI) for few mineral species (Calcite, Aragonite, Gypsum, Anhydrirte, Fluorite, Halite), TDI/EC and Ca/HCO3 ratio on the selected springs in November and may

Spring	Date	$SI_{Calcite}$	$SI_{Aragonite}$	$SI_{Dolomite}$	SI_{Gypsum}	$SI_{Anhydrite}$	$SI_{Fluorite}$	SI_{Halite}	TDI/EC_{25}	Ca/HCO_3
SAN 4	13/11/09	-2.3	-2.4	-5.3	-2.9	-3.2	-3.3	-9.5	1.31	0.48
SAN 5	13/11/09	-2.8	-3.0	-6.1	-3.2	-3.4	-3.6	-9.5	0.93	0.34
SAN 6	13/11/09	-2.2	-2.4	-5.2	-2.8	-3.1	-3.1	-9.5	1.46	0.39
SAN 7	13/11/09	n.d.	n.d.	n.d.	n.d.	n.d.	n.d.	n.d.	n.d.	n.d.
SAN 8	13/11/09	-2.8	-3.0	-6.3	-2.9	-3.2	-3.1	-9.3	0.68	1.48
SAN 9	13/11/09	-2.8	-2.9	-6.4	-2.8	-3.0	-3.2	-9.3	0.97	0.80
SAN 1	13/11/09	-2.7	-2.8	-5.9	-2.8	-3.0	-3.2	-9.7	0.73	1.32
SAN 4	18/5/10	-3.0	-3.2	-6.5	-3.2	-3.5	-4.4	-9.8	0.44	0.60
SAN 5	18/5/10	-3.2	-3.4	-6.9	-3.3	-3.5	-4.1	-9.8	0.43	0.48
SAN 6	18/5/10	-3.3	-3.5	-7.1	-3.2	-3.5	-4.1	-9.8	0.43	0.75
SAN 7	18/5/10	-3.9	-4.0	-8.2	-3.2	-3.4	-4.1	-8.8	0.47	1.10
SAN 8	18/5/10	-3.5	-3.7	-7.6	-3.2	-3.4	-4.1	-8.8	0.46	1.42
SAN 9	18/5/10	-3.5	-3.7	-7.5	-3.2	-3.4	-4.1	-8.9	0.45	1.44
SAN 1	18/5/10	-4.0	-4.1	-8.3	-3.1	-3.3	-4.1	-9.7	0.51	2.04

Obviously with a decreasing of the Total Dissolved Ions (TDI) also the saturation indexes (SI) decrease in essentially all the springs in May, even if the effect on the TDI is not visible on the EC. The ratio TDI/EC is in fact different in November (drought period) and May (humid period), as shown in Table 6.3.

Two ions show noticeably decrease in May: calcium (Ca^{++}) and the hydrogen bicarbonates (HCO_3^-) that derive from the calcite and dolomite dissolution; the ratio Ca/HCO_3 is lower in the first group of springs, higher for the second group (Figure 6.8 and Table 6.3).

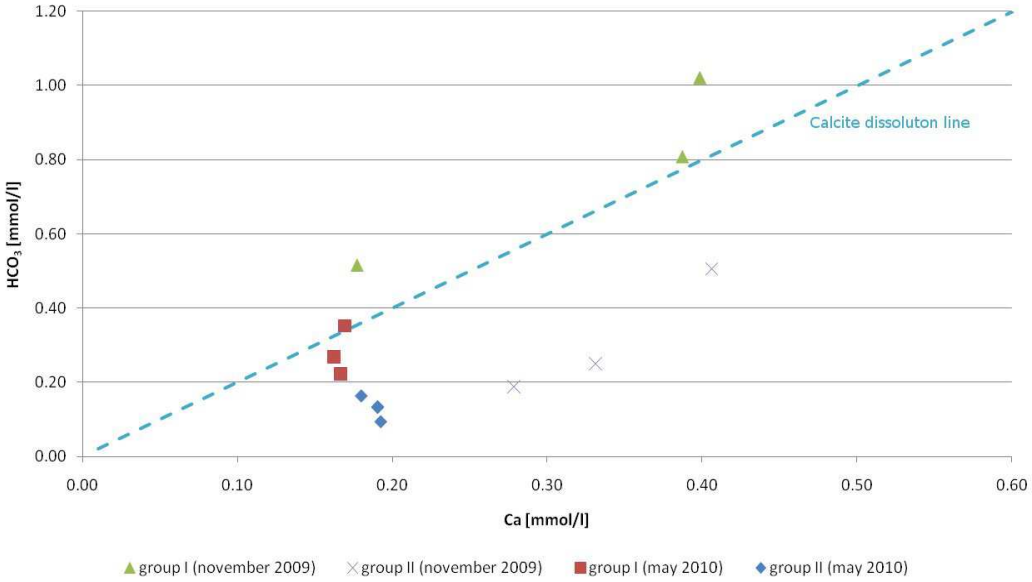

Figure 6.8 - Plot of molar concentrations of Ca vs. HCO3. Samples lie parallel to a line representing 1Ca : 2 HCO as expected from dissolution of calcite (calcite dissolution line).

The halite is the only mineral the saturation index of which increases in May, at least in the springs of the second group. It has indeed been already noted that, for these springs, is clearly visible the effect of the dilution of salt used for winter road maintenance.

- *Stable isotopes of oxygen and hydrogen*

Concerning δ^2H and $\delta^{18}O$ values, both the yearly average (equation 6.1) and seasonal trends (Figure 6.6) were considered.

As shown in Figure 6.9, all samples have meteorological origin. On the $\delta^{18}O$ and δ^2H plot, they are placed between the Mediterranean and Locarno meteorological water lines. In particular the data are close to the Ticino MWL obtained on the basis of precipitation data coming from 6 stations in southern Switzerland (see chapter 2). The higher deuterium excess is due to the difference between stable isotope signature of precipitation (rain and snow) and the effective groundwater recharge that is only a small percentage of rainout water. These differences are due to seasonal effects on infiltration that is higher during the more humid and hot season and practically null in the drier winter season. In fact, in winter the soil is frozen and precipitation occurs mainly in the form of snowfalls. Moreover, the melt of the snowpack for the most part produces run off and directly sublimates, while only in a small part infiltrates, with different δ^2H and $\delta^{18}O$ of snowmelt respect of that of measured in the snowfall (Taylor et al, 2001; Lee et al. 2010) and reported in Figure 6.9.

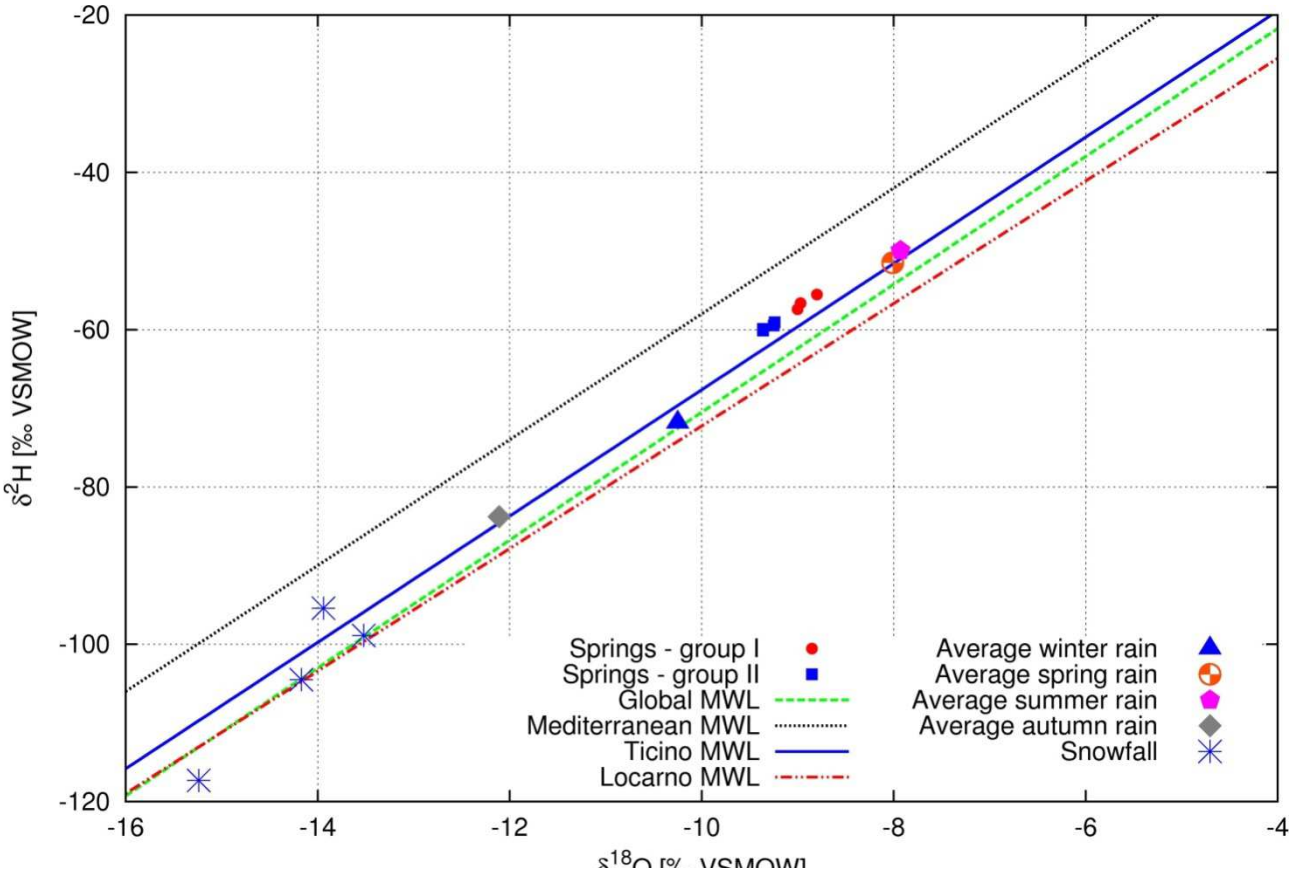

Figure 6.9 - $\delta^{18}O$ vs $\delta^{2}H$ in the monitored springs compared with local (Locarno and Ticino and Mediterranean) and global MWLs. Average seasonal rain data and snowfalls collected in few selected rain gauges (see chapter 2) are also reported as comparison.

On the basis of mean annual $\delta^{2}H$ and $\delta^{18}O$, mean altitude water infiltration can be calculated (Blavoux and Letolle, 1995). Springs from group I (SAN4, SAN5, SAN6), even if located at higher elevation above sea level, are characterized by a higher heavy isotope content ($\delta^{18}O \approx -8.92$, $\delta^{2}H \approx -56.5$) with respect to the second group of springs ($\delta^{18}O \approx -9.30$, $\delta^{2}H \approx -59.6$). An altitude gradient of about -0.12‰/100 m for ^{18}O and of -1.03‰/100 m for ^{2}H can be calculated on the basis of rain data collected in 6 stations of the Ticino canton (see chapter 2 and appendix B). Therefore a difference in average altitude of groundwater recharge, between the two groups of springs of about 250 m was estimated, being higher for group II.

In particular, using the altitude stable isotope relationships specifically obtained for the groundwaters of Monte Ceneri region (chapter 2) and reported in the following equations (*6.5*) and (*6.6*), the mean altitude of infiltrations of springs' groundwaters can be estimated.

$$\delta^{2}H = -10.80‰ \cdot H[\text{m a.s.l.}] - 52.83‰ \qquad (6.5)$$

$$\delta^{18}O = -1.29‰ \cdot H[\text{m a.s.l.}] - 8.36‰ \qquad (6.6)$$

Springs of group I seem to originate by an average infiltration at the elevation of about 600 m a.s.l., just behind the springs (Table 6.1). Conversely, the springs of group II seem to be due to groundwater recharged at higher altitudes (average infiltration height: ~800 m a.s.l.).

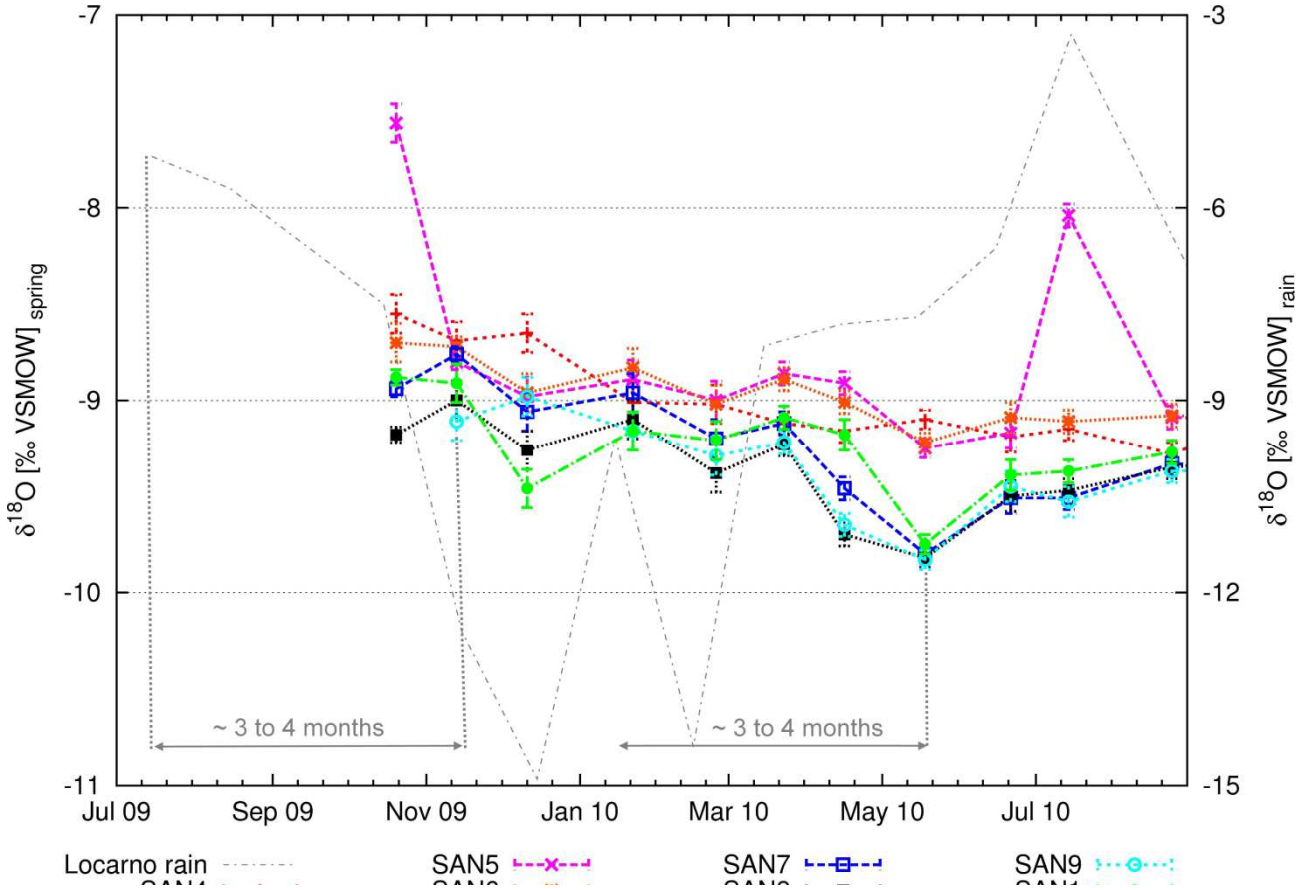

Figure 6.10 - Seasonal trend of $\delta^{18}O$ in the selected springs compared with Locarno rain data (Swiss network NISOT, Schürch, 2003)

Variability of $\delta^{18}O$ and $\delta^{2}H$ (Figure 6.9) is generally low within a range of 17.26 ‰ (from -64.29 to -47.02) for the $\delta^{2}H$ values, and 2.27 ‰ (from -9.83 to -7.56) for the $\delta^{18}O$. Seasonal variations in stable isotope compositions are not clearly visible, such as it is possible to expect in case of recently recharged groundwater (Eichinger et al., 1984; Rank et al. 1992; Maloszeski et al., 2002). Nevertheless, two different behaviors can be observed:

- Group I (SAN4, SAN5, SAN6): seasonal effects are not visible. This fact could be related to the presence of a water reservoir, even if poor, in the underground, and to the occurrence of a consistent (in proportion to the discharge rates) mixing of groundwater. Recharge is probably focused in a shorter period of time, especially in the spring and summer months. Concerning the SAN5 spring, two higher peaks in $\delta^{18}O$, as well of $\delta^{2}H$ have been observed in October 2009 and July 2010; they are the probable signal of a quick and local infiltration of rain water from the surface into the springs.
- Group II (SAN7, SAN8, SAN9, SAN1) seasonal variations, even though attenuated, are visible. In particular, an increase of stable heavy isotope content was observed in the fall of 2009 and a decrease during the spring of 2010. This decrease and the delay with respect to the stable isotope signature of rain collected in Locarno is clearly evidenced in Figure 6.10.

Table 6.4 summarizes all the considerations done in this section at the light of the results of the water spring monitoring on the two groups of springs:

Table 6.4 - Summary of the observations coming from the spring monitoring.

Parameter	Group I (SAN 4, SAN5, SAN6)	Group II (SAN 7, SAN8, SAN 9, SAN 1)
Discharge	Low discharge (predominantly VII Meinzer class), variability high for the SAN 4 and 5, not for the SAN 6 (DVI_{2010}=24%).	Low discharge but higher than group I (predominantly VI Meinzer class), variability always high.
Electrical conductivity	Dilution effect due to intense rain.	Piston effect due to intense rain.
Temperature	Stable temperature, low variation.	Temperature variations noticeable.
Major ions	Ca-HCO3 groundwater typical of shallow crystalline aquifers.	Ca-HCO3-SO4 groundwater with higher presence of Cl- ion (salt normally used for winter road maintenance).
δ^2H vs $\delta^{18}O$	Stable isotopes of oxygen and hydrogen show a meteorological origin of the spring's water. Seasonal effects in stable isotope composition are not visible. Mean annual stable isotope signature higher ($\delta^{18}O \approx -8.92$, $\delta^2H \approx -56.5$).	Stable isotopes of oxygen and hydrogen show a meteorological origin of the spring's water. Seasonal effects on the stable isotope composition, even if attenuated, are visible. Mean annual stable isotope signature lower ($\delta^{18}O \approx -9.30$, $\delta^2H \approx -59.6$).

6.5.2 Geoelectrical surveys

Figure 6.11 shows geoelectrical surveys (ERT) performed in correspondence of the two groups of selected springs. The results for two groups are described in separate sections.

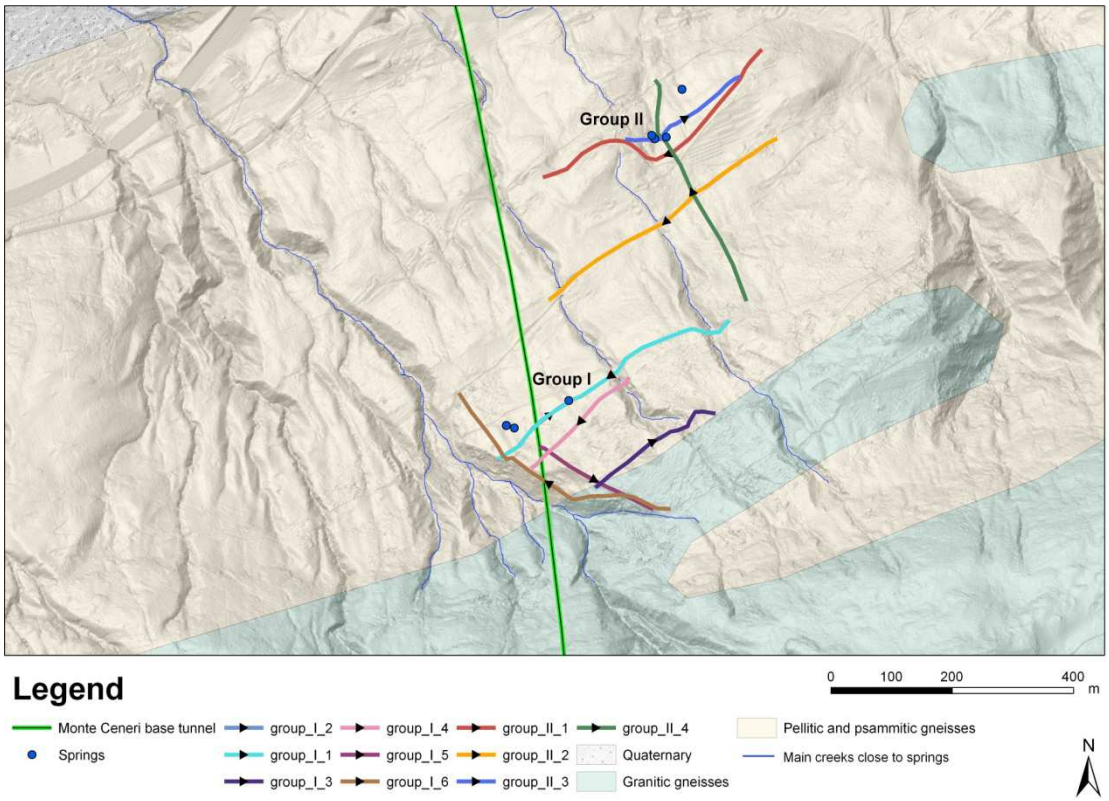

Figure 6.11 - Selected springs at south of Vigana (see Figure 6.5) and carried out geoelectrical surveys.

- *Group I: SAN4, SAN5, SAN6*

Six 2D geoelectrical surveys were performed within the watershed of the springs of group I. Four surveys (pp. 1 to 4) have been carried perpendicular to maximum slope direction, at different distances upstream from the springs; while the last two (pp. 5 & 6) have been realized following the slope direction. The springs are located at the right bank of a creek (Figure 6.11), beyond a watershed line and the interconnection between the creek and the springs aquifer is possible, at least from a morphological point of view.

From the 2D resistivity sections an increase in electrical conductivity with depth is visible in profiles perpendicular to slope direction (Figure 6.12) close to the springs (pp 1-2). At greater

distance, low resistivity values have been detected, also at higher depth and with an irregular distribution (pp. 3-4).

A more conductive zone in correspondence of the springs seems lightly visible in the upper layers of the rock from geoelectrical section profile 6 (Figure 6.13). Hydrogeological connection between the creek and the springs can be confirmed also by the surveys realized on the slope direction on the ridge that separates the springs' basin from the creek (pp. 5-6), where higher electrical conductivities have been detected at a depth corresponding approximately to the elevation of the creek (Figure 6.14).

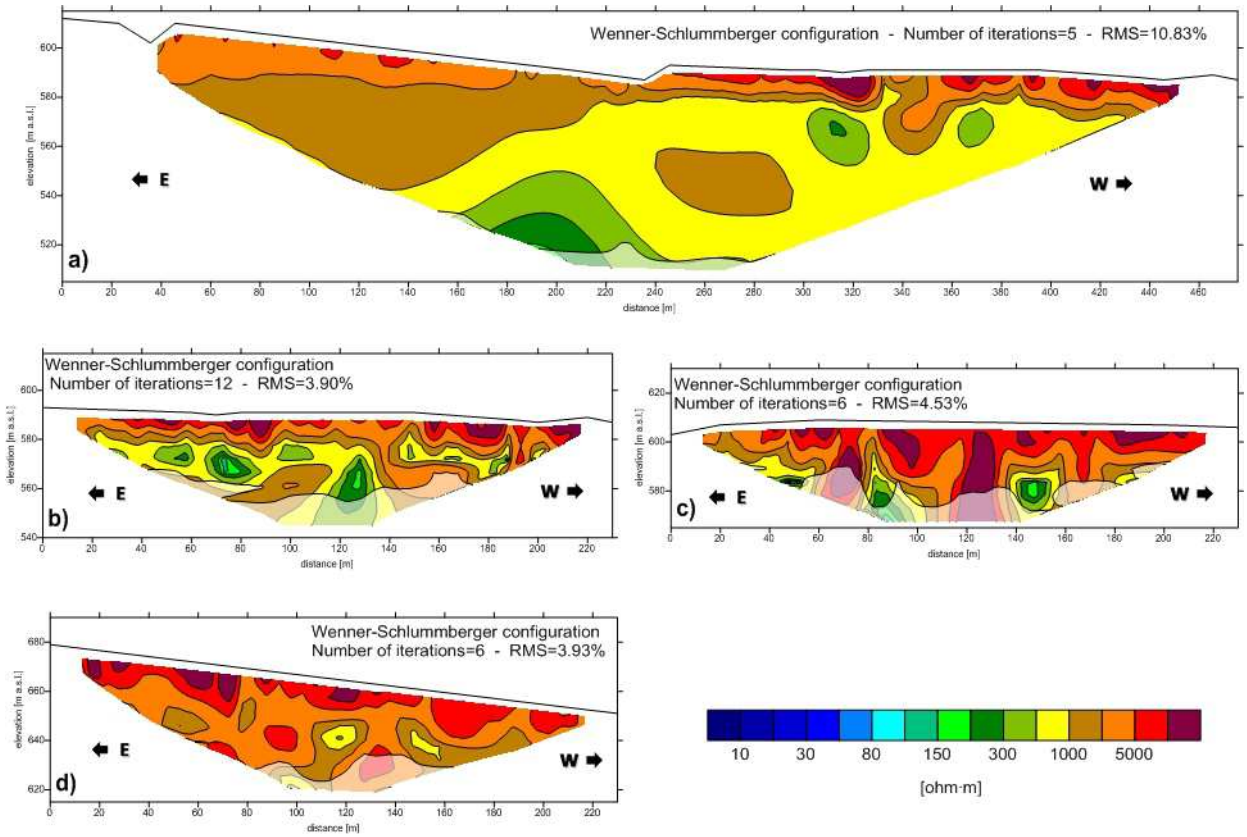

Figure 6.12 - The four resistivity 2D sections realized parallel to the slope (*a*- group_I_1, *b*- group_I_2, *c*- group_I_3, *d*- group_I_4).

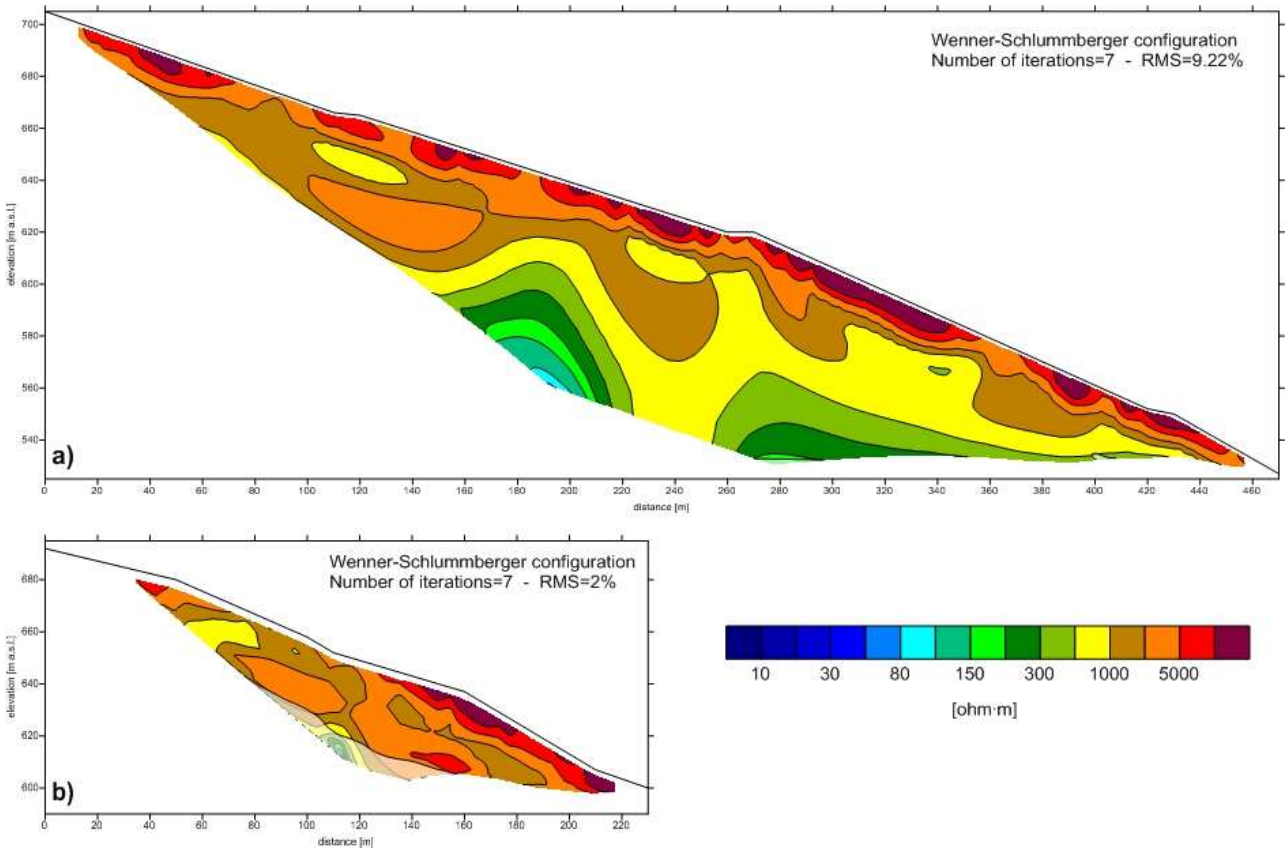

Figure 6.13 - The two resistivity 2D sections realized in the slope direction (*a*- group_I_6, *b*- group_I_5).

A hydrogeological interpretation available from the resistivity sections shown in the previous Figure 6.12 and Figure 6.13 is proposed in the following Figure 6.14.

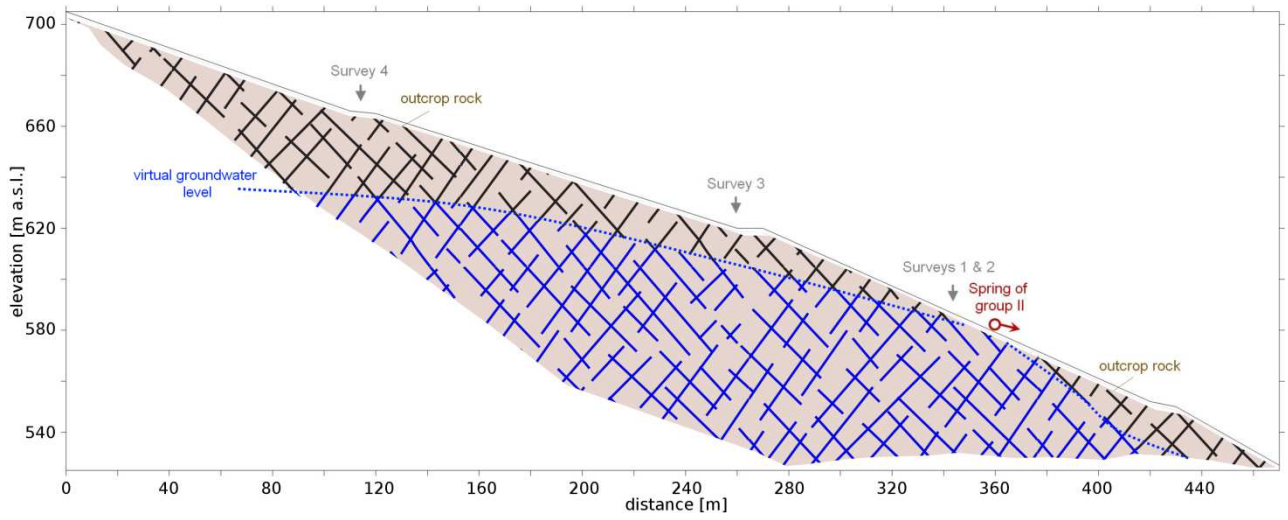

Figure 6.14 - Hydrogeological interpretation available from ERT surveys conducted above the first group of springs (SAN4, SAN5, SAN6).

- *Group II: SAN7, SAN8, SAN9, SAN1*

4 geoelectrical profiles were performed within watershed feeding springs of the second group. Three of them (pp. *1*, *2*, *3*) were carried out upstream parallel to the slope, while the fourth has been carried out along the slope direction, starting about 200 m a.s.l. upstream. The most interesting profiles (pp 1, 3 and 4) are shown in the following Figure 6.15.

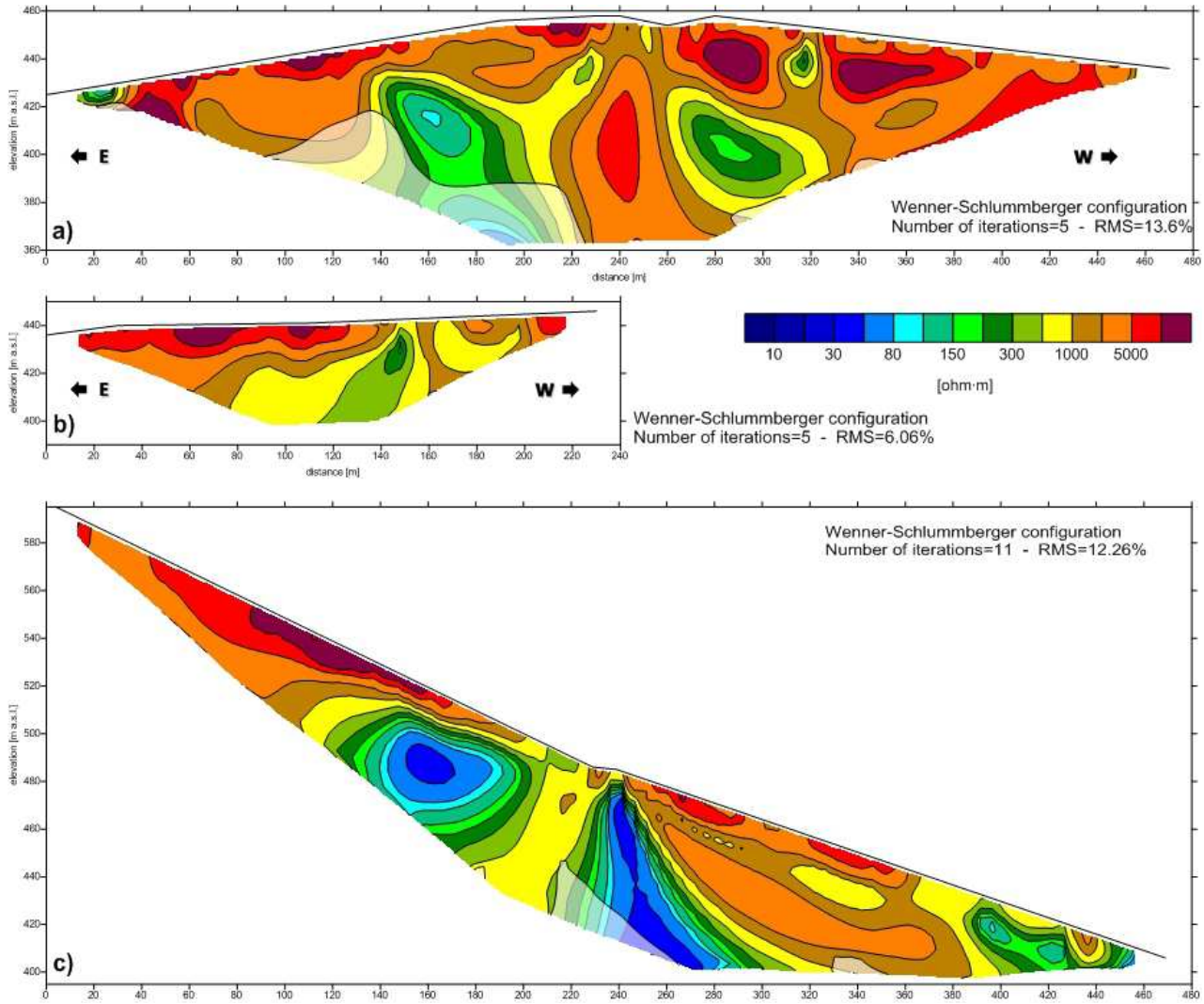

Figure 6.15 - Three resistivity 2D section collected close to the second group of springs (*a*- group_II_1, *b*- group_II_3, c-group_II_4).

Resistivity sections resulting from surveys perpendicular to maximum slope direction (Figure 6.15 *a*,*b*), denotes the presence of localized conductive zones. They can be interpreted as fractures and or fractured/weathered rock volumes carrying groundwater. The ERT profile acquired along the slope direction (Figure 6.15 *c*) shows clearly the presence of three conductive zones in the underground. The first one upstream reaching the ground surface in the middle of the profile is placed in correspondence of a small spring showing variable discharge in response to hydrologic conditions (Bestenheider, 2009). A reasonable hypothesis is that groundwater present in the fractured rock come to surface in correspondence of fine and impermeable layer of soil (probably clay). This layer is evidenced by the presence of a steep deeping conductive area shown in the resistivity section. The last conductive zone is placed in correspondence with the springs of group II and it represents the surfacing of groundwater. Unlike springs of group I, in this case groundwater seem circulate through few localized fractures, as shown by profiles 1 and 3 (Figure 6.15 *a*,*b*).

A hydrogeological interpretation available from the resistivity sections shown in the previous Figure 6.15 is proposed in the following Figure 6.16.

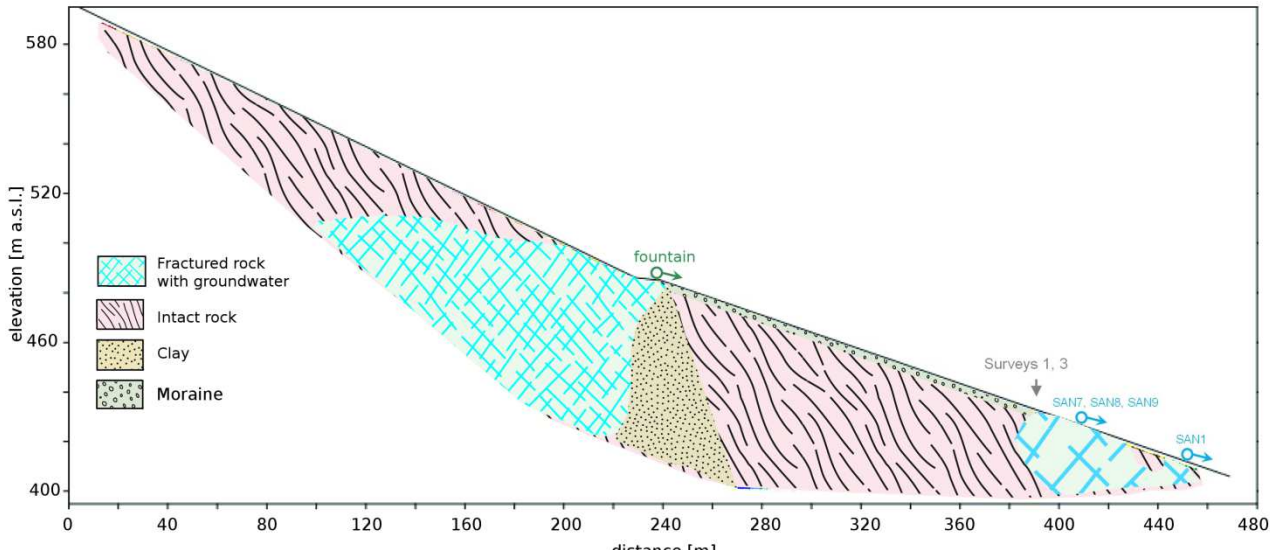

Figure 6.16 - Hydrogeological interpretation available from ERT surveys conducted above the first group of springs (SAN4, SAN5, SAN6).

6.6 Discussion

6.6.1 Resulting Conceptual Hydrogeological Model (HCM)

Combining all collected information coming from hydrogeological measurements and geoelectrical 2D surveys, a data supported HCM of groundwater flow systems was formulated. The low discharges (VI and VII Meinzer class), high discharge variability and the low electrical conductivity values registered in both groups of springs, are typical of shallow aquifers in fractured crystalline rocks. A detailed analysis of monitored parameters (chemico-physical parameters and stable isotope of hydrogen and oxygen ratios) and 2D geoelectrical surveys does, however, demonstrate that the groundwater flow systems of the two groups of springs are different.

In particular, springs of group I have less groundwater recharge areas as evidenced by low discharge. The δ^2H and $\delta^{18}O$ data mean annual values are higher than δ^2H and $\delta^{18}O$ measured in the other springs, indicating that groundwater infiltration happens probably at lower elevation. Groundwater circulates within the first layer of terrain, through a thin layer of moraine deposits and underlying fractured gneiss, as shown by results of geoelectrical surveys and also confirmed by the dilution effect in EC values in response to meteorological events.

The springs of group II have on the contrary wider recharge areas, as evidenced by the higher discharge rates. The deuterium and oxygen-18 relative mean annual abundances are lower respect of the other springs denoting that groundwater infiltration happens probably at higher elevation. Comparing seasonal variations in δ^2H and $\delta^{18}O$ of springs and rain (Figure 6.9), these springs can be related to rapid flows through the main fractures of the gneiss crystalline rocks of recently infiltrated groundwaters having a residence time of about 3-4 months. Moreover the increase of EC values in correspondence of the discharge's peak, like as the results of 2D geoelectrical tomography, seem to demonstrate that the groundwater probably circulate through a few major fractures. In Figure 6.17, the elaborated HCM for the selected springs is shown.

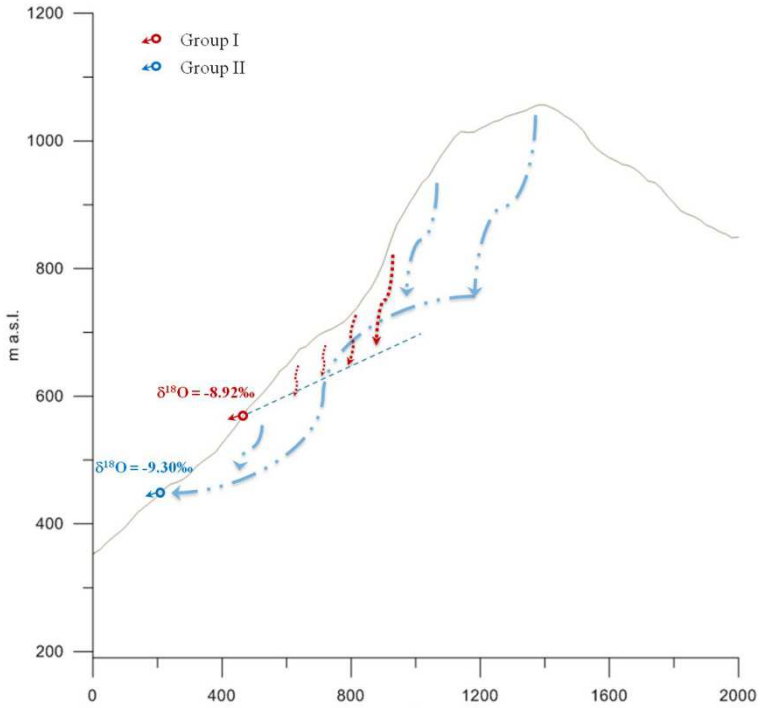

Figure 6.17 - HCM of the two group of analyzed springs coming from the hydrogeochemical monitoring and from geoelectrical realized surveys.

6.6.2 Drawdown hazard evaluation

The resulting HCM was hence used to apply a parametric method (De Matteis et al. 2001, Torri et al., 2007; De Matteis 2008) in order to define the aquifer depletion hazard in the specific case study.

Both groups are the result of a shallow groundwater flow system (*spring type* parameter), and using the parameters proposed by Torri et al. (2007), with numerical values reported in the following Table 6.5, a moderate drawdown hazard index values for both groups has been obtained.

Table 6.5 - DHI of the analyzed springs and corresponding classes according to De Matteis method.

Spring	FF	MK	OV	PZ	IF	ST	DT	DHI	DHI classes
Group I	0.1	0.33	0.1	0	0	0	1	0.26	Moderate hazard
Group II	0.1	0.33	0.2	0	0.5	0	0.4	0.31	Moderate hazard

Therefore, on the basis of available information it is possible to conclude that both the springs of group I and II are not particularly vulnerable to the possible tunnel drainage effects.

It is important to notice two more general things about the application of parametric method. First, the correct definition of the spring hydrogeological parameters used by the method and described in the previous sections, is otherwise impossible, without the collection of a bare minimum hydrogeological dataset. Moreover a parametric method lend itself to improvement of the original formulation; thus, it is possible to add or conveniently change the spring parameters, adapting them to the available hydrogeological information with the aim to better define the groundwater flow systems.

6.7 Conclusions and remarks

The hydrogeological interpretation of the spring's groundwater flow systems is often difficult, especially in fractured rock where water table contour are normally not available. Developing an hydrogeological conceptual model (HCM) is a natural progression from geological observations in field, geomorphological surveys and hydrogeochemical data analysis. The collected data should

give an understanding of how the spring occurs, the physical factors governing flow to the spring, the possible sources of recharge and other peculiarity (Kreye et al.1996).

In this paper, the usefulness of hydrogeochemical and stable isotope data to obtain a reliable model of the water springs has been demonstrated. The use of geoelectrical surveys in addition, can give precious informations to validate the hypothesis, because often there is more than one plausible interpretation of the various hydrogeochemical informations.

Often analyzing a single hydrogeological parameter is meaningless and could lead to erroneous deductions. Only combining all the available data, and considering the unavoidable uncertainties, it is possible obtain a well-founded interpretation of the different groundwater flow systems. The obtained HCM, though being a hypothesis, is, however, the main input of the parametric methods that are frequently used to understand the possible impact of tunneling on the groundwater, using a stochastic approach that, in this domain of uncertainty, is suggested.

In our case study, for instance, considering all the observation summarized in Table 6.4 and the resistivity sections obtained from ERT surveys, it is possible to formulate a HCM for the groundwater flow system (Figure 6.17) and obtain corresponding indication concerning drawdown hazard (Table 6.5). In this paper, just a possible standard approach to collect requested input of parametric approaches from all the available data and resulting information, is presented. The parameters of the used method can be specifically modified in each case, adapting them to the available data.

Finally, some logistical considerations of general relevance, concerning the monitoring scheduling and geoelectrical surveys can be given.

Concerning physico-chemical measurements (Q, EC, T and pH), a monthly measuring interval is the bare minimum in order to have a reliable representation of the discharge and mineralization seasonal trends in quite humid climate like as the south-alpine. Could be however appreciable, even if not necessary, to have few series of data with an higher temporal frequency, e.g. using a physical sound connected to a data logger in order to register the data in a few selected springs.

Concerning stable isotope sampling, four measures at the different seasons of the year are generally enough in order to obtain mean yearly values, due to the low variability of springs groundwater, nevertheless, if the objective is to observe seasonal trends, also in this case a monthly sampling is needed.

Concerning geoelectrical surveys, from a theoretical point of view, it should be necessary to try to place the profiles perpendicular to the body to be studied. Nevertheless, not always the structure positions are known and, especially in the mountainous regions, not always it is possible place the profile in the desired direction. It is thence difficult formulate universal rules, but it is advisable to possibly realize the surveys along the two main directions, that are parallel and along the slope, in order to facilitate the interpretation of resistivity profiles with an almost 3D model. A detailed analysis of the underground infrastructures that intersect the survey line and could negatively affect the measurements is finally highly advised.

Acknowledgments

The authors would like to thank the *Commissione Federale di Stima 13° Circondario* and the Geol. Jean Claude Bestenheider for the provided data concerning springs and the precious suggestions and informations. Special thanks are due for all the colleagues of Institute of Earth Science (M. Baruffini, S. Beatrizzotti, M. Pozzoni, and L. Soma) that assist us in the field work and to Dr. Eng. Ludovic Baron of Institute of Geophysics (Unil) for the technical support.

References

Begert M., Schlegel T., Kirchhofer W. (2005). Homogeneous Temperature and Precipitation Series of Switzerland from 1864 to 2000. International Journal of Climatology 25: 65-80.

Bestenheider J.C. (2005). Commissione federale di stima 13° circondario, “Galleria di base del Ceneri (senza cunicolo di prospezione di Sigirino) – Misure a futura memoria delle sorgenti, 2° rapporto annuale N 24/05, 11pp.

Bestenheider J.C. (2009). Commissione federale di stima 13° circondario, "Galleria di base del Ceneri Misurazioni delle sorgenti durante i lavori di scavo, 1° rapporto annuale N9B/09 – Misurazioni dell'anno 2008, 14pp.

Blavoux B., Letolle R. (1995) Apport des techniques isotopiques à la connaissance des eaux souterraines, Géochroniques 54, 12-15

Buergi C., Parriaux A., Franciosi G., Rey J.Ph. (1999). Cataclastic rocks in underground structures – terminology and impact on the feasibility of projects (initial results), Engineering geology 51:225-235

Cesano D., Olofsson B., Bagtzoglou A.C. (2000). Parameters regulating groundwater inflows in hard rock tunnels – a statistical study of the Bolmen tunnel in Southern Sweden, Tunneling and Underground Space Technology 15,2:153-165

Colombi A., Baumer A. (1995). Galleria di base del Monte Ceneri, Situazione idrogeologica, Rapporto idrogeologico, Tecnhnical report of the "Studio di geologia Dr. A. Baumer"

De Matteis A. (1995). Typologie géochimique des eaux des aquifères carbonatés des chaînes alpines d'Europe centrale et méridionale. Ph.D. thesis EPFL No.1419, Lausanne, 226 pp.

De Matteis A., Kalamaras G., Eusebio A. (2001). A System approach for evaluating springs drawdown due to tunneling, Proceedings of the AITES-ITA 2001 World Tunnel Congress, Milano

De Matteis A. (2008). Come prevenire e gestire venute d'acqua in galleria, Strade & Autostrade, Milano, 1:66-70

Derron, M.-H. (1999). L'interaction eau-roche-sol à basse température dans les Alpes. Ph.D.thesis University of Lausanne, 209 pp.

Di maio R., Piegari E., Scotellaro C., Soldovieri MG. (2007). Resistivity tomographies to define thickness and water content of pyroclastic covers at Mt. di Vezzi (Ischia island, Italy). Italian Journal of Engineering Geology and Environment, 2:65-72

Dubois, J.D. (1992). Typologie des aquifères du cristallin: exemple des massifs des Aiguilles Rouges et du Mont-Blanc (France, Italie et Suisse). - Thèse EPFL, no 950, Lausanne, 324pp

El Tani, M. (2003). Circular tunnel in a semi-infinite aquifer. Tunnelling and Underground Space Technology 18(1):49–55

Eichinger L., Merkel B., Nemeth B., Salvamoser J., Stichler W. (1984). Seepage velocity determinations in unsaturated Quaternary gravel; Recent Investigations in the Zone of Aeration, Symposium Proceedings, Munich, October 1984, pp. 303-313

Fazzito S.Y., Rapalini A.E., Cortés J.M., Terrizzano C.M. (2009). Characterization of Quaternary faults by electric resistivity tomography in the Andean Precordillera of Western Argentina. Journal of South American Earth Sciences, 28:217-228

Gargini A., Vincenzi V., Piccinini L., Zuppi G.M., Canuti P. (2008). Groundwater flow systems in turbuidites of the Northern Appennines (Italy): natural discharge and high speed railway tunnel drainage , Hydrogeology Journal 16:1577-1599

Goodman R.F., Moye D.G., Van Schaikwyk A., Javandel I. (1965). Ground water inflows during tunnel driving. Bulletin of the International Association of Engineering Geologists 2(1): 39–56

Hesske S. (1995). Typologie des eaux souterraines de la molasse entre Chambéry et Linz (France, Suisse, Allemagne, Autriche) – PhD Thesis EPFL, no 1417, Lausanne, 374 pp

Högl O. (1980). Die Mineral- und Heilquellen der Schweiz. - Haupt, Bern, Stuttgart, 322pp.

IST (2010). Annuario idrologico del canton Ticino 2009, Istituto scienze della terra, SUPSI

Lee J., Feng X., Faiia A.M., Posmentier E.S.. Kirchner J. W., Osterhuber R., Taylor S. (2010). Isotopic evolution of a seasonal snowcover and its melt by isotopic exchange between liquid water and ice, Chemical Geology 270:126-134

Lei S. (1999). An analytical solution for steady flow into a tunnel. Ground Water 37:23–26

Kies A., Hofmann H., Tosheva Z., Hoffmann L., Pfister L. (2005). Using ^{222}Rn for hydrograph separation in a micro basin (Luxembourg). Annals of geophysics. 48(1):101-107

Kirsch R. (2006). Groundwater Geophysics - A Tool for Hydrogeology, Springer-Verlag Berlin Heidelberg, 548 pp.

Kolymbas D., Wagner P. (2007). Groundwater ingress to tunnels – The exact analytical solution Tunnelling and Underground Space Technology 22:23–27

Kreye R., Wei M., Reksten D. (1996). Defining the source area of water supply springs, Hydrology Branch, British Columbia, Environment 28pp.

Maloszeski P., Stichler W., Zuber A., Rank D. (2002). Identifying the flow systems in a karstic-fissured-porous aquifer, the Schneealpe, Austria, by modelling of environmental 18O and 3H isotopes. Journal of hydrology 256:48-59

Maréchal J.C., Etcheverry D. (2003). The use of 3H and 18O tracers to characterize water inflows in Alpine tunnels. Applied Geochemistry 18:339-351

Marzocchi R., Pera.S, (2009). Groundwater and tunneling: implementation of a geochemical monitoring network in Southern Switzerland, VII Swiss Geoscience Meeting, Neuchatel 20-21 November

Marzocchi R., Pera S., Pfeifer H.R. (2010). Hydrogeological interferences in tunneling - A comprehensive study, Aquamundi 1(3):1-14

Masset O., Loew S. (2010). Hydraulic conductivity distribution in crystalline rocks, derived from inflows to tunnels and galleries in the Central Alps, Switzerland. Hydrogeology Journal 18: 863–891

Meinzer O.F. (1923). The occurrence of groundwater in the United States. USGS Water Supplyt Paper 489

MeteoSwiss, IDAWEB data service – Free available data for research project

Ofterdinger U.S. (2001). Ground water flow systems in the Rotondo Granite, Central Alps (Switzerland), Phd Thesis of Natural Science, Swiss federal institute of technology (ETH) – Zurich, 177 pp.

Pancescu M. (2006). Phreatic aquifers vulnerability for Mostistea Plain using GIS technology, Proceedings International Conference Hydrology and Ecology: The Groundwater/Ecology Connection 11–14 September 2006, Karlovy Vary, Czech Republic, 267-272

Parkhurst D.L., Appelo C.A.J. (1999). User's guide to PHREEQC (version 2) - a computer program for speciation, reaction-path, 1D-transport, and inverse geochemical calculations. U S Geological Survey Water-Resources Investigations Report 99-4259, 312p

Perrochet P., Dematteis A. (2007). “Modeling transient discharge into a tunnel drilled in a heterogeneous formation”. Ground Water, 45(6):786-790.

Piegari E., Cataudella V., Di maio R., Milano L., Nicodemi M., Soldovieri M.G. (2009). Electrical resistivity tomography and statistical analysis in landslide modeling: a conceptual approach. Journal of Applied Geophysics, 68, 151-158

Pini O., Rossi D. (2009). The Ceneri railway base tunnel (15.4 km) in the southern Swiss alps (Gotthard Alptransit). Proceedings of the ITA–AITES World Tunnel Congress (WCG`09). Budapest, Hungary 23-28 May

R Development Core Team (2011). R: A Language and Environment for Statistical Computing, R Foundation for Statistical Computing - Vienna, Austria (http://www.R-project.org)

Rank D., Völkl G., Maloszewski P., Stichler W., (1992). Flow dynamics in an Alpine karst massif studied by means of environmental isotopes. Isotope Techniques in Water Resources Development 1991. IAEA, Vienna pp. 327–343

Schurch M., Kozel R., Schotterer U., Tripet JP, (2003). Observation of isotopes in the water cycle: the Swiss National Network (NISOT), Environmental geology 45(1):1-11

Schmassmann H., Balderer W., Kanz W., Pekdeger A. (1984). Beschaffenheit der Tiefengrundwässer in der zentralen Nordschweiz und angrenzenden Gebieten. - NAGRA, NTB 84-21, Baden, 335pp

Schmid S.M., Fügenschuh B., Kissling E., Schuster R. (2004). Tectonic map and overall architecture of the Alpine orogen. Eclogae Geologicae Helvetiae. 97:93–117

Tassone A., Santomauro M., Menichetti M. Cerredo M.E., Remesal M.B., Lippai H., Lodolo E., Vilas J.F., (2010). Imaging subsurface lithological and structural features by resistivity tomography: North Beagle Channel (Tierra del Fuego, Argentina). Revista Mexicana de Ciencias Geológicas 27(3):562-572

Taylor S., Feng X. Kirchner J.W., Osterhuber R., Klaue B., Renshaw C. E. (2001). Isotopic evolution of a seasonal snowpack and its melt. Water resources research 37(3):759-769

Torri, R., Dematteis, A., Delle Piane, L. (2007). "Drawdown hazard of springs and wells in tunneling: predictive model and Verification". Proc. XXXV IAH Congress, Groundwater and Ecosystems, Lisbon 17-21 Sept. 2007, 10 pp.

Vincenzi V., Piccinini L., Gargini A., Sapigni M. (2010). Parametric and numerical modelling tools to forecast hydrogeological impacts of a tunnel Aquamundi 1(2):135-153

Zeileis A., Grothendieck G. (2005). Zoo: S3 Infrastructure for Regular and Irregular Time Series. Journal of Statistical Software, 14(6):1-27.

7. Conclusions

A main scientific issue related to the excavation of tunnels is constituted by their impacts on water resources, especially on groundwater flow. In fact, tunnel drilling may cause a drawdown of piezometric levels and/or affect spring's discharge rate; while inflows may be a problem during excavation or tunnel service. Unlike porous homogeneous media, where impacts can be easily predicted, fractured rock masses are a specific and particularly complex case. In fact these environments are extremely heterogeneous and their hydrogeological behaviour is highly influenced by structural elements like fault zones and other discontinuities. Two tunnels under construction in the southern Switzerland were selected as case studies: *(i)* the Monte Ceneri base tunnel (Alptransit) and *(ii)* the San Fedele tunnel (Federal Roads Office - FEDRO). In particular, concerning the first one, two were the accessible segments: *(i.1)* the northern portal, placed near the Vigana town, and *(i.2)* the Sigirino access tunnel. Both areas are mainly constituted by metamorphic rocks (gneiss), usually considered impervious; however fractures and discontinuities locally increase permeability allowing water flow.

A comprehensive approach integrating *geochemical* and *geophysical* methods was used in this work to formulate data supported Hydrogeological Conceptual Models (HCM) for case studies giving information about *(i)* spring vulnerability to the tunnel drilling, *(ii)* water-bearing zones assessment during tunnel drilling; and *(iii)* in order to understand origin and groundwater flow.

Water of springs and tunnel inflows were monitored on a monthly basis for chemico-physical data (discharge, temperature, electrical conductivity, pH) and stable isotopes of hydrogen and oxygen (δ^2H and $\delta^{18}O$). Analyses of major ions, and, in selected cases, *(iv)* analyses of noble gases (He, Ne, Ar, Kr, Xe) and their isotopes (^3He, ^4He, ^{20}Ne) concentrations were also carried out. These data were integrated with several geophysical surveys carried out using two different techniques: *(i)* the 2D electrical resistivity tomography (ERT), and *(ii)* the very low frequency electromagnetic (VLF-EM). From the analyzed case studies the following general conclusions can be drawn.

Concerning groundwater circulation within rock masses, monitored springs of the region surrounding the northern portal of the Ceneri base tunnel (chapter 6) shows low mineralized water and highly variable discharges reacting to meteoric events. Noble gas concentrations are found at solubility equilibrium with the atmosphere. Moreover, seasonal variations are noticed in electric conductivity (EC) and stable isotope values (δ^2H and $\delta^{18}O$). In particular, in monitored springs, EC is related with discharge: in a few cases EC values increase with increasing discharge, while in other cases they decrease with increasing discharge. Concerning stable isotope values, springs having increasing EC with discharge show small and irregular fluctuations, while in springs having negative correlation with discharge, regular seasonal variations in stable isotope values are found with 2- 3 months of delay respect to precipitation. Geoelectrical surveys show that the watershed feeding the monitored springs is relatively shallow, limited to the first 10 – 20 meters, where rocks are fractured by decompression and/or thin sediment strata are present and evidenced by low resistivity values. However, some major fractures were identified, giving structural control on the position of a few springs and acting as preferential pathways for water circulation. Finally, mean annual stable isotope compositions in springs, compared with those of rain and snow, gave an indication of groundwater recharge. Recharge is probably focused in a shorter period of time, from April to November, and not during all the year. Moreover, using the mean annual stable isotope composition and considering that, as a rule, the isotopic composition of precipitations and thence of infiltrated groundwater becomes more depleted in ^2H and ^{18}O at higher elevations, the mean altitude of infiltration of different springs was estimated. A few springs are fed by water infiltrated directly above them, while the others seem fed by water infiltrated about 400 m above them. On the basis of previously given information, it is possible to conclude that springs are fed by shallow circulation circuits. However a distinction can be made about flow dynamics: piston flow conditions are likely to occur in springs having less variable stable isotope composition and where EC rise with the discharge; while total mixing flow conditions are likely to occur in springs showing seasonal

isotopic variations and negative correlation of EC with discharge. In both cases vulnerability to tunnel drilling is low, as observed applying a parametric specifically designed method (Figure 7.1).

The drilling of tunnels is conducted frequently in about dry conditions for most of their length; in fact rock masses are often almost impervious. Nevertheless the presence of water-bearing fractures may constitute a problem; in fact consistent and sudden water inflows in a tunnel may be present while crossing cataclastic structures or local discontinuities. The application of geophysical methods (ERT and VLF-EM) was demonstrated useful for the detection of such water bearing fractures that can cause the tunnel inflows. In particular ERT give more reliable results, being less affected by noise with respect to VLF-EM. Different arrangements were tested for both geoelectrical and electromagnetic methods, obtaining useful indications in order to optimize the methods' pertinence. These arrangements are discussed in detail in the thesis; while below a few interesting results can be summarized.

In the San Fedele tunnel, geological logs confirmed the hydrogeological interpretation of geophysical surveys. In fact, the most consistent water inflows were situated at the rock/unconsolidated material interface. Moreover ERT profiles have successfully predicted that the crossing of the Traversagna valley, which is a major fault in the area limiting two different tectonic domains, would be on dry conditions at the designed depth. Finally they have also correctly foreseen that the general conditions of drilling would have been dry, except for small inflows related to local discontinuities, too little to be detected by used methods.

In the northern portal of the Ceneri base tunnel, using geoelectrical 2D surveys, water bearing fractures that act as preferential pathways for groundwater flow were identified, especially in the upper zone of the gneiss where the northern portal has been excavated. Also in this case, geophysical results were confirmed by geological logs during drilling; moreover the application of a tracer test confirms the formulated hypothesis linking a local perched aquifer at surface and inflows in the tunnel.

Concerning the Sigirino access tunnel area, on the basis of geophysical surveys (chapter 3), fractures at surface, which were also recognized during tunnel drilling, were identified. In this case, at the tunnel depth, the fractures are filled by fine-grained and low permeable material; thence no consistent water inflows were noticed, but only lateral dripping from the wall were associated with its presence.

On the basis of geochemical and geophysical measurements a HCM, representative of the hydrogeological conditions in the studied region, was developed integrating information of all case studies. Three different groundwater flow systems have been identified:

i) highly mineralized old and deep groundwater, strongly enriched in helium of crustal origin. This water circulates through deep discontinuities having low permeability and poor connection with the surface;
ii) low mineralized, recently recharged groundwater, with noble gas isotopic composition at atmospheric equilibrium. This water contributes to spring discharge and was also sampled in the tunnel where it circulates through major discontinuities and faults connected to the surface or being able to receive recharge;
iii) a mixing between them, having enough time within the system to accumulate tritiogenic ^{3}He.

The integration of geophysical and geochemical methods is a good approach in order to understand the groundwater flow dynamics in fractured rock masses, giving information about possible impacts of tunneling on the hydrogeology of touched regions. On the basis of obtained information, vulnerability of springs to tunnel drilling was assessed and possible inflow areas were identified.

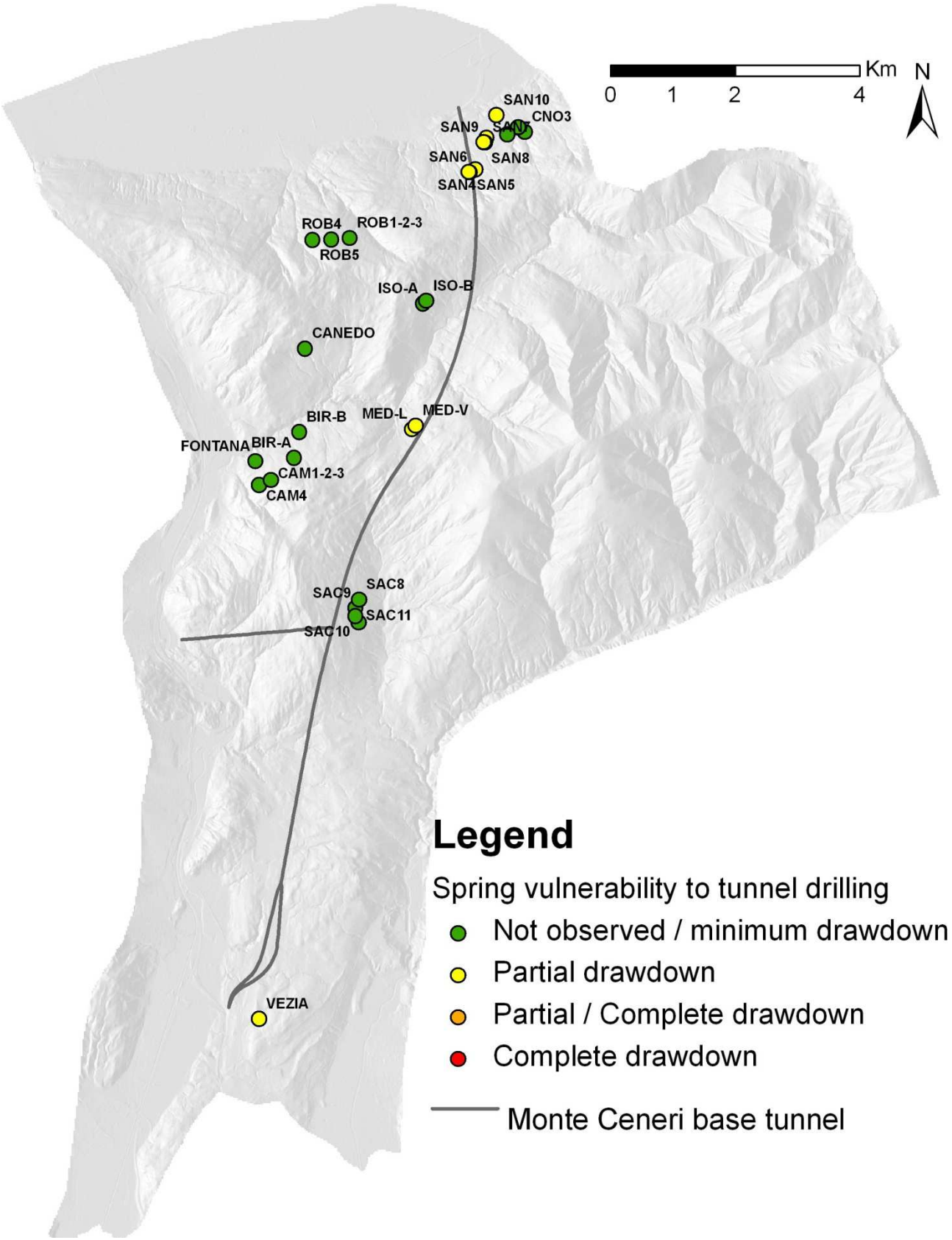

Figure 7.1 - Vulnerability of analyzed springs in the region surrounding the Monte Ceneri base tunnel using the De Matteis parametric methods. Spring nomenclature and all the monitored parameters are presented in Appendix B.2, while parametric method has been presented in chapter 1.

Appendix A

Marzocchi R., Pera S., Pfeifer H.R. (2010). Hydrogeological interferences in tunneling - A comprehensive study, Aquamundi 1(3):1-14

Hydrogeological interferences in tunneling - A comprehensive study.

*Roberto Marzocchi[1], Sebastian Pera[1] & Hans-Rudolf Pfeifer[2]
[1]Istituto Scienze della Terra (IST-SUPSI), Via Trevano C.P. 72 CH-6952 Canobbio (Switzerland),

roberto.marzocchi@supsi.ch

[2] IMG-Centre d'Analyse Minérale, Faculté des Géosciences et de l'Environnement, Université de Lausanne,

Anthropole, CH-1015 Lausanne

Abstract

The interference of groundwater with tunneling is both an environmental and an engineering problem. In fractured rocks, the prediction of tunnel water inflows is of primary importance, but unfortunately it is very complex, even impossible without the development of a well-founded Conceptual Hydrogeological Model (CHM). For this purpose, a comprehensive study is ongoing in the region of Monte Ceneri close to Lugano (Ticino, Switzerland), where a tunnel of 16 km in length is under construction in metamorphic rocks (gneiss and amphibolites). In particular, we are integrating the structural geological informations, commonly used for tunnel design, with geophysical surveys (VLF electromagnetic and resistivity) and physico-chemical data (discharge, temperature, electric conductivity, pH, ionic and stable isotope composition) of water collected at the surface and within the tunnel actually in construction. The theoretical frameworks and the preliminary results of the research are presented.

Résumé (French)

L'interférence d'eaux souterraines avec des tunnels pose des problèmes d'ingénierie et environnementaux. Dans des roches fracturées, savoir prédire les arrivées potentielles d'eau est primordiale, mais est très complexe, voire impossible sans disposer d'un modèle hydrogéologique conceptuel. Dans ce but, une étude importante est en route dans la région du Monte Ceneri près de Lugano, Canton Tessin, Suisse), où une tunnel de 16 km de longueur est en construction dans des roches métamorphiques de type gneiss et amphibolites. Notre étude intègre des données géologiques-structurales avec des mesures géophysiques (VLF, électromagnétisme et résistivité) et des données physico-chimiques (débit, température, conductivité, pH, composition ionique et isotopique) des eaux échantillonnées à l surface et dans le tunnel en construction. Ici on présente l'approche théorique et les résultats préliminaires.

Long abstract

Le acque sotterranee costituiscono circa il 98% delle risorse acquifere allo stato liquido nel mondo, e la loro conservazione è una questione di primario interesse.

In particolare nel Canton Ticino (Svizzera) le acque sotterranee sono la principale risorsa di acqua potabile: circa il 90% di esse deriva infatti dagli acquiferi vallivi o dalle sorgenti. La necessità di nuove vie di comunicazione europee (strade e ferrovie) ha determinato l'esigenza di costruire nuove gallerie in difficili condizioni geologiche. In particolare il Nord Italia e la Svizzera sono regioni strategiche per i trasporti Europei; esse sono infatti una via obbligata tra il Mar Mediterraneo e l'Europa del Centro Nord.Nelle regioni alpine infatti, molte infrastrutture sia in superficie che sotterranee sono state costruite anni fa (ad es. la ferrovia e l'autostrada del Gottardo), mentre molte altre sono ad oggi in costruzione, come la nuova ferrovia ad alta velocità del Gottardo, che permetterà un collegamento più veloce tra Zurigo e Milano ed è certamente una delle più importanti attualmente in costruzione. Nell'ambito di questa nuova infrastruttura, denominata Alptransit, in particolare, le gallerie del S. Gottardo e del Monte Ceneri, rispettivamente lunghe circa 57 e 16 km, sono attualmente in fase di costruzione.

Per queste ragioni, attualmente c'è un'esigenza crescente di coordinare tutti gli aspetti idrogeologici durante la costruzione della nuova galleria al fine di migliorare la sostenibilità ambientale. Inoltre lo scavo di questa galleria è un'opportunità unica per acquisire una buona conoscenza geologica e idrogeologica del sito.

Specialmente per le regioni montuose la corretta previsione del flusso delle acque nella matrice rocciosa non è infatti semplice, in quanto la permeabilità primaria delle rocce cristalline è praticamente nulla e solo la presenza di fratture, faglie e altre cavità permette il flusso delle acque. Pertanto la corretta valutazione dei parametri acquiferi delle rocce fratturate è difficile o impossibile senza studi idrogeologici di dettaglio. Per questo scopo, intendiamo utilizzare indagini

geochimiche, tra cui le metodologie isotopiche, e geofisiche per comprendere meglio il deflusso idraulico sotterraneo in roccia fratturata e ottenere un affidabile modello idrogeologico concettuale.
Abbiamo quindi intrapreso unan ricerca nel Canton Ticino, in particolare nella zona vicina a Lugano, dove si sta attualmente scavando la galleria di base del Monte Ceneri. Quest'area è principalmente costituita da rocce metamorfiche (gneiss e anfiboliti), generalmente considerate impermeabili, tuttavia le fratture e i processi legati agli agenti atmosferici localmente aumentano la permeabilità, permettendo il flusso delle acque.
In questo articolo intendiamo descrivere per prima cosa gli assetti geologici ed idrogeologici dell'area di studio, per poi illustrare l'approccio geochimico e geofisico concepito ed i risultati preliminari delle prime applicazioni.

KEYWORDS: Groundwater – Tunneling – Conceptual model – Geochemical method – Geophysical survey – Southern Switzerland

Geological and hydrogeological settings of the area

The Ceneri base tunnel is entirely located within the crystalline basement of southern Alps. From a tectonic point of view, this geological zone is separated from the Penninic nappes of the Central Alps by the *Insubric Line* (known also as *Periadriatic Line*), which is one of the main tectonic features of the Alpine chain.

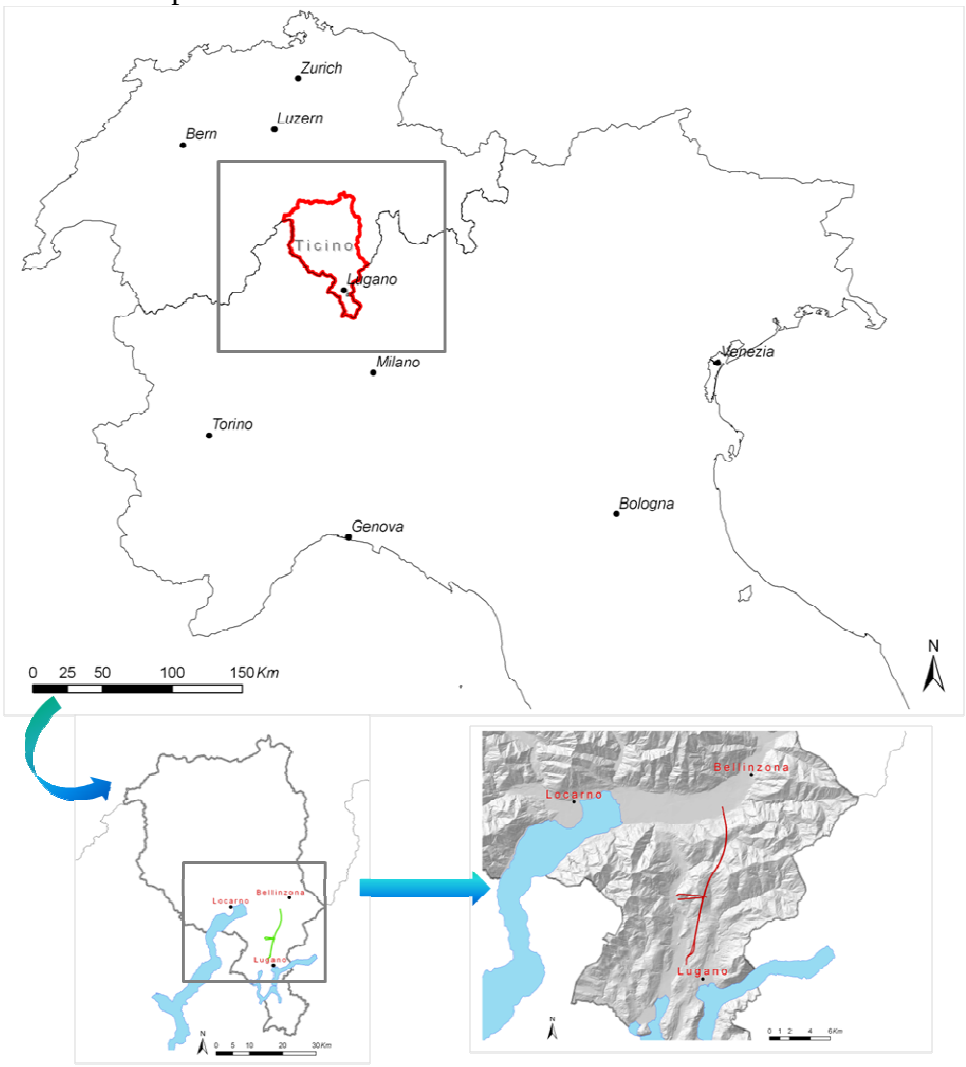

Figure 1. Area of Ticino Canton where the Monte Ceneri base tunnel is drilled

The Southalpine basement extends along the whole length of the tunnel from the Vigana north portal (Magadino alluvial plain), to the Vezia south portal (Vedeggio alluvial plain).

The part of tunnel drilling is mainly constituted by metamorphic rocks (gneisses and amphibolites). However it is possible to subdivide the area where tunnel will be drilled in two

different zones [Pini et al. 2007], that are separated by a fault, the *Val Colla Line* (the black broken line that intersect the tunnel in figure 4):

the Ceneri zone, in the north, 10.2 km long;

the Val Colla zone, in the south, 4.6 km long.

In particular, the first zone is essentially constitute by ortho- and paragneisses, Ceneri orthogneisses and other heterogeneous gneisses of Giumello-type, greenschists, amphibolites and serpentinites, i.e. basic and ultrabasic rocks present in a small area under Gola di Lago. The zone of Val Colla is essentially constituted by the following main lithologies: metasedimentary rocks, S. Bernardo orthogneisses, Stabiello paragneisses and schists.

The main schistosity is nearly parallel to the slope in the northern area, while in the southern part it is south or south/east dipping. The deformations associated to the alpine orogenesis are of destructive nature with several clastic structures, such as fault zones and fractures, which in the overlying landscape, morphologically correspond to incisions in the slope.

The topographic elevation of the gneiss bodies of the Ceneri zone ranges from 300 and 1100 m a.s.l., while in the Val Colla zone it ranges from 300 and 500 m a.s.l. The Ceneri base tunnel passes through the gneiss bodies at an elevation of about 250 m a.s.l.

In figure 5 all expected lithologies of the tunnel are shown, while figure 4 illustrates a horizontal cut through the tunnel and a geological sketch map (scale 1:250000), which also contains the most important known disturbed zones.

All the crystalline rocks crossed by tunnel, are usually considered impervious (low absolute permeability), however fractures and other alteration processes locally increase the effective permeability, allowing water flow in the rock matrix. It is not simple to assign values to the permeability index *k*. In fact it depends substantially of the fracture abundance and of their interconnection. Several studies have investigated the permeability range of the crystalline rocks. In particular Beatrizzotti [1996] has studied the permeability of the rock in the Ticino Canton. With a series of pumping tests, he measured a value of $k = 1.7 \cdot 10^{-6}$ m/s in the Ceneri gneiss, and $k = 1 \cdot 10^{-6} \div 4 \cdot 10^{-6}$ m/s in the Stabiello gneiss in the zone of Val Colla.(all these data refer to surface rocks).

Several literature studies have shown a depth-dependency of the hydraulic conductivity in crystalline rocks such as gneisses, not confirmed instead in other crystalline rocks such as granites and basalts. In particular, in gneiss, a hydraulic discontinuity has generally been observed under the uppermost 100-200 m. In fact, close to the surface substantially higher conductivities are registered, due to higher fracture density and higher apertures; while stress release, weathering processes and gravitationally induced weakening of the bedrock along steep slopes cause a decrease of the permeability with depth. Therefore in gneiss it is so possible distinguish an uppermost zone [Ofterdinger, 2001; Maréchal and Etcheverry, 2003], often named “decompressed”, and, deep down, an other zone that is named “deeper” and is characterized by a lower permeability (fig.2).

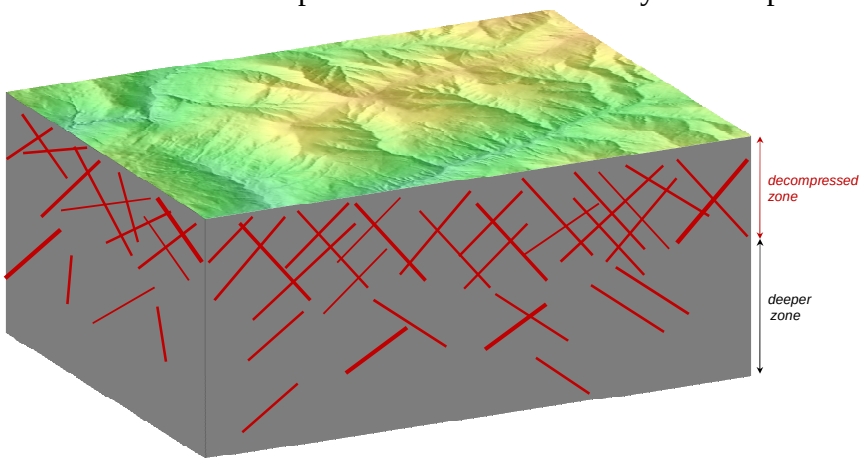

Figure 2. Simplified pattern of the hypothetical presence of fractures in gneissic rocks.

This evidence is described by a number of literature studies performed in the crystalline rocks of the Alps. In particular, Maréchal and Etcheverry [2003], on the basis of the data collected in the M. Blanc massif and in other Alpine crystalline basements, propose an exponential decrease of hydraulic conductivity described by equation 1, that is commonly adopted for the design of structures in the deep rocks, such as tunnels or underground nuclear waste disposals.

$$k = k_0 \cdot e^{a \cdot C} \qquad (1)$$

Where k_0 [m/s] represents the hydraulic conductivity at the surface, C is the overburden [m] and α is a parameter that Marechal and Etcheverry define as shown in table 1.

Zone	α (m^{-1})
Uppermost decompressed zone (0-100 m)	0.05
Intermediate decompressed zone (100 - 600 m)	0.015
Deeper zone (>600 m)6	0.005

Table 1. Values of the *a* parameter of equation 1.

Therefore, the values of *k* at the tunnel depth, estimated on the basis of geological knowledge, drilling, Lugeon tests, pumping tests and variable head tests performed by tunnel designer, are in the range of $1.8 \cdot 10^{-7} \div 7.5 \cdot 10^{-10}$ m/s. They are defined for different homogeneous intervals, that are the tunnel shares with similar geological features.

The total drainage due to tunnel excavation has been estimated within the geological design using the following the Muskat or Goodman formulation of formula 2 [El Tani, 2003] applied to homogeneous intervals.

$$Q = 2\pi \cdot k \frac{h}{\ln\left(2h / r_e\right)} \qquad (2)$$

where r_e is the equivalent radius (8 m as estimated by designers) and *h* is the overburden above the tunnel. The drainage water is so evaluated using the value of *k* above discussed, and the most probable total discharge forecasted for both the base tunnel and the Sigirino exploration tunnel is 49 l/s (about 16 l/min/100m), while the conservative evaluation is 84 l/s (about 28 l/min/100m). In figure 3 the measured water inflows in the geological investigation tunnel of Sigirino, registered in the excavation phases, which is now monthly recorded are shown. Due to the high tunnel overburden and the good state of rocks, the inflows in the Sigirino tunnels are indeed very low.

From a qualitative point of view, the permeability of rocks crossed by the Ceneri base tunnel is generally low.

On the basis of the geological inspections (geomorphological and surface geological surveys, drilling inspections, previous geological informations, etc.) the tunnel excavation will be conducted in essentially dry conditions.

One of the most important disturbed zone, the Val Colla Line (figg. 4 & 5), from drilling inspections seem be mainly composed by mylonites, that are fine grained shists, often with an high mica content and therefore essentially low permeable. A possible disturbed zone more permeable is localized under the Isone town (fig 5), and finally the most important water inflows are expected close to the north and south portals, where the tunnel will be excavated in the decompressed zone.

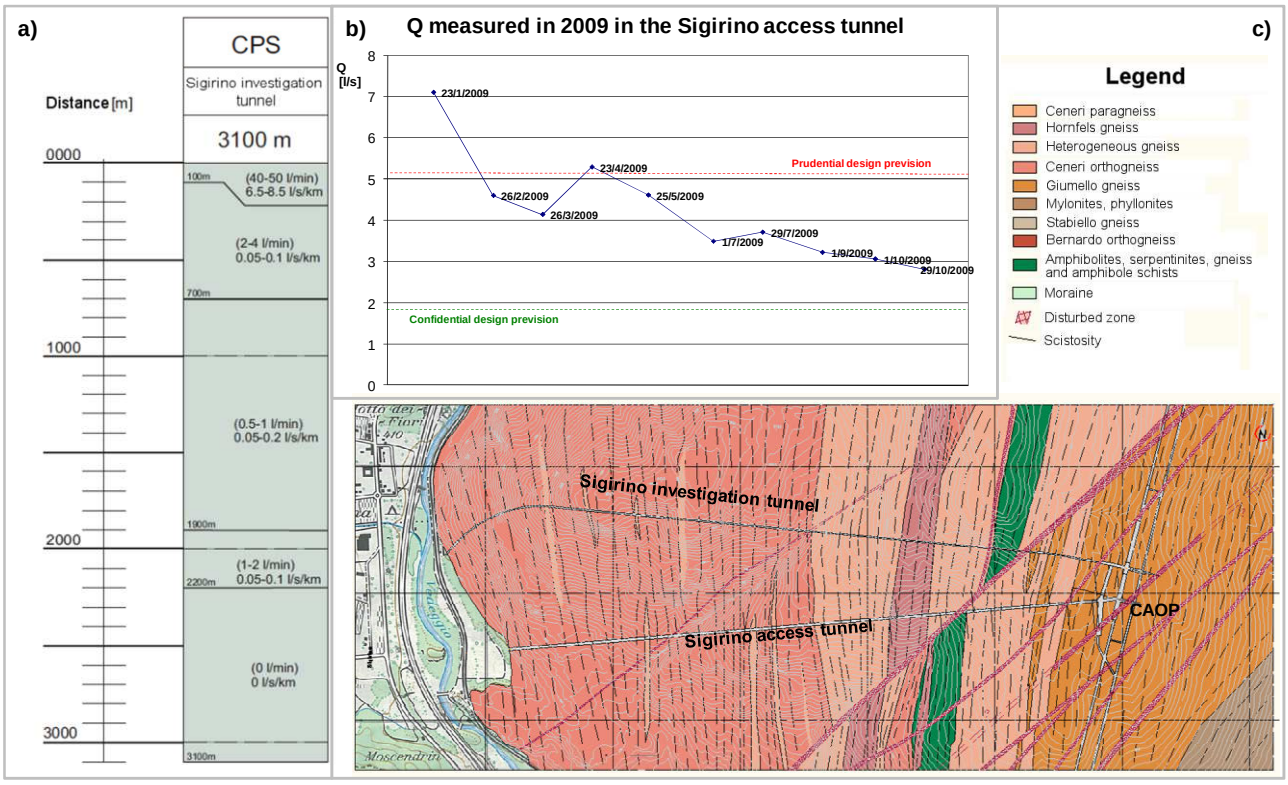

Figure 3. Water inflows registered in the geological investigation tunnel during drilling phases(a) and actually (b) and corresponding lithologies crossed (c) [*data kindly offers by Alptransit Inc*].

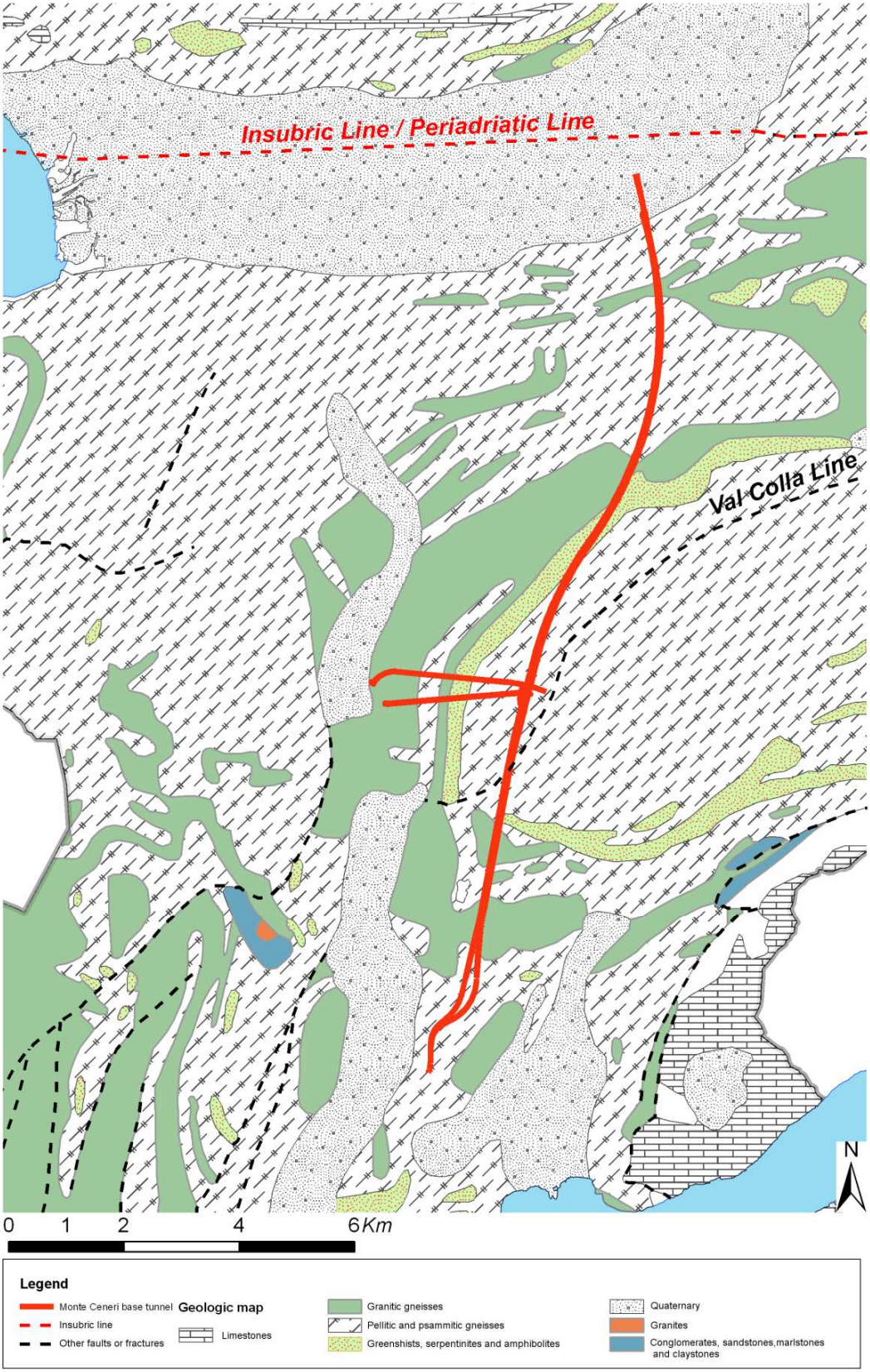

Figure 4. Geological sketch map of the Monte Ceneri base tunnel area.

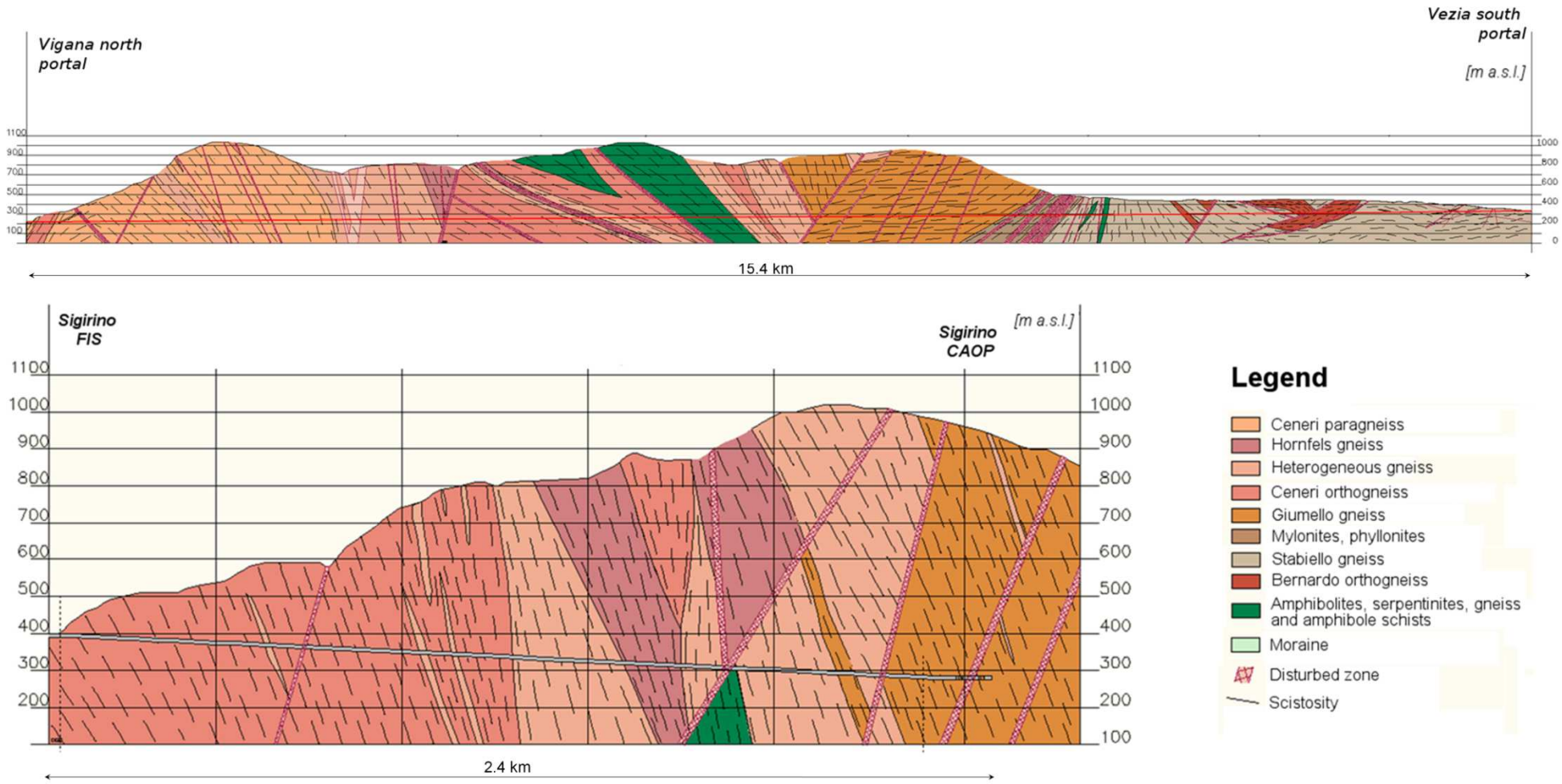

Figure 5. Expected geological profile of the Ceneri base tunnel (upper side) and Sigirino exploration tunnel (below). Now only the latter has been drilled [*data kindly offers by Alptransit Inc.*].

Geochemical methods

Geochemical methods consisted in monitoring springs and, if possible, water inflows in tunnel, for discharge, electric conductivity, pH and in collecting water samples for geochemical and isotopic analysis.

Both conductivity values, that are mostly related with Total Dissolved Solids (TDS), or the sum of major ions, allow defining different hydrogeological facies and can be an useful indicator of interactions between water and rocks, and thus of the water flows in the fractured rocks. Also discharge and temperature variability during the year, their comparison with rain events and mean monthly air temperature data can give further informations about spring types (e.g. deep or shallow groundwater systems).

The knowledge of the stable isotopic composition of atmospheric precipitations is an important research tool in the fields of hydrology, as well as of climatology and paleoclimatology. In fact, the water may be divided into light ($^1H_2{}^{16}O$) and heavy ($^1H^2H^{16}O$ and $^1H_2{}^{18}O$) molecules and the isotopic fractionation that occurs during chemical reactions and physical hydrological processes is a tool to understand the water provenance [Sheppard, 1986]. For geochemical purposes, the isotopic compositions are expressed in terms of deviations relative to a standard material. Consequently, δ-values are used to express stable isotope abundance as follows:

$$\delta = \frac{R_{sample} - R_{VSMOW}}{R_{VSMOW}} \times 1000 \qquad (3)$$

where R are the isotope ratios ($^2H/^1H$; $^{18}O/^{16}O$) respectively of sample and standard (expressed in terms of Vienna Standard Mean Ocean Water isotope composition).

A basic concept, useful for hydrogeological studies, is the *meteoric isotopic line* [Craig, 1961], that is a linear correlation between the δ^2H *(‰VSMOW)* and the $\delta^{18}O$ *(‰VSMOW)* values of the meteoric waters. Since 1961 the isotopic meteoric composition data were collected by the International Atomic Energy Agency (IAEA) Water Resource Program and by the World Meteorological Organization (WMO), that created the *Global Network of Isotopes in Precipitation* (*GNIP*). Moreover in Switzerland, since 1993, the Network for the Observation of Isotopes in the Water Cycle (*NISOT*) of the national groundwater observation program NAQUA is the institution commissioned to survey the content of hydrogen and oxygen isotopes in precipitation [Schürch et al, 2003]. It is managed by the Federal Office for the Environment (FOEN) in conjunction with the Climate and Environmental Physics group at the University of Bern.

In particular, the variations in δ^2H and $\delta^{18}O$ in precipitations can be better understood if we consider the two main processes in the global water cycle: *(i)* the evaporation of surface water characterized by the isotopic fractionation effect between various water vapor molecules, and *(ii)* the progressive raining out of the vapor masses as they move towards regions. Therefore, rain has a specific isotopic signature; in particular it depends on the origin of vapor, the amount of precipitation, the temperature and altitude effects and it is stable in the water, even after flow in the underground. For this reason the knowledge of the isotopic signature of water is very interesting in order to investigate groundwater flows in crystalline fractured rock.

For example, *seasonal effect* (fig. 6) can be useful in order to understand aquifer recharge, transit time of water in the rock, attenuation and flow rates [Eichinger et al., 1984; Maloszewski et al., 1990]. For instance, in our study we will compare the seasonal variations of isotopic signature of the rain of Canton Ticino and the isotopic signature of monitored springs. From this type of data, that we are now collecting in the region surrounding the Monte Ceneri, we expect interesting information about water provenance and transit time. Investigating the *Altitude effect* is another interesting and widely used application in isotope hydrology. It consists of the identification of the elevation at which groundwater recharge takes place. In fact, as a rule, the isotopic composition of precipitations changes with the altitude of the terrain and it becomes more and more depleted in ^{18}O and ^2H at higher elevations. The observed effect on the ^{18}O abundance generally varies between –0.1‰ and -0.6‰ per 100 m of altitude. Values in this range have also been reported for other

mountainous regions in Switzerland [Pearson et al. 1991]. However, the altitude effect is variable from region to region and unfortunately Pearson et al. in their technical report (fig.7) did not report any specific relationship that correlate elevation and isotopic abundance in Southern Switzerland. From a literature review, we found three possible relationships $H\text{-}\delta^{18}O$ obtained for areas close to the Ticino canton (fig.8). The first is obtained by Ofterdinger et al [2001] and it is applied for the Gotthard region; it is certainly valid for the central Swiss Alps for data of that area, but probably not suitable for ours:

$$\delta^{18}O = -(0.0023 \pm 0.0003)z - (9.4 \pm 0.5)‰ \quad (4)$$

A second relationship has been described by Pastorelli et al. [1999] for the Blenio Valley, but unfortunately on the basis of too few samples and it is most likely not valid for our area:

$$\delta^{18}O = -0.00192 \cdot z - 7.51‰ \quad (5)$$

A third is obtained by Bestenheider [2006] also applied for the Blenio Valley on the basis of data collected until 2003 in the stations of Locarno-Monti, Riazzino (Ticino river) and Grimsel.

$$\delta^{18}O = -0.0024 \cdot z - 6.97‰ \quad (6)$$

Probably, not any of these relationships is reliable for our region. This lack may be a problem; in fact, in the alpine regions, it is necessary to take into account at least two different altitude gradients, because of the climatic contrast between the northern and southern sides of the mountains [Marechal and Etcheverry, 2003]. For instance for the Southern Alps, Novel et al. [1999] have calculated an altitude gradient on 8 stations of precipitations lying between 315 and 3500 m in the Aosta Valley (Italy) during the 1993-1994 period. The relationship between the average annual content of ^{18}O of precipitation and altitude is thus:

$$\delta^{18}O = -(0.0018 \pm 0.0002)z - (8 \pm 0.5)‰ \quad (7)$$

While for the Northern Alps it is seems possible to use the following relationship obtained by samples collected between the stations at Thonon les Bains (385 m) and Grimsel (1980 m):

$$\delta^{18}O = -0.0027 \; z - 8.4‰ \quad (8)$$

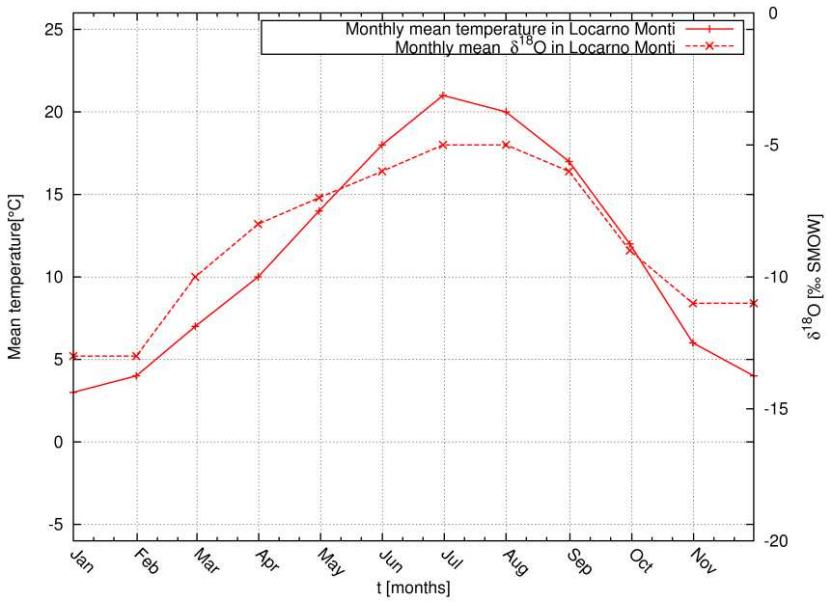

Figure 6.Monthly mean isotopic composition of rain and temperature in Locarno

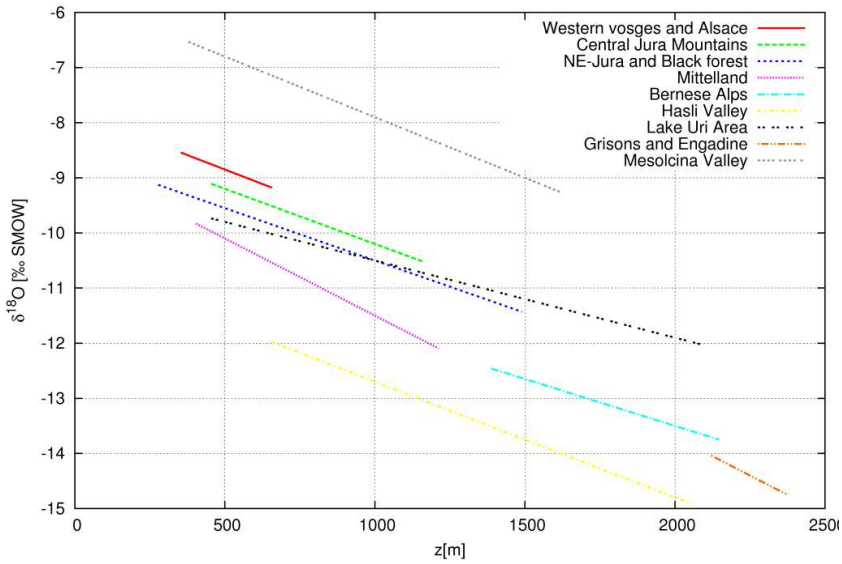

Figure 7. Stable isotope-recharge altitude relationship for Northern Switzerland [elaborated from data reported in Pearson et al., 1991]

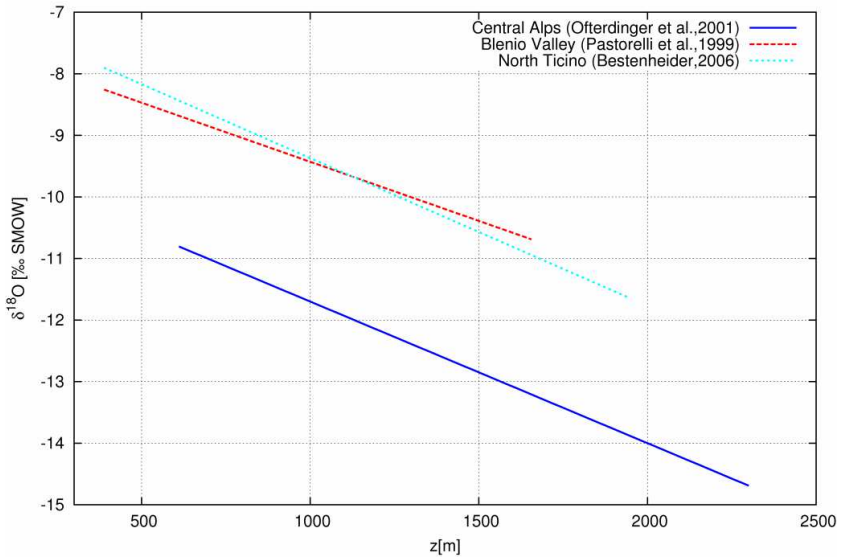

Figure 8.Stable isotope-recharge altitude relationships obtained with data of area close to the Canton Ticino.

The difference in altitude gradients, between two regions at similar latitude and orography, but with a rain system that differs a lot, is considerable (fig.9). Therefore, it is clear that to obtain a good indication about mean altitude recharge, we need to find a valid relationship between altitude and isotopic composition of our rain.

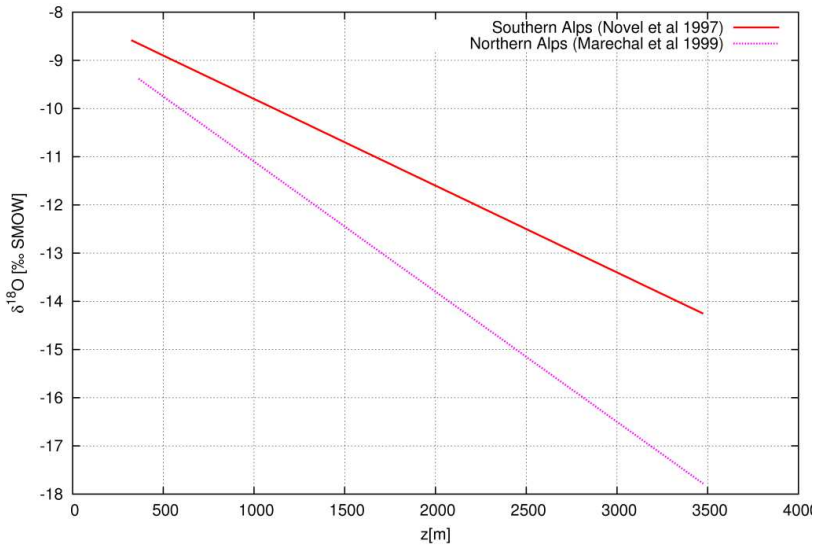

Figure 9.Stable isotope-recharge altitude relationships for northern and southern Alps

For this reason, we have densified the monitoring network of rain isotopic data for the Ceneri zone. In a first step we will measure data even in the Arosio rain gauge (fig.10), that is located at 860 m a.s.l. and is close to the M. Ceneri base tunnel area. The data collected, that will be correlated with that collected in Locarno Monti (379 m a.s.l.) and eventually with others data, coming from GNIP stations, will hopefully allow us to obtain a reliable value for altitude gradient curve for the Monte Ceneri base tunnel area. Unfortunately, there is not yet a good collection neither of data for Northern Italy, where the only precipitation data actually available was sporadically collected in the 2002-2004 years and are reported in Longinelli et al. [2006].

Due to the lack of neighborhood data, recently we have increased the precipitation monitoring network with more five stations located at different altitude in the Ticino Canton to get a better data set for the Southern Switzerland. Concerning data are not yet available, to this reason the stations will be present in further specific reports.

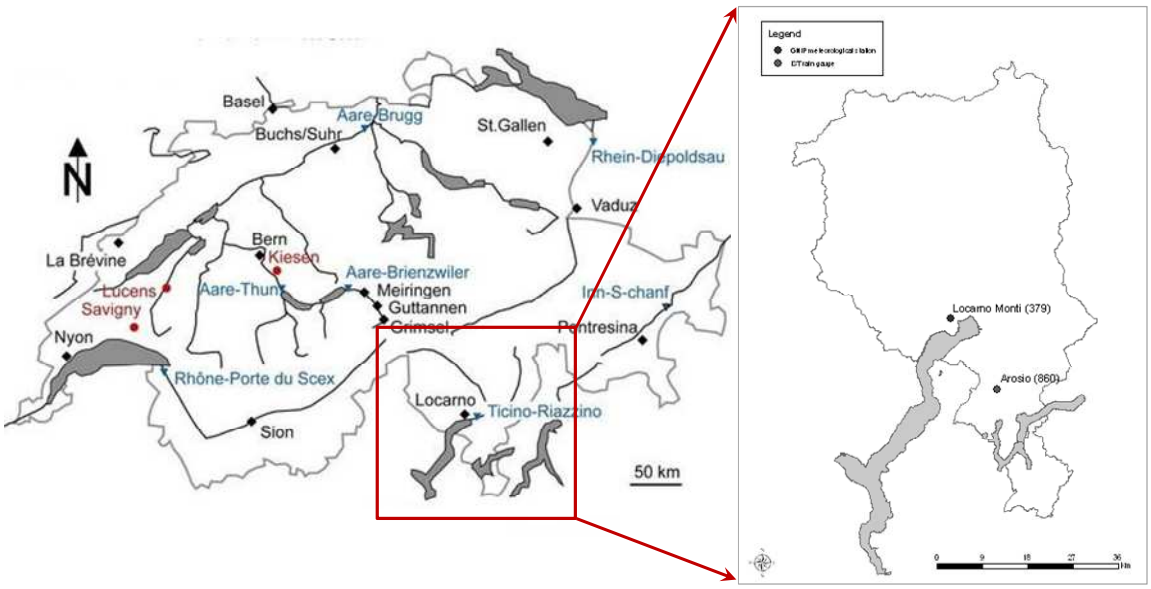

Figure 10.Localization of precipitation isotope measurement stations of GNIP network and of Isone rain gauge of Institute of Earth Sciences (SUPSI), used for this research project.

The tritium (^{3}H) is a further isotopic element useful to obtain information about groundwater age, flow paths and velocities. It is first of all a radioactive heavy isotope of hydrogen, that is naturally formed in the upper atmosphere from a nuclear reaction between atmospheric nitrogen and thermal neutrons. The ^3H thus formed enters the hydrologic cycle after an oxidation that forms "tritiated waters" $^1H^3HO$, and it finally decays to form helium ^{3}He, that is named tritiogenic helium. The rate of radioactive decay is by convention expressed as the half-life $T_{1/2}$, defined as the time span during which a given concentration of the radioelement atoms decay to half the initial value. The half-life of tritium was calculated by Lucas and Unterweger [2000] as 12.32 years. Under undisturbed natural conditions the ^{3}H concentration in precipitations would be probably about 5 TU; however following the nuclear weapon tests of the early sixties, the ^3H content in precipitation temporarily increased by a 1000-fold in the northern hemisphere. Since 1963, due to the end of the era of thermonuclear bomb testing in the atmosphere, this extreme ^3H content has decreased to essentially natural values in winter when a large part of ^{3}H stay in the stratosphere, while it increases about twice natural values in summer, when this part of ^{3}H returns to the troposphere (fig.11).

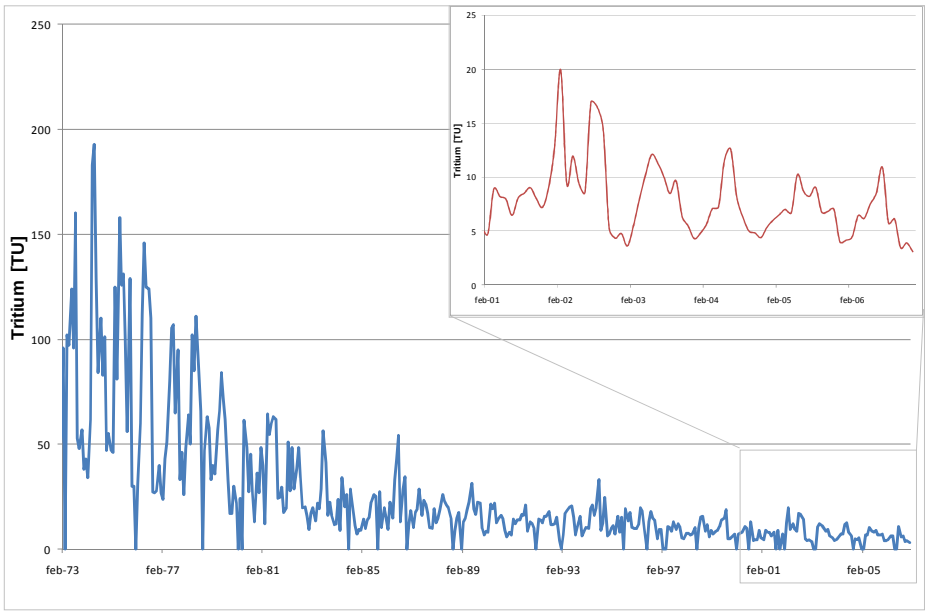

Figure 11. Monthly values of tritium concentrations since 1972 in Locarno precipitations.

Actually the use of only tritium data is probably not able to give us detailed information on groundwater, especially in case of modern water, allowing only a qualitative interpretation of groundwater mean residence times. Rather the use of the tritium/helium-3 (^{3}H/^{3}He) method [Schlosser et al., 1988; 1989; Aeschbach-Hertig et al., 1998; Althaus et al, 2009; Holzner et al, 2009] should have the additional advantage of providing, in case of modern water, a "*discrete age*" for the sampled water, even though it needs complex and expensive measuring techniques and to this reason we will try to apply this method only as last check of our conceptual model.

Geophysical investigations

In addition to geochemical methods we are interested in the use of geophysical approaches, in order to (*i*) predict the presence of fractures and discontinuities that are the preferable hydraulic pathways of the rock masses, (*ii*) forecast the possible water inflows in the tunnel, and (*iii*) investigate the hydrogeological behaviour of the water springs in the regions surrounding the new tunnel actually in construction. In our research project, we use a Very Low Frequency electromagnetic (VLF-EM) instrument and an Inductive Polarized (IP) Electrical Resistivity Tomography (ERT) equipment. Our aim is to better understand the possible application of the two

approaches to investigate the interaction of tunnel with groundwater in the rock masses domain, discuss benefits and disadvantages and make a comparison of these methods.

The VLF-EM method is useful for the detection of elongated, steeply dipping high-conductivity bodies, that can be due not only to water trapped in rock fractures and cavities, but also due to conductive bodies in the underground. The instrument utilizes the magnetic component of the electromagnetic field generated by long-distance radio transmitters in the very low frequency band (15-30 kHz), that are used mostly for long-distance communications. Conductive structures on the surface, but also in the underground, even when buried with a thick overburden, affect locally the direction and strength of the magnetic field normally generated by the transmitted radio signal. A weak secondary field builds up around the geological underground structure, and the instrument is capable to measure this radio signal distortion (fig.12).

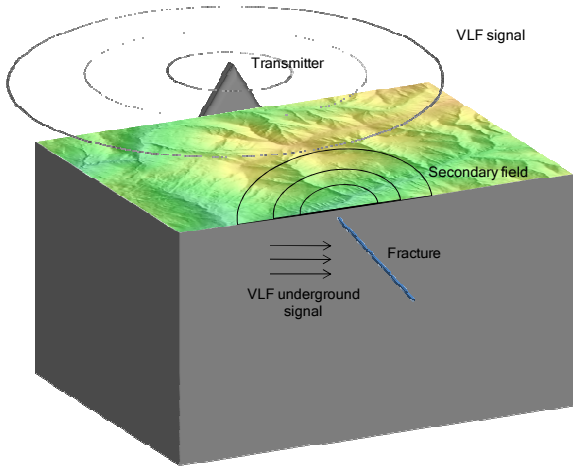

Figure 12.Scheme of the VLF technique functioning

Therefore, VLF method has been often used in hydrogeology for the detection of fractures in rocks [Macedo and Lima, 2004]. Few works have been carried out some years ago at Institute of Earth Sciences (IST-SUPSI) to find faults and fractures over tunnel [Pagano, 1996], in order to study hydrothermal flow of groundwater, or simply to test the instrument [Ghirlanda,1996]. Actually we want to test this method and to compare it with other geophysical methods. For this purpose, we use a WABEM® WADI VLF instrument of Institute of Earh Science (IST-SUPSI) of Lugano. The maximum depth capacity of the instrument is about 100 m, under ideal undisturbed conditions, and in particular it depends on the mean resistivity of the field rock. For a steeply dipping conductor, the typical anomaly will appear in the following manner: a maximum occurs to the left, and a minimum to the right of the conductor (fig.13a). The above sketched anomaly can be imagined to be the real part, that is the part of the resulting field which are in phase with the primary field from the VLF transmitter. The instrument will also measure an imaginary component, which are 90° out of phase with the primary field. This way of plotting the VLF anomaly reached by the instrument, makes the interpretation of data difficult, especially in case of complicated geology. Various types of filtering techniques have been used to extract interesting information; in particular the WADI VLF instrument uses a filter designed by Karous an Hjelt [ABEM, 1993] to purify the data. The output from this filter is an equivalent current density at a certain depth in the ground, that is named “anomaly” and is represented by a single peak right above the conductor (fig.13b). For the interpretation of recorded VLF data, we could use the RAMAG 2.2 software. It allows to download data from the instrument and to transform field data into line graphs of original and filtered data, and more understandable cross sections with % of in-phase response of underground to electrical current flow.

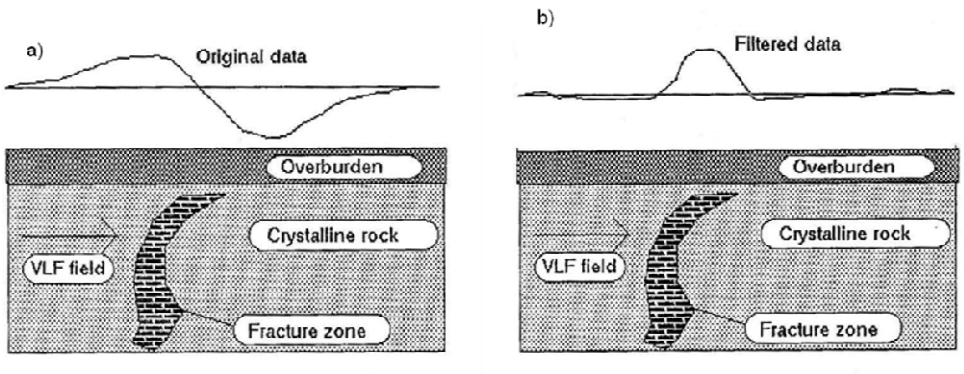

Figure 13.Typical behaviour of an VLF anomaly like reached by the instrument (a) and after a filtering process of data

(b)

We are also performing some 2D geoelectrical surveys in order to test their application for the detection of fractures that could intersect the underground infrastructure, causing consistent water inflows within the tunnel actually excavating. The purpose of Electrical Resistivity Tomography (ERT) is to determine the subsurface resistivity distribution, by making more simple measurements on the ground surface (fig.14). The resistivity ρ is the physical property which determines the aptitude of a material to oppose to the passage of the electrical current. In field geology, it is related to various ground parameters, such as the mineral and fluid content. In particular, knowing the geology and the resistance expected from a rock, often, the conductivity skill is mainly controlled by voids presence and by the water which they contain. For this reason, geoelectrical techniques are frequently used in the hydrogeological domain [Giudici et al 2003].

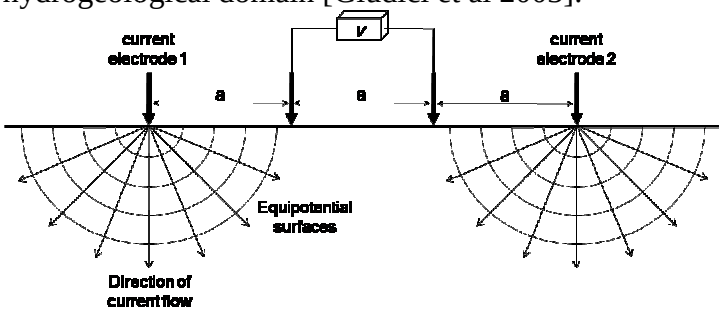

Figure 14.Simplify pattern of resistivity acquisition. Two electrodes are used as electrical input, while two electrodes

measure the difference of potential.

A 2D acquisition uses a great number of electrodes connected to a multicore cable and placed along the desired profile. In the field we obtain values of terrain *apparent resistivity*, that is the resistivity of a homogeneous underground that will give the same resistance value for the same electrode arrangement. After both a filtering and an inversion process, the result is a modeled profile of terrain resistivity. In particular, using different configurations (fig. 15), it is possible to analyze the superimposed horizontal layers of a terrain or the presence of vertical structures, such as faults or fractures in the rock components.

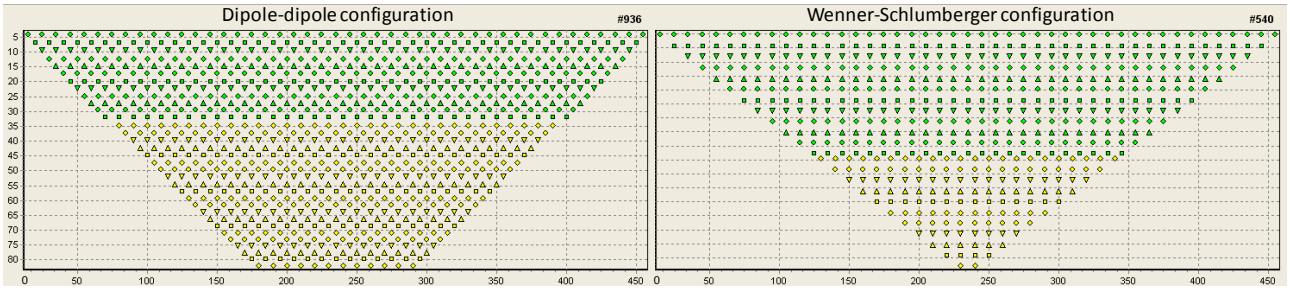

Figure 15.Two possible configurations used to acquire the apparent resistivity values along a profile using 48 electrodes interspaced 10 m

In the Ceneri Zone, due to the high elevation of the terrain above the tunnel, it is impossible to directly find the intersection between the eventually detected disturbed zones and the tunnel in construction; nevertheless geoelectrical surveys, connected with geomorphologic observations, can be useful in order to obtain information about location and properties of fractures or faults, even only in the shallow decompressed zone. To test it, we are using a 10 channel resistivity meter for resistivity and IP measurements (*Syscal Pro*) kindly provided by the Institute of Geophysics of University of Lausanne. For the download and the inversion of field data we are using the RES2DINV inversion software [Locke, 2004].

Preliminary results of geochemical analysis

For the region surrounding the new infrastructure of the Ceneri base tunnel there are about 750 springs registered in the cantonal hydrogeological database. On the basis of criteria of relevance (use and discharge), distance from the tunnel and chemico-physical preliminary characterization, a number of springs have been classified at high risk and selected for monthly measurements in the tunnel geological design [Colombi & Baumer, 1995]. We have used this official classification, in order to implement our monitoring network for isotopes measurements (fig.16); in total, we are monitoring 29 springs. Monthly sampling of water of the selected springs for isotopic abundance data, we have performed also, if possible, physical measurements (discharge, conductivity, pH, air and water temperature). The monitoring will be performed for one year.

The spring waters come from different aquifers, most of which are silicate rocks (ortho- and paragneisses, micaschists, amphibolites, etc). Average annual discharges of monitored springs (1994-2009) vary from 15 to 300 l/min, electric conductivities from 50 to 300 µS/cm at 25°C. These are typical values of water with low and very low ion concentrations with pH-values from 6 to 7.5, that are typical values of neutral waters. Discharge vary from season to season and recently increased, in consideration of that the last years (2008-2009) were very humid if compared with the standard Swiss precipitation rates (calculated on the 30 years between 1961 and 1990).

Spring code	Town	z [m a.s.l.]
104_3	Camorino	462
104_4	Camorino	425
104_5	Camorino	425
109_2	Isone	940
109_3	Isone	935
111_2	Medeglia	900
111_4	Medeglia	800
111_5	Medeglia	805
117_1	Sant'Antonino	340
117_108	Sant'Antonino	568
117_109	Sant'Antonino	560
117_2	Sant'Antonino	420
117_3	Sant'Antonino	448
117_4	Sant'Antonino	582
117_5	Sant'Antonino	430
117_75	Sant'Antonino	435
117_76	Sant'Antonino	438
120_55	Cadenazzo	825
120_57	Cadenazzo	790
120_96	Cadenazzo	870
525_1	Bironico	562
525_15	Camignolo	745
525_18	Camignolo	758
525_2	Bironico	562
525_7	Bironico	751
526_226	Capriasca	780
526_227	Capriasca	810
526_228	Capriasca	790
591_6	Vezia	400

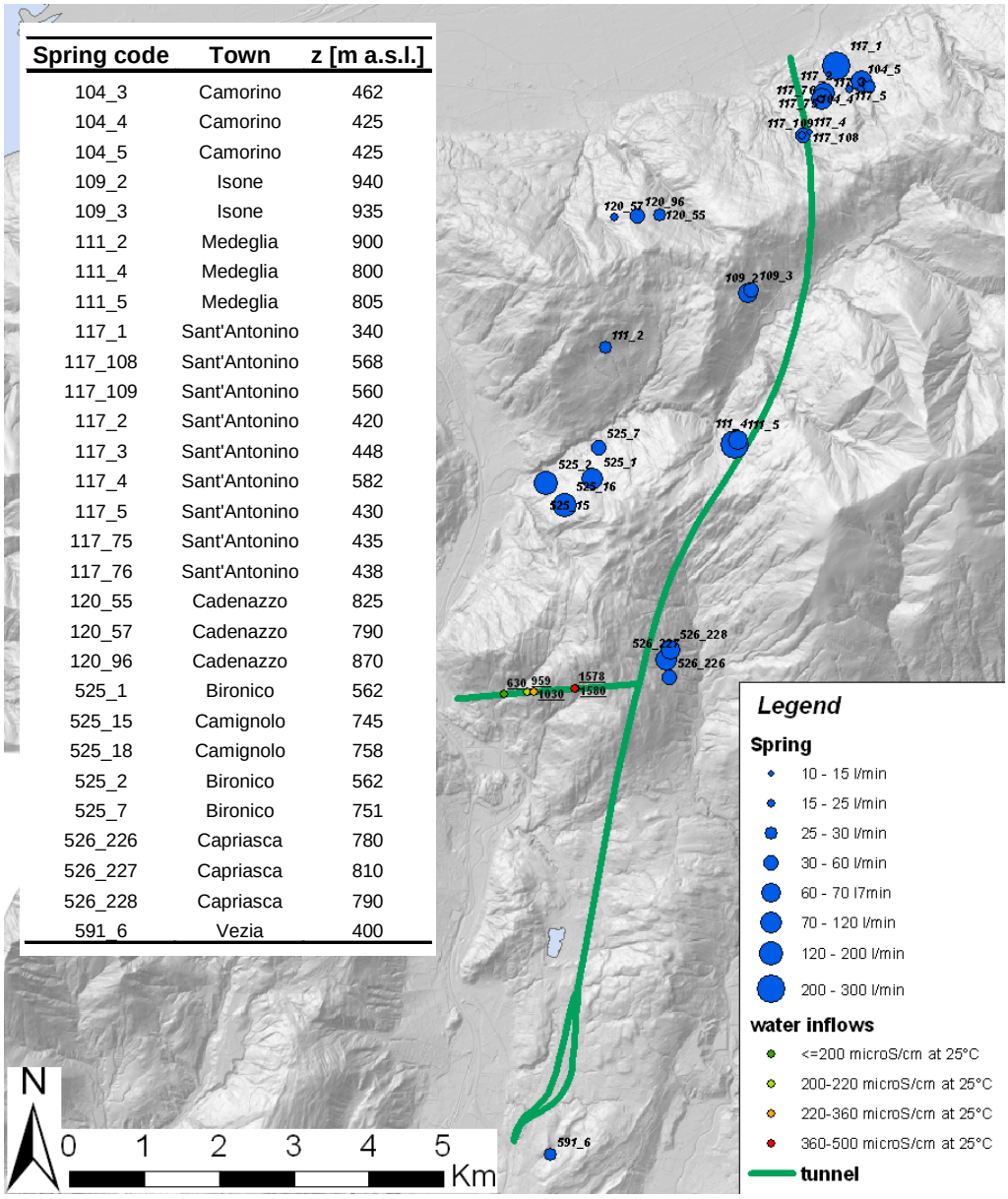

Figure 16.Spring and water inflows monitored.

A number of chemical measurements (table 2) for a few of the selected springs in the region surrounding the Monte Ceneri base tunnel are available on the basis of geological structure of the tunnel [Colombi & Baumer, 1995]. Other chemical measurements were carried out in November 2009 for all the selected springs (table 3). In addtion to the general parameters (EC, T, discharge and pH) that were monthly monitored, we performed also geochemical analyses of major ions, total nitrogen, organic and inorganic carbon. These analyses were carried out in the classical geochemistry laboratory of University of Lausanne (IMG-Centre d'Analyse Minerale). In particular F^-, Cl^-, NO_2^-, NO_3^{2-}, SO_4^-, Li^+, Na^+, NH_4^+, K^+, Mg^+, Ca^+ have been determined by Ion Chromatography, while HCO_3^- is determined by mass balance with the total inorganic carbon, that is analyzed by a C-analyzer (LiquiTOC Elementar), together with organic carbon and total nitrogen.

From the position on the Piper diagram, we note that most of the springs are Ca-SO_4 or Ca-HCO_3–type waters (fig.17 & 18), which are typically shallow groundwaters that flow through crystalline sulfide-bearing rocks; moreover this indication is confirmed by the low EC values. In particular it is possible distinguish between the Camorino and Sant'Antonino springs located above the northern portal, and the other waters, as well shown by figure 18.

Spring ID	*104_3*	*117_1*	*117_3*	*117_5*	*117_75*	*525_18*	*525_2*	*525_7*	*526_227*	*526_228*	*591_6*
Flow [l/min]	8.4	62.7	21	6	11	51	150	40	80	190	33
T[°C]	8.5	11.6	10.2	11.3	8.2	7	7.5	9.1	10	9.5	11.4
pH	6.6	6.2	6.3	6.4	6.7	7.3	7.1	7.1	6.8	6.6	6.3
Cond [µS/cm 20 °C]	66	105	62	76	63	113	140	66	81	77	55
O [%]			92	78					91		
Ca [mg/l]	7.2	10.1	6.7	7.8	6.7	20.8	26	10	10.5	10.4	6
Mg [mg/l]	1.3	2	1.1	1.9	0.8	0.8	2.4	0.9	1.5	1.1	0.9
Na [mg/l]	2.2	4.9	3.2	4	2.4	1.2	2	2.4	2.7	3.3	2.1
K [mg/l]	1.8	2.9	3.2	0.8	1.4	1.4	2.1	1.3	1.7	1.5	< 1
NH4 [mg/l]	0.03	0.02	0.03	0.04	0.02	0.02	0.02	0.02	0.03	< .015	0.03
HCO3 [mg/l]	9	16.1	6.7	10.9	6.3	42.6	51.4	25.9	22.5	20	11.2
SO4 [mg/l]	14.4	14.1	15.3	20.2	12.2	4.4	17.7	7.7	13.4	19.4	2.2
NO3 [mg/l]	< 1	8.4	2.1	< 1	3.1	3.5	< 1	1.5	2	1.4	1.6
Cl [mg/l]	1.6	4.2	1.5	1.1	1.9	1.9	2.4	1.6	1.4	1.4	3.6
NO2 [mg/l]		< .05	< .05	< .05				< .05	< .05	< .05	
F [mg/l]		< .1	< .1	< .1				< .1	< .1	< .1	
SIO2 [mg/l]		12.7	12.9	15.2				12.4	10.6	10.5	
TDS [mg/l]	38.5	75.6	52.9	63.1	34.8	76.6	105.0	63.9	66.5	69.2	28.6
Water Type (PHREEQC software)	Ca-SO4-HCO3	Ca-Na-SO4-NO3-HCO3	Ca-Na-SO4	Ca-Na-Mg-SO4-HCO3	Ca-SO4	Ca-HCO3	Ca-HCO3-SO4	Ca-HCO3-SO4	Ca-HCO3-SO4	Ca-SO4-HCO3	Ca-Na-HCO3-Cl

Table 2.Results of chemico-physical analysis on springs [*from Colombi et al.,1995*]

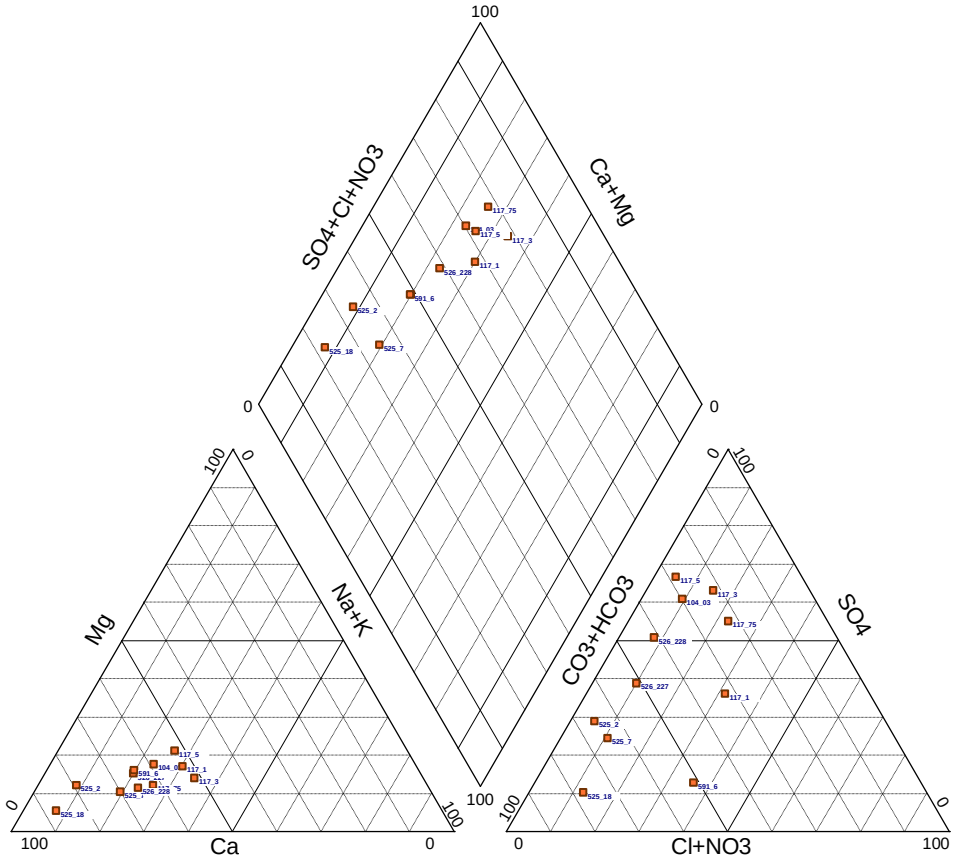

Figure 17.Piper diagram of spring analyzed [*elaborated from Colombi et al.,1995*]

We are also collecting a number of samples of the water inflows in the accessible tunnel (Sigirino exploration tunnel) and in the part of the tunnel actually in construction. Concerning the Sigirino access tunnel, we have a few of samples that were collected in the excavation phases by Alptransit geologists; that kindly allow us, from now on, every two months, where possible, to sample the few residual water inflows. For the remaining parts of the tunnel, that are now drilled, we can collect also, samples of water inflows compatible with excavations works. This concerns in

particular the few months of excavation at the northern portal, while the drilling at the southern portal will start in april 2010.

Spring	Date [2009]	pH	T [°C]	Cond [µS/cm 25 °C]	Q [l/min]	Na [mg/l]	K [mg/l]	Mg [mg/l]	Ca [mg/l]	F [mg/l]	Cl [mg/l]	NO3 [mg/l]	SO4 [mg/l]	HCO3 [mg/l]	TDS [mg/l]	Water Type (PhREEQC software)
104_3	13/11	6.70	10.1	80	12	3.08	0.86	2.11	7.10	0.12	0.65	2.60	22.45	1.94	40.94	Ca-Mg-Na-SO4
104_4	13/11	6.60	12.1	98	105	3.72	1.54	2.62	16.90	0.11	1.35	3.78	26.40	18.41	74.86	Ca-SO4-HCO3
104_5	13/11	6.60	9.9	80	14	3.08	0.84	2.16	14.31	0.13	0.65	2.48	23.08	39.47	86.23	Ca-HCO3-SO4
109_2	25/11	6.67	9.5	42	17.6	2.54	1.05	1.38	12.40	0.05	1.16	4.60	7.13	40.50	70.83	Ca-HCO3
109_3	25/11	6.75	9.5	75	n.d.	3.17	1.14	2.50	17.85	0.06	1.34	5.04	6.78	66.97	104.88	Ca-HCO3
111_2	25/11	6.60	11.1	69	12.5	2.47	1.22	1.26	7.51	0.06	0.68	3.27	5.54	28.98	51.02	Ca-HCO3
111_4	25/11	7.60	8.7	96	n.d.	1.58	0.48	2.34	12.55	0.05	0.67	5.68	6.11	49.27	78.75	Ca-HCO3
111_5	25/11	7.50	11	97	30	1.63	0.82	4.25	14.05	0.16	0.75	5.71	8.01	53.09	88.50	Ca-Mg-HCO3
117_1	13/11	6.50	11.6	118	150	5.79	2.48	2.69	9.76	0.13	7.27	7.04	20.40	25.71	81.30	Ca-Na-Mg-SO4-NO3-Cl
117_2	13/11	6.50	11.6	118	150	3.53	1.60	2.38	13.28	0.12	1.98	5.53	20.02	15.27	63.74	Ca-SO4-HCO3
117_108	13/11	6.60	9.8	72	32	3.82	0.92	2.00	7.11	0.10	2.34	5.63	13.47	31.51	66.94	Ca-HCO3-SO4-NO3
117_109	13/11	6.60	9.9	73	10	3.87	0.93	2.11	15.97	0.12	2.34	5.20	13.72	62.29	106.59	Ca-HCO3-SO4
117_5	13/11	6.80	10.6	90	12	3.94	0.87	2.66	8.07	0.15	0.79	0.65	24.66	21.55	63.37	Ca-Mg-SO4-HCO3
117_75	13/11	6.80	10.7	78	8	4.07	0.81	1.82	11.16	0.11	4.25	3.56	16.08	11.49	53.39	Ca-Na-SO4-HCO3
117_76	13/11	6.40	10.4	80	15	4.08	0.91	1.91	16.28	0.11	4.13	3.71	15.90	30.87	77.93	Ca-HCO3-SO4
120_55	16/11	6.98	8.5	56	38.8	2.32	0.89	1.06	11.69	0.07	0.51	9.56	9.89	36.46	72.47	Ca-HCO3-NO3-SO4
120_57	16/11	6.36	8.8	50	23.1	2.08	0.75	1.02	8.50	0.06	0.55	6.20	4.24	24.84	48.26	Ca-HCO3-NO3
120_96	16/11	6.89	8.2	70	40.1	2.23	0.71	1.01	12.21	0.06	0.41	6.21	6.12	35.98	64.97	Ca-HCO3-NO3
525_1	25/11	7.30	8.4	73	50	2.31	1.02	1.47	10.36	0.13	0.67	3.38	5.78	49.91	75.05	Ca-HCO3
525_15	25/11	7.70	8.3	130	80	2.28	0.66	1.52	21.35	0.27	0.61	5.04	11.93	47.27	90.96	Ca-HCO3
525_18	25/11	7.60	7.6	120	2.8	2.17	0.88	1.42	19.86	0.28	0.57	5.39	11.58	57.12	99.28	Ca-HCO3
525_2	25/11	7.40	9	157	n.d.	2.94	1.98	2.86	24.52	0.19	0.84	1.59	24.85	55.51	115.31	Ca-HCO3-SO4
525_7	25/11	7.40	8.7	133	n.d.	3.05	1.90	2.84	19.93	0.12	0.84	2.75	12.04	59.76	103.26	Ca-HCO3
526_226	19/11	6.80	10.1	95	85.3	3.35	1.39	2.11	10.05	0.08	0.86	2.85	18.97	33.23	72.91	Ca-HCO3-SO4
526_227	19/11	6.80	9.8	99	60	2.91	1.47	2.05	10.56	0.07	1.09	4.03	16.73	32.64	71.57	Ca-HCO3-SO4
526_228	19/11	6.75	9.7	93	85.7	3.02	1.58	2.18	20.80	0.07	0.85	2.83	20.26	44.59	96.21	Ca-HCO3-SO4
591_6	25/11		11.7	85	23.1	3.82	0.81	2.35	14.81	0.25	2.10	3.54	9.23	47.28	84.95	Ca-HCO3

Table 3.Results of chemico-physical analysis on springs (november 2009)

What the isotopes concern, as first stage, using the least squares fit linear correlation method on 204[2] samples of water collected in Locarno Monti meteorological station, we have found a best fit line, which we can be defined as "Locarno meteoric line" (fig. 19). It is expressed by the following linear correlation:

$$\delta^{2}H = 7.79\,\delta^{18}O + 5.65 \qquad (9)$$

With a correlation coefficient r^2 value of 0.96.

[2] 49 of these were monthly sporadically collected by IAEA in the years since 1983 to 1991, 155 were monthly regularly collected by NISOT, that kindly offers our these data, in the years since 1992 to 2006.

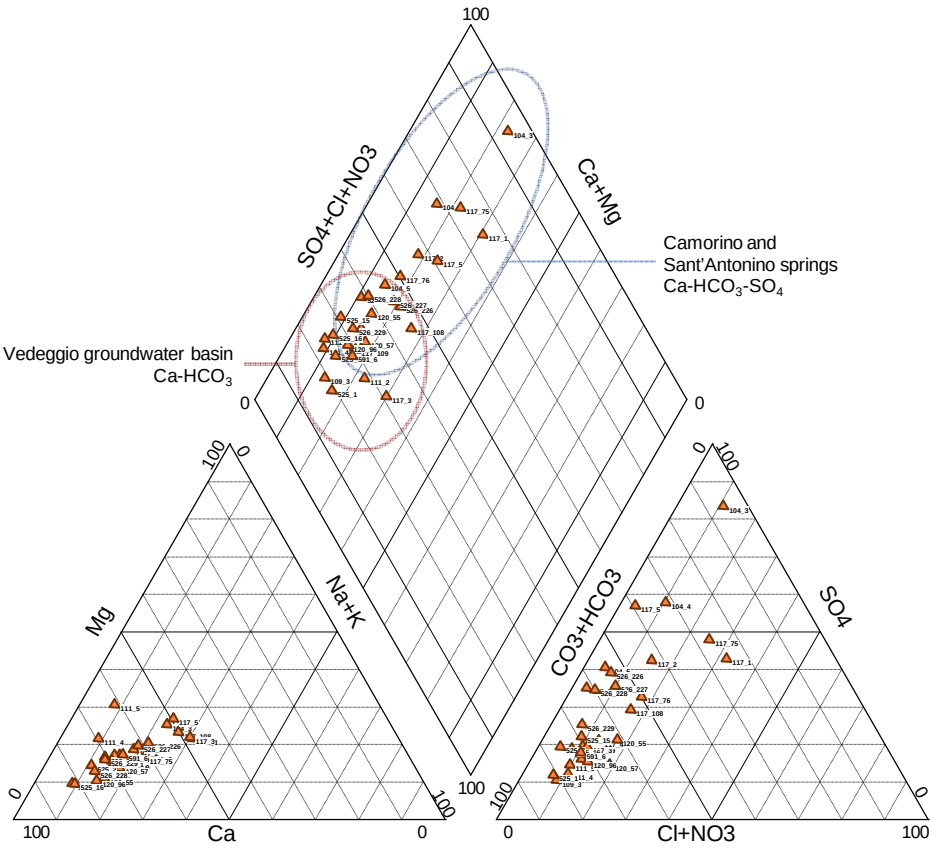

Figure 18.Piper diagram of spring analyzed monitored [*data of November 2009*]

Actually, we have only analyzed stable isotopes in a few of the water collected on the surface springs and within the tunnel. Deuterium and oxygen-18 analyses were performed at the Stable Isotopes Laboratory of the University of Lausanne, using a Wavelength-Scanned Cavity Ring Down Spectroscopy (WS-CRDS) based analyzer that perform together deuterium and oxygen-18 analysis. For seasonal feedbacks and mean altitude recharge evaluation it is necessary to complete the scheduled year of observation; nevertheless a preliminary comparison with meteorological water lines, and a distinction between isotopic composition of spring water and that of the inflows in the Sigirino prospection tunnel is possible using a δ^2H and $\delta^{18}O$ graphic correlation (fig.20). In particular Sigirino tunnel data (red star) are almost all displaced between the Mediterranean and the global or local (Locarno) meteoric water lines. Nevertheless considering the interpolation process which are used in order to obtain the Locarno meteoric line, and the altitude effect on the Monte Ceneri area, these are, reasonably, the typical meteoric water of our region, with relative small residence time. We also try to distinguish between the Camorino and Sant'Antonino springs (black square) located above the northern portal, and the other groundwaters of the Vedeggio hydrogeological basin (blue circle), but there is no clear difference, as shown also by three different correlation lines reported in table 4. All the data analyzed up to now are collected between June and November 2009, and are characterized by relative high values in δ^2H and $\delta^{18}O$ compared to winter precipitation values, that are well shown by figure 21.

Water type	Correlation lines	Correlation coefficient
Tunnel inflows	$\delta^2H = 6.73 \cdot \delta^{18}O + 3.81$	r^2=0.92
Camorino and Sant'Antonino springs	$\delta^2H = 6.68 \cdot \delta^{18}O + 3.19$	r^2=0.95
Vedeggio groundwater basin springs	$\delta^2H = 6.71 \cdot \delta^{18}O + 3.81$	r^2=0.97

Table 4. Different correlation lines for stable isotopic composition of springs and tunnel inflows. There is no clear distinction between various waters.

Also the few precipitation samples, collected in the Arosio rain gauge are analyzed and the obtained stable isotope abundance values are also reported on the δ^2H and $\delta^{18}O$ diagram (fig.21). A first correlation between data is possible:

$$\delta^2H = 8.32\,\delta^{18}O + 18.35 \qquad (10)$$

where correlation coefficient value r^2 is 0.97; obviously the quality is not good, because of the lack of the necessary number of samples (at least one year of observation).

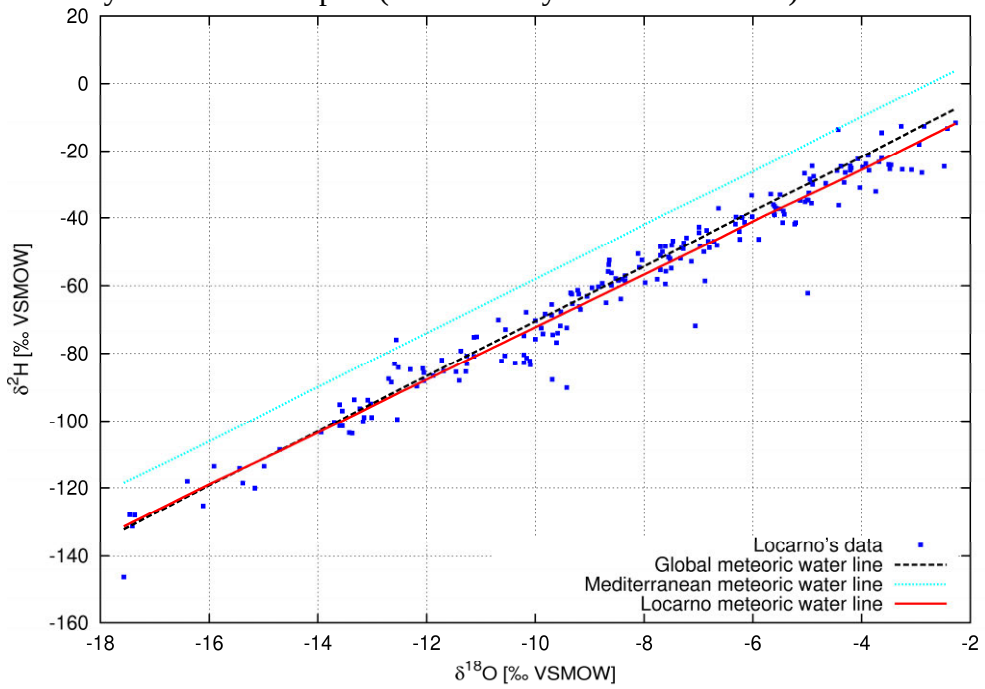

Figure 19. Stable isotopes composition in Locarno precipitations. Local data are fitted by equation 9 and compared with the Vienna Meteoric Water Line [Rozanski et al., 1993]

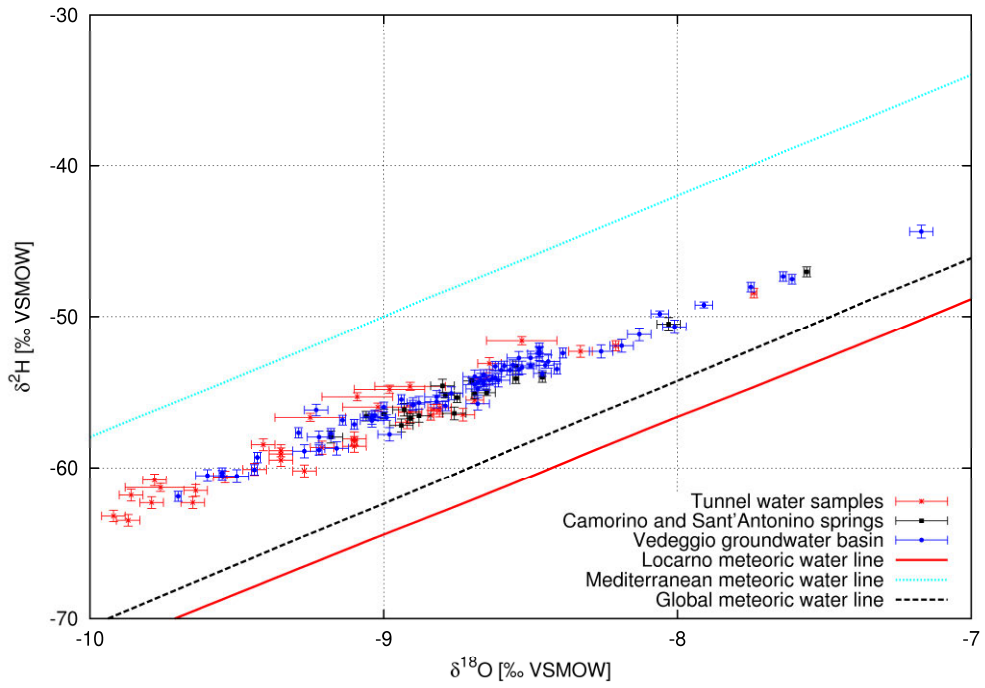

Figure 20.Stable isotopic composition of spring's water and Sigirino tunnel inflows.

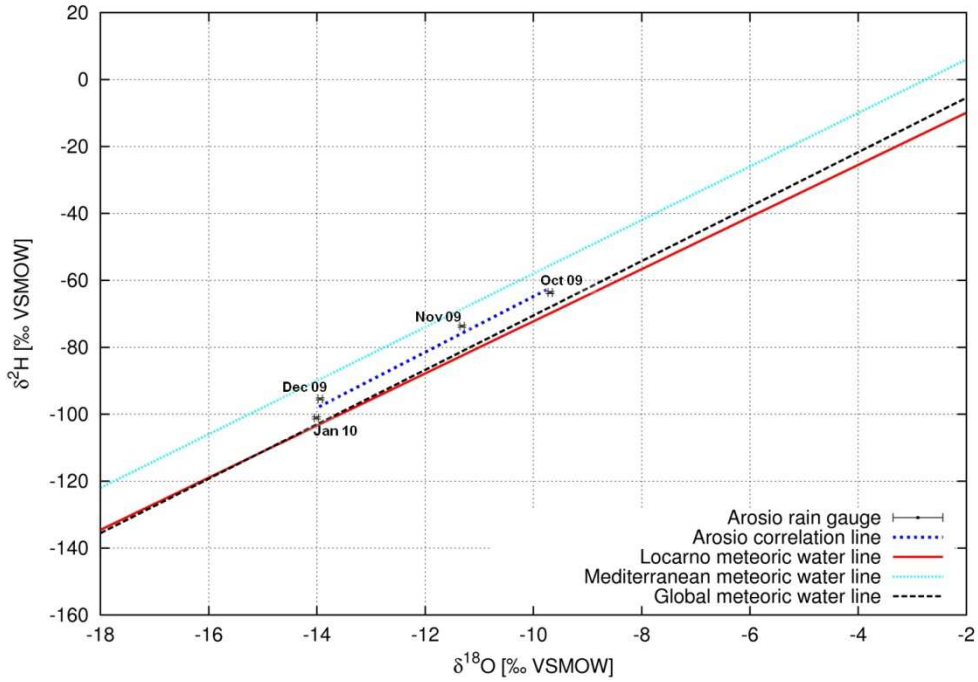

Figure 21. Stable isotopes composition in Arosio precipitations compared with existent meteoric water lines.

Preliminary results of geophysical surveys

Initially, in spring and summer 2009, we have carried out some tests about the applications of two geophysical methods above mentioned. Obtaining good results, we have performed an out-and-out geophysical survey in October 2009 in the Monte Ceneri base tunnel area, specifically designed for the detection of the possible discontinuities of the rock masses that are the preferential hydraulic pathways in this geological medium. The eight realized profiles are shown in figure 22. For each profile, we have done both the VLF electromagnetic profile and the 2D geoelectrical tomography. In particular, where possible, we have investigated with our surveys both the Val Colla line and the region close to the Isone town where the most important disturbed zones are expected. In the next months we will realize also two other geophysical campaigns designed for the water inflows prediction and hydrogeological characterization of water springs.

The detailed results of the carried out geophysical surveys will be presented in further specific publications. In this paper we restrict ourselves to few preliminary considerations about the hydrogeological use of these methods, putting the emphasis on their benefits and disadvantages. Geoelectrical surveys are more expensive with respect to VLF electromagnetic profiles. In fact, ERT method request three or four people for the displacement of electrical cables and instrument, while VLF surveys request only a single operator, because it is a lighter instrument. Nevertheless geoelectrical results, in our opinion, are more reliable. In fact a 2D resistivity model of the underground is given, inverting, with an iterative procedure, the apparent resistivity values that the instrument reads in field. For each resistivity profile, an index of the goodness of the data is given by the RMS error, that is the difference between the real apparent resistivity values recorded in field by the instrument and that calculated on the hypothetical model of underground resistivity. Therefore RMS errors lower than 10 are typical of a very good model, values between 10 and 20 are indicative of discrete model of resistivity, while RMS errors higher than 20 are typical for a bad terrain model.

Contrarily, the VLF results are less clear. In fact there is not always a direct correlation between the resulting profile and the geology. The instrument simply detects and maps electrical conductive zones. Data units are expressed in percentage of the in-phase response produced by the subsurface matrix; obviously the % of in-phase answer is linked with the degree of conductivity of rock masses or soil, but there is no direct correlation between % in-phase response and resistivity of

the underground as in the resistivity method. Finally, unlike the ERT method, VLF results do not have an index of the goodness of data; the user is the only subject that is able to check the quality of field data and look for signs of noise and interferences, directly showing the data downloaded by the instrument.

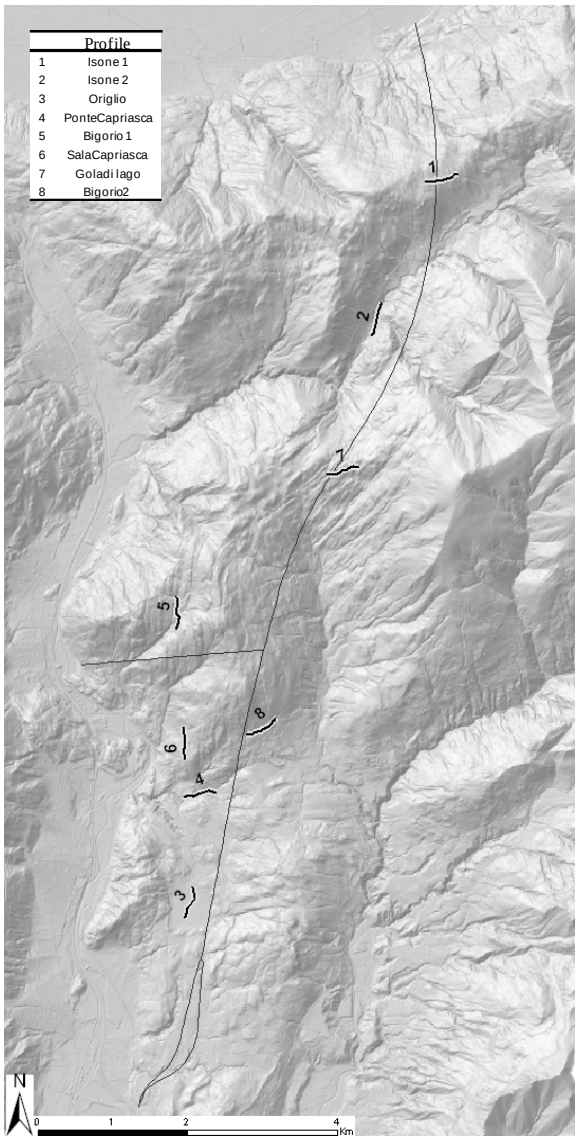

Figure 22.Geophysical profiles location

As mentioned above, resistivity surveys are, in our opinion, more reliable to perform hypotheses on the underground geology. In fact resistivity values of crystalline rock, (such as gneiss, paragneiss, orthogneiss and amphibolites) are in general higher than 1000 ohm·m; therefore the presence of fractures, or in general disturbed zones with water is clearly indicated on geoelectrical profiles by an high increase of conductivity. Obviously there are also some critical situations; for example the presence of a moraine deposit is not always predictable, because different types of sediments produce also a heterogeneity in resistivity values. In particular, sands and gravels should cause an increase in conductivity, while the presence of rock inside the deposit can increase the resistivity values. Also the occurrence of water, for example of a water table within the glacial deposit, is another factor that complicates the geophysical interpretations in this geological environment. On the contrary, in any cases a difference in electrical response is even observable, between two type of rocks, such as in the Bigorio 2 survey (fig.23) that we show here as example of the obtained geophysical results. In this case, we have measured the profile intersecting the previous cited Val Colla disturbed zone, where the geological map which shows a transition

from Giumiello to Stabiello gneisses (fig 23a). Results of ERT(fig 23b), even more disturbed with respect to other profiles (RMS error is 13.9 %, while in the other profiles is always less than 10%), show very well the central presence of a zone characterized by high conductivity values, that is probably the Val Colla fault. Moreover a slight difference is visible at the right and left of this fault; Stabiello gneiss, in particular, seems to have an higher resistivity value compared with Giumiello gneiss.

VLF profiles are instead more disturbed. Data are expressed in % in-phase. As shown by figure 23c for the Bigorio 2 profile, some interfaces between different geological matrices seem perceptible, but there is not a clear correlation between geoelectrical and electromagnetic results, and these latter seem worse than ERT results.

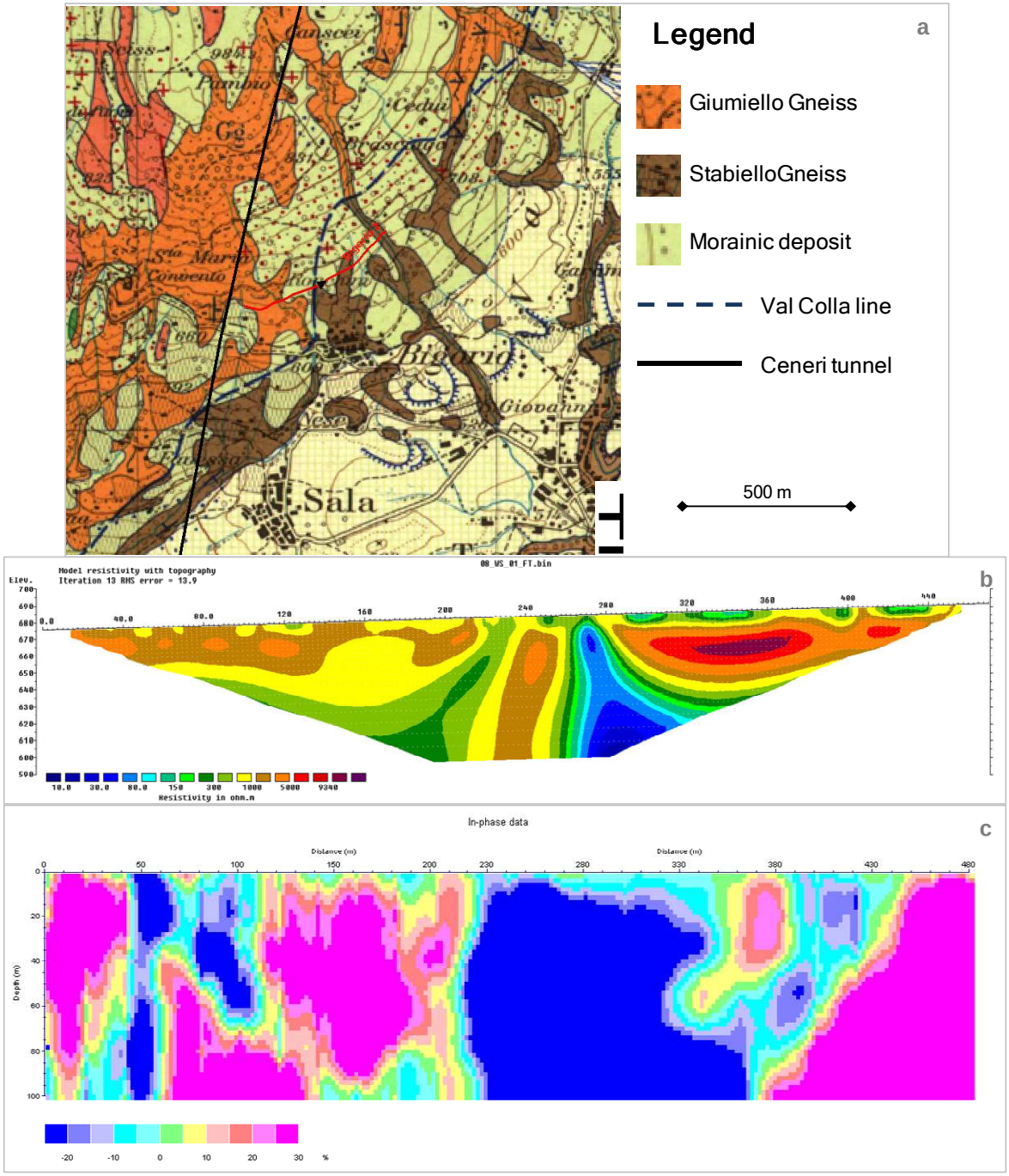

Figure 23.Profile 8: a) trace of geophysical profile on the geological map (1:25000); b)resistivity profile; c) VLF electromagnetic profile.

Considerations and perspectives

To study large scale flow systems in fractured crystalline rocks, a comprehensive study is actually ongoing in southern Switzerland (Canton Ticino), taking advantage of the availability of a large amount of geological and hydrogeological data collected in the region of Monte Ceneri, for the current construction of the railway base tunnel. A monitoring network of spring, rain and tunnel waters has been carried out for geochemical, physical, oxygen and hydrogen isotopic water composition data, and the monitoring is currently underway. Moreover, we have performed few geophysical surveys to understand the availability of VLF-EM and ERT methods to detect fractures and faults in the underground, that could be the hydraulic pathways of the rock masses.

Physical (discharge, conductivity, pH and temperature), and chemical measurements are nowadays the only available and reasonable methods, with which we can obtain indications about groundwater system before the drilling of a new infrastructure starts, and therefore to understand the possible interaction between the tunnel and the groundwater flows in the fractured rock matrix. The collection of data, with an appropriate monitoring network is always possible, not expensive and very functional.

Moreover we expect also useful information from the application of isotopic techniques. In fact, the monthly collection of stable isotopes of hydrogen and oxygen will give us indication on (i) water origin, (ii) type of recharge and (iii) residence time of water in the underground.

Actually the application of geophysical methods to detect discontinuities that constitute the preferential hydraulic pathways in the rock masses is not able to give us a physical validation of results obtained, because the tunnel will not be excavated exactly below the survey locations. Nevertheless, especially for the resistivity method, comparing them with geological existing map, geomorphological and surface geological observations, and deeper tunnel indications, we have obtained reliable results. VLF electromagnetic data are generally more disturbed and not always appear reliable, even if, considering the manageability of this technique, it could be applied as indication method, at least in a preliminary stage of a construction of a new tunnel. Besides, more detailed considerations and a specific comparison between the two methodology will be carried out near the north portal where the tunnel excavation will take place at a lower depth and using a new smaller case study where seismic methods have been already been applied, allowing a better physical validation of the geophysical hypothesis, that is otherwise impossible.

This paper present only the preliminary steps of a comprehensive study that we are carrying out in the Southern Switzerland, where few tunnels are actually excavating in metamorphic rocks. In particular, we have shown the configuring of the stable isotope monitoring network, the preliminary geochemical outcomes, and just an example of the results coming from the VLF-EM and the ERT methods; while in further publications the complete results of geochemical and isotope analysis and of geophysical surveys will be detailed presented. Nevertheless, summarizing we could make some preliminary considerations.

Firstly, the low mineralization of spring waters like as the first geochemical analysis denote that all the springs are originated by shallow groundwater systems with a relative small residence time. The underground flows seem localized in the upper part of the rock masses that is characterized by an higher fracturation, confirmed also by the results of the first campaign of geoelectrical and electromagnetic surveys. Moreover, on the basis of the preliminary geochemical outcomes from collected samples, it is possible distinguish between two slightly different hydrochemical facies; one is typical of the springs located above the Vigana northern portal, and one of the other springs belonging to Vedeggio groundwater basin.

A second observation is that the rock mass fracturation and thence the hydraulic permeability decrease with the depth as shown by drilling inspections. This evidence is also confirmed by the excavation of the Sigirino access tunnel. In fact this part of tunnel has been excavated in dry conditions and moreover they are big differences between the hydrogeological facies of the spring waters and that of the inflows in the Sigirino access tunnel, that, although not presented in this paper, are typical of deeper aquifers.

Finally, due to these remarks, we could conclude that the possible interferences between the tunnel actually in construction and the most important water springs seem weak. Instead we could expect an interference with the surface water discharge, at least close to the north portal of the tunnel and in the high Vedeggio hydrological basin, where we expect few humid faults that could be a fast interconnection between the surface and the tunnel.

More detailed informations about the underground flows will be available after completing the stable isotope monitoring currently underway (until September 2010), from the tritium analysis, perhaps combined with helium, and thanks to the further applications of the geophysical surveys.

Acknowledgements

We will like to thank Alptransit San Gottardo Inc and in particular the Dr. Geol Pierre-François Erard and Geol. François Ghirlanda for the time expend for us, the helpfulness demonstrate and the data provided; the Dr. Eng. Ludovic Baron and Prof. Klaus Holliger of Institute of Geophysics (Unil) that kindly give us the geoelectrical instruments and the theoretical supports; and the Dr. Laurent Decrouy and Prof. Torsten Vennemann of the Stable Isotopes Laboratory (Unil) for the availability of the measurement instruments.

References

ABEM (1993) Abem Wadi® VLF Instruction manual.

AESCHBACH-HERTIG W, SCHLOSSER P, STUTE M, SIMPSON HJ, LUDIN A, CLARK JF, A 3H/3He study of ground water flow in a fractured bedrock aquifer, Ground Water 36(4):661-670

ALTHAUS R, KLUMP S., ONNIS A., KIPFER R., PURTSCHERT R. STAUFFER F. KINZELBACH W. (2009) Noble gas tracers for characterisation of flow dynamics and origin of groundwater: A case study in Switzerland, Journal of Hydrology 370 (2009) 64–72

BEATRIZZOTTI G. (1996) Cantone Ticino - Valutazione della permeabilità delle rocce. 17pp

BESTENHEIDER J.C., (2006), Captazioni nella Galleria OFIBLE, a 300 m e a 1210 m dal portale della finestra di Torre, Hydogeogical study for the Torre Town (Ticino-CH)

COLOMBI A, BAUMER A (1995) Galleria di base del Monte Ceneri, Situazione idrogeologica, Rapporto idrogeologico, Tecnhnical report of the "Studio di geologia Dr. A. Baumer"

CRAIG H., (1961) Isotopic variations in meteoric waters, Science, 133, 1702-1703

EICHINGER L, MERKEL B, NEMETH G, SALVAMOSER J, STICHLER W (1984) Seepage Velocity Determinations in Unsaturated Quarternary Gravel. Recent investigations in the Zone of Aeration, Munich 303–313.

EL TANI M (2003) Circular tunnel in a semi-infinite aquifer, Tunnelling and Underground Space Technology, 18(1):49-55

GHIRLANDA F (1996) Test effettuato con il VLF WADI ABEM. Internal report of IST

GIUDICI M, MANERA M, ROMANO E (2003), The use of hydrological and geoelectrical data to fix the boundary conditions of a ground water flow model: a case study, Hydrology and Earth System Sciences, 7(3):297-303

HOLZNER CP, AESCHBACH-HERTIG W, SIMONA M, VERONESI M, IMBODEN DM, KIPFER R (2009) Exceptional mixing events in meromictic Lake Lugano (Switzerland/Italy), studied using environmental tracers 54(4):1113–1124

LOKE M.H. (2004), Tutorial:2-D and 3-D electrical imaging surveys Copyright (1966-2004)M.H.Loke 136pp.

LONGINELLI A, ANGLESIO E, FLORA O, IACUMIN P, SELMO E (2006) Isotopic composition of precipitation in northern Italy: reverse effect of anomalous climatic events. J. of Hydrology329:471-476

LUCAS LL, UNTERWEGER MP (2000) Comprehensive review and critical evaluation of the half-life of tritium. J. Res. Natl. Inst. Stand. Technol. 105:541-549

MACEDO L, LIMA AS, (2004) Groundwater exploration by VLF techniques: a case study in granitic terrains of Northwestern Portugal. In: Proceedings of the "2004 Fractured Rock Conference", National Ground Water Association, USA

MALOSZEWSKI P, MOSER H, STICHLER W, BERTLEFF B, HEDIN K, (1990) Modelling of groundwater pollution by river bank filtration using oxygen-18 data Groundwater monitoring and management IAHS Publ. no 173:153-161

MARÉCHAL J.C. & ETCHEVERRY D., (2003), The use of ^{3}H and ^{18}O tracers to characterize water inflows in Alpine tunnels, Applied Geochemistry 18:339-351

NOVEL J.P., DRAY M., FERHI A., JUSSERAND C., NICOUD G., OLIVE P., PUIG J.M. & ZUPPI G.M., (1999), Homogénéisation des signaux isotopiques, ^{18}O et ^{3}H, dans un système hydrologique de haute montagne: la Vallée d'aoste (Italie), Revue des sciences de l'eau 12(1):3-21

OFTERDINGER US, (2001), Ground water flow systems in the Rotondo Granite, Central Alps (Switzerland), Phd thesis of Natural Science, Swiss federal institute of technology (ETH) – Zurich

PAGANO A, (1996) Indagine geofisica VLF (Very Low Frequncy) preliminare allo scavo della galleria per Mergoscia, Cantone Ticino. Tecnical reports of IST

PASTORELLI S (1999), Low enthalpy geothermal resources of the western alps. Geochemical and isotopic considerations and tectonic constraints. Examples from the cantons of Ticino and Bern (Switzerland), Phd thesis, Faculty of Geoscience, University of Lausanne

PEARSON F.J., BALDERER W., LOOSLI H.H., LEHMANN B.E., MATTERA., PETERS T., SCHMASSMANN H. & GAUTSCHI A., (1991), Applied Isotope Hydrogeology – A case study in Northern Switzerland, NAGRA Technical Report 88-01

PINI O., ERARD P.F. & DEL COL A. (2007), Percer la base du Ceneri. Traces 22:16-22

SCHLOSSER P, STUTE M, DORR H, SONNTAG C, MUNNICH KO (1988) Tritium/^{3}He dating of shallow groundwater, Earth and Planetary Science Letters, 89:353-362

SCHLOSSER P, STUTE M, SONNTAG C, MUNNICH KO, (1989) Tritiogenic ^{3}He in shallow groundwater, Earth and Planetary Science Letters, v. 94, pp. 245-256

SCHURCH M., KOZEL R.; SCHOTTERER U., TRIPET JP, (2003) Observation of isotopes in the water cycle: the Swiss National Network (NISOT), Environmental geology 45(1):1-11

SHEPPARD S.MF (1986) Characterization and isotopic variations in natural waters. In: J.W. Valley, H.P. Taylor, Jr. and J.R. O'Neil, Editors, Stable Isotopes in High Temperature Geological Processes Reviews in Mineralogy, Mineralogical Society of America 16:165–183

Appendix B

B.1 Stable isotope composition of rain data

Name	East	North	z	Link
Arosio	713130	100610	860	http://www.ist.supsi.ch/index.php?page=arosioPG
Camedo	690050	112110	558	http://www.ist.supsi.ch/index.php?page=CamedoPG
Canobbio- Trevano	717900	98520	342	http://www.ist.supsi.ch/index.php?page=trevanoPG
Chiasso	722690	77090	240	http://www.ist.supsi.ch/index.php?page=chiassoPG
Gnosca	721880	122072	247	http://www.ist.supsi.ch/index.php?page=gnoscaPG
Olivone	715410	54120	909	http://www.ist.supsi.ch/index.php?page=olivonePG

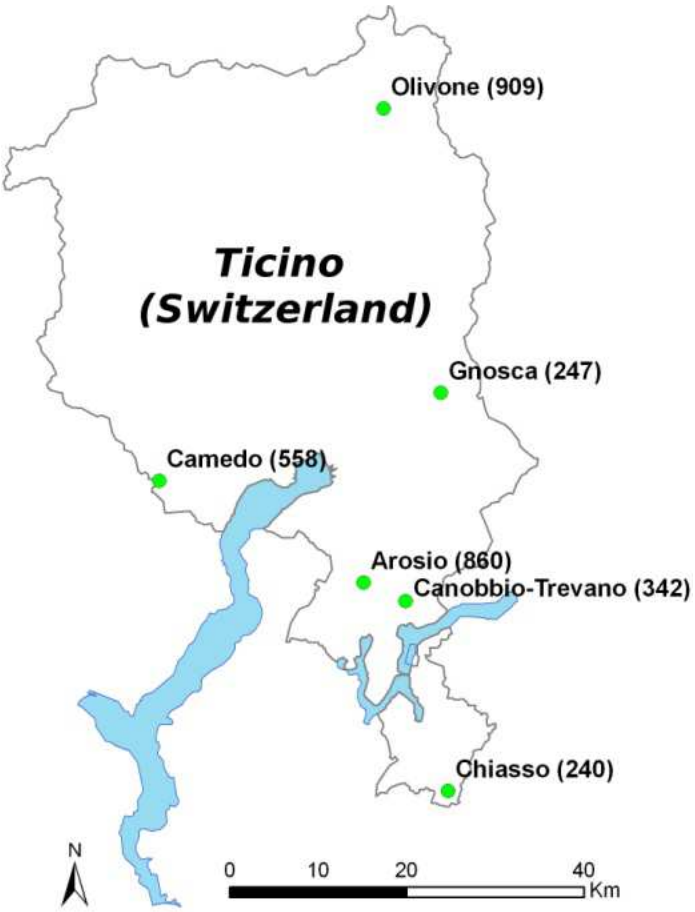

Arosio

Date	δ^2H (‰ VSMOW)			$\delta^{18}O$ (‰ VSMOW)			d-excess (‰ VSMOW)	T_{air} [°C]	Rain amount [mm]
15/03/2010	-9.15	±	0.05	-61.47	±	0.4	11.7	4	135.5
15/04/2010	-7.68	±	0.05	-45.57	±	0.4	15.8	8.9	93
15/05/2010	-8.02	±	0.05	-51.45	±	0.4	12.7	11.4	362.3
15/06/2010	-8.13	±	0.10	-51.50	±	1.0	13.6	16.7	156.6
15/07/2010	-4.51	±	0.10	-22.66	±	1.0	13.5	20.8	87
15/08/2010	-11.84	±	0.10	-82.72	±	1.0	12.0	17.4	214.2
15/09/2010	-8.30	±	0.06	-50.18	±	0.5	16.2	13.8	210.3
15/10/2010	-11.39	±	0.06	-76.16	±	0.5	15.0	8.5	189.1
15/11/2010	-12.18	±	0.06	-83.89	±	0.5	13.5	4.1	277.8
15/12/2010	-11.67	±	0.06	-84.49	±	0.5	8.9	-0.7	143.8
15/01/2011	-6.13	±	0.06	-35.16	±	0.5	13.8	0.9	49.9
15/02/2011	-14.89	±	0.06	-107.64	±	0.5	11.5	3.6	71.4

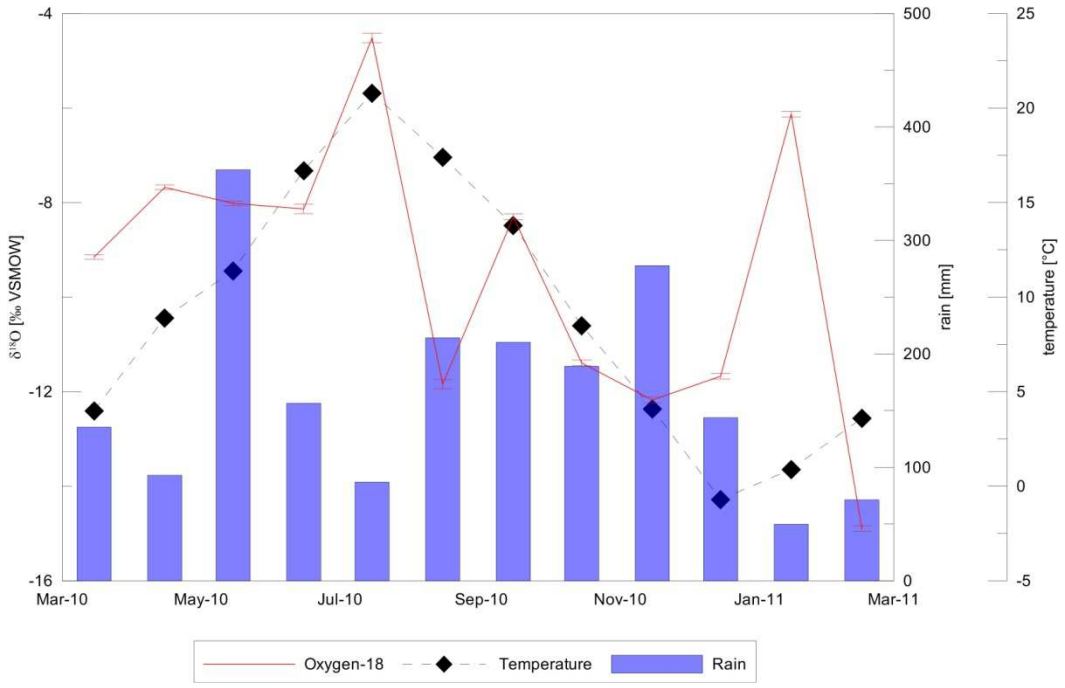

Camedo

Date	δ^2H (‰ VSMOW)			$\delta^{18}O$ (‰ VSMOW)			d-excess (‰ VSMOW)	T_{air} [°C]	Rain amount [mm]
15/03/2010	-8.73	±	0.06	-57.68	±	0.5	12.1	6.3	235.6
15/04/2010	-7.85	±	0.06	-48.52	±	0.5	14.3	11.2	110.8
15/05/2010	-9.08	±	0.05	-60.40	±	0.4	12.2	13.7	367.5
15/06/2010	-6.38	±	0.10	-39.01	±	1.0	12.0	18.7	253.7
15/07/2010	-5.16	±	0.10	-29.81	±	1.0	11.5	22.7	66.7
15/08/2010	-12.99	±	0.10	-88.60	±	1.0	15.4	19.5	223.7
15/09/2010	-6.78	±	0.06	-36.80	±	0.5	17.4	15.8	128.8
15/10/2010	-11.25	±	0.06	-75.02	±	0.5	15.0	10.3	291.2
15/11/2010	-12.67	±	0.06	-88.26	±	0.5	13.1	6	321.1
15/12/2010	-13.13	±	0.06	-97.40	±	0.5	7.6	1.1	133.1
15/01/2011	-4.49	±	0.06	-31.41	±	0.5	4.5	2.3	35.2
15/02/2011	-14.52	±	0.06	-106.93	±	0.5	9.2	5	37.7

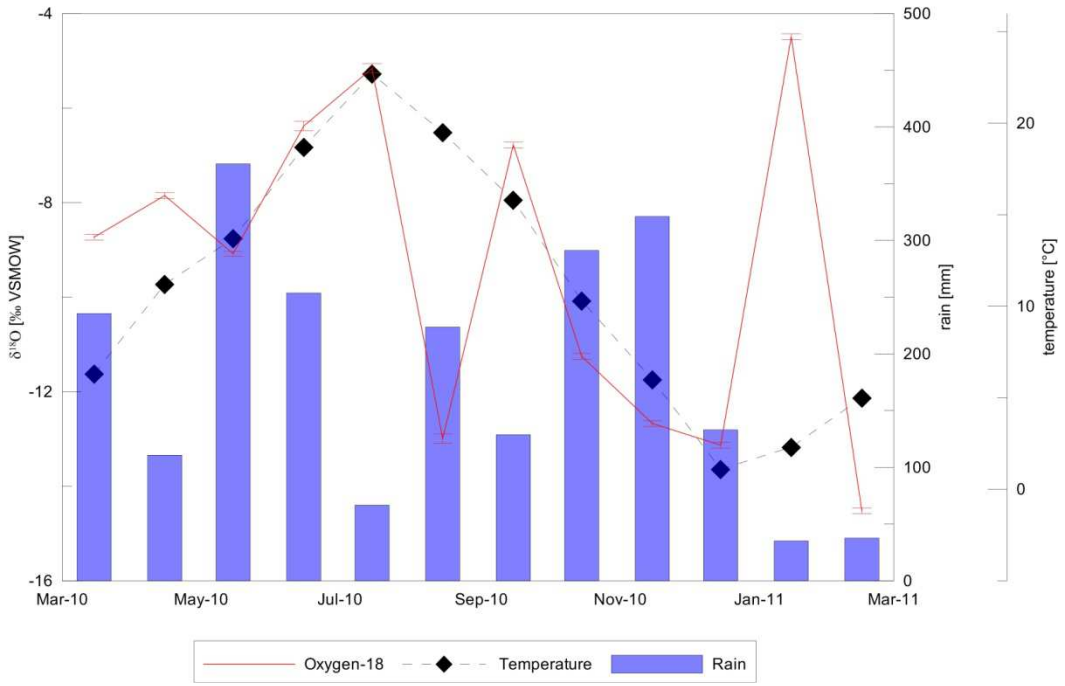

Canobbio-Trevano

Date	δ^2H (‰ VSMOW)			$\delta^{18}O$ (‰ VSMOW)			d-excess (‰ VSMOW)	T_{air} [°C]	Rain amount [mm]
15/03/2010	-8.99	±	0.06	-61.17	±	0.5	10.8	7.29	106.6
15/04/2010	-8.17	±	0.06	-49.63	±	0.5	15.7	12.15	58.8
15/05/2010	n.a.			n.a.			n.a.	15.05	342.8
15/06/2010	-6.87	±	0.10	-43.80	±	1.0	11.2	20.38	118
15/07/2010	-4.18	±	0.10	-20.75	±	1.0	12.7	24.37	121.4
15/08/2010	-10.68	±	0.10	-72.27	±	1.0	13.2	20.54	176.8
15/09/2010	-7.88	±	0.06	-49.09	±	0.5	13.9	16.48	174.8
15/10/2010	-10.41	±	0.06	-69.81	±	0.5	13.5	10.83	161.2
15/11/2010	-11.78	±	0.06	-81.02	±	0.5	13.2	6.89	232.6
15/12/2010	-11.74	±	0.06	-82.52	±	0.5	11.4	1.36	132.4
15/01/2011	-6.36	±	0.06	-38.04	±	0.5	12.8	2.12	42.6
15/02/2011	-14.95	±	0.06	-107.09	±	0.5	12.5	4.80	42

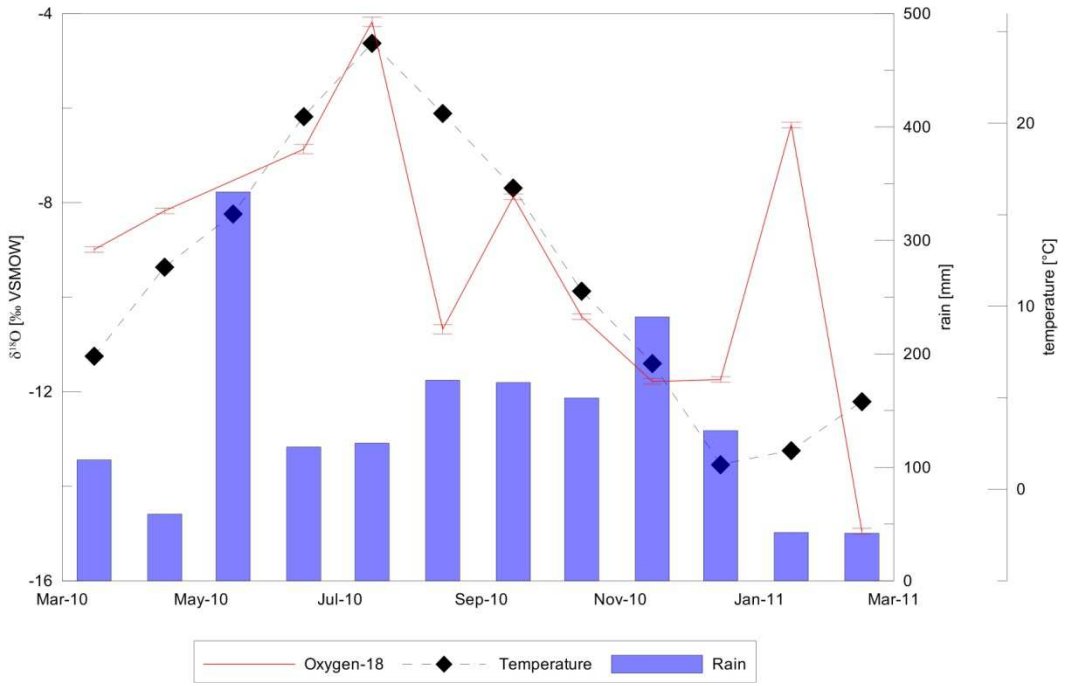

Chiasso

Date	δ^2H (‰ VSMOW)			$\delta^{18}O$ (‰ VSMOW)			d-excess (‰ VSMOW)	T_{air} [°C]	Rain amount [mm]
15/03/2010	-8.46	±	0.06	-57.46	±	0.5	10.2	7.8	78.8
15/04/2010	-6.96	±	0.06	-42.28	±	0.5	13.4	12.5	102.4
15/05/2010	-7.05	±	0.05	-43.77	±	0.4	12.6	15.8	459.1
15/06/2010	-8.42	±	0.10	-55.44	±	1.0	11.9	21.2	141.1
15/07/2010	-5.02	±	0.10	-30.60	±	1.0	9.6	25	84.2
15/08/2010	-9.55	±	0.10	-60.90	±	1.0	15.5	21.6	246.4
15/09/2010	-8.24	±	0.06	-50.87	±	0.5	15.1	17.3	243.7
15/10/2010	-10.39	±	0.06	-67.89	±	0.5	15.3	11.6	216
15/11/2010	-10.78	±	0.06	-70.67	±	0.5	15.6	7.8	374.1
15/12/2010	-11.11	±	0.06	-74.85	±	0.5	14.0	1.9	164.7
15/01/2011	-6.77	±	0.06	-41.88	±	0.5	12.3	2.3	49.9
15/02/2011	-13.38	±	0.06	-94.48	±	0.5	12.5	5.1	71.4

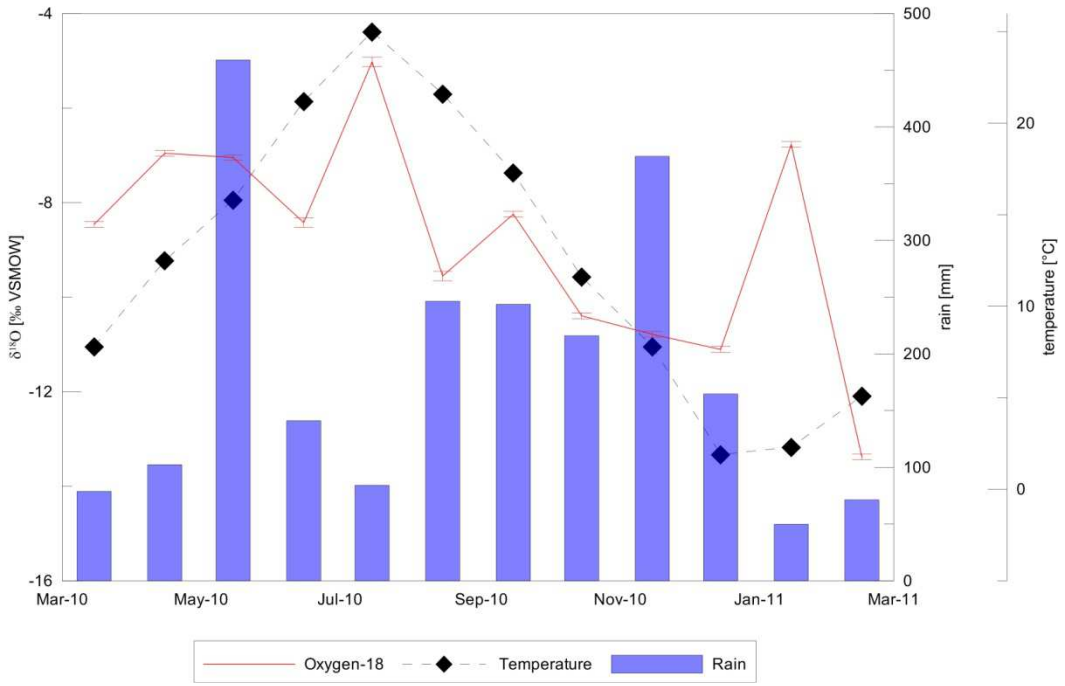

Gnosca

Date	δ^2H (‰ VSMOW)			$\delta^{18}O$ (‰ VSMOW)			d-excess (‰ VSMOW)	T_{air} [°C]	Rain amount [mm]
15/03/2010	-7.69	±	0.06	-51.40	±	0.5	10.1	7.8	90.1
15/04/2010	-8.49	±	0.06	-55.21	±	0.5	12.7	12.5	70.6
15/05/2010	-9.50	±	0.05	-65.36	±	0.4	10.6	15.2	387.9
15/06/2010	-5.93	±	0.10	-35.25	±	1.0	12.2	20.5	150.1
15/07/2010	-4.87	±	0.10	-27.30	±	1.0	11.7	24.3	47.1
15/08/2010	-11.07	±	0.10	-75.11	±	1.0	13.4	20.9	257
15/09/2010	-7.67	±	0.06	-49.33	±	0.5	12.0	16.8	100.9
15/10/2010	-12.15	±	0.06	-85.64	±	0.5	11.5	11.2	114.5
15/11/2010	-13.62	±	0.06	-96.29	±	0.5	12.7	6.5	222.4
15/12/2010	-13.47	±	0.06	-95.47	±	0.5	12.3	1	101.2
15/01/2011	-6.08	±	0.06	-37.54	±	0.5	11.1	1.8	37.9
15/02/2011	-14.91	±	0.06	-111.94	±	0.5	7.4	4.7	38.5

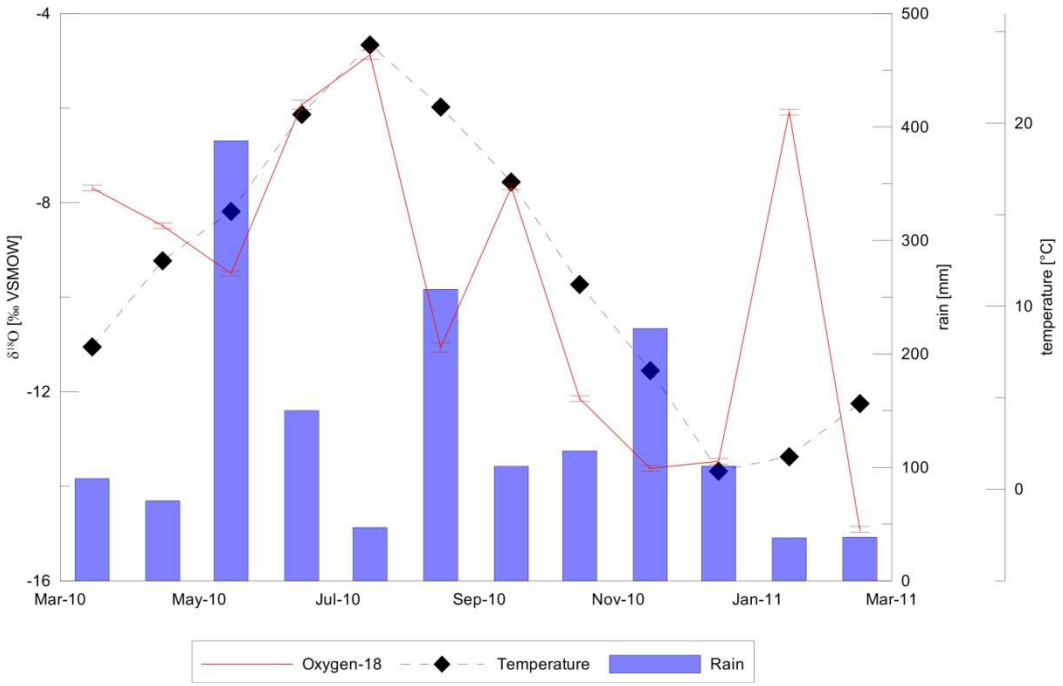

Olivone

Date	δ^2H (‰ VSMOW)			$\delta^{18}O$ (‰ VSMOW)			d-excess (‰ VSMOW)	T_{air} [°C]	Rain amount [mm]
15/03/2010	-8.92	±	0.06	-60.08	±	0.5	11.3	3.3	78.1
15/04/2010	-10.29	±	0.06	-70.69	±	0.5	11.6	8.2	64.9
15/05/2010	-11.31	±	0.05	-80.67	±	0.4	9.8	10.8	258.8
15/06/2010	-6.06	±	0.10	-36.78	±	1.0	11.7	15.8	135.7
15/07/2010	-4.69	±	0.10	-25.95	±	1.0	11.6	19.3	79.2
15/08/2010	-11.24	±	0.10	-76.99	±	1.0	13.0	16.2	216
15/09/2010	-8.13	±	0.06	-49.05	±	0.5	16.0	12.4	94.6
15/10/2010	-12.97	±	0.06	-91.44	±	0.5	12.3	7.1	125.6
15/11/2010	-14.50	±	0.06	-101.52	±	0.5	14.5	2.9	189.2
15/12/2010	-14.17	±	0.06	-104.50	±	0.5	8.9	-2.2	85.5
15/01/2011	-6.58	±	0.06	-46.36	±	0.5	6.3	-0.3	16.8
15/02/2011	-15.31	±	0.06	-112.79	±	0.5	9.7	2.7	26.1

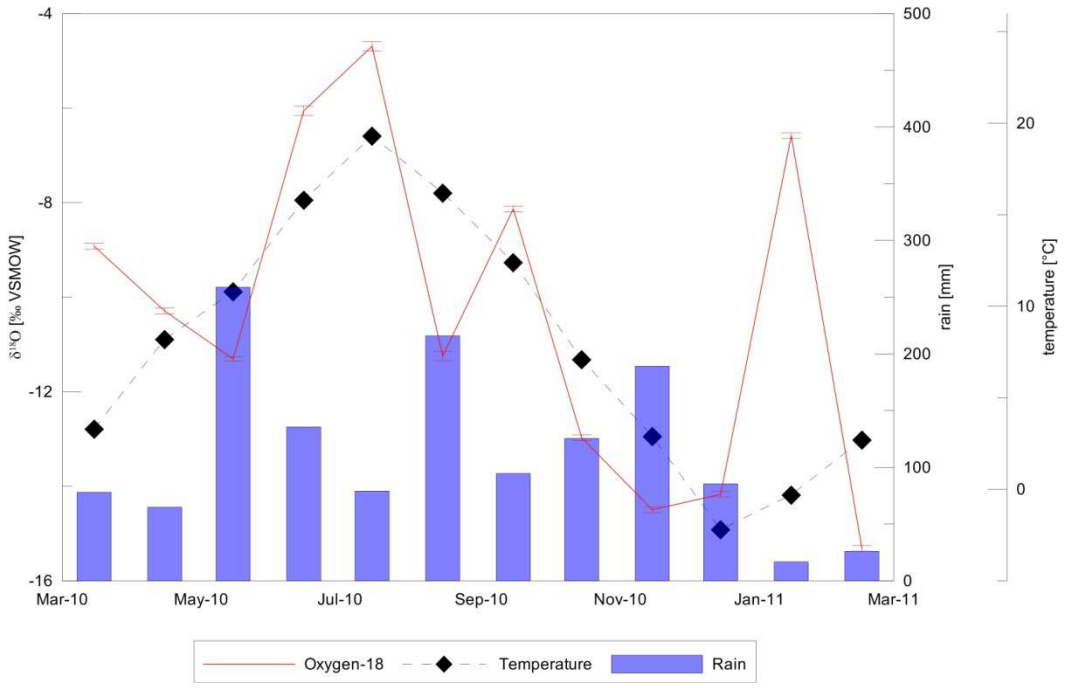

B.2 Monte Ceneri springs

Chemico-physical monitoring of Monte Ceneri springs

For the region surrounding the new infrastructure of the Ceneri base tunnel there are about 750 springs registered in the cantonal hydrogeological database. On the basis of criteria of relevance (use and discharge), distance from the tunnel and chemico-physical preliminary characterization, a number of springs have been classified at high risk and selected for monthly measurements in the tunnel geological design [Colombi & Baumer, 1995]. We have used this official classification, in order to implement our monitoring network for isotopes and geochemical measurements; in total, we are monitoring 30 springs.

Spring code	z [m a.s.l.]	Town
CNO3	462	CAMORINO
CNO2	425	CAMORINO
CNO5	425	CAMORINO
ISO-A	940	ISONE
ISO-B	935	ISONE
CANEDO	900	MEDEGLIA
MED-L	800	MEDEGLIA
MED-V	805	MEDEGLIA
SAN10	340	SANT'ANTONINO
SAN5	568	SANT'ANTONINO
SAN6	560	SANT'ANTONINO
SAN1	417	SANT'ANTONINO
SAN7	448	SANT'ANTONINO
SAN4	582	SANT'ANTONINO
SAN11	430	SANT'ANTONINO
SAN8	435	SANT'ANTONINO
SAN9	438	SANT'ANTONINO
ROB1-2-3	825	CADENAZZO
ROB5	790	CADENAZZO
ROB4	870	CADENAZZO
BIR-A	562	CAMIGNOLO
CAM4	745	CAMIGNOLO
CAM1-2-3	758	CAMIGNOLO
FONTANA	595	CAMIGNOLO
BIR-B	751	CAMIGNOLO
SAC11	780	CAPRIASCA
SAC9	810	CAPRIASCA
SAC8	790	CAPRIASCA
SAC10	810	CAPRIASCA
VEZIA	400	VEZIA

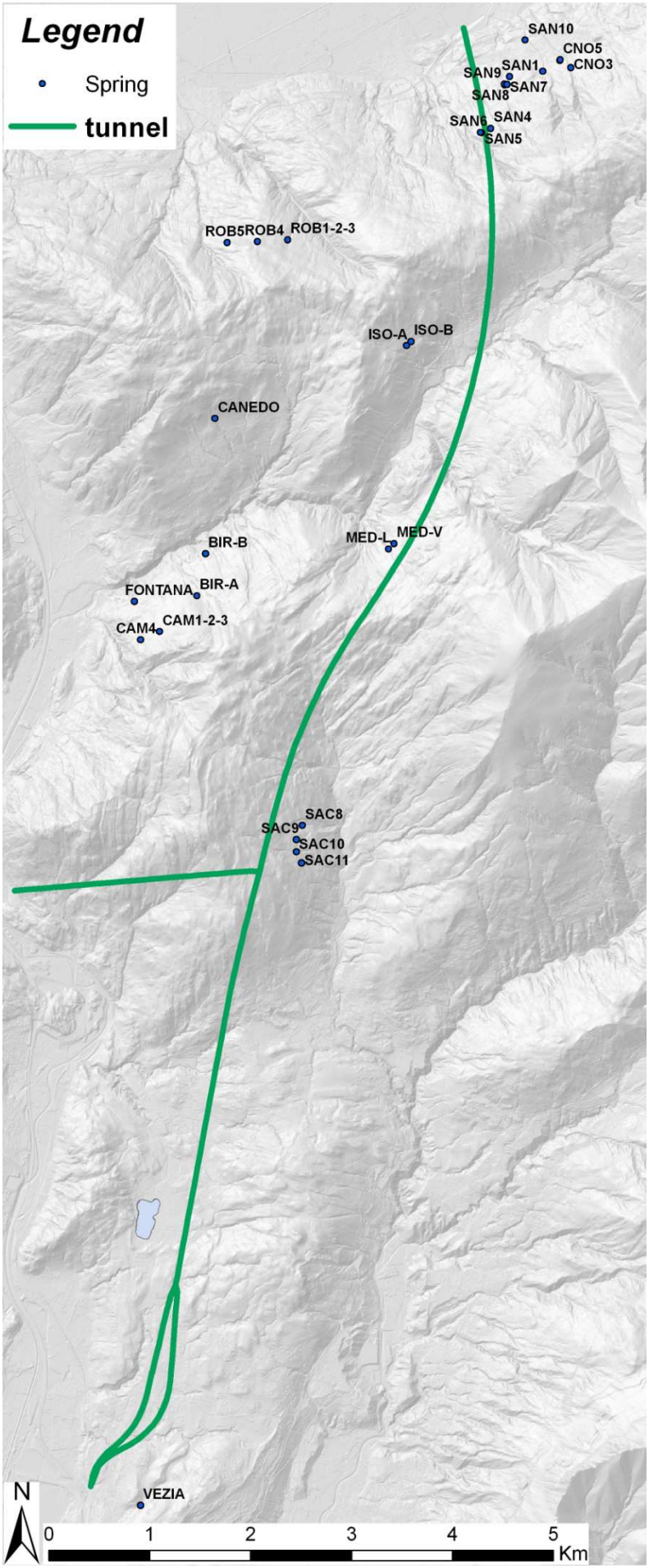
Legend
Spring
tunnel
SAN10
CNO5
CNO3
SAN1
SAN9
SAN7
SAN8
SAN6
SAN4
SAN5
ROB5
ROB4
ROB1-2-3
ISO-A
ISO-B
CANEDO
BIR-B
MED-I
MED-V
FONTANA
BIR-A
CAM4
CAM1-2-3
SAC8
SAC9
SAC10
SAC11
VEZIA
N
0
1
2
3
4
5
Km

Monitoring of physico-chemical parameters (discharge, temperature, pH, EC, $\delta^{18}O$ and $\delta^{2}H$)

Name	Date	Q [l/min]	T_{air} [°C]	T_{water} [°C]	pH	EC_{25} [µS/cm]	$\delta^{18}O$ [‰ VSMOW]			$\delta^{2}H$ [‰ VSMOW]		
BIR-A	25/6/2009			9.6	7.4	117	-8.46	±	0.04	-53.65	±	0.4
CAM4	25/6/2009			9.8	8	135	-8.69	±	0.04	-53.96	±	0.4
CAM1-2-3	25/6/2009			10.2	7.7	135	-8.47	±	0.1	-52.08	±	1
FONTANA	25/6/2009			10.1	7.6	167	-8.39	±	0.1	-52.41	±	1
BIR-B	25/6/2009			10.6	7.6	134	-7.64	±	0.1	-47.33	±	1
ISO-A	15/7/2009						-9.5	±	0.04	-60.54	±	0.4
ISO-B	15/7/2009						-9.22	±	0.04	-58.01	±	0.4
SAC11	22/7/2009	98	20	9.8	6.9	88	-8.63	±	0.1	-54.09	±	1
SAC9	22/7/2009	157	20	10.1	6.9	89	-8.66	±	0.1	-54.27	±	1
SAC8	22/7/2009	105	21	9.7	6.9	90	-8.69	±	0.04	-54.48	±	0.4
ROB1-2-3	27/7/2009						-9.14	±	0.1	-56.89	±	1
ROB5	27/7/2009						-9.04	±	0.04	-56.92	±	0.4
ROB4	27/7/2009						-9.18	±	0.1	-57.76	±	1
BIR-A	28/7/2009			9.7	7.4	105	-8.44	±	0.04	-52.97	±	0.4
CAM4	28/7/2009			9.6	8.3	147	-8.53	±	0.04	-53.37	±	0.4
CAM1-2-3	28/7/2009			9.3		127	-8.54	±	0.04	-52.74	±	0.4
FONTANA	28/7/2009			10.5	7.6	200	-8.53	±	0.05	-52.93	±	0.4
BIR-B	28/7/2009			10.1	7.8	155	-8.06	±	0.1	-49.82	±	1
VEZIA	29/7/2009	99.1		12.1		65	-8.98	±	0.04	-57.82	±	0.4
CANEDO	4/8/2009	33.3	16.7	11.7	6.4	56	-9.1	±	0.1	-57.17	±	1
MED-L	4/8/2009	600	15	8.8	7.2	77	-8.6	±	0.04	-53.54	±	0.4
MED-V	4/8/2009	93	15	9.9	7.2	78	-8.47	±	0.04	-52.47	±	0.4
ROB1-2-3	31/8/2009						-9.11	±	0.05	-56.37	±	0.4
ROB5	31/8/2009						-9.29	±	0.1	-57.72	±	1
ROB4	31/8/2009						-8.82	±	0.04	-55.31	±	0.4
ISO-A	1/9/2009	120	18.4	11	6.4	339	-9.55	±	0.1	-60.32	±	1
ISO-B	1/9/2009		17.7	10.6	6.5	77	-9.55	±	0.1	-60.5	±	1
CANEDO	1/9/2009	14.3	22.2	13.3	6.3	63	-9.7	±	0.1	-61.89	±	1
MED-L	1/9/2009		19.5	9.9	7.6	108	-9.04	±	0.04	-56.73	±	0.4
MED-V	1/9/2009	34.3	19.5	9.9	7.5	106	-8.9	±	0.04	-55.8	±	0.4
BIR-A	1/9/2009	75	18.5	9.6	7.3	78	-8.67	±	0.04	-54.18	±	0.4
CAM4	1/9/2009		18.6	9.5	7.7	125	-8.57	±	0.01	-53.54	±	0.3
CAM1-2-3	1/9/2009	120	18.5	10.2	7.8	124	-8.62	±	0.05	-53.23	±	0.4
FONTANA	1/9/2009		22.5	10.4	7.5	156	-8.46	±	0.05	-52.74	±	0.4
BIR-B	1/9/2009	92.3	18.5	10.3	7.6	146	-8.61	±	0.05	-53.59	±	0.4
SAC11	21/9/2009	52	15	9.9	6.8	79	-8.77	±	0.04	-55.07	±	0.4
SAC9	21/9/2009	109	18.5	11.1	6.7	100	-8.61	±	0.04	-54.2	±	0.4
SAC8	21/9/2009	60	18.4	10.2	6.7	104	-8.54	±	0.1	-53.52	±	1
ISO-A	24/9/2009		20	11.5		62.3	-9.6	±	0.04	-60.54	±	0.4
ISO-B	24/9/2009		20	10.3		66.5	-8.01	±	0.04	-50.65	±	0.4
CANEDO	24/9/2009	8.2	20	13.5		53.6	-9.44	±	0.1	-60.12	±	1
MED-L	24/9/2009		19.9	10.3		84.2	-9.05	±	0.05	-56.54	±	0.4
MED-V	24/9/2009	43.4	19.9	10.4		77.6	-8.68	±	0.1	-54.34	±	1
BIR-A	24/9/2009	68.2	16.1	9.5		79.7	-8.65	±	0.05	-54.07	±	0.4
CAM4	24/9/2009	138.2	16.7	9.2		116.5	-8.66	±	0.01	-53.83	±	0.3
CAM1-2-3	24/9/2009		15.2	10		115.7	-8.64	±	0.05	-53.81	±	0.4
FONTANA	24/9/2009		17	9.8		156	-8.13	±	0.04	-51.17	±	0.4
BIR-B	24/9/2009	107.1	16	10		126.6	-8.47	±	0.1	-52.31	±	1
ROB1-2-3	19/10/2009	37.2	4	7.5		50	-8.82	±	0.04	-55.63	±	0.4
ROB5	19/10/2009	22.2	3	7.8	6.6	44	-9.23	±	0.04	-56.2	±	0.4
ROB4	19/10/2009	40	3	6.8	6.9	50	-8.9	±	0.1	-55.88	±	1
CNO4	20/10/2009	9.2	7.5	10.2		79	-8.03	±	0.04	-50.49	±	0.4
CNO2	20/10/2009	45.7	7	12.7		96	-8.55	±	0.1	-53.27	±	1
CNO5	20/10/2009	14.1	7.5	10.1		79	-8.93	±	0.04	-56.18	±	0.4
SAN10	20/10/2009	150	7	11.9		117	-8.65	±	0.1	-55.03	±	1
SAN5	20/10/2009	36	6	9.9	6.6	79	-7.56	±	0.1	-47.02	±	1
SAN6	20/10/2009	10.5	6	10.4	6.4	81	-8.7	±	0.1	-54.25	±	1
SAN1	20/10/2009	32.8	7	10.9	6.7	84	-8.88	±	0.04	-56.59	±	0.4
SAN7	20/10/2009	51	7	10.2	6.5	80	-8.94	±	0.04	-57.24	±	0.4
SAN4	20/10/2009	2.4	6	9.5	6.8	77	-8.55	±	0.1	-54.09	±	1
SAN11	20/10/2009	9	7	10.2	7.2	89						
SAN8	20/10/2009	7.5	7	10.7	6.8	77	-9.18	±	0.04	-58	±	0.4
SAN9	20/10/2009	20	7	10.8	6.5	79						
SAC11	27/10/2009	88.5	6	10.1		94	-8.46	±	0.1	-53.75	±	1
SAC9	27/10/2009	70.5	6	9.9		98	-8.45	±	0.1	-53.21	±	1
SAC8	27/10/2009	80	6	9.9		92	-8.66	±	0.04	-54.44	±	0.4
SAC10	27/10/2009	80	6	9.9		92	-7.91	±	0.1	-49.25	±	1
ISO-A	29/10/2009	18	10.7	10.4		68	-9.16	±	0.04	-58.74	±	0.4

Name	Date	Q [l/min]	T_{air} [°C]	T_{water} [°C]	pH	EC_{25} [µS/cm]	$\delta^{18}O$ [‰ VSMOW]			$\delta^{2}H$ [‰ VSMOW]		
ISO-B	29/10/2009		10.7	9.8		80	-8.41	±	0.1	-53.46	±	1
CANEDO	29/10/2009	5.1	14	11.4		60	-9.43	±	0.1	-59.33	±	1
MED-L	29/10/2009		12	8.8		96	-9.03	±	0.1	-56.55	±	1
MED-V	29/10/2009	30	12	9.1		95	-8.9	±	0.05	-55.45	±	0.4
BIR-A	29/10/2009	45	11	9.1		58	-8.62	±	0.1	-53.29	±	1
CAM4	29/10/2009		12	9.5		123	-8.59	±	0.01	-53.27	±	0.3
CAM1-2-3	29/10/2009	3.2	12	9.2		120	-8.5	±	0.04	-52.73	±	0.4
FONTANA	29/10/2009		13	9.6		162	-7.61	±	0.1	-47.51	±	1
BIR-B	29/10/2009	76.9	11	9.5		133	-8.26	±	0.04	-52.3	±	0.4
VEZIA	29/10/2009	23.4	17.7	13.4		84	-8.68	±	0.04	-55.78	±	0.4
BIR-A	25/11/2009	50	6.5	8.4		73	-8.5	±	0.1	-53.25	±	1
BIR-B	25/11/2009	75	5	8.7		133	-8.19	±	0.04	-51.92	±	0.4
CAM1-2-3	25/11/2009	2.8	6.5	7.6		120	-8.56	±	0.1	-53.19	±	1
CAM4	25/11/2009	80	7	8.3		130	-8.72	±	0.05	-54.08	±	0.4
CANEDO	25/11/2009	12.5	12	11.1		69	-9.27	±	0.04	-58.93	±	0.4
CNO2	13/11/2009	105	8	12.1		98	-8.46	±	0.1	-54	±	1
CNO4	13/11/2009	12	9	10.1		80	-8.79	±	0.1	-55.2	±	1
CNO5	13/11/2009	14	9	9.9		80	-9.06	±	0.1	-56.62	±	1
FONTANA	25/11/2009		5	9		157	-7.17	±	0.04	-44.36	±	0.4
ISO-A	25/11/2009	17.6	7	9.5		42	-9.22	±	0.1	-58.85	±	1
ISO-B	25/11/2009		7	9.5		75	-8.99	±	0.1	-56.71	±	1
MED-L	25/11/2009		11	8.7		96	-9.04	±	0.1	-56.64	±	1
MED-V	25/11/2009	30	11	8.8		97	-7.75	±	0.1	-48.05	±	1
ROB1-2-3	16/11/2009	38.8	10	8.5		56	-8.94	±	0.1	-55.49	±	1
ROB4	16/11/2009	40.1	10	8.2		70	-8.96	±	0.1	-57.31	±	1
ROB5	16/11/2009	23.1	10	8.8		50	-9	±	0.1	-56	±	1
SAC10	19/11/2009	85.7	6	9.7		93	-8.62	±	0.1	-54.08	±	1
SAC11	19/11/2009	85.3	5.5	10.1		95	-8.68	±	0.04	-54.77	±	0.4
SAC8	19/11/2009	85.7	6	9.7		93	-8.75	±	0.05	-54.44	±	0.4
SAC9	19/11/2009	60	6	9.8		99	-8.64	±	0.1	-54.2	±	1
SAN1	13/11/2009	37.5	7	10.8	6.6	87	-8.91	±	0.1	-56.78	±	1
SAN10	13/11/2009	150	8	11.6		118	-8.59	±	0.1	-54.8	±	1
SAN11	13/11/2009	12	9	10.6		90	-8.75	±	0.1	-55.37	±	1
SAN4	13/11/2009	3	5	9	6.7	78	-8.69	±	0.1	-55.11	±	1
SAN5	13/11/2009	32	5	9.8	6.5	72	-8.8	±	0.04	-54.57	±	0.4
SAN6	13/11/2009	10	5	9.9	6.7	73	-8.72	±	0.05	-54.51	±	0.4
SAN7	13/11/2009	2.6	6.5	10.1	6.5	82	-8.76	±	0.04	-56.43	±	0.4
SAN8	13/11/2009	8	6.5	10.7	6.5	78	-9	±	0.1	-56.47	±	1
SAN9	13/11/2009	15	6.5	10.4	6.4	80	-9.11	±	0.1	-56.93	±	1
VEZIA	25/11/2009	23.1	12	11.7		85	-8.79	±	0.1	-55.92	±	1
CNO4	11/12/2009	32	10	10	6.5	77	-8.9	±	0.1	-56.52	±	1
CNO2	11/12/2009	166.5	10	11.1	6.7	91	-8.74	±	0.1	-58.07	±	1
CNO5	11/12/2009	28	10	10	6.5	78	-8.49	±	0.1	-55.33	±	1
SAN10	11/12/2009	285.4	10	11.6	6.6	123	-9.42	±	0.1	-58.98	±	1
SAN5	11/12/2009	60	9	9.7	6.5	78	-8.98	±	0.1	-55.69	±	1
SAN6	11/12/2009	7.5	9	9.7	6.5	77	-8.96	±	0.1	-55.96	±	1
SAN1	11/12/2009	112.5	10	10.6		88	-9.46	±	0.1	-59.57	±	1
SAN7	11/12/2009	144.3	9	10.6	6.6	90	-9.06	±	0.1	-58.72	±	1
SAN4	11/12/2009	6	9	9.1	6.7	78	-8.65	±	0.1	-55.33	±	1
SAN11	11/12/2009	30.8	10	10.4	6.6	74	-8.91	±	0.1	-56.36	±	1
SAN8	11/12/2009	28	9	9.8	6.4	84	-9.26	±	0.1	-58.56	±	1
SAN9	11/12/2009	35	9	9.8	6.2	76	-8.98	±	0.1	-57.68	±	1
SAC11	11/12/2009	49	10	9.3	6.9	93	-8.61	±	0.1	-55.78	±	1
SAC9	11/12/2009	150	10	9.6	6.9	93						
SAC8	11/12/2009	79	10	9.6	6.8	101						
SAC10	11/12/2009	74	10	9.7	7.2	97						
ROB1-2-3	14/12/2009	150	1	8	7	55	-9.13	±	0.05	-56.32	±	0.4
ROB5	14/12/2009	23.1	1	8.4	6.6	91	-9.29	±	0.05	-57.74	±	0.4
ROB4	14/12/2009	100	1	8.1	6.9	83	-9.17	±	0.05	-56.98	±	0.4
ISO-A	16/12/2009	120	0	9.5	6.7	68	-9.47	±	0.05	-60.65	±	0.4
ISO-B	16/12/2009		0	9.6	6.8	80	-9.12	±	0.1	-59.69	±	1
CANEDO	16/12/2009		2	9.7	6.7	50	-9.48	±	0.1	-59.99	±	1
MED-L	16/12/2009											
MED-V	16/12/2009											
BIR-A	16/12/2009	75	1	8.2	7.4	85	-8.73	±	0.05	-53.95	±	0.4
CAM4	16/12/2009	150	0	8.6	7.7	120	-8.87	±	0.05	-55.15	±	0.4
CAM1-2-3	16/12/2009	3.2	0				-8.67	±	0.1	-53.19	±	1
FONTANA	16/12/2009		0	9	7.4	161	-8.46	±	0.05	-52.83	±	0.4
BIR-B	16/12/2009	150	0	9.2	7.5	129	-8.5	±	0.1	-54.08	±	1
VEZIA	16/12/2009	88.2	4	10.9	7	62	-9.15	±	0.1	-57.47	±	1
CANEDO	19/1/2010	16.7	2	8.4	6.8	66.5	-9.52	±	0.1	-61.3	±	1
BIR-A	19/1/2010	200	2	9	7.5	124	-8.66	±	0.1	-54.13	±	1
CAM4	19/1/2010	150	0	8.5	7.6	147	-8.76	±	0.1	-54.63	±	1
CAM1-2-3	19/1/2010	3.4	0	6.8	7.6	124	-8.69	±	0.1	-53.76	±	1
FONTANA	19/1/2010		2	9	7.3	156	-8.21	±	0.1	-52.34	±	1

Name	Date	Q [l/min]	T_{air} [°C]	T_{water} [°C]	pH	EC_{25} [µS/cm]	$\delta^{18}O$ [‰ VSMOW]			$\delta^{2}H$ [‰ VSMOW]		
BIR-B	19/1/2010	89.8	1	7.9	7.3	108	-8.63	±	0.1	-54.13	±	1
VEZIA	19/1/2010	120	5	10.4	7.2	61	-9.18	±	0.1	-59.51	±	1
SAC11	20/1/2010	120	-2	9.8		90	-8.68	±	0.06	-54.86	±	0.5
SAC9	20/1/2010	206.5	-2	9.3	6.7	91	-9.05	±	0.1	-55.76	±	1
SAC8	20/1/2010	144.6	-2	9.5		92	-8.86	±	0.1	-56.16	±	1
SAC10	20/1/2010	94.9	-2	9.4		93	-8.8	±	0.1	-56.3	±	1
CNO4	22/1/2010	20	-1	9.5		76	-8.88	±	0.1	-57.38	±	1
CNO2	22/1/2010	120	-1	7.5		80	-9.27	±	0.1	-59.83	±	1
CNO5	22/1/2010	20	-1	9.5		77	-9.33	±	0.1	-58.43	±	1
SAN10	22/1/2010	260.6	-1	10.5		129	-9.44	±	0.1	-60.71	±	1
SAN5	22/1/2010	48.6	-2	9.4	6.6	78	-8.89	±	0.1	-56.12	±	1
SAN6	22/1/2010	10.5	-2	8.8	6.6	78	-8.83	±	0.1	-56.3	±	1
SAN1	22/1/2010	104.5	-1.5	10.4	6.5	82	-9.16	±	0.1	-58.57	±	1
SAN7	22/1/2010	92.7	-1.5	10.5	6.3	79	-8.96	±	0.1	-58.28	±	1
SAN4	22/1/2010	6	-2	8.8	6.5	76	-9.01	±	0.1	-56.52	±	1
SAN11	22/1/2010	48	-1	9.8		71	-8.83	±	0.06	-56.13	±	0.5
SAN8	22/1/2010	15	-1.5	8.7	6.8	82	-9.1	±	0.1	-58.76	±	1
SAN9	22/1/2010	30	-1.5	9.1	6.4	81	-9.16	±	0.1	-58.91	±	1
ISO-A	23/2/2010	27.3	8	9.3	6.6	57	-9.55	±	0.1	-61.53	±	1
ISO-B	23/2/2010		8	9.6	6.9	72	-9.23	±	0.1	-59.48	±	1
CANEDO	23/2/2010	13	8	7.9	6.5	53	-9.63	±	0.1	-61.7	±	1
BIR-A	23/2/2010	67.2	6.5	8.1	8	75	-8.98	±	0.1	-56	±	1
CAM4	23/2/2010											
CAM1-2-3	23/2/2010											
FONTANA	23/2/2010	100	6.5	9.3	7.9	157	-8.58	±	0.1	-55.19	±	1
BIR-B	23/2/2010	120	6.5	9.1	7.9	12	-8.55	±	0.1	-54.67	±	1
VEZIA	23/2/2010	60	10	10.6	7.1	59	-9.39	±	0.1	-61.22	±	1
CNO4	24/2/2010	15.6	8	8.7	6.8	90	-9.17	±	0.1	-59.58	±	1
CNO2	24/2/2010	129	7	6.5	6.2	90	-9.57	±	0.1	-62.33	±	1
CNO5	24/2/2010	24	7	9.5	6.5	83	-9.3	±	0.1	-58.72	±	1
SAN10	24/2/2010	228.1	7	11	6.7	136.7	-9.39	±	0.1	-61.13	±	1
SAN5	24/2/2010	40	2.5		6.5	78	-9	±	0.1	-57.03	±	1
SAN6	24/2/2010	10.5	2.5		6.5	80	-9.02	±	0.1	-57.93	±	1
SAN1	24/2/2010	84.3	3	8.8	6.7	92	-9.21	±	0.1	-59.7	±	1
SAN7	24/2/2010	64.6	2.5	9.5	6.4	81	-9.2	±	0.1	-59.54	±	1
SAN4	24/2/2010	4	2.5		6.7	79	-9.02	±	0.1	-59.02	±	1
SAN11	24/2/2010	30	8	9.5	6.5	79	-9.02	±	0.1	-57.26	±	1
SAN8	24/2/2010	12	2.5	7.5	6.7	92	-9.38	±	0.1	-60.07	±	1
SAN9	24/2/2010	30	2.5	8.2	6.7	100	-9.29	±	0.1	-59.83	±	1
SAC11	24/2/2010	69.8	9	8.8	6.9	90	-8.79	±	0.06	-54.86	±	0.5
SAC9	24/2/2010	130.4	9	8	7	118	-8.91	±	0.06	-55.52	±	0.5
SAC8	24/2/2010	109.1	9	8.7	6.7	98	-8.78	±	0.06	-55.82	±	0.5
SAC10	24/2/2010	75	9	9	7.2	99	-8.94	±	0.06	-55.77	±	0.5
CNO4	23/3/2010	21	12	9.9	6.3	77	-9.19	±	0.06	-58.37	±	0.5
CNO2	23/3/2010	126.1	14.5	7.8	6.3	87	-9.28	±	0.06	-59.71	±	0.5
CNO5	23/3/2010	22.5	12	9.7	6.5	78	-9.17	±	0.06	-58.46	±	0.5
SAN10	23/3/2010	212.8	14.5	10.7	6.4	123	-9.4	±	0.06	-60.59	±	0.5
SAN5	23/3/2010	46.2	9.1	9.7	6.5	79	-8.86	±	0.06	-55.59	±	0.5
SAN6	23/3/2010	12.2	9.1	9	6.5	78	-8.89	±	0.06	-56.09	±	0.5
SAN1	23/3/2010	77.9	11	10.7	6.5	84	-9.09	±	0.06	-57.89	±	0.5
SAN7	23/3/2010	68.9	10	10.4	6.2	81	-9.12	±	0.06	-58.7	±	0.5
SAN4	23/3/2010	6	8.9	9.3	6.6	78	-9.12	±	0.06	-58.32	±	0.5
SAN11	23/3/2010	20	12	10.1	6.7	76	-8.9	±	0.06	-56.37	±	0.5
SAN8	23/3/2010	13	10	9.3	6.4	84	-9.23	±	0.06	-59.02	±	0.5
SAN9	23/3/2010	30	10	9.4	6.3	83	-9.22	±	0.06	-59.06	±	0.5
BIR-A	24/3/2010	67.5	15	8.4	7.4	81.5	-8.73	±	0.06	-54.62	±	0.5
CAM4	24/3/2010	124.4	15	8.8	7.3	122	-8.93	±	0.06	-54.84	±	0.5
CAM1-2-3	24/3/2010	3.6	15	8.5	7.9	113	-8.63	±	0.06	-53.9	±	0.5
FONTANA	24/3/2010	111.1	15	10.3	7.6	159	-8.5	±	0.06	-53.17	±	0.5
BIR-B	24/3/2010	122.9	15	9.8	7.3	128.5	-8.58	±	0.06	-53.62	±	0.5
SAC11	24/3/2010	89.6	12	9.7	6.4	90	-8.87	±	0.06	-55.84	±	0.5
SAC9	24/3/2010	161.9	11	9.9	6.6	97	-8.84	±	0.06	-56.23	±	0.5
SAC8	24/3/2010	76.1	11	9.3	6.6	99	-8.88	±	0.06	-55.99	±	0.5
SAC10	24/3/2010	93.8	12	9.6	6.8	94	-8.95	±	0.06	-56.42	±	0.5
ISO-A	29/3/2010	113.9	9	9.6	6.4	56	-9.54	±	0.06	-61.41	±	0.5
ISO-B	29/3/2010		9	9.6	6.7	74	-9.19	±	0.06	-58.24	±	0.5
CANEDO	29/3/2010	32.3	9	9.2	6.2	48	-9.87	±	0.06	-63.51	±	0.5
MED-L	29/3/2010		10	7.8	7.1	72	-9.87	±	0.06	-63.28	±	0.5
MED-V	29/3/2010	75	10	8.1	7.1	65	-9.9	±	0.06	-64.16	±	0.5
ROB1-2-3	29/3/2010	300	8	7.4	6.7	53						
ROB5	29/3/2010	27.3	7	7.8	6.5	58						
ROB4	29/3/2010	300	7	7.3	6.5	57						
CNO4	16/4/2010	37	11.5	9.7	6.4	74	-9.44	±	0.08	-59.17	±	0.5
CNO2	16/4/2010	184	11.5	8.3	6.4	76	-9.56	±	0.06	-61.99	±	0.5
CNO5	16/4/2010	26	11.5	9.6	6.5	77	-9.39	±	0.06	-60.38	±	0.5

Name	Date	Q [l/min]	T_{air} [°C]	T_{water} [°C]	pH	EC_{25} [µS/cm]	$\delta^{18}O$ [‰ VSMOW]			$\delta^{2}H$ [‰ VSMOW]		
SAN10	16/4/2010	343	11.5	10.6	6.3	140	-9.64	±	0.06	-62.83	±	0.5
SAN5	16/4/2010	68.2	9	9.6	6.6	77	-8.91	±	0.06	-56.21	±	0.5
SAN6	16/4/2010	12	9	9	6.6	73	-9.01	±	0.06	-57.03	±	0.5
SAN1	16/4/2010	170	11	10.7	6.4	82	-9.18	±	0.08	-58.61	±	0.5
SAN7	16/4/2010	172.9	10	9.7	6.3	84	-9.46	±	0.06	-60.81	±	0.5
SAN4	16/4/2010	15	9	9.3	6.6	73	-9.16	±	0.06	-57.74	±	0.5
SAN11	16/4/2010	62	11.5	9.9	6.4	64	-9.25	±	0.06	-59.4	±	0.5
SAN8	16/4/2010	18.2	10	9.4	6.4	88	-9.7	±	0.06	-61.75	±	0.5
SAN9	16/4/2010	36	10	9.3	6.4	86	-9.65	±	0.06	-62.18	±	0.5
SAC11	16/4/2010	146.3	15	9.3	6.8	64	-9.11	±	0.05	-57.48	±	0.7
SAC9	16/4/2010	330	15	9.6	6.8	89	-9.08	±	0.06	-57.49	±	0.5
SAC8	16/4/2010	242.5	15	9.8	6.8	83	-9.22	±	0.06	-58.79	±	0.5
SAC10	16/4/2010	255	15	9.3	7	81	-9.22	±	0.06	-58.46	±	0.5
ROB1-2-3	19/4/2010	120	9	8.1	7	52.5						
ROB5	19/4/2010	23.4	8	7.6	6.5	41						
ROB4	19/4/2010	60	8	7.9	6.6	50						
ISO-A	28/4/2010	85.7	16	10.2	6.4	57	-9.86	±	0.08	-63.4	±	0.5
ISO-B	28/4/2010		16	9.7	6.8	67	-9.41	±	0.06	-59.85	±	0.5
CANEDO	28/4/2010	16.9	15	10.2	6.3	45.8	-10.13	±	0.06	-64.81	±	0.5
MED-L	28/4/2010	45.5	10	8.3	7.4	74.5	-9.57	±	0.08	-60.47	±	0.5
MED-V	28/4/2010	36.6	10	8	7.2	79.8	-9.48	±	0.06	-60.12	±	0.5
BIR-A	28/4/2010	104.3	20	8.7	7.5	80.8	-8.79	±	0.06	-55.37	±	0.5
CAM4	28/4/2010	150	20	9.2	7.8	113.5	-8.96	±	0.06	-55.86	±	0.5
CAM1-2-3	28/4/2010	15.4	20	8.8	8	95.6	-8.64	±	0.08	-53.63	±	0.5
FONTANA	28/4/2010	300	20	10.2	7.6	96.4	-8.56	±	0.08	-53.82	±	0.5
BIR-B	28/4/2010	150	20	9.6	7.7	93.6	-8.61	±	0.06	-54.01	±	0.5
BIR-A	31/5/2010	130	20	8.8	7.4	60	-9.05	±	0.05	-55.85	±	0.7
BIR-B	31/5/2010	204	20	9.7	7.9	76	-8.87	±	0.05	-54.67	±	0.7
CAM1-2-3	31/5/2010	15	16	8.5	7.9		-8.86	±	0.05	-54.55	±	0.7
CAM4	31/5/2010	180	16		7.5		-9.23	±	0.05	-57.29	±	0.7
CANEDO	31/5/2010	15.8	20	10.7	6.1	43	-10.25	±	0.05	-66.84	±	0.7
CNO2	18/5/2010	293	15	9.6	6.8	73	-9.83	±	0.05	-63.71	±	0.7
CNO4	18/5/2010	72.3	16	9.7	6.5	71	-9.66	±	0.05	-62.72	±	0.7
CNO5	18/5/2010	42	16	9.6	6.3	72	-9.68	±	0.05	-62.69	±	0.7
FONTANA	31/5/2010	540	20	9.8	7.5	92	-8.8	±	0.05	-54.61	±	0.7
ISO-A	31/5/2010	129	18	11	6.3	58	-10.17	±	0.05	-66.05	±	0.7
ISO-B	31/5/2010		18	9.9	6.7	75	-9.7	±	0.05	-61.78	±	0.7
MED-L	31/5/2010		20	8.9	7.3	83	-9.66	±	0.05	-61.4	±	0.7
MED-V	31/5/2010	37.5	20	8.5	7	74	-9.58	±	0.05	-60.33	±	0.7
ROB1-2-3	17/5/2010	335.7	10	8.1	7	50.5	-9.68	±	0.05	-61.49	±	0.7
ROB4	17/5/2010	160	10	7.5	6.5	39	-9.98	±	0.05	-64.12	±	0.7
ROB5	17/5/2010	25	10	7.4	6.5	36	-10	±	0.05	-63.97	±	0.7
SAC10	18/5/2010	255	10	9.3	7	73	-9.6	±	0.05	-61.48	±	0.7
SAC11	18/5/2010	510	16	9.6	6.9	75	-8.97	±	0.08	-56.43	±	0.5
SAC8	18/5/2010	370.4	10	9.2	6.9	68	-9.58	±	0.05	-61.8	±	0.7
SAC9	18/5/2010	530.7	10	9.8	10	80	-9.38	±	0.05	-59.97	±	0.7
SAN1	18/5/2010	463.6	10	10.7	6.3	85	-9.75	±	0.05	-62.77	±	0.7
SAN10	18/5/2010	790	15	10.6	6.3	138	-9.63	±	0.05	-62.44	±	0.7
SAN11	18/5/2010	300	16	10.4	6.6	49	-9.55	±	0.05	-61.5	±	0.7
SAN4	18/5/2010	26.5	10	9.3	6.7	70	-9.1	±	0.05	-57.72	±	0.7
SAN5	18/5/2010	141.7	10	9.9	6.4	72	-9.25	±	0.05	-57.73	±	0.7
SAN6	18/5/2010	12.8	10	9.5	6.3	71	-9.22	±	0.05	-58.18	±	0.7
SAN7	18/5/2010	255	10	9.4	6.3	90	-9.8	±	0.05	-63.12	±	0.7
SAN8	18/5/2010	21.4	10	9.9	6.5	89	-9.82	±	0.05	-63.95	±	0.7
SAN9	18/5/2010	45	10	10	6.5	86	-9.83	±	0.05	-64.29	±	0.7
VEZIA	21/5/2010	161	13.1	11.1		65	-9.97	±	0.05	-65.94	±	0.7
VEZIA	14/6/2010	50	20.1	11.7		80	-9.64	±	0.08	-63.41	±	0.5
CNO4	21/6/2010	21	22	9.9	6.6	73	-9.56	±	0.08	-61.43	±	0.5
CNO2	21/6/2010	146.3	25	11.8	6.5	78	-9.19	±	0.08	-58.64	±	0.5
CNO5	21/6/2010	25	22	10	6.4	74	-9.52	±	0.08	-61.21	±	0.5
SAN10	21/6/2010	214.3	25	11	6.3	111	-9.45	±	0.08	-61.39	±	0.5
SAN5	21/6/2010	52.2	19	9.8	6.4	79	-9.17	±	0.08	-57.39	±	0.5
SAN6	21/6/2010	11	19	10.1	6.4	77	-9.09	±	0.08	-57.5	±	0.5
SAN1	21/6/2010	156.9	21	10.7	6.3	80	-9.39	±	0.08	-60.01	±	0.5
SAN7	21/6/2010	127.5	20	9.5	6.2	77	-9.51	±	0.08	-61.08	±	0.5
SAN4	21/6/2010	5.7	20	9.9	6.5	76	-9.19	±	0.08	-58.5	±	0.5
SAN11	21/6/2010	26.1	23	10.5	7.3	68	-9.3	±	0.08	-59.27	±	0.5
SAN8	21/6/2010	13.5	20	10.8	6.3	80	-9.5	±	0.08	-61.03	±	0.5
SAN9	21/6/2010	36	20	10.7	6.3	84	-9.45	±	0.08	-61.54	±	0.5
SAC11	28/6/2010	15.9	22	10.2	6.8	85	-8.93	±	0.08	-56.58	±	0.5
SAC9	28/6/2010	170	22	10.8	6.8	88	-9.27	±	0.08	-58.66	±	0.5
SAC8	28/6/2010	300	22	9.5	6.7	86	-9.31	±	0.08	-59.28	±	0.5
SAC10	28/6/2010	82.3	22	10.1	7.1	90	-9.34	±	0.08	-59.17	±	0.5
CANEDO	30/6/2010	80	25	11.5	6.4	46	-9.93	±	0.08	-64.99	±	0.5
MED-L	30/6/2010	400	22	8.9	7.3	84	-9.52	±	0.08	-60.65	±	0.5

Name	Date	Q [l/min]	T_{air} [°C]	T_{water} [°C]	pH	EC_{25} [µS/cm]	$\delta^{18}O$ [‰ VSMOW]			$\delta^{2}H$ [‰ VSMOW]		
MED-V	30/6/2010	37.5	22	9.1	7.4	81	-9.35	±	0.08	-59.41	±	0.5
BIR-A	30/6/2010	90.6	26	9.8	7.5	72	-8.91	±	0.08	-55.83	±	0.5
CAM4	30/6/2010	121.4	26	9.4	7.5	118	-8.89	±	0.08	-56.06	±	0.5
CAM1-2-3	30/6/2010	3.1	26	10.3	7.8	121	-8.74	±	0.08	-54.4	±	0.5
FONTANA	30/6/2010	161.5	26	10.7	7.4	149	-8.76	±	0.08	-54.17	±	0.5
BIR-B	30/6/2010	133.3	26	9.8	7.5	118	-8.69	±	0.08	-54.54	±	0.5
CNO4	14/7/2010	18.7	26	10.3	6.3	76	-9.55	±	0.06	-61.06	±	0.5
CNO2	14/7/2010	162	26	12.5	6.4	78	-9.23	±	0.06	-58.95	±	0.5
CNO5	14/7/2010	18	26	10.9	6.1	76	-9.48	±	0.06	-61.59	±	0.5
SAN10	14/7/2010	62	26	12.9	6.4	87	-9.3	±	0.06	-60.82	±	0.5
SAN5	14/7/2010	39.5	26	10.2	6.4	74	-8.04	±	0.06	-54.3	±	0.5
SAN6	14/7/2010	11.9	26	10.6	6.8	70	-9.11	±	0.06	-57.2	±	0.5
SAN1	14/7/2010	55.4	26	10.8	6.9	82	-9.37	±	0.06	-59.88	±	0.5
SAN7	14/7/2010	44.3	26	10.1	6.3	85	-9.51	±	0.06	-59.94	±	0.5
SAN4	14/7/2010	3.2	26	10.9	6.5	73	-9.15	±	0.06	-58.25	±	0.5
SAN11	14/7/2010	12	26	12.4	6.5	81	-9.13	±	0.06	-59	±	0.5
SAN8	14/7/2010	9.2	26	10.8	6.4	78	-9.47	±	0.06	-60.71	±	0.5
SAN9	14/7/2010	20	26	10.8	6.4	82	-9.53	±	0.08	-60.61	±	0.5
SAC11	14/7/2010	65	25	9.7	7	86	-8.89	±	0.06	-56.45	±	0.5
SAC9	14/7/2010	103	25	10.2	6.7	90	-9.26	±	0.08	-58.91	±	0.5
SAC8	14/7/2010	80	25	9.7	6.4	87	-9.21	±	0.08	-58.31	±	0.5
SAC10	14/7/2010	63	25	10.6	6.7	91	-9.23	±	0.08	-59.35	±	0.5
ISO-A	30/7/2010	21.4	20	10.2	6.5	56	-9.98	±	0.08	-64.41	±	0.5
ISO-B	30/7/2010		20	10	6.7	75	-9.55	±	0.08	-60.93	±	0.5
CANEDO	30/7/2010	5.2	21	13.4	6.4	56	-9.84	±	0.08	-63.02	±	0.5
MED-L	30/7/2010	216	20	8.7	7.5	103	-9.37	±	0.08	-59.26	±	0.5
MED-V	30/7/2010	25.9	20	9.3	7.4	89	-9.29	±	0.08	-58.92	±	0.5
BIR-A	30/7/2010	58	22	9.1	7.5	75	-8.94	±	0.08	-55.19	±	0.5
CAM4	30/7/2010	108	22	9.3	7.7	119	-8.86	±	0.08	-55.8	±	0.5
CAM1-2-3	30/7/2010	2.8	22	9.8	7.8	121	-8.78	±	0.08	-54.55	±	0.5
FONTANA	30/7/2010	73	22	10.1	7.5	148	-8.65	±	0.08	-53.85	±	0.5
BIR-B	30/7/2010	100	22	9.8	7.6	121	-8.73	±	0.08	-54.54	±	0.5
VEZIA	30/7/2010	23.1	24	12.9	7	67	-9.59	±	0.08	-62.06	±	0.5
CNO4	24/8/2010	10.5	25	10.6	6.2	79	-9.42	±	0.06	-60.61	±	0.5
CNO2	24/8/2010	52	25	13.6	6.3	99	-9.47	±	0.06	-61.2	±	0.5
CNO5	24/8/2010	12	25	11.1	6.4	79	-9.48	±	0.06	-60.1	±	0.5
SAN10	24/8/2010	123	25	12.3	6.2	116	-9.27	±	0.06	-59.89	±	0.5
SAN5	24/8/2010	28	25	10.3	6.5	103	-9.09	±	0.06	-57.39	±	0.5
SAN6	24/8/2010	10.6	25	11	6.6	90	-9.08	±	0.06	-57.29	±	0.5
SAN1	24/8/2010	30	25	11	6.5	87	-9.27	±	0.06	-59.38	±	0.5
SAN7	24/8/2010	45	25	10	6.3	81	-9.33	±	0.06	-60	±	0.5
SAN4	24/8/2010	5.5	25	10.7	6.6	121	-9.28	±	0.06	-59.76	±	0.5
SAN11	24/8/2010	6	25	13.1	6.7	88	-9.03	±	0.06	-58.31	±	0.5
SAN8	24/8/2010	8.7	25	11.7	6.6	93	-9.35	±	0.06	-60.53	±	0.5
SAN9	24/8/2010	24	25	12.2	6.4	85	-9.37	±	0.06	-60.21	±	0.5
SAC11	24/8/2010	42	21	9.8	6.5	89						
SAC9	24/8/2010	102	21	10.1	6.4	91	-9.16	±	0.06	-58.64	±	0.5
SAC8	24/8/2010	69	21	10.2	6.6	93	-9.07	±	0.06	-57.98	±	0.5
SAC10	24/8/2010	64	21	10.3	6.7	93	-9.2	±	0.06	-59.17	±	0.5
ISO-A	26/8/2010	18.9	24	10.3	6.5	56	-9.82	±	0.06	-63.53	±	0.5
ISO-B	26/8/2010		24	9.7	6.8	76	-9.51	±	0.06	-60.41	±	0.5
CANEDO	26/8/2010	6.99	26	13.6	6.4	56	-9.81	±	0.06	-62.71	±	0.5
MED-L	26/8/2010	54	26	9.8	7.4	84	-9.49	±	0.06	-60.76	±	0.5
MED-V	26/8/2010	28.6	26	9.6	7.4	89	-9.32	±	0.06	-59.86	±	0.5
BIR-A	26/8/2010	44.1	28	9.3	7.5	78	-8.85	±	0.06	-55.22	±	0.5
CAM4	26/8/2010	90.8	28	8.9	7.5	121	-9.16	±	0.06	-59.09	±	0.5
CAM1-2-3	26/8/2010	2.7	28	10.2	7.8	122	-8.81	±	0.06	-54.44	±	0.5
FONTANA	26/8/2010	48.4	28	10.5	7.6	149	-8.62	±	0.06	-53.96	±	0.5
BIR-B	26/8/2010	83	28	10	7.6	121	-8.76	±	0.06	-54.72	±	0.5
ISO-A	21/9/2010	8.6	18	10.5	6.8	60	-9.84	±	0.06	-63.21	±	0.5
ISO-B	21/9/2010	50	18	9.8	6.8	74	-9.39	±	0.06	-60.55	±	0.5
CANEDO	21/9/2010	5.9	21	12.5	6.3	57	-9.73	±	0.06	-62.94	±	0.5
MED-L	21/9/2010	600	18	9	7.5	96	-9.25	±	0.06	-59.77	±	0.5
MED-V	21/9/2010	37.5	18	9.3	7.2	87	-9.15	±	0.06	-59.25	±	0.5
BIR-A	21/9/2010	345.6	21	9.1	7.5	78	-8.83	±	0.06	-55.59	±	0.5
CAM4	21/9/2010	94.7	21	9.1	7.7	123	-8.93	±	0.06	-55.29	±	0.5
CAM1-2-3	21/9/2010	2.5	21	9.3	7.9	122	-8.76	±	0.06	-53.39	±	0.5
FONTANA	21/9/2010	50	22	10		153	-8.72	±	0.06	-53.96	±	0.5
BIR-B	21/9/2010	85.7	24	9.8	7.7	123	-8.74	±	0.06	-55.11	±	0.5
CNO4	22/9/2010	6.1	17	10.5	6.3	80	-9.43	±	0.06	-59.76	±	0.5
CNO2	22/9/2010	56.5	17	13.1	6.2	101	-9.1	±	0.06	-58.2	±	0.5
CNO5	22/9/2010	12	17	10.9	6.1	81	-9.37	±	0.06	-59.71	±	0.5
SAN10	22/9/2010	82	17	12.4	6.1	121	-9.14	±	0.06	-59.36	±	0.5
SAN5	22/9/2010	30.6	18	9.9	6.1	79	-9.09	±	0.06	-57.4	±	0.5
SAN6	22/9/2010	10.7	18	10.4	6.4	80	-9.08	±	0.06	-57.48	±	0.5

Name	Date	Q [l/min]	T_{air} [°C]	T_{water} [°C]	pH	EC_{25} [µS/cm]	$\delta^{18}O$ [‰ VSMOW]	$\delta^{2}H$ [‰ VSMOW]
SAN1	22/9/2010	20	18	10.9	6.9	86		
SAN7	22/9/2010	27	18	9.9	6.1	80	-9.36 ± 0.06	-59.84 ± 0.5
SAN4	22/9/2010	3	18	10	6.3	78	-9.14 ± 0.06	-58.47 ± 0.5
SAN11	22/9/2010	3	17	12.8	6.8	91	-9.08 ± 0.06	-58.72 ± 0.5
SAN8	22/9/2010	7.7	18	11.1	6.5	79	-9.32 ± 0.06	-59.94 ± 0.5
SAN9	22/9/2010	15	18	10.9	6.2	80	-9.36 ± 0.06	-60.09 ± 0.5
SAC11	22/9/2010	37.5	18	9.9	6.3	90	-8.96 ± 0.06	-56.67 ± 0.5
SAC9	22/9/2010	121	12	10	6.6	90	-9.12 ± 0.06	-58.86 ± 0.5
SAC8	22/9/2010	60	12	10.2	7.6	94	-9.09 ± 0.06	-57.75 ± 0.5
SAC10	22/9/2010	63	18	10.4	7.5	92	-9.19 ± 0.06	-58.96 ± 0.5
VEZIA	22/9/2010	45.5	20	13		77	-9.45 ± 0.06	-61.84 ± 0.5
CNO4	19/10/2010	16.5	12	10	6.6	78		
CNO2	19/10/2010	52	12	12.4	6.2	99		
CNO5	19/10/2010	14.2	12	10.1	6.1	79		
SAN10	19/10/2010	111.5	12	11.8	7.4	121		
SAN5	19/10/2010	34.1	10	9.7	7.1	79		
SAN6	19/10/2010	10.1	10	10.1	6.4	81		
SAN1	19/10/2010	47	12	10.8	7	88		
SAN7	19/10/2010	54	10	9.9	6.4	83		
SAN4	19/10/2010	4	10	9.5	6.2	79		
SAN11	19/10/2010	6	12	10.4	7.4	88		
SAN8	19/10/2010	9.7	10	10.6	6.8	82		
SAN9	19/10/2010	20	10	10.5	6.5	82		
SAC11	19/10/2010	35.3	9	9.4	7.2	91		
SAC9	19/10/2010	80	9	9.5	6.8	91		
SAC8	19/10/2010	56.3	9	9.6	6.7	96		
SAC10	19/10/2010	45	9	9.7	7.1	96		
ISO-A	20/10/2010	15.2	12	10	6.9	58		
ISO-B	20/10/2010	54.9	12	9.9	6.9	74		
CANEDO	20/10/2010	13.9	12.5	10.9	6.5	52		
MED-L	20/10/2010	700	13	8.7	7.4	88		
MED-V	20/10/2010	32.3	13	9.1	7.2	86		
BIR-A	20/10/2010	44.9	7	8.8	7.6	80		
CAM4	20/10/2010	99.1	7.5	8.9	7.8	122		
CAM1-2-3	20/10/2010	2.8	7.5	8.5	7.9	121		
FONTANA	20/10/2010	31.6	7	9.3	7.6	183		
BIR-B	20/10/2010	76.1	7	9.6	7.6	124		
CNO4	17/11/2010	58.6	10	10.4	6.6	72		
CNO2	17/11/2010	200	10	11.4	6.6	89		
CNO5	17/11/2010	42	10	10.4	6.6	72		
SAN10	17/11/2010	286	7.5	11.6	6.6	133		
SAN5	17/11/2010	80	9.5	9.8	7	71		
SAN6	17/11/2010	12.7	9.5	10	6.8	70		
SAN1	17/11/2010	400	10	10.6	6.4	86		
SAN7	17/11/2010	280	10	10.5	6.4	85		
SAN4	17/11/2010	24	9.5	9.4	6.9	69		
SAN11	17/11/2010	128	10	10.6	6.6	63		
SAN8	17/11/2010	23.2	10	10	6.5	86		
SAN9	17/11/2010	60	10	10	6.6	84		
SAC11	17/11/2010	99	7.5	9.9	6.9	92		
SAC9	17/11/2010	310	7.5	9.6	6.8	91		
SAC8	17/11/2010	191	7.5	9.7	6.8	98		
SAC10	17/11/2010	269	7.5	10	6.9	92		
CNO4	14/12/2010	40	1.5	9.6	6.4	74		
CNO2	14/12/2010	116	2	8.8	6.4	77		
CNO5	14/12/2010	20	1.5	9.5	6.2	74		
SAN10	14/12/2010	273	2	11.4	6.3	124		
SAN5	14/12/2010	45	0.5	9.6	6.3	76		
SAN6	14/12/2010	12.1	0.5	9.1	6.3	75		
SAN1	14/12/2010	129	1.5	10.5	6.2	82		
SAN7	14/12/2010	108	1	10.5	6.1	80		
SAN4	14/12/2010	7.2	0.5	9	6.5	72		
SAN11	14/12/2010	41	1.5	9.3	6.7	66		
SAN8	14/12/2010	16	1	9.2	6.3	87		
SAN9	14/12/2010	40	1	8.9	6.2	84		
SAC11	14/12/2010	125	-3	9.7	6.7	87		
SAC9	14/12/2010	227	-3	9.3	6.7	87		
SAC8	14/12/2010	191	-3	8.4	6.7	84		
SAC10	14/12/2010	150	-3	9.2	6.7	89		
BIR-A	15/12/2010	130	0	8.2	7.6	73		
CAM4	15/12/2010	180	0	8.8	7.5	112		
CAM1-2-3	15/12/2010	6.8	-1	7.8	7.4	118		
FONTANA	15/12/2010	209	0.5	9	7.5	149		
BIR-B	15/12/2010	200	0	9.1	7.2	120		
CNO4	18/1/2011	30.9	2	9.5	6.6	74		

Name	Date	Q [l/min]	T_{air} [°C]	T_{water} [°C]	pH	EC_{25} [µS/cm]	$\delta^{18}O$ [‰ VSMOW]	$\delta^{2}H$ [‰ VSMOW]
CNO2	18/1/2011	167	2	7.8	6.2	76		
CNO5	18/1/2011	30	2	9.5	6.6	78		
SAN10	18/1/2011	212	2	10.8	6.4	122		
SAN5	18/1/2011	51	1	9.6	6.3	76		
SAN6	18/1/2011	11.4	1	8.7	6.3	75		
SAN1	18/1/2011	119	1	10.4	6.1	81		
SAN7	18/1/2011	95	1	10.3	6.1	80		
SAN4	18/1/2011	7.8	1	9.1	6.4	72		
SAN11	18/1/2011	42	2	9.6	6.6	67		
SAN8	18/1/2011	15.41	1	8.7	6.3	89		
SAN9	18/1/2011	40	1	8.7	6.1	86		
SAC11	18/1/2011	133	-0.5	9.7	6.5	86		
SAC9	18/1/2011	213	-0.5	9.4	6.3	89		
SAC8	18/1/2011	195	-0.5	8.7	6.4	86		
SAC10	18/1/2011	165	-0.5	9.2	6.5	86		

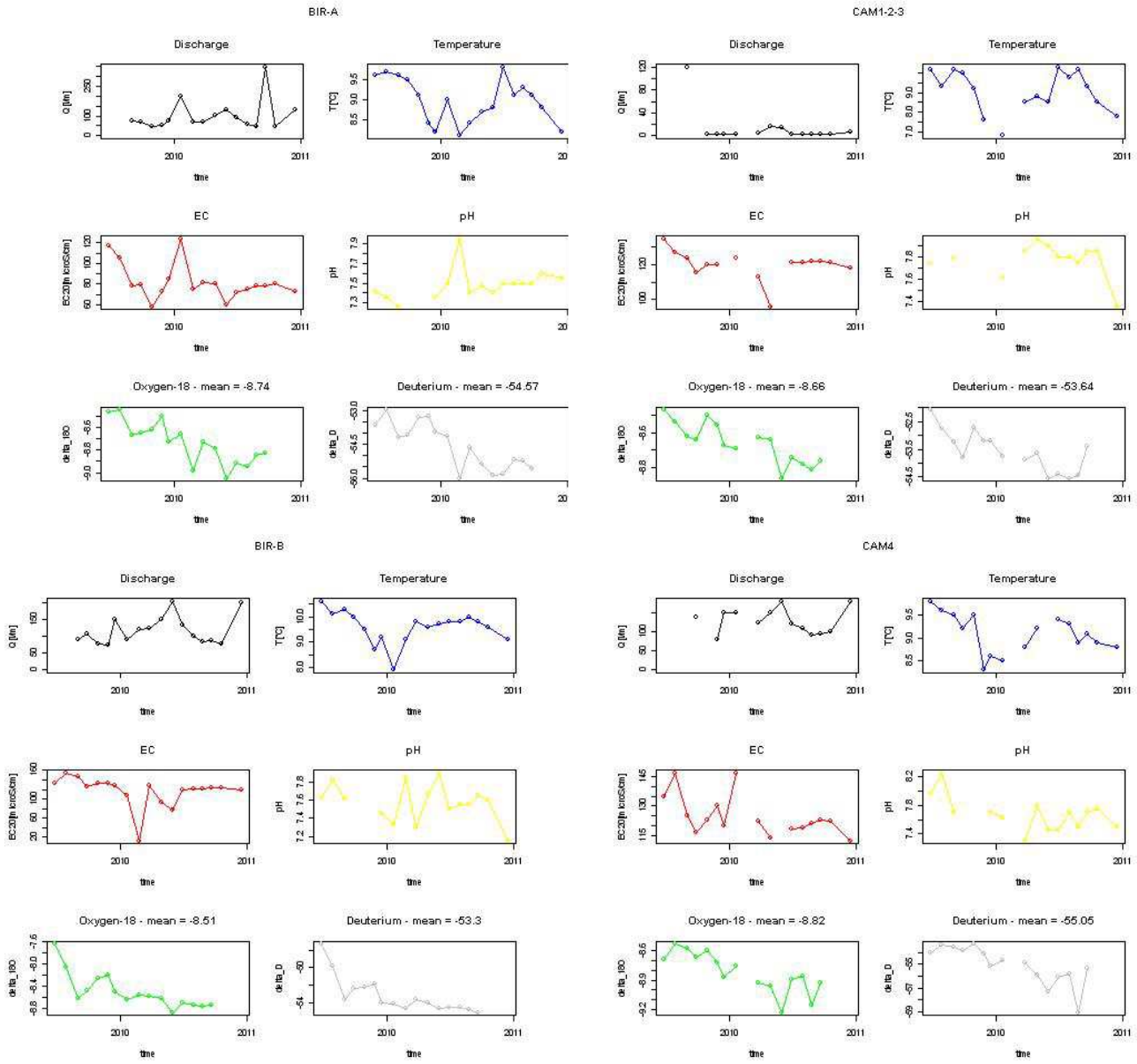

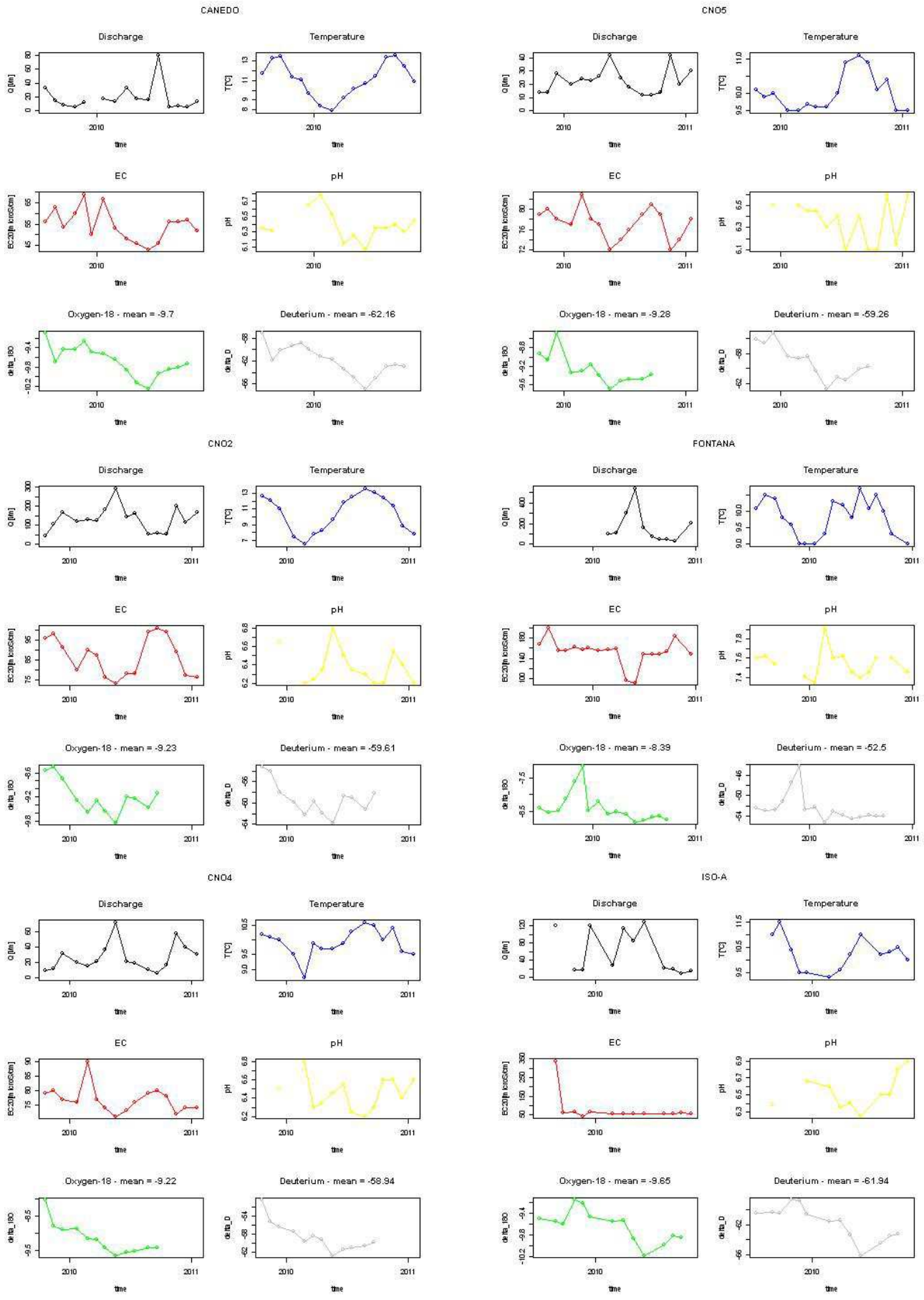
CANEDO
Discharge
Temperature
EC
pH
Oxygen-18 - mean = -9.7
Deuterium - mean = -62.16
CNO5
Discharge
Temperature
EC
pH
Oxygen-18 - mean = -9.28
Deuterium - mean = -59.26
CNO2
Discharge
Temperature
EC
pH
Oxygen-18 - mean = -9.23
Deuterium - mean = -59.61
FONTANA
Discharge
Temperature
EC
pH
Oxygen-18 - mean = -8.39
Deuterium - mean = -52.5
CNO4
Discharge
Temperature
EC
pH
Oxygen-18 - mean = -9.22
Deuterium - mean = -58.94
ISO-A
Discharge
Temperature
EC
pH
Oxygen-18 - mean = -9.65
Deuterium - mean = -61.94
time

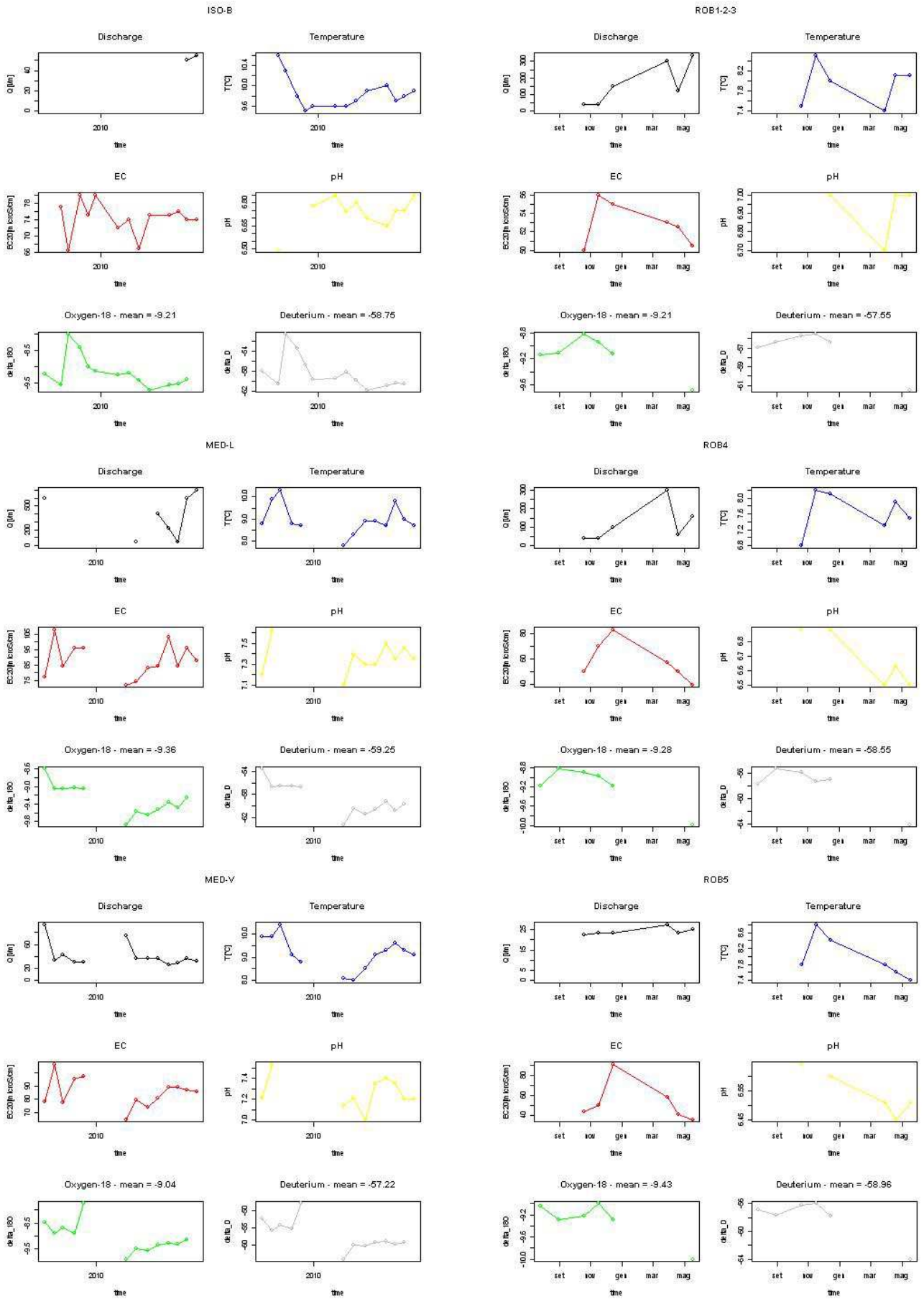
ISO-B
Discharge
Q [l/m]
Temperature
T [°C]
EC
EC 20 [µs cm-1 S/cm]
pH
Oxygen-18 - mean = -9.21
delta_18O
Deuterium - mean = -58.75
delta_D
time
ROB1-2-3
Discharge
Q [l/m]
Temperature
T [°C]
EC
EC 20 [µs cm-1 S/cm]
pH
Oxygen-18 - mean = -9.21
delta_18O
Deuterium - mean = -57.55
delta_D
set
nov
gen
mar
mag
time
MED-L
Discharge
Q [l/m]
Temperature
T [°C]
EC
EC 20 [µs cm-1 S/cm]
pH
Oxygen-18 - mean = -9.36
delta_18O
Deuterium - mean = -59.25
delta_D
2010
time
ROB4
Discharge
Q [l/m]
Temperature
T [°C]
EC
EC 20 [µs cm-1 S/cm]
pH
Oxygen-18 - mean = -9.28
delta_18O
Deuterium - mean = -58.55
delta_D
set
nov
gen
mar
mag
time
MED-V
Discharge
Q [l/m]
Temperature
T [°C]
EC
EC 20 [µs cm-1 S/cm]
pH
Oxygen-18 - mean = -9.04
delta_18O
Deuterium - mean = -57.22
delta_D
2010
time
ROB5
Discharge
Q [l/m]
Temperature
T [°C]
EC
EC 20 [µs cm-1 S/cm]
pH
Oxygen-18 - mean = -9.43
delta_18O
Deuterium - mean = -58.96
delta_D
set
nov
gen
mar
mag
time

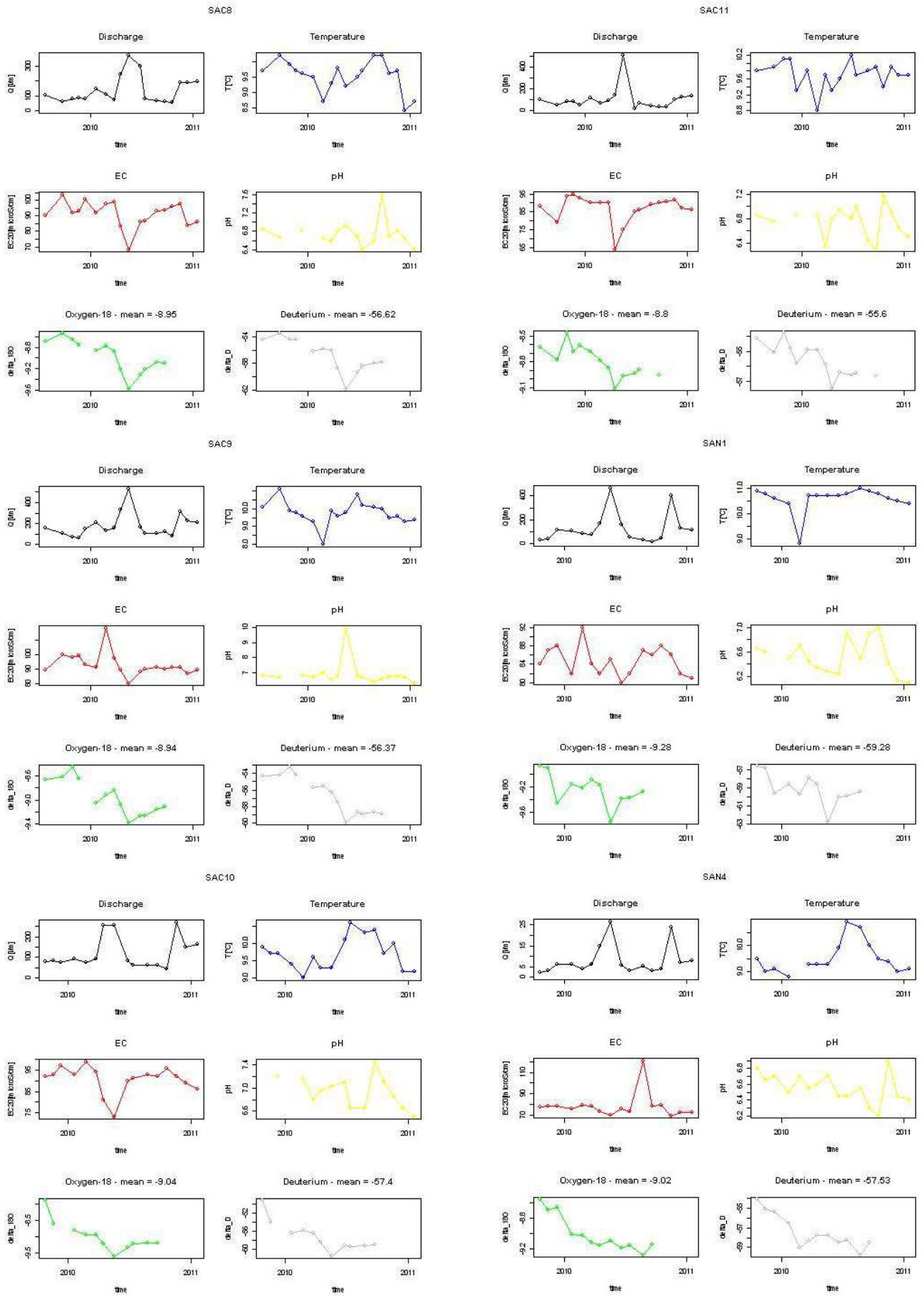
SAC8
Discharge
Q [l/m]
Temperature
T [°C]
EC
EC 20 [µs /cm]
pH
Oxygen-18 - mean = -8.95
delta_18O
Deuterium - mean = -56.62
delta_D
time
SAC11
Discharge
Q [l/m]
Temperature
T [°C]
EC
EC 20 [µs /cm]
pH
Oxygen-18 - mean = -8.8
delta_18O
Deuterium - mean = -55.6
delta_D
time
SAC9
Discharge
Q [l/m]
Temperature
T [°C]
EC
EC 20 [µs /cm]
pH
Oxygen-18 - mean = -8.94
delta_18O
Deuterium - mean = -56.37
delta_D
time
SAN1
Discharge
Q [l/m]
Temperature
T [°C]
EC
EC 20 [µs /cm]
pH
Oxygen-18 - mean = -9.28
delta_18O
Deuterium - mean = -59.28
delta_D
time
SAC10
Discharge
Q [l/m]
Temperature
T [°C]
EC
EC 20 [µs /cm]
pH
Oxygen-18 - mean = -9.04
delta_18O
Deuterium - mean = -57.4
delta_D
time
SAN4
Discharge
Q [l/m]
Temperature
T [°C]
EC
EC 20 [µs /cm]
pH
Oxygen-18 - mean = -9.02
delta_18O
Deuterium - mean = -57.53
delta_D
time

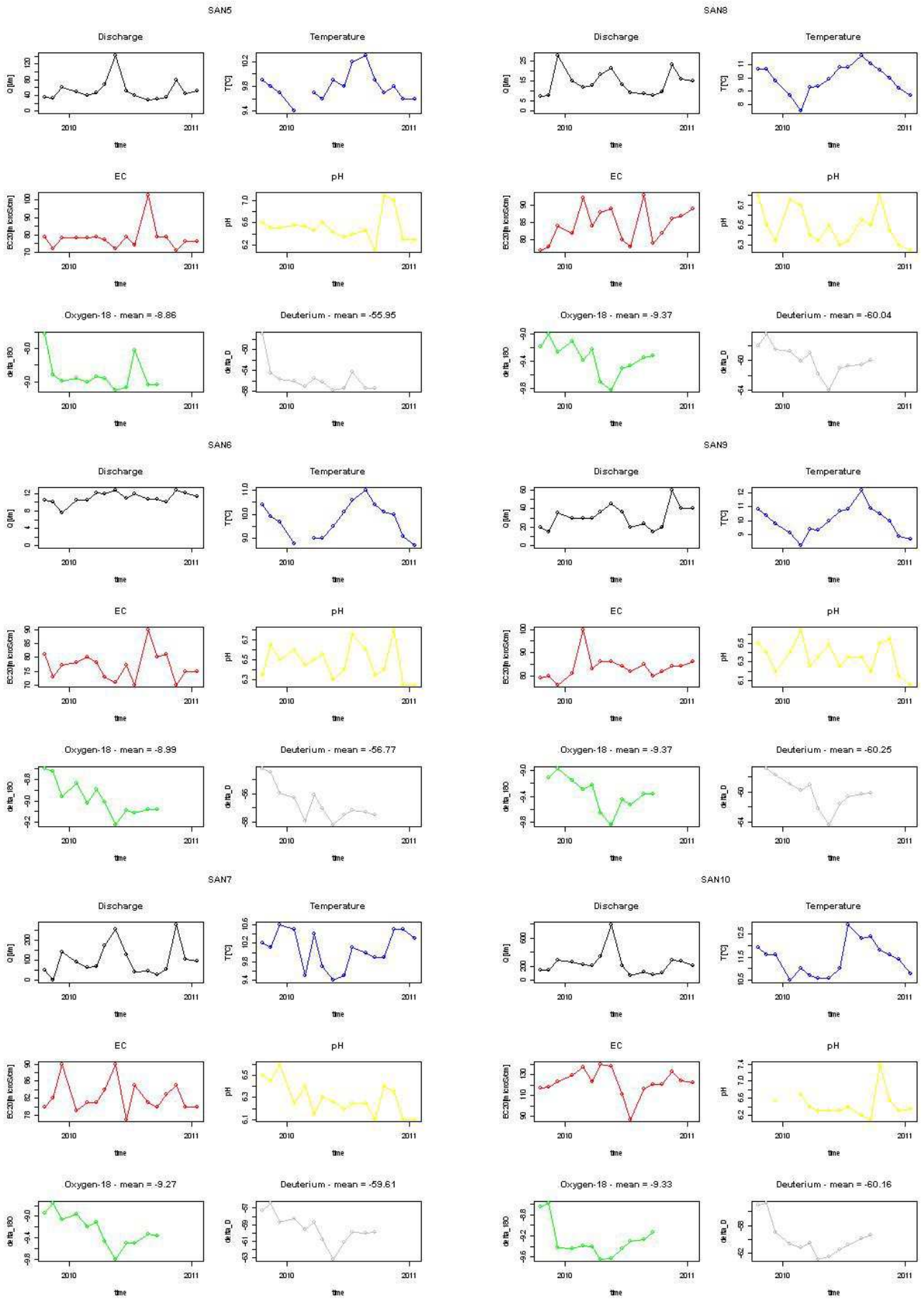
SAN5
Discharge
Q [l/m]
Temperature
T [°C]
EC
EC 20 [in µs/cm]
pH
Oxygen-18 - mean = -8.86
delta_18O
Deuterium - mean = -55.95
delta_D
time
SAN8
Discharge
Q [l/m]
Temperature
T [°C]
EC
EC 20 [in µs/cm]
pH
Oxygen-18 - mean = -9.37
delta_18O
Deuterium - mean = -60.04
delta_D
time
SAN6
Discharge
Q [l/m]
Temperature
T [°C]
EC
EC 20 [in µs/cm]
pH
Oxygen-18 - mean = -8.99
delta_18O
Deuterium - mean = -56.77
delta_D
time
SAN9
Discharge
Q [l/m]
Temperature
T [°C]
EC
EC 20 [in µs/cm]
pH
Oxygen-18 - mean = -9.37
delta_18O
Deuterium - mean = -60.25
delta_D
time
SAN7
Discharge
Q [l/m]
Temperature
T [°C]
EC
EC 20 [in µs/cm]
pH
Oxygen-18 - mean = -9.27
delta_18O
Deuterium - mean = -59.61
delta_D
time
SAN10
Discharge
Q [l/m]
Temperature
T [°C]
EC
EC 20 [in µs/cm]
pH
Oxygen-18 - mean = -9.33
delta_18O
Deuterium - mean = -60.16
delta_D
time

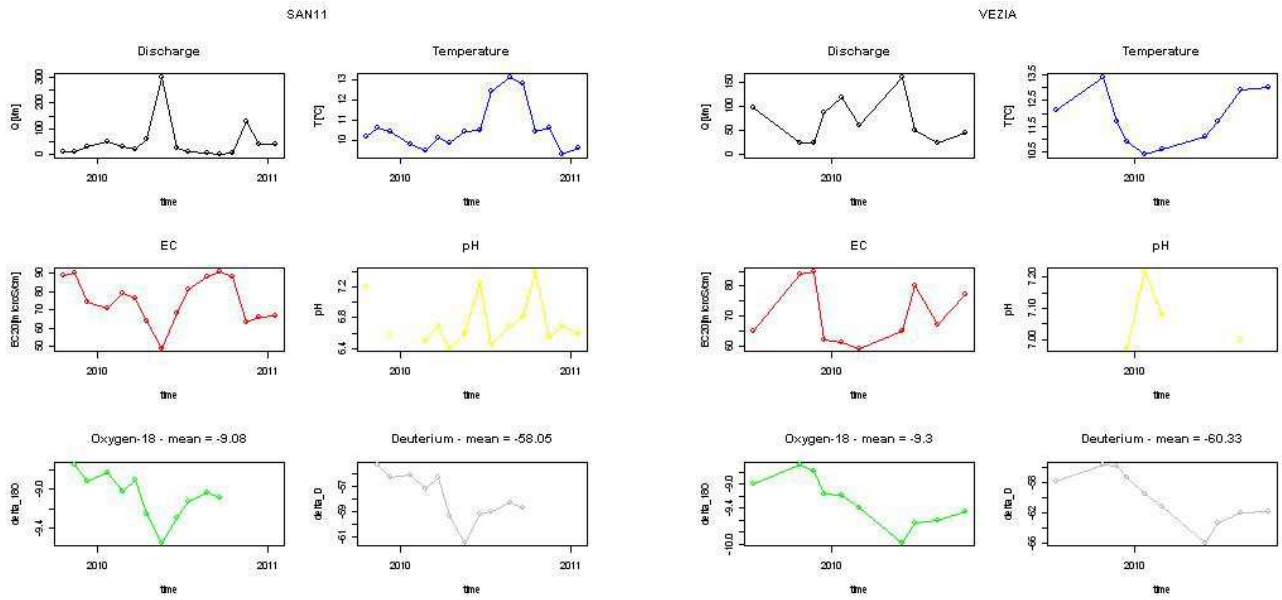

Annual mean values of δ^2H and $\delta^{18}O$

Spring	δ^2H [‰ VSMOW]	Standard deviation (monthly δ^2H)	$\delta^{18}O$ [‰ VSMOW]	Standard deviation (monthly $\delta^{18}O$)
CNO4	-58.94	3.31	-9.22	0.46
CNO2	-59.61	3.12	-9.23	0.42
CNO5	-59.26	2.27	-9.28	0.32
ISO-A	-61.94	2.19	-9.65	0.29
ISO-B	-58.75	3.20	-9.21	0.48
CANEDO	-62.16	2.58	-9.70	0.31
MED-L	-59.25	2.67	-9.36	0.34
MED-V	-57.22	4.52	-9.04	0.61
SAN10	-60.16	2.55	-9.33	0.34
SAN1	-59.28	1.71	-9.28	0.25
SAN7	-59.61	1.79	-9.27	0.30
SAN4	-57.53	1.75	-9.02	0.24
SAN11	-58.05	1.84	-9.08	0.23
SAN8	-60.04	1.94	-9.37	0.24
SAN9	-60.25	2.07	-9.37	0.25
SAN5	-55.95	2.91	-8.86	0.50
SAN6	-56.77	1.26	-8.99	0.16
ROB1-2-3	-57.55	2.40	-9.21	0.31
ROB5	-58.96	3.22	-9.43	0.39
ROB4	-58.55	3.40	-9.28	0.46
BIR-A	-54.57	1.02	-8.74	0.18
FONTANA	-52.50	2.78	-8.39	0.43
BIR-B	-53.30	2.09	-8.51	0.31
CAM4	-55.05	1.55	-8.82	0.20
CAM1-2-3	-53.64	0.72	-8.66	0.11
SAC11	-55.60	1.10	-8.80	0.18
SAC9	-56.37	2.23	-8.94	0.29
SAC8	-56.62	2.35	-8.95	0.29
SAC10	-57.40	3.25	-9.04	0.44
VEZIA	-60.33	3.36	-9.30	0.40

Major ion analysis[3]

- *November 2009*

Spring	Date [2009]	Na [mg/l]	NH_4 [mg/l]	K [mg/l]	Mg [mg/l]	Ca [mg/l]	HCO_3 [mg/l]	F [mg/l]	Cl [mg/l]	NO_2 [mg/l]	NO_3 [mg/l]	SO_4 [mg/l]	TDI [mg/l]	Ionic Balance [mg/l]
CNO 3	13-11	3.08	n.a.	0.86	2.11	7.10	1.94	0.12	0.65	n.a.	2.60	22.45	40.91	9.5
CNO 2	13-11	3.72	n.a.	1.54	2.62	16.90	18.41	0.11	1.35	n.a.	3.78	26.40	74.83	13.7
CNO 5	13-11	3.08	n.a.	0.84	2.16	14.31	39.47	0.13	0.65	n.a.	2.48	23.08	86.20	-6.4
ISO-A	25-11	2.54	n.a.	1.05	1.38	12.40	40.50	0.05	1.16	n.a.	4.60	7.13	70.80	-2.8
ISO-B	25-11	3.17	n.a.	1.14	2.50	17.85	66.97	0.06	1.34	n.a.	5.04	6.78	104.85	-3.7
CANEDO	25-11	2.47	n.a.	1.22	1.26	7.51	28.98	0.06	0.68	n.a.	3.27	5.54	50.99	-3.7
MED-L	25-11	1.58	n.a.	0.48	2.34	12.55	49.27	0.05	0.67	n.a.	5.68	6.11	78.73	-7.5
MED-V	25-11	1.63	n.a.	0.82	4.25	14.05	53.09	0.16	0.75	n.a.	5.71	8.01	88.47	-0.6
SAN 10	13-11	5.79	n.a.	2.48	2.69	9.76	15.27	0.13	7.27	n.a.	7.04	20.40	70.83	1.2
SAN 5	13-11	3.82	n.a.	0.92	2.00	7.11	31.51	0.10	2.34	n.a.	5.63	13.47	66.91	-14.9
SAN 6	13-11	3.87	n.a.	0.93	2.11	15.97	62.29	0.12	2.34	n.a.	5.20	13.72	106.56	-11.4
SAN 1	13-11	3.53	n.a.	1.60	2.38	13.28	25.71	0.12	1.98	n.a.	5.53	20.02	74.14	3.2
SAN 7	13-11	4.29	n.a.	0.95	1.87	6.79	73.21	0.11	4.90	n.a.	3.75	16.06	111.94	-42.3
SAN 4	13-11	3.45	n.a.	0.77	2.11	15.52	49.32	0.10	2.81	n.a.	5.18	12.39	91.64	-4.9
SAN 11	13-11	3.94	n.a.	0.87	2.66	8.07	21.55	0.15	0.79	n.a.	0.65	24.66	63.34	-5.3
SAN 8	13-11	4.07	n.a.	0.81	1.81	11.16	11.49	0.11	4.25	n.a.	3.56	16.08	53.34	12.3
SAN 9	13-11	4.08	n.a.	0.91	1.91	16.28	30.87	0.11	4.13	n.a.	3.71	15.90	77.90	6.9
ROB 1-2-3	16-11	2.32	n.a.	0.89	1.06	11.69	36.46	0.07	0.51	n.a.	9.56	9.89	72.45	-10.2
ROB 5	16-11	2.08	n.a.	0.75	1.02	8.50	24.84	0.06	0.55	n.a.	6.20	4.24	48.24	0.4
ROB 4	16-11	2.23	n.a.	0.71	1.01	12.21	35.98	0.06	0.41	n.a.	6.21	6.12	64.94	-1.4
BIR-A	25-11	2.31	n.a.	1.02	1.47	10.36	49.91	0.13	0.67	n.a.	3.38	5.78	75.03	-14.2
CAM 4	25-11	2.28	n.a.	0.66	1.52	21.35	47.28	0.27	0.61	n.a.	5.04	11.93	90.94	7.0
CAM 1-2-3	25-11	2.17	n.a.	0.88	1.42	19.86	57.12	0.28	0.57	n.a.	5.39	11.58	99.26	-2.8
FONTANA	25-11	2.94	n.a.	1.98	2.86	24.52	55.51	0.19	0.84	n.a.	1.59	24.85	115.28	4.9
BIR-B	25-11	3.05	n.a.	1.90	2.84	19.93	59.76	0.12	0.84	n.a.	2.75	12.04	103.22	3.9
SAC 11	19-11	3.35	n.a.	1.39	2.11	10.05	33.23	0.08	0.86	n.a.	2.85	18.97	72.89	-8.4
SAC 9	19-11	2.91	n.a.	1.47	2.05	10.56	32.64	0.07	1.09	n.a.	4.03	16.73	71.55	-6.6
SAC 8	19-11	3.02	n.a.	1.58	2.18	20.80	44.59	0.07	0.85	n.a.	2.83	20.26	96.17	6.3
SAC 10	19-11	2.46	n.a.	1.54	2.16	15.87	50.66	0.06	0.74	n.a.	4.06	14.89	92.44	-4.8
VEZIA	25-11	3.82	0.73	0.81	2.35	14.81	47.28	0.25	2.10	n.a.	3.52	9.23	84.90	2.8

[3] n.a. < 0.01 (Lithium (Li^+), phosphates (PO_4^-) and Bromium (Br^-) are analyzed but not founded in a representative quantity (all samples n.a.).

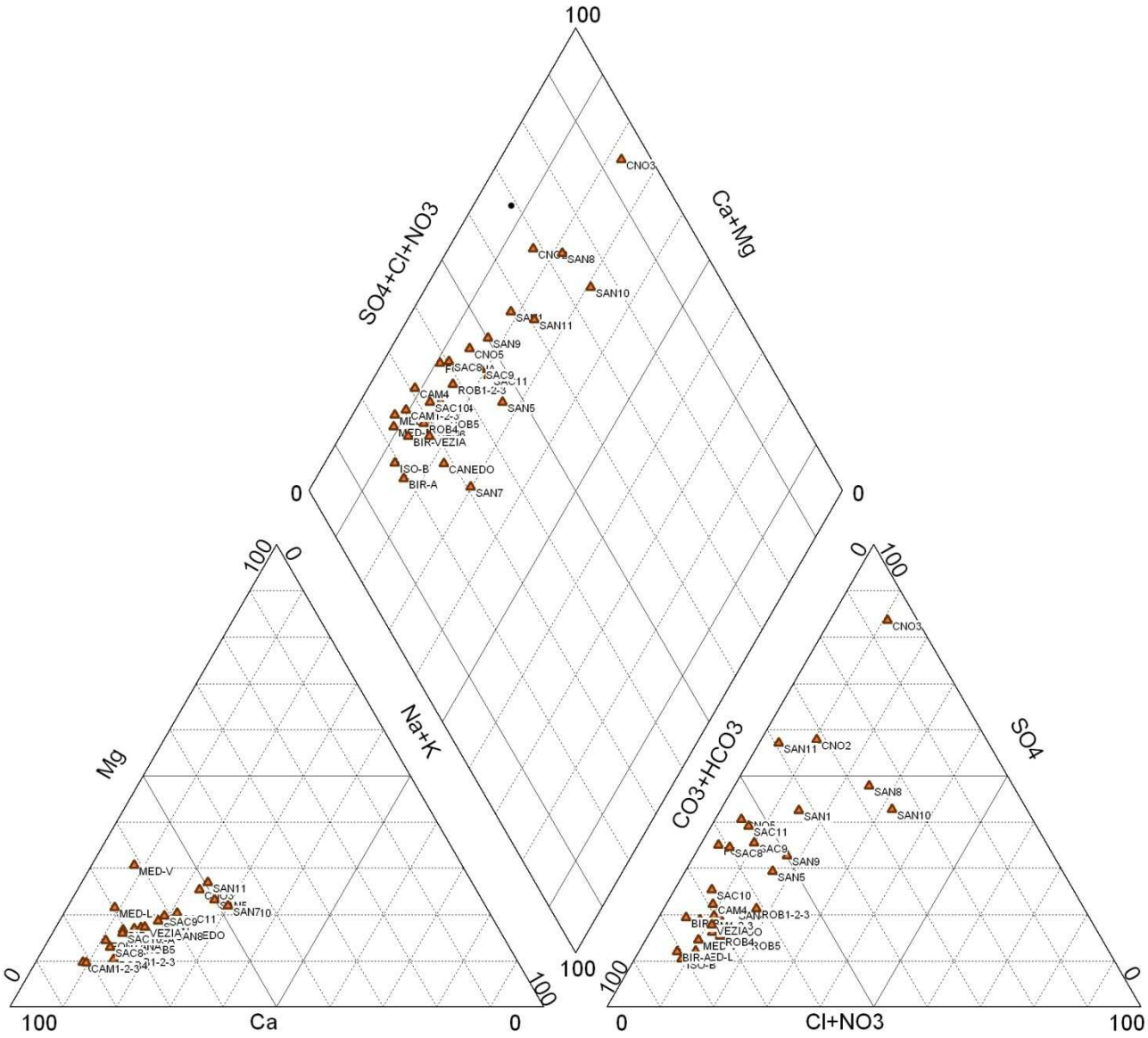
SO4+Cl+NO3
Ca+Mg
Na+K
CO3+HCO3
SO4
Cl+NO3
Mg
Ca
100
0
CNO3
CNO4
SAN8
SAN10
SAN1
SAN11
SAN9
CNO5
SAC9
SAC11
CAM4
ROB1-2-3
SAC10
SAN5
BIR-VEZIA
ISO-B
CANEDO
BIR-A
SAN7
CNO2
SAN11
SAN8
SAN10
SAN1
SAC11
SAC9
SAN9
SAN5
SAC10
CAM4
ROB1-2-3
ROB4
ROB5
BIR-AED-L
MED-V
MED-L
SAN11
SAN710
CAM1-2-3

- *May 2010*

Spring	Date [2010]	Na [mg/l]	NH_4 [mg/l]	K [mg/l]	Mg [mg/l]	Ca [mg/l]	HCO_3 [mg/l]	F [mg/l]	Cl [mg/l]	NO_2 [mg/l]	NO_3 [mg/l]	SO_4 [mg/l]	TDI [mg/l]	Ionic Balance [mg/l]
CNO3	18-5	3.54	n.a.	0.84	2.21	6.23	17.47	0.06	0.25	n.a.	2.92	n.a.	61.19	-5.1
CNO2	18-5	4.10	n.a.	1.16	1.89	6.37	14.41	0.07	2.82	n.a.	2.36	n.a.	56.06	3.9
CNO5	18-5	3.45	n.a.	0.83	2.25	6.55	12.59	0.06	0.26	n.a.	2.71	n.a.	53.68	0.7
ISO-A	31-5	2.96	n.a.	1.41	1.46	5.89	15.60	0.03	0.81	n.a.	5.39	n.a.	44.67	30.7
ISO-B	31-5	3.87	0.46	2.19	2.43	7.61	22.24	0.03	1.54	0.05	5.11	n.a.	64.56	36.5
CANEDO	31-5	2.14	n.a.	0.56	0.81	5.20	7.95	0.02	0.19	n.a.	5.92	n.a.	27.80	18.4
MED-L	31-5	1.88	n.a.	0.50	2.53	11.63	33.54	0.03	0.22	n.a.	4.30	n.a.	87.97	10.0
MED-V	31-5	2.04	n.a.	0.67	3.71	7.80	23.83	0.05	0.23	n.a.	3.83	n.a.	65.87	37.9
SAN10	18-5	6.83	0.03	2.67	3.46	11.78	18.96	0.06	14.03	n.a.	8.94	n.a.	89.16	3.5
SAN5	18-5	4.17	0.13	0.98	1.95	6.78	21.48	0.06	1.30	n.a.	4.16	n.a.	62.86	1.4
SAN6	18-5	4.07	n.a.	0.82	1.92	6.68	13.57	0.06	1.24	n.a.	4.25	n.a.	51.51	9.6
SAN1	18-5	3.92	0.12	1.71	2.57	7.71	5.75	0.06	1.59	n.a.	10.71	n.a.	51.87	12.6
SAN7	18-5	6.43	0.14	1.29	2.03	7.21	9.94	0.06	8.25	0.20	3.61	n.a.	56.10	7.1
SAN4	18-5	3.90	n.a.	0.72	1.92	6.50	16.42	0.04	1.40	n.a.	4.29	n.a.	57.37	3.4
SAN11	18-5	3.26	n.a.	0.49	1.47	3.91	6.71	0.05	0.27	n.a.	2.08	n.a.	33.30	9.8
SAN8	18-5	5.89	n.a.	0.91	1.99	7.63	8.19	0.06	8.66	0.22	3.46	n.a.	53.37	8.6
SAN9	18-5	5.41	n.a.	0.98	2.03	7.63	8.07	0.06	7.03	0.04	3.08	n.a.	51.00	11.4
ROB1-2-3	17-5	2.61	n.a.	0.71	0.98	4.74	8.85	0.04	0.17	n.a.	5.80	n.a.	36.48	10.0
ROB5	17-5	1.85	0.04	0.48	0.82	3.36	3.65	0.03	0.09	n.a.	4.75	n.a.	21.09	23.2
ROB4	17-5	2.22	n.a.	0.54	0.81	3.77	6.79	0.02	0.13	n.a.	3.79	n.a.	25.34	17.4
BIR-A	31-5	2.78	n.a.	1.00	1.40	9.09	25.18	0.07	0.14	n.a.	1.23	n.a.	66.04	29.7
CAM4	31-5	2.88	n.a.	0.79	1.47	17.79	38.79	0.10	0.21	n.a.	3.01	n.a.	106.81	15.3
CAM1-2-3	31-5	2.84	n.a.	0.88	1.55	19.70	38.71	0.14	0.14	n.a.	3.16	n.a.	112.88	17.0
FONTANA	31-5	3.31	n.a.	1.92	2.87	20.94	42.72	0.11	0.29	n.a.	1.51	n.a.	132.25	11.7
BIR-B	31-5	3.49	n.a.	1.86	2.89	16.69	43.16	0.06	0.30	n.a.	1.42	n.a.	119.92	13.2
SAC11	18-5	3.65	n.a.	1.31	1.85	8.13	16.86	0.04	0.45	n.a.	2.38	n.a.	61.58	29.6
SAC9	18-5	3.09	n.a.	1.32	1.93	9.58	19.92	0.03	0.33	n.a.	3.26	n.a.	66.75	10.8
SAC8	18-5	2.69	0.04	1.25	1.59	7.91	17.59	0.06	0.23	n.a.	2.02	n.a.	58.57	7.4
SAC10	18-5	2.70	n.a.	1.54	1.71	9.07	23.76	0.03	0.39	n.a.	2.83	n.a.	71.33	5.7
VEZIA	21-5	3.51	n.a.	0.54	1.47	5.16	10.09	0.13	0.90	n.a.	2.13	n.a.	38.49	18.7

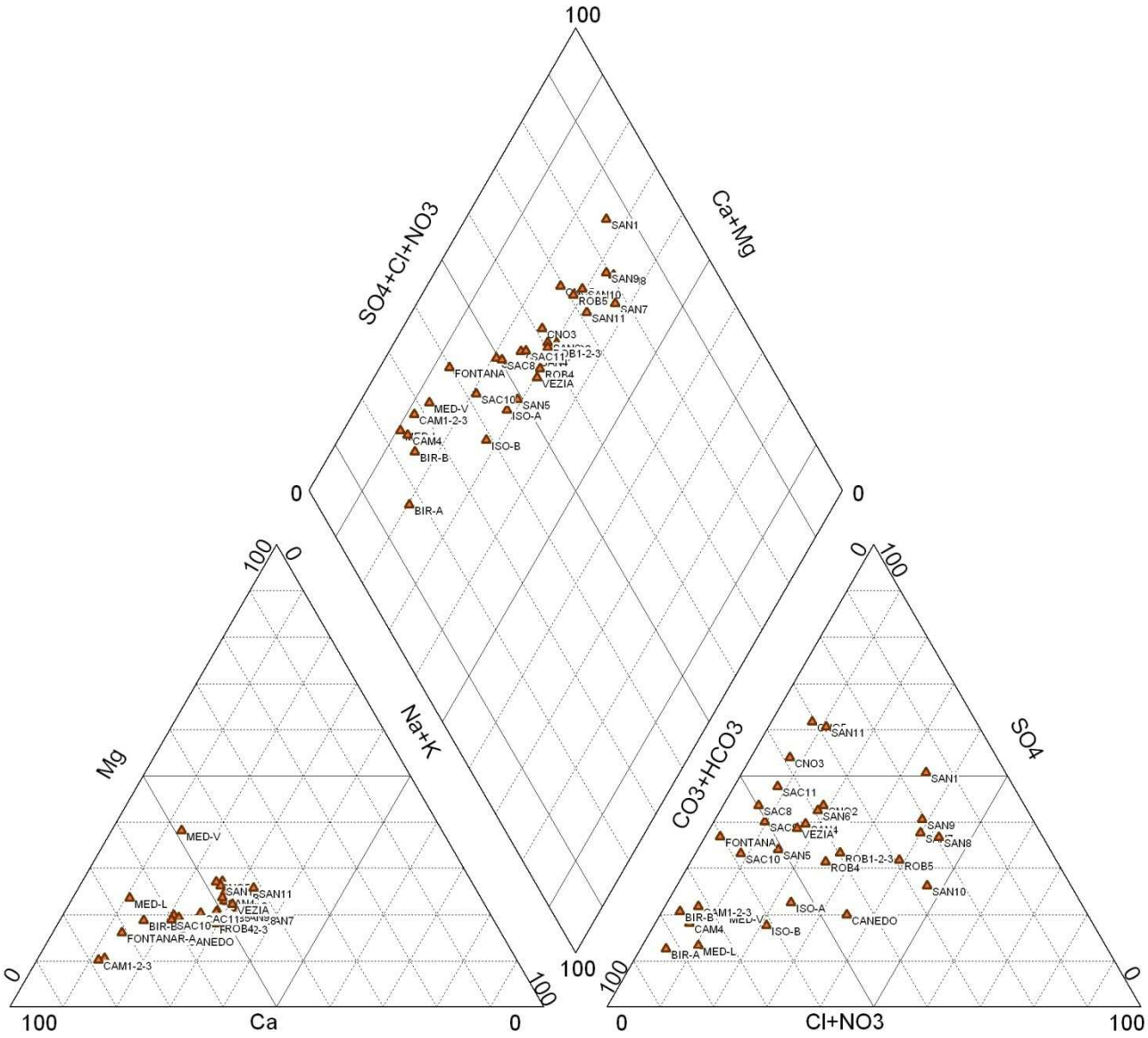
SO4+Cl+NO3
Ca+Mg
Na+K
CO3+HCO3
Mg
Ca
SO4
Cl+NO3
100
0
SAN1
SAN9
SAN8
SAN10
ROB5
SAN7
SAN11
CNO3
SAC11
SAC8
SAC4
ROB1-2-3
FONTANA
ROB4
VEZIA
SAC10
SAN5
MED-V
CAM1-2-3
ISO-A
CAM4
ISO-B
BIR-B
BIR-A
SAN6
ROB5
SAN10
CANEDO
MED-L
FONTANAR-A

B.3 Monte Ceneri inflows

Sigirino access tunnel

One year of steady state monitoring of lateral dripping at different distance from the portal, as shown by the following map:

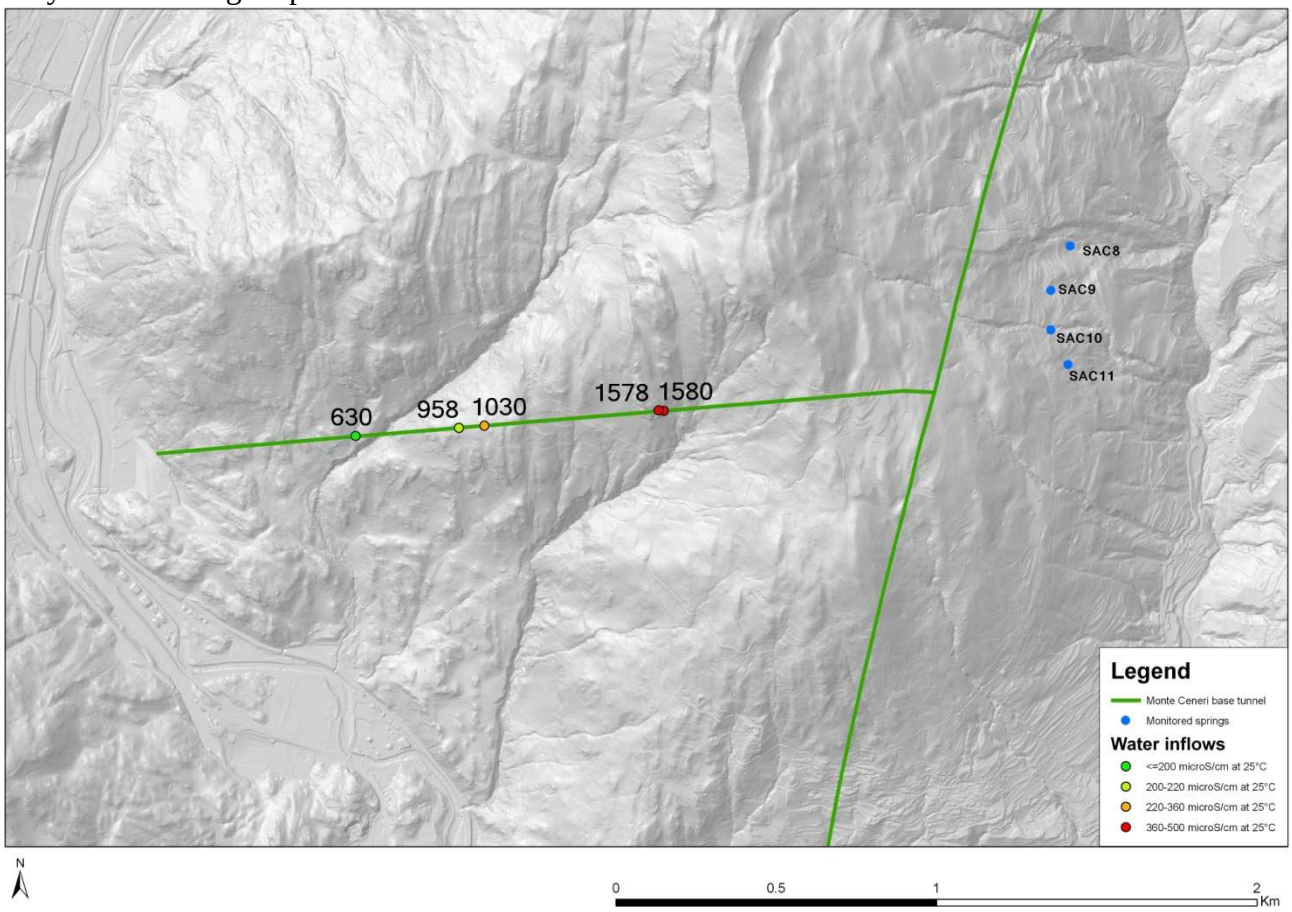

Distance from the portal [m]	Date	T [°C]	pH	EC_{25} [µS/cm]	Na [mg/l]	NH_4 [mg/l]	K [mg/l]	Li [mg/l]	Mg [mg/l]	Ca [mg/l]	HCO_3 [mg/l]	CO_3 [mg/l]	F [mg/l]	Cl [mg/l]	NO_2 [mg/l]	NO_3 [mg/l]	SO_4 [mg/l]	Ionic Balance [mg/l]	$\delta^{18}O$ [‰ VSMOW]	$\delta^{2}H$ [‰ VSMOW]
630	1/8/2009			182	28.09	5.22	1.77	n.a.	0.90	11.26	45.30	1.31	1.54	0.98	n.a.	1.03	8.64	34%	-8.21 ± 0.10	-51.93 ± 1.00
630	1/10/2009	17.4		191	30.12	0.04	0.92	0.02	0.61	11.47	61.71	1.77	3.35	0.74	n.a.	0.29	16.75	9%	-8.91 ± 0.04	-56.33 ± 0.43
630	1/12/2009	14.0	8.7	197	30.76	n.a.	0.83	0.02	0.57	11.69	67.31	1.47	3.43	0.74	n.a.	0.03	16.95	8%	-8.91 ± 0.04	-56.35 ± 0.43
630	1/2/2010	13.5	9.0	196	30.54	0.10	1.01	0.01	0.59	15.20	49.97	1.96	3.28	1.00	0.07	0.11	17.14	20%	-8.51 ± 0.05	-54.47 ± 0.4
630	1/2/2010	15.4		213	33.11	0.09	1.88	0.02	1.02	17.10	55.12	0.02	3.51	1.33	n.a.	3.09	18.42	22%	-8.96 ± 0.05	-56.86 ± 0.4
630	1/5/2010	16.0	8.7	188	30.54	0.07	0.64	0.02	0.60	12.32	55.12	1.18	3.33	0.49	n.a.	0.03	17.25	15%	-8.96 ± 0.05	-56.71 ± 0.4
630	1/7/2010	21.4	8.6	181	30.38	0.02	1.36	n.a.	0.31	11.79	40.41	0.71	3.82	1.64	n.a.	1.49	18.00	19%	-8.97 ± 0.10	-57.35 ± 1.00
958	1/8/2009			205	36.88	0.05	0.69	0.03	0.21	7.91	43.01	1.25	4.07	2.95	n.a.	0.06	29.61	10%	-8.69 ± 0.10	-55.54 ± 1.00
958	1/8/2009			138	22.90	0.45	1.56	n.a.	0.92	11.81	17.72	0.51	1.41	2.80	n.a.	0.72	13.11	40%	-7.74 ± 0.10	-48.46 ± 1.00
958	1/10/2009	17.0		213	35.27	n.a.	0.47	0.02	0.12	9.95	45.13	1.29	3.81	1.57	n.a.	6.82	30.42	7%	-8.81 ± 0.04	-56.05 ± 0.43
958	1/12/2009	15.3	8.8	200	35.30	n.a.	0.22	0.02	0.07	7.17	40.92	1.16	4.11	1.67	n.a.	n.a.	32.79	7%	-8.81 ± 0.04	-56.25 ± 0.43
958	1/2/2010	15.6	8.6	201	35.90	0.11	0.39	0.02	0.08	9.28	43.18	0.78	3.65	1.31	n.a.	0.04	29.44	13%	-8.90 ± 0.05	-56.72 ± 0.4
958	1/5/2010	16.5	8.2	193	35.13	n.a.	0.34	0.02	0.16	9.16	44.39	0.30	3.66	1.13	n.a.	0.48	25.84	14%	-9.10 ± 0.05	-58.64 ± 0.4
958	1/7/2010	21.5	8.5	212	34.55	1.71	0.51	0.02	0.09	10.82	35.93	0.51	4.07	1.81	0.06	9.33	27.22	15%	-9.29 ± 0.10	-59.65 ± 1.00
1030	1/8/2009			305	44.85	0.29	1.53	0.03	0.77	15.10	17.68	0.53	4.72	7.67	0.02	0.24	81.74	7%	-8.84 ± 0.10	-56.56 ± 1.00
1030	1/8/2009			294	41.83	0.06	1.11	0.03	0.51	18.11	14.78	0.45	4.76	4.67	n.a.	0.22	81.41	9%	-8.73 ± 0.04	-56.52 ± 0.43
1030	1/10/2009	17.4		407	62.09	n.a.	1.00	0.02	0.34	18.82	28.14	0.86	6.50	13.39	0.04	0.17	109.63	3%	-8.83 ± 0.10	-56.16 ± 1.00
1030	1/12/2009	15.0	9.4	374	55.84	n.a.	0.39	0.02	0.10	16.14	15.59	1.69	6.12	9.23	n.a.	0.12	109.30	1%	-8.92 ± 0.04	-57.02 ± 0.43
1030	1/2/2010	15.8	9.5	348	52.95	n.a.	0.29	0.02	0.08	15.35	13.69	2.03	5.82	7.75	n.a.	n.a.	97.31	3%	-9.05 ± 0.05	-57.66 ± 0.4
1030	1/5/2010	16.5	9.5	331	52.24	0.05	0.42	0.02	0.09	12.06	14.44	2.07	5.81	7.14	n.a.	0.04	91.52	3%	-9.10 ± 0.05	-57.75 ± 0.7
1030	1/7/2010	19.4	9.3	320	51.46	0.01	0.91	0.02	0.07	11.07	13.91	1.38	6.44	7.40	n.a.	1.64	84.78	3%	-9.22 ± 0.10	-58.73 ± 1.00
1578	1/8/2009			456	100.49	n.a.	3.92	0.05	0.37	4.12	153.70	4.76	12.65	2.93	n.a.	1.51	28.56	8%	-9.27 ± 0.04	-60.2 ± 0.39
1578	1/10/2009	17.4		497	112.31	0.10	1.99	0.06	0.54	4.20	156.72	4.81	16.35	6.66	n.a.	0.07	27.89	9%	-9.10 ± 0.10	-58.29 ± 1.00
1578	1/12/2009	13.5	9.2	512	113.14	n.a.	2.40	0.05	0.22	2.83	173.17	11.58	15.88	2.95	n.a.	1.98	24.39	5%	-9.10 ± 0.04	-58.10 ± 0.43
1578	1/2/2010	14.7	9.3	471	109.95	n.a.	2.05	0.05	0.18	2.05	135.98	11.18	15.47	2.39	n.a.	0.10	24.33	11%	-9.19 ± 0.05	-58.86 ± 0.4
1578	1/5/2010	16.8	8.2	484	113.07	n.a.	5.68	0.05	0.23	2.22	140.42	1.04	15.70	5.41	n.a.	9.30	25.66	13%	-9.14 ± 0.05	-58.61 ± 0.7
1578	1/7/2010	19.5	9.2	462	110.58	0.08	1.62	0.05	0.22	2.31	101.71	8.22	16.05	3.04	10.34	0.54	25.17	16%	-9.03 ± 0.10	-57.84 ± 1.00
1580	1/12/2009	14.9	9.0	473	107.93	n.a	0.57	0.05	0.30	1.99	156.83	7.64	15.10	1.47	n.a.	0.09	28.50	6%	-9.21 ± 0.04	-58.69 ± 0.43
1580	1/10/2009			437	97.02	0.11	3.06	0.06	0.32	3.29	148.95	4.58	13.83	4.38	n.a.	0.74	20.89	7%	-9.41 ± 0.04	-58.5 ± 0.39
1580	1/2/2010	15.5	9.3	451	105.88	n.a	0.57	0.05	0.20	2.07	127.50	10.92	14.33	1.28	n.a.	0.05	26.76	11%	-9.26 ± 0.05	-58.60 ± 0.4
1580	1/5/2010	17.2	8.7	443	108.45	n.a	0.72	0.05	0.24	2.10	129.89	3.05	14.73	1.43	n.a.	0.11	27.91	15%	-9.27 ± 0.05	-59.23 ± 0.7
1580	1/7/2010	21.1	9.1	426	105.81	0.01	0.53	0.05	0.20	1.74	99.39	6.86	15.15	2.21	n.a.	0.95	26.62	18%	-9.13 ± 0.10	-58.87 ± 1.00

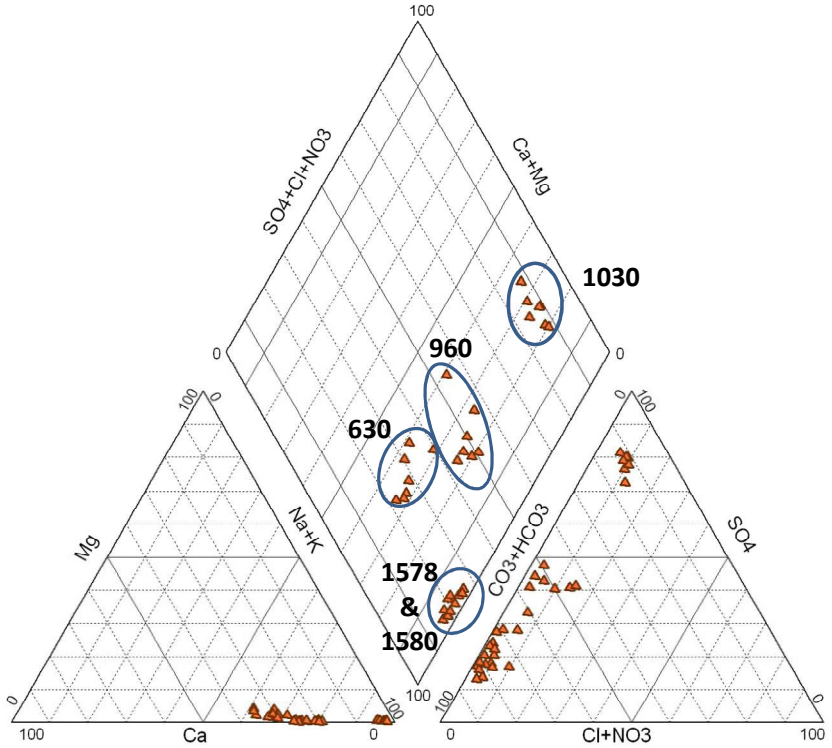

- *Average values*

Distance from the portal [m]	T [°C]	pH	EC_{25} [µS/cm]	Na [mg/l]	NH_4 [mg/l]	K [mg/l]	Li [mg/l]	Mg [mg/l]	Ca [mg/l]	HCO_3 [mg/l]	CO_3 [mg/l]	F [mg/l]	Cl [mg/l]	NO_3 [mg/l]	SO_4 [mg/l]	$\delta^{18}O$ [‰ VSMOW]	$\delta^{2}H$ [‰ VSMOW]
630	16	8.74	193	30.51	0.92	1.20	0.02	0.66	12.98	53.56	1.20	3.18	0.99	0.87	16.16	-8.77	-55.71
958	17	8.52	206	33.70	0.58	0.60	0.02	0.23	9.44	38.61	0.83	3.54	1.89	2.91	26.92	-8.76	-55.90
1030	17	9.42	329	51.61	0.10	0.81	0.02	0.28	15.24	16.89	1.29	5.74	8.18	0.40	93.67	-8.96	-57.20
1578	16	8.96	466	109.92	0.09	2.94	0.05	0.30	2.96	143.62	6.93	15.35	3.90	2.25	26.00	-9.14	-58.65
1580	17	9.03	470	105.02	0.06	1.09	0.05	0.25	2.24	132.51	6.61	14.63	2.16	0.39	26.14	-9.26	-58.78

- *Main ions abundance*

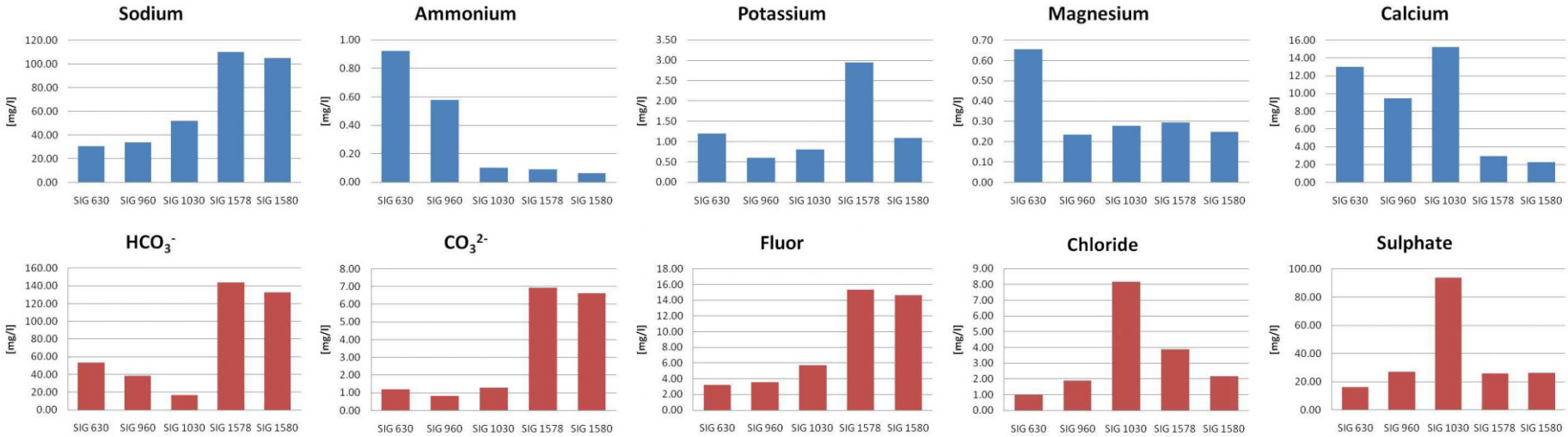

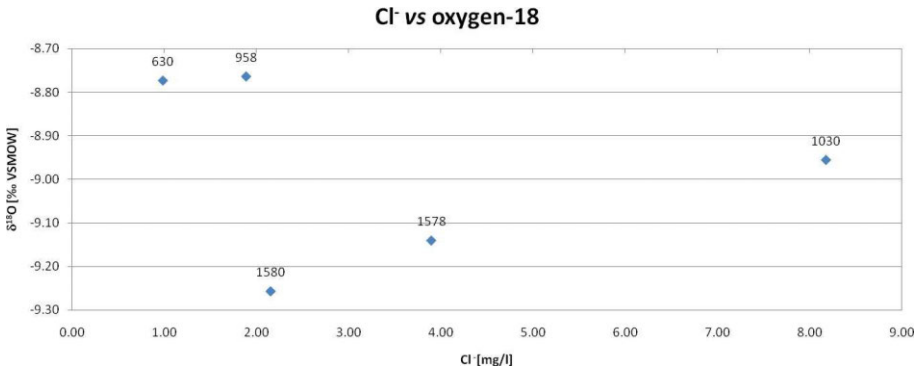

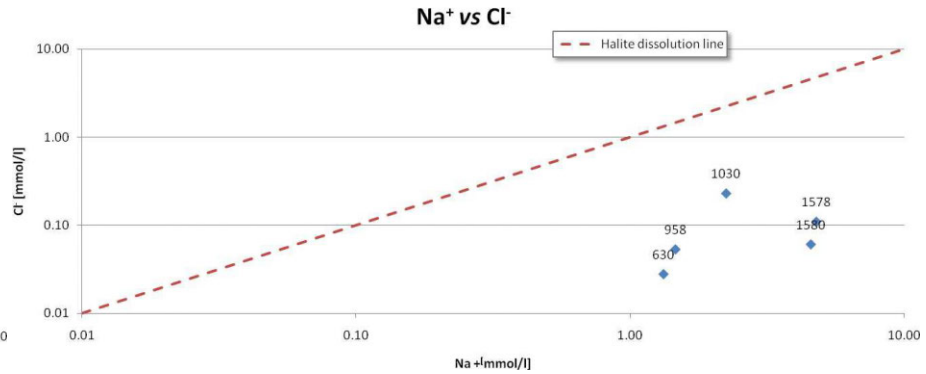

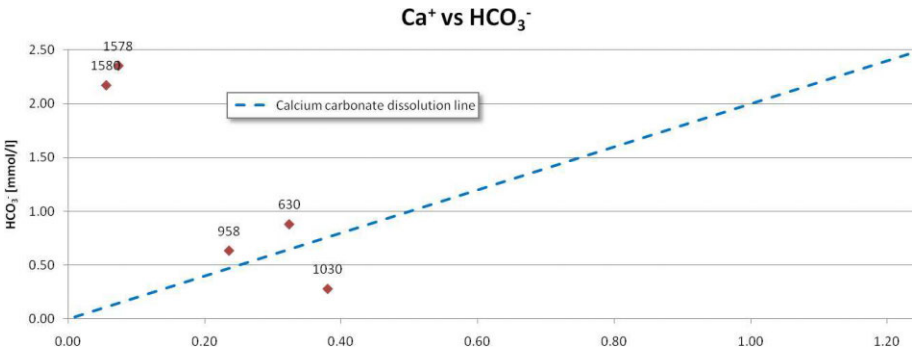
Ca+ vs HCO3-
HCO3- [mmol/l]
Calcium carbonate dissolution line
1578
1580
630
958
1030
0.00
0.50
1.00
1.50
2.00
2.50
0.00
0.20
0.40
0.60
0.80
1.00
1.20

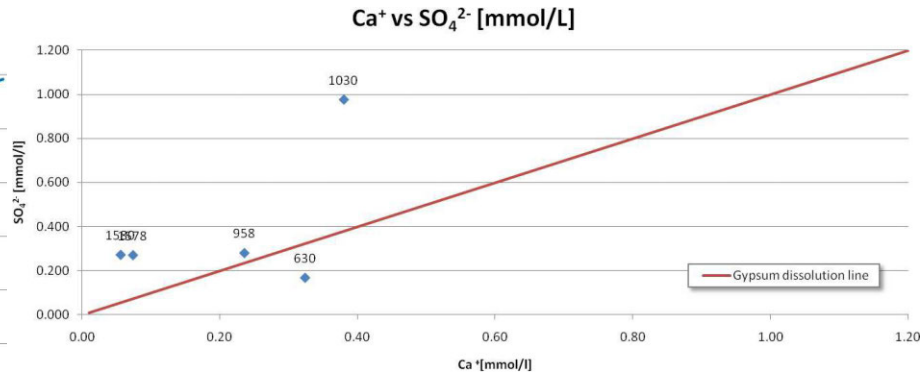
Ca+ vs SO4 2- [mmol/L]
SO4 2- [mmol/l]
Ca +[mmol/l]
Gypsum dissolution line
1030
958
630
0.000
0.200
0.400
0.600
0.800
1.000
1.200
0.00
0.20
0.40
0.60
0.80
1.00
1.20

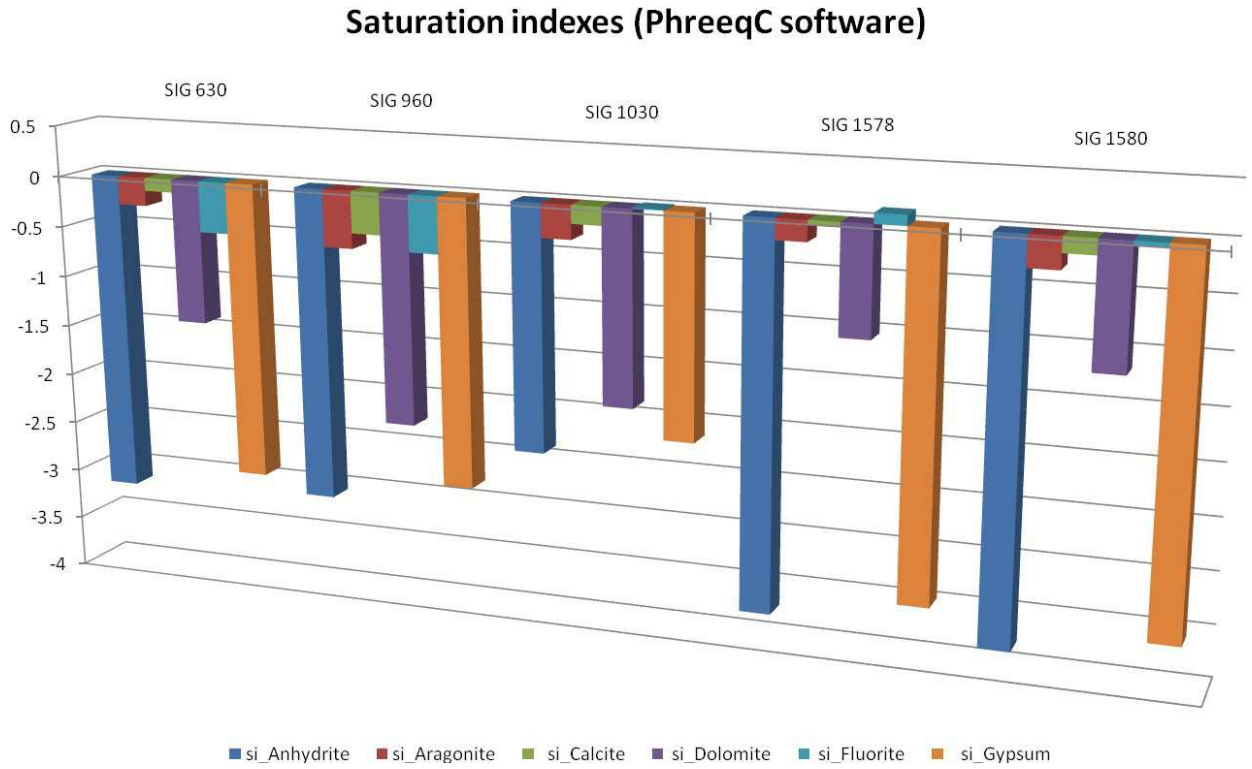
Saturation indexes (PhreeqC software)
SIG 630
SIG 960
SIG 1030
SIG 1578
SIG 1580
0.5
0
-0.5
-1
-1.5
-2
-2.5
-3
-3.5
-4
si_Anhydrite
si_Aragonite
si_Calcite
si_Dolomite
si_Fluorite
si_Gypsum

Vigana north portal

Distance from the portal [m]	Date	T [°C]	pH	EC_{25} [µS/cm]	Na [mg/l]	NH_4 [mg/l]	K [mg/l]	Li [mg/l]	Mg [mg/l]	Ca [mg/l]	HCO_3 [mg/l]	CO_3 [mg/l]	F [mg/l]	Cl [mg/l]	NO_2 [mg/l]	NO_3 [mg/l]	SO_4 [mg/l]	Ionic Balance [mg/l]	$\delta^{18}O$ [‰ VSMOW]	$\delta^{2}H$ [‰ VSMOW]
200	8/2/2010	12.2	8.23	210	8.11	0.16	3.44	n.a.	4.01	29.33	48.13	0.33	0.11	8.65	n.a.	n.a.	32.82	12.81	-8.97 ± 0.05	-57.21 ± 0.7
192	11/2/2010		8.61	258	8.14	n.a.	2.84	0.01	3.98	32.36	43.11	0.97	0.41	7.44	n.a.	0.02	36.86	15.41	-8.96 ± 0.05	-57.30 ± 0.7
204	19/2/2010	12.2	7.74	182	7.40	n.a.	2.41	0.01	3.54	25.78	38.67	0.09	0.15	2.73	n.a.	0.06	33.76	15.87	-9.11 ± 0.05	-58.15 ± 0.7
220	3/3/2010	12.5	7.92	172	6.52	n.a.	2.34	0.01	3.48	24.66	37.11	0.12	0.12	1.24	n.a.	0.08	33.61	15.77	-9.14 ± 0.05	-58.25 ± 0.7
276	22/4/2010	13.6	7.86	161	6.06	0.13	1.68	n.a.	3.49	22.34	33.32	0.10	0.19	0.39	n.a.	0.02	35.37	13.53	-9.30 ± 0.05	-60.14 ± 0.7
170	12/5/2010	12.8	9.52	349	14.33	0.62	9.20	0.02	6.07	45.80	31.34	4.44	0.06	38.37	n.a.	6.76	28.70	20.01	-9.57 ± 0.05	-62.06 ± 0.7
300	12/5/2010	13.5	8.68	162	6.48	0.04	2.92	n.a.	3.42	21.74	30.53	0.60	0.21	1.07	n.a.	n.a.	36.02	13.61	-9.38 ± 0.05	-59.91 ± 0.7
320	12/5/2010	12.9	8.76	160	6.17	0.09	1.66	n.a.	3.45	23.16	32.91	0.77	0.2888	1.103	n.a.	n.a.	37.4529	11.58	-9.21 ± 0.05	-58.84 ± 0.7
290	12/5/2010	12.9	8.70	178	6.70	0.17	7.00	n.a.	3.31	22.54	30.18	0.62	0.2985	5.7115	0.0537	0.0984	35.6827	13.26	-9.13 ± 0.05	-58.96 ± 0.7
310 (east)	27/5/2010	13.3	8.50	167	6.43	0.07	4.41	n.a.	3.38	21.95	30.11	0.39	0.2943	3.117	n.a.	n.a.	37.3958	12.07	-9.34 ± 0.05	-59.71 ± 0.7
310 (west)	27/5/2010	13.8	8.67	164	6.26	0.11	3.47	n.a.	3.46	22.47	33.00	0.64	0.2505	2.5254	n.a.	n.a.	36.7593	11.33	-9.22 ± 0.05	-58.87 ± 0.7

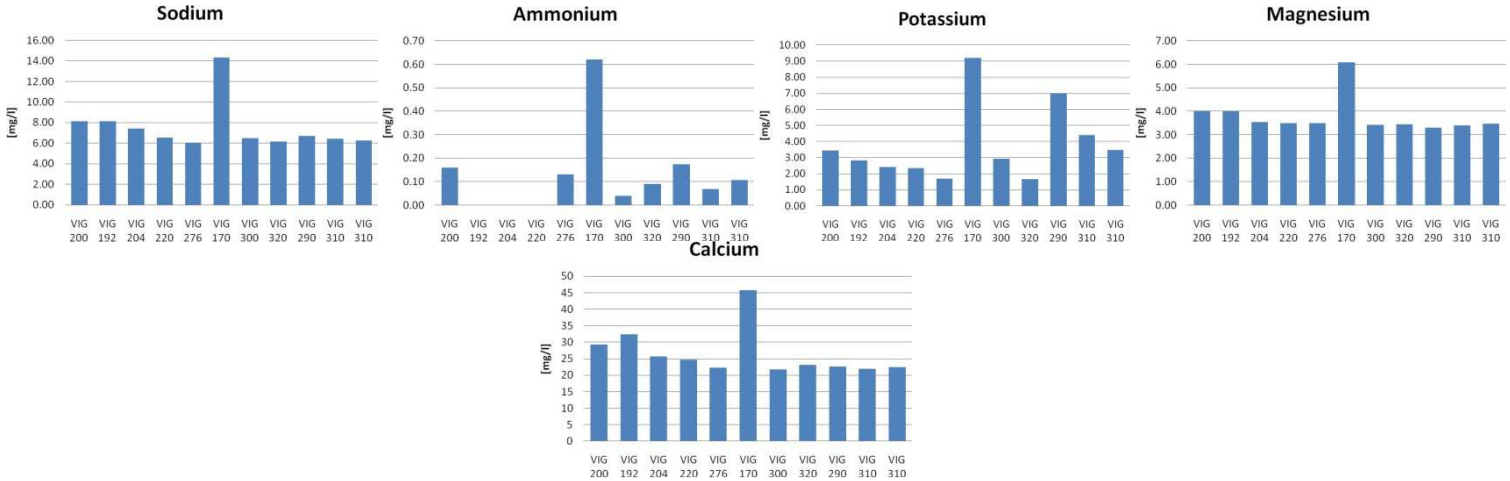

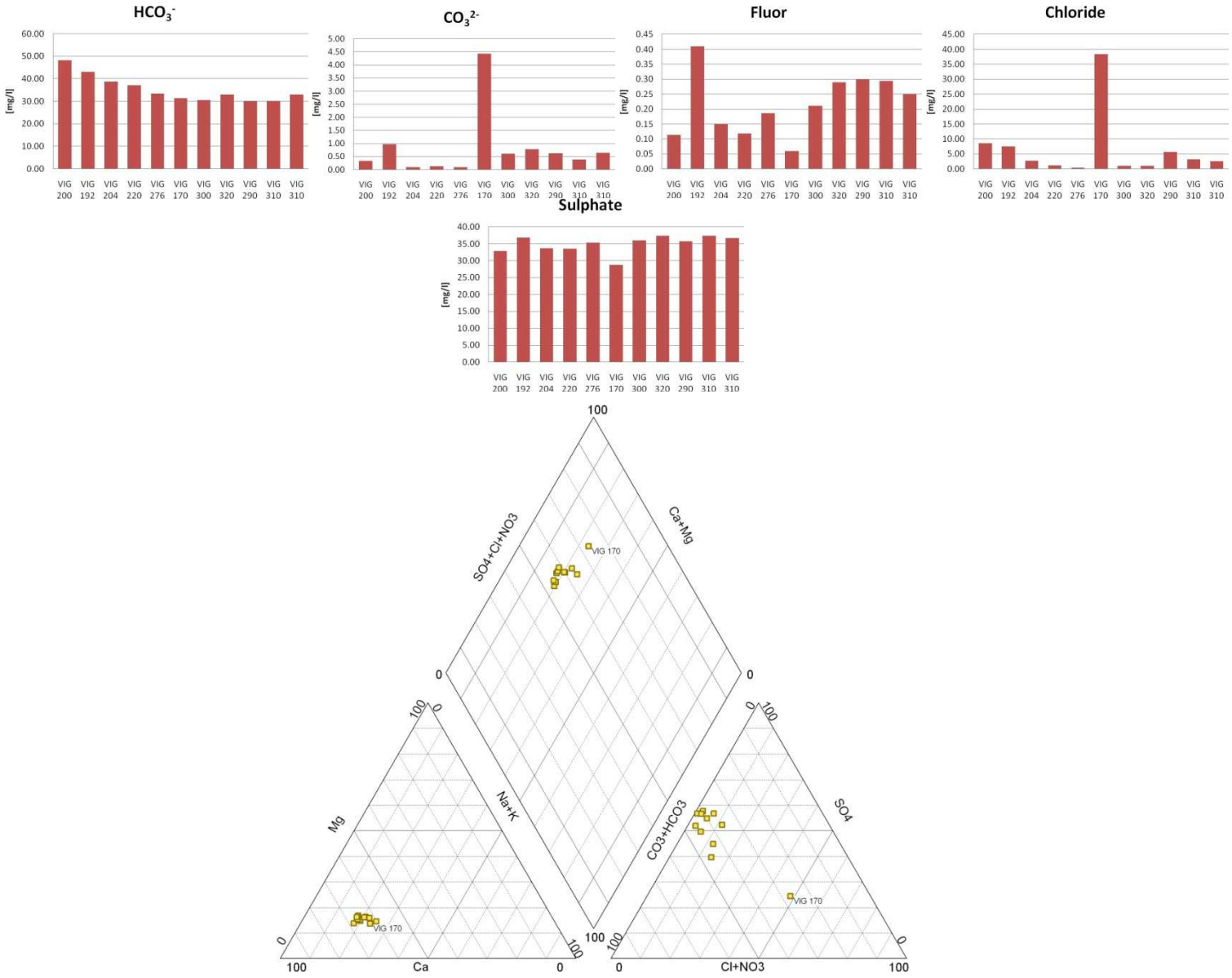
HCO3-
CO32-
Fluor
Chloride
Sulphate
[mg/l]
VIG 200
VIG 192
VIG 204
VIG 220
VIG 276
VIG 170
VIG 300
VIG 320
VIG 290
VIG 310
SO4+Cl+NO3
Ca+Mg
Mg
Na+K
CO3+HCO3
SO4
Ca
Cl+NO3
0
100

B.4 Roveredo (GR) springs

In the region surrounding the San Fedele tunnel (Roveredo – GR) 8 springs are individuated for a monthly/bi-monthly physico-chemical monitoring.

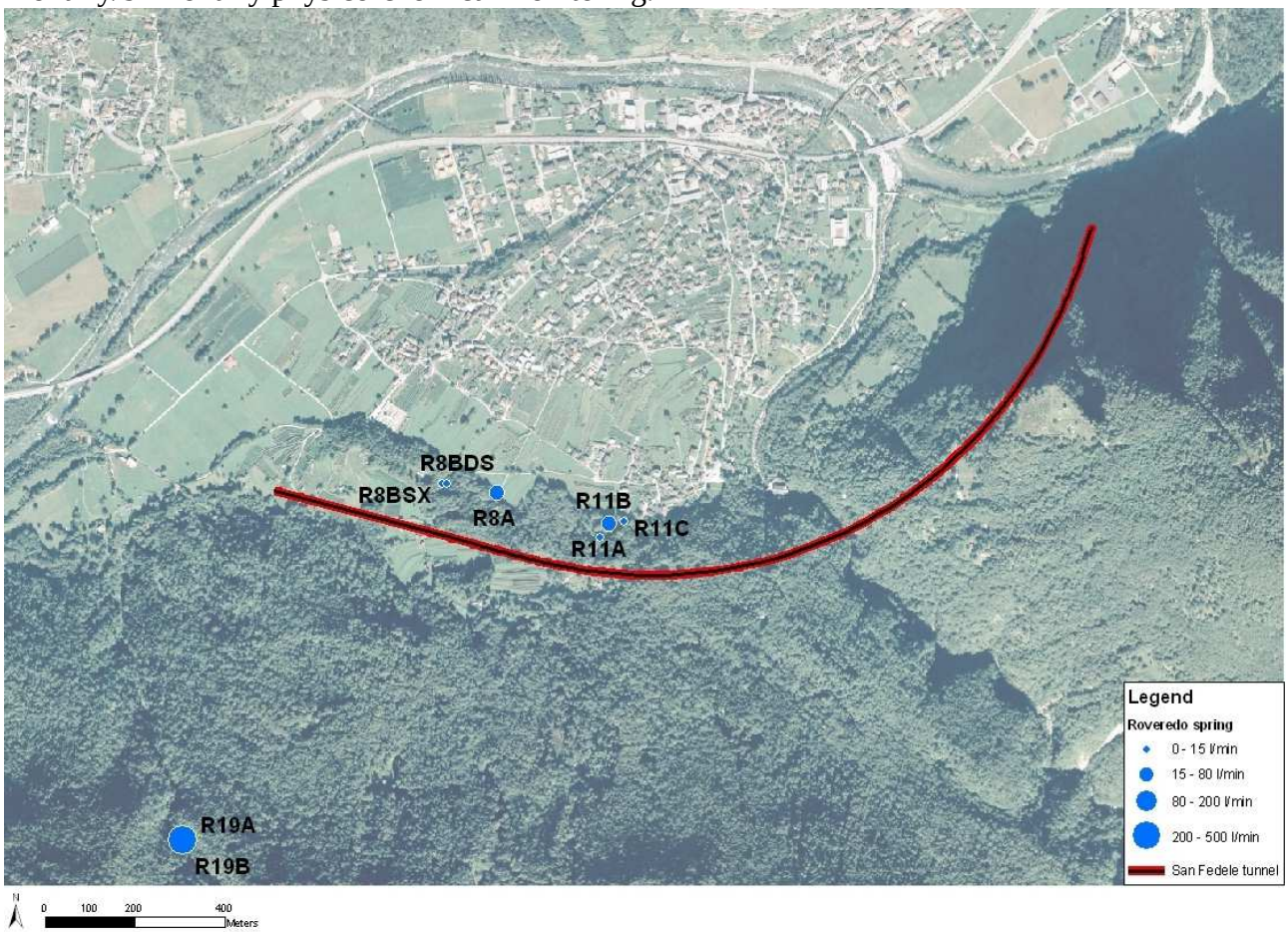

Spring code	z [m a.s.l.]
R8A	350
R8BSX	320
R8BDS	320
R11A	360
R11B	360
R11C	360
R19A	580
R19B	580

Physico-chemical monitoring

Spring	Date	Q [l/min]	T [°C]	EC20 [mS/cm]
R11A	26/3/2008	3	9.3	71.3
R11B	26/3/2008	5	8.6	70.3
R11C	26/3/2008	0	8.6	70.7
R19A	26/3/2008	300	8.7	153
R19B	26/3/2008	16	8.3	157
R8A	26/3/2008	22	6.6	149
R8BDS	26/3/2008	8	7.9	126
R11A	30/4/2008	3	10.5	74
R11B	30/4/2008	12.5	10.9	71.5
R11C	30/4/2008	0	9	76.1
R8A	30/4/2008	42	10.1	145.4
R8BDS	30/4/2008	12	8.9	122.3
R8BSX	30/4/2008	7	9.5	119.4
R11A	30/5/2008	2.5	11.8	74.1
R11B	30/5/2008	50.4	11.3	76.6
R11C	30/5/2008	0	9.7	88
R19A	30/5/2008	600	9.2	147.3
R19B	30/5/2008	46.2	9.1	111.8
R8A	30/5/2008	78.4	12.4	137.8
R8BDS	30/5/2008	36	10.3	112.6
R8BSX	30/5/2008	18.3	12.6	112.3
R11A	25/6/2008	2.8	11.1	70.5
R11B	25/6/2008	53.09	11.9	69
R11C	25/6/2008	8.82	10	84.8
R8A	25/6/2008	80.53	13.9	159.4
R8BDS	25/6/2008	10.71	11.3	126.8
R8BSX	25/6/2008	14.84	13.5	115.3
R19A	9/7/2008	600	9.1	147.2
R19B	9/7/2008	74	9.1	127.5
R11A	6/8/2008	2.5	11.4	69.6
R11B	6/8/2008	80.5	11.6	66.1
R11C	6/8/2008	28.6	10.8	72
R8BDS	6/8/2008	16.7	12.6	113
R8BSX	6/8/2008	13.3	15.2	117.1
R11A	21/8/2008	2.4	11.2	66.8
R11B	21/8/2008	56.1	11.7	65.1
R11C	21/8/2008	11.4	11.1	73.4
R8A	21/8/2008	78.4	13.9	189.2
R8BDS	21/8/2008	12.6	12.9	131.1
R8BSX	21/8/2008	6.7	14.8	123.4
R11A	10/9/2008	3	11.5	48
R11B	10/9/2008	54.5	11.7	65.4
R19A	10/9/2008	521.7	9	153
R19B	10/9/2008	86.7	9	141.4
R11C	11/9/2008	0	12	52.5
R8A	11/9/2008	27.4	13.4	173.7
R8BDS	11/9/2008	22.2	13.2	130.41
R8BSX	11/9/2008	16.5	14.9	123.2
R8A	2/10/2008	17.2	12	168.7
R8BDS	2/10/2008	12	12.5	133
R8BSX	2/10/2008	27.3	12.9	120.1
R11A	6/10/2008	1.5	10.5	66.9
R11B	6/10/2008	59.4	10.5	65.5
R11C	6/10/2008	12.5	11.2	68.8
R11A	19/11/2008	7.8	10.3	67.3
R11B	19/11/2008	92.3	9.8	68.5
R11C	19/11/2008	36.3	11	68.8
R8A	19/11/2008	200	9.3	145.5
R8BDS	19/11/2008	20.9	11.3	121.7
R8BSX	19/11/2008	23.1	9.2	110
R11A	22/12/2008	3.6	9.9	68.8
R11B	22/12/2008	70.6	9.4	67.2
R11C	22/12/2008	35.3	10.6	67.8
R8A	22/12/2008	125	7.8	166.1
R8BDS	22/12/2008	14.4	9.6	115.6
R8BSX	22/12/2008	17.6	6.3	107.6
R11A	16/2/2009	6.8	10	66.4
R11B	16/2/2009	43.5	8.3	65.3
R11C	16/2/2009	13.19	9.9	64.9
R8A	16/2/2009	60	5.9	164.9
R8BDS	16/2/2009	9	4.1	109
R8BSX	16/2/2009	9.6	4.1	164.9
R19A	17/2/2009	545.5	8.6	158.7
R19B	17/2/2009	61.9	8.6	151.5
R11A	20/3/2009	12.9	10.3	65.7
R11B	20/3/2009	39.7	9.2	64.8
R11C	20/3/2009	15.2	9.6	65.4
R8A	20/3/2009	65.2	7.6	166.3
R8BDS	24/3/2009	15.7	6.4	111.5
R8BSX	24/3/2009	15	7.8	118.3
R11A	21/4/2009	11.71	10.7	64.8
R11B	21/4/2009	27.52	11.9	63.7
R11C	21/4/2009	2.31	9.6	66
R19A	21/4/2009	352.9	9.5	163
R19B	21/4/2009	40	9.1	164.4
R8A	21/4/2009	50.42	10.7	167.7
R8BDS	21/4/2009	15	9.1	119.6
R8BSX	21/4/2009	7.8	9.4	119.8
R11A	22/5/2009	16.5	10.8	66.5
R11B	22/5/2009	49.6	12	66
R11C	22/5/2009	14.3	10	69.5
R8A	22/5/2009	37	13	160.1
R8BDS	22/5/2009	16.3	10	121.1
R8BSX	22/5/2009	18	11.7	117.4
R11A	18/6/2009	8.9	10.8	65.4
R11B	18/6/2009	45.3	13.1	66.1
R11C	18/6/2009	5.6	11.5	70
R19A	18/6/2009	600	9.1	163
R19B	18/6/2009	64	9	161.6
R8A	18/6/2009	46.2	14	178.3
R8BDS	18/6/2009	11.5	11.5	128.6
R8BSX	18/6/2009	8.8	13.4	125.2
R11A	23/7/2009	8.6	10.9	65.3
R11B	23/7/2009	31.7	12.3	66
R11C	23/7/2009	0	12.3	71.7
R8A	23/7/2009	32.2	14.6	174.9
R8BDS	23/7/2009	13.3	12.5	135.7
R8BSX	23/7/2009	11.3	14.5	133.7
R11A	25/8/2009	7.9	11.1	65.8
R11B	25/8/2009	30	12.9	66.4
R11C	25/8/2009	0.8	11.6	80.5
R19A	25/8/2009	300	9.3	166.6
R19B	25/8/2009	52.86	9.3	171.4
R8A	25/8/2009	50	15.5	171.5
R8BDS	25/8/2009	11.5	13.7	142
R8BSX	25/8/2009	9.2	15.4	141.6
R11A	17/9/2009	9	10.9	67.1
R11B	17/9/2009	26.2	12.5	66.6
R11C	17/9/2009	0.15	12	93.1
R8A	17/9/2009	44.4	14.2	168
R8BDS	17/9/2009	13.1	13.5	143.7
R8BSX	17/9/2009	8.9	14.4	145
R11A	20/10/2009	9.1	10.3	
R11B	20/10/2009	15.5	10	
R11C	20/10/2009	0	10.5	
R19A	20/10/2009	400	9	
R19B	20/10/2009	50	8.8	
R8A	20/10/2009	4.7	10	
R8BDS	20/10/2009	8.4	12.7	
R8BSX	20/10/2009	5.6	11	
R11A	17/11/2009	7.9	9.4	62.4

R11B	17/11/2009	12	9.3	62.8
R11C	17/11/2009	0	10.3	67.3
R8A	17/11/2009	0.2	10.2	158
R8BDS	17/11/2009	10.3	10.4	127
R8BSX	17/11/2009	5.14	9.7	110
R11A	28/12/2009	11.4	8.7	61.3
R11B	28/12/2009	1.7	6.8	60.8
R11C	28/12/2009	0	8.5	59.6
R19A	28/12/2009	300	5.6	147
R19B	28/12/2009	32.7	6.7	138.1
R8A	30/12/2009	23.1	4.5	133.5
R8BDS	30/12/2009	13.3	8.2	105.1
R8BSX	30/12/2009	12.6	5	103.8
R11A	29/1/2010	11	8.4	60.5
R11B	29/1/2010	18.3	6.3	60
R11C	29/1/2010	0	8	53.2
R8A	29/1/2010	20.7	3.2	131.7
R8BDS	29/1/2010	10.9	6	111.2
R8BSX	29/1/2010	9.4	3	102.4
R19A	12/2/2010	400	7.7	149.4
R19B	12/2/2010	28	7.5	157.8
R11A	17/2/2010	9.6	9	63
R11B	17/2/2010	21.4	7.4	59.1
R11C	17/2/2010	0	9.2	50.8
R8A	17/2/2010	26.1	4.4	128
R8BDS	17/2/2010	8.5	6.6	93.3
R8BSX	17/2/2010	10.7	4.4	103.8
R11A	17/3/2010	9.6	9	62
R11B	17/3/2010	15.8	8.4	62
R11C	17/3/2010	0	8.5	55
R19A	17/3/2010	300	8	142
R19B	17/3/2010	30	8	153.4
R8A	17/3/2010	4.2	6	133.4
R8BDS	17/3/2010	8.6	7	110
R8BSX	17/3/2010	5.8	5.7	101.8
R11A	26/3/2010	9.6	9.3	62.3
R11B	26/3/2010	17.1	8.8	62
R11C	26/3/2010	0	9	55.6
R19A	26/3/2010	333.3	8.5	148
R19B	26/3/2010	33.3	8.2	157
R8A	26/3/2010	12.1	7.6	134.3
R8BDS	26/3/2010	9.2	7.3	83.3
R8BSX	26/3/2010	7.1	6.8	106
R11A	9/4/2010	8.7	9.2	62.1
R11B	9/4/2010	18.8	9.8	60.6
R11C	9/4/2010	0	8.6	58.6
R19A	9/4/2010	400	8.7	142.4
R19B	9/4/2010	47.4	8.3	127.6
R8A	9/4/2010	7.4	10	133
R8BDS	9/4/2010	13.3	8.1	111.6
R8BSX	9/4/2010	7.7	8.1	104.3
R11A	30/4/2010	18.9	9.6	63.6
R11B	30/4/2010	24.5	10	63.2
R11C	30/4/2010	0	9	59
R19A	30/4/2010	368.1	8.7	145.1
R19B	30/4/2010	36.5	8.3	151.3
R8A	30/4/2010	7.5	10.8	132
R8BDS	30/4/2010	9.2	8.5	111.4
R8BSX	30/4/2010	4.4	9.7	116.9
R11A	27/5/2010	33.3	9.5	63.9
R11B	27/5/2010	83.3	10	63.2
R11C	27/5/2010	28.6	8.9	71.9
R8A	27/5/2010	127.7	11.4	124
R8BDS	27/5/2010	16.7	9.5	108.2
R8BSX	27/5/2010	26.4	11	101.7
R19B	14/6/2010	70.4	8.5	146.2
R8A	14/6/2010	42.9	12.6	161.4
R8BDS	14/6/2010	14.6	10.7	112.9
R8BSX	14/6/2010	15	13.2	113.7
R19A	19/6/2010	394.7	8.5	142.4
R11A	28/6/2010	25.3	10	57.4
R11B	28/6/2010	46.7	10.6	57.6
R11C	28/6/2010	4.3	9	67.6
R11A	31/7/2010	13.9	10.1	56.6
R11B	31/7/2010	22.9	11.1	52.2
R11C	31/7/2010	0	10	64.3
R8A	31/7/2010	3.4	14.6	165.5
R8BDS	31/7/2010	4.4	12.9	124.1
R8BSX	31/7/2010	0.45	14.5	99.7
R19A	3/8/2010	375	10	176
R19B	3/8/2010	53	9.3	155
R11A	31/8/2010	9.8	10	57.3
R11B	31/8/2010	15.8	10.8	58.1
R11C	31/8/2010	0	10.8	74.1
R8A	31/8/2010	0.95	12.6	169.3
R8BDS	31/8/2010	6.2	12.3	130.4
R8BSX	31/8/2010	1.01	12	128.9
R11A	16/9/2010	11.1	10	55.2
R11B	16/9/2010	13.3	11	45.4
R11C	16/9/2010	0	12	75.1
R8A	16/9/2010	1.4	13.9	162.2
R8BDS	16/9/2010	5.8	12.6	128
R8BSX	16/9/2010	1.2	13.5	87.5
R11A	13/10/2010	9.3	10	53.8
R11B	13/10/2010	10.7	10.3	56.8
R11C	13/10/2010	0	10.8	81.7
R19A	13/10/2010	400	8.4	143.9
R19B	13/10/2010	40.5	8.3	156
R8A	13/10/2010	3.8	12	155.9
R8BDS	13/10/2010	6.9	11.9	80.4
R8BSX	13/10/2010	2.4	12	128.7
R11A	27/11/2010	24.3	9.1	59.4
R11B	27/11/2010	47.4	8.1	58.1
R11C	27/11/2010	0	9.5	55.4
R8A	27/11/2010	24.3	4.9	139
R8BDS	27/11/2010	12.7	8.5	104
R8BSX	27/11/2010	18.5	5.5	103.5
R11A	24/12/2010	25.5	9.2	57.7
R11B	24/12/2010	61.5	7.8	56.2
R11C	24/12/2010	9.4	9.4	57.8
R19A	24/12/2010	428.6	7.7	137.3
R19B	24/12/2010	52.2	7.5	127.7
R8A	24/12/2010	50	4.9	107.2
R8BDS	24/12/2010	37.5	4.2	89
R8BSX	24/12/2010	16.4	7.6	99.4
R11A	28/1/2011	24	9	59.9
R11B	28/1/2011	47.5	7.7	59.1
R11C	28/1/2011	6.2	9	60.2
R8A	28/1/2011	49.2	4.5	144
R8BDS	28/1/2011	9.5	6.5	109.1
R8BSX	28/1/2011	7.7	4	98.6

R8BSX

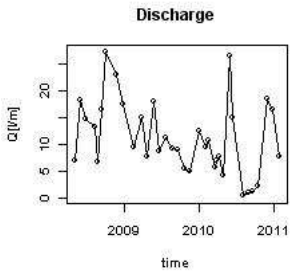

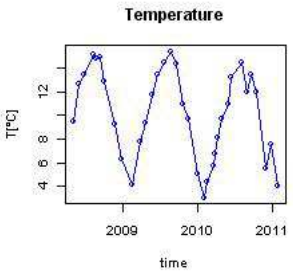

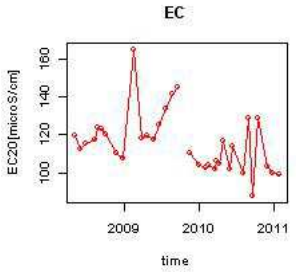

R11A

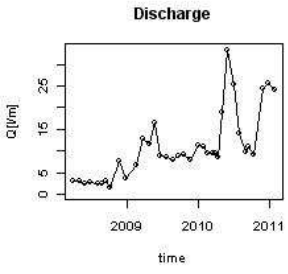

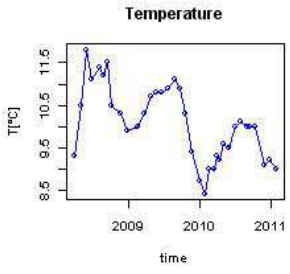

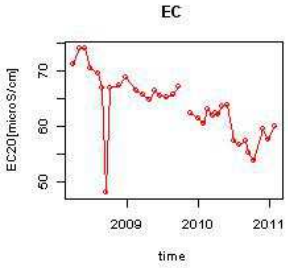

R8BSX

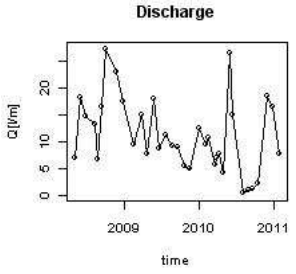

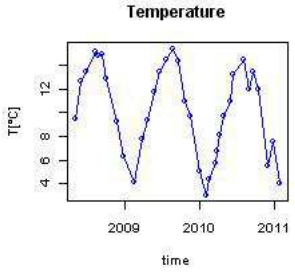

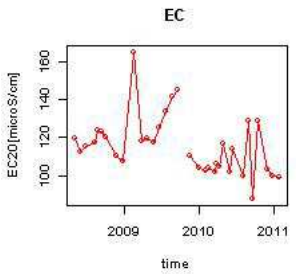

R11B

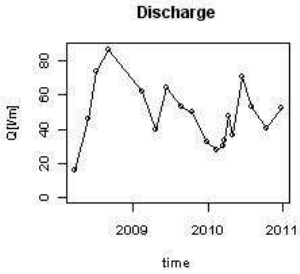

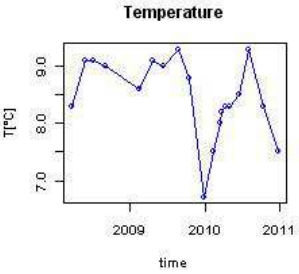

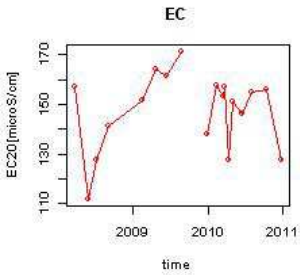

R8A

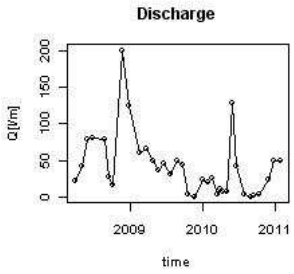

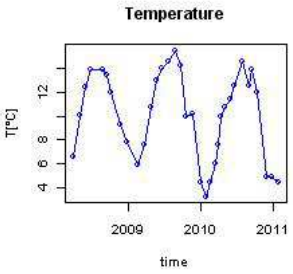

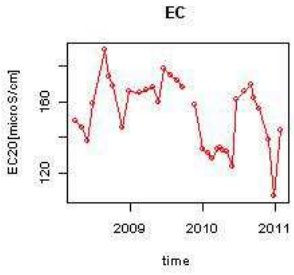

R8BDS

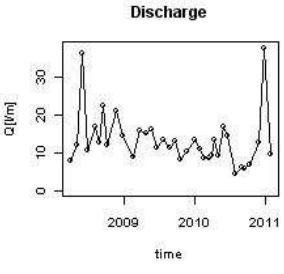

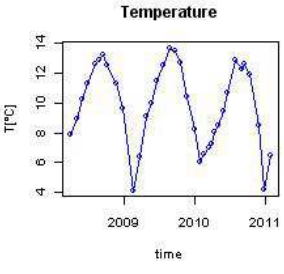

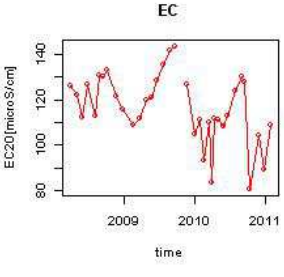

R11C

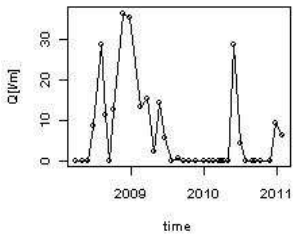

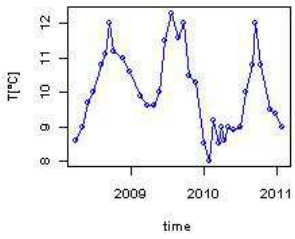

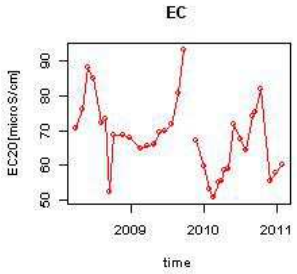

R19A

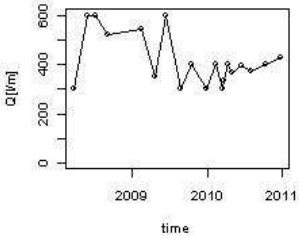

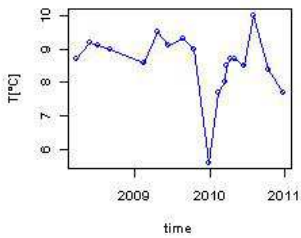

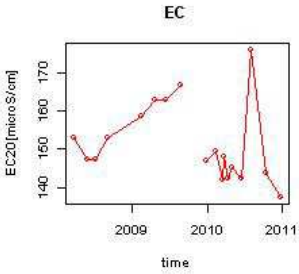

R19B

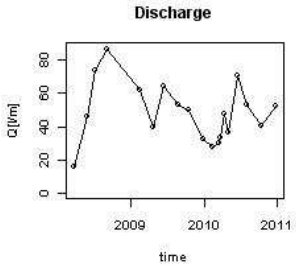

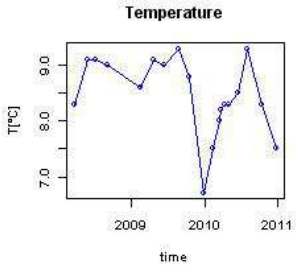

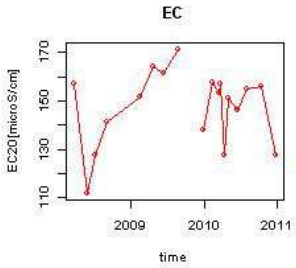

Major ion analysis

Spring	Li [mg/l]	Na [mg/l]	NH_4 [mg/l]	K [mg/l]	Mg [mg/l]	Ca [mg/l]	HCO_3 [mg/l]	CO_3 [mg/l]	F [mg/l]	Cl [mg/l]	NO_2 [mg/l]	NO_3 [mg/l]	SO_4 [mg/l]	TDI [mg/l]	Ionic Balance [mg/l]
R19A	0.01	2.29	0.01	2.01	1.98	31.85	49.74	0.17	0.10	0.44	n.a.	2.23	12.81	103.63	25
R19B	n.a.	2.32	0.02	2.05	2.07	33.78	52.65	0.14	0.09	0.44	n.a.	2.08	14.34	110.00	25
R11B	0.00	3.29	0.35	1.30	1.80	9.27	19.10	0.02	0.07	0.85	n.a.	0.59	3.66	40.31	31
R11C	0.01	3.04	0.02	1.27	1.74	8.92	19.56	0.00	0.06	0.88	n.a.	0.80	3.61	39.90	27
R8A	0.00	2.68	0.02	1.72	2.04	36.72	57.79	0.29	0.06	4.00	n.a.	2.75	5.74	113.82	27
R8BDS	n.a.	2.88	0.02	3.13	2.21	25.15	42.34	0.04	0.06	3.02	n.a.	3.01	6.44	88.31	26
R8BSX	n.a.	2.94	0.03	3.04	2.21	26.76	50.44	0.16	0.14	3.40	n.a.	2.77	5.15	97.05	23

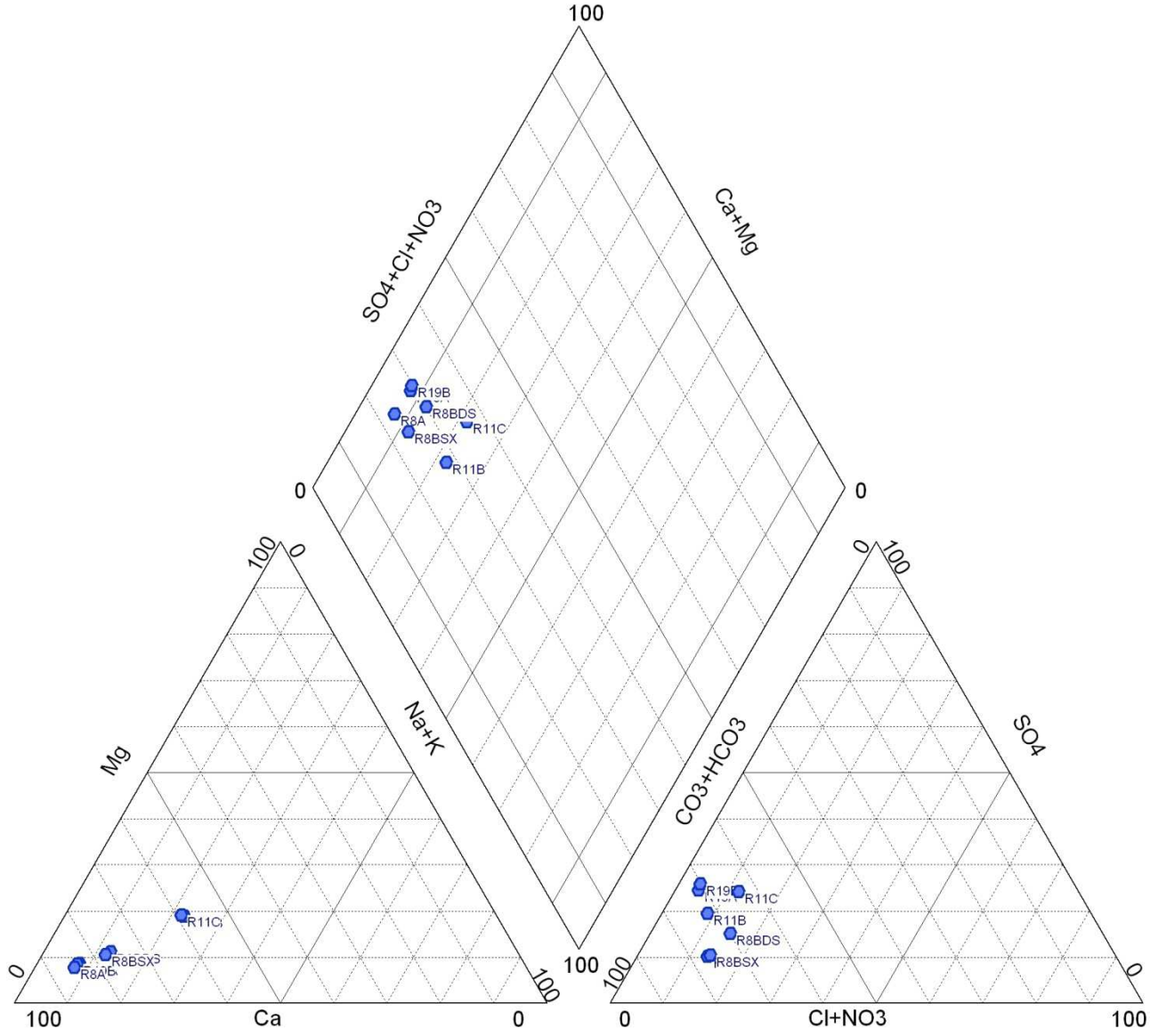

Stable isotope compositions of oxygen and hydrogen

Name	Date	$\delta^{18}O$ [‰ VSMOW]			$\delta^{2}H$ [‰ VSMOW]		
R11A	02/2010	-8.66	±	0.06	-55.77	±	0.5
R11A	03/2010	-8.70	±	0.06	-56.58	±	0.5
R11A	04/2010	-8.88	±	0.06	-56.78	±	0.5
R11A	07/2010	-9.22	±	0.10	-60.54	±	1.0
R11A	08/2010	-9.28	±	0.06	-60.70	±	0.5
R11A	09/2010	-9.36	±	0.06	-60.49	±	0.5
R11B	02/2010	-9.16	±	0.06	-59.20	±	0.5
R11B	03/2010	-8.76	±	0.06	-56.52	±	0.5
R11B	04/2010	-8.87	±	0.08	-57.14	±	0.5
R11B	07/2010	-9.45	±	0.10	-60.81	±	1.0
R11B	08/2010	-9.35	±	0.06	-60.55	±	0.5
R11B	09/2010	-9.31	±	0.06	-60.45	±	0.5
R11C	02/2010	-10.12	±	0.06	-67.43	±	0.5
R11C	03/2010	-9.14	±	0.06	-61.93	±	0.5
R11C	04/2010	-9.20	±	0.06	-60.11	±	0.5
R11C	07/2010	-9.36	±	0.10	-61.13	±	1.0
R11C	08/2010	-9.31	±	0.06	-61.20	±	0.5
R11C	09/2010	-9.22	±	0.06	-59.99	±	0.5
R19A	03/2010	-9.41	±	0.06	-61.54	±	0.5
R19A	04/2010	-9.41	±	0.06	-61.37	±	0.5
R19A	07/2010	-9.60	±	0.10	-61.20	±	1.0
R19B	03/2010	-9.38	±	0.06	-61.40	±	0.5
R19B	04/2010	-9.42	±	0.06	-61.63	±	0.5
R19B	07/2010	-9.38	±	0.10	-60.92	±	1.0
R8A	02/2010	-8.89	±	0.06	-58.18	±	0.5
R8A	03/2010	-8.86	±	0.06	-58.15	±	0.5
R8A	04/2010	-9.01	±	0.06	-59.08	±	0.5
R8A	07/2010	-9.02	±	0.10	-58.98	±	1.0
R8A	09/2010	-9.11	±	0.06	-59.50	±	0.5
R8BDS	02/2010	-9.08	±	0.06	-59.38	±	0.5
R8BDS	03/2010	-9.44	±	0.06	-61.92	±	0.5
R8BDS	04/2010	-9.53	±	0.08	-61.86	±	0.5
R8BDS	07/2010	-9.73	±	0.10	-64.09	±	1.0
R8BDS	08/2010	-9.68	±	0.06	-64.29	±	0.5
R8BDS	09/2010	-9.67	±	0.06	-63.34	±	0.5
R8BSX	02/2010	-9.33	±	0.06	-60.79	±	0.5
R8BSX	03/2010	-9.48	±	0.06	-62.08	±	0.5
R8BSX	04/2010	-9.47	±	0.06	-62.34	±	0.5
R8BSX	07/2010	-9.67	±	0.10	-63.66	±	1.0
R8BSX	08/2010	-9.74	±	0.06	-64.56	±	0.5
R8BSX	08/2010	-9.59	±	0.06	-63.98	±	0.5
RB8SX	09/2010	-9.70	±	0.06	-63.10	±	0.5

B.5 San Fedele (Roveredo) tunnel inflows

Distance from the W portal [m]	Date	T [°C]	pH	EC_{25} [µS/cm]	Na [mg/l]	NH_4 [mg/l]	K [mg/l]	Li [mg/l]	Mg [mg/l]	Ca [mg/l]	HCO_3 [mg/l]	CO_3 [mg/l]	F [mg/l]	Cl [mg/l]	NO_2 [mg/l]	NO_3 [mg/l]	SO_4 [mg/l]	Ionic Balance [mg/l]	$\delta^{18}O$ [‰ VSMOW]	$\delta^{2}H$ [‰ VSMOW]
345	16/2/2010	11.6	8.00	206	3.12	n.a.	3.33	n.a.	3.25	28.20	53.977248	0.20	0.0837	4.6813	0.0276	1.8802	8.7805	21	-9.06 ± 0.05	-59.04 ± 0.7
387.5	22/2/2010	12.9	7.76	284	4.42	0.06	2.40	n.a.	3.23	28.87	60.119389	0.13	0.1059	2.2683	n.a	0.9347	11.1638	20	-9.03 ± 0.05	-59.13 ± 0.7
399	22/2/2010	13.1	8.04	439	4.74	0.07	2.75	n.a.	3.60	27.87	60.658171	0.26	0.1348	2.3477	n.a	1.0612	11.4623	19	-9.08 ± 0.05	-59.02 ± 0.7
402	22/2/2010	12.6	8.01	171	4.95	0.04	3.27	n.a.	4.10	31.26	57.55717	0.23	0.1354	2.0729	n.a	0.8983	12.0441	26	-8.46 ± 0.05	-57.43 ± 0.7
500	26/2/2010		8.09	133	5.38	n.a.	2.82	n.a.	2.22	17.66	40.663302	0.25	0.1341	0.3914	n.a		12.2038	18	-9.33 ± 0.05	-62.14 ± 0.7

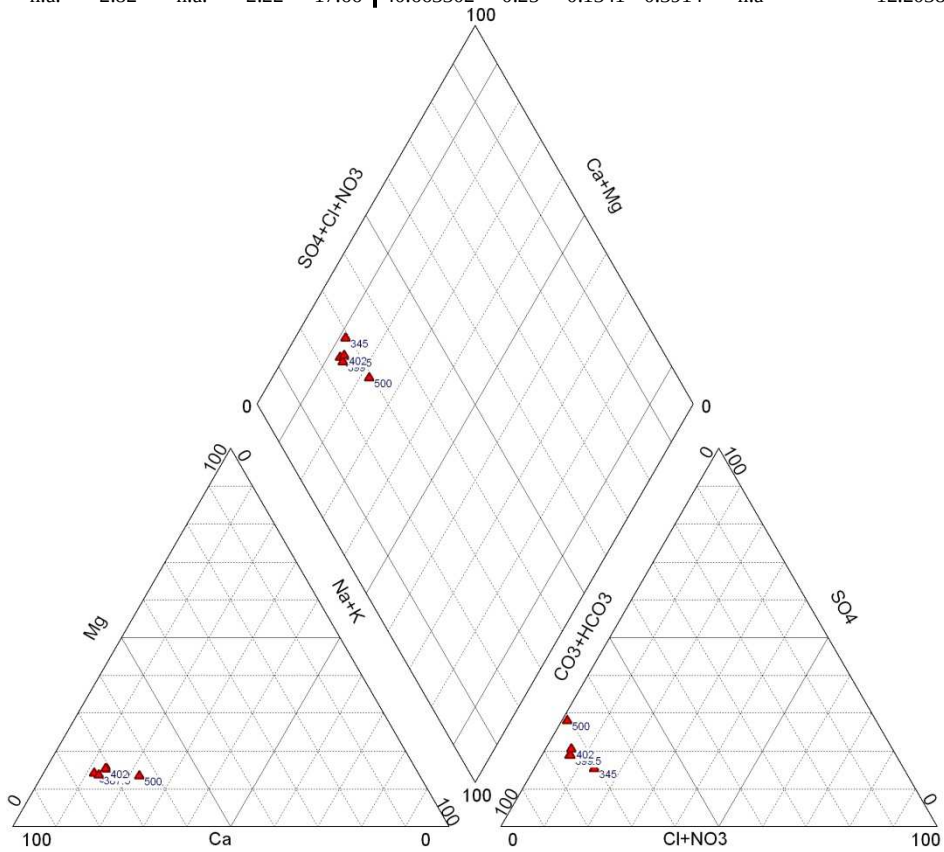

B.6 IAEA-WMO programme on isotopic composition of precipitation: global network of isotopes in precipitation (GNIP) technical procedure for sampling[4]

I. Introduction

The International Atomic Energy Agency in cooperation with the World Meteorological Organization has organized for many years a global network of stations for the collection of monthly precipitation samples for the determination of the isotopic composition. The meteorological and isotope data collected in the programme through this network of stations and National Networks are stored in a database available through INTERNET. The isotopes, the content variations of which are determined, are the stable isotopes oxygen-18 and hydrogen-2 (deuterium) and the radioactive isotope hydrogen-3 (tritium). These data are used as background information for isotopic hydrological investigations and for meteorological and climatological studies.

To obtain reliable isotopic data it is essential that the sampling procedure described below be followed in all detail. Above all evaporation should be avoided, because during evaporation the isotopic composition of the water sample is strongly affected. It is therefore essential to use tight bottles to preserve, ship and store the precipitation samples collected for isotopic analysis. It is advisable to use the bottles provided by IAEA, which have been checked for their tightness. Also during the collection, the water should be removed from the rain collector soon after the rain, or it should protected against evaporation with medicinal paraffin oil.

II. Technical Procedure for Precipitation Sampling for Isotopic Analyses

1. Each sample must represent the integrated precipitation for a one-month period, beginning on the first day of the month and continuing until the end of the month.

2. The bottles provided by IAEA have a volume of 1/2 liter (for tritium analysis) and 50 ml (for stable isotope analysis), which are considered the optimal amounts of water required for isotopic analysis. A minimum amount of about 300 ml of water is needed to perform tritium, deuterium and oxygen-18 analysis. If sometimes less than this amount is available (for instance because the precipitation was scarce), send anyhow the available water to the laboratory in charge of the isotopic analyses, which in this case will carry out only some of them. If tritium and stable isotopes are analysed in different laboratories, fill up 50 ml bottle for the stable isotope analysis and use the rest of water to fill the 1/2 1 bottle (or part of it if the sample is insufficient) for the tritium analysis.

3. The rain water is collected in the standard rain gauge which is read and emptied as soon as possible after each rain event, if practicable, or each morning. After reading the gauge the precipitation should be poured into a 5-litre plastic bottle with a good cap to avoid evaporation. Keep this container in a cool, dark place. It is very important that the cap on the large bottle should be kept tightly closed: evaporation, in fact modifies the isotope composition of water, and therefore all precautions should be taken to prevent it.

4. It is absolutely essential that the water be transferred after every precipitation or every day and the rain collector be dried again with a clean dry cloth or tissue before returning it to its collecting position.

5. If the rain water should remain several days in the rain collector (which can consist simply of a plastic bottle with a funnel) before being transferred to a tight container, then it is necessary to put medicinal paraffin oil, available in a pharmacy, in the rain collector to prevent evaporation. The medicinal paraffin oil layer floating over the water should have a thickness of about 0.5 cm. The rain water with the paraffin oil can be transferred periodically into the tight container. The water is separated from the oil at the end of the month with a separation funnel, or simply by siphoning out the oil.

6. At the end of the month, all the water in the container must then be shaken before filling the bottles to be sent for analysis. If medicinal paraffin oil is present, then the container should not be shaken, but left aside for a week, before filling the bottles. This will ensure mixing but avoid that the oil forms an emulsion with water, which later would make its separation difficult.

7. If the amount of water collected in any month exceeds 5 litres, then a second 5-litre bottle should be used to accumulate the excess water. At the end of the month all the water from both containers must then be mixed before filling the bottles with samples. The operations described in paragraph 3 to 7 should be carried out as rapidly as possible, in order to reduce the time during which the sample is exposed to the atmosphere and thus the risk of evaporation.

8. If the medicinal paraffin oil is used and its separation from water is not possible at the station, then this separation will be made at the laboratory in charge of the isotopic analysis. In this case, try to minimize the amount of oil present in the bottles shipped and be sure that the amount of water largely exceeds that of oil. Remember that an amount of at least 300 ml of water is needed for tritium, deuterium and oxygen-18 analysis.

[4] From a document available online at the www.naweb.iaea.org site.

9. At the end of the month when the bottles with samples are filled, the 5-litrecontainer should be dried again before using it for the next month's precipitation.

10. Never fill any plastic bottle completely. Always leave a slight air gap (~ 5% of bottle volume) to allow for water expansion due to possible temperature increase or decrease below the freezing point. Always be sure to use the bottles provided by IAEA, and ensure the cap is secured tightly.

11. Information concerning the station, month and amount of total precipitation should be clearly marked on the labels provided by IAEA. The bottles should always be marked immediately on filling.

12. There should be no sharp objects in the box when samples are returned (e.g. screws, nails, wood splinters). These can puncture the plastic bottles.